RIFT VALLEY FEVER VIRUS REPLICATION IN MOSQUITO CELLS

STEPHEN ROBERT WELCH

Submitted in fulfillment of the requirements for the Degree of
Doctor of Philosophy in Molecular Virology

Institute of Infection Immunity & Inflammation
College of Medical, Veterinary and Life Sciences
University of Glasgow

September, 2014

© Stephen R. Welch, 2014

Abstract

Rift Valley fever virus is a mosquito-borne pathogen capable of causing severe disease in both humans and ruminants. The disease was first recognised in 1931, and is now endemic in large areas of Africa, and more recently the Arabian peninsula. The tripartite genome consists of two negative-sense (L and M) and one ambisense (S) segments encoding four structural and three non-structural proteins. Whilst the viruses has been extensively studied in the mammalian host, characterisation is less defined in the mosquito vector species.

The results presented herein describe the characterisation of several rMP12 infected mosquito cell lines. Compared to rMP12 infected mammalian cells differences in viral replication, S segment-encoded protein expression and mRNA transcript levels, and phenotypic presentation of the non-structural protein NSs are described. These differences were also observed between the individual mosquito cells lines. Using reverse genetics a virus was generated in which the N and NSs coding sequences on the ambisense S segment were switched, yielding rMP12:SSwap virus. This virus demonstrated altered levels of protein expression and RNA transcription in infected cells, and replication was cytotoxic in mosquito cell lines. By developing a strand specific qRT-PCR assay I was able to show that infection with rMP12:S-Swap led to a differential packaging ratio of genomic and antigenomic polarity S segment RNA into progeny virions. To investigate replication and transcription of RVFV in mosquito cells a minireplicon assay was developed, which demonstrated differences in viral protein activity and segment-specific promoter activity when compared to a mammalian cell based minireplicon assay. Activation of the RNAi pathway in rMP12 and recombinant virus infected mosquito and mammalian cells was also investigated.

My results highlight the numerous differences between RVFV replication in mammalian and mosquito cells. The development of two assays described here open the way for more detailed comparison of arbovirus replication in mammalian and mosquito cells, and the RNAi research described will broaden our understanding of mosquito antiviral RNAi responses.

Table of Contents

List of Tables

List of Figures

Publications based on project research

Brennan, B., Welch, S. R., McLees, A., & Elliott, R. M. (2011). Creation of a recombinant Rift Valley fever virus with a two-segmented genome. Journal of Virology, 85(19), 10310–10318. doi:10.1128/JVI.05252-11

Brennan, B., Welch, S. R., & Elliott, R. M. (2014). The consequences of reconfiguring the ambisense S genome segment of Rift Valley fever virus on viral replication in mammalian and mosquito cells and for genome packaging. PLoS Pathogens, 10(2), e1003922. doi:10.1371/journal.ppat.1003922

Acknowledgements

Firstly, thanks must go to my supervisor Professor Richard Elliott for giving me the opportunity to do a PhD, and the support and patience he had shown over the last four years. And to everyone past and present in the RME lab: Agnieszka, Angela, Basma, Ben, Beryl, Daisy, Elya, Felix, Gillian, Gjon, Gustavo, Ing, Jill, Junjie, Ping, Natasha, Sandra, Sophie, Veronica, and Xiaohong – thank you for all the coffee breaks, birthday cakes and nights out. I am not sure it will feel like Christmas anymore unless I get to paint my face and dress up in a ridiculous costume.

Special thanks however must go to Ben and Agnieszka however for their advice and support throughout this project. I would like to thank my assessors Professors Rick Randall and Martin Ryan at St Andrews University, and Dr. Alain Kohl and Professor Sarah Cleaveland at Glasgow University for helpful discussions of my work. I am also indebted to Dr. Esther Schnettler and Dr. Mick Watson for their help and advice with the RNAi research. I also would like to thank previous colleagues at Porton Down for teaching me how science is done, and giving me the experiences I needed to make this PhD a success. Whilst there are too many to name individually special thanks must go out to Dr. Jane Osborne and Professor Patricia Cane for their advice and support. Thanks also to Professors David Nokes and Kevin Marsh and everyone at the KEMRI-Wellcome Trust Unit in Kilifi for the opportunity to experience the academic research environment again, without which I would never have considered doing a PhD.

To ex-teammates in the Whipping Boys football team, to past and present Bionet members, and to all other friends, colleagues and flat mates at both universities I would like to say thank you for making my time out of the lab so much fun. Lastly, the final thank you must go to Alex for her support and encouragement during the past three years.

Declaration

I, Stephen Robert Welch, declare that, except where explicit reference is made to the contribution of others, that this thesis is the result of my own work and has not been submitted for any other degree at the University of Glasgow or any other institution.

Signature _____

Printed name _____

List of abbreviations

General:

(e)GFP	(enhanced) green fluorescent protein
ACDP	Advisory Committee on Dangerous Pathogens
cDNA	complementary DNA
CDS	coding sequence
CIAP	calf intestinal alkaline phosphatase
CPE	cytopathic effect
CRE	cis-acting replication element
ct	crossing threshold
Dcr-2	Dicer-2 protein
DI	defective interfering
DIVA	differentiating infected and vaccinated animals
DMEM	Dulbeccos modified Eagles media
DNA	deoxyribonucleic acid
dsRNA	double stranded RNA
DTT	dithiothreitol
EDTA	ethylenediaminetetraacetic acid
EM	electron microscopy
ER	endoplasmic reticulum
FCS	foetal calf serum
FFLuc	firefly luciferase
GMEM	Glasgow modified Eagles Media
Gn/Gc	glycoproteins Gn and Gc
h p.i.	hours post infection
h p.t.	hours post transfection
HF	haemorrhagic fever
HFRS	haemorrhagic fever with renal syndrome
HPLC	high-performance liquid chromatography
HPS	hantavirus pulmonary syndrome
ICTV	International Committee on Taxonomy of Viruses
IFN	interferon

IRES	internal ribosome entry site
L	L protein (viral polymerase) or large genomic segment
M	medium genomic segment
MEM	modified Eagles media
M-MLV RT	Moloney murine leukemia virus reverse transcriptase
MOI	multiplicity of infection
mRNA	messenger RNA
N	nucleoprotein
NCS	newborn calf serum
NE	nephropathia epidemica
NSm	non-structural protein encoded on M segment
NSs	non-structural protein encoded on S segment
NSV	negative strand virus
nt	nucleotide
ORF	open reading frame
PBS	phosphate buffered saline
PCR	polymerase chain reaction
pfu	plaque forming units
piRNA	PIWI-induced RNA
QC	quick-change PCR
qPCR	quantitative PCR
RCF	relative centrifugal force (g)
RdRp	RNA-dependent RNA-polymerase
RISC	RNA-induced silencing complex
Rluc	*Renilla* luciferase
RNA	ribonucleic acid
RNAi	RNAI interference
RNP	ribonucleocapsid protein
rpm	revolutions per minute
RT	reverse-transcription
RT-PCR	reverse-transcription PCR
S	small genomic segment
SDS	sodium dodecyl sulfate
siRNA	small interfering RNA

T7RNAP	T7 RNA polymerase
Tm	melting temperature
TPB	tryptose phosphate broth
UPS	ubiquitin-proteasome system
UTR	un-translated region
viRNA	virus induced RNA
VLP	virus-like particle

Virus abbreviations:

AKAV	Akabane virus
ANDV	Andes virus
BAV	Bayou virus
BCCV	Black Creek Canal virus
CCHFV	Crimean-Congo haemorrhagic fever
CVV	Cache Valley virus
DENV	dengue virus
DOBV	Dobrava-Belgrade virus
DUGV	Dugbe virus
FMDV	foot and mouth disease virus
HTNV	Hantaan virus
JCV	Jamestown Canyon virus
JEV	Japanese encephalitis virus
JUNV	Junin virus
LACV	La Crosse virus
LASV	Lassa virus
LCMV	lymphocytic choriomeningitis virus
NSDV	Nairobi sheep disease virus
ONNV	O'nyong'nyong virus
OROV	Oropoche virus
PHV	Prospect Hill virus
PUUV	Puumula virus
RSV	respiratory syncytial virus

RVFV	Rift Valley fever virus
SBV	Schmallenberg virus
SEOV	Seoul virus
SFTSV	severe fever with thrombocytopenia syndrome virus
SFV	Semliki Forest virus
SINV	sin nombre virus
SNV	Sindbis virus
TSWV	tomato spotted wilt virus
TULV	Tula virus
UUKV	Uukuniemi virus
VSV	vesicular stomatitis virus
WEEV	western equine encephalitis virus
WNV	West Nile virus

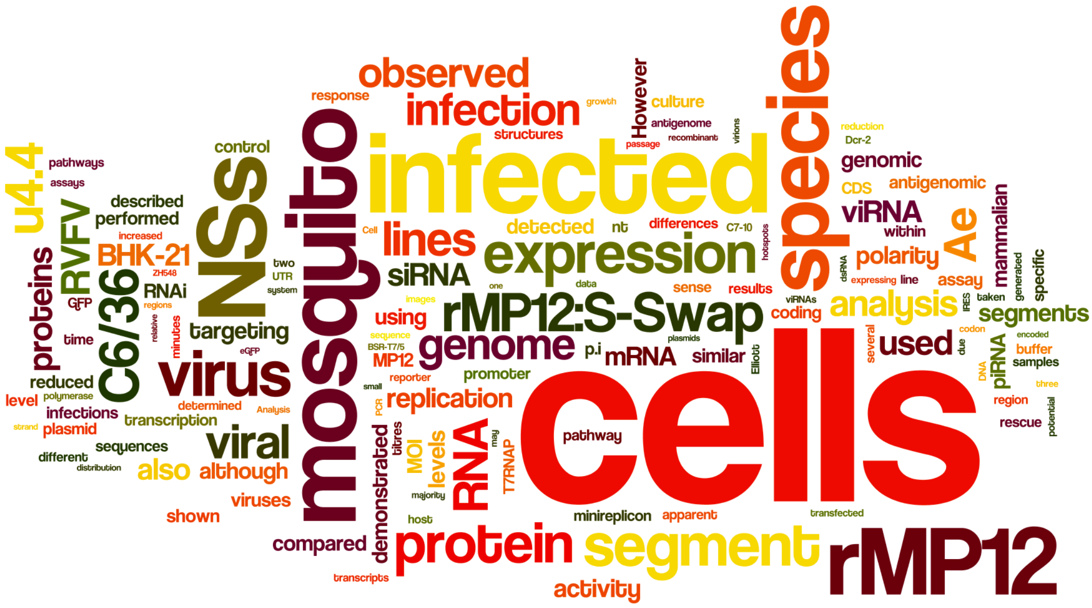

cells
infected
mosquito
species
rMP12
NSs
expression
rMP12:S-Swap
segment
protein
virus
C6/36
infection
observed
lines
genome
RNA
u4.4
RVFV
proteins
viral
analysis
Ae
replication
BHK-21
siRNA
viRNA
polarity
segments
used
targeting
mRNA
detected
also
although
shown
viruses
compared
activity
demonstrated
levels
MOI
T7RNAP
pathway
minireplicon
promoter
similar
genomic
antigenomic
mammalian
piRNA
specific
control
described
performed
reduced
infections
plasmid
transcription
sequences
different
level
time
RNAi
GFP
two
UTR
system
response
structures
However
culture
antigenome
differences
nt
C7-10
sense
results
coding
using
MP12
p.i
Elliott
several
rescue
region
buffer
samples
assay
CDS
within
Dcr-2
reduction
pathways
assays
increased
determined
Analysis
polymerase
strand
distribution
apparent
host
majority
transcripts
transfected
reporter
titres
may
growth
passage
recombinant
virions
hotspots
dsRNA
expressing
line
taken
generated
encoded
codon
due
IRES
DNA
three
potential
data
one
images
sequence
BSR-T7/5
eGFP
small
PCR
Cell
ZH548
regions
relative
minutes
plasmids
viRNAs

Chapter 1

GENERAL INTRODUCTION

1 General introduction

1.1 Bunyaviruses

1.1.1 Classification

The *Bunyaviridae* family comprises over 350 viruses sharing common morphological, genetic, and replicative characteristics (Elliott & Schmaljohn 2013). First established as a separate family by the International Committee on Taxonomy of Viruses (ICTV) in 1975, sub-classification of member viruses based on serological cross-reactivity, similar morphological and biochemical characteristics, and conserved genomic sequences has led to the establishment of five genera (King et al. 2012). These genera are *Orthobunyavirus*, *Phlebovirus*, *Nairovirus*, *Hantavirus*, and *Tospovirus*. With the exception of hantaviruses, bunyaviruses are all arboviruses primarily transmitted by mosquitoes, although a wide range of haematophagous invertebrate species such as ticks and phlebotomine sandflies also act as competent vectors. Whilst the majority of *Bunyaviridae* infections are innocuous, several cause high impact diseases in both humans and animals (Table 1-1). The orthobunyavirus Bunyamwera (BUNV) is the family prototype, and the first bunyavirus whose genome was sequenced (Elliott & Schmaljohn 2013).

1.1.2 Genera

1.1.2.1 Orthobunyavirus

The *Orthobunyavirus* genus is the largest of the *Bunyaviridae*, comprising over 170 species. Currently 18 serogroups and 44 species are recognised by the ICTV, although classification remains complex due to the occurrence of natural re-assortants and a lack of extensive sequence data. All known orthobunyaviruses are arboviruses, comprising a vertebrate host and mosquito vector lifecycle. Within the genus are a number of important human and animal pathogens. La Crosse viruses (LACV) and Jamestown Canyon virus (JCV) are the leading cause of viral encephalitis in North America (McJunkin et al. 2001). Oropouche virus (OROV) in Brazil is second only to dengue virus (DENV) for incidence of arboviral morbidity, and is increasing recognised as a major public health issue across Central and South America (Mourãão et al. 2009; Azevedo et al. 2007). Cache Valley

Table 1-1: Notable virus species in the *Bunyaviridae* family

Genus and Species	Vector	Disease manifestations	Geographic Distribution
Orthobunyavirus			
Bunyamwera	Mosquito/Tick	Acute febrile illness, encephalitis	Africa
La Crosse	Mosquito	Fever, headache, encephalitis	North America
Oropouche	Midge	Fever, myalgia, arthralgia, anorexia, encephalitis	South America
Tahyna	Mosquito	Acute febrile illness, pneumonia, occasional encephalitis	Central Europe, Asia
Phlebovirus			
Rift Valley fever	Mosquito	Hepatitis, retinitis, encephalitis, haemorrhagic fever	Africa, Arabia
SFTSV$^{\Phi}$	Tick	Fever, thrombocytopenia, leukocytopenia	China, SE Asia
Toscana	Sandfly	Fever, myalgia, conjunctivitis, nausea	Mediterranean Europe
Nairovirus			
CCHFV$^{\Psi}$	Tick	Haemorrhagic fever	Africa, Europe, Asia
Nairobi Sheep Disease	Mosquito/Tick	Haemorrhagic gastroenteritis in sheep and goats	Africa
Hantavirus			
Hantaan	Field Mouse	Haemorrhagic fever with renal syndrome (HFRS)	Europe, Asia
Seoul	Brown Rat	Haemorrhagic fever with renal syndrome (HFRS)	Europe, Asia, Americas
Puumula	Bank Vole	Nephropathia epidemica (NE)	Europe
Sin Nombre	Deer Mouse	Hantavirus cardio-pulmonary syndrome (HCPS)	North America
Tospovirus			
Tomato Spotted Wilt	Thrip	Spotting and wilting of tomato plant leaves	Worldwide

Φ- Severe fever with thrombocytopenia syndrome virus
Ψ- Crimean-Congo haemorrhagic fever virus
NB – all disease manifestation are for human infection unless otherwise stated

(CVV) and Akabane (AKAV) virus are responsible for economically important diseases of livestock in North America and Australia respectively, with abortion and congenital deformities common clinical presentations (Kittelberger et al. 2013; Blackmore & Grimstad 2008). The rapid spread of Schmallenberg virus (SBV) throughout Europe was a major problem between 2011-13 (Afonso et al. 2014).

1.1.2.2 Phlebovirus

The *Phlebovirus* genus comprises over 80 named viruses classified into two serogroups and nine antigenic complexes. They derive their name from the phlebotomine sandflies which act as the primary vectors for the majority of species, although several notable exceptions exist. The newly emerging severe fever with thrombocytopenia syndrome virus (SFTSV) in South East Asia is transmitted by *Haemaphysalis* species ticks (Liu et al. 2014). Infection results in considerable morbidity, with clinical presentations including high fever, thrombocytopenia, leukocytopenia, gastrointestinal symptoms, and lymphadenopathy (D. Li 2013). Case fatality rate is 10-15% and associated with multi organ failure (Liu et al. 2014). Uukuniemi virus (UUKV) is associated with *Ixodes* species ticks and is used as a laboratory model for phleboviruses. Rift Valley fever virus (RVFV) is transmitted by mosquito species, and is responsible for both human and livestock disease in Africa and areas of the Middle East (Grobbelaar et al. 2011).

1.1.2.3 Nairovirus

Members of the *Nairovirus* genus are almost exclusively tick-borne, are maintained in the arthropod host via transovarial transmission. Vertebrate species are infected via tick bites, and are thought to play an important amplifying role in the viral lifecycle (Elliott & Schmaljohn 2013). Crimean-Congo haemorrhagic fever virus (CCHFV) is endemic within tick populations in several African, Asian and European regions (Gergova et al. 2012; Bente et al. 2013). While it results in an asymptomatic infection of livestock and wild herbivores, human infection can result in significant morbidity and progress to severe haemorrhagic fever with a case fatality rate ranging from 5-30% (Bente et al. 2013). A second important species is Nairobi sheep disease virus (NSDV) which infects sheep and goats in Africa and Asia. Clinical presentations include abortion and acute haemorrhagic

gastroenteritis, and case fatality rates greater than 90% have been reported (Marczinke & Nichol 2002; M. C. Smith & Sherman 2011).

1.1.2.4 Hantavirus

Hantaviruses are unique amongst the bunyaviruses as they are not associated with an invertebrate vector stage in their viral lifecycle. Instead the virus is associated with, and maintained in nature by. various rodent, insectivore, and bat species (Weiss et al. 2012; Gu et al. 2014; Sumibcay et al. 2012; Jonsson et al. 2010). Virus is shed in body excretions (urine, saliva, feaces etc.) and transmitted between rodents via the inhalation route (Jonsson et al. 2010). Infection of the rodent host is asymptomatic, but symptomatic in humans. Two distinct clinical presentations are recognised, dependent on whether infection is with Old or New World hanatavirus species. Infection with Old world hantaviruses such as Hantaan (HTNV), Seoul (SEOV), Dobrava-Belgrade (DOBV), and Puumala (PUUV) virus is associated with disease classified as haemorrhagic fever with renal syndrome (HFRS). Infection with New World hantaviruses such as Sin Nombre (SINV), Andes (ANDV), Black Creek Canal (BCCV) and Bayou (BAV) virus found in the Americas presents as hantavirus cardio-pulmonary syndrome (HCPS). This is characterised by non-specific febrile illness which can progress to severe non-cardiogenic pulmonary edema and cardiogenic shock, with a case fatality rate of approximately 35% (Núñez et al. 2014; MacNeil et al. 2011).

1.1.2.5 Tospovirus

Named after the prototype tomato spotted wilt virus (TSWV), members of the *Tospovirus* genus are plant viruses transmitted by thrip species insect vectors. Over 82 plant families are susceptible to tospovirus infection, and several of these such as peanut, tobacco, potato, pepper and tomato species have significant agricultural importance (Prins & Goldbach 1998). Despite there being over 5,000 thrips species, only 14 have been identified as virus vectors (Riley et al. 2011). The geographical distribution of competent thrips species is worldwide (Pappu et al. 2009). Disease presentations include leaf and stem necrotic spots, wilted leaves, reduced vegetative output and eventual plant death (Jones 2005).

1.1.3 Virion structure

Ultrastructure characteristics of bunyaviruses have been primarily determined using cryoelectron microscopy methods. Individual virions have a pleomorphic or spherical appearance, with diameters between the genera ranging from 80-120 nm (Elliott & Schmaljohn 2013). Virions have a lipid envelope 5-7 nm thick derived from the viral morphogenic origin site, primarily the Golgi cisternae. The viral envelope contains the viral glycoproteins Gn and Gc, arranged as heterodimers with a 1:1 molar ratio (Gentsch et al. 1977; Obijeski, Bishop, Murphy, et al. 1976a). They project 5-10 nm from the envelope surface, forming spike structures visible by electron microscopy (EM) (Talmon et al. 1987; Obijeski, Bishop, Murphy, et al. 1976a; Hewlett & Chiu 1991) (Figure 1-1). Bunyaviruses do not encode a matrix protein, and instead virion morphology is thought to be strongly influenced glycoprotein envelope arrangement (Överby et al. 2008; Huiskonen et al. 2009). The glycoprotein organisation is distinct between the genera. Members of *Orthobunyavirus*, *Tospovirus*, and *Nairovirus* genera generally have a disordered arrangement of the Gn/Gc heterodimers throughout the envelope, although a tripodal glycoprotein spike has recently been described for BUNV (M. L. Martin et al. 1985; Bowden et al. 2013). Viruses in the *Phlebovirus* genus exhibit a more ordered T-12 icosahedral lattice arrangement of Gn/Gc heterodimers, giving the virions a more distinct spherical morphology (Freiberg et al. 2008; Huiskonen et al. 2009). The hantavirus Gn/Gc heterodimers are also distinctly ordered, but the heterodimers are further arranged four-fold in a grid-like arrangement (Battisti et al. 2011; M. L. Martin et al. 1985; Huiskonen et al. 2010). The viral genome consists of RNA genomic segments encapsidated by viral nucleoprotein N to form ribonucleocapsid protein (RNP) structures. RNPs are also associated with a small amount of viral polymerase protein L (Obijeski, Bishop, Murphy, et al. 1976a). There is no overt organisation to the virion interior, although interactions between RNPs and Gn cytoplasmic tails have been described (Battisti et al. 2011; Överby et al. 2008; Huiskonen et al. 2009; Raymond et al. 2010; Overby et al. 2007).

1.1.4 Genome structure and coding strategy

The bunyavirus genome consists of three single-stranded RNA segments termed L, M, and S according to their nucleotide length. The segment lengths vary between the separate genera (Table 1-2). All bunyaviruses employ a predominantly negative sense coding

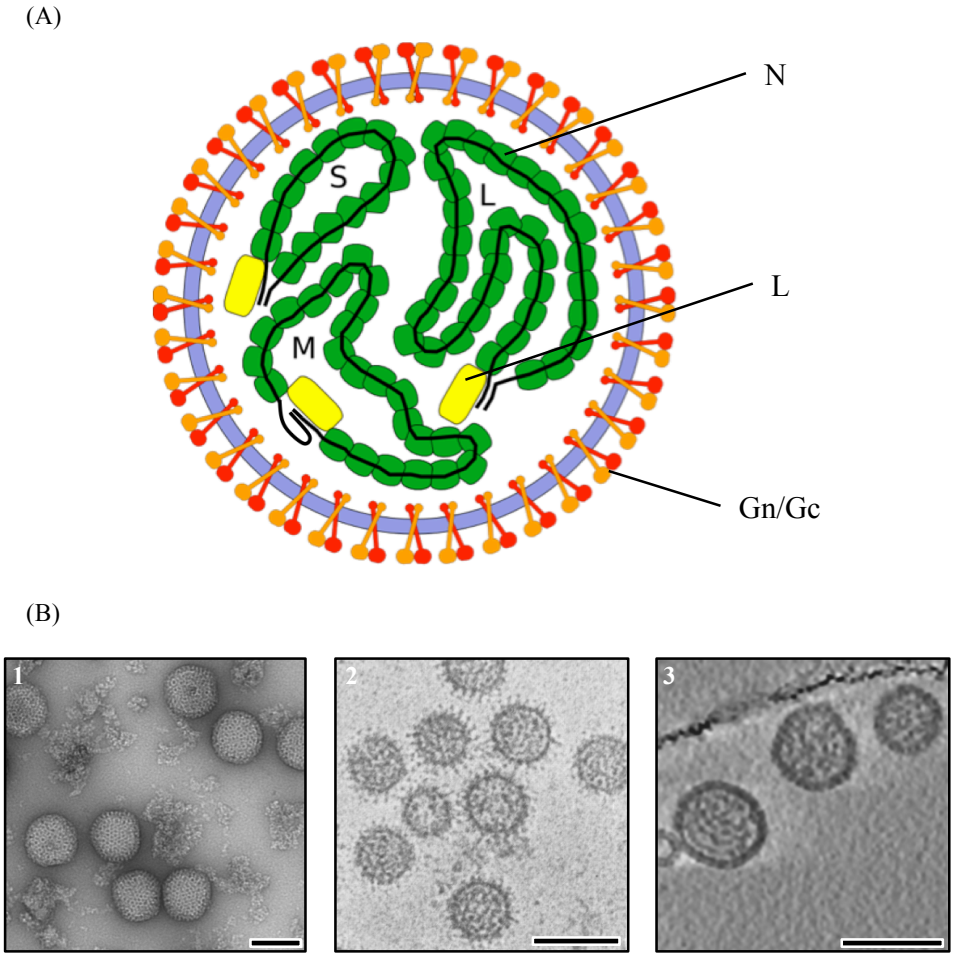

Figure 1-1: Structures of typical bunyavirus virions
(A) A schematic representation of a virion, consisting of a lipid envelope (blue) in which the viral glycoproteins Gn (red) and Gc (orange) are inserted as heterodimers. Interior of the virion comprises three ribonucleocapsid protein (RNP) complexes, which consist of genome RNA (black) encapsidated by nucleocapsid protein N (green). Each RNP complex is associated with small amounts of viral polymerase L (yellow) and adopt circular conformations due to complementary UTR sequences. (B) Cryo-electron micrographs of Rift Valley fever virus (1), La Crosse virus (2), and Tula virus (3), taken from Huiskonen *et al*, 2009, Talmon *et al*, 1987, and Huiskonen *et al*,2010 respectively. Bar represent 100 nm.

Table 1-2: Differences between viral genome sizes in members of the *Bunyaviridae* genera

	Genus				
Segment	***Orthobunyavirus***	***Phlebovirus***	***Nairovirus***	***Hantavirus***	***Tospovirus***
L	6.9	6.5	12.2	6.4	8.9
M	4.5	3.6	4.9	3.5	4.8
S	1.0	1.7	1.7	1.7	2.9
Total	12.4	11.8	18.8	11.6	16.6

NB - sizes given in kb
Adapted from (Elliott & Schmaljohn 2013)

strategy. However, the S and M segments of tospoviruses and S segment of phleboviruses encode non-structural proteins by an ambisense coding strategy. Four structural proteins are encoded: the viral polymerase (L) on L segment; the envelope glycoproteins Gn and Gc on M segment; and the nucleoprotein (N) on S segment. Non-structural proteins are also encoded on S and M segments of orthobunyavirus, tospovirus, and phlebovirus, and the S segment of certain hantaviruses (Table 1-3). The S segment non-structural proteins (termed NSs) are encoded in an overlapping reading frame for orthobunyaviruses and hantaviruses, but phleboviruses and tospoviruses use an ambisense strategy to encode the protein in a separate coding sequence (CDS). Open reading frames (ORFs) encoding potential NSs proteins are also present in certain hantaviruses (SINV, PUUV, Tula (TULV), Prospect Hill (PHV) and ANDV viruses), but have only been empirically detected in PUUV and TULV infected cells (Elliott & Schmaljohn 2013; Jääskeläinen et al. 2007; Vera-Otarola et al. 2012). M segment encoded non-structural protein (NSm) species are encoded in negative sense for orthobunyavirus and phlebovirus species, but again an ambisense strategy is employed by the tospoviruses (Figure 1-2). The CDSs are flanked 3' and 5' by untranslated regions (UTRs). UTR length varies widely between bunyavirus species, but terminal sequences show a high degree of conservation within genera for the S, M, and L segments (Elliott & Schmaljohn 2013). The terminal sequences of the 3' and 5' UTRs are complementary, and base-pairing between them causes panhandle structures to form. This gives the RNPs a circular conformation, a feature confirmed by EM analysis (Obijeski, Bishop, Palmer, et al. 1976b; Hewlett et al. 1977; Reguera et al. 2013). UTR sequences are though to contain *cis*-acting signals responsible for regulating both replication and transcription processes (Lowen et al. 2005; Gauliard et al. 2006).

1.1.5 Bunyavirus gene products

1.1.5.1 Viral polymerase

Bunyavirus L segment encodes an RNA-dependent RNA-polymerase (RdRp). Amino acid sequence alignments of bunyavirus L proteins demonstrate minimal homology, although several highly conserved motifs are observed (Aquino et al. 2003; H. Jin & Elliott 1991; Reguera et al. 2010; Muller et al. 1994). Four domains were recognised as the 'polymerase module' common in all RdRp enzymes encoded by positive, negative and double stranded

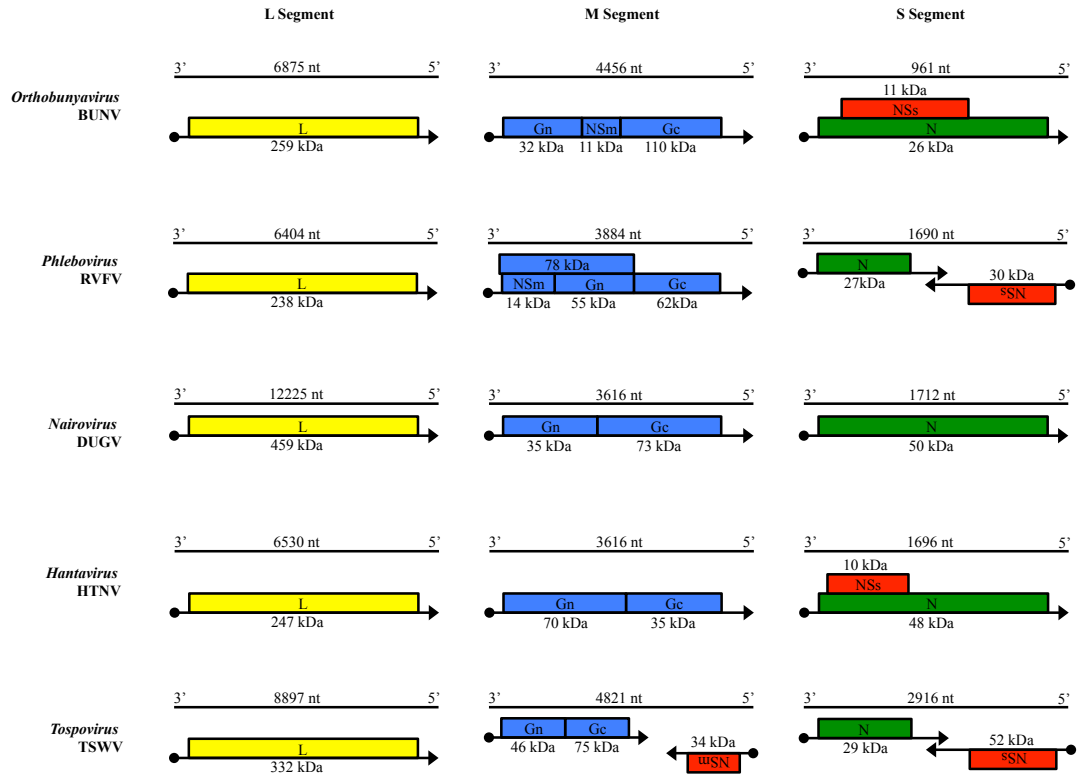

Figure 1-2: Coding strategies of genome segments for the prototypes virus species of each *Bunyavirus* genera.

Schematic representation of the L, M, and S segment for: Bunyamwera virus (BUNV); Rift Valley fever virus (RVFV); Dugbe virus (DUGV); Hantaan virus (HTNV); and tomato spotted wilt virus (TSWV). Genome strand represented by naked line with 3' and 5' ends shown, with genome length in nucleotides (nt) indicated above. Lines below the genome strands represent mRNA with 5' cap (•) and direction of transcription (5' to 3'). Coloured boxes represent encoded protein products: L - viral polymerase; Gn and Gc - envelope glycoproteins; N - nucleocapsid protein; NSm and NSs - non-structural proteins. Sizes are indicated in kilo Daltons (kDa).

Table 1-3: Differences between protein sizes encoded by viruses in the *Bunyaviridae* family

	Genus				
Protein	***Orthobunyavirus***	***Phlebovirus***	***Nairovirus***	***Hantavirus***	***Tospovirus***
L	260	240	460	250	330
Gn	35	55-70	35	70	50
Gc	110	65	75	55	75
NSm	15-18	14 and 78	78-115	none	35
N	25	30	50	50	30
NSs	10-13	30	none	none or 7-12	52

NB - sizes given in kDa
Adapted from (Elliott & Schmaljohn 2013) and (Plyusnin et al. 2012).

RNA viruses (Poch et al. 1989). Two domains unique to bunyaviruses and arenaviruses were identified, although no known biological function has yet been ascribed to these (Muller et al. 1994). Research with BUNV L protein using recombinant vaccinia virus expressing L confirmed its function as the RNA polymerase responsible for both RNA transcription and replication activity (H. Jin & Elliott 1991; H. Jin & Elliott 1993). Mutagenesis analysis of the conserved motifs comprising the polymerase module demonstrated the critical role they play in polymerase activity (H. Jin & Elliott 1992). Analysis of coding sense viral RNA transcripts revealed the presence of cell-derived sequences at the 5' terminal ends, suggesting an exonuclease activity for L protein (H. Jin & Elliott 1993). The presence of an N-terminal PD-(D/E)XK motif demonstrating exonuclease activity *in vitro* has been described for LACV, and bioinformatics analysis revealed this motif was highly conserved amongst all *Bunyaviridae* (Reguera et al. 2010). This domain is similar to motifs located in the PA protein subunit of influenza virus polymerase complex, suggesting a common origin for the cap-snatching mechanism employed by both virus families to initiate transcription of viral RNA sequences (Dias et al. 2009). The unusually large Nairovirus L contains motifs suggesting helicase, topoisomerase, and gyrase activities (Honig et al. 2004; Kinsella et al. 2004). Another region contains an ovarian tumor-like protease motif, with research suggesting a role for this enzyme in overcoming host innate immune defenses (Capodagli et al. 2011; Frias-Staheli et al. 2007). Exact functions for the other extra domains remain to be described.

A cytoplasmic localization of L protein during infection has been demonstrated for several bunyavirus species (Shi & Elliott 2009; Brennan et al. 2011; Kukkonen et al. 2004; Di Bonito et al. 1999; Rossier et al. 1986). Co-localisation with N has been shown for BUNV and RVFV, suggesting the location of "viral factory" structures representing areas of intense replication activity (Brennan et al. 2011; Shi & Elliott 2009; Fontana et al. 2008).

1.1.5.2 Envelope glycoproteins

The M segment encodes two structural envelope glycoproteins, termed Gn and Gc based on their respective position in the coding sequence (Lappin et al. 1994). Translated as a polyprotein precursor from a single mRNA, cleavage is thought to occur co-translationally as no full length polyprotein has been detected in bunyavirus infected cells (Fazakerley et al. 1988). For the majority of bunyaviruses the Gn and Gc CDSs are preceded by signal

sequences thought to mediate precursor cleavage by host cell signal peptide peptidases (Elliott & Schmaljohn 2013). The resultant Gn and Gc proteins demonstrate considerable variability between genera (Table 1-3). Both are class I membrane proteins, with the carboxyl-terminus interior to the virion and modified by *N*-glycosylation at asparagine residues. The cysteine content ranges from 4-7%, with the position of these residues highly conserved between viruses within a genus. This suggests disulphide bonds play important roles in determining correct protein folding (Shi & Elliott 2004; Persson & Pettersson 1991; Shi et al. 2005). For BUNV, Golgi-targeting and retention signals reside only within Gn, meaning Gc requires interaction with Gn to be correctly transported within the cytoplasm to sites of viral assembly (Shi & Elliott 2004).

1.1.5.3 Nucleoprotein

The nucleoprotein (N) for all bunyaviruses is encoded on S segment in a negative sense orientation. It is the most abundant protein expressed during infection. The primary function is encapsidation of viral genome strands to form the helical ribonucleocapsid protein (RNP) complexes, protecting RNA from degradation (Elliott & Schmaljohn 2013). Only encapsidated RNA can be transcribed or replicated by L. Minimal homology between N proteins from different genera is observed, although similar functionality is evident in all.

The RNA binding characteristics of several N proteins have been studied, with evidence of preferential binding of BUNV and HTNV N to 5' genomic RNA strands (Osborne & Elliott 2000; Severson et al. 2001). Further studies have revealed N specifically recognises the panhandle structures of genome segments, with genus specific recognition demonstrated (Mir et al. 2006). Oligomerisation of N is critical to facilitate RNA binding. The characteristics of this varies between the genera, with dimer subunits and trimer subunits recognized for phlebovirus and hantavirus N respectively (Kaukinen et al. 2003). N proteins of tospoviruses and orthobunyaviruses do not form subunits, and instead form oligomers by addition of single N proteins in a head-to-head, tail-to-tail multimerisation model (Uhrig et al. 1999; Eifan & Elliott 2009). Interactions with L and the glycoproteins have been described, although specific biological functions for these remain undefined.

1.1.5.4 NSm

Non-structural proteins encoded on M segment have been recognised in viral species from all genera aside from hantaviruses. In orthobunyaviruses NSm is cleaved from the polyprotein precursor along with Gn and Gc. Expression assays with BUNV showed NSm localised to the Golgi independent of Gn and Gc, although both will localise to Golgi in the absence of NSm (Lappin et al. 1994; Shi et al. 2006). Further evidence has suggested the N-terminal region of BUNV NSm plays a role in viral assembly (Shi et al. 2006). Phlebovirus NSm proteins are similarly co-translationally cleaved from a precursor. The roles these proteins play during infection remain poorly characterised, although their presence in mosquito-borne and absence in tick-borne viral species suggests a role in determining vector specificity. Whilst dispensable for infection, RVFV mutants lacking NSm are attenuated in mosquitoes (Crabtree et al. 2012). The NSm proteins encoded by nairoviruses are similarly cleaved co-translationally from a polyprotein precursor. However, further cleavage of preGn and preGc precursors is believed to occur to form several other NSm proteins. The functions of these remain uncharacterised (Sanchez et al. 2006). Contrasting the strategy of other bunyaviruses, tospoviruses employ an ambisense coding strategy to express NSm. The functions of these proteins are well characterised, and have been shown to mediate cell-to-cell spread of TSWV in infected plants (W. Li et al. 2009b).

1.1.5.5 NSs

Orthobunya- and hantavirus S segment-encoded non-structural proteins are encoded in an overlapping reading frame within the N CDS. Expression occurs from a second initiation codon in the same mRNA transcript via a ribosomal leaky-scanning mechanism (Vera-Otarola et al. 2012). In phlebo- and tospoviruses an ambisense coding strategy is employed for expression. Very little homology is observed for NSs protein between genera, and even within a genus there is a high degree of variation. However, the proteins all appear to play similar roles in antagonising anti-viral pathways. Orthobunyavirus NSs proteins are the best characterised. While NSs is non-essential for BUNV, LACV, and AKAV replication in cell culture, virus mutants lacking NSs are attenuated *in vitro*. NSs has interferon (IFN) antagonistic activities, and also contributes to a global dampening of host cell transcription during infection (Elliott & Schmaljohn 2013). NSs has been shown to inhibit BUNV, LACV, and AKAV minireplicon assays in a dose-dependent manner,

suggesting a role in regulating L activity (Blakqori & Weber 2005; Bridgen et al. 2001; Ogawa, Kato, et al. 2007a), (Ogawa, Sugiura, et al. 2007b). RVFV NSs has also been extensively studied, displaying similar activities as those observed for orthobunyavirus NSs. RVFV NSs will be discussed in more detail in a later section. Tospovirus NSs proteins are not well characterised, although a role in suppressing RNAi activity has been suggested for TSWV NSs (Oliveira et al. 2011). NSs proteins have been identified in several hantavirus species, with evidence suggesting similar interferon antagonistic properties for TULV and PUUV NSs (Jääskeläinen et al. 2007; Jääskeläinen et al. 2008).

1.1.6 Bunyavirus replication cycle

The bunyavirus replication cycle is exclusively cytoplasmic, and comprises four principle stages: 1) viral attachment and entry; 2) primary transcription and translation; 3) genome replication; and 4) viral assembly and release of progeny virions. These stages are summarised in Figure 1-3.

1.1.6.1 Viral attachment and entry

Bunyaviruses employ mechanisms for cell attachment and entry common to the majority of enveloped viruses. Attachment involves interactions between the viral envelope glycoproteins and specific cellular receptor molecules on the cell surface. Gc protein is thought to be the major attachment protein for orthobunyaviruses in both mosquitos and vertebrate hosts (Plassmeyer et al. 2005; Hacker et al. 1995). However studies with LACV indicate a more important role for Gn in viral attachment in the mosquito vector (Ludwig et al. 1991; Ludwig et al. 1989). Gn is similarly the more important glycoprotein for tospovirus TSWV attachment to thrips cells (Whitfield et al. 2004). In all tospoviruses glycoproteins are required only for infection of the invertebrate vector and not for plant cell infection (Elliott & Schmaljohn 2013). Cellular receptors for the bunyaviruses remain poorly characterised, with only those for hantaviruses and phleboviruses identified. Hantavirus glycoproteins interact with β1- and β3-integrin family proteins to mediate attachment (Gavrilovskaya et al. 1998; Gavrilovskaya et al. 1999). Two further proteins, DAF/CD55 and gC1qR/p32, have been shown to be required for HTNV and PUUV virus infection (Krautkrämer & Zeier 2008; Choi et al. 2008). RVFV, SFTSV, and UUKV

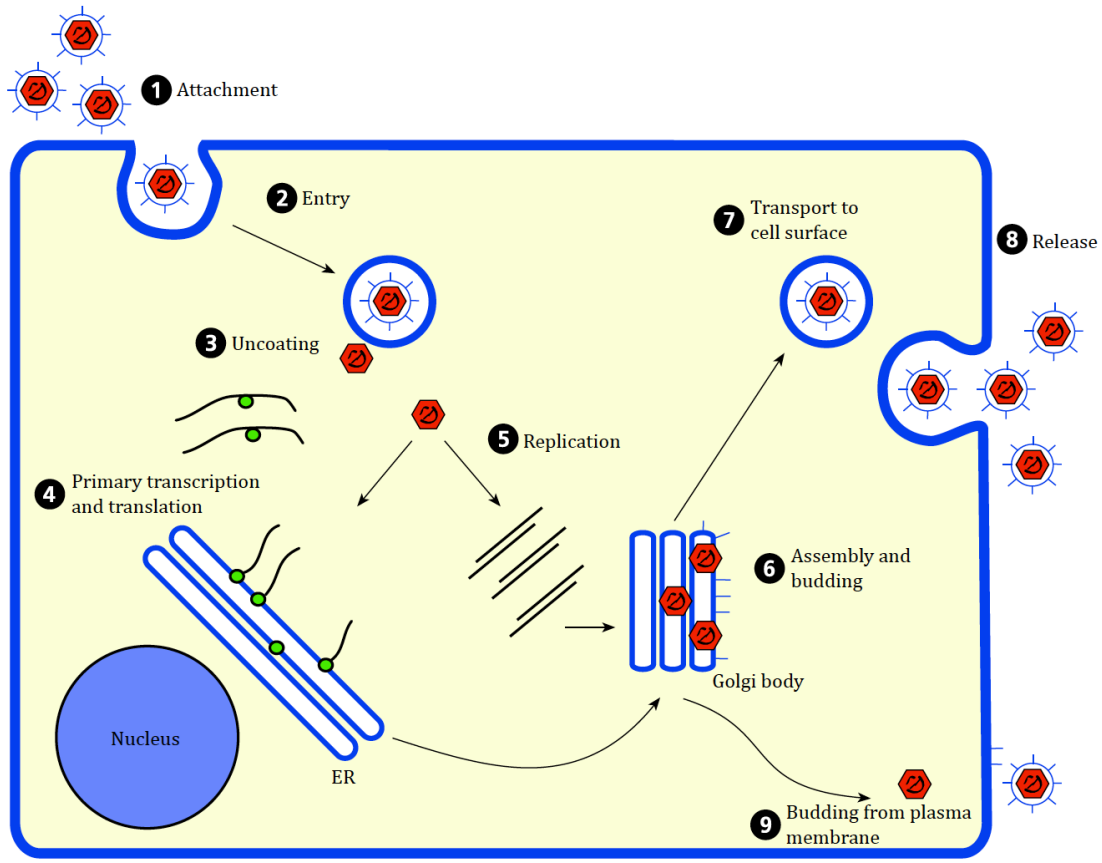

Figure 1-3: Bunyavirus replication cycle
Schematic representation of the viral lifecycle of a typical bunyavirus. Represents the following stages: 1. Attachment mediated by interaction between viral envelope glycoproteins and cell surface proteins; 2. Clathrin-dependent receptor-mediated endocytosis; 3. Low pH induced fusion of viral and vesicle membranes causes viral uncoating; 4. Primary transcription of viral mRNA and simultaneous translation of viral proteins on cytoplasmic (L and S segment encoded) and membrane bound (M segment encode) ribosomes; 5. Replication of viral genome and antigenome strands by viral polymerase forming numerous ribonucleocapsids (RNP) complexes; 6. Accumulation of viral glycoproteins and RNPs at Golgi smooth membranes, and assembly and budding from Golgi cisternae; 7. Transport of progeny virions to cell surface via exocytic vesicles; 8. Fusion of vesicle membrane with plasma membrane resulting in release of progeny virions into extracellular space; 9. Some bunyavirus species can bud directly from the plasma membrane.

(Figure adapted from (Elliott & Schmaljohn 2013)

attachment is mediated by DC-SIGN, a C type lectin mannose binding protein thought to interact with the glycosylated residues of both Gn and Gc (Lozach et al. 2011; Hofmann et al. 2013). After attachment, the majority of bunyavirus species are internalised through a clathrin-dependent receptor-mediated endocytosis process, a process described for HTNV, OROV and CCHFV (Simon et al. 2009; Santos et al. 2008; M. Jin et al. 2002). An exception is UUKV which utilises a clathrin-independent endocytosis pathway (Lozach et al. 2010). Once internalized, membrane fusion between viral and vesicle envelopes is mediated by acidification of the endocytic vesicle causing conformational changes in Gn and/or Gc (Lozach et al. 2010; Hacker & Hardy 1997; Rossier et al. 1986; M. Jin et al. 2002). This releases the RNP complexes into the cytoplasm.

1.1.6.2 Primary transcription and translation

After uncoating, primary transcription from the RNPs is initiated by virion-associated L protein interacting with 3' UTRs of the genome segments. Minireplicon experiments have shown that L and N are both necessary and sufficient for this activity, and naked RNA cannot act alone as a template for transcription (Lopez et al. 1995; Dunn et al. 1995). Bunyaviruses utilise the exonuclease activity of L to removed the capped 5' termini of cellular mRNAs, which are then used to prime viral mRNA transcription (H. Jin & Elliott 1991; Reguera et al. 2010). A role in this "cap-snatching" mechanism has also been suggested for SINV N protein (Mir et al. 2008). Viral mRNA transcripts are not poly-adenylated at the 3' termini (Vera-Otarola et al. 2010). Viral transcripts terminate prior to the 5' end of the template, indicating the presence of transcription termination sequences. Genome segments with ambisense coding arrangements have termination signals located within the intergenomic regions (IGRs). No consensus termination signal has been identified for bunyaviruses, although sequences responsible for transcription termination have been identified for several individual species (Barr et al. 2006; Blakqori et al. 2012; Ikegami et al. 2007). Translation is initiated before transcription is completed (Figure 1-4). Translation of proteins encoded on L and S segment occurs on free cytoplasmic ribosomes. The M segment proteins are translated by membrane-bound ribosomes, before transportation to Golgi cisternae where viral assembly occurs (Elliott & Schmaljohn, 2013).

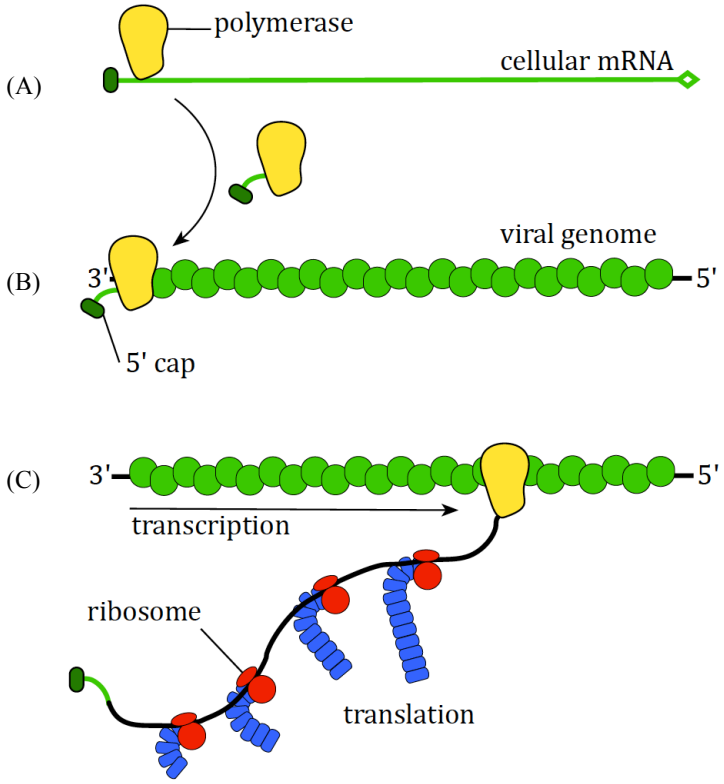

Figure 1-4: Viral mRNA transcription initiation
Viral polymerase exonuclease activity cleaves the 5' cap structure from cellular mRNAs (A) which is then used to initiate transcription of viral mRNA transcripts from viral genome strands (B). As transcription occurs the nascent mRNA stand associates with ribosomes to initiate translation of viral protein products (C).

Adapted from (Mir et al. 2008).

1.1.6.3 Replication

The next stage of infection is replication of the viral genome. This process requires the generation of exact copies of the negative sense genomes, yielding positive sense antigenome strands. Genome replication is cap-independent, produces full-length copies of template, and nascent RNA transcripts are immediately encapsulated by N thus preventing translation (Elliott & Schmaljohn, 2013). Viral polymerase is responsible for both transcription and replication activity, although the process or processes responsible for regulating the switch between the two activities is unclear. However, for another RNA virus respiratory syncytial virus (RSV) the cellular level of N has been shown to be important in regulating the change in polymerase activity (Noton et al. 2010). Analysis with BUNV demonstrated that mutants of N exhibited variations in their transcriptional and replicative abilities, suggesting N protein plays a role in regulating the synthesis of the different RNA species (Eifan & Elliott 2009). It is thought that encapsidation by N may serves as an anti-termination signal for the polymerase, similar to what is seen in other negative strand viruses (NSVs) such as the rhabdovirus vesticular stomatitis virus (VSV) and the paramyxovirus Sendai virus (Elliott & Schmaljohn, 2013). The antigenome RNA transcripts act as templates for further replication of negative sense genome segments. In segments with ambisense coding strategies the positive sense antigenomes also act as templates for transcription (Figure 1-5).

1.1.6.4 Virus assembly and release

Bunyavirus assembly occurs at the Golgi smooth membrane in contrast to many other NSVs which bud at the plasma membrane. However, budding at both the Golgi and plasma membranes has been described for the hantaviruses SINV and BCCV, and the phlebovirus RVFV (Anderson & J. F. Smith 1987; Ravkov et al. 1997). Viral glycoproteins accumulate in these membranes, and viral proteins and RNP complexes are trafficked to these locations. Studies with BUNV have identified unique structures at the assembly site involving both cellular and viral proteins, with the complexes termed viral factories (Fontana et al. 2008).Virions are formed by budding into the Golgi cisternae, followed by transport to the cell surface via the exocytic pathway and release of progeny virions into the extracellular space.

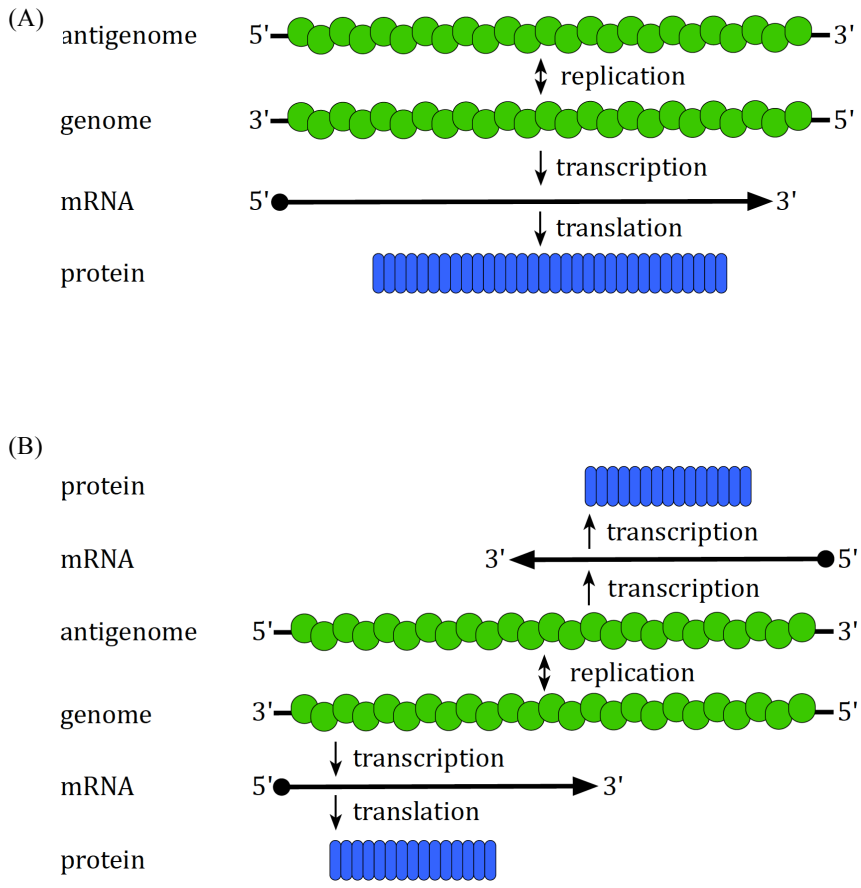

Figure 1-5: Bunyavirus transcription and replication strategies for negative and ambisense genome segments
(A) mRNA is transcribed directly from genome (negative) sense segments. Antigenome (positive) sense segments are replicated using genome sense template strands. (B) On ambisense segments proteins encoded in the negative sense are translated as shown in (A). mRNA for protein encoded in the positive sense is transcribed from after the genome is replicated, using the antigenome strand as template.

1.2 Rift Valley fever virus

1.2.1 Epidemiology

Rift Valley fever virus (RVFV) is a member of the *Phlebovirus* genus primarily transmitted by mosquitos. It is the causative agent of Rift Valley fever (RVF), a potentially severe disease of both livestock and humans. It was first isolated during an 1931 outbreak of unexplained sudden death and abortion in sheep near to Lake Niavasha in the Rift Valley region of Kenya (Daubney & Hudson 1931). The traditional endemic range of the virus was limited to sub-Saharan Africa, but several ”virgin-soil” outbreaks of epidemic disease have subsequently expanded the geographic range of the virus. The 1977-1979 epidemic in Egypt was the first time the virus was isolated north of the Sahara (Meegan et al. 1979). It was isolated for the first time outside of the African continent during a 1979 disease outbreak in Madagascar (Morvan et al. 1992; Morvan et al. 1991). It has more recently been recognised in the Arabian peninsular during a 2000 outbreak in Yemen and Saudi Arabia (Jup et al. 2002; Shoemaker et al. 2002). The virus has now been isolated in over 30 countries, including the majority of countries in Africa (Rolin et al. 2013) (Figure 1-6).

Unlike the majority of arboviruses that exhibit a narrow range of permissive vectors, RVFV has the potential to infect an extremely broad range of vectors species. Epidemiological surveys have isolated RVFV from a large number of different mosquito species (Table 1-4), and the ability to infect certain tick and fly species has also been documented (Pepin et al. 2010; Fontenille et al. 1998; Labuda & Nuttall 2004; Chevalier et al. 2010). Vector species of RVFV are broadly split into two classes, the maintenance vectors and the amplifying vectors. The maintenance vectors are predominately *Aedes* species, with virus sustained in nature through transovarial transmission. The classical endemic regions in East Africa are climatically atypical for an equatorial latitude, being generally temperate and dry. Time between periods of significant rainfall can be substantial, and *Aedes* mosquitos can survive these drought intervals due to their desiccation-resistant eggs (Gargan et al. 1988). Seasonal rainfall creates areas of localised and semi-permanent fresh-water flooding, dehydrating and hatching the *Aedes* eggs. Flood water also attracts host species for RVFV (buffalo, cattle, sheep, goats) to the area which

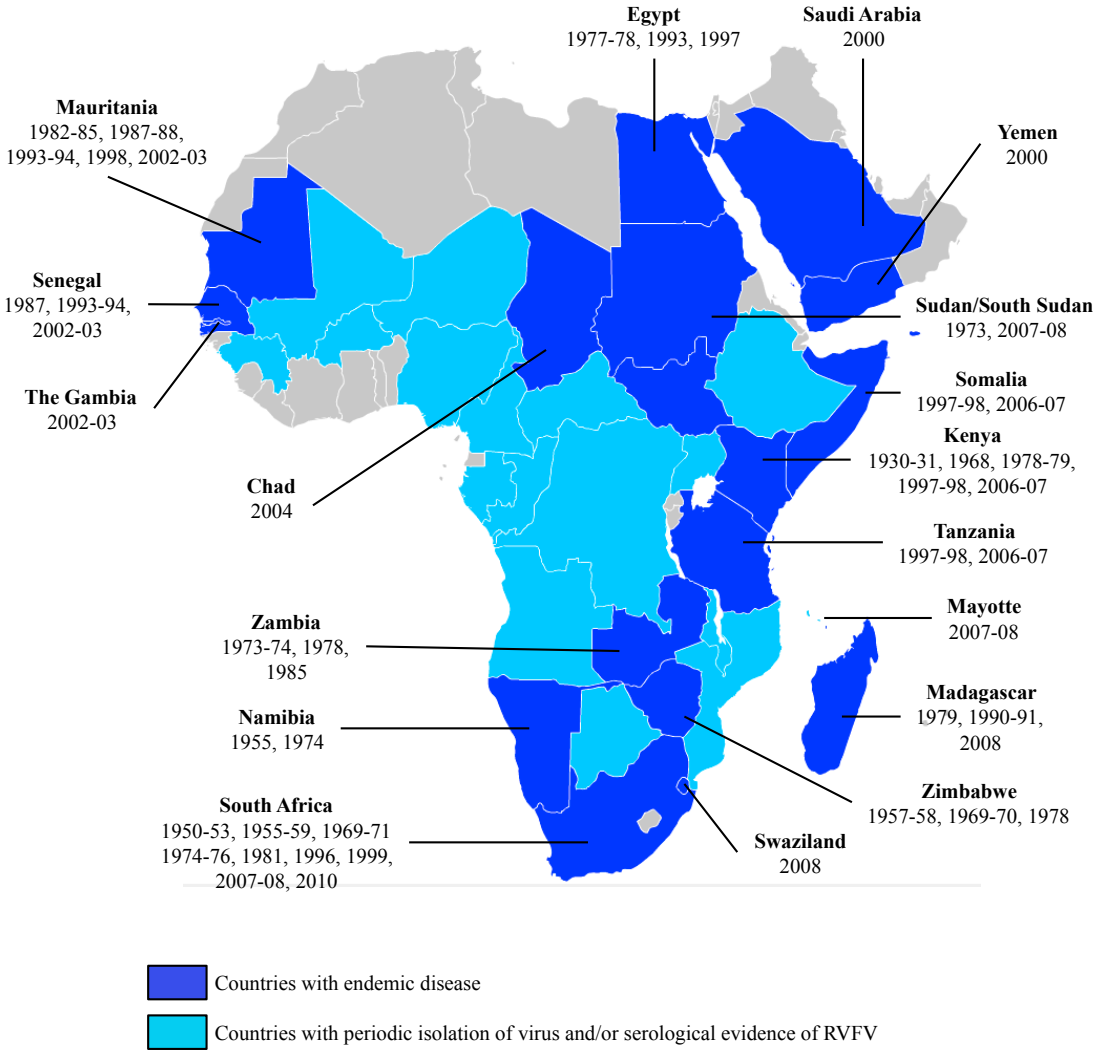

Figure 1-6: Geographic distribution of Rift Valley fever virus
Map showing the geographic distribution of RVFV in Africa and the Arabian peninsular, with known epizootic outbreaks of disease indicated. Figure adapted from (Rolin et al. 2013).

Table 1-4: Arthropods naturally infected with Rift Valley fever virus

Genus	Species	Survey region (year)
Aedes (Aedimorphus)	*cumminsii*	Kenya (1981-1984)
		Burkina Faso (1983)
	dalzieli	Senegal (1974, 1983)
	dentatus	Zimbabwe (1969)
	durbanensis	Kenya (1937)
	ochraceus	Senegal (1993)
	tarsalis	Uganda (1944)
	vexans arabiensis	Senegal (1993) Saudi Arabia (2000)
Aedes (Neomelaniconion)	*circumluteolus*	Uganda (1955) South Africa (1955, 1981)
	mcintoshi	Zimbabwe (1969) South Africa (1974-1975) Kenya (1981-1984)
	palpalis	Central African Republic (1969)
Ochlerotatus (Ochlerotatus)	*caballus*	South Africa (1953)
	caspius	Suspected, Egypt (1993)
	juppi	South Africa (1974-1975)
Aedes (Stegomya)	*africanus*	Uganda (1956)
	demeilloni	Uganda (1944)
Aedes (Diceromya)	*furcifer group*	Burkina Faso (1983)
Anopheles (Anopheles)	*coustani*	Zimbabwe (1969) Madagascar (1979)
	fuscicolor	Madagascar (1979)
Anopheles (Cellia)	*chrityi*	Kenya (1981-1984)
	cinereus	South Africa (1974-1975)
	pauliani	Madagascar (1979)
	pharoensis	Kenya (1981-1984)
Culex (Culex)	*spp.*	Madagascar (1979)
	antennatus	Nigeria(1967-1970) Kenya (1981-1984)
	neavi	South Africa (1981)
	pipiens	Egypt (1977)
	poicilipes	Senegal (1998, 2003)
	theileri	South Africa (1970) Zimbabwe (1969)
	tritaeniorhynchus	Saudi Arabia (2000)
	vansomereni	Kenya (1981-1984)
	zombaensis	South Africa (1981) Kenya (1981-1984, 1989)
Culex (Eumelanomya)	*rubinotus*	Kenya (1981-1984)
Eretmapodites	*chrysogaster*	Uganda (1944)
	quinquevittatus	South Africa (1971) Kenya (1981-1984)
Coquillettidia	*fuscopennata*	Uganda (1959)
	grandidieri	Madagascar (1979)
Mansonia (Mansoniodes)	*africana*	Uganda (1959, 1968) Central African Republic (1969) Kenya (1989)
	uniformis	Uganda (1959) Madagascar (1979)

Taken and adapted from (Chevalier et al. 2010).

subsequently become infected. These events create localised disease outbreaks. Viremia in the infected vertebrates is short lived however (2-7 days), suggesting that that chronic infection in the local *Aedes* mosquito population plays the greater role in maintaining endemicity than the infected vertebrates (McIntosh et al. 1973; Davies & Karstad 1981; Olaleye et al. 1996; Pepin et al. 2010). Atypical rainfall patterns result in heavy localised flooding and creation of fresh-water reservoirs that can persist for several months. These flooded areas attract *Culex* mosquitos, species whose eggs cannot survive desiccation. *Culex* species reproduction and subsequent feeding on viremic vertebrates results in an explosion in mosquito numbers infected with RVFV. Furthermore, whilst *Aedes* species remain close to their hatching site, *Culex* species tend to disperse more widely. The increased range of *Culex* species results in a greater dissemination of the virus (Figure 1-7). Increased rainfall associated with El Niño events has been correlated to several RVFV epidemics in Africa (Gould & Higgs 2009). Human activity has also resulted in epidemics, with the large Egyptian outbreak in 1977-79 linked to both an increase in available vertebrate hosts and fresh-water availability due to the construction of the Aswan High Dam across the Nile (Meegan 1981; Johnson et al. 1978). The large outbreak in 2000 in the Arabian Peninsular was caused by the importation of infected ruminants into Saudi Arabia. Competent mosquito vector species are common to the region, and feeding on these viremic hosts established the virus in the local mosquito population where it has persisted (Jupp et al. 2002; Shoemaker et al. 2002). This introduction to a previously RVFV-free region is of concern to areas of Europe, the Americas and Asia as competent vectors for RVFV are common to all these regions (Chevalier et al. 2010; Elliott 2009; Rolin et al. 2013).

1.2.2 Pathogenicity and transmission

Numerous vertebrate species are susceptible to RVFV infection. A clear dichotomy is apparent in the mortality rates for RVFV infection of young and old animals, especially in *Bovidae* species such as buffalo, cattle, sheep and goats. In juvenile animals mortality rates approach 100%, whereas in the adult animal this is reduced to about 20% (Pepin et al. 2010). The classical hallmark of RVFV infection is simultaneous abortion events in a herd, termed “abortion storms”. Transmission can occur either via the bite of an infected mosquito or via contact with infected biological tissues. Aborted foetal tissues contain

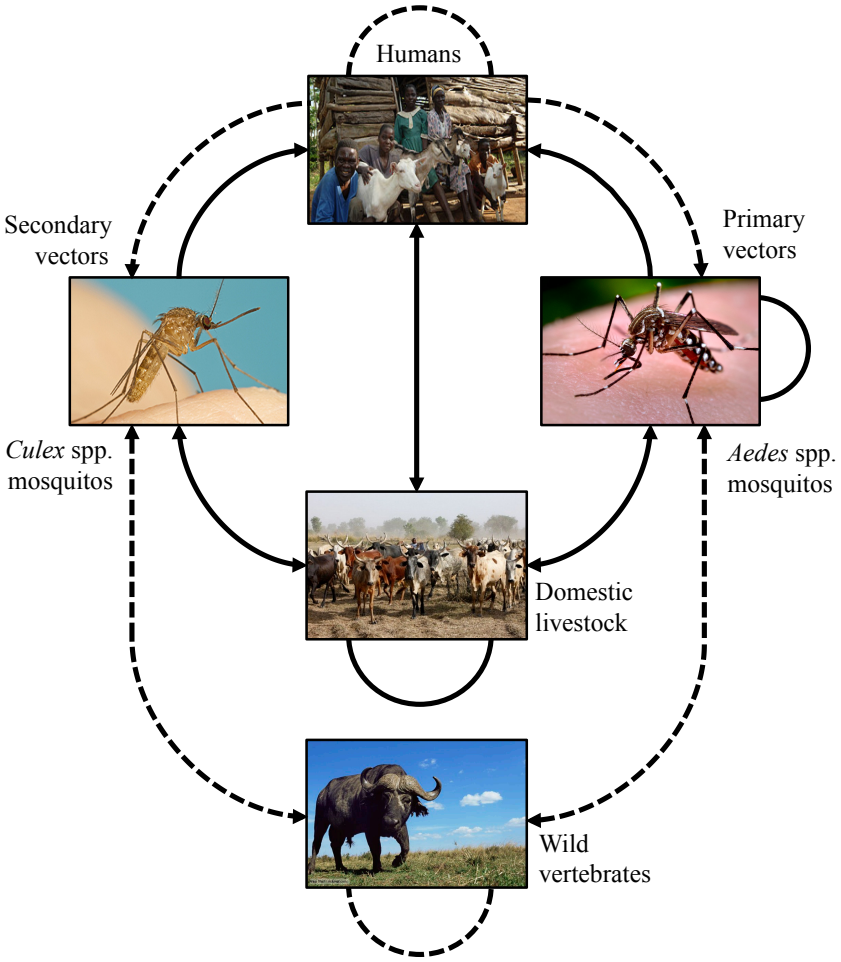

Figure 1-7: Transmission cycle of Rift Valley fever virus
Solid lines represent experimental established transmission route (arrows represent direction). Dashed lines represent suspected routes of transmission yet to be verified. Primary vectors such as the *Aedes* species mosquito are responsible for maintaining the virus in endemic areas during normal seasonal environmental conditions. During periods of unusual rainfall the secondary vectors usually, *Culex* species, are responsible for extended dissemination of the virus.

Adapted from (Chevalier et al. 2010)

high titres of infectious virus and interaction with these materials is a significant transmission route. Infected animals remain highly viremic for between 2-7 days after infection, acting as amplifying hosts for continued infection of biting vectors (Meegan 1979). Human infection generally results in a self-limiting febrile illness. Some patients however develop more serious symptoms including neurological disorders, encephalitis, vision loss, and haemorrhagic fever (HF). Treatment options are entirely supportive (Bouloy & Weber 2010). The overall case fatality rate is estimate to be between 0.5-2.5%, although progression to HF disease is associated with an increased risk of fatality (Pepin et al. 2010; Madani et al. 2003). Cause of death in patients with haemorrhagic presentations is generally a result of complications arising from acute hepatic injury, renal failure or disseminated intravascular coagulations (or a combination of these) (Imam et al. 2009; Al-Khuwaitir et al. 2004). While transmission of RVFV via a mosquito vector has been reported, the major transmission route for human infection is exposure to infected animal tissues and bodily fluids (Davies & V. Martin 2003; Swanepoel & Coetzer 2004). Humans are considered a dead-end host for RVFV, with limited potential as an amplifying host (Chevalier et al. 2010).

1.2.3 Disease control

It is an unfortunate fact that the impact of RVFV is felt most keenly in countries least able to cope with the significant problems associated with the disease. As well as the social impact associated with human morbidity and mortality, the high mortality in economically important livestock species such as cattle and sheep creates additional burdens. Public and animal health agencies are prioritising the development of a RVFV vaccine for both humans and livestock, although this has proven more challenging than anticipated (Mandell & Flick 2011; Bouloy & Weber 2010; Bird et al. 2009). An ideal vaccine would be safe, efficacious, allow for the differentiation between natural and vaccine infection (DIVA), and ultimately inexpensive to the end-user. Genetic engineering of RVFV has created several mutant strains that are highly attenuated and potential ideal vaccine candidates, although fears remain over both reversion to virulence or the potential for re-assortants (Ikegami & Makino 2009; McElroy et al. 2009; Hunter et al. 2002; Morrill & Peters 2011; Bird et al. 2008). The currently licensed vaccine available for animal use is a partially attenuated live vaccine strain (Smithburn strain), but evidence of abortion and teratology when given to pregnant animals precludes its use in non-endemic regions.

Formalin inactivation of the virus removes these complications, but reduces efficacy and increases cost due to need for booster vaccinations (Mandell & Flick 2011)

Effective surveillance protocols remain an important tool in preventing the spread of disease. Numerous inexpensive and effective diagnostic assays based on nucleic acid and antibody/antigen detection are available, although the need for specialist facilities to handle suspected RVFV samples reduces their overall effectiveness in the developing world. Furthermore, increasing knowledge of the climatic factors that trigger outbreaks allows use of remote sensing satellite techniques as an early-warning system, predicting environmental conditions that could be favourable to RVFV disease spread. This could be used in conjunction with other control techniques such as selective vaccination of at risk animals, eradication of mosquito breeding sites, and restrictions in animal movements to prevent future epidemics.

1.2.4 Introduction and establishment in non-endemic regions

Movement of viremic host species, either through intentional (trade) or natural (migration) sources, is thought to be a major risk factor in the dissemination of RVFV to new geographic areas. Transport of infected cattle from Egypt is believed to have caused the 2000 Saudi Arabian outbreak (Shoemaker et al. 2002; Abdo-Salem et al. 2011; Chevalier et al. 2010). However the risk of RVFV entry into the EU or USA through this method is believed to be low (Kasari et al. 2008; Chevalier et al. 2010; Pfeiffer et al. 2005). Animal importation into the USA is banned from foot and mouth disease virus (FMDV) endemic areas, which serendipitously coincide with RVFV endemic areas. Animal importation to the EU is required by law to be from RVFV-free countries, with transportation through endemic areas also banned (Pfeiffer et al. 2005; Chevalier et al. 2010). Transfer of susceptible wild animal species between zoological parks is also considered to be a risk factor, although quarantine measures for imported animals in both the USA and Europe are believed to make this risk negligible (Kasari et al. 2008).

Movement of infected vector species is also considered to be a risk factor for RVFV introduction to non-endemic areas. Of note are the large number of susceptible vector species (30+) capable of support RVFV replication and transmission, and their associated extensive geographic distribution (Seufi & Galal 2010). The dispersal of infected vector

species have been implicated in the spread of numerous arboviruses, included Japanese encephalitis virus (JEV), bluetongue virus (BT) and SBV (Chevalier et al. 2004; Tarlinton et al. 2012). Inherent vector biology makes wind-borne dispersal or powered vector flight across the Mediterranean Sea from Northern Africa to Southern Europe unlikely, although it could potentially occur across the narrow gap between Morocco and Spain (Lopez-Velez & Molina Moreno 2005). It is thought unlikely that even the most extreme wind conditions could move mosquito species across the Atlantic Ocean from Africa to the Americas (Kasari et al. 2008). Whilst mechanical dispersal of mosquito species via aeroplanes and ships has been demonstrated from *Plasmodium* infected mosquitos, this is a low risk factor for RVFV introduction as susceptible local amplifying host species would have to be involved to initiate a local cycle of transmission (Guillet et al. 1998).

1.3 RVFV genetic engineering

1.3.1 Reverse genetics systems

Reverse genetics techniques allow extensive manipulation of a viral genome, and subsequent observation of the resultant phenotypic variations. Various methods have been used for investigations with RVFV resulting in a greater understanding of individual steps in the replication cycle.

Minireplicon assays involve replacement of some or all of the coding sequences on the genome segments with reporter genes. The most common of these reporter genes involve expression of a protein which can be enzymatically induced to produce a quantifiable reading. Minireplicon reporter segments can also be used in conjunction with glycoproteins to produce virus-like particles (VLPs) which can be used to infect naïve cells. Finally, reverse genetics techniques can be employed to rescue fully infectious virions from cloned cDNA copies of the genome segments. This was first demonstrated for segmented NSVs for BUNV (Bridgen & Elliott 1996). Several further segmented NSVs have since been rescued including LACV (Blakqori & Weber 2005), influenza A and B (Fodor et al. 1999; Neumann et al. 1999; E. Hoffmann et al. 2000; E. Hoffmann et al. 2002), Lymphocytic Choriomeningitis Virus (LCMV) (Sánchez & la Torre 2006), AKAV (Ogawa, Sugiura, et al. 2007b), influenza C (Crescenzo-Chaigne & van der Werf 2007),

Lassa virus (LASV) (Albariño et al. 2011; Carnec et al. 2011), Junin virus (JUNV) (Emonet et al. 2011), and SBV (Elliott et al. 2013; Varela et al. 2013).

Reverse genetic experiments require a way of transcribing genome segments and expressing viral proteins *in vitro*. One method utilises the T7 RNA polymerase (T7RNAP) enzyme from T7 bacteriophage to generate RNA copies of cDNA templates. For the initial BUNV rescue T7RNAP was expressed by co-infection with a recombinant vaccinia virus, although later rescue methods employed the BSR-T7/5 cell line which constituently expresses T7RNAP. T7RNAP can also be supplied to a cell line via transfection with an expression plasmid. The use of T7RNAP has many advantages in that it can be expressed in a broad range of cell types and localises to the cytoplasm where the majority of replicative activity for bunyaviruses occurs. However, while T7RNAP is extremely specific for efficient transcription, it requires a guanoside residue +1 from the 3' end of the promoter sequence, which is incorporated into the RNA transcript. While this additional nucleotide is seemingly tolerated for some virus rescues, it may affects viral polymerase recognition and activity levels as 3' and 5' terminal ends would differ from parental viral sequences. Transcription termination is also not precise, so self-trimming ribozyme structures are incorporated into the RNA transcripts to maintain exact terminal sequences. A second method employs cellular DNA-dependent RNA-polymerase (Pol-I) to transcribe the genome copies. Pol-I transcription is more precise than that for T7RNAP, although promoter sequences must be tailored to the species of the cell line employed. Furthermore, Pol-I based systems require co-transfection with helper plasmids containing cell specific Pol-II promoters to express the L and N proteins needed for viral transcription and replication.

1.3.2 Rift Valley fever virus reverse genetics

Minireplicon experiments and associated VLP assays have been utilised to gain a greater understanding of the various stages of the RVFV replication cycle. It has been used to study cell attachment, transcription and translation processes, genome replication, and virion packaging and release from the cell (Ikegami et al. 2005; Gauliard et al. 2006; Habjan et al. 2009a; Brennan et al. 2011). Reverse genetics systems for RVFV have been developed using several separate methodologies. Groups have employed both a T7RNAP only method to rescue infectious (Ikegami et al. 2006; Gerrard et al. 2007), or a

combination of Pol-1 and T7RNAP (Billecocq et al. 2008; Habjan et al. 2008) (Figure 1-8). The establishment of the RVFV reverse genetics systems has allowed the study of RVFV molecular biology, replication, and pathogenesis characteristics in ways that were not possible before.

1.3.3 RVFV non-structural proteins

RVFV NSs has been extensively studied, and acts in a broadly similar way to other bunyavirus NSs proteins. Namely, it acts as the major virulence factor during infection, antagonising the antiviral IFN responses and establishing a cellular environment beneficial to viral replication (Vialat et al. 2000; Billecocq et al. 2004; Bouloy et al. 2001). IFN antagonism occurs through two distinct mechanisms. A specific mechanism is initiated by interaction with SAP30, one of several transcription factors involved in the regulation of IFN-β expression (Huang et al. 2003; Weill et al. 2003). By sequestering SAP30 NSs inhibits the formations of the SAP30/NCor/HDAC repressor complex required to initiate transcription of the IFN-β gene. Using reverse genetics a RVFV mutant was generated in which the NSs protein lacked the SAP30 binding domain. Unlike the wildtype virus, this mutant was unable to kill mice as IFN-β expression was induced (Le May *et al.*, 2008). NSs has also been shown to target the antiviral IFN-induced protein kinase PKR (Habjan et al. 2009b; Ikegami et al. 2009). Viral RNA activates PKR which mediates a stop in viral protein translation (Sadler & Williams 2008). Reverse genetics was again used to generate mutants strains lacking NSs in which PKR degradation was not observed (Habjan et al. 2009a). NSs also suppresses host cell transcription capabilities by sequestering p44 protein, a required sub-unit of TFIIH basal transcription factor. Failure of TFIIH to form leads to a drastic reduction in host cell gene expression (Le May et al. 2004; Billecocq *et al.*, 2004).

RVFV encodes two non-structural protein on the M segment. mRNA transcribed from M segment contains five in-frame initiation codons with NSm1 (78 kDa) translated from the first and NSm2 (14 kDa) from the second. Signal sequences mediating host cell signal peptidase cleavage produce the two proteins (Gerrard & Nichol 2007). The NSm proteins

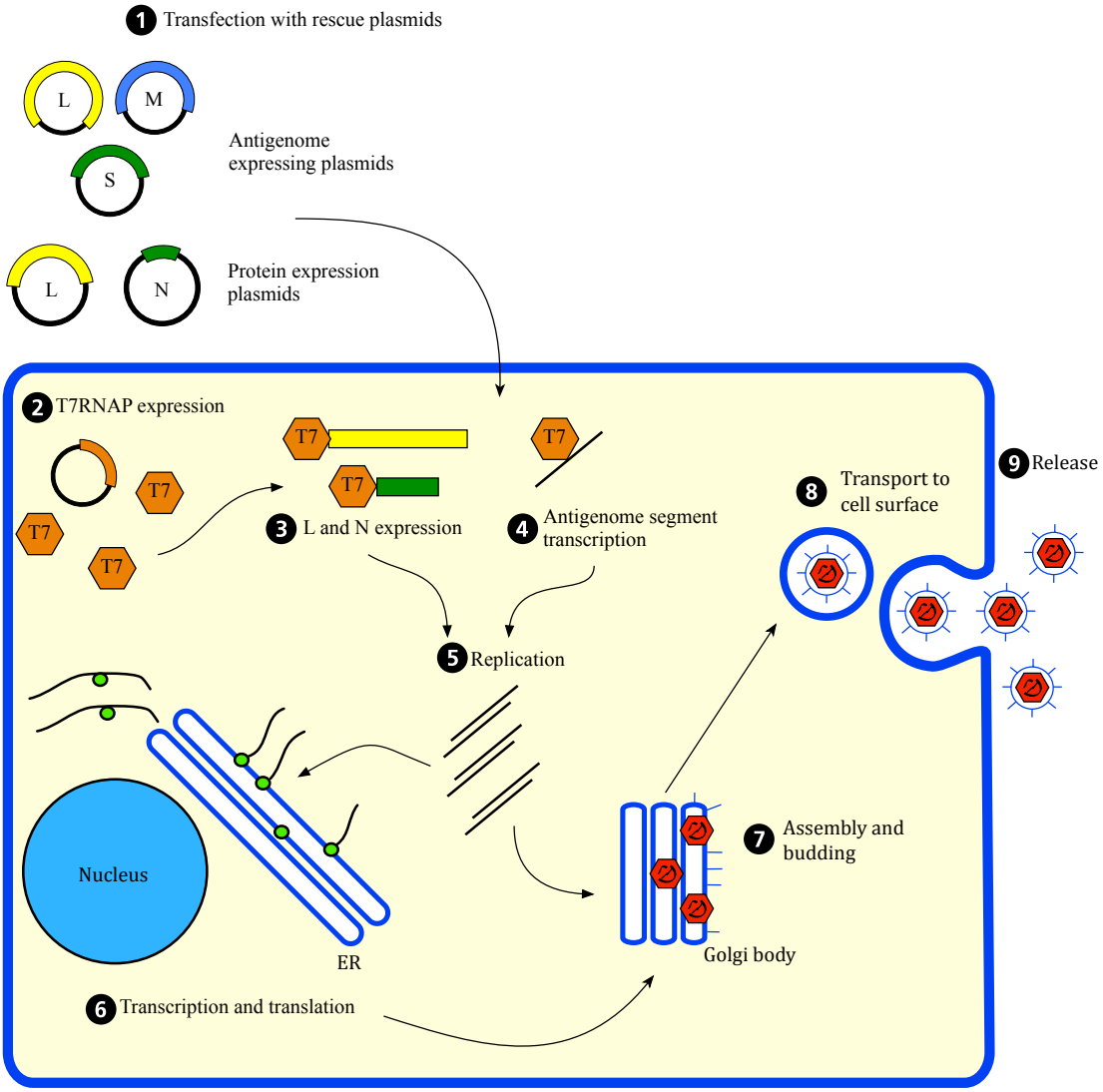

Figure 1-8: Reverse genetics rescue system used for RVFV
Schematic representation of the rescue of infectious RVFV from plasmids:1. Transfection of BSR-T7/5 cells with the plasmids containing nucleotide sequences for the three genome segments in antigenomic orientation, and the coding sequences for L and N, all under control of the T7 promoter; 2. BSR-T7/6 cell constituently express T7 RNA polymerase (T7RNAP); 3. Expression of L and N protein from T7RNAP transcripts, with expression enhanced by presence of EMCV IRES element; 4. T7RNAP-driven transcription of RVFV antigenome polarity L, M, and S segments; 5. Replication of genome and antigenome segment copies; 6. Transcription and viral mRNA and translation of proteins; 7. Assembly and budding of progeny virions at the Golgi body; 8. Transport of progeny virions in vesicle to the cell surface via the exocytic pathway; 9. Fusion of vesicle and plasma membrane to release progeny virus to the extracellular space.

have been less well studied although several groups have published research indicating putative roles for them. A role for NSm2 as a suppressor of the host cell apoptosis by inhibiting caspase-8 activation has been described (Won et al. 2007). Pathogenicity studies indicated the RVFV mutants lacking the NSm proteins retain the ability to cause serious disease *in vivo* (Bird *et al.*, 2007), whereas RVFV mutants lacking both NSm and NSs are attenuated (Crabtree et al. 2012; Bird et al. 2008).

1.4 Mosquito innate immunity

Consequences of RVFV infection in the vertebrate host and invertebrate vector are very different. Whilst severe pathology can be observed in susceptible vertebrate species, the infection in mosquitoes appears benign in nature. Similar observations are made for many other arboviruses, and suggests effective and efficient antiviral control measures are present in invertebrate species (Karpf & Brown 1998). Understanding of the mosquito immune system has grown in recent years, although it still lags behind our knowledge of the vertebrate antiviral immune pathways (Randall & Goodbourn 2008). The overwhelming majority of information regarding invertebrate immunity arises from the extensive research conducted with the model insect *Drosophila melanogaster* (Kemp & Imler 2009; Lemaitre & J. A. Hoffmann 2007). Malaria research dissecting the immune response to the *Plasmodium* parasite has benefited arboviral research as it has ultimately culminated in the publishing of complete annotated genome sequences for several mosquito species (Christophides et al. 2002; Holt et al. 2002; Nene et al. 2007). Orthologues to many proteins with characterised antiviral activities in *D. melanogaster* have subsequently been identified in mosquito species. Current understanding of the mosquito antiviral response involves three areas: immune signaling pathways; apoptosis; and RNA interference (RNAi).

1.4.1 Immune signaling pathways

Three invertebrate immune signaling pathways have been characterised: Toll; immune deficiency and c-Jun N-terminal kinase (IMD/JNK); and Janus kinase signal transducers and activators of transduction (JAK/STAT). Originally investigated for their role in response to microbial infection, results from *D. melanogaster* research have also implicated these pathways as playing a role in the control of viral infections (Dostert et al.

2005; Zambon et al. 2005). One major disadvantage for mosquito research is the lack of mutants for immune signaling pathways genes such as those available for *D. melanogaster*, leaving research on these pathways in mosquito species lacking (Waterhouse et al. 2007; Xi et al. 2008). Whilst limited data regarding RVFV infection in mosquitoes are available, investigations on relative gene expression levels pre and post infection have identified numerous differentially regulated genes for several other arboviral infections. Up-regulation of the Toll and IMD/JNK pathways was observed in sindbis virus (SNV) infected mosquitoes, and similar up-regulation of Toll and the JAK/STAT pathways was observed in DENV infected *A. aegyptii* (Sanders et al. 2005; Xi et al. 2008). Mederious *et al* (2004) described activation of multiple immune pathways in *Frankliniella occidentalis* thrips after infection with TSWV. Additional genes encoding various antiviral immune molecules were also up-regulated following viral infection, including heat-shock protein cognate 70B with O'nyong'nyong (ONNV) in *Anopheles gambiae* (Sims et al. 2010), and serine proteases with SNV infection in *D. melanogaster* (Lemaitre & J. A. Hoffmann 2007).

Mechanisms by which viruses counteract these pathways have been described for several species. STAT phosphorylation, a vital step in the activation of the JAK/STAT pathway, is inhibited in JEV infected mosquito cells (Lin et al. 2004). Toll-signaling is suppressed in SNV infected mosquitoes by inhibition of Cactus and Dif activation, two proteins of the mosquito Toll pathway (Sanders et al. 2005). DENV virus replication has been shown to inhibit both the Toll and IMK pathways in A.aegypti cells (Sim & Dimopoulos 2010). In vertebrate cells the general dampening of host cell transcription has been described for several viruses, including for RVFV via the actions of NSs (Bouloy & Weber 2010). This activity would constrain the effectiveness of the immune signaling pathways. A reduction in host cell RNA levels in SNV infected *A. albopictus* cells was reported by Sarver and Stollar (1977), and more recently for Semilki Forest virus (SFV) infected U4.4 cells (Fragkoudis et al. 2008). Fragkoudis *et al* (2008) further showed that in SFV infected *A .albopictus* cells STAT, IMD and Toll pathway activities were strongly reduced via a global reduction in host cell transcription rather than through targeted suppression by the virus. However, activation of these pathways by a bacterial infection prior to SFV infection resulted in reduced SFV titres, demonstrating potential antiviral properties for these pathways. The majority of research on mosquito immune signaling pathways has been described for positive-strand RNA viruses, such as the alphaviruses and flaviviruses. One

example of viral-induced host cell transcription inhibition has been described for a negative-strand RNA virus, namely VSV infection of *A. albopictus* cells (Gillies & Stollar 1982).

1.4.2 Arbovirus-induced apoptosis

Apoptosis in response to viral infection has been described in vertebrate cell infections, and is thought to be a way to limit virus replication and dissemination within the host (Best 2008). Apoptosis has been shown to be an active antiviral defense in DNA viruses, but its role in controlling arboviral infections which are mainly RNA viruses remains ill defined (McLean et al. 2008; Clarke & Clem 2003). Differences are observed in cell culture where arboviral infection of mosquito cell lines generally results in a persistent infection, in contrast to the cytolytic infection of vertebrate cells (Karpf & Brown 1998). Cytolytic infections of *A. albopictus* cell lines have been described for SNV and SFV although these were unusual and dependent on particular arbovirus-cell line combinations (Condreay & Brown 1988; Stalder et al. 1983). A similar observation has been described for RVFV infection of *A .albopictus* C6/36 cells, where infection with virulent ZH548 strain was cytolytic (Léger et al. 2013). The reasons behind there differences remain unclear. Pathology associated with viral replication in the mosquito model has been described in *Aedes* species for SNV and SFV (Mims et al. 1966; Bowers et al. 2003), and for West Nile virus (WNV) and Western equine encephalitis virus (WEEV) in *Culex* species mosquitoes (Weaver et al. 1992; Girard et al. 2005; Vaidyanathan & Scott 2006). Sites of pathology were both the midgut epithelium and salivary glands, areas known to be potential barriers to infection and dissemination within the mosquito (Mellor 2000). Apoptosis has been suggested as a mechanism to disrupt the cells within these organs to affect viral replication, and also to play a role in determining vector competence. Experiments with SNV infected mosquitoes in which apoptosis was inhibited demonstrated both reduced midgut viral titres and virus dissemination (Wang et al. 2012). More research is needed before the exact role virus-inducted apoptosis plays in controlling an arboviral infection.

1.4.3 RNAi antiviral defense

The RNA interference (RNAi) response is a evolutionarily conserved gene regulatory process in eukaryotes in which short RNA strands are employed to silence translation

through degradation of mRNA (Carthew 2001; Bernstein, Denli, et al. 2001b). It also functions as the major antiviral defense mechanism in insects (Sanchez-Vargas et al. 2004) (van Mierlo et al. 2011; Blair 2011). Two separate pathways have been classified as responding to viral infection, the small interfering RNA (siRNA) and the PIWI-interacting RNA (piRNA) pathways (Sanchez-Vargas et al. 2004; Yan et al. 2011; Siomi et al. 2011).

The siRNA pathway has been extensively studied in *D. melanogaster*, and activation requires the presence of intracellular dsRNA structures (Figure 1-9). During infection viral dsRNA is thought to arise from either RNA secondary structure inherent to the genome segments or mRNA strands, or through replicative intermediate duplexes. These structures are recognized by the RNase-III enzyme Dicer 2 (Dcr-2), and in conjunction with R2D2 protein cleaved to form 21 nucleotide small virus-derived RNA duplexes (viRNAs) (Bernstein, Caudy, et al. 2001a). The viRNA duplexes are loaded into the RNA-interfering silencing complex (RISC), and one "passenger strand" of the viRNA is degraded via the exonuclease activity of the RISC associated protein Argonaute 2 (Ago-2) in conjunction with C3PO (Rand et al. 2005; Matranga et al. 2005; Tomari et al. 2007). The remaining viRNA strand, termed the "guide strand", is utilised by the RISC to recognise cognate RNA sequences within the cell, which are enzymatically cleaved by Ago-2 to silence that message. Intercellular spread of viRNA populations has been described for SFV infected mosquito cells which suggests a systemic dissemination of viRNAs to "prime" surrounding cells in an anti-viral state (Attarzadeh-Yazdi et al. 2009).

The piRNA pathway has only recently been recognised as being activated by viral infection of insects (Tchurikov & Kretova 2011; Reynolds & Ruohola-Baker 2009; Malone et al. 2009; C. Li et al. 2009a) (Morazzani et al. 2012). Piwi-induced RNAs (piRNAs) are generated in a Dicer-independent method from ssRNA templates. They exhibited a broader size range than those for siRNAs of between 24-30 nucleotides, and are produced by cleavage of the target by the PIWI subclass of the Argonaute family (piwi, Argonaute-3, and aubergine) (Siomi et al. 2011). They were originally believed to function only in germ cell lines to protect against retrotransposon activation. However, their expression and detection has recently been described in somatic cells of *D. melanogaster*, mosquito and midges species (Yan et al. 2011; Léger et al. 2013; Vodovar et al. 2012) (Figure 1-10). Biogenesis of piRNAs involves a "ping-pong" amplification mechanism

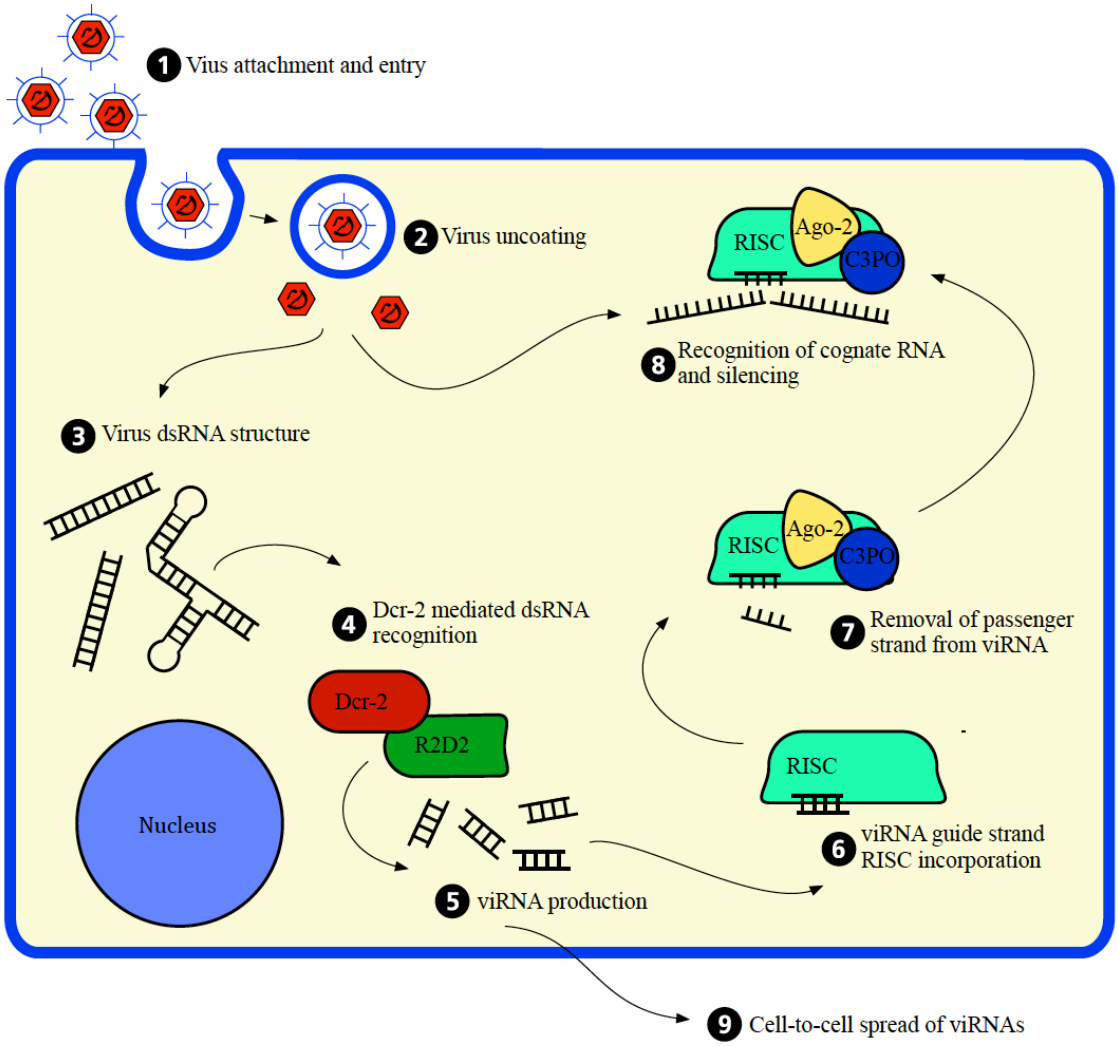

Figure 1-9: RNAi response to viral infection
The typical anti viral RNAi response is a multi-step process: 1. Viral attachment and entry into the cell; 2. Un-coating of viruses releases the genome into the cytoplasm; 3. Viral dsRNA structures, either from replicative intermediates, mRNA secondary structures or mRNA:genome hybrids are recognized by the cellular protein Dcr-2; 4. Dcr-2 in conjunction with R2D2 protein processes the dsRNA into small virus-derived RNA duplexes (viRNAs); 4. A viRNA duplex is incorporated into the RNA-induced silencing complex (RISC); The RISC incorporates the Argonaute-2 (Ago-2) and C3PO proteins which remove the "passenger strand" of the viRNA and expose the "guide strand"; 8. Cognate RNA strands are loaded into the RISC where they are cleaved, effectively "silencing" expression or replication processes; 9. Cell-to-cell spread of the viRNAs primes uninfected cells prior to entry of virus, increasing the speed and effectiveness of the response.

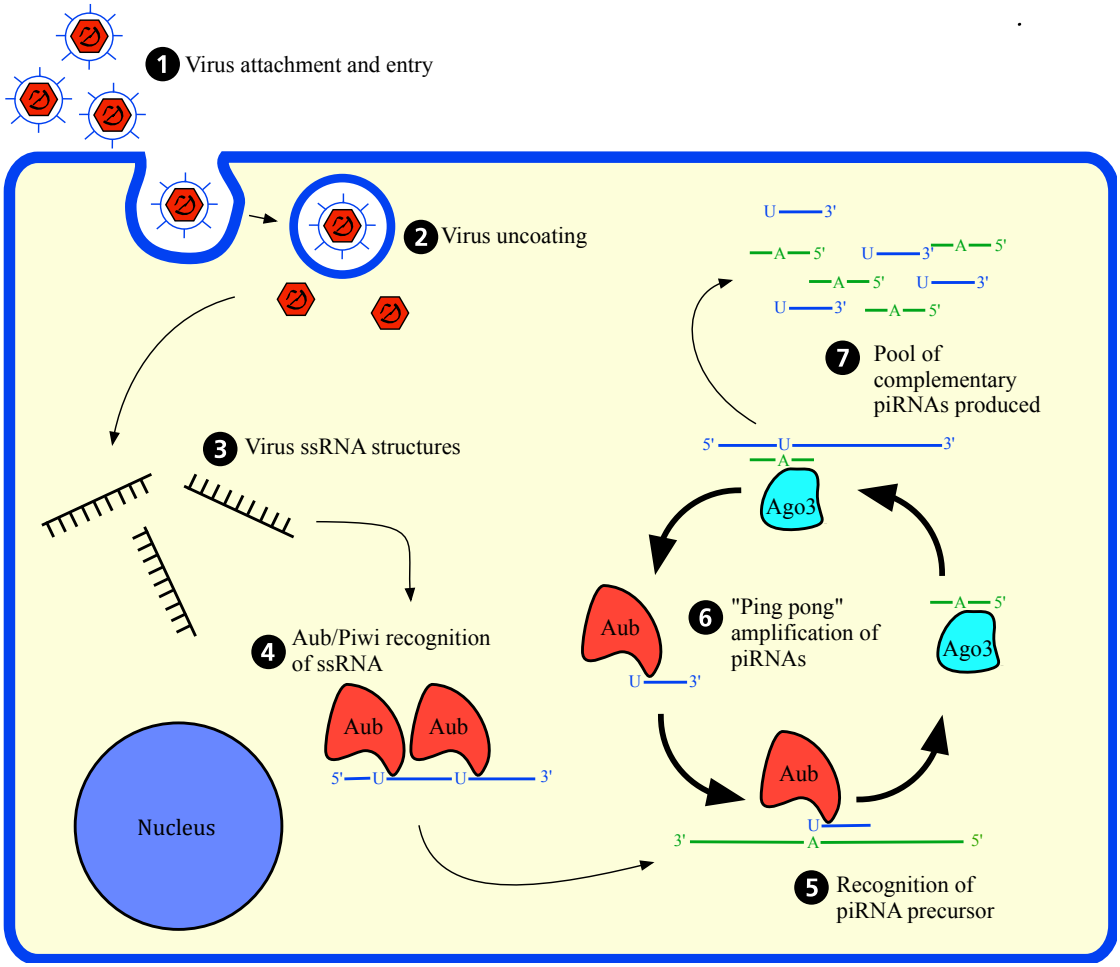

Figure 1-10: piRNA pathway in infected mosquito cells

piRNA species are thought to arise from ssRNA viral targets, typically of one polarity. Although the exact process of biogenesis is poorly understood, it is thought that the target is initially recognized by the aubergine (Aub) protein which cleaves the RNA leaving a 5' uracil residue, resulting in a piRNA precursor. This initiates a ping-pong amplification cycle in association with another PIWI subclass of the Argonaute protein Argonaute-3 (Ago-3), and the associated cleavage activities of these proteins results in a pool of piRNA species with characteristic nucleotide biases. The aubergine –associated piRNA contain a strong bias for uracil at nucleotide position 1, and the Argonaut3-3 –associated piRNAs a strong bias for adenine at nucleotide position 10. Unlike siRNA species complementarity between the piRNA species is generally limited to the first 10 nucleotides.

(Siomi et al. 2011) . Unlike siRNA which are complementary across their full length, piRNAs only possess complementarity in their first 10 nucleotides. Biogenesis creates a 5' uridine bias in the primary transcripts, and the amplification cycle generates a pool of piRNA with a specific signature of uridine at position 1 and adenosine at position 10 (Brennecke et al. 2007).

Orthologues to many of the proteins identified in the *D. melanogaster* RNAi pathways have subsequently been recognized in mosquito species whose genomes are available, such as *A. gambiae*, *C. pipiens*, and *A. aegypti* (Campbell, Black, et al. 2008a). Activation of the RNAi pathways in mosquitos has been described for multiple viruses species including SNV, LACV, ONNV, DENV, and RVFV (Blakqori et al. 2007; Sanchez-Vargas et al. 2009; Khoo et al. 2010; Léger et al. 2013; Vodovar et al. 2012; Keene et al. 2004). responses have been hampered by the unavailability of knockout mutants like those employed to study the response in *D. melanogaster r*. However, knock-down experiments can be performed in mosquitoes by introduction of dsRNA to silence expression of specific proteins of RNAi pathway components (Campbell, Keene, et al. 2008b; Keene et al. 2004; Sanchez-Vargas et al. 2009). These results demonstrated that inhibition of the RNAi pathway resulted in increased viral replication and titres. This suggests the RNAi pathways play an important role in controlling viral replication within the arbovirus vector.

Although it has been shown that RNAi pathways are activated by viral infection, the specific templates recognised by the cell are currently not well characterised. Positive-sense viruses have highly structures genomes in which dsRNA secondary structures acts as internal ribosome entry sites (IRES) and *cis*-acting replication elements (CREs) (Simmonds et al. 2004). The observation that the positive-sense *Flaviviridae* sequester dsRNA structure behind double-membraned intracellular vesicles termed replication complexes suggest that this is done in a way to avoid RNAi activation (Uchil & Satchidanandam 2003). Negative sense RNA viruses do not have naked-RNA genomes, instead they are heavily encapsidated with nucleoprotein which limits secondary structure formation (Elliott & Schmaljohn 2013). However, as both siRNAs and piRNAs have been detected in both LACV and RVFV infected mosquito cells it suggest intercellular dsRNA is present (Blakqori et al. 2007; Léger et al. 2013). Potential targets for siRNA activity in NSV infected cells include cryptic structures within encapsidated genome, secondary structures within viral mRNA transcripts, or replicative intermediate structures. The viral

substrates that activate the piRNA response are much less well understood, as is any potential anti-viral activity they may possess (Vodovar et al. 2012). Whilst clues relating to specific targets can be garnered by examining the polarity of viRNA populations, it will undoubtedly require extensive bioinformatics analysis of several viral species infections before the origins of arbovirus induced viRNA can be accurately defined.

Chapter 2

MATERIALS

2 Materials

2.1 Cell culture

2.1.1 Eukaryotic cell lines

The C6/36, u4.4, and C7-10 cell lines were derived from *Aedes albopictus* mosquito neonatal larvae. The Ae cell line was derived from *Aedes aegypti* mosquito neonatal larvae. All mosquito cell lines were maintained in L-15 cell culture medium (Life Technologies) supplemented with 10% (v/v) foetal calf serum (FCS) and 10% (v/v) tryptose phosphate broth (TPB) (Life Technologies).

BHK-21 clone 13 cell line was derived from baby hamster kidney cells and maintained in Glasgow modified Eagle's medium (GMEM) (Life Technologies) with 10% (v/v) newborn calf serum (NCS) and 10% (v/v) TPB.

BSR-T7/5 cell line is a derivative of BHK-21 cells constitutively expressing the T7 bacteriophage T7 RNA polymerase (T7RNAP) (Buchholz et al. 1999). Cells were maintained in GMEM with 10% (v/v) FCS and 10% (v/v) TPB. Continued selection of cells expressing T7RNAP was maintained through addition of 1 mg/ml G418 to cell culture media at each split.

Vero-E6 cell line was derived from African Green Monkey kidney cells and was maintained in Dulbeccos modified Eagle's medium (DMEM) (Life Technologies) with 10% (v/v) FCS.

2.1.2 Bacterial strains

The bacterial strain used for growth and maintenance of plasmid stocks was *Escherichia coli* strain JM109: *end*A1, *rec*A1, *gyr*A96, *thi*, *hsd*R17 (r_k^- m_k^+), *rel*A1, *sup*E44, Δ*pro-lac*AB), [F' *tra*D36, *pro*AB, *laq*I^qZΔM15]. Competent JM109 bacteria used in transformations were generated using Mix & Go *E. coli* Transformation Kit & Buffer Set (Zymo Research, USA). Bacteria were cultured in liquid phase using LB broth and in solid phase using LB Agar.

2.1.3 Antibiotics

Ampicillin (100 mg/ml) and Kanamycin (50 mg/ml) were used for bacterial transformant selection (Sigma-Aldrich). Hygromycin B (200 mg/ml) was used for maintenance of mosquito cell lines constitutively expressing plasmids of interest (Invitrogen).

2.2 Virus strain

RVFV strain MP12 rescued using reverse genetic techniques, termed rMP12, was used for this research. Plasmids were supplied by Institut Pasteur, Paris. Rescue methodology is described in Billecocq *et al*, 2008. rMP12 served as the template for all further virus mutants rescued.

2.3 Molecular biology

2.3.1 Oligonucleotides

All synthetic oligonucleotides were purchased from Integrated DNA technologies. Primers for PCR were ordered at 25 nM scale with standard desalt purification. Primers for qPCR were ordered at 100 nM scale with HPLC purification.

2.3.2 Enzymes

GoTaq® DNA polymerase family enzymes (Promega) and KOD Hot Start DNA Polymerase (Novagen, Merck Millipore International) were used for PCR. MML-V Reverse Transcriptase (Promega) and Superscript III Reverse Transcriptase enzymes were used for RT reactions. MESA BLUE Mastermix Plus for SYBR® Assay was used for quantitative PCR (Eurogentech).

All restriction enzymes used were supplied by New England BioSystems or Promega unless otherwise stated.

MAXIscript® SP6/T7 Transcription Kit and MEGAscript® T7 Kit were used for in-vitro transcription of RNA probes and qPCR genomic and anti-genomic standards (Ambion).

2.3.3 Cloning

For restriction digest cloning reactions T4 DNA ligase was used (Roche). For restriction free cloning In-Fusion® HD Cloning Plus kit was used (Clonetech, Takara Bio).

2.3.4 Plasmids

Table 2-1: Plasmids used during project

Plasmids	Description	Source
pTVT7-GS, pTVT7-GM, pTVT7-GL	Plasmids containing RVFV MP12 anti-genome S, M and L segment sequences respectively under control of the T7 promoter. Contains a single G +1 upstream of the T7 promoter, and a hepatitis D ribozyme element at the antigenome segment 3' end to cleave T7RNAP transcripts at the correct position.	*M.Bouloy, Institut Pasteur*
pTM1-L, pTM1-N	Plasmids containing CDS for RVFV MP12 L and N proteins respectively under control of the T7 promoter. The transcript includes the encephalomyocarditis virus (EMCV) internal ribosome entry site (IRES) element upstream of the CDS to allow protein expression in mammalian cells expressing T7RNAP.	*M.Bouloy, Institut Pasteur*
pTVT7-GSΔNSs:KpnI	Modified pTVT7-GS plasmid in which the complete NSs CDS has been replaced with three consecutive restriction sites (PmlI-KpnI-SpeI).	*B.Brennan, Glasgow University*
pTVT7-GSΔNSs:eGFP	Modified pTVT7-GS plasmid in which the NSs CDS has been replaced with that for eGFP CDS.	*Made during PhD*
pTVT7-GSΔNSs:ZH548NSs	Modified pTVT7-GS plasmid in which the NSs CDS has been altered to include non-synonymous mutations allowing expression of ZH548 NSs. Synonymous nucleotide changes between MP12 and ZH548 were not introduced.	*B.Brennan, Glasgow University*
pTVT7-GMΔNSm	Modified pTVT7-GM plasmid in which the CDS downstream from 4th ATG initiation site has been removed. The downstream Kozak sequence is also altered to make it stronger	*Made during PhD*
pTVT7-GS:S-Swap	Modified pTVT7-GS plasmid in which the N and NSs CDSs have been swapped, leaving the UTR and IGR region unaltered.	*B.Brennan, Glasgow University*
pTVT7-GS:S-SwapΔNSs:eGFP	Modified pTVT7-GS:S-Swap plasmid in which the NSs CDS has been replaced with that for eGFP CDS.	*B.Brennan, Glasgow University*

Plasmids	Description	Source
pTVT7-GL3V5 tag	Modified pTVT7-GL plasmid in which the PIV-5 V5 epitope has been inserted into L CDS (at nt 5574-5 vcRNA in plasmid). This allows use of the V5 antibody to detect L protein.	*B.Brennan, Glasgow University*
pTVT7-GSco, pTVT7-GMco, pTVT7-GLco	Plasmids containing modified RVFV MP12 anti-genome S, M and L segment sequences under control of a T7 promoter. Identical to the template pTVT7-Gx rescue plasmids except S, M, and L derived protein CDSs have been altered so that they are codon optimized for protein expression in *Aedes* species cell lines.	*Made during PhD*
pUC-GSco, pUC-GMco, pUC-GLco	Plasmids containing the modified MP12 S, M, and L segment in which the CDSs for all viral protein were replaced with those for *Aedes* species codon optimised CDSs.	*Designed during PhD, produced by GenScript, USA*
pTM1-Lco, pTM1-Nco, pTM1-Gn/Gcco	Plasmids containing the *Aedes* species codon optimized CDSs for MP12 L protein, N protein, and Gn/Gc polyprotein respectively under control of the T7 promoter. The transcript includes an EMCV IRES element upstream of the CDS to allow protein expression in mammalian cell lines expressing T7RNAP.	*Made during PhD*
pTM1-R-L, pTM1-R-N, pTM1-R-Gn/Gc	Plasmids containing the CDSs for MP12 L, N, and Gn/Gc polyprotein respectively under control of the T7 promoter. The transcript includes an Rhopalosiphum padi virus (RhPV) IRES element upstream of the CDS to allow protein expression in insect cell lines expressing T7RNAP.	*Made during PhD*
pTM1-R-Lco, pTM1-R-Nco, pTM1-R-Gn/Gcco	Modified version of pTM1-RhPV-L, pTM1-RhPV-N, pTM1-RhPV-Gn/Gc in which the CDSs have been replaced with those for CDSs codon optimised for *Aedes* species.	*Made during PhD*
pST-IRES polyUB hyg -GFP DCR2 HA N-tag	Plasmid that produces a bi-cistronic RNA transcript under control of the polyubiquitin promoter. Primary CDS is for *Aedes albopictus* Dcr-2 containing the HA tag at the N terminus, followed by the RhPV IRES and the secondary CDS for hygromycin B resistance protein fused with GFP at the C terminus.	*K.Myles, Virginia Tech*
pSTI-T7RNAP IRES H/G	Modified pST-IRES polyUB hyg -GFP DCR2 HA N-tag plasmid in which the primary CDS is replaced with the T& polymerase CDS.	*Made during PhD*
pSTI-N, pSTI-NSs pSTI-L	Plasmids containing the CDS for MP12 N, NSs, and L respectively under control of the polyubiquitin promoter found in pST-IRES polyUB hyg -GFP DCR2 HA N-tag. The IRES and second ORF have been removed.	*Made during PhD*
pMT-Ren, pMT-GL3	Plasmids containing the *Renilla* luciferase gene, and Firefly luciferase gene respectively, under a $CuSO_4$ inducible promoter. Used to express luciferase in cells treated with $CuSO_4$.	*J. van Mierlo, Radboud University*

Plasmids	Description	Source
pTVT7-SRENg pTVT7-MRENg pTVT7-LRENg	Plasmids containing the *Renilla* luciferase gene. A negative polarity transcript is produced by T7 polymerase. From this a positive polarity transcript is produced under control of the S, M, and L MP12 3' genomic UTR respectively.	*Made during PhD*
pTVT7-SRENag	Plasmids containing the *Renilla* luciferase gene. A negative polarity transcript is produced by T7 polymerase. From this a positive polarity transcript is produced under control of the S 3' antigenomic UTR.	*Made during PhD*
pSTI-GL3	Plasmids containing the Firefly luciferase gene under control of the polyubiquitin promoter.	*Made during PhD*

2.3.5 Antibodies

Table 2-2: Primary antibodies

		Dilution	
Target	Antibody	Western Blot	IF
RVFV N	Rabbit anti-RVFV N (Eurogentech)	1:10 000	1:300
RVFV NSs	Rabbit anti-RVFV NSs (Eurogentech)	1:10 000	1:300
Tubulin	Mouse anti-tubulin (Sigma)	1:25 000	-
Tubulin	Mouse anti-tubulin (Calbiochem)	-	1:100
GFP	Rabbit anti-GFP (Invitrogen)	1:10 000	-
V5 epitope	Mouse anti-SV5 V5 epitope (Life Technologies)	-	1:200

Table 2-3: Secondary antibodies

		Dilution	
Target	Antibody	Western Blot	IF
Rabbit IgG	Anti-rabbit IgG HRP-linked (Cell signaling)	1:1000	-
Mouse IgG	Anti-mouse IgG HRP-linked (Sigma)	1:1000	-
Rabbit IgG	Anti-Rabbit IgG FITC (Sigma)	-	1:200
Mouse IgG	Anti-mouse IgG CY5-linked (Sigma)	-	1:200

2.4 Chemicals and buffers

2.4.1 Cell culture

- **2X MEM -** 20% (v/v) 10X Modified Eagle's media (MEM) (Invitrogen), 2% (v/v) L-glutamine, 0.435% (v/v) sodium bicarbonate, 4% NCS, diluted in H_20.
- **Avicell overlay 0.6% (w/v) -** 1.2% (w/v) of Avicell in 100ml of H_20. Autoclaved and stored at rt until use. Prior to use in plaque assay diluted 50:50 with 2X MEM.
- **Crystal violet stain buffer -** 20% (v/v) ethanol, 1% (v/v) methanol, 0.1% (w/v) crystal violet, diluted in H_20.
- **Formaldehyde fixing buffer -** 8% (v/v) formaldehyde.
- **LB Agar -** 4% (w/v) LB-Agar-Miller (Formedium) diluted in de-ionised H_20.
- **LB Broth -** 2.5% (w/v) LB-Broth-Agar-Miller (Formedium) diluted in de-ionised H_20.
- **Phosphate buffered saline (PBS) -** 137 mM NaCl, 15 mM KCL, 10 mM Na_2HPO_4/KH_2PO_4; pH 7.4.

2.4.2 Immunofluorescence

- **Mounting Media -** VECTORSHIELD hardset mounting medium with DAPI (Vector Laboratories).
- **Permeabilisation buffer -** 0.1% (v/v) Triton X-100 diluted in PBS.

2.4.3 Protein analysis

- **LI-COR blocking buffer -** 5% skimmed milk powder diluted in PBS
- **Membrane transfer buffer -** 20X NuPAGE transfer buffer (Novex, Life technologies) diluted in H_20.
- **MES SDS running buffer -** 20X MES SDS NuPAGE running buffer (Invitrogen) diluted in H_20.
- **Protein Disruption Buffer (PDB) -** 0.125 M Tris-HCl (pH 6.8), 4% (w/v) SDS, 25% (v/v) glycerol, 0.02% (w/v) bromophenol blue. Prior to use mix with DTT 1M in a 4:1 ratio (v/v), with 5 µl Benzonase (≥250 units/µl) per 1 ml PDB.

- **Western blot blocking buffer -** 5% skimmed milk powder diluted in PBS 0.1% Tween-20.
- **Western blot washing buffer-** PBS 0.1% (v/v) Tween-20.

2.4.4 DNA analysis

- **10**X **TAE buffer -** 0.4 M Tris, 1.142% (v/v) acetic acid, 0.01 M EDTA, diluted in H_20. Diluted to 1X in H_20 prior to use.
- **10**X **TBE buffer -** 1 M Tris, 0.9 M boric acid, 0.01 M EDTA, diluted in H_20. Diluted to 1X in H_20 prior to use.
- **Agarose -** 0.8-2% (w/v) molecular grade agarose (Bioline) diluted in either 1× TAE or 1X TBE buffer depending on application.

2.4.5 RNA analysis

- **50% Formamide hybridization buffer -** 50% (v/v) de-ionised formamide, 5X (v/v) SSC, 0.1% (w/v) n-lauroyl sarcosine, 0.02% (w/v) SDS, 2% (v/v) blocking solution, diluted in H_20.
- **Antibody buffer -** 1X blocking buffer diluted in maleic acid, 1:10 000 dilution of anti-digoxigenin-AP Fab fragments.
- **Blocking buffer 10**X **-** 10% (w/v) blocking reagent (Roche) diluted in maleic acid buffer.
- **Detection buffer -** 0.1 M NaCl, 0.1 M Tris; pH 9.5.
- **Maleic acid buffer -** 0.15 M NaCl, 0.1 M Maleic acid; pH 7.5.
- **RNA loading dye 10**X **-** 50 mM Tris-HCl, 0.25% (v/v) Bromophenol blue, 60% (v/v) glycerol.
- **SSC buffer 20**X **-** 3 M NaCl, 0.3 M Tri-sodium citrate; pH 7.
- **Washing Buffer -** 0.15 M NaCl, 0.1 M Maleic acid, 0.3% (v/v) Tween-20; pH 7.5.

2.5 Radiochemical

Protein radiolabeling used the EasyTag^{TM} EXPRESS ^{35}S Protein Labeling Mix [^{35}S] (2 mCi), specific activity of 74 MBq (purchased from Perkin Elmer).

Chapter 3

METHODS

3 Methods

3.1 Cell culture

3.1.1 Insect cell culture

Mosquito cell lines were maintained in non-vented 75 cm^2 cell culture flasks (Corning, with Greiner coating) and split every 5-7 days at 100% confluency. To split cells the monolayer was washed gently once with PBS, and then cell detached by cell scraper (C6/36, C7-10) or by forceful agitation of the flask (u4.4 and Ae). Cells were re-suspended in 10 ml fresh L-15 media split into new flasks in the ratio 1 in 10 for C6/36 cells and 1 in 5 for u4.4, C7-10, and Ae cells. All cells were incubated at 28°C with no supplementary CO_2 in a non-humidified atmosphere.

3.1.2 Mammalian cell culture

Cells were maintained in either 75 cm^2 or 175 cm^2 vented flasks depending upon usage, and were split every 3-4 days as required. To split cell the cell culture media was removed and cell monolayer washed three times with PBS before the addition of 1X trypsin (Gibco). Flasks plus trypsin were incubated at 37°C for 5 minutes to detach cells. before they were re-suspended fresh cell culture media. For general maintenance all mammalian cell lines were split 1 in 10 into new flasks and incubated at 37°C in 5% supplementary CO_2 in a humidified atmosphere.

3.1.3 Transfection of mammalian and mosquito cells

Mammalian cell lines transfections were carried out when the cells were at 60-80% confluency, and mosquito cell lines when they were at 50-60% confluency. Transfection reagent was Lipofectamine 2000 (Invitrogen).

Experiments at ACDP category 2 were performed in cell culture plates. The required amount of plasmid DNA was aliquoted into polystyrene tubes with half the required volume of Optimem serum-free cell culture media (Gibco) (Table 3-1). The remaining volume of Optimem media was added to the calculated Lipofectamine 2000 volume and added to the Optimem/DNA mix. Due to the cell toxicity associated with Lipofectamine

2000 each cell culture vessel had a maximum volume of Lipofectamine 2000 that could be used, even if DNA amounts exceeded this. This was then incubated for 15 minutes at room temperature. Immediately prior to transfection, cell culture media was removed from the monolayer and the transfection mix overlaid. Cells were then incubated for two hours at 37°C (mammalian cell lines) or 28°C (insect cell lines) before the transfection mix was removed and replaced with fresh cell culture media.

Table 3-1: Transfection volumes for cell culture vessels used

Cell culture vessel	Surface area of one well (cm2)	Cell culture media volume (ml)	Transfection mix volume (µl)	Max. Lipofectamine 2000 volume (µl)
24-well plate	2	0.5	100	1.25
12-well plate	4	1.0	200	2.5
6-well plate	9	2.0	250	5.0
T25 flask	25	5.0	1000	10.0

Transfection experiments at ACDP category 3 were performed in sealed cell culture vessels such as T25 flasks. The two Optimem mixes (Optimem/DNA and Optimum/Lipofectamine 2000) were prepared as at ACDP category 2 but combined only at ACDP category 3. Reactions then continued as at ACDP category 2.

3.1.4 Rescue of virus

The rescue method used throughout this project was based on the published five-plasmid method for rescuing infectious RVFV (Billecocq et al. 2008). Briefly, plasmid mixes were prepared using 1 µg of each genomic plasmid (pTVT7-GS, pTVT7-GM, pTVT7-GL) and 0.5 µg of each support plasmid (pTM1-L, pTM1-N). This was mixed with 250 µl Optimem, and in a separate tube 250 µl of Optimem was mixed with 3 µl Lipofectamine 2000 per 1 µg DNA.

At ACDP Category 3 the Optimem/DNA and Optimem/Lipofectamine 2000 mix tubes were combined and incubated at room temperature for 15 minutes. Cell culture media in a T25 flask of sub-confluent BSR-T7/5 cells was replaced, and the transfection mix added directly to the cell culture media. Flasks were incubated at 37^0C for between five to seven days until widespread cytopathic effects (CPE) and/or cell death was observed. The cell

culture media was then removed and centrifuged at 3,000 rpm (500 g) for 5 minutes at 4°C to pellet any cell debris. The remaining supernatant was then separated into 1 ml aliquots (termed the p0 rescue stock) and stored at -80°C. Viral titres of p0 stocks were obtained through plaque assay on BHK-21 cells.

3.1.5 Creating elite p1 viral stocks

All virus stocks were grown in BHK-21 cells infected with p0 rescue stocks at MOI 0.01. Briefly, cell culture media from a sub-confluent flask of BHK-21 cells was removed and replaced with a minimal volume of PBS 2% v/v NCS with diluted virus to cover the monolayer. This was incubated at 33°C for one hour, after which cell culture media was added. Flasks were then incubated at 33°C for five to seven days until signs of viral replication were observed. The media was the removed and centrifuged at 3,000 rpm (500 g) for 5 minutes at 4°C to pellet any cell debris. The remaining supernatant was then stored in 1 ml aliquots at -80°C.

3.1.6 Experimental viral infections

All rMP12 infections were performed at ACDP category level 3 conditions to ensure effective biocontainment. Cells were seeded into cell culture vessels at $2.5x10^5$ (mammalian) or $1x10^6$ (mosquito) cells per cm^2 12 to 18 hours prior to infection. To infect cells the cell culture media was removed and a volume of virus diluted in PBS 2% (v/v) NCS added to the monolayer. After one hour incubation to allow virus adsorption to the cell monolayer the virus diluent was removed and replaced with fresh cell culture medium. In all experiments this time point was 0 h p.i..

3.1.7 Determination of viral titre by plaque assay

BHK-21 cells were seeded at $7x10^5$ per well in 6-well cell culture plates 12 to 18 hours prior to use. Serial 10-fold dilutions of virus diluted in PBS 2% (v/v) NCS were prepared. Cell culture media was removed from the BHK-21 cell monolayers and replaced with 200 µl of virus dilution. After one hour incubation at 37°C the cell monolayer was overlaid with 0.6% Avicell solution and incubated at 37°C for a further 72 hours. The cell monolayers were then fixed by immersion of the 6-well plate in formaldehyde fixing

buffer, also inactivating the virus. After a four hour fixation the plates were removed, rinsed with H_20, and the plaques visualised by addition of crystal violet stain buffer. Viral titres were calculated using the formula t=(p/d)x5, where t = titre in pfu/ml, p = plaque number, and d = dilution factor of counted well.

3.1.8 Immunofluorescence studies

Cells were seeded in 12-well cell culture plates containing 30 mm circular coverslips at the required density for infection: Vero-E6 cells at $1x10^5$ cells per well; mosquito cells at $5x10^5$ cells per well. Infections were performed as in 3.1.7 with 100 µl of virus diluted to required MOI in PBS 2% (v/v) NCS. At the end of the experiment cell monolayers were fixed in formaldehyde fixing buffer by immersion of plate for four hours before being removed from the ACDP Category 3 laboratory.

Cells were treated with permeabilisation buffer for 30 minutes at room temperature. The coverslips were washed three times in PBS before being blocked in PBS 2% (v/v) NCS for 30 minutes. Coverslips were exposed to primary antibody diluted in PBS 2% (v/v) NCS for one hour at room temperature, washed five times in PBS 2% (v/v) NCS, before exposure to secondary antibody diluted in PBS 2% (v/v) NCS for 1 hour at room temperature. Antibody incubations were performed in the dark. After incubation the coverslips were washed five times in PBS 2% (v/v) NCS before being mounted on slides using VECTORSHIELD mounting solution. Slides were stored at -20°C until use.

3.2 Nucleic acid manipulation and cloning

3.2.1 Bacterial transformation and plasmid preparation

Competent E. coli bacteria were prepared using the Z-Competent E. coli Transformation kit and Buffer Set (Zymo Research) and stored in aliquots of 100 µl at -80°C. Prior to transformation competent cells were defrosted on ice for five minutes before being transformed with required concentration of plasmid DNA. After five minutes incubation on ice bacteria were plated on LA agar plates with selective antibiotic and incubated at 37°C overnight. If applicable, colony PCR was performed on selected colonies to confirm

suitability before bacteria were propagated by incubation in 5 ml of LB broth with selective antibiotic at 37°C overnight in a shaking incubator (225 rpm).

Small scale plasmid DNA preparations were performed using the Qiagen QIAprep Spin Miniprep kit (Qiagen, Germany) according to the manufacturers protocol. For large scale plasmid preparations a colony was inoculated into 10 ml LB broth and incubated at 37°C for 8 hours in a shaking incubator (225 rpm). The 10 ml culture was added to 140 ml LB broth and incubated at 37°C overnight in a shaking incubator (225 rpm). Plasmid DNA extraction was then performed using either the Qiagen QIAprep Spin Maxiprep kit (Qiagen, Germany) or the NucleoBond Xtra midiprep kit (Macherey-Nagel, Germany) following the manufacturers protocol. The one exception of this was for propagation of plasmids containing sequences based on MP12 M segment. All incubations in these cases were performed at room temperature with incubation times were doubled to compensate for slower growth of bacteria.

3.2.2 Total cellular RNA and virion RNA extraction

Total RNA was extracted from cell monolayers by first removing cell culture medium from cell monolayers before addition of Trizol reagent (Invitrogen). The volume of Trizol reagent used was determined by manufacturers recommendations. After 15 minutes incubation at room temperature the Trizol solution was removed and stored at -80°C until extraction.

Trizol samples were first added to pre-spun phase-lock heavy gel tubes (5Prime Inc., VWR) with 0.2 volumes of chloroform before being mixed by inverting 5-10 times. The sample was centrifuged at >13,000 rpm (>15,000 g) for 10 minutes before the aqueous layer was removed to a tube containing 250 µl of isopropanol. After mixing the tube was incubated at room temperature for 15 minutes before centrifugation at >13,000 rpm for 30 minutes at 4°C. Supernatant was carefully removed and the pellet washed in 750 µl of ice-cold ethanol before further centrifugation at >13,000 rpm (>15,000 g) for 10 minutes at 4°C. Supernatant was removed and the pellet allowed to air-dry before being resuspended in 50 µl nuclease-free water. Concentrations of RNA were determined using a NanoDrop spectrophotometer (Thermo Scientific).

Extraction of virion RNA was performed using the QIAamp Viral RNA mini kit (Qiagen), with manufacturers recommendation followed. RNA was eluted in 50 µl nuclease-free water and concentrations of RNA again determined using a NanoDrop spectrophotometer.

3.2.3 PCR

PCRs were performed using KOD polymerase (Novagen, Merck Millipore). Reaction volumes of 50 µl were prepared containing: 5 µl 10X PCR reaction buffer; 5 µl dNTP mix (2 mM each); 3 µl $MgSO_4$ solution (25 mM); 0.3 mM (final concentration) of both forward and reverse primer; 1 µl of template DNA (1-10 ng/µl); 1 U of KOD hot start DNA polymerase; and 32 µl of nuclease-free water. Reaction conditions were as follows: initial denaturation of 5 minutes at 95°C; 30 cycles of denaturing at 95°C for 30 seconds, primer annealing at 45-60°C for 30 seconds, extension at 70°C; final extension of 70°C for 5 minutes; hold at 4°C. Primer annealing temperature was determined by primer Tm. Extension time was determined by the length of the amplicon, using an amplification speed of KOD polymerase set at 25 seconds per 1 kB of amplicon size.

3.2.4 RT-PCR

1 µl of RNA (2 ng/µl) was added to 12 µl DNase/RNase-free water with 1 µl of RT primer (10 µM/ml). The reaction was then heated to 65°C for 5 minutes before rapidly cooling on ice. Then 4 µl M-MLV 5X buffer, 1 µl 10 mM 4xdNTPs, 40 U (1 µl) of RNasin, and 200 U of M-MLV RT were added to the reaction mix and the reaction incubated at 42°C for 1 hour. Samples then heated to 90°C for 10 minutes to inactive enzyme before being stored at -20°C until used for the PCR reaction.

3.2.5 Real time qPCR

Each real-time PCR reaction consisted of 8.4 µl of MESA Blue qPCR Mastermix Plus (Eurogentec), 0.3 µl of each primer and 1 µl of cDNA from the appropriate RT-PCR. Reactions were performed on either a ABI 7300 (Applied Biosystems) or a TOpitcal (Biometra) machine. Cycle conditions were 95°C for 10 minutes followed by 40 cycles of 95°C for 15 seconds and 60°C for 1 minute. A melt curve analysis at the end of each assay

consisted of 95°C for 15 seconds, 60°C for 1 minute before increasing temperature to 95°C at 0.1°C per second.

3.2.6 Quick-change PCR

Quick-change PCR methods allowed the introduction of nucleotide mutations at specific points. Complementary 30-35 nt primers were designed targeting the region where the change was to be made. The specific mutations to be introduced were contained in the central region of the primer sequence, with flanking regions complementary to target sequence. The PCR was set up as in 3.2.3 but contained only 1 ng of DNA template and a reduced cycle number of 18 was used. The reaction was then treated with 1 U of DpnI and incubated for 1 hour at 37°C. A 1 in 10 dilution of the reaction in nuclease-free water was used transform competent JM109 bacteria as in 3.2.1.

3.2.7 Restriction digest

Restriction digests were used to confirm correct sequences through restriction profile analysis, or to perform cloning reactions. Reactions were set up to final volumes of 20-50 µl dependent of application. Each reaction contained: 1X final concentration of appropriate enzyme buffer; 1 U of restriction enzyme per 1 µg of DNA (up to maximum 3 µg DNA in 50 µl reaction); acetylated BSA (10 µg/µl) when needed; made up final reaction volume with nuclease-free water. Reactions were incubated at 37°C for between 1 to 4 hours. Digested DNA used in subsequent cloning procedures was purified from agarose electrophoresis gels.

3.2.8 DNA ligation

Vector and insert ligations were performed using the Rapid DNA Ligation kit (Roche). After linearisation the plasmid was dephosphorylated with CIAP (calf intestinal alkaline phosphatase) (Promega) by addition of CIAP Reaction buffer and 0.1 U CIAP per µl (final volume). Reactions were incubated at 37°C for 1 hour before being purified from an agarose gel after electrophoresis. The ligation reaction was performed as per the manufacturers instructions, using a 1:3 molar ratio of vector to insert.

3.2.9 Restriction free cloning

Restriction free cloning was used to subclone a PCR product into a plasmid at a specific location, and used as an alternative to restriction enzyme based cloning. Plasmids were either linearised using restriction enzymes, or by excision PCR to remove a specific sequence. Excision PCR uses primers aligning to the flanking regions of the region to be deleted, in such an orientation that the 5' end of one primer anneals to the 3' boundary of the region to be deleted, and the 5' end of the other primer anneals to the 5' boundary of the region to be deleted. These excision primers were designed to incorporate the terminal 15 nt of the sequence to be subcloned at the 5' ends. A second pair of primers were designed to produce an PCR amplicon of the insert sequence, and these primers also included the 15 nts of the boundary regions at their 5' end. These PCRs creates two amplicons with complementary 30 nt sequences at each end. Using the In Fusion HD Cloning Kit (Clonetech Laboratories Inc.) the following reaction mix was used: 100 ng of insert; 50 ng of vector; 2 µl 5X In Fusion enzyme pre-mix; volume made up to 10 µl with nuclease-free water. The reaction was incubated at 50°C for 15 minutes before being placed on ice. All 10 µl was then transformed into competent JM109 bacteria and standard transformation protocols followed.

3.2.10 Colony PCR

Colony PCR was used to confirm presence or absence of an insert within a plasmid construct. Selected colonies were resuspended in 13.5 µl of DNase free water and heat-shocked at 95°C for 5 minutes before cooling on ice. To this was added 6.5 µl of PCR master mix (GoTaq, Promega) with specific primers to amplify the insert and distinguish it from re-ligated plasmid or incorrectly cloned inserts. The master mix contained (for 1 reaction): 4 µl 5X PCR buffer, 0.4 µl dNTP mix (10 mM), 1 µl forward primer (10 mM), 1µl reverse primer (10 mM), and 0.1 µl GoTaq polymerase. Standard PCR conditions were: initial denaturation at 95°C for 5 minutes; 30 cycles of denaturation at 95°C for 30 seconds, primer anneal for 30 seconds, extension at 72°C final extension at 72°C for 10 minutes; followed by cooling and storage at 4°C. The primer annealing temperature was determined by the primer characteristics and the extension time was determined by the PCR amplicon size (1 minute per 1 kb amplicon size).

3.2.11 Agarose gel electrophoresis

Agarose gel electrophoresis was used to separate DNA fragments for either visual analysis or gel purification. Gel electrophoreses was performed in horizontal slab gel gels consisting of either TAE or TBE agarose gels. TAE gels were used if DNA bands were to be purified post electrophoresis, TBE gels were used in all other cases. Loading dye was added to samples (1:6 ratio of dye to sample) and the volume loaded ranged from 5-50 µl dependent of procedure. Gels were run at 100 V for 30 minutes (or until ideal separation was achieved) using 1X TAE as the running buffer. After electrophoresis DNA fragments were visualized using a UV transilluminator. DNA bands were purified from agarose gels using the Wizard® SV Gel and PCR Clean-Up System (Promega), with manufacturers recommendations followed.

3.2.12 In-vitro transcription

Up to 1 µg of linearised plasmid in 20 µl of DNase and RNase-free water was combined with 2 µl of T7 or SP6 10X reaction buffer, 2 µl of each of the dNTP solutions (75 mM) and 2 µl of the T7 or SP6 enzyme mix. The reaction buffer was incubated at 37°C for 4 hours. After 4 hours, 1 µl of TURBO DNase (2 U/µl) was added to the reaction and incubated at 37^0C for a further 30 minutes. To terminate the reaction and recover the RNA transcripts 115 µl of DNase and RNase free water and 15 µl of ammonium acetate stop solution (5 M ammonium acetate, 100 mM EDTA) was added. To this two volumes of ice-cold ethanol were added, the reaction was mixed well and incubated at -20°C for 30 minutes. The reaction was then centrifuged at 4°C at >3,000 rpm (>15,000 g) for 15 minutes to pellet the precipitated RNA. The supernatant was removed and RNA re-suspended in 50 µl of RNase and DNase free water.

3.2.13 Northern blot analysis

Samples were prepared to a final minimum volume of 60% de-ionised formamide, 10X RNA loading dye and 10 µg ethidium bromide to ensure 4 µg of RNA in each sample. Sample were denatured at 65°C for 5 minutes before being placed on ice for a further 5 minutes. RNA was electrophoresed through a 1.2% TAE agarose gel at 75 V. The agarose gel was washed twice in 10X SSC under constant agitation before blotting to nitrocellulose

membrane in 10X SSC overnight. After blotting the membrane was twice washed in 2X SSC before being dried at room temperature. RNA was cross-linked to membrane by exposure to a 302 nm UV light source for 3 minutes.

Membranes were incubated in pre-warmed 50% formamide hybridisation buffer at 68°C for 30 minutes (under constant agitation in hybridisation tube). RNA specific DIG-labeled probes were heat-denatured by incubating at 99°C for 5 minutes before cooling on ice for 5 minutes. Pre-hybridisation buffer was removed from the hybridisation tube, replaced with approximately 150 ng of probe diluted in 4 ml fresh pre-warmed 50% formamide hybridisation buffer and incubated overnight at 68°C.

After probe hybridisation membranes were washed twice in 2X SSC and 0.1% SDS at room temperature for 10 minutes, washed twice in 0.1X SSC and 0.1% SDS at 68°C for 25 minutes, and rinsed twice in washing buffer at room temperature for 5 minutes (all under constant agitation). The membrane was blocked with 1X blocking buffer for 45 minutes under constant agitation. Blocking buffer was removed and replaced with antibody buffer and incubated at room temperature for 45 minutes under constant agitation. After incubation membrane was washed twice in washing buffer for 30 minutes before being incubated in detection buffer for 5 minutes at room temperature. To visualise the RNA:DIG probe hybridisations membranes were treated with an alkaline phosphatase chemiluminescent substrate (CPD-Star, Roche) before exposure to X-ray film.

3.2.14 Small RNA isolation and deep sequencing analysis

Sequencing of the small RNAs was performed by ARK-Genomics (The Roslin Institute, University of Edinburgh) on the Illumina Solexa platform (HiSeq 2000). Illumina adapters and sequencing primers were removed using cutadapt (Martin 2011), and trimmed sequences were aligned to the reference genomes using Novoalign. Graphs and reports were produced in R (RCore 2012) using the viRome package (Watson et al. 2013). Sequence logo analysis was plotted using the seqLogo package (Bembom 2008) from Bioconductor (Gentleman et al. 2004).

3.3 Protein analysis

3.3.1 Western blot analysis

Cell lysates were prepared by addition of protein disruption buffer (PDB) to cell monolayers (30 µl/cm^2 cell monolayer area). Prior to SDS-PAGE samples were boiled at 100°C for 5 minutes before being placed immediately on ice. 15 µl of sample was added per well of NuPAGE 4-12% Bis-Tris gels (Invitrogen) along with 5 µl PageRule Plus pre-stained protein ladder (Fermentans). Protein separation was achieved by electrophoresis at 180 V for 50 minutes in MES SDS running buffer. Proteins were transferred to a nitrocellulose membrane (Amersham) using membrane transfer buffer. Transfer were performed using semi-dry blotting methodology, and transferred at 10 V for 50 minutes.

The membrane was blocked post transfer for 1 hour in western blot blocking buffer at room temperature. All antibody dilutions were performed in 5% milk solution diluted in PBS 0.1% (v/v) Tween-20. Antibody incubations on membranes were performed at room temperature for 1 hour under constant agitation. The membrane was washed with western blot washing buffer after each antibody incubation step.

Visualisation of detected proteins was achieved using SuperSignal West Pico chemiluminescent substrate (Thermo Scientific) followed by exposure to x-ray film.

3.3.2 LI-COR analysis

Protein samples for LI-COR analysis were separated on NuPAGE 4-12% Bis-Tris gels as with chemiluminescent analysis although only 1 µl of PageRule Plus pre-stained protein ladder was used to prevent signal saturation during analysis. Membranes were blocked post transfer for 1 hour in LI-COR blocking buffer. Antibody incubations on membranes were performed at room temperature for 1 hour under constant agitation. All antibody dilutions were performed in western blot washing buffer, and incubated at room temperature for 1 hour in a sealed box. Membranes were washed with western blot washing buffer after each antibody incubation step, with a final wash in PBS prior to visualization.

3.3.3 Metabolic labeling of mammalian and mosquito cells

Mammalian cells were starved of methionine for 2 hours prior to treatment by replacement of cell culture media with DMEM (Met-) media (Sigma). The DMEM (Met-) media was then replaced with DMEM (Met-) media containing 15 µCi of [^{35}S]-methionine per 200 µl (for a 12-well cell culture plate). Mosquito cell culture medium lacking methionine was not available. Therefore mosquito cells were starved by replacement of media with PBS, and treated with 15 µCi of [^{35}S]-methionine in PBS. After 2 hours incubation the DMEM (Met-) or PBS volumes were removed and cell monolayers carefully washed with PBS before addition of PDB to lyse the monolayer. Cell lysates were then removed and stored at -20^{0}C until analysed. Labeled protein were separated as in 3.3.1, before the gel was dried and analysed by autoradiography.

3.3.4 Luciferase assays

Luciferase assay were performed using either the Dual-Luciferase® Reporter System or *Renilla* Luciferase® Assay System (both Promega), with manufacturers recommendations followed. Reactions were performed in triplicate in 24-well cell culture plates. Luciferase activities were determined using a GloMax® 20/20 Single Tube Luminometer (Promega) using manufacturers recommended protocol for each kit, with 10 second integration periods chosen for both.

3.4 Software packages

3.4.1 Bioinformatics

Sequence analysis, primer design, and *in silico* plasmid design were performed using CLC Main Workbench (Ver. 6.8.3) (CLC bio, www.clcbio.com).

3.4.2 Graphing and statistical analysis

Performed using GraphPad Prism version 5.0a for Mac OS X (GraphPad Software, La Jolla California USA, www.graphpad.com).

3.4.3 Imaging programs

LI-COR analysis was performed using Image Studio Software (www.licor.com).

Chapter 4

AIMS

4 Aims

The general aim of this project was to examine rMP12 replication in the available mosquito cell lines, and to use to the reverse genetics system to create recombinant viruses to help with these investigations.

Specifically I investigated the following areas of research:

1) To characterise RVFV rMP12 infection in a range of mosquito cell lines, and compare and contrast aspects of the replication to that in mammalian cells. I aimed to create rMP12 recombinants and use them to examine the effects of (a) removing genes coding for the non-structural proteins; (b) the introduction of foreign genes into the genome segments; and (c) how alterations to the coding strategy of rMP12 S segment were tolerated

2) I aimed to design and develop a strand-specific qRT-PCR assay to examine variances in genome packaging between the mosquito and mammalian cells when the coding strategy of the rMP12 S segment was altered.

3) To use the available molecular tools and reverse genetics methodologies to investigate the development of minireplicon systems and rescue methods in mosquito cell lines.

4) To investigate the RNAi responses in mosquito cells when infected with rMP12 and recombinant viruses.

Chapters 5-8

RESULTS

5. Characterisation of Rift Valley fever virus in mosquito cells

5.1 Introduction

5.1.1 Mosquito cell culture

A wide range of mosquito species have been described as viable vectors capable of RVFV transmission (Chevalier et al. 2010). One of the primary species responsible for transmitting the virus and maintaining disease endemicity are those of the *Aedes* genus, from which several cell lines have been derived (Pepin et al. 2010; Ikegami & Makino 2011). The mosquito cell lines employed throughout this project were all originally generated from neonate larval samples. Cell line preparation involved mechanical disruption of freshly hatched mosquito larvae, followed by propagation of the resultant primary cells until a continuous cell line was obtained via spontaneous immortalisation. Mosquito cell cultures in common experimental use today are derived from clones of these cells that demonstrated preferred characteristics during infection, such as rapid cell proliferation, minimal CPE, and generation of high viral titres.

C6/36 and U4.4 cells were derived from the original *A. albopictus* cell line created by Singh *et* al. (1967). The C6/36 cell line was selected from multiple clones for its ability to generate higher DENV and chikungunya virus titres compared with the original Singh line (Igarashi 1978). It remains the most widely used *A. albopictus* cell line available to researchers today. A further *A. albopictus* cell line U4.4 was selected during experiments to examine SNV growth in the original Singh cell line (Condreay & Brown 1986). Although they originate from the same species, differences have been observed when comparing the replication of BUNV in C6/36 and U4.4 cells (Szemiel et al. 2012) Two cell lines derived from *A. aegypti* (Ae and A20) were initially used in this project. They were developed during work to expand the number of mosquito cell lines available to researchers (Pudney et al. 1979). However, after several months it became apparent from repeated experiments that there was no variation in how either *A. aegypti* cell line responded to RVFV infection. Therefore it was decided to use just Ae cells as the representative *A. aegypti* cell line.

5.1.2 RVFV strain MP12

This attenuated RVFV strain was created by serially passaging the virulent ZH548 strain, obtained during the 1977-79 Egyptian epidemic, in MRC-5 human diploid fibroblast cells in the presence of the mutagen 5-fluorouracil (Caplen et al. 1985). Subsequent sequencing of the MP12 genome revealed a total of 9, 12, and 4 nucleotide substitutions in the L, M and S segments respectively. These mutations resulted in 3 amino acid changes in the L protein, 7 amino acid changes in the M segment-encoded proteins, and 1 amino acid change in the NSs protein (Vialat et al. 1997). The reverse genetics rescue system employed throughout this project was based on the MP12 strain, and rescued virus termed rMP12 (Billecocq et al. 2008).

5.2 Aims

The primary aims of this section of the thesis were to characterise rMP12 replication in mosquito cells, and to compare and contrast the results with that for infection in mammalian cells. Secondly, rMP12 recombinants were to be used to investigate the importance of the non-structural proteins for mosquito cell replication.

5.3 Results

5.3.1 Phenotypic observation of uninfected mosquito cell lines

The mosquito cells grew more slowly, were physically smaller, and exhibited a less homogeneous morphology than the BHK-21 cells selected as the comparative mammalian cell line. Fully confluent C6/36 cells exhibited moderate contact inhibition with minimal areas of overgrowing cells at 100% confluency. U4.4 cells did not exhibit contact inhibition and clumps of cells were visible in the monolayer if left to overgrow. Ae cell monolayers also formed cell clumps when fully confluent, although not to the extent seen in U4.4 cells (Figure 5-1).

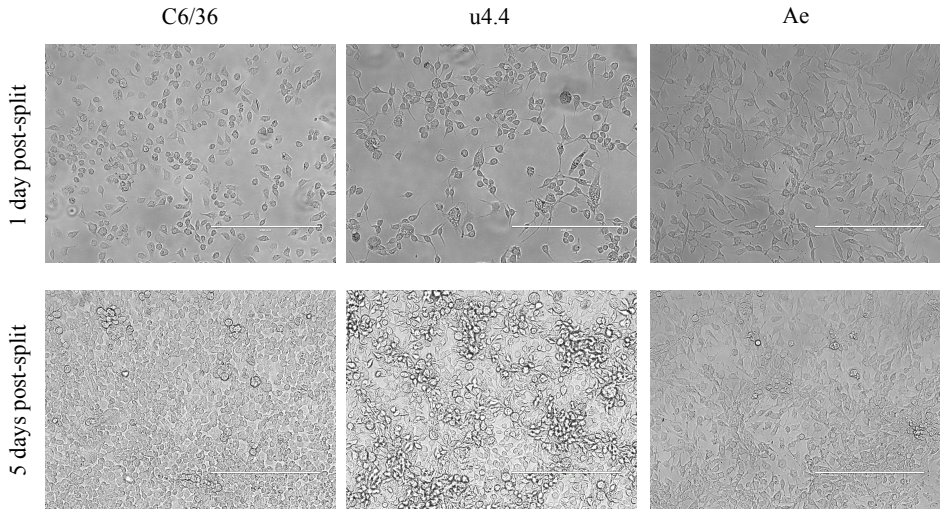

Figure 5-1: Uninfected mosquito cell monolayers.
Phase contrast light microscope images of C6/36, U4.4, and Ae cells (20x magnification). The cells were passaged with a 1:10 split ratio when 100% confluent (day 0), and imaged on day 1 and 5 post split.

5.3.2 rMP12 replication in mosquito cells

Initial experiments were performed to assess the permissiveness of mosquito cell lines to support rMP12 replication. BHK-21 cells were used as the mammalian cell comparative control, and infections performed at MOI 1. rMP12 replication was apparent in all mosquito cell lines (Figure 5-2.A). C6/36 cells were the most permissive, yielding $7x10^8$ pfu/ml by 48 h p.i.. The growth rate in U4.4 cells was similar to that observed for C6/36 cells, but the total yield was a slightly reduced $8x10^7$ pfu/ml. Viral replication was slowest in Ae cells and the yield was also the lowest, reading $4x10^7$ pfu/ml. In BHK-21 cells the virus reached a maximum titre of $4x10^8$ pfu/ml by 24 h p.i., and by 48 h p.i. cytolytic effects of infection were considerable. Small perturbations in mosquito cell phenotypes were noted during early in the time course (< 24 h p.i.), but no CPE or cell death was observed by 96 h p.i..

Western blot analysis for N and NSs protein demonstrated further differences between cell lines (Figure 5.2.B). N and NSs were detected in BHK-21 cells at 6 h p.i., and their levels increased until 18 h p.i. after which they remained stable until completion of the time course. In C6/36 cells N was first detected at 9 h p.i., and the level increased throughout the time course. NSs was first detected at 12 h p.i., and the level similarly increased over time. In U4.4 and Ae cells N was detected at 18 h p.i., but no NSs was detected at any time. In all mosquito cell lines N seemed to accumulate throughout the time course.

5.3.3 Immunofluorescence studies of rMP12 replication

Immunofluorescence studies were performed on rMP12 infected mosquito cells to investigate the cellular localisation of N and NSs during infection. Cells were infected at MOI 1, and at 48 h p.i. stained with anti-N, anti-NSs, and anti-tubulin antibodies. As both the anti-N and anti-NSs antibodies were rabbit-derived, co-staining for these two proteins could not be performed on the same sample. Therefore the experiments were performed on duplicate cell monolayers.

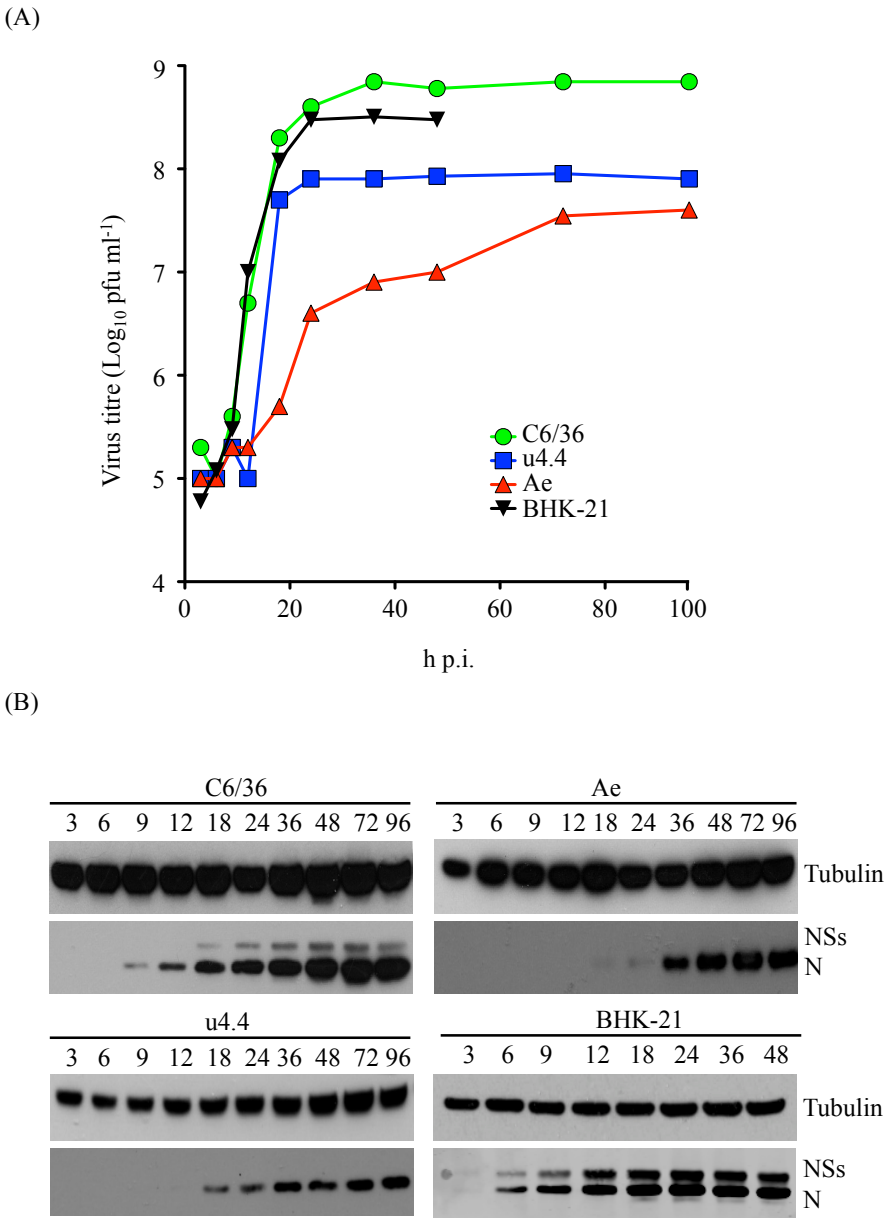

Figure 5-2: Characterisation of rMP12 replication in C6/36, U4.4, Ae, and BHK-21 cell lines
(A) Growth curves in rMP12 infected C6/36, U4.4, Ae, and BHK-21 cell lines at MOI 1. rMP12 infection of BHK-21 cells was cytolytic past 48 h p.i. and sample collection stopped, but mosquito cell monolayers remained intact by 96 h p.i.. (B) Western blot analysis of proteins synthesised in rMP12 infected mosquito and BHK-21 cells lines. Total cell lysates were taken at the same time points as for the growth curve analysis, indicated at the top of each track. Antibodies targeting RVFV N and NSs were used to probe for viral proteins, and anti-tubulin antibody was used to detected tubulin as loading control for each sample.

In infected mammalian cells, RVFV N protein was expressed in large quantities and was localised exclusively to the cytoplasm (Brennan et al. 2011; Benferhat et al. 2012). In infected C6/36 (Figure 5-3.A) and U4.4 (Figure 5-4.A) cells N was localised to the cytoplasm, and displayed a punctate staining pattern. In infected Ae cells however N was more uniformly distributed throughout the cytoplasm with no punctate staining observed (Figure 5-5.A). A characteristic feature of the RVFV NSs protein is that it forms intranuclear filaments (Swanepoel & Blackburn 1977; Kohl et al. 1999; Yadani et al. 1999; Billecocq et al. 2004; Mansuroglu et al. 2010). NSs expression was most apparent in C6/36 cells (Figure 5-3.B), and only detectable in a very small minority of U4.4 (Figure 5-4.B) and Ae (Figure 5-5.B) cells. Although NSs was localised exclusively to the nucleus, no filamentous structures were observed. Rather, NSs existed as irregular amorphous bodies, with no regular or repeating structures detected.

rMP12 N has been shown to co-localise with the L protein in infected mammalian cells (Brennan et al. 2011). To investigate whether similar co-localisation occurs in mosquito cells C6/36, U4.4 and Ae cells were infected with rMP12:L3V5, a recombinant virus expressing a V5-epitope tag in the L protein (Brennan et al. 2011). Cells were infected at MOI 1 and stained at 48 h p.i. with anti-N, anti-V5, and anti-tubulin antibodies. L protein was detected exclusively in the cytoplasm, and analysis of the merged images demonstrated a high degree of N and L co-localisation within the cytoplasm (Figure 5-6).

Although no NSs nuclear filaments were observed with rMP12 infections, previous results have described their formation in mosquito cells infected with the ZH548 strain (Léger et al. 2013). To investigate whether the differences between rMP12 and ZH548 NSs were responsible for this observation, an rMP12 recombinant was rescued in which the MP12 NSs CDS was replaced with that for ZH548 NSs. This virus was named rMP12ΔNSs:NSs_{ZH548}. C6/36 cells were the only cell line used in this experiment as NSs expression in rMP12 infected U4.4 and Ae cells was minimal. Cells were infected at MOI 1 with rMP12ΔNSs:NSs_{ZH548} and fixed and stained at 48 h p.i.. A significant difference in NSs phenotype was observed between the two viral infections. Infection with rMP12ΔNSs:NSs_{ZH548} resulted in nuclear NSs structures that were more consistent with the filaments observed in mammalian cells, and for the published data examining ZH548 infection in mosquito cells (Léger et al. 2013) (Figure 5-7). These structures were not as

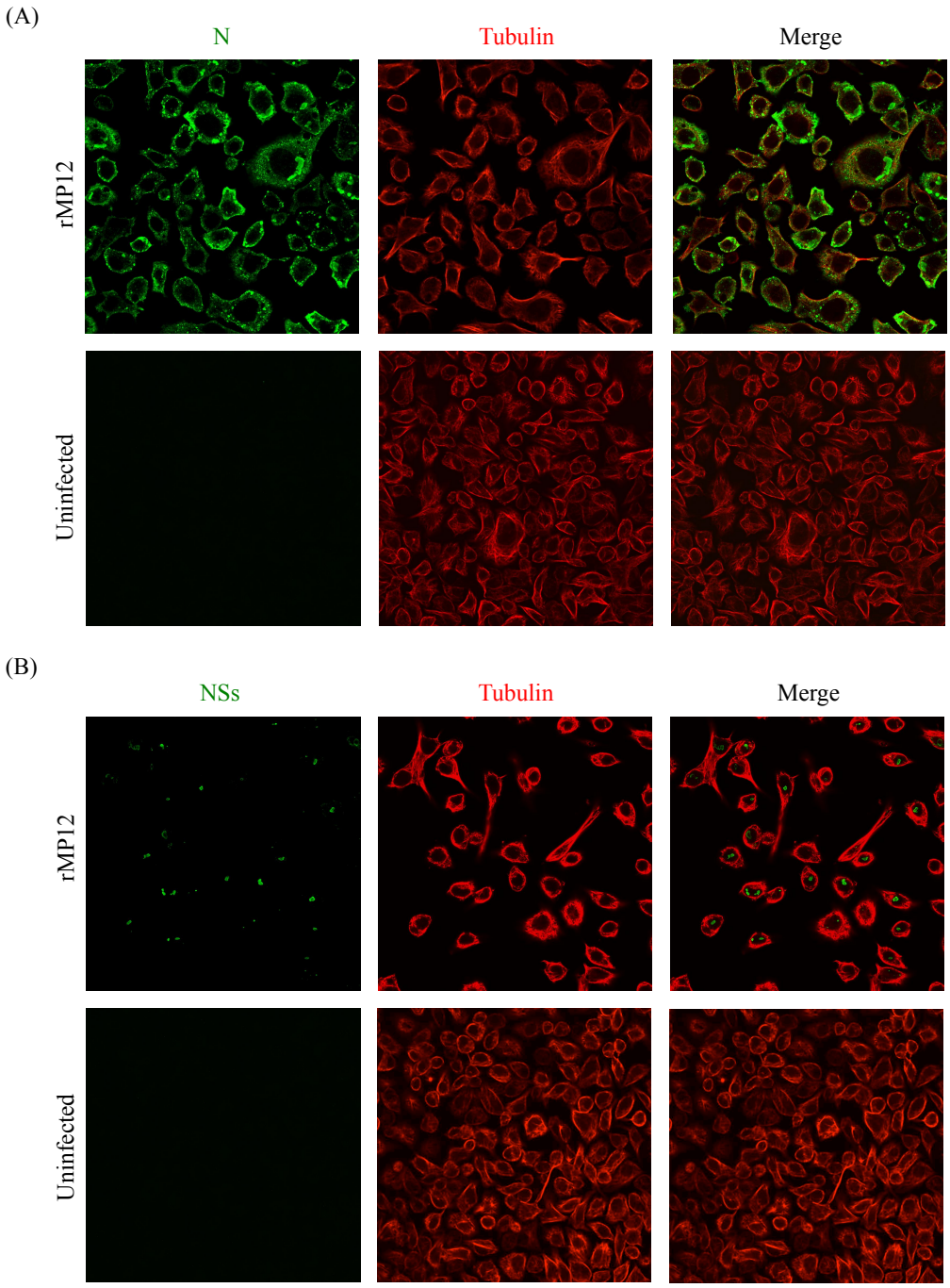

Figure 5-3: Detection of N and NSs protein in rMP12 infected C6/36 cells.
Detection of (A) N and (B) NSs protein by immunofluorescent staining of rMP12 infected C6/36 cells. Cells were infected at MOI 1 and fixed and stained at 48 h p.i. with anti-N (green), anti-NSs (green), and anti-tubulin (red) antibodies. Also shown are the uninfected control cells. All images were taken using the 63x objective.

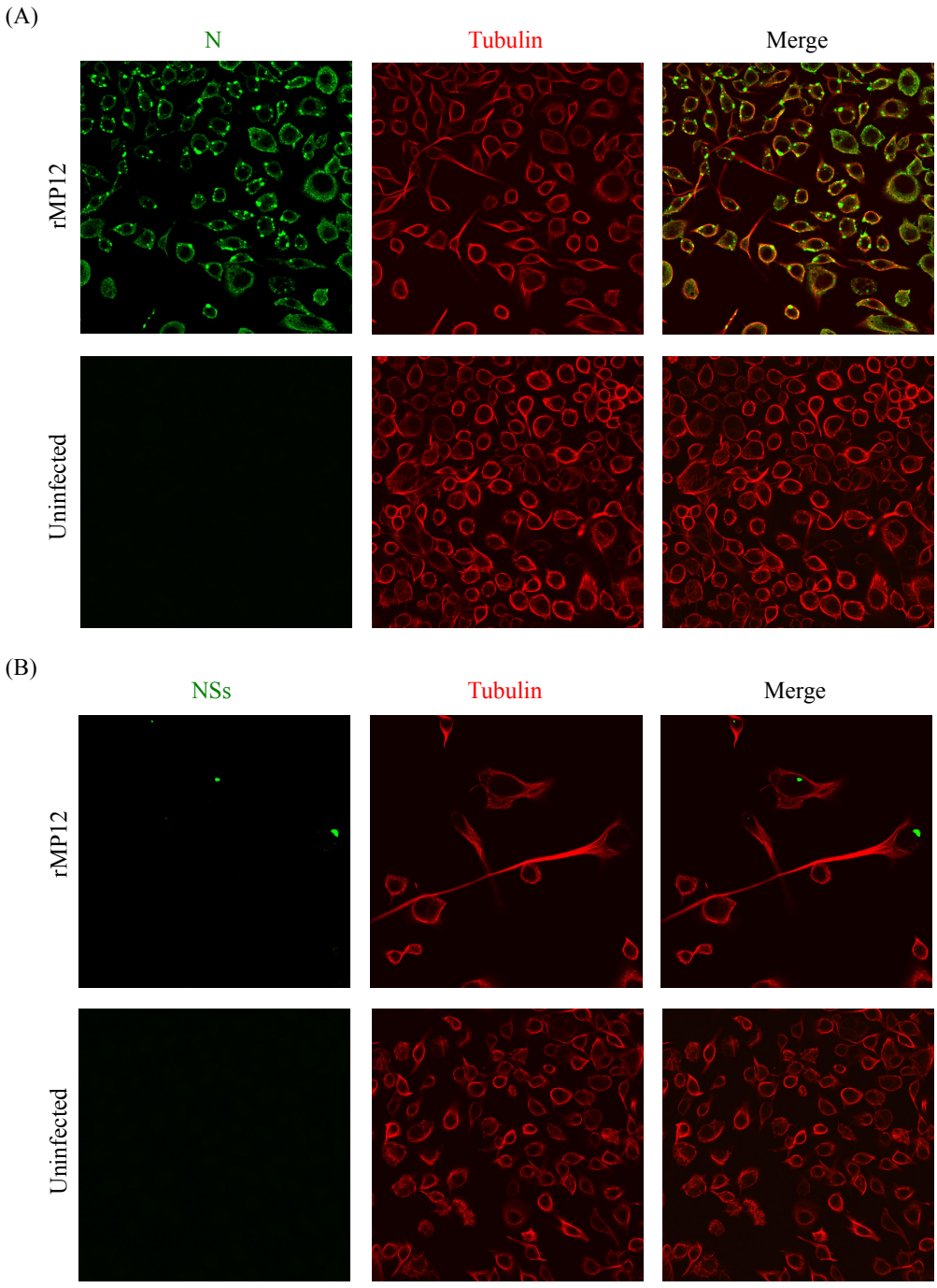

Figure 5-4: N and NSs in rMP12 infected U4.4 cells.
Detection of (A) N and (B) NSs protein by immunofluorescent staining of rMP12 infected U4.4 cells. Cells were infected at MOI 1 and fixed and stained at 48 h p.i. with anti-N (green), anti-NSs (green), and anti-tubulin (red) antibodies. Also shown are the uninfected control cells. All images were taken using the 63x objective.

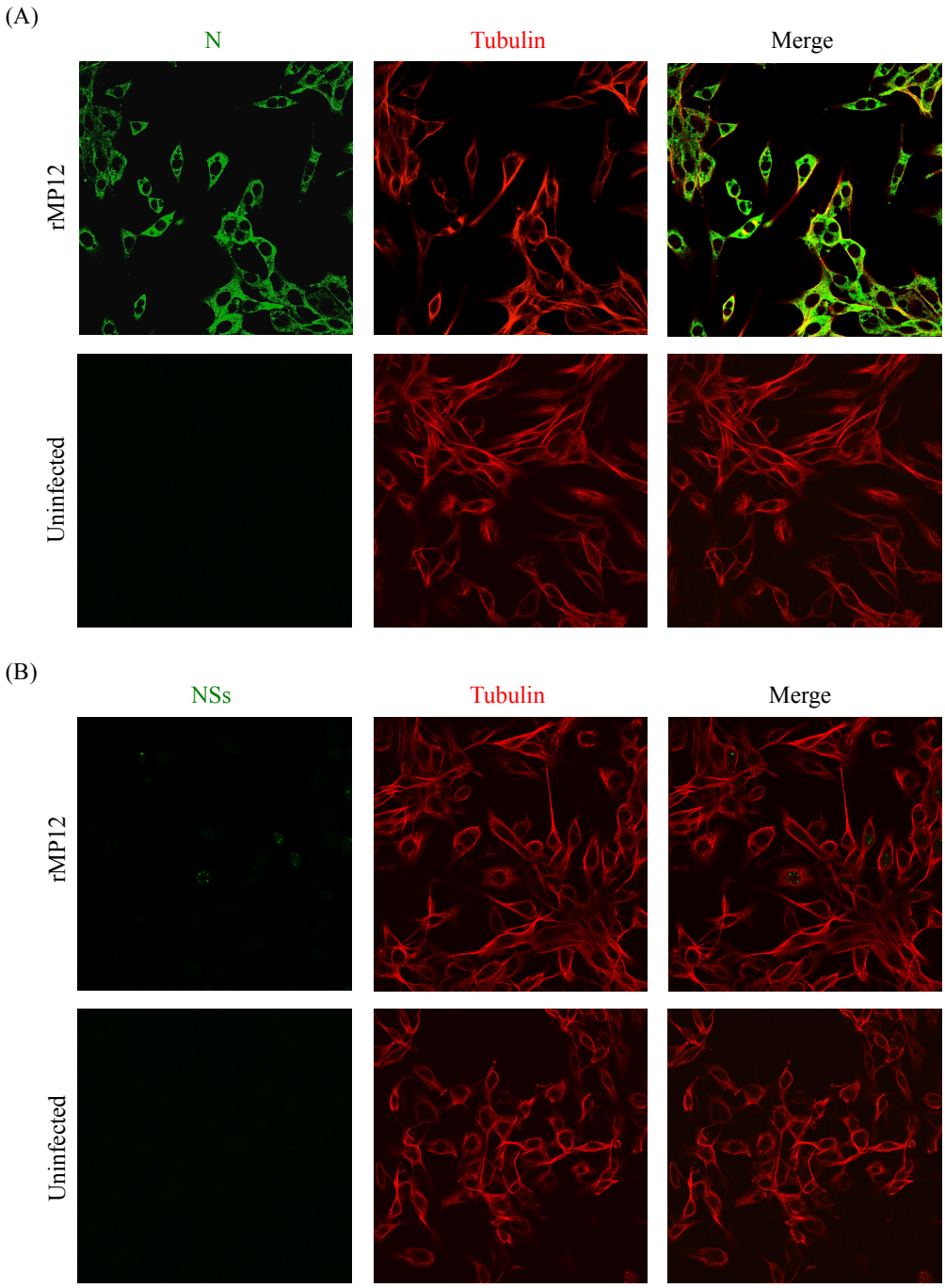

Figure 5-5: N and NSs in rMP12 infected Ae cells.
Detection of (A) N and (B) NSs protein by immunofluorescent staining of rMP12 infected Ae cells. Cells were infected at MOI 1 and fixed and stained at 48 h p.i. with anti-N (green), anti-NSs (green), and anti-tubulin (red) antibodies. Also shown are the uninfected control cells. All images were taken using the 63x objective.

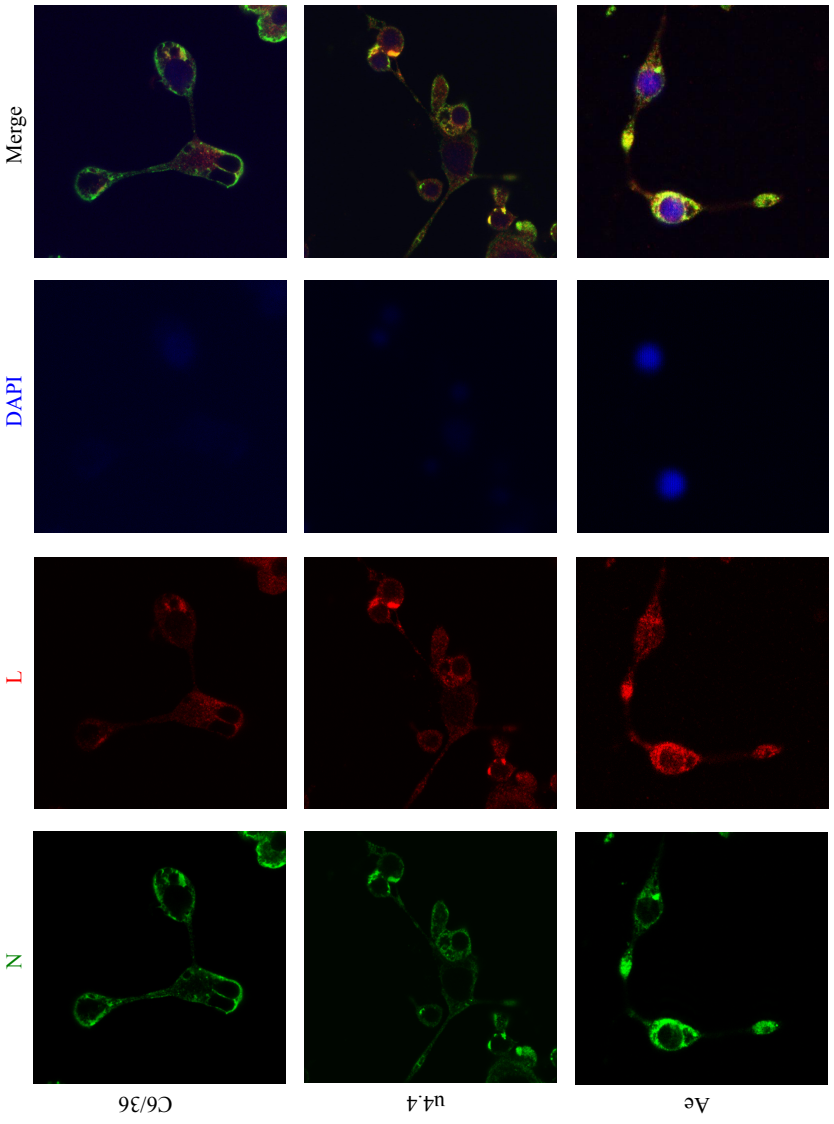

Figure 5-6: Detection of N and L proteins in rMP12:LV5 infected mosquito cells
C6/36, U4.4 and Ae cells were infected with rMP12:LV5, a recombinant virus expressing a V5-epitope tag in the L protein, at MOI. Cells were fixed and stained 48 h p.i. with anti-N (green) and anti-V5 (red) antibodies. Cover slips were mounted in Movial which contained DAPI. All images were taken using the 63x objective.

(A) Examples rMP12 infected C6/36 cells

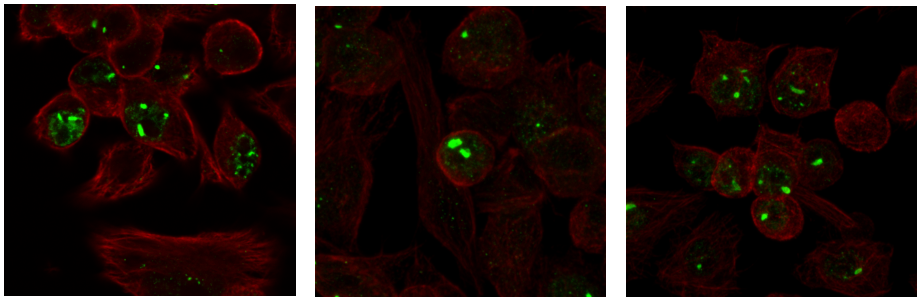

(B) Examples rMP12ΔNSs:NSs_{ZH548} infected C6/36 cells

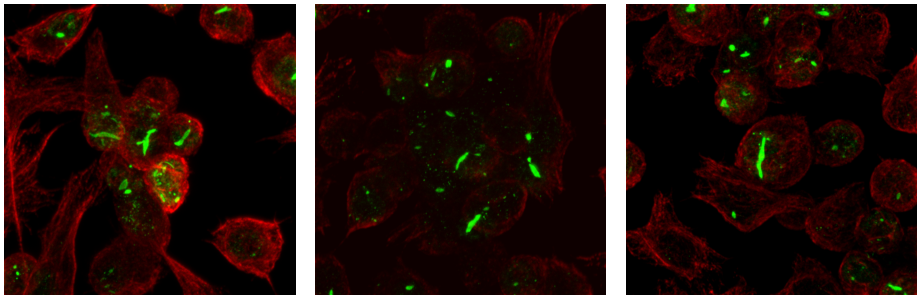

Figure 5-7: NSs structures in rMP12 or rMP12ΔNSs:NSs_{ZH548} infected C6/36 cells.
Immunofluorescence images showing three examples of merged images for either (A) rMP12 or (B) rMP12ΔNSs:NSs_{ZH548} infected C6/36 cells. Cells were infected at MOI 1 and fixed and stained at 48 h p.i. with anti-NSs (green) and anti-tubulin (red) antibodies. All images were taken using the 63x objective.

defined or as regular as those observed in mammalian cells, being generally thicker and shorter. Whilst there are three nucleotide substitutions between the rMP12 and ZH548 NSs CDSs, only one of these results in an amino acid change (Vialat et al. 1997).

5.3.4 Persistence and infection of mosquito cells

Arbovirus infection of invertebrate cell lines generally manifests as a persistent rather than cytolytic infection (Newton et al. 1981; Brown 1984; Elliott & Wilkie 1986; Scallan & Elliott 1992). Published research using ZH548 showed that although persistence could be maintained in U4.4 cells and the *A. aegypti* cell line Aag-2, it could not be continually passaged in C6/36 cells as infection was cytolytic (Léger et al. 2013). Experiments were undertaken to determine if this pattern was repeated for rMP12 infected mosquito cells. C6/36, U4.4 and Ae cells were infected at MOI 0.01, split 1:5 at 100% confluency, and then maintained like uninfected mosquito cells. All cell lines were maintained for 10 consecutive passages and at each split, cell culture supernatant and total cell protein samples obtained to analyse the persistence of virus.

The virus titres demonstrated that persistence was maintained throughout the 10 passages in all cell lines, although titres reduced as passage number increased (Figure 5-8.A). No obvious CPE was observed in the cell monolayers throughout the 10 passages (Figure 5-8.B). Compared to uninfected cells progression to 100% confluency was marginally slower, but this was more apparent in the early passages, with the effect lost after passage 3. Western blot analysis confirmed N was expressed at each passage, with a reduction in level that correlated with the lower titres. NSs protein was detected only in C6/36 cells, but the level reduced with each passage becoming undetectable from passage 3 onwards (Figure 5-9). This correlated with a 100-fold reduction in titre between passages 2 and 3.

To investigate whether the reduction in viral titres and loss of NSs expression were due to accumulated mutations, virus derived from persistently infected cells at passages 5 and 10 was used to infect BHK-21 cells at MOI 1. The titres in BHK-21 cells at 48 h p.i. were reduced between 100- and 10,000-fold when compared to a control infection with the elite rMP12 stock (Figure 5-10.A). Despite this large reduction in titre N and NSs expression

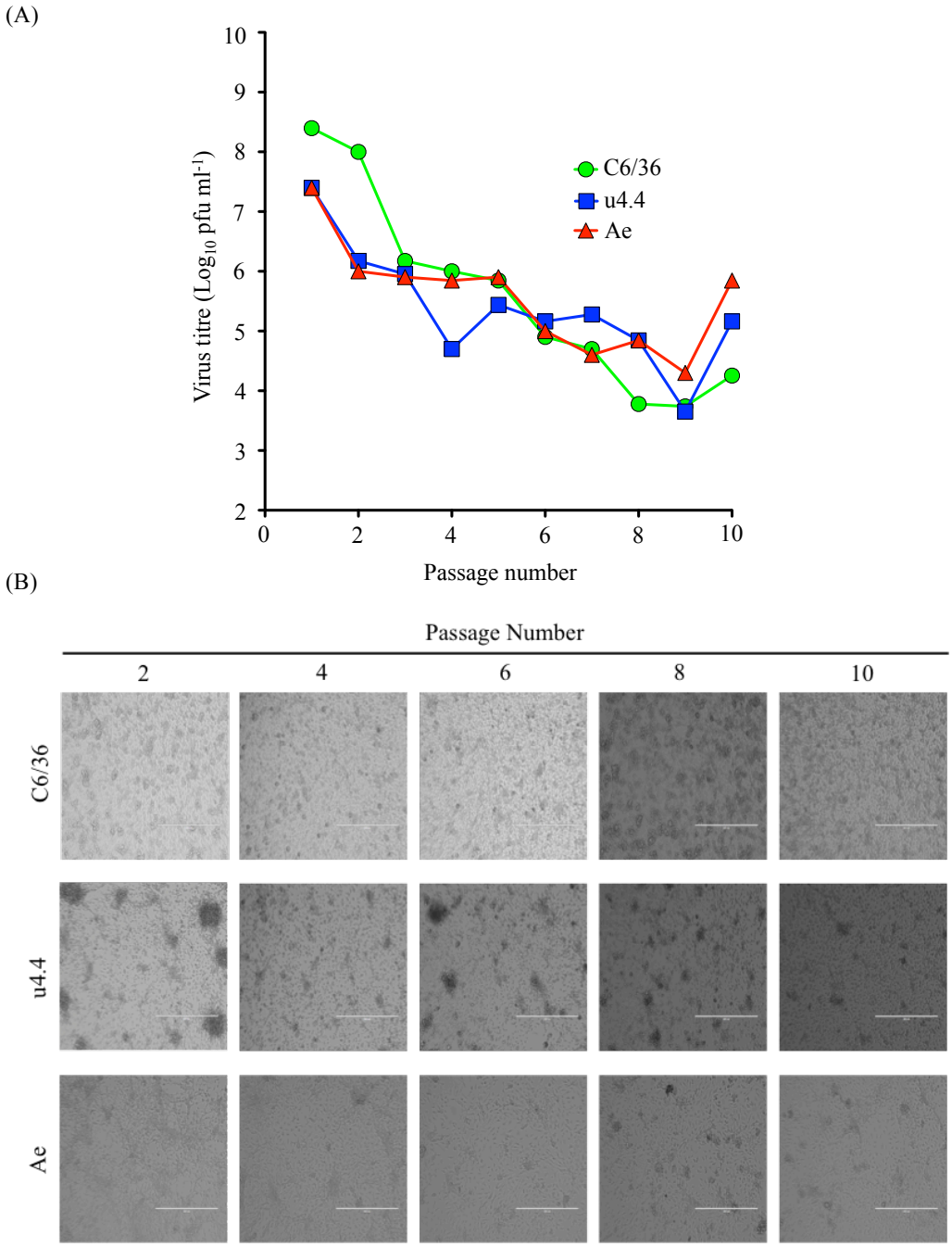

Figure 5-8: Persistent rMP12 infection in C6/36, U4.4, and Ae cell lines.
(A) Titres of rMP12 obtained from the persistently infected mosquito cells at each passage. Cell culture supernatant was harvested prior to each passage and titre determined by plaque assay on BHK-21 cells. (B) Phase contrast light microscope images of mosquito cell monolayers were taken at x10 magnification. Images were taken immediately prior to passage.

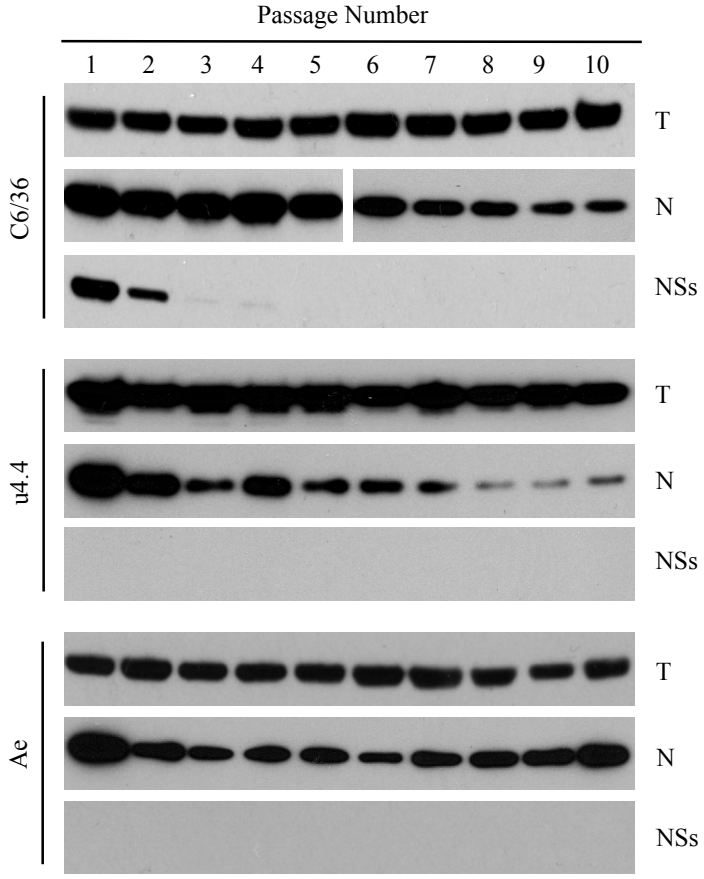

Figure 5-9: N and NSs production in rMP12 persistently infected mosquito cell lines.
Western blot analysis of proteins expressed in rMP12 persistently infected C6/36, U4.4 and Ae cells lines. At each split 20% of the cells were used to seed the next passage. The remaining 80% of cells were pelleted and re-suspended in PDB. Antibodies targeting RVFV N and NSs were used to probe for viral proteins, and anti-tubulin antibody was used to detect tubulin (T) as a loading control for each sample.

was observed in all samples (Figure 5-10.B). Sequence analysis of the N and NSs CDS of the p5 and p10 virus from each mosquito cell line demonstrated they were identical to that of the elite rMP12 stock.

5.3.5 Characterisation of rMP12ΔNSs:eGFP and rMP12ΔNSm

To investigate the importance of NSs in a mosquito cell infection, an rMP12 recombinant was rescued in which the NSs CDS was replaced with that for eGFP, yielding rMP12ΔNSs:eGFP virus. A second rMP12 recombinant was rescued which was unable to express both NSm and 78kDa. The pTVT7-GMΔNSm rescue plasmid was constructed using excision PCR to remove the M segment CDS from nucleotide position 21 to 410 (antigenome segment) leaving only the Gn and Gc CDS. The rescued virus was termed rMP12ΔNSm (Figure 5-11). C6/36, U4.4, and Ae cell lines were infected with rMP12, rMP12ΔNSs:eGFP or rMP12ΔNSm at MOI 5. BHK-21 cells were used as the mammalian cell line for comparison.

Similar to the previously described rMP12 infection, no CPE was observed in the mosquito cell monolayers during the time course. The CPE in rMP12ΔNSs:eGFP infected BHK-21 cells was similar to that observed with rMP12 infected cells, although it was markedly reduced in the rMP12ΔNSm infected cells. GFP expression in the rMP12ΔNSs:eGFP infected cells was analysed by fluorescent microscopy at each time point. In infected BHK-21 cells GFP expression was detected first at 6 h p.i., and the level increased at each time point. However, in mosquito cells no GFP expression was detected at any time point (Figure 5-12). Titres of rMP12 and rMP12ΔNSs:eGFP in U4.4 and Ae cells were similar, and no differences in growth rates or yields were apparent. A 10-fold yield reduction for rMP12ΔNSs:eGFP in C6/36 cells was observed however. BHK-21 cells infected with rMP12ΔNSs:eGFP demonstrated only minor differences in growth rates, and yields were comparable to those of rMP12 infected cells. Titres of rMP12ΔNSm were reduced 100-fold in U4.4 and Ae cells, and 1000-fold in C6/36 cells when compared to rMP12. In BHK-21 cells infected with rMP12ΔNSm there was an approximate 10-fold reduction in titre when compared to rMP12 (Figure 5-13).

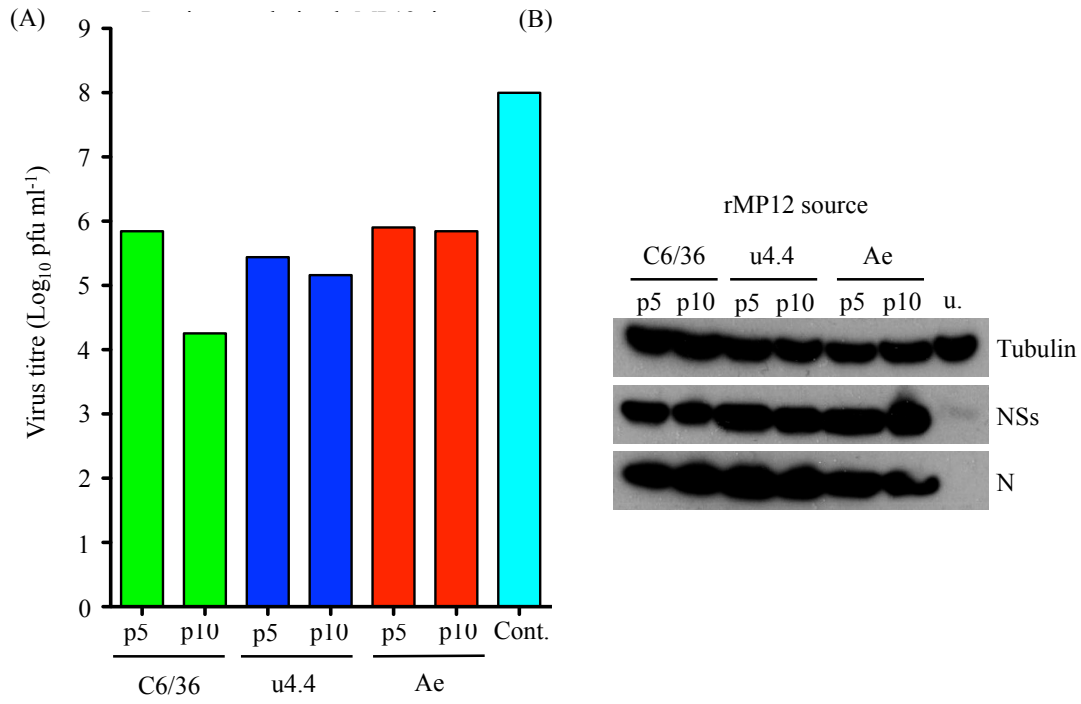

Figure 5-10: Replication of rMP12 from persistently infected mosquito cells in BHK-21 cells.
rMP12 harvested from persistently infected C6/36, U4.4, and Ae cells at passages 5 and 10 was used to infect BHK-21 cells. (A) Cell culture supernatant was taken at 48 h p.i. and titres determined by plaque assay. Also shown is the titre of elite stock rMP12 as a control (Cont.) (B) Cell monolayers were treated with PDB and protein expression determined by western blot. Antibodies targeting RVFV N and NSs were used to probe for viral proteins, and anti-tubulin antibody was used to detected the tubulin loading control for each sample. Also shown are uninfected BHK-21 cells (u.).

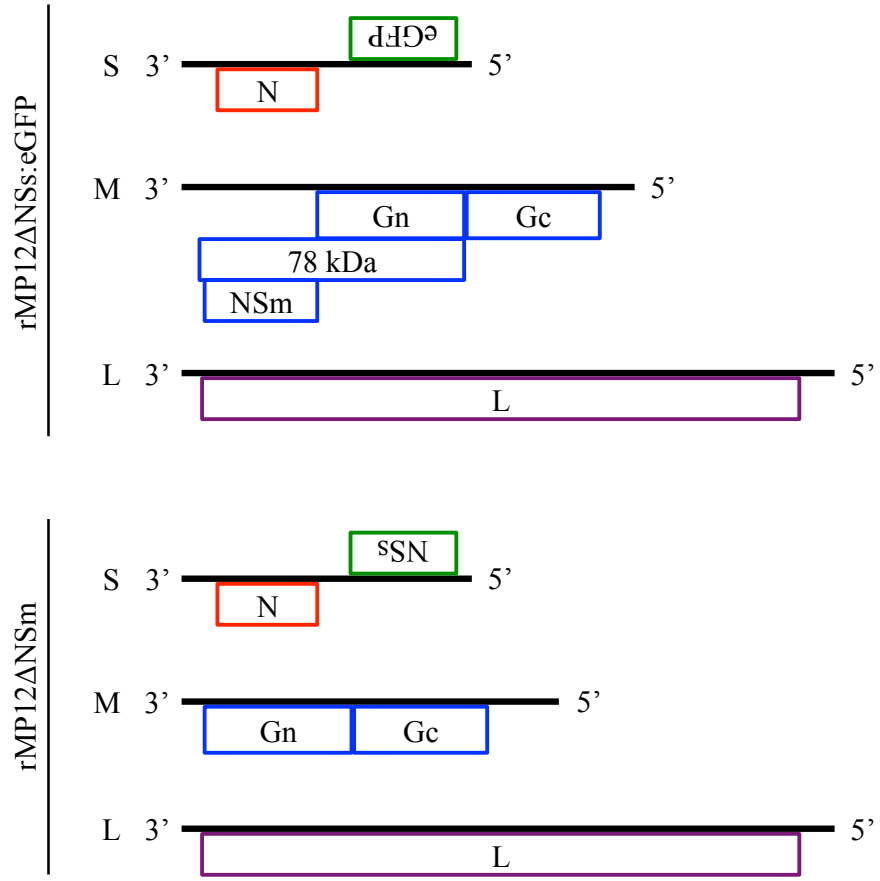

Figure 5-11: Genome organisation of rMP12 recombinant viruses
Schematic diagrams representing the genome organisation on the S, M, and L segments of rMP12ΔNSs:eGFP and rMP12ΔNSm viruses (not to scale). Boxes represent the CDS for nucleocapsid protein (N), humanised green fluorescent protein (eGFP), 78kDa protein, NSm, Gn, Gc, and L protein. Segments are represented in the genomic polarity (negative sense).

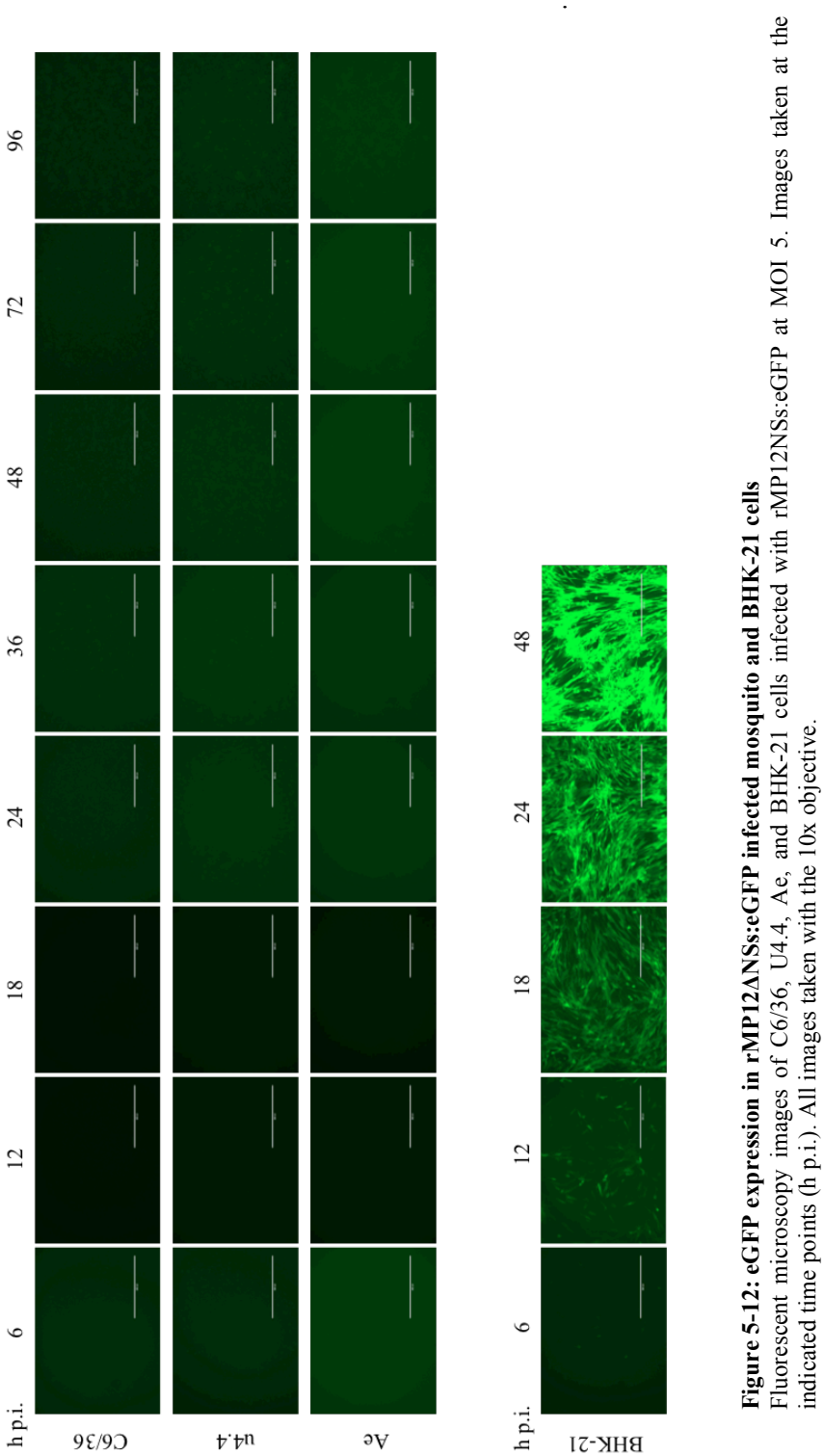

Figure 5-12: eGFP expression in rMP12ΔNSs:eGFP infected mosquito and BHK-21 cells
Fluorescent microscopy images of C6/36, U4.4, Ae, and BHK-21 cells infected with rMP12NSs:eGFP at MOI 5. Images taken at the indicated time points (h p.i.). All images taken with the 10x objective.

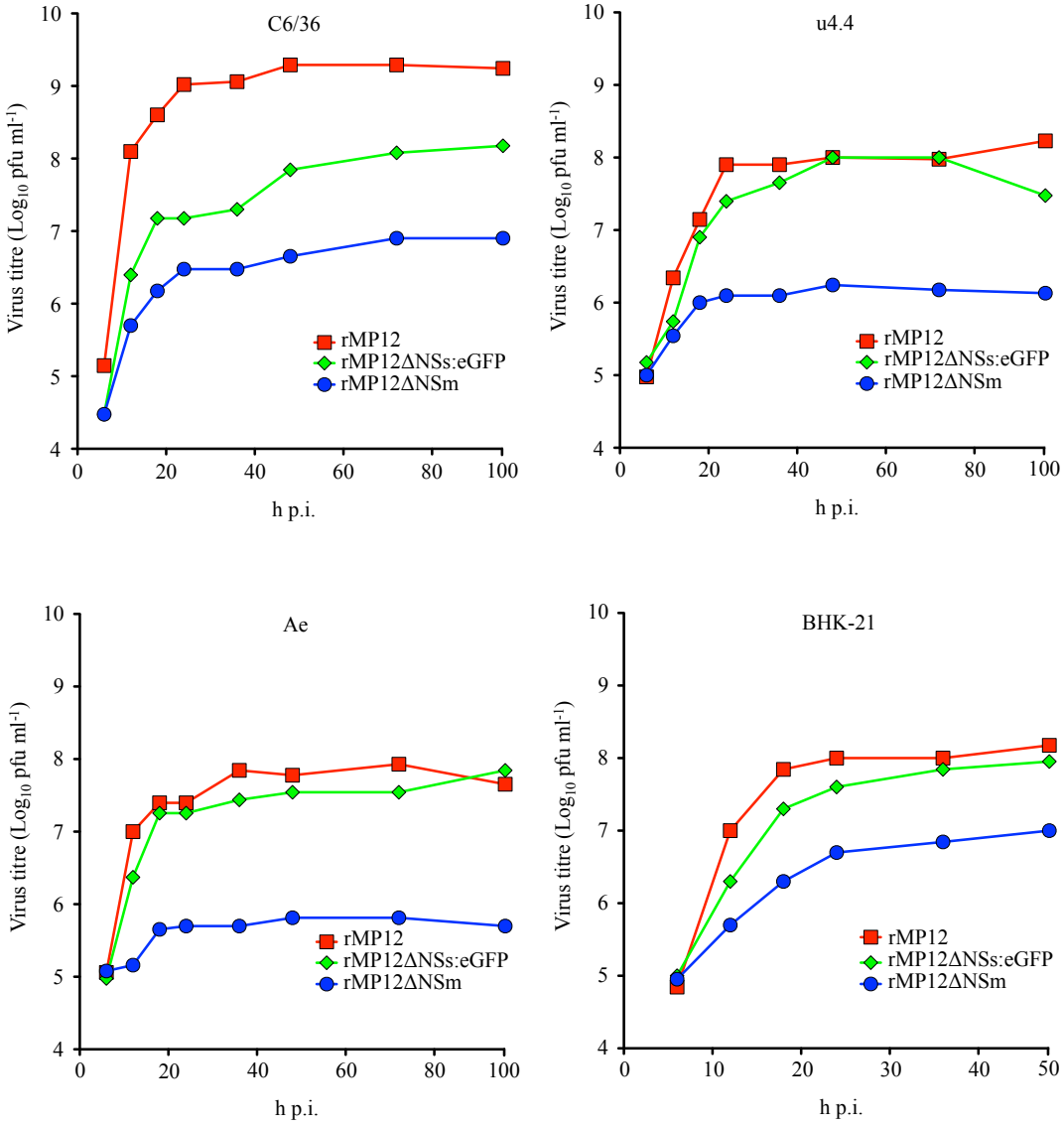

Figure 5-13: Growth curves of rMP12 and recombinant viruses
C6/36, U4.4, Ae and BHK-21 cell lines were infected with rMP12, rMP12ΔNSs:eGFP, or rMP12ΔNSm at MOI 5. Cell culture supernatant samples were taken at the indicated time points and titres obtained by plaque assay on BHK-21 cells.

N protein was detected in all rMP12 infected cell lines by 12 h p.i., with higher levels detected in C6/36 cells compared to U4.4 and Ae cells (Figure 5-14). NSs protein was detected in all rMP12 infections, although the expression profile varied between the cell lines. In C6/36 cells NSs was first detected at 12 h p.i., and remained detectable over 96 hours. In U4.4 cells NSs was also first detected at 12 h p.i. but at a lower level to that observed in C6/36 cells. By 36 h p.i. the level of NSs had reduced compared to earlier time points, and by 72 h p.i. could not be detected. In Ae cells NSs was first detected at 18 h p.i., but at a much lower level to that observed in the other mosquito cell lines. The level peaked at 24 h p.i. before decreasing to an undetectable level by 48 h p.i.. In rMP12ΔNSs:eGFP infected cells N expression level was comparable to that in rMP12 infected cells. GFP expression however was not detected at any point. N and NSs expression levels in rMP12ΔNSm infected C6/36 cells were lower that that of rMP12, and NSs was detected later in the time course. N expression was also at a lower level in U4.4 and Ae cells, and NSs expression was not observed at any time point.

5.3.6 RVFV protein detection at different MOIs

One observation taken from the previous experiments described here was that in rMP12 infected U4.4 and Ae cells NSs expression was detectable in infections at MOI 5, but not at MOI 1. To determine whether NSs expression in infected mosquito cells was linked to MOI, C6/36, U4.4, and Ae cells infected with rMP12 at MOIs of 10, 7, 3 and 0.1. Results were combined with previous experiments performed at MOIs of 5 and 1 (Figure 5-15).

For N the overall picture was one of delayed and decreased expression levels at the lower MOIs. In C6/36 cells detection was first noted at 12 h p.i. at MOIs ≥ 3, and 18 h p.i. at MOI 1 and 0.1. The pattern was similar in U4.4 and Ae cells although a more pronounced reduction in N level was observed at MOI 1 and 0.1 compared to C6/36 cells. NSs was detected in C6/36 cells at all MOIs, and the level of expression increased at the higher MOIs. In U4.4 cells NSs was detected at MOIs ≥ 3, but the level decreased as the time course progressed. This pattern was repeated in the Ae cells, but NSs expression levels were lower and degradation of the protein more pronounced.

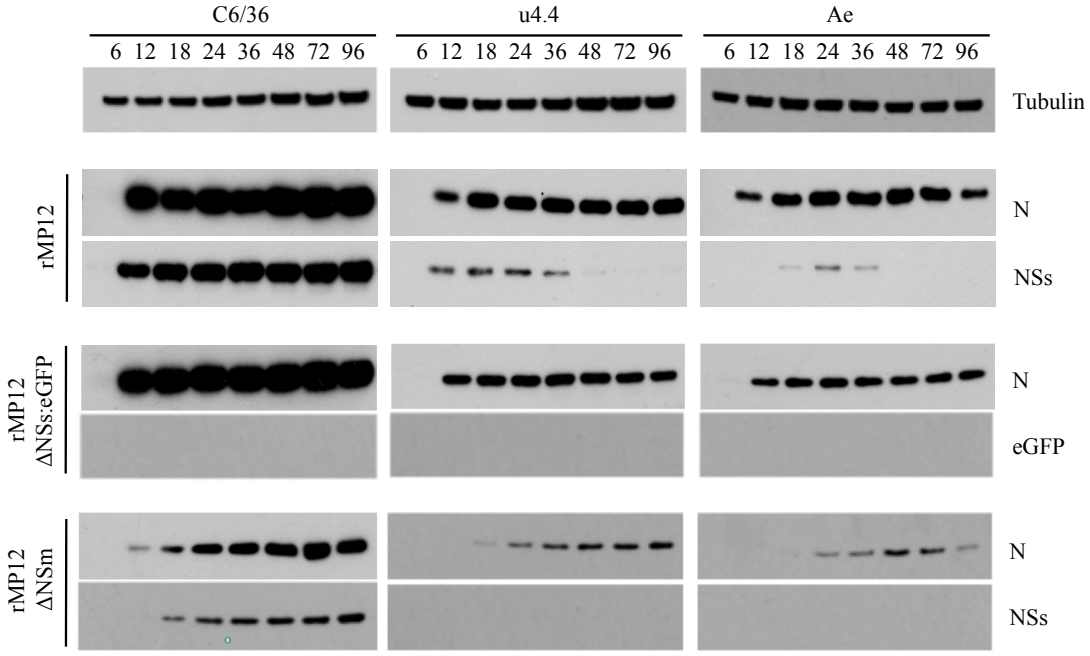

Figure 5-14: Protein production in mosquito cells infected with rMP12 recombinant viruses.
Western blot analysis of proteins expressed in C6/36, U4.4, Ae, and BHK-21 cells infected with rMP12, rMP12ΔNSs:eGFP, or rMP12ΔNSm at MOI 5. Total cell lysate samples were taken at the same time points as for the growth curve analysis. Antibodies targeting RVFV N and NSs were used to probe for viral proteins, anti-eGFP was used to detect GFP, and anti-tubulin antibody was used to detect tubulin as loading control for each sample.

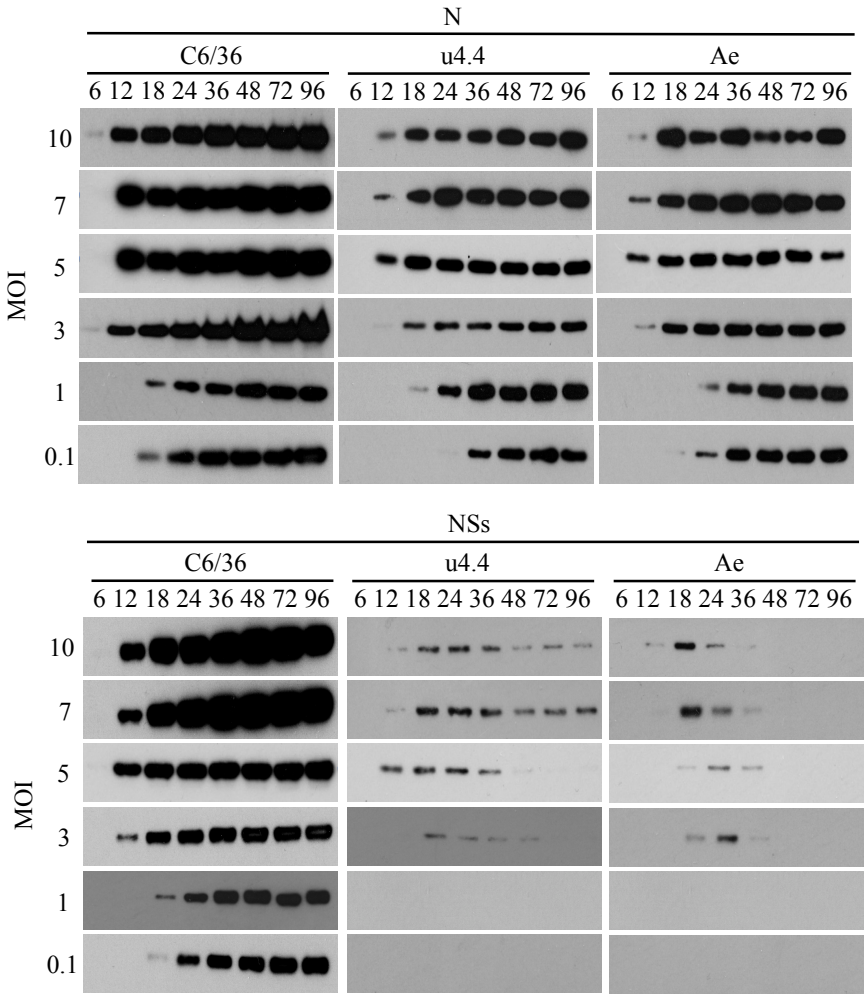

Figure 5-15: Effect of MOI on N and NSs protein expression.
C6/36, U4.4, and Ae cell lines were infected with rMP12 at MOIs of 10, 7, 3, or 0.1. Cell lysates were taken at each time point and analysed for presence of RVFV N and NSs. This figure combines results from experiments also performed at MOIs of 5 and 1. Polyclonal antibodies targeting RVFV N and NSs were used to probe for viral proteins.

Consistent with previous observations, titres were higher in the C6/36 cells compared to the U4.4 and Ae cells. Viral growth rate was slower at the lower MOIs, although final yields were independent of MOI in the infected C6/36 and U4.4 cells. Maximum yields in the Ae cells were similar to U4.4 cells except for cells infected at MOI 1 and 0.1. Here viral growth rate was markedly slower that the other mosquito cell lines, with total yields reduced 10-fold (Figure 5-16).

5.3.7 Transcriptional regulation role of NSs

NSs expression in mammalian cells results in a global inhibition of host cell protein synthesis. NSs inhibits at both a transcriptional level by disrupting TFIIH formation, and at a translational level through degradation of PKR (Le May et al. 2004; Kalveram et al. 2011; Habjan et al. 2009; Ikegami et al 2009b). Experiments were performed to investigate whether analogous reductions in host cell protein synthesis were observed in infected mosquito cells. C6/36, U4.4 and Ae cells were infected with rMP12 or rMP12ΔNSs:eGFP at MOI 3, and cells labeled with [^{35}S] methionine/cysteine for 2 hours prior to cell lysate collection. For this experiment A549 cells were used as the mammalian control cell line.

In infected mosquito cells, N was observable at 16 h p.i., although NSs was not detected at any time point. In these cells lines there was no reduction in radiolabel incorporation into host proteins compared to the mock infected cells. There was also no difference in host cell protein synthesis observed between rMP12 and rMP12ΔNSs:eGFP infected cells. By contrast, in rMP12 infected A549 cells both N and NSs protein were observed at 24 h p.i., and a marked reduction in host cell protein synthesis was observed as the infection progressed. No reduction in host cell protein synthesis was apparent in A549 cells infected with the rMP12ΔNSs:eGFP virus unable to express NSs protein (Figure 5-17).

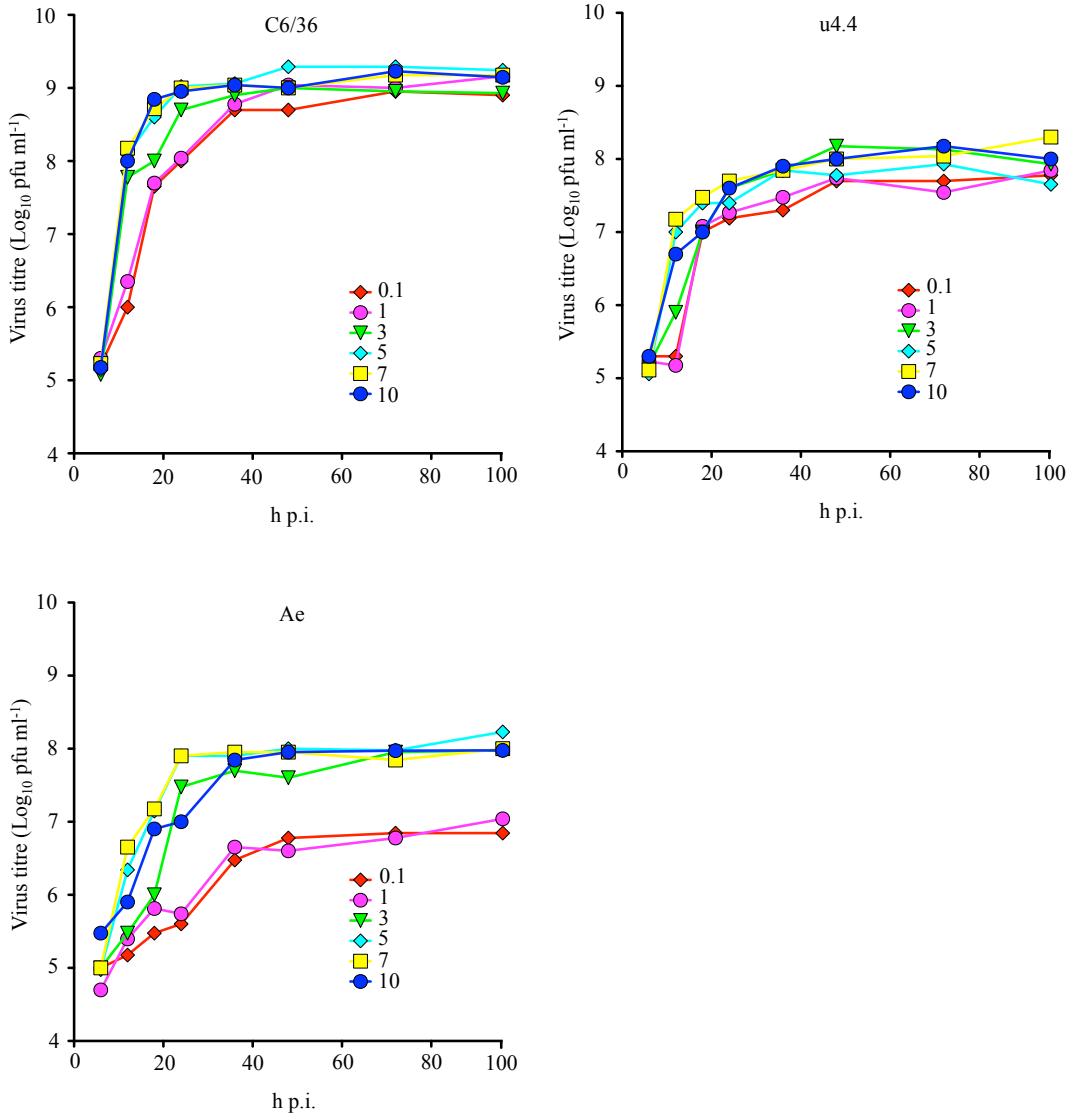

Figure 5-16: Growth of rMP12 in mosquito cells infected at different MOIs.
Growth curves of rMP12 in C6/36, U4.4, and Ae cells infected with rMP12 at MOIs of 10, 7, 3, and 0.1. Included are results from previous experiments performed at MOI 5 and 1. Titres determined by plaque assay in BHK-21 cells.

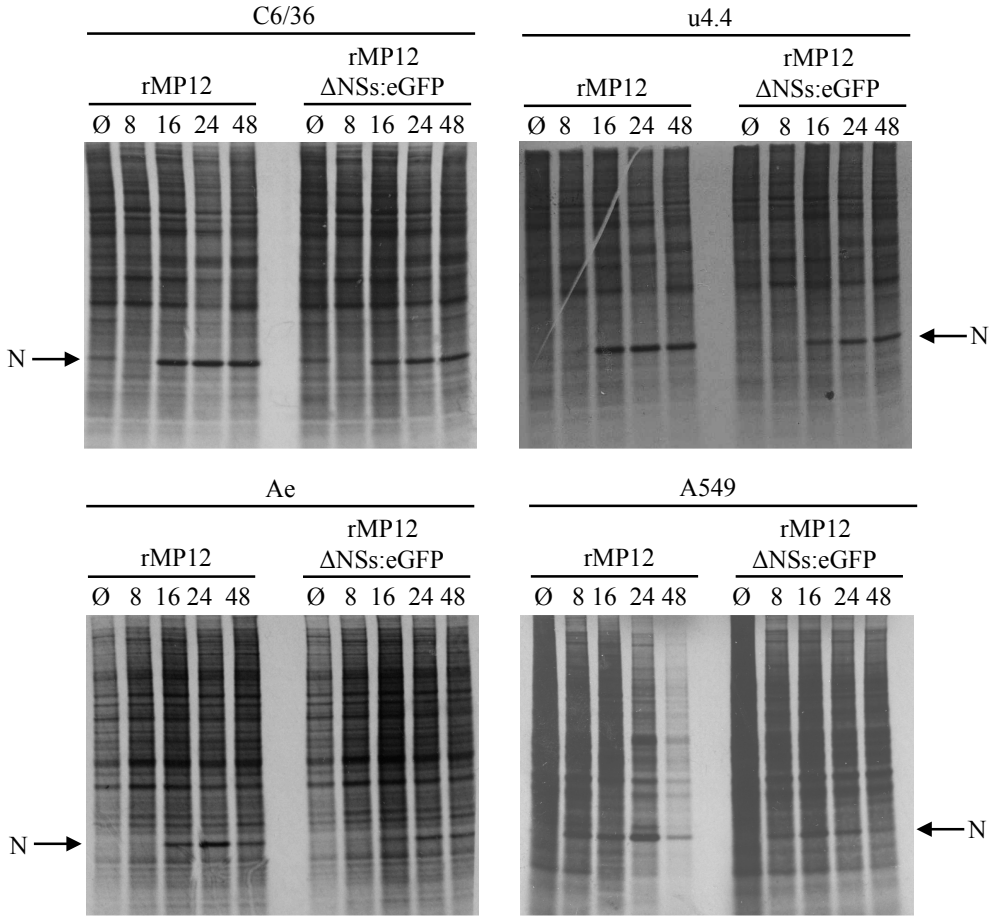

Figure 5-17: Host cell protein synthesis in cells infected with rMP12 or rMP12ΔNSs:eGFP.
C6/36, U4.4, Ae, and A549 cells were infected with rMP12 or rMP12ΔNSs:eGFP at MOI 3. Cells were labeled with 15 µCi [^{35}S] methionine/cysteine for 2 hours prior to harvesting of cells at 8, 16, 24 and 48 h p.i.. Also shown are mock infected cells harvested at 48 h p.i..

5.4 Discussion

The experiments reported above demonstrated that although rMP12 replication was supported in all the cell lines, differences were noted in replication kinetics and protein expression profiles. These disparities were observed between both the individual mosquito cell lines, and also when compared to the mammalian cell lines. Viral titres and growth rates were consistently higher in C6/36 cells compared to both U4.4 and Ae cells. The increased permissiveness of C6/36 cells over other mosquito cell lines for arbovirus replication have previously been described, for the ZH548 strain of RVFV as well as several other arboviral species such as BUNV and DENV (Léger et al. 2013; Scott et al. 2010; Szemiel et al. 2012).

NSs is the main virulence factor during vertebrate cell infection, acting both as an interferon antagonist and inhibitor of host cell transcription (Won et al. 2007; Billecocq et al. 2004; Habjan et al. 2009; Ikegami et al. 2009a; Ikegami et al. 2009b). However, analogous biological roles for NSs in mosquito cells are unknown, and research on the subject is limited. NSs is known to be important for successful infection of vertebrate species, and RVFV strains unable to express NSs are highly attenuated (Bouloy et al. 2001; Vialat et al. 2000). An example of this is the naturally occurring Clone 13 strain which has a large deletion in the NSs gene, with its attenuation advocating its potential as a possible vaccine candidate (Muller et al. 1995; Dungu et al. 2010). However, NSs is dispensable for replication in cell culture, providing the cell line is IFN deficient. The results described here have demonstrated that NSs was also non-essential for rMP12 replication in mosquito cells. Recombinants unable to express NSs suffered no significant impact on growth kinetics or maximum yields. The only difference was a 10-fold reduction in the rMP12ΔNSs:eGFP yield from C6/36 cells, which brought them to the level observed in infected U4.4 cells. This was contrasted by the significant impact on viral growth and titres observed in cells infected with the rMP12 recombinant unable to express both NSm and 78kDa proteins. It has been suggested that these proteins are important for viral dissemination in mosquito cells (Kading et al. 2014). My results support this, with slower growth and a 100-fold reduction in yields observed in all rMP12ΔNSm infected mosquito cell lines. This attenuation was less pronounced in mammalian cells with only a 10-fold reduction in titres observed, suggesting that NSm and 78 kDa protein were less vital for a successful infection of mammalian cells. Furthermore, there was no demonstrable effect on host cell protein synthesis levels caused by NSs expression in mosquito cells. Taken

together these data suggest that the effects of NSs expression in mammalian cells are not manifest in mosquito cells. Whether this is due to fundamental biological differences between the two cell types, or a consequence of the much reduced NSs expression level requires further experimental validation.

Disparities in the NSs expression level between invertebrate and mammalian cell lines during RVFV infection have previously been described by Vaughn *et al* (2010), and were confirmed here for rMP12 by my results. The variations observed in rMP12 NSs expression level between the mosquito cell lines were similar to the results described for ZH548 infection (Léger et al. 2013). In C6/36 cells infected with ZH548 at MOI 5 NSs remained detectable throughout the time course, whereas in U4.4 and Aag-2 cells NSs expression was apparent only at early time points before becoming undetectable. A similar pattern for rMP12 NSs expression was described here, although my results have demonstrated that this expression was correlated to MOI. Whilst NSs remained detectable in infections at all MOIs in C6/36 cells, evidence of delayed expression and degradation of the protein was apparent in the infected U4.4 and Ae cells. Western blot analysis examines the accumulation of protein over time, meaning loss of detection represents degradation of that protein. Published results have described the role the RNAi responses play in reducing NSs expression in ZH548 infected mosquito cells (Léger et al. 2013). The Dcr-2 mediated siRNA response is active in U4.4 and Ae cells but defective in C6/36 cells. While differences in the siRNA response could explain lack of NSs expression in U4.4 and Ae cells, it does not address the degradation of NSs in these cells. However, previous results from the laboratory have described the involvement of the ubiquitin-proteasome system (UPS) in the removal of BUNV NSs from infected C6/36 cells (van Knippenberg et al. 2013). It is possible that interplay between the siRNA response and UPS are responsible for both the reduced expression level and degradation of NSs observed here in infected U4.4 and Ae cells. Infections at a higher MOI were accompanied by an increased growth rate, and this may have overwhelmed the RNAi and UPS pathways to a point where NSs expression became detectable by western blot. However, as infection progressed the siRNA response silenced any further NSs expression with remaining intracellular protein degraded via the UPS.

Differences in the NSs expression level were also observed during analysis of the persistently infected mosquito cells. Interestingly NSs expression in C6/36 cells was only

apparent during early passages, with expression level reducing with each passage until it became undetectable at p3. As an arbovirus, RVFV naturally has to alternate between a vertebrate host and mosquito vector. Published results demonstrated for RVFV that this alternation between host species was necessary to maintain genetic stability of the virus, with forced passage in one cell type resulting in an accumulation of deleterious mutations within the NSs gene (Moutailler et al. 2011). However, the NSs CDS in viruses taken at p5 and p10 showed no evidence of mutations compared to the parental rMP12, and NSs expression was detected in BHK-21 cells infected with these viruses. The experiment performed by Moutailler *et al* (2011) was carried out with ZH548 over 30 passages, with mutations first appearing at p10. It is therefore possible that the experiment performed here did not continue for long enough for any mutations to arise. An interesting observation was the reduction in titre observed in BHK-21 cells when infected with virus produced by persistently infected mosquito cells. Results for DENV demonstrated that continued passage in C6/36 cells resulted in a fitness gain in that cell type, and an associated loss of fitness in Huh-7 cells (Vasilakis et al. 2009). Although no mutations were observed in the N and NSs genes, it is possible that mutations elsewhere in the genome may have affected the ability of the virus to replicate in BHK-21 cells.

The observation that rMP12 NSs did not form nuclear filament structures in mosquito cells was unexpected given that they were apparent in ZH548 infected cells (Léger et al. 2013). The NSs bodies associated with rMP12 demonstrated no apparent organised structure, with variations in size, length and number in individual cells observed. C6/36 cells infected with the rMP12 recombinant expressing ZH548 NSs did however exhibit the filamentous NSs phenotype, although not as pronounced as that observed in mammalian cells, or in ZH548 infected C6/36 cells. It is unclear why the one amino acid difference between rMP12 and ZH548 NSs proteins results in this difference in NSs phenotype. Yadani *et al.* (1999) demonstrate that NSs filaments are composed of NSs dimers, and that if expressed alone will spontaneously form nuclear filaments in mammalian cells. It has also been reported that, although the majority of nuclear DNA is excluded from filaments, NSs will selectively bind cellular factors such as SAP30 allowing further interaction with specific host cell DNA regions such as pericentromeric γ-satellite or IFN-β promoter sequences (Le May et al. 2008). There is no difference in filament formation between mammalian cells infected with either ZH548 or rMP12. This therefore suggests that the host cell factors interacting with NSs proteins are different in mosquito cells compared to mammalian cells.

The localisation of N within rMP12 infected mosquito cells was similar to that described for infected mammalian cells. N was localised to the cytoplasm where it exhibited the same punctate staining pattern observed in infected Vero-E6 cells (Brennan et al. 2011). It was also shown that N and L co-localise in the cytoplasm of infected cells. It is likely that these areas of co-localisation represent viral factories, complexes of Golgi stacks, mitochondria, and rough ER components constructed around Golgi bodies in the cytoplasm (Novoa et al. 2005b; Novoa et al. 2005a; Salanueva et al. 2003). Similarities between viral assembly structures in mammalian and arthropod species remain to be determined, although the co-localisation results presented here suggest as least some commonality between the two.

In conclusion, the results described here demonstrated the numerous differences apparent in rMP12 replication between mosquito cells and mammalian cells. Of particular note where variations in NSs expression level observed between cell lines. Although shown to be dispensable in cell culture NSs was expressed in all mosquito cell lines although at levels that varied significantly between the mosquito cell lines. Expression was shown to be correlated to MOI, and also to the growth rate of virus during replication. One consideration not examined in this work was the possibility that the effective MOI differed between mammalian and mosquito cell lines, and that an MOI calculated using infected BHK-21 cells would not correlate to the same MOI in mosquito cells. It must be noted that in immunofluorescence experiments at MOIs of greater than 5 all cells species infected with rMP12 displayed evidence of N expression indicating infection. However, investigations into the variances in infectivity level at MOIs lower than this between the cell species requires further validation. Further investigations into the roles that the RNAi response and segment-specific promoters play in these observations are examined in later chapters. The reported severe attenuation in viral replication for RVFV recombinants lacking both NSm and 78 kDa proteins was repeated here for rMP12 in mosquito cells. Finally, immunofluorescence studies demonstrated that NSs filaments were not present in rMP12 infected mosquito cells, although replacement of the NSs CDS with that for the ZH548 NSs did result in their formation. It is unknown why the one amino acid difference between the protein would result in such a variation in phenotype, but it suggests the mutation site is maybe important in binding particular mosquito cell factors.

5.5 Summary

- rMP12 replicated to high titres in all mosquito cells analysed. Unlike with BHK-21 cells, infection of the mosquito cells was non-cytolytic and persistence could be maintained for at least 10 passages.

- NSs expression profiles varied between the mosquito cells lines. NSs was always expressed in rMP12 infected C6/36 cells, but only in U4.4 and Ae cells when infected at high MOIs. Western blot data further suggested evidence of NSs degradation in U4.4 and Ae cells.

- NSs was dispensable for rMP12 replication in mosquito cells lines, although an rMP12 recombinant lacking both NSm and 78 kDa protein was severely attenuated.

- rMP12 NSs did not form intranuclear filament structures in infected mosquito cells, contrasting to those observed in the infected BHK-21 cells. However, an rMP12 recombinant expressing the ZH548 NSs protein did form filament-like structures in the nuclei of infected C6/36 cells.

- rMP12 N and L proteins co-localise in the cytoplasm of rMP12 infected mosquito cells, suggesting the presence of viral assembly structures similar to those observed in mammalian cells.

6. Consequences of reconfiguring the coding strategy of MP12 S segment

6.1 Introduction

Phleboviruses, along with tospoviruses and arenaviruses, are unique among NSVs in their utilisation of ambisense coding strategies. For RVFV, this method is employed to express the S segment-encoded proteins N and NSs. One explanation for this strategy was that it allowed for temporal control over protein production, with NSs expression occurring later during the replication cycle than N (Bishop 1986b; Bishop 1989; Bishop 1986a; Nguyen & Haenni 2003; Ihara et al. 1984; Simons et al. 1990; Giorgi et al. 1991). However, given our current knowledge of the role NSs plays as the main virulence factor during infection, it seems incongruous that delayed expression would be beneficial to the virus lifecycle. To better understand the S segment coding strategy a recombinant was rescued using reverse genetics in which the N and NSs CDSs were swapped, leaving the terminal UTR and IGR sequences unaltered (Figure 6-1). This virus was termed rMP12:S-Swap virus. A further recombinant was generated in which the rMP12:S-Swap NSs CDS was replaced with that for eGFP (termed rMP12:S-SwapΔNSs:eGFP) Together with rMP12 and rMP12ΔNSs:eGFP, these viruses were used to investigate the consequences of this altered coding strategy on viral replication in mosquito cells.

As well as examining viral protein expression, these viruses were also used to investigate potential differences in virion genome packaging. Progeny virions must contain a copy of each genome segment to be viable, and therefore packaging mechanisms must be robust and reliable. In addition, the packaged segments must be of the correct polarity. However research into phlebovirus packaging has revealed that RVFV and UUKV progeny virions do not always contain three negative sense genome segments (Simons et al. 1990; Ikegami et al. 2005). Rather, both polarities of genome can be packaged into progeny virions. The genomic to antigenomic polarity ratio for genome strands in RVFV virions was shown to range from 5:1 to 100:1 depending on the cell line used to propagate the virus. Furthermore, it was shown that antigenome S segment packaged into virions can be employed directly to transcribe NSs mRNA upon infection (Ikegami et al. 2005).

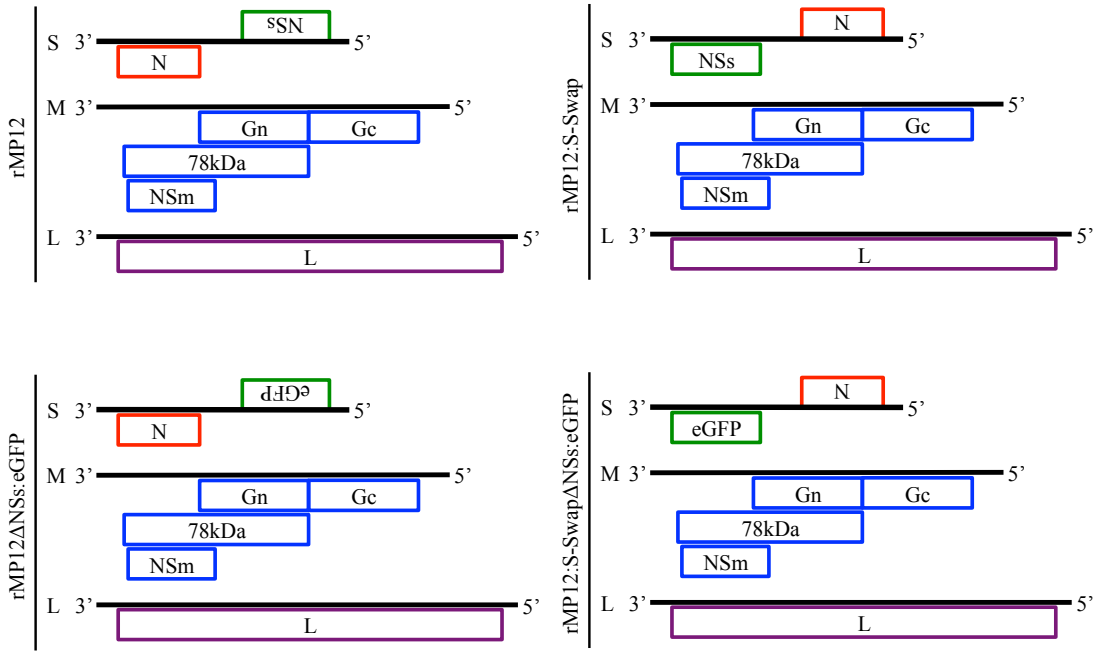

Figure 6-1: Schematic representation of MP12 and recombinant viruses
Represented are the individual coding sequences encoded by rMP12, rMP12:S-Swap, rMP12ΔNSs:eGFP, and rMP12:S-SwapΔNSs:eGFP virus. Shown are genomic polarity S, M and L genome segments, with CDSs below the segment negative sense (non coding) and above the segment positive sense (coding). The coding sequences represented are nucleocapsid (N), non-structural proteins (NSs, NSm, 78kDa), the glycoproteins (Gn, Gc), and the RNA-dependent RNA-polymerase (L).

Previously our laboratory investigated the different RNA species in RVFV virions and infected cells by using DIG-labeled RNA probes in northern blot analysis. This demonstrated differences between the ratios of genomic to antigenomic polarity RNA species present in rMP12 or rMP12:S-Swap infected cells. The experimental hypothesis was that the different coding strategy in rMP12:S-Swap subsequently caused an altered packaging phenotype compared to rMP12. Specifically, the S segment genome and antigenome ratios in progeny virions were different between the two viruses. However, these differences were difficult to quantify due to variations in binding efficiencies between the RNA probes used in the northern blots. An qRT-PCR assay was therefore designed which would allow accurate quantification of genome to antigenome ratios present in rMP12 or rMP12:S-Swap virus infected cells.

6.2 Aims

The aims of this section of the thesis were to investigate the different characteristics of rMP12:S-Swap virus infection in mosquito cells, and to compare and contrast them to rMP12 infected cells. This involved comparative analysis of the growth kinetics and protein expression profiles in BHK-21 and mosquito cells lines.

Investigations into the genome packaging variations between the two viruses involved the design and validation of a strand specific real-time qRT-PCR assay This would be used to accurately determine genomic to antigenomic polarity ratios of genome segments present in infected mammalian and mosquito cell lines, as well as in the progeny virions produced.

6.3 Results

6.3.1 Characterisation of rMP12:S-Swap growth in mosquito cells.

The ideal method of virus characterisation involves one-step growth curve analysis at MOI 7 or higher to ensure all cells are infected simultaneously (Flint et al. 2008). However, this was not possible for rMP12:S-Swap or rMP12:S-SwapΔNSs:eGFP as maximum titres of these viruses were on average 100- to 1,000-fold lower than those of the parental rMP12. Infection was therefore performed at MOI 1, the maximum achievable for all viruses in

both the mammalian and mosquito cell lines. Samples were taken at various time points to determine viral titre and analyse protein expression.

Both rMP12:S-Swap and rMP12:S-SwapΔNSs:eGFP virus replicated in all the mosquito cell lines, as well as in the control BHK-21 cells (Figure 6-2). rMP12 and rMP12ΔNSs:eGFP titres were consistently higher in all cell lines compared to those of rMP12:S-Swap and rMP12:S-SwapΔNSs:eGFP. In BHK-21 cells virus yields for rMP12 and rMP12ΔNSs:eGFP were similar at approximately $4x10^8$ pfu/ml, as were yields for rMP12:S-Swap and rMP12:S-SwapΔNSs:eGFP at approximately $3x10^6$ pfu/ml. As well as the lower titres, viral growth was also markedly slower in the rMP12:S-Swap and rMP12:S-SwapΔNSs:eGFP infected cells. Infection with the rMP12:S-Swap recombinants was markedly less cytopathic than that observed for rMP12 infection, with the cell monolayer largely intact at 48 h p.i.. In infected mosquito cells maximum titres of rMP12 and rMP12ΔNSs:eGFP were reached by 48-72 h p.i., although growth in Ae cells was slower than that observed in C6/36 and U4.4 cells (Figure 6-2). This corroborates the data obtained in Chapter 5. An approximate 5-fold reduction between rMP12 and rMP12ΔNSs:eGFP yields was apparent in C6/36 cells, although titres for both were higher than those in U4.4 and Ae cells. rMP12:S-Swap and rMP12:S-SwapΔNSs:eGFP growth was similar between mosquito cell lines, but markedly slower compared to the rMP12 and rMP12ΔNSs:eGFP viruses. In C6/36 and U4.4 cells there was a 10-fold increase in titre by 96 h p.i., but in Ae cell only a minimal increase in titre was observed over the time course.

Similar to previous results, mosquito cells infected with rMP12ΔNSs:eGFP did not express GFP. This was in direct contrast to the infected BHK-21 cells in which GFP fluorescence was first detectable by 18 h p.i. with levels increasing as the time course progressed (Figure 6-3). However, in mosquito cells infected with rMP12:S-SwapΔNSs:eGFP extensive GFP expression was apparent. Levels were highest in both the *A. albopictus* cell lines, detected first by 24 h p.i. and increasing through the time course. Expression level was reduced by comparison in the Ae cells, although the level similarly increased as the time course progressed. The level of GFP expression in rMP12:S-SwapΔNSs:eGFP infected BHK-21 cell was significantly higher that that observed for the rMP12ΔNSs:eGFP infection.

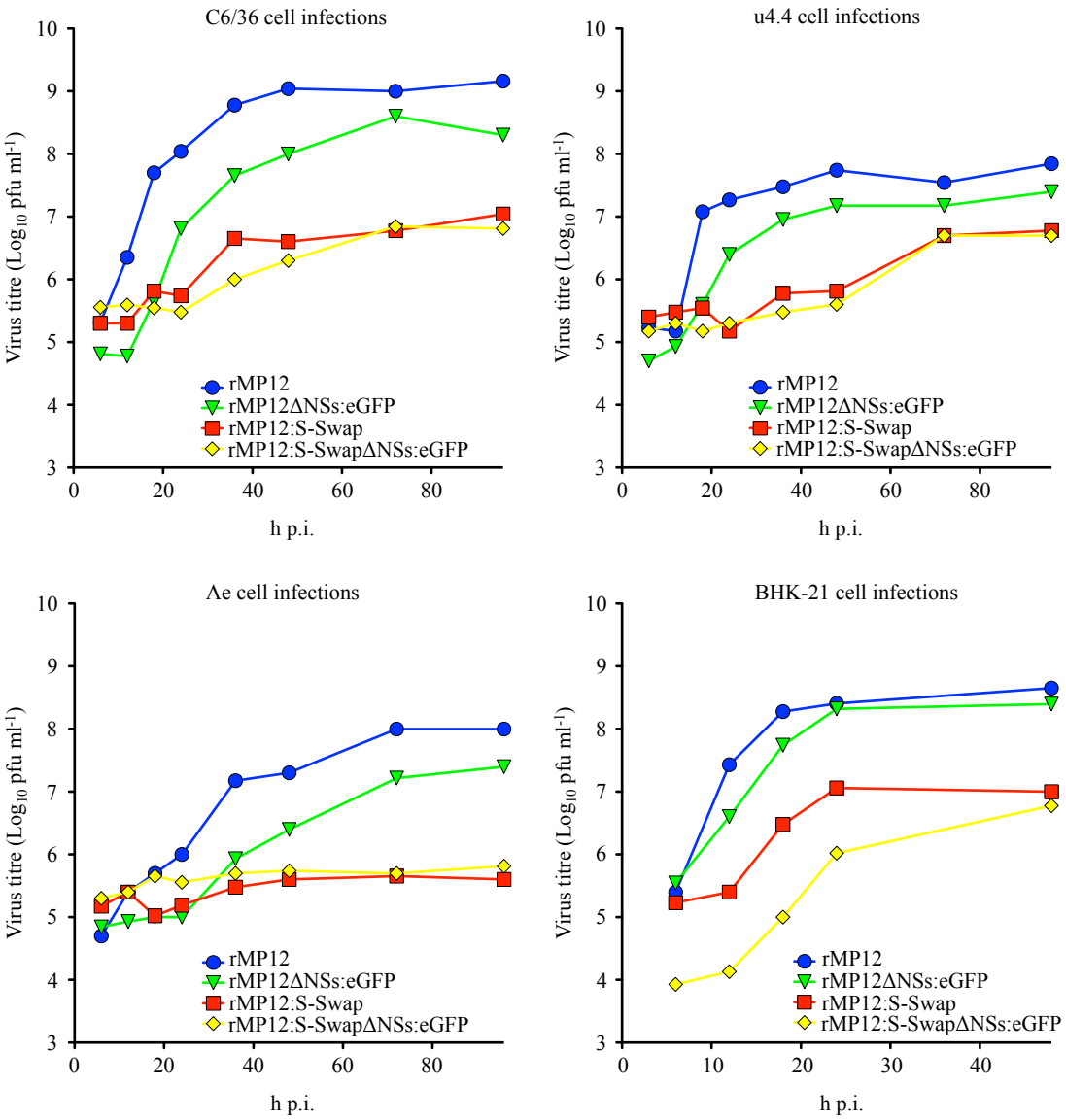

Figure 6-2: Growth curves of rMP12 and recombinant viruses in BHK-21 and mosquito cell lines
C6/36, U4.4, Ae, and BHK-21 cells were infected with rMP12, rMP12NSs:eGFP, rMP12:S-Swap or rMP12:S-SwapNSs:eGFP at MOI 1. Cell culture supernatant samples were taken at the indicated time points and titres obtained by plaque assay on BHK-21 cells

Figure 6-3: GFP expression in rMP12NSs:eGFP and rMP12:S-SwapNSs:eGFP infected cells
C6/36, U4.4, Ae, and BHK-21 cells were infected with rMP12NSs:eGFP or rMP12:S-SwapNSs:eGFP at MOI 1. At the indicated time points cell monolayers were observed for GFP fluorescence. All images taken at 10x magnification.

Protein analysis demonstrated the temporal variation in N and NSs expression in rMP12 infected cells. In rMP12 infected BHK-21 cells N was detectable by 12 h p.i., with NSs only faintly detectable at this time. The intensity of both bands increased throughout the time course. The opposite was true in rMP12:S-Swap infected cells where NSs was detected by 12 h p.i., but the band for N barely detectable. The level of NSs increased throughout the time course, but the level of N remained barely detectable at all the time points (Figure 6-4). At all points past 12 h p.i. a higher level of N was observed in rMP12 infected cells compared to those infected with rMP12:S-Swap, and visa versa for NSs protein. This differential protein expression profile was also apparent in the rMP12ΔNSs:eGFP and rMP12:S-SwapΔNSs:eGFP infected cells, although differences in the GFP expression levels were less pronounced that those observed for the analogous NSs levels.

The expression profiles of N, NSs and GFP in rMP12 or rMP12ΔNSs:eGFP infected mosquito cells were comparable to those previously described, with NSs expression detectable only in rMP12 infected C6/36 cells and no GFP expression observed in any rMP12ΔNSs:eGFP cell line (Figure 6-5). In rMP12:S-Swap infected cells the expression profiles of N and NSs were similar to those observed for BHK-21 cells. In infected C6/36 cells NSs expression was earlier and at a higher level compared to rMP12, with a lower level of N expression apparent. Unlike infection with rMP12 NSs expression was detected in rMP12:S-Swap infected U4.4 and Ae cells, although at lower levels than that of C6/36 cells. No N expression was detected in rMP12:S-Swap infected Ae cells, indicating minimal levels of viral replication. This confirms the results described in Figure 6-2 showing minimal viral growth in rMP12:S-Swap infected Ae cells. In rMP12:S-SwapΔNSs:eGFP infections GFP was detected in all mosquito cells, correlating to the levels of GFP fluorescence in the infected cells observed in Figure 6-3.

6.3.2 Northern blot analysis of RNA species in infected mosquito cells

To determine what mRNA species were present in the infected mosquito cells, northern blot analysis was performed using strand specific DIG-labeled RNA probes specific for sequences contained in the N, NSs, or eGFP CDSs. Probe polarity was such that the following mRNA species were detected: N(+) probe detected N mRNA of rMP12 and

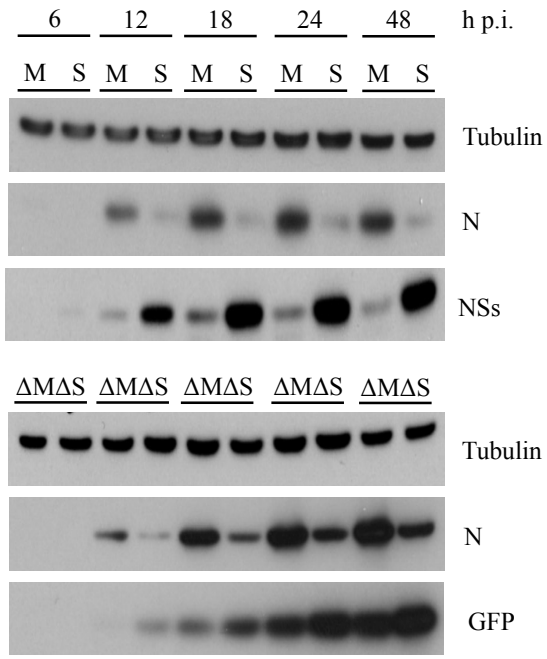

Figure 6-4: Protein production in rMP12 and recombinant virus infected BHK-21 cells
BHK-21 cells were infected with (M) rMP12, (S) rMP12:S-Swap, (ΔM) rMP12ΔNSs:eGFP, or (ΔS) rMP12:S-SwapΔNSs:eGFP at MOI 1. At the indicated time points (h p.i.) cell monolayer lysates were taken and analysed for viral protein production. Antibodies targeting RVFV N and NSs, and eGFP were used to probe for virally expressed proteins, and anti-tubulin antibody was used to detected the tubulin loading control for each sample

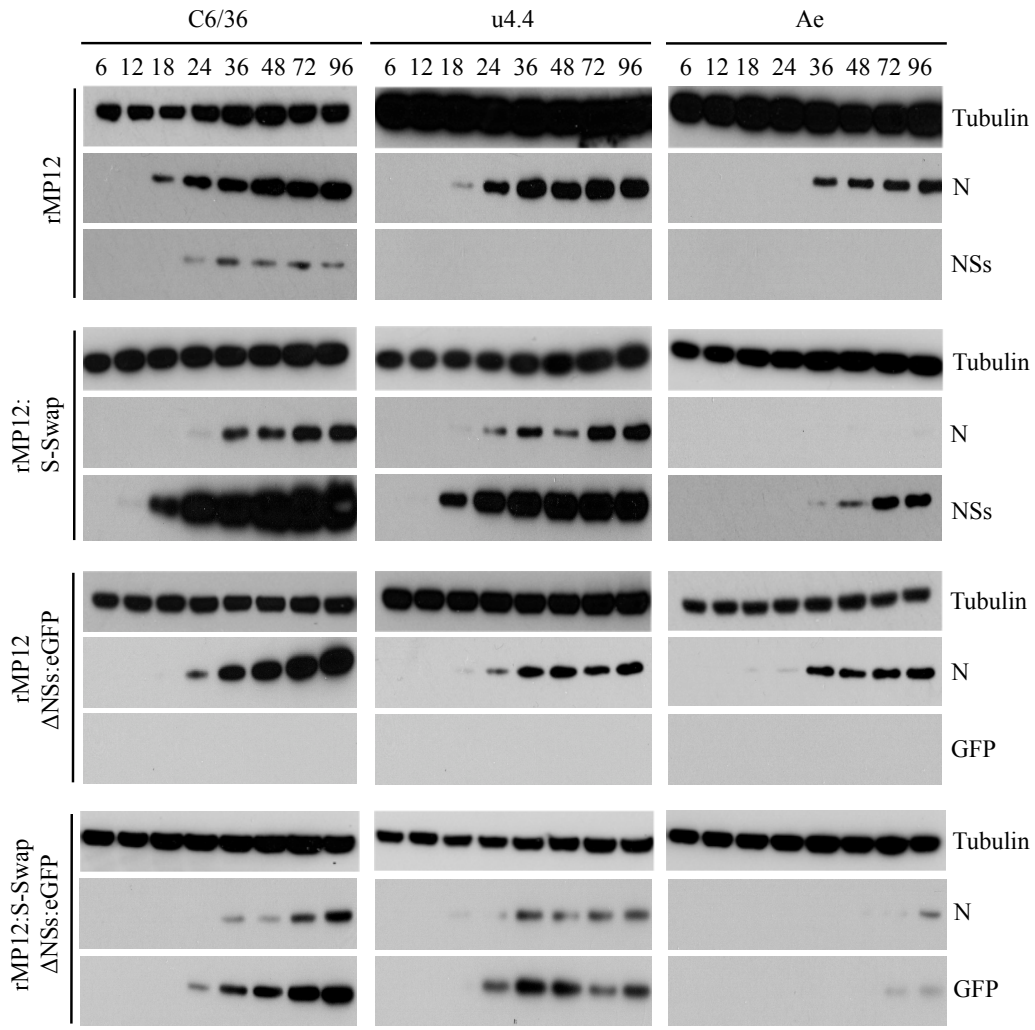

Figure 6-5: Protein production in rMP12 recombinant virus infected mosquito cell lines
C6/36, U4.4, and Ae cells were infected with rMP12, rMP12:S-Swap, rMP12ΔNSs:eGFP, or rMP12:S-SwapΔNSs:eGFP at MOI 1. At the indicated time points cell lysates were taken and analysed for viral protein production. Antibodies targeting RVFV N and NSs, and eGFP were used to probe for virally expressed proteins, and anti-tubulin antibody was used to detected the tubulin loading control for each sample.

rMP12ΔNSs:eGFP virus; N(-) probe detected N mRNA of rMP12:S-Swap and rMP12:S-SwapΔNSs:eGFP virus; NSs(-) probe detected NSs mRNA of rMP12 virus; NSs(+) probe detected NSs mRNA of rMP12:S-Swap virus; GFP(-) probe detected eGFP mRNA of rMP12ΔNSs:eGFP virus; and GFP(+) probe detected eGFP mRNA of rMP12:S-SwapΔNSs:eGFP virus. C6/36, U4.4, and Ae cells were infected with rMP12, rMP12:S-Swap, rMP12ΔNSs:eGFP, or rMP12:S-SwapΔNSs:eGFP virus at MOI 1 and at 24 hour time points total cellular RNA was extracted for northern blot analysis.

The results showed that the presence or absence of protein determined in Figure 6-5 directly correlated with presence or absence of its associated mRNA (Figure 6-6). In rMP12 infected C6/36 cells NSs mRNA was detectable, whereas in U4.4 and Ae cells levels were significantly reduced. No GFP mRNA was detectable in rMP12ΔNSs:eGFP infected mosquito cells. Differences in the expression levels of N and NSs in rMP12:S-Swap infected mosquito cells determined by western blot analysis were mirrored here by the northern blot results. A reduced level of N mRNA and a markedly increased level of NSs mRNA was detectable in all mosquito cells. GFP mRNA was detectable in rMP12:S-SwapΔNSs:eGFP infected C6/36 and U4.4 cells, but not in infected Ae cells although GFP expression was detected via microscopy. However, the GFP fluorescence was reduced compared to that observed for both C6/36 and U4.4 cells, suggesting this anomaly was likely due to differences in the relative sensitivities of these two detection methods. These results suggest that the variations in protein expression levels observed between mosquito cells were due to differences at a transcriptional level, rather than any defect in translation.

6.3.3 Immunofluorescence analysis of N and NSs protein in rMP12:S-Swap infected mosquito cells

As western blot data demonstrated a higher level of NSs expression in rMP12:S-Swap infected mosquito cells compared to rMP12, experiments were performed to investigate any potential variations in intracellular location and structural phenotypes of the protein. C6/36, U4.4 , and Ae cells were infected with rMP12:S-Swap virus at MOI 1. At 48 h p.i. cell monolayers were fixed and stained with anti-N, anti-NSs, and anti-tubulin antibodies. As with the previous experiments, because co-staining for N and NSs could not be performed on the same sample they were performed on duplicate cell monolayers.

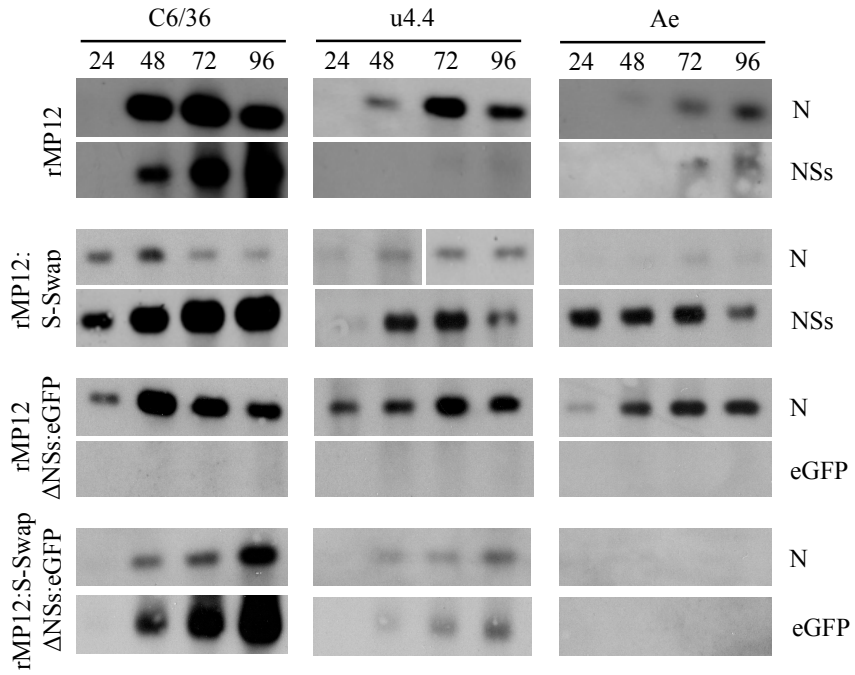

Figure 6-6: Analysis of viral RNA species in RVFV recombinant virus infected mosquito cell lines
C6/36, U4.4 and Ae cells were infected with rMP12, rMP12:S-Swap, rMP12ΔNSs:eGFP, or rMP12:S-SwapΔNSs:eGFP at MOI 1. At 24, 48, 72, and 96 h p.i. cell were lysed and total RNA extracted for northern blot analysis of S segment derived mRNA species: N and NSs mRNA from rMP12 and rMP12:S-Swap; and N and eGFP mRNA from rMP12ΔNSs:eGFP and rMP12:S-SwapΔNSs:eGFP.

As with rMP12, in rMP12:S-Swap infected cells N was confined to the cytoplasm (Figure 6-7). N expression levels were reduced when compared to the rMP12 infected cells, something most apparent in the Ae cells where only approximately 30% of cells demonstrated expression. As expected, NSs was more abundant in the rMP12:S-Swap infected cells compared to that seen for rMP12, although it remained exclusively intranuclear and no filamentous structures were detected (Figure 6-8). Examination was performed on individual cells to better determine the various morphologies NSs exhibited within infected mosquito cell nuclei (C6/36 in Figure 6-9, U4.4 in Figure 6-10, and Ae in Figure 6-11). This demonstrated that although NSs expression levels were higher in the rMP12:S-Swap infected cells, it did not result in any drastic alteration to the NSs phenotype. The same amorphous protein bodies were observed in all cell lines, although these were increased in size over those observed in the rMP12 infected cells presumably due to the higher expression level of protein.

6.3.4 rMP12:S-Swap persistence in mosquito cells

Mosquito cells were previously shown to support persistent infection with rMP12. To investigate whether the differences in growth characteristics and protein expression in rMP12:S-Swap infected cells altered the establishment of persistence, similar experiments were performed. C6/36, U4.4 and Ae cells were infected with r;MP12:S-Swap at MOI 0.01. When the cells reached 80-100% confluency they were split 1:5, with cell culture supernatant and cell lysates collected at each passage to determine viral titres and protein production.

Persistence of rMP12:S-Swap in infected mosquito cells was different to that observed for rMP12. In C6/36 cells a dramatic over-expression of NSs was observed as passage number increased, and N expression level was reduced at all passage numbers compared with C6/36 cells persistently infected with rMP12. Furthermore, as passage number increased cell viability noticeably decreased, and at p3 the majority of cells were detached from the substrate (Figure 6-12). Attempts to maintain cells beyond this passage were unsuccessful. A similar pattern of NSs over-expression and reduced cell viability was observed in the U4.4 cells (Figure 6-13). Although a majority of cells were similarly dead at

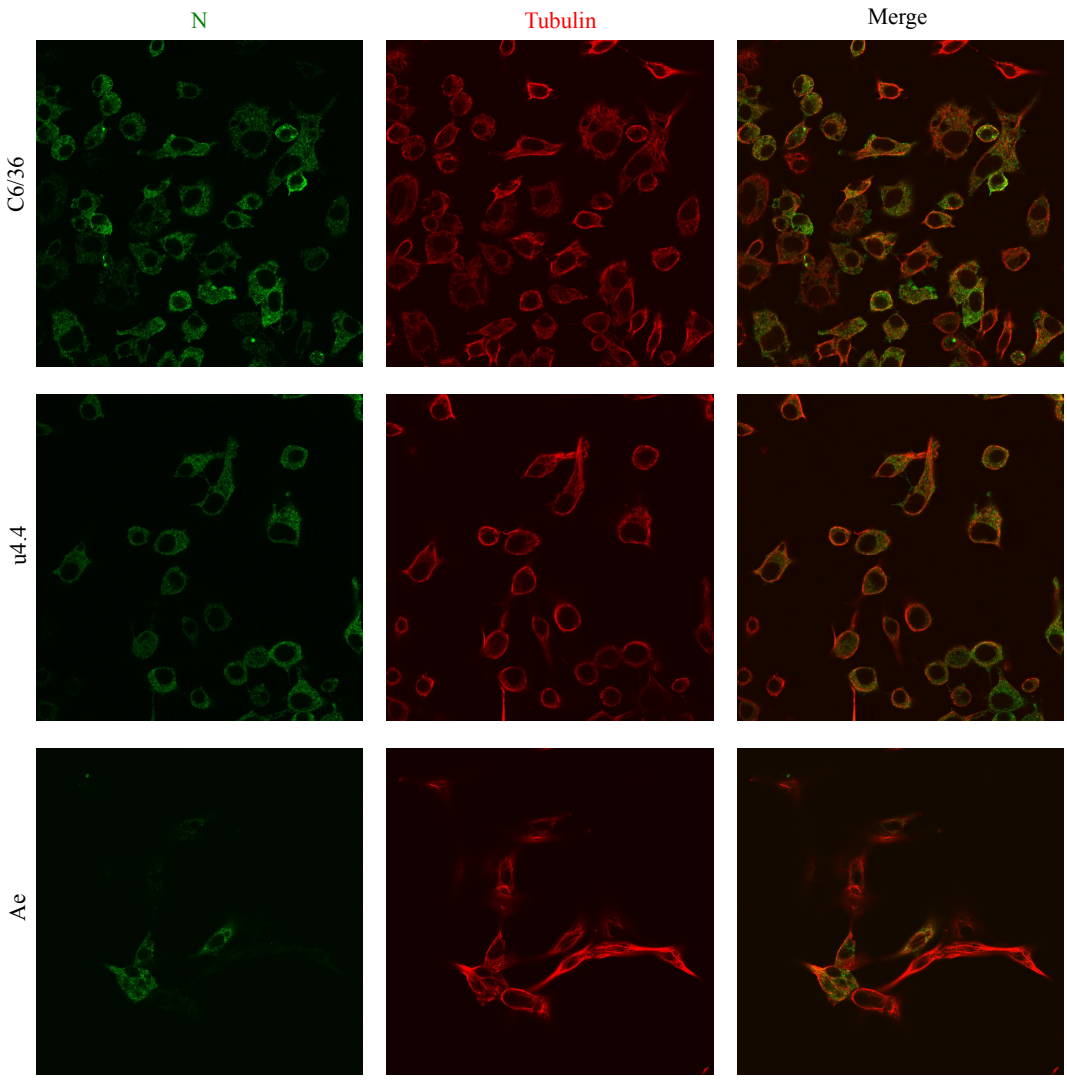

Figure 6-7: Intracellular location of rMP12:S-Swap N protein in infected mosquito cells.
Immunofluorescence images of N in rMP12:S-Swap infected mosquito cells. C6/36, U4.4 and Ae cells were infected at MOI 1 and fixed 48 h p.i. with 4% formaldehyde. Co-staining was performed with anti-N (green) and anti-tubulin (red) antibodies. All images are taken at 63x magnification. Images were taken at the same times as those for Figure 5-3 to 5-5, and uninfected control images are presented for these images in that chapter.

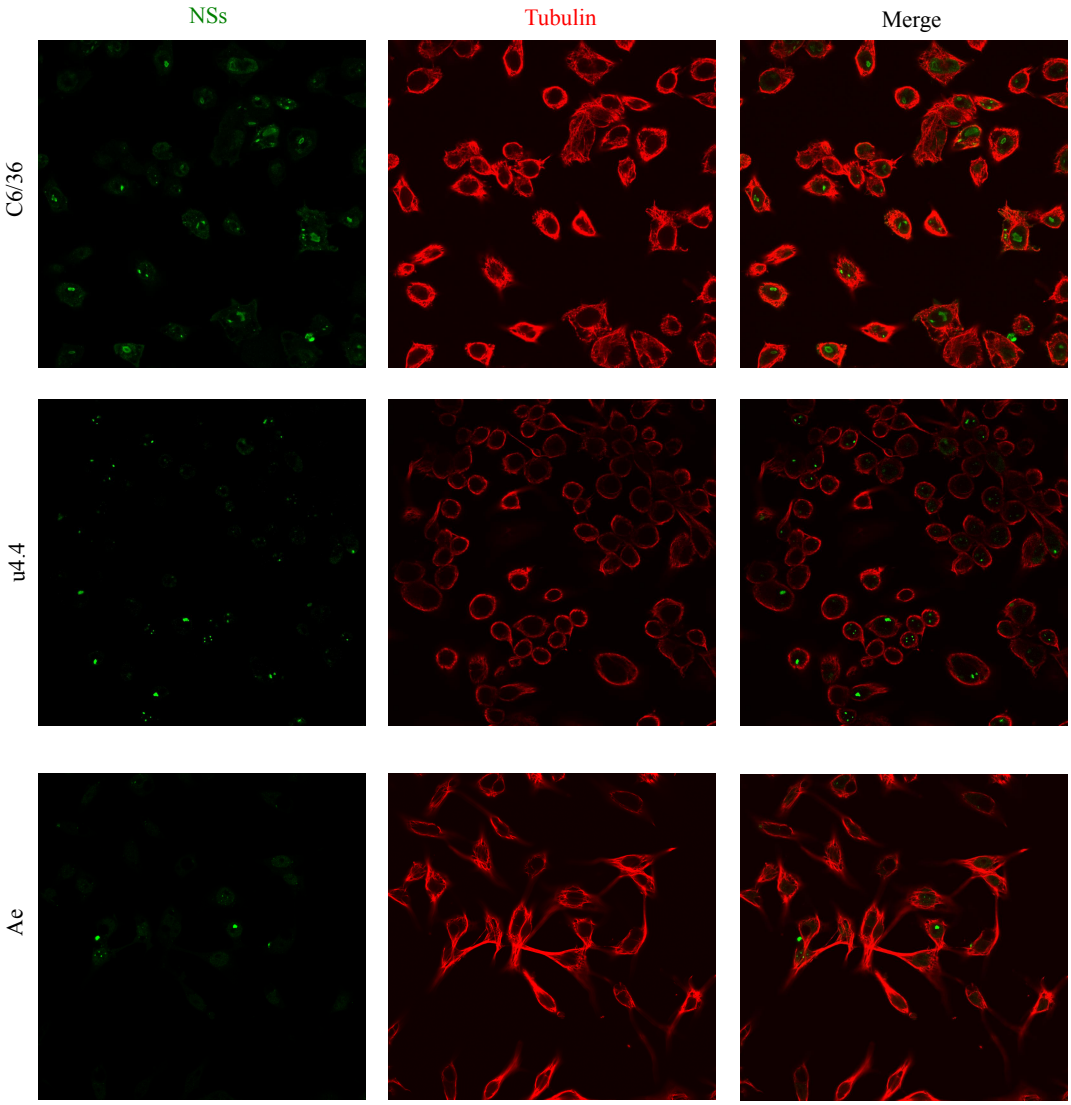

Figure 6-8: Intracellular location of rMP12:S-Swap NSs protein in infected mosquito cells
Immunofluorescence images of NSs in rMP12:S-Swap infected mosquito cells. C6/36, U4.4 and Ae cells were infected at MOI 1 and fixed 48 h p.i. with 4% formaldehyde. Co-staining was performed with anti-NSs (green) and anti-tubulin (red) antibodies. All images are taken at 63x magnification. Images were taken at the same times as those for Figure 5-3 to 5-5, and uninfected control images are presented for these images in that chapter.

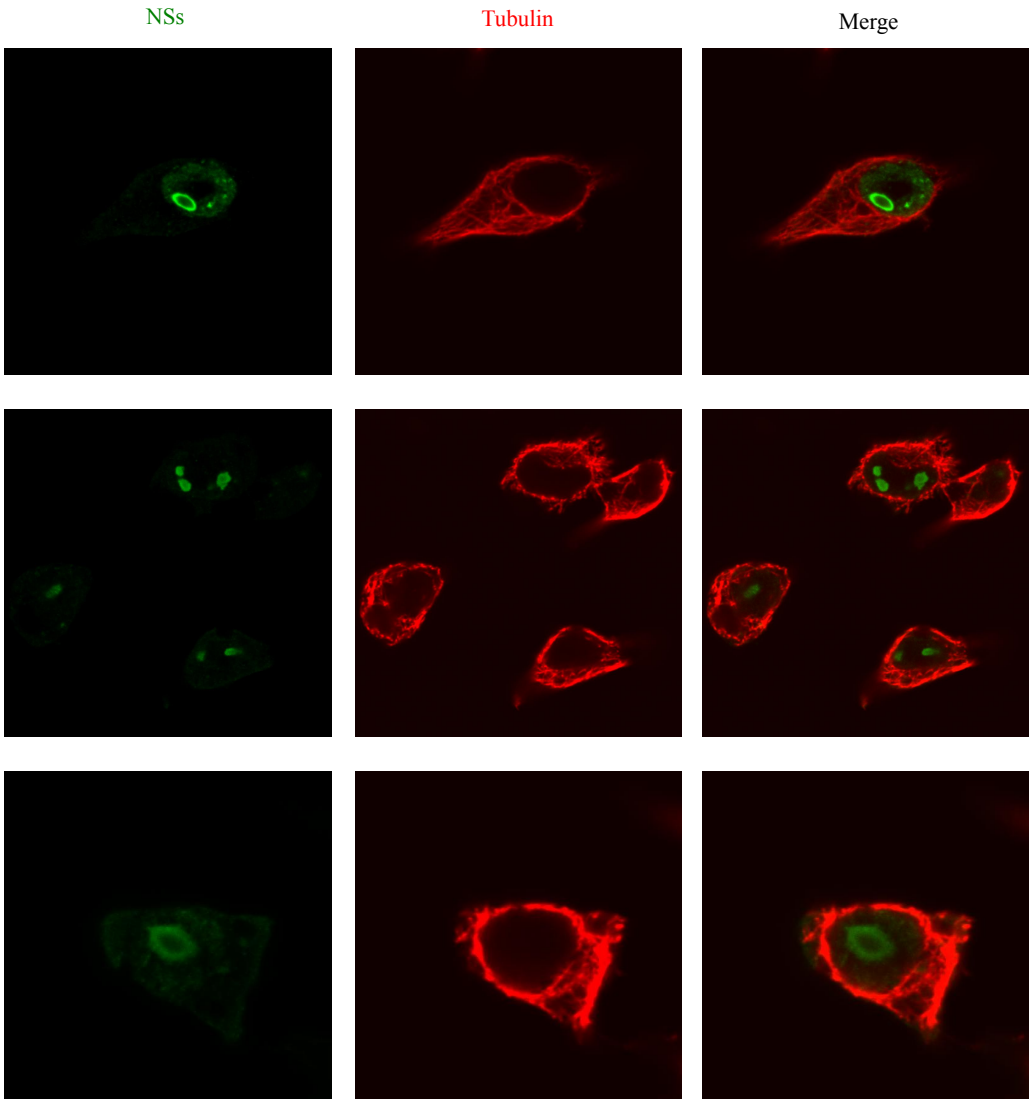

Figure 6-9: Single cell analysis of rMP12:S-Swap NSs structures within the nuclei of infected C6/36 cells

Analysis of NSs expression and intranuclear phenotypic formations individual C6/36 cells infected with rMP12:S-Swap taken from previous immunofluorescent analysis (Figure 6-8). Shown are three independent images. All images are taken at 63x magnification. Images were taken at the same times as those for Figure 5-3, and uninfected control images are presented for these images in that chapter.

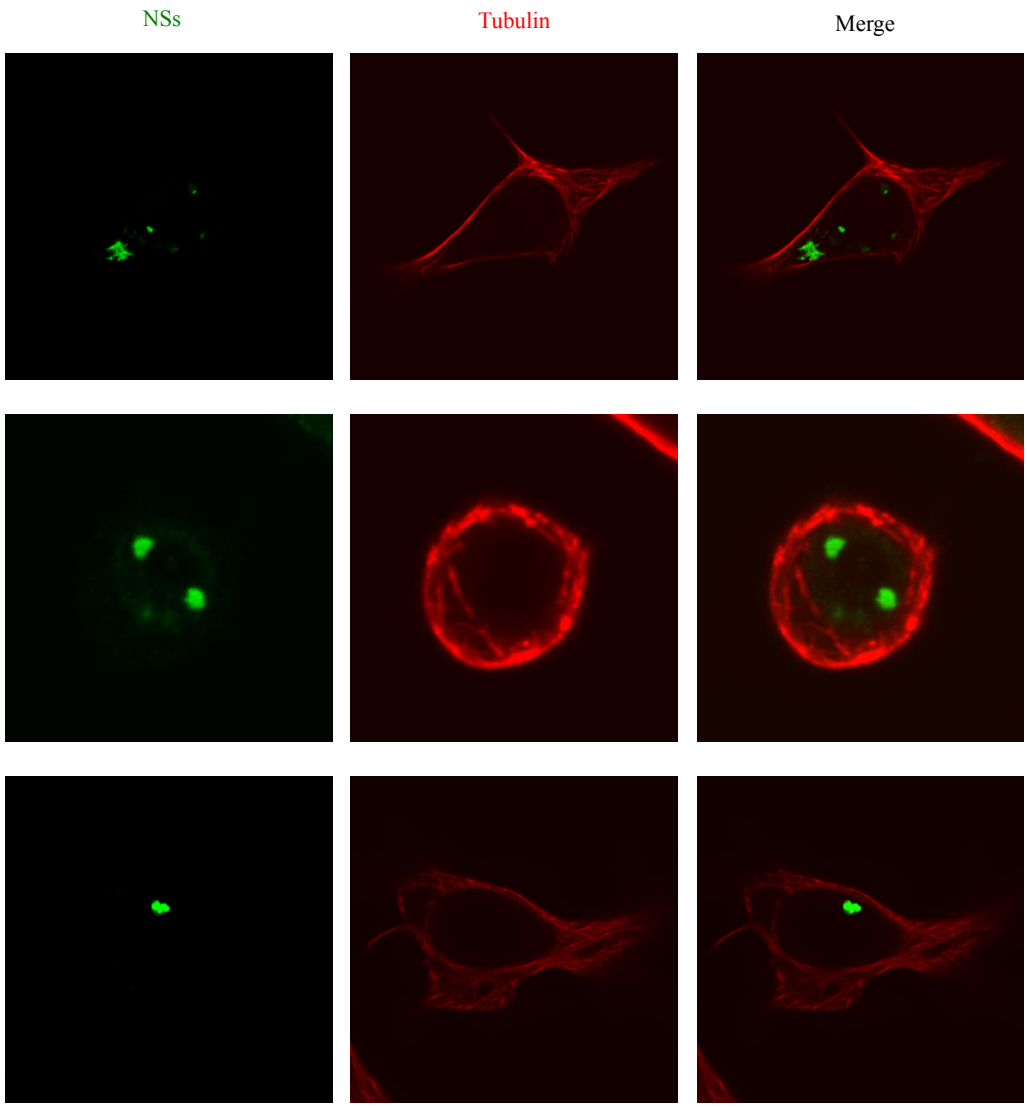

Figure 6-10: Single cell analysis of rMP12:S-Swap NSs structures within the nuclei of infected U4.4 cells

Analysis of NSs expression and intranuclear phenotypic formations individual U4.4 cells infected with rMP12:S-Swap taken from previous immunofluorescent analysis (Figure 6-8). Shown are three independent images. All images are taken at 63x magnification. Images were taken at the same times as those for Figure 5-4, and uninfected control images are presented for these images in that chapter.

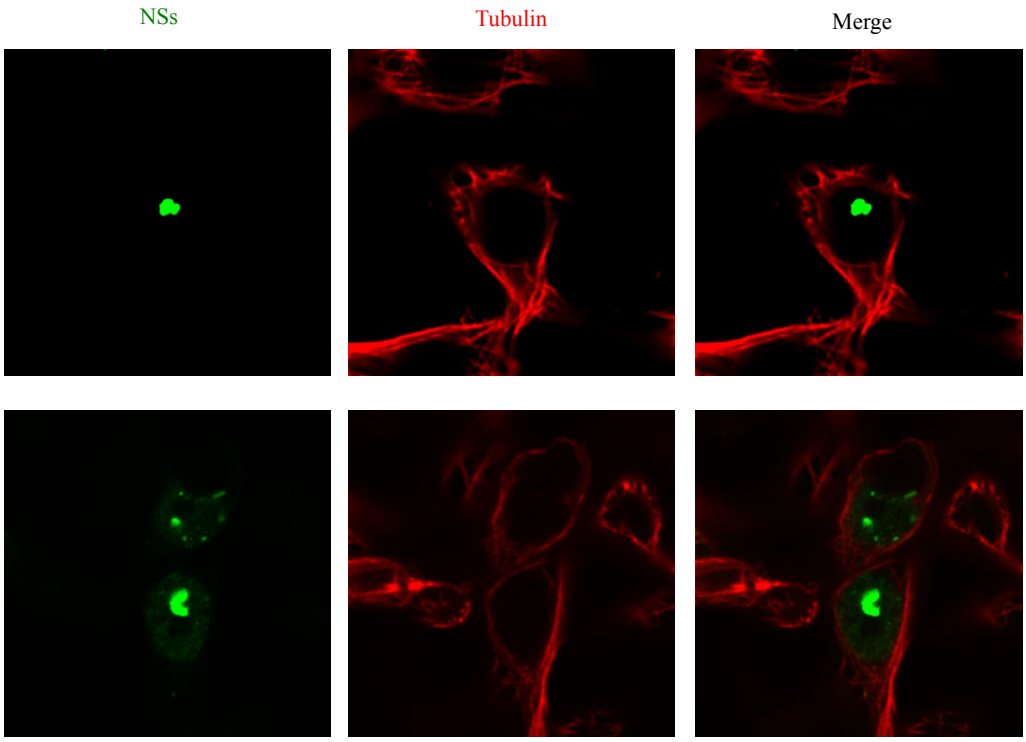

Figure 6-11: Single cell analysis of rMP12:S-Swap NSs structures within the nuclei of infected Ae cells
Analysis of NSs expression and intranuclear phenotypic formations individual Ae cells infected with rMP12:S-Swap taken from previous immunofluorescent analysis (Figure 6-8). Shown are three independent images. All images are taken at 63x magnification. Images were taken at the same times as those for Figure 5-5, and uninfected control images are presented for these images in that chapter.

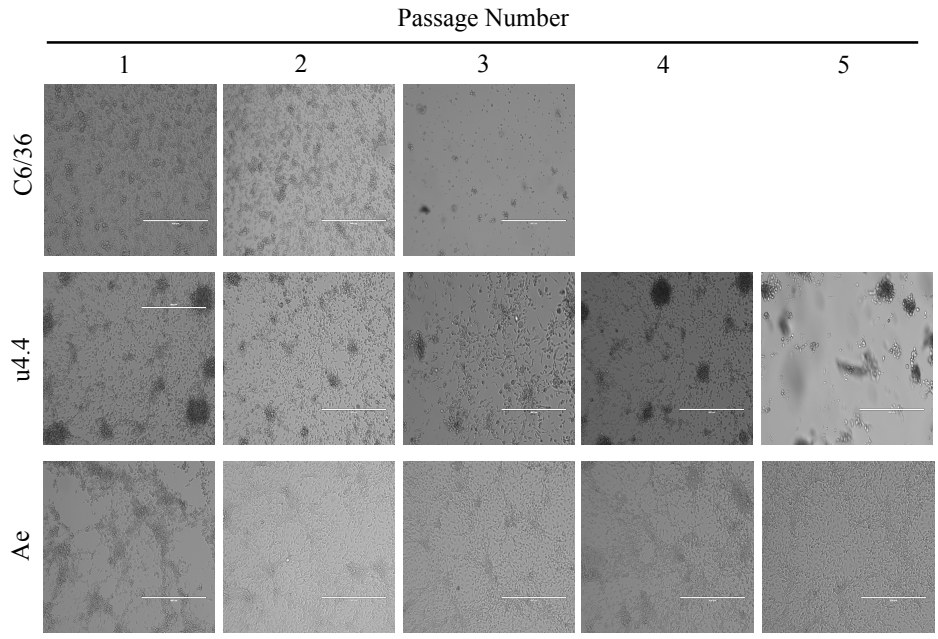

Figure 6-12: Analysis of mosquito cell monolayers persistently infected with rMP12:S-Swap
C6/36, U4.4, and Ae cells were infected with rMP12:S-Swap at MOI 0.01. When cells reached 80-100% confluency the culture was split 1:5 to continue passage. Phase contrast light microscopy images of cell monolayers taken prior to each cell split at 10x magnification. No passage 4 or 5 could be achieved for infected C6/36 cells.

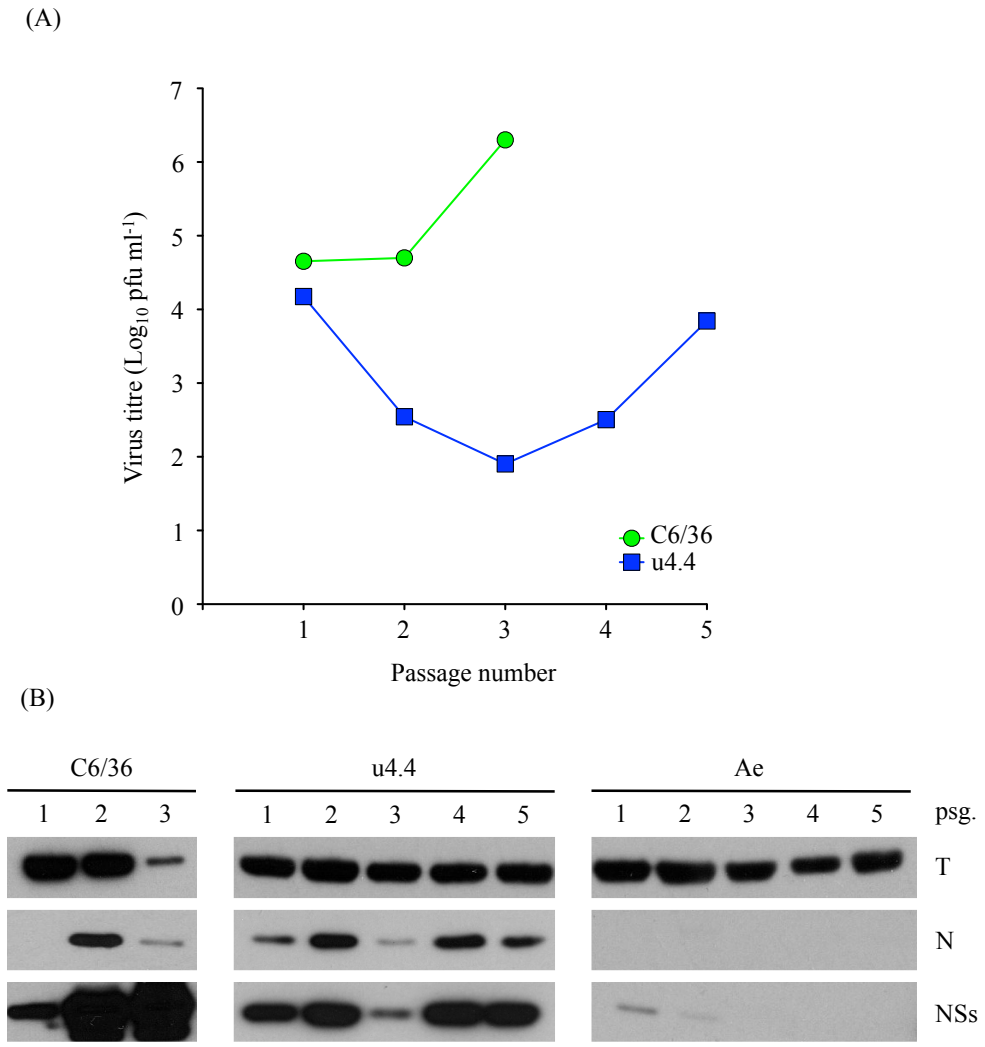

Figure 6-13: rMP12:S-Swap viral titres and protein production in persistently infected cells
(A) Cell culture supernatant was harvested prior to each cell passage and titres determined by plaque assay on BHK-21 cells. (B) Western blot analysis of proteins synthesised in rMP12:S-Swap persistently infected mosquito cells lines during each passage. Antibodies targeting RVFV N and NSs were used to probe for viral proteins, and anti-tubulin antibody was used to detected the tubulin loading control for each sample

p3, enough viable cells remained to successfully continue passaging. However, cell viability continued to decrease continued passage past p5 was unsuccessful. These patterns were not observed in the Ae cells, and lack of N expression after p1 suggested these cells did not become persistently infected. Viral titres in infected C6/36 cells rose as passage number increased, and in infected U4.4 cells a dip in titre correlated to the number of viable cells in the experiment. In both cell lines the virus yields were similar to that determined in Figure 6-2 for an MOI 1 infection.

As with the rMP12 persistence analysis, characteristics of persistently derived virus were examined in mammalian cells. BHK-21 cells were infected with virus from persistently infected C6/36 and U4.4 cells obtained at p3 and p5 respectively. Unlike with rMP12 virus there was no reduction in titre observed when compared to an infection with elite p1 rMP12:S-Swap virus. Protein analysis demonstrated both N and NSs were expressed at expected levels in the infected BHK-21 cells (Figure 6-14). Sequence analysis of the N and NSs CDS's in both persistently derived viruses revealed no mutations compared to the elite rMP12:S-Swap virus stock.

6.3.5 The effect of multiplicity of infection on virus yield

Our laboratory had previously demonstrated that for certain viruses the MOI used affected virus yield. In these examples a higher MOIs resulted in a reduced yield compared to infection at a lower MOI. This phenomenon is thought to be due to generation of defective interfering virus particles (DIs) (Kascsak & Lyons 1978; Brennan, Welch, Mclees, et al. 2011c). Results for BHK-21 cells infected with rMP12 virus at different MOIs demonstrated little effect on final yields. However, increased titres were observed in the lower MOI rMP12:S-Swap infection (Brennan et al. 2014). To investigate if similar effects were observed in mosquito cells C6/36, U4.4, and Ae cells were infected with rMP12 or rMP12:S-Swap at MOIs of 1, 0.1, 0.01, 0.001, and 0.0001. At 72 h p.i. cell culture supernatant was removed and virus titre determined by plaque assay.

For rMP12 infected C6/36 cells the MOI made little difference to the final yield obtained (Figure 6-15).. In infected U4.4 and Ae cells the yields for infections performed at lower MOIs were reduced compared to the higher MOI infections. In rMP12:S-Swap infected

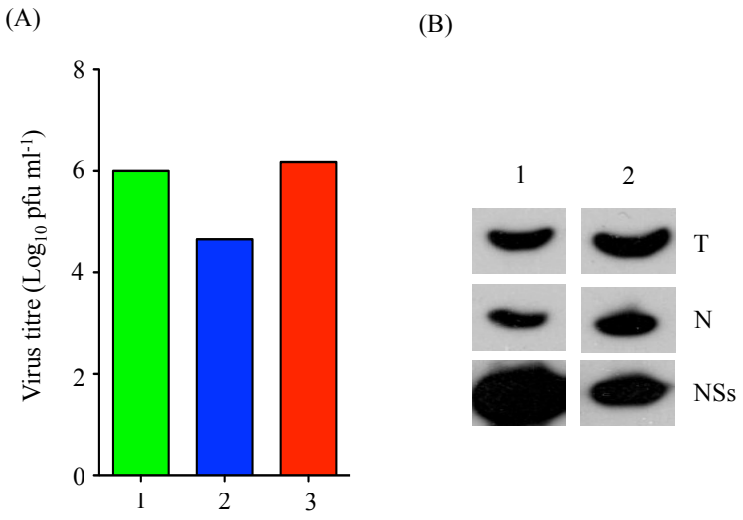

Figure 6-14: Growth of rMP12:S-Swap in BHK-21 cells infected with virus generated from persistently infected mosquito cells

rMP12:S-Swap taken from persistently infected (1) C6/36 cells at passage 3, and (2) U4.4 cells at passage 5 was used to infect BHK-21 cells at MOI 1. Samples were harvested at 48 h p.i. (A) Viral titres were determined by plaque assay and compared to that for (3) p1 elite stock. (B) BHK-21 cell monolayers infected with the (1) C6/36 p3 and (2) U4.4 p5 derived rMP12:S-Swap were analysed for presence of viral protein by western blot. Antibodies targeting RVFV N and NSs were used to probe for viral proteins, and anti-tubulin antibody was used to detected the tubulin loading control for each sample

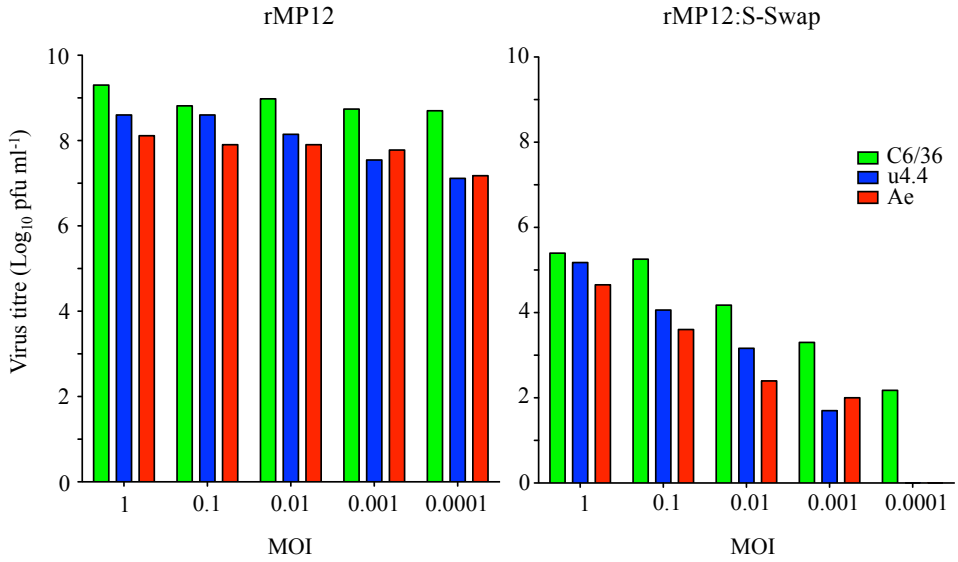

Figure 6-15: Virus yields in mosquito cells infected with rMP12 or rMP12:S-Swap at different MOIs
C6/36, U4.4, and Ae cells were infected with rMP12 or rMP12:S-Swap at MOI 1, 0.1, 0.01, 0.001, and 0.0001. At 96 h p.i. cell culture supernatant was removed and viral titres determined by plaques assay.

C6/36 cells yields were similar when infected at MOI 1 and 0.1, but after this progressively declined with decreasing MOI. In U4.4 and Ae cells the decline was more pronounced at all MOIs, and no virus growth detected for either cell line when infected at MOI 0.0001. The reduction in yield in rMP12:S-Swap infected cells is likely due to the reduced level of N expression affecting the replication and transcription potential of the virus.

6.3.6 Experimental design of a strand specific qRT-PCR assay for MP12

The second aim of this chapter was to develop an assay which could quantify relative levels of both RVFV genome and antigenome strands during an infection. Specific assays were designed for both S and M segment. Standard curves were used to validate the individual assays and also to correct for differences in sensitivity between the genome and antigenome specific assays. Therefore, by comparing qPCR crossing threshold (ct) values from both assays the relative ratio of genomic to antigenomic polarity strands within a sample was determined.

Initially the assay was designed to employ sequence-specific RT primers unique to sites on the genomic and antigenomic polarity strands. However, this approach was not successful due to a lack of polarity specificity shown by the primers during the RT reaction. It was thought that RNA secondary structures in the samples were recognized by the RT enzyme, priming non-specific cDNA formation. This lack of specificity meant that polarity-specific RNA ratios could not be resolved using the subsequent qPCR assay. This problem was solved by designing the strand-specific primers with an unique sequence tag incorporated at the 5' end, ensuring that any resultant cDNA would also contain the sequence tag. qPCR was then performed using primers targeting both the specific strand and the unique tag sequence. This ensured non-specific cDNA would not be amplified during the qPCR assay, and therefore not interfere with the relative quantification calculations (Figure 6-16). The RT primers targeting S segment were designed to be complementary to sequences wholly contained within the N or NSs CDSs of rMP12, allowing for the same assay to also be used in rMP12:S-Swap samples. RT primers were designed to be non-complimentary to mRNA transcripts, ensuring only genome strands were targeted. The unique sequence tag used was taken from the assay published by Kawakami et al (2011). The term genome and antigenome were based on the 3' UTR sequence of the target segment, with the reference being the parental S and M segments of rMP12.

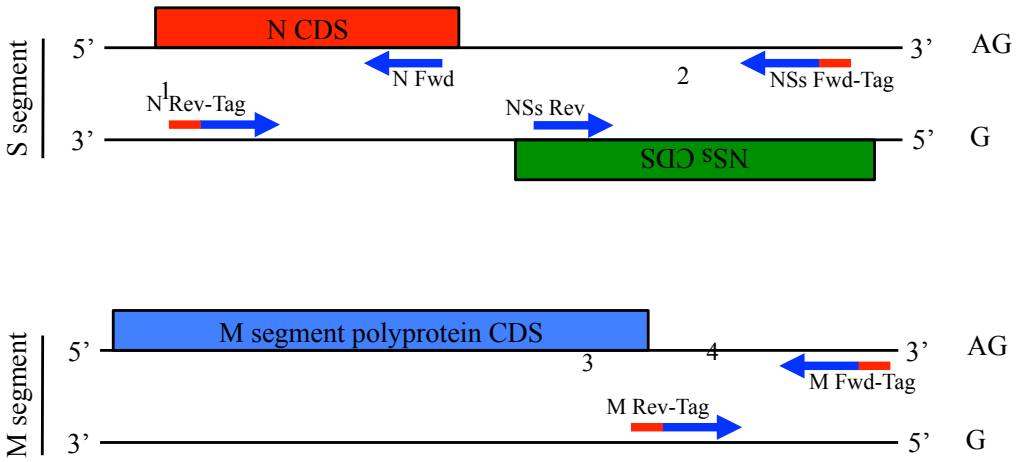

Figure 6-16: Genome schematic showing primer binding sites for the RVFV strand specific RT and qPCR assays

Schematic diagram showing the position of the primers used in the reverse transcription (RT) and qPCR assays on RVFV S and M segments. The primers were specific to either genome (G) or antigenome (AG) strands (blue arrow) and incorporated a unique sequence tag (red). RT reactions produce strand-specific cDNA incorporating the unique sequence tag. During PCR the cDNA is amplified using a primer complementary to the tag sequence and a further strand specific primer. See Table-6-1 for primer details.

The RT reactions were performed using a single tagged primer (Table 6-1). Four RT reactions were performed for each RNA sample extracted from either infected cells or virions (summarised in Table 6-2). Each qPCR was performed in triplicate with a mean ct value calculated post-assay. As a further quality check, melt curve analyses were performed at the end of each qPCR assay. The Tm of each amplicon was determined during assay optimisation, was referenced after each qPCR to ensure the correct amplicon was generated. This was to guard against false positives arising from non-specific amplification or primer dimerisation.

6.3.7 Assay validation

To determine the specificity and efficiency of the individual qRT-PCR assays, RNA transcripts of MP12 S and M segment genome and antigenome strands were generated using *in vitro* transcription. pTVT7 based MP12 rescue plasmids contain full length segments in antigenomic orientation under control of a T7 promoter, while a SP6 promoter at the opposite end of the insert allows transcription of a genomic polarity segment. Plasmids were linearised with either SapI or SalI to generate genomic or antigenomic sense RNA transcripts respectively by run-off transcription (Figure 6-17). RNA transcripts for both MP12 S and M segment were generated using the pTVT7-GS and pTVT7-GM plasmids. RNA copy numbers of genome and antigenome strands were calculated, and standards containing 10^{10} to 10^{0} RNA copies/µl were made.

The M segment assay displayed a wider dynamic range than both S segment assays, detecting genome and antigenome targets in the 10^{10} to 10^{2} RNA copies/µl range before losing sensitivity. The S genome and antigenome assays were both accurate within the range of 10^{10} to 10^{4} RNA copies/µl. Within their dynamic range all standard curves had an R^2 value of >0.99, and the amplification efficiencies were comparable within between the segment-specific assays: S segment assay = 103% vs. 104%; M segment assay = 94% vs. 93% (Figure 6-18). The assay for S antigenome was more sensitive than that for S genome, with a ct difference between the assays across their dynamic range of 4. Therefore, normalisation by subtracting 4 from the genome assay ct values allowed direct comparison with results for the antigenome assay. The M segment assay ct values for both genome and antigenome samples at the same copies/µl were identical, and could therefore be compared

Table 6-1: Primer sequences
Table showing the primers used for both the RT and qPCR assays.

Primer Name	Sequence (5' – 3')	Genome Position
N Fwd	AACTCTACGGGCATCAAACC	1539-1558[a]
N Rev	AAGAGCTTGCGATCCAGTTT	1620-1639[a]
NSs Fwd	GGACTCCTTTGCTGGCTTAC	502-521[a]
NSs Rev	GCACTGTACGTGAGCAACCT	597-616[a]
N Rev-Tag	**GGCCGTCATGGTGGCGAAT**AAGAGCTTGCGATCCAGTTT	-
NSs Fwd-Tag	**GGCCGTCATGGTGGCGAAT**GGACTCCTTTGCTGGCTTAC	-
M Fwd	CCGGTGCAACTTCAAAGAGT	10-29[b]
M Rev	AGGCAGCAGCAGTCTCAAGT	90-109[b]
M Fwd-Tag	**GGCCGTCATGGTGGCGAAT**CCGGTGCAACTTCAAAGAGT	-
M Rev-Tag	**GGCCGTCATGGTGGCGAAT**AGGCAGCAGCAGTCTCAAGT	-
Tag Primer	**GGCCGTCATGGTGGCGAAT**	-

Unique sequence tag is shown in bold
Genome position is based on genomic polarity segment
[a] From Rift Valley fever virus strain MP12 S segment, NCBI accession number DQ380154
[b] From Rift Valley fever virus strain MP12 M segment, NCBI accession number DQ380208

Table 6-2: Primer combinations for strand specific RT and qPCR assays

	rMP12		rMP12:S-Swap	
Target	**RT**	**qPCR**	**RT**	**qPCR**
S segment genome	N Rev-Tag	Tag Primer + N Fwd	NSs Rev-Tag	Tag Primer + NSs Fwd
S segment antigenome	NSs Fwd-Tag	Tag Primer + NSs Rev	N Fwd-Tag	Tag Primer + N Rev
M segment genome	M Rev-Tag	Tag Primer + M Fwd	M Rev-Tag	Tag Primer + M Fwd
M segment antigenome	M Fwd-Tag	Tag Primer + M Rev	M Fwd-Tag	Tag Primer + M Rev

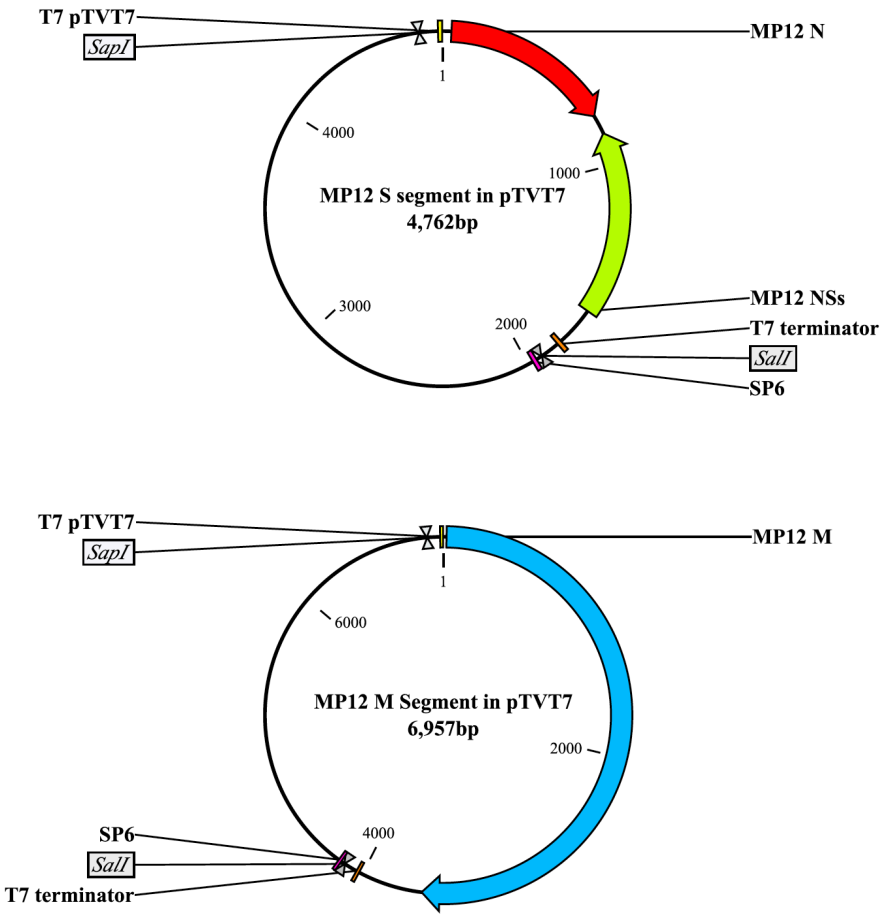

Figure 6-17: Generation of *in vitro* transcripts for standard curves
Key: MP12 N – nucleocapsid CDS; MP12 NSs – non-structural protein NSs CDS; MP12 M – M segment polyprotein CDS; T7 pTVT7 – T7 promoter site; T7 terminator – T7 termination site; SP6 – SP6 polymerase promoter; SapI – restriction enzyme recognition site for SapI enzyme; SalI – restriction enzyme recognition site for SalI enzyme. To generate the RNA used for standards in the qRT-PCR assay pTVT7-GS and pTVT7-GM were linearised with either SapI or SalI. T7 polymerase was used to generate antigenome segment RNA transcripts in SalI linearised plasmids, and SP6 polymerase was used to generate genome segment RNA transcripts in SapI linearised plasmids.

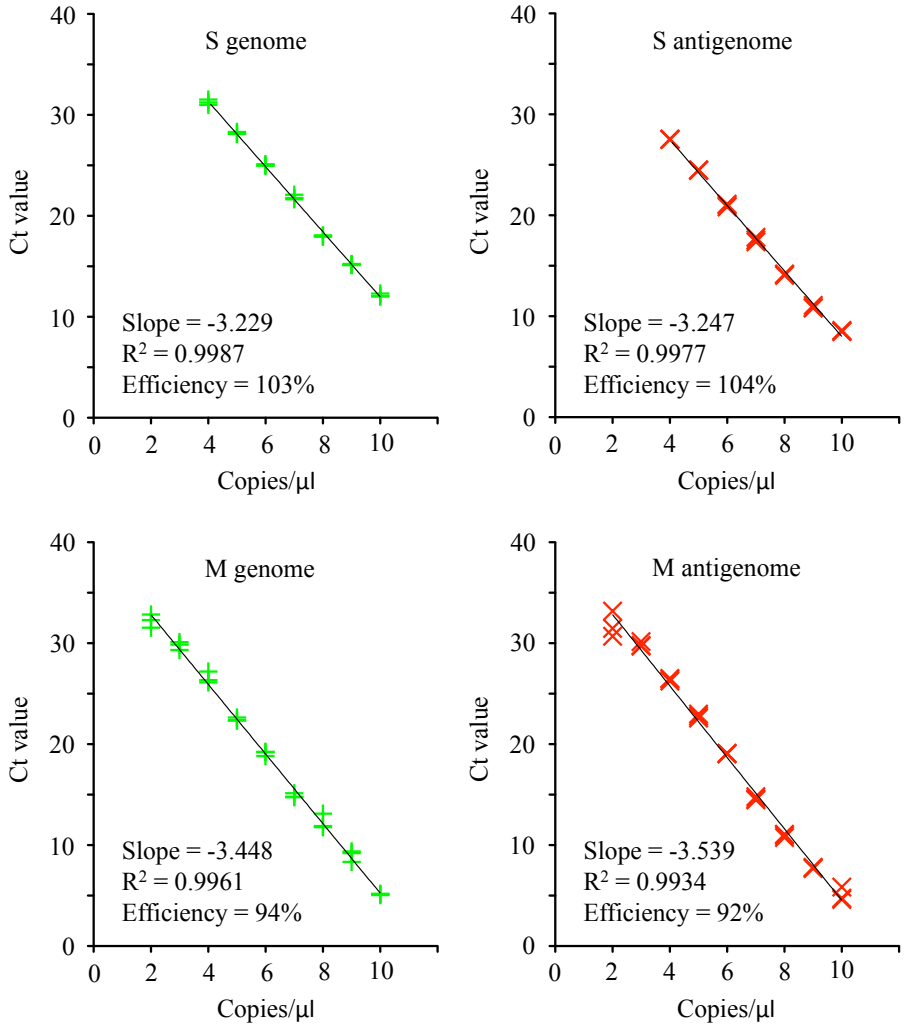

Figure 6-18: Standard curve analysis of the S and M segment strand-specific qRT-PCR assay
Standard curves for the RVFV S and M segment genome and antigenome qRT-PCR assays. Serial 10 fold dilutions from an *in-vitro* transcription generated control were used to construct the curves. Dilutions from 10^{10} to 10^{4} copies/µl are shown for the S segment assays and 10^{10} to 10^{2} copies/µl are shown for the M segment assays. Slope and R^2 value were calculated using linear regression software in GraphPad Prism. Amplification efficiency was calculated using the following formula: $E = -1+10^{(-1/slope)}$

directly with no normalisation. Melt curve analysis of qPCR amplicons demonstrated that a single product was amplified by each reaction, with no evidence of primer dimer formation or non-specific binding detected (Figure 6-19). The Tm's of S segment genome and antigenome assays amplicons were 80.8°C and 82.3°C respectively, and 79.3^0C for the amplicon from both M segment assays.

The ct values obtained with genome and antigenome specific assays in the same sample were compared to determine the ratio of genomic to antigenomic polarity strands present. Once ct values had been normalised, the difference in ct value was calculated (genome ct – antigenome ct). As only positive values could be used in the equations, an inverse function (square-root of the square) was used to remove any negative values. Using the formula $x = e^{(0.6931y)}$,where y was the difference in ct values, gave a value for the relative amount difference between genomic and antigenomic polarity strands (x), equivalent to the ratio of genome strands to 1 antigenome strand. From this value the percentage of genome segment that was of genomic polarity in the original RNA sample could be calculated using the formula (%genome = x/(x+1)). This value was used in all further statistics and figures. One-way ANOVA with Tukey's multiple comparison post test statistical analysis was performed, with significance set at $p < 0.05$.

6.3.8 Variations in RNA species between rMP12 and rMP12:S-Swap infected cells

BHK-21, C6/36, U4.4, and Ae cells were infected with rMP12 or rMP12:S-Swap at MOI 1. At 48 h p.i. cell culture supernatant was removed and cells lysed to obtain total RNA. The cell culture supernatant was clarified by centrifugation, and RNA extraction performed on the virions. A minimum of five independent infections were performed for each combination of cell line and virus, and percentage genome for S and M segment calculated for each RNA sample. These data are summarised for rMP12 infected mosquito cells in Appendix Table 10-2, for rMP12:S-Swap infected mosquito cells in Appendix Table 10-3, and for rMP12 and rMP12:S-Swap infected cells in Appendix Table 10-4.

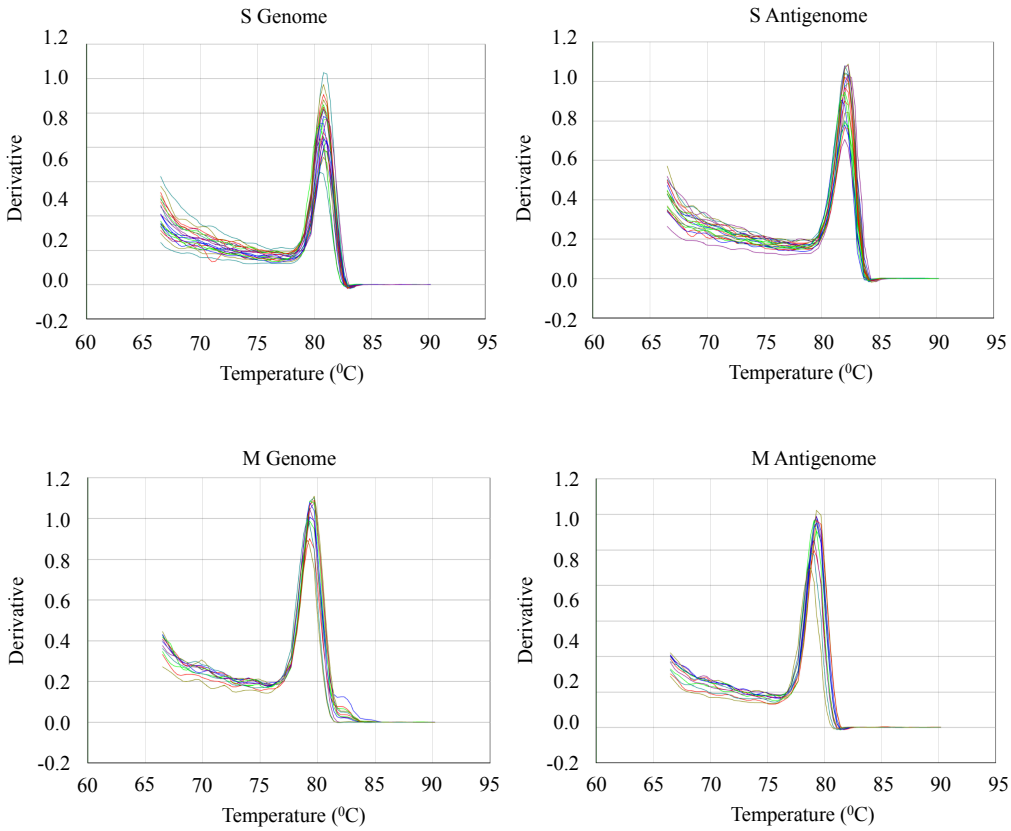

Figure 6-19: Melt curve analysis of the S and M strand-specific assay amplicons
Melt curve analysis on the qPCR amplicons for S and M segment genome and antigenome assays. The Tm's of the S segment genome and antigenome assays were 80.8°C and 82.3°C respectively. The M segment genome and antigenome assays utilized the same primers and produced similar PCR products with identical Tm's 79.3°C

The results demonstrated significant differences in the relative amounts of genomic and antigenomic polarity S segment detected in both the virion and cellular RNA samples taken from rMP12 or rMP12:S-Swap infected cells. A significant decrease in the percentage of genomic sense S segment packaged into nascent virions in rMP12:S-Swap infection was observed (Figure 6-20). On average approximately 80% of rMP12 S segment detected in both virions and infected cells was of genomic polarity. No significant difference was observed between the individual cell lines, or between the virion and cellular RNA samples. However, in rMP12:S-Swap infected cells the majority of both cellular and virion S segment was of antigenomic polarity. Levels of M genomic polarity RNA species were measured for each samples as a control. Unlike the S segment results there was no significant difference in the proportions of M genome and antigenome segments packaged in virions when comparing rMP12 and rMP12:S-Swap virus infected cells (Figure 6-21). There were however significant differences determined for M genomic polarity segment levels between the rMP12 and rMP12:S-Swap viruses for certain cell lines (Table 6-3). However, these were not as pronounced at the almost opposite ratios observed between the viruses for S segment.

6.4 Discussion

Definite reasons as to why certain members of the *Bunyaviridae* and *Arenaviridae* genera have evolved ambisense coding strategies remain unanswered (Bishop 1986a). One theory is that the common *Bunyaviridae* ancestor once employed an ambisense coding strategy, a feature eventually lost in the majority through evolutionary selective pressures (Nguyen & Haenni 2003). A contrasting idea is that ambisense genes were acquired at various points in the viruses evolutionary history conferring fitness advantages (Elliott 1996). Given our current understanding of the roles that RVFV NSs plays during infection, namely its antagonistic actions toward host immunity, it is unclear why a coding strategy that effectively delays expression of NSs would be maintained. rMP12:S-Swap therefore proved a useful tool allowing study of the virus lifecycle in a context where temporal regulation of N and NSs was reversed

Growth curves demonstrated attenuation of both rMP12:S-Swap and rMP12:S-SwapΔNSs:eGFP viruses in all cell lines evaluated, with attenuation greatest in mosquito

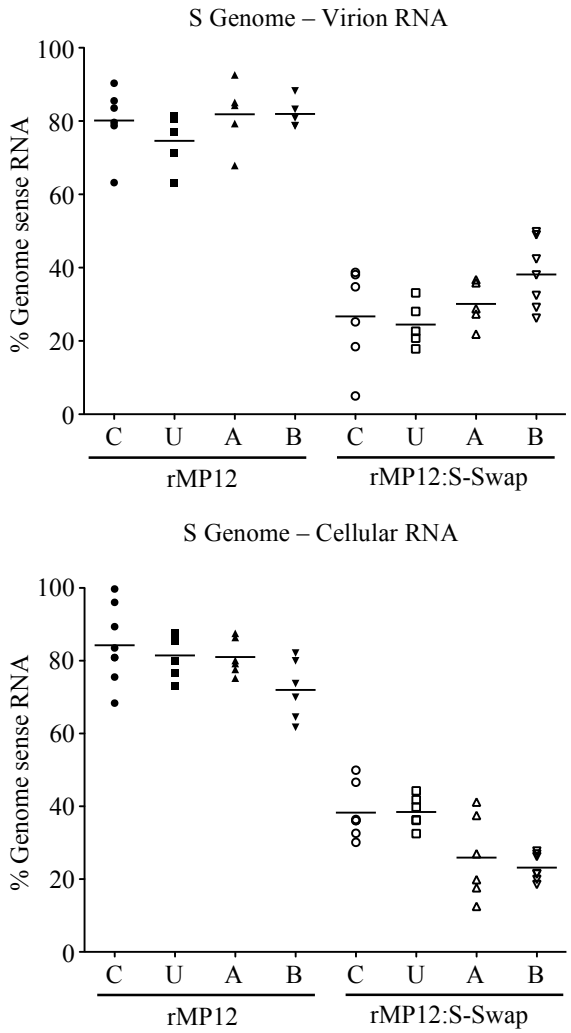

Figure 6-20: qRT-PCR assays for S segment in rMP12 and rMP12:S-Swap infected cell lines
Quantitative RT-PCR on RNA extracted from rMP12 or rMP12:S-Swap virions or infected cell monolayers. Cell lines infected were (C) C6/36), U) U4.4, (A) Ae, and (B) BHK-21. Data points are from separate independent infections, and show the percentage genomic sense S segment packaged into progeny virions or detected in cellular RNA. Mean values are represented as a line.

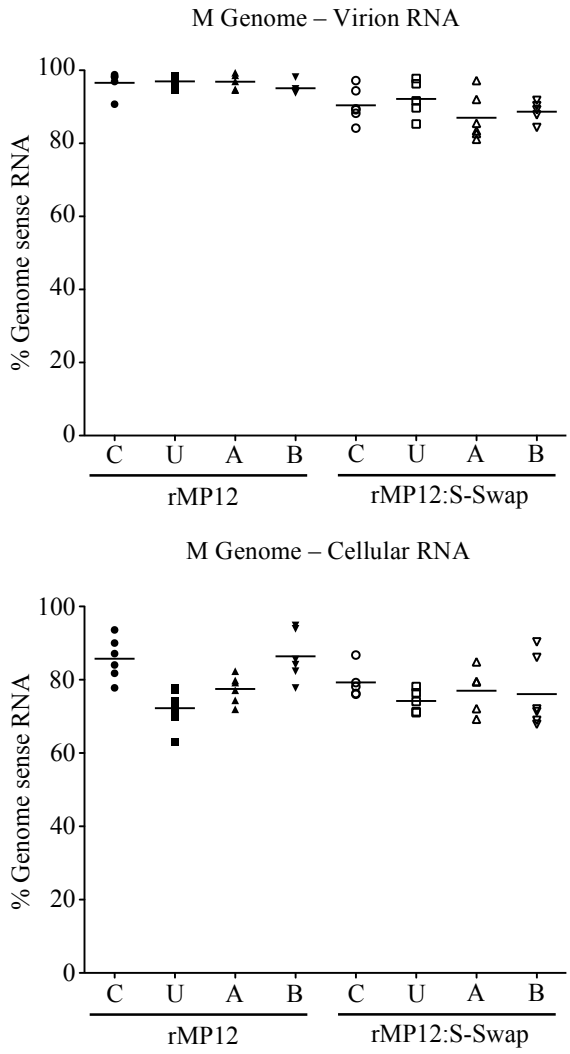

Figure 6-21: qRT-PCR assays for M segment in rMP12 and rMP12:S-Swap infected cell lines
Quantitative RT-PCR on RNA extracted from rMP12 or rMP12:S-Swap virions or infected cell monolayers. Cell lines infected were (C) C6/36), U) U4.4, (A) Ae, and (B) BHK-21. Data points are from separate independent infections, and show the percentage genomic sense M segment packaged into progeny virions or detected in cellular RNA. Mean values are represented as a line.

Table 6-3: Statistical summary of qRT-PCR analysis

	S Segment			
Samples Compared	**C6/36**	**U4.4**	**Ae**	**BHK-21**
rMP12 Virion vs. rMP12:S-Swap Virion	YES[a]	YES	YES	YES
rMP12 Virion vs. rMP12 Cellular	NO[b]	NO	NO	NO
rMP12:S-Swap Virion vs. rMP12:S-Swap Cellular	NO	NO	NO	NO
rMP12 Cellular vs. rMP12:S-Swap Cellular	YES	YES	YES	YES

	M Segment			
Samples Compared	**C6/36**	**U4.4**	**Ae**	**BHK-21**
rMP12 Virion vs. rMP12:S-Swap Virion	NO	NO	NO	NO
rMP12 Virion vs. rMP12 Cellular	NO	YES	YES	NO
rMP12:S-Swap Virion vs. rMP12:S-Swap Cellular	YES	YES	NO	YES
rMP12 Cellular vs. rMP12:S-Swap Cellular	NO	NO	NO	NO

[a] statistically significant difference in percentage genomic sense RNA ($p = <0.05$), analysis by one-way ANOVA with Tukey's multiple comparison post test
[b] not statistically significant difference in percentage genomic sense RNA

cell lines. This attenuation was most probably due to the significantly reduced N expression level observed in infected cells. Reduced N levels would impact numerous important stages in the replication cycle, including the viral transcription and replication processes (Lopez et al. 1995; Jin & Elliott 1991). As reduction in N levels were most apparent in the mosquito cells, titres here were more keenly affected. It was originally thought that reduced N expression in rMP12:S-Swap infected BHK-21 cells was a result of the increased NSs expression. Increasing levels of NSs have previously been shown to be inhibit a *Renilla*-based RVFV minireplicon reporter assay, and NSs is known to cause a reduction in host cell protein synthesis (Brennan, Li, et al. 2011a; Ikegami et al. 2009; Le May et al. 2008). The hypothesis was that the earlier and greater levels of NSs expression reduced host cell protein expression levels to a point where transcription and replication was constrained by lack of N and L protein. However, hyper-expression of NSs in BHK-21 cells was subsequently shown to have no effect on the overall level of host cell protein synthesis inhibition (Brennan et al. 2014). This also did not explain the reduced N expression in mosquito cell lines as NSs expression was previously shown to have no effect on host cell synthesis in these cells.

It was therefore suggested that both the reduced N and increased NSs expression levels observed in rMP12:S-Swap infected cells were more likely due to inherent differences in the genomic and antigenomic UTR promoter strengths of S segment. Western blot analysis demonstrated that NSs was expressed at a higher level in BHK-21 cells compared to the mosquito cells, suggesting transcription from the parental NSs promoter in BHK-21 cells was more efficient than in mosquito cells. The higher level of N in rMP12:S-Swap infected BHK-21 cells compared to that in infected mosquito cells could account for the differences in viral titres observed. A comparison between S segment promoter strengths can also be inferred by evaluating differences in GFP expression level between rMP12ΔNSs:eGFP and rMP12:S-SwapΔNSs:eGFP infected cells. BHK-21 cells infected with rMP12ΔNSs:eGFP demonstrate GFP expression, but mosquito cells did not even at the higher MOI 5 infections. In contrast, GFP expression was significantly greater in rMP12:S-SwapΔNSs:eGFP infected BHK-21 cells, and now apparent in the infected mosquito cells. This was in spite of the significantly reduced viral titres, presumably again due to reduced N protein levels. Cell line variations in UTR promoter strengths would also explain the differences in NSs expression level observed between rMP12 infected mammalian and

mosquito cells. The relative promoter strengths of genome and antigenome segments between mammalian and mosquito cells are more extensively investigated in Chapter 7.

A possible reason explaining why NSs expression level is constraint in mosquito cells was demonstrated by the rMP12:S-Swap persistence experiments. Persistent rMP12 infections were characterised by the loss of NSs expression in C6/36 cells as passage number increased. However, persistent infection with rMP12:S-Swap virus resulted in NSs hyper-expression accompanied by compromised cell growth and reduced cell viability. NSs hyper-expression also resulted in an increase in intranuclear accumulation of the protein compared to rMP12 infection. In mammalian cells NSs accumulation in the nucleus has been shown to lead to DNA damage such as chromosome cohesion and segregation defects, factors linked to the pathogenicity associated with RVFV infections (Josse et al. 2012; Mansuroglu et al. 2010). Therefore, analogous DNA damage in the rMP12:S-Swap infected mosquito cells resulting from NSs hyper-expression may be responsible for the observed cell death. The cytotoxic effect of NSs may be a reason why mosquito cells target the NSs mRNA via the previously described siRNA pathway (Léger et al. 2013). Down regulation of NSs may be necessary for RVFV to maintain persistence in mosquito cells. Investigations into the RNAi pathway responses in mosquito cells infected with rMP12 and rMP12:S-Swap are investigated in Chapter 8.

Viral genome packaging in some viruses is well characterised, and several control mechanisms have been identified. These include segment specific packaging signals in UTR and ORF terminal regions for influenza (Gao et al. 2012), secondary structures formed between separate genome copies in HIV (Heng et al. 2012; Lu et al. 2011), and interactions between matrix proteins and genome strands (Overby, Popov, et al. 2007b). However, the methods by which RVFV packages the three genomic segments into progeny virions are currently not extensively characterised. However, as BUNV has been reported to have a particle to pfu ratio approaching 1:1, this suggests a tightly regulated process is involved to ensure correct distribution of bunyavirus genome strands to progeny virions (Lowen et al. 2005). Bunyaviruses do not encode a matrix protein to assist with viral maturation and genome packaging, and therefore packaging must involve alternative viral architectures. Recent research with bunyaviruses has identified structures in the glycoprotein tail of UUKV, and in the Gn protein of RVFV as important for genome encapsidation and packaging (Overby, Popov, et al. 2007b; Overby, Pettersson, et al.

2007a; Raymond et al. 2010). A putative mechanism for RVFV genome packaging involving specific intermolecular interactions among the three genomic RNA molecules has been described (Terasaki et al. 2011). Specifically, a sequence identified in the 5' UTR of M segment was demonstrated to play a critical role in packaging of all three segments. However, the recovery a two segmented RVFV by reverse genetics lacking the M segment entirely indicates that the processes involved are more complex than just one sequence alone, and potentially involve multiple interacting mechanisms (Brennan, Welch, McLees, et al. 2011b).

Results described here demonstrated that the altered coding strategy of rMP12:S-Swap also affected the genome packaging phenotype. This effect was predominantly limited to the modified S segment, as M segment genome packaging ratios were not significantly altered. The virion population produced by rMP12:S-Swap infected cells contained a significantly higher proportion of antigenomic polarity S segment than those from in rMP12 infected cells. S segment RNA populations within the infected cells were also significantly altered in a similar way. However, in both rMP12 and rMP12:S-Swap infected cells the S segment genome and antigenome populations between virions and cells were not significantly different from each other. This suggested that the mechanisms responsible for packaging S segment into virions may not be directed processes, and instead merely a stochastic representation of the RNA species contained within an infected cell. These results also suggest that the panhandle structures formed by the 3' and 5' UTR regions in S segment are not the only prerequisite for packaging correct polarity as has previously been proposed, as UTR regions were identical between the two viruses (Piper et al. 2011; Murakami et al. 2012). For M segment packaging significant differences between genome proportions in virion and infected cell RNA were noted in some cell types. These differences were observed in both rMP12 and rMP12:S-Swap infected cells, and therefore unlikely a result of the altered S segment. Taken together these results could suggest that directed mechanisms are responsible for packaging the M segment, but none are apparent for the S segment. Another explanation is that specific genome strand:strand interactions are involved in the packaging processes. If these regions residing on the S segment were altered in the generation of the rMP12:S-Swap S segment then correct packaging may have been disrupted. Additional work is currently underway to investigate genome packaging in RVFV further.

In conclusion, rescue of a MP12 recombinant virus in which the N and NSs coding sequencing have been transposed was shown to be possible. However, the resulting virus was highly attenuated in both mammalian and mosquito cells. Whilst lack of N may be a potential cause of this attenuation by reducing both transcriptional and replicative processes, over expression of NSs may also negatively impact cellular function and viability. As well as altering protein and mRNA transcription levels, the proportion of genome and antigenome S segment strands packaged into progeny virions was significantly altered. The use of rMP12:S-Swap or derivatives there of as a vaccine candidate for RVFV has been suggested (Brennan et al. 2014). If protective immunity is induced, then the over expression of a second antigenic protein located under the NSs promoter could provide immunity to a further pathogen. This could even be tailored to specific geographical regions. Conversely, if overexpression of NSs result in mosquito death then this would also be advantageous.

6.5 Summary

- Transposing the N and NSs CDSs on S segment generated a virus with attenuated growth characteristics in mammalian and mosquito cells lines. Changes were observed for N and NSs at both the transcriptional and translation level.

- Unlike with rMP12, a prolonged persistent infection of C6/36 and U4.4 cells with rMP12:S-Swap virus was not possible due to the cytotoxic effects of replication. Of note was the hyper expression of NSs. However, even with the increased levels of protein, intranuclear NSs filaments were not observed in infected mosquito cells.

- A strand-specific qRT-PCR assay was designed, capable of determining ratios of genomic to antigenomic strands for S and M segments. Significant differences were described in the ratios of genomic to antigenomic polarity S segment genome strands packaged into progeny virions when samples of rMP12 or rMP12:S-Swap virus infected cells were compared

7 Development of minireplicon and reverse genetics systems in mosquito cells

7.1 Introduction

Minireplicon assays are a powerful tool to analyse viral replication and transcriptional activities. They function in a similar way to the previously described reverse genetics rescue system, except viral protein CDSs are replaced with those for reporter genes (Elliott 2012). This allows for assessment of viral protein activity levels, as well as evaluation the regulatory elements involved in controlling replication and transcription processes (Ikegami et al. 2005; Gauliard et al. 2006). Two different systems have been described to generate the RNA transcripts and express the proteins required in the assay. T7RNAP alone can be utilised to generate RNA acting as both the synthetic genomes and mRNA transcripts from which proteins can be expressed. T7RNAP transcripts are neither 5' capped or 3' poly-adenylated and therefore IRES elements are used to enhance translation. These systems require that the T7RNAP be supplied *in trans*, preferentially from a constitutively expressing cells such as the BSR-T7/5 cell line (Buchholz et al. 1999). A second system uses cellular RNA-polymerase I promoters to transcribe RNA genome copies. Unlike with the T7RNAP system, minireplicon assays using Pol-1 require the use of helper plasmids. These plasmids can either be T7RNAP based, or use RNA polymerase-II promoters to transcribe capped and poly-A tailed mRNA transcripts to express the N and L proteins (Bouloy & Weber 2010). For RVFV minireplicon and rescue based assays, both T7RNAP and Pol I/II based systems have been described, and been shown to have similar efficiencies (Ikegami et al. 2006; Gerrard et al. 2007; Habjan et al. 2008; Billecocq et al. 2008)

Published research to date investigating RVFV has focused on the development of both rescue and minireplicon systems in mammalian cell lines. The relative activities and functions of viral proteins, and the relative strengths of the genome segment UTR promoter sequences remain undetermined in mosquito cells. Variances in protein expression levels and viral yields between mosquito and mammalian cells have been described here in previous results. Possible theories proposed to explain these differences included disparities in N and/or L activity in the cell lines, or cell-specific variations in responses to the regulatory sequences within the UTRs. The development of a minireplicon

system functional in mosquito cell lines could be used to investigate these factors. It could also be used as the basis for a reverse genetics system in these cells. In mosquito cells supplied with a source of T7RNAP *in trans*, the same pTVT7- based plasmids used in BSR-T7/5 cells could utilised. However, expression of N and L protein in mosquito cells would require different promoters and IRES elements to those used in the established mammalian cell system. In this chapter I therefore investigated several invertebrate-specific promoters which could be utilised for viral protein expression. The effectiveness of an invertebrate-specific IRES element in enhancing protein expression was also examined.

It was also hypothesised that if viral coding sequences were codon optimised for *Aedes* species, it may result in an increase in the protein expression levels from transfected plasmids. Codon usage bias relates to differences in the frequency of specific non-synonymous codons utilised between species, and is related to the relative abundance of specific tRNA species (Behura & Severson 2013). Altering CDS codon biases in invertebrate genomes has previously been shown to affect the expression level of that protein (Carlini & Stephan 2003). As increased expression levels could boost efficiencies of both minireplicon and rescue attempts, the effects viral proteins of codon optimised for mosquito cell expression were also investigated.

7.2 Aims

The aims of this section were to firstly develop an efficient minireplicon assay for MP12 which would be functional in the range mosquito cell lines available. This assay would then be used to investigate the activity of both N and L proteins in mosquito and mammalian cells., and to examine UTR promoter strengths. Codon optimised N and L proteins would be used to investigate whether the different protein expression level altered minireplicon activity levels. The second aim was to use the results from the minireplicon experiments to develop a reverse genetics system for mosquito cells in which rMP12 and recombinants thereof could be rescued .

7.3 Results

7.3.1 Evaluation of promoters and IRES elements in mosquito cells

Three candidates were identified to drive expression of viral proteins in mosquito cells. The pIB plasmids have been previously utilised by our research group for mosquito cell expression of BUNV proteins (Kohl et al. 2004). Plasmids containing the pAC actin promoter have been used to express proteins in *D. melanogaster* cells, and the highly conserved nature of the actin gene in invertebrate species made it a candidate here (Gunning et al. 1984; Firtel 1981). pSTI based plasmids contained a specific *A. aegypti* polyubiquitin promoter known to function in C6/36 cells (Anderson et al. 2010), although the expression potential of this promoter in the U4.4 and Ae cell lines required experimental validation. The mammalian promoter used in phRL based plasmids (pCMV) was used as a control (Promega, GenBank accession#: AF362549). The origins of the different promoters are described in Table 7-1.

GFP was used as a reporter gene to evaluate the protein expression level from the promoters described above. The eGFP CDS was subcloned into plasmids under control of the four promoters, and C6/36, U4.4, and Ae cells transfected with 1 μg of plasmid. GFP expression levels were assessed over 96 hours using fluorescent microscopy (Figure 7-1). In all cell lines the highest GFP expression levels were observed in cells transfected with pSTI-eGFP. GFP expression at 24 hours post transfection (h p.t.) was greater than that observed in both pIB-eGFP and pAC-eGFP transfected cells at 96 h p.t.. GFP expression with pSTI-eGFP was also at a higher level in C6/36 compared to U4.4 and Ae cells. GFP expression from pAC-eGFP was observable in C6/36 cells, although levels were minimal in U4.4 and Ae cells. The expression level from pIB-eGFP transfected cells was minimal in all cell lines. The mammalian promoter used in pCMV-eGFP appeared to be non-functional in mosquito cells.

An invertebrate-specific IRES element was required to enhance protein expression from the T7RNAP transcripts, with the Rhopalosiphum padi virus (RhPV) 5' IRES element

Table 7-1: Origin of the promoter sequences used for mosquito cell protein expression

Promoter	Plasmid	Details	Source
OpIE2	pIB	Baculovirus immediate early promoter OpIE2 from Orgyia pseudotsugata multicapsid nuclear polyhedrosis virus.	RME lab
Actin 5C	pAC	Proximal promoter of the *Drosophilia melanogaster* actin 5C gene.	Plasmids supplied by J. van Mierlo, Radboud University (van Cleef et al. 2011)
Polyubiquitin	pSTI	Promoter of the *Aedes* aegypti polyubiquitin gene.	Plasmid supplied by Prof. Kevin Myles, Virginia Tech (Anderson et al. 2010)
CMV	phRL	CMV immediate early enhancer/promoter	Promega (NCBI accession# AF362549)

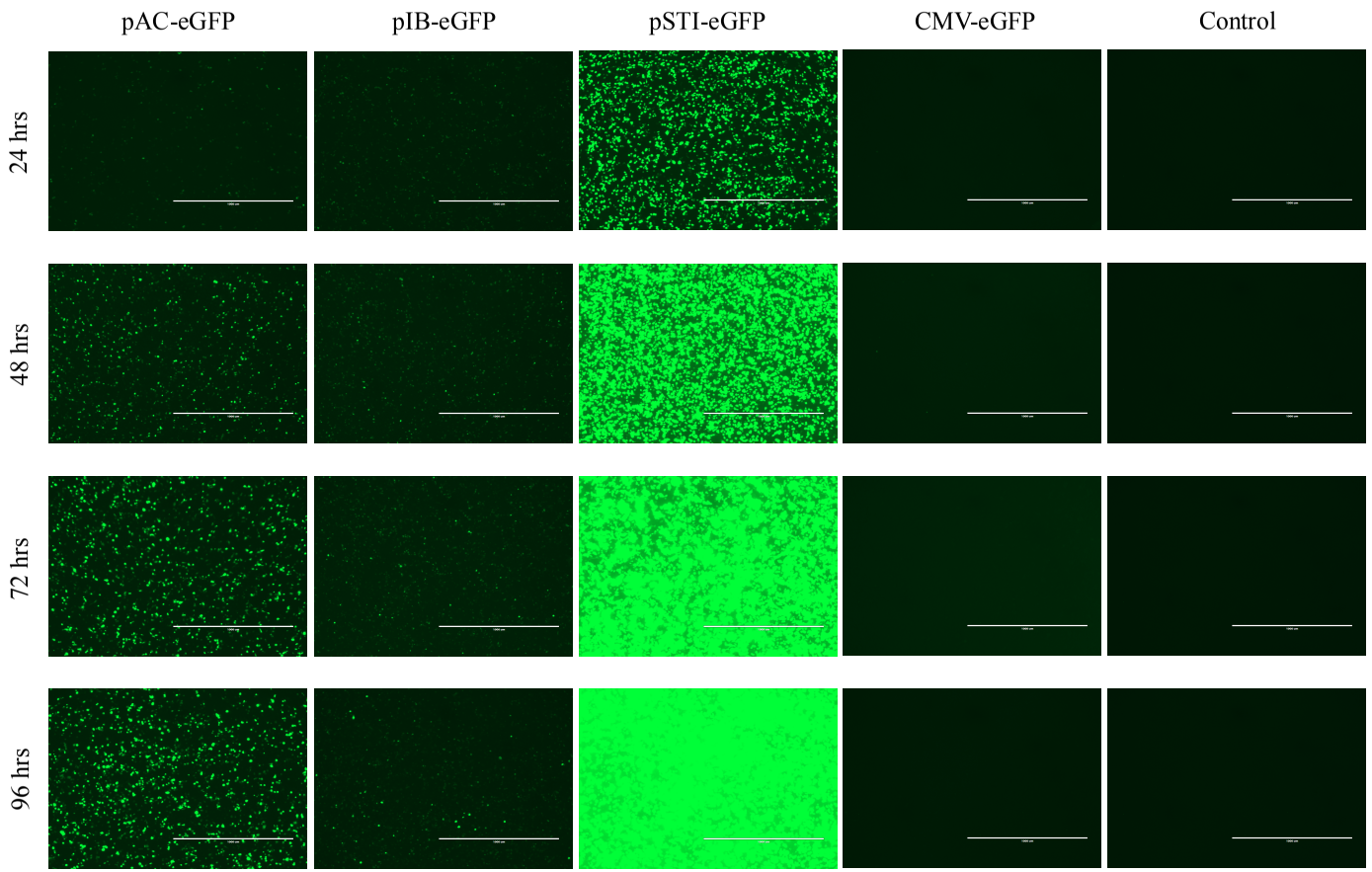

Figure7-1: Evaluation of protein expression levels in mosquito cell lines using invertebrate-specific promoter elements
C6/36, U4.4, and Ae cells were transfected with 1 µg of pAC-eGFP, pIB-eGFP, pSTI-eGFP, or pCMV-eGFP plasmids. GFP expression was recorded at 24, 48, 72, and 96 h p.t.. Shown here are the images recorded for (A) C6/36,(B) U4.4, and (C) Ae cell lines. All images taken at x10 magnification.

(A) C6/36 cells

Control
CMV-eGFP
pSTI-eGFP
pIB-eGFP
pAC-eGFP
24 hrs
48 hrs
72 hrs
96 hrs
(B) U4.4 cells

Control
CMV-eGFP
pSTI-eGFP
pIB-eGFP
pAC-eGFP
24 hrs
48 hrs
72 hrs
96 hrs
(C) Ae cells

contained in pST-IRES polyUB hyg-GFP DCR2 HA N-tag plasmid used (Anderson et al. 2010). To investigate functionality in all the cell lines a plasmid was constructed from pST-IRES polyUB hyg -GFP DCR2 HA N-tag (Figure 7-2.A) in which the first and second CDSs were changed to those for TagRFP and eGFP CDSs respectively, yielding pSTI-TagRFP-RhPV-eGFP (Figure 7-2.B). C6/36, U4.4, and Ae cells were transfected with 1 µg of this plasmid and expression of both TagRFP and eGFP assessed at 48 h p.t. using fluorescent microscopy (Figure 7-3). The expression level of both proteins was again greatest in C6/36 cells although the IRES was functional in all three mosquito cell lines, with the overwhelming majority of cells co-expressing both proteins.

These results established C6/36 cells as the best candidate for rescue attempts in mosquito cells. Transfection efficiency was consistently higher in these cells compared to U4.4 and Ae cells, and previous results described here have noted the increased permissiveness of viral replication in this cell line. Transfection efficiencies with the plasmids varied between the mosquito cell lines, from C6/36 to U4.4 to Ae cells (highest to lowest). However, even after optimisation of transfection procedures the maximum transfection rate (based on GFP expression) in mosquito cells was limited to between 30-50%. The RhPV IRES was shown to be functional in all mosquito cell lines meaning it could be used to enhance translation from the T7RNAP transcripts.

7.3.2 Codon optimisation of MP12 viral proteins

Using the reference MP12 genome segments in GenBank (NCBI accession numbers: L segment – DQ375404; M segment – DQ380208; S segment – DQ380154) coding sequences for the RdRp (L segment), M polyprotein (M segment), and N and NSs proteins (S segment) were codon optimised for *A. albopictus* using the Entelechon web software (www.Entelchon.com) in conjunction with the codon usage table at www.kazusa.or.jp. The UTR and IGR sequences remained unchanged. DNA sequences containing the codon optimised CDSs for the three genome segments were designed *in silico* to be flanked 5' and 3' in the antigenomic sense by the T7 promoter (with a single G +1 upstream) and the hepatitis D ribozyme respectively. Plasmids were produced by GenScript (GenScript, USA) and supplied in a pUC19 backbone. However, there were concerns regarding the pUC19 plasmid being experimentally unverified in viral rescue attempts. Therefore the

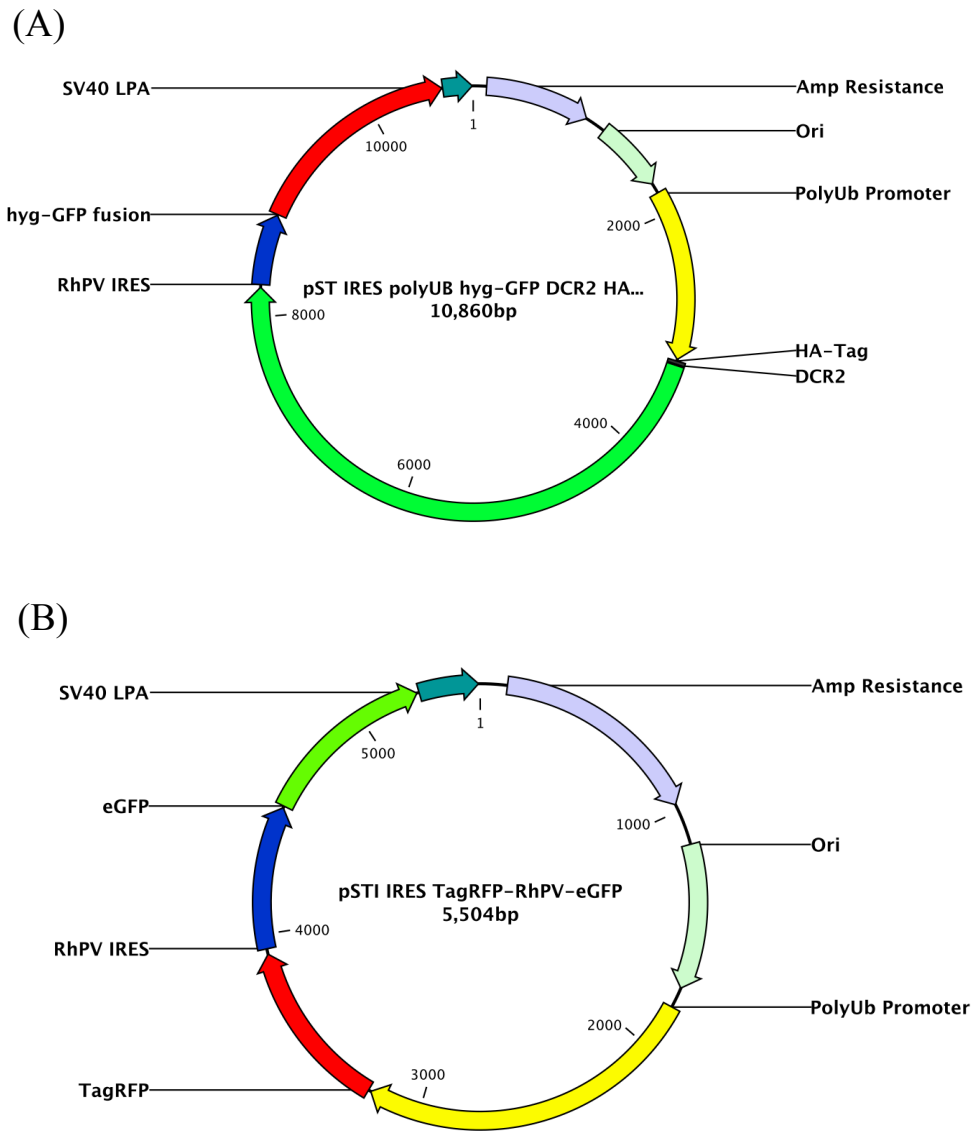

Figure 7-2: Schematic representation of the plasmids employed in assay development
Represented is the (A) original plasmid pST IRES polyUB hyg-GFP DCR2 HA N-Tag. This contains the *A. aegypti* polyubiquitin promoter which transcribes a bicistronic message containing CDS for Dcr-2 and a CDS for hygromycin resistance protein fused with GFP. Translation from the second coding sequence in enhanced by the presence of the RhPV IRES element. This plasmid was used to create (B) pSTI TagRFP-RhPV-eGFP in which the first and second CDS have been replaced with those for TagRFP and eGFP respectively. This was to evaluate the effectiveness of the IRES in the mosquito cell lines.

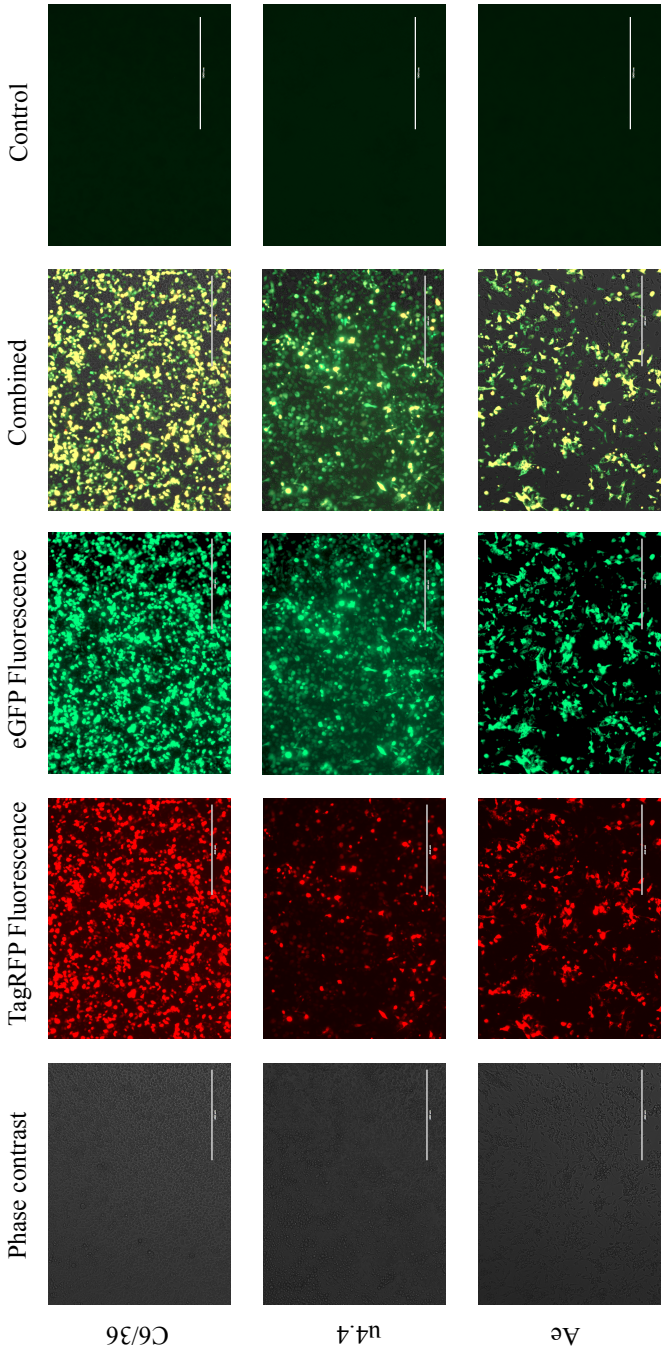

Figure7-3: Evaluation of the RhPV IRES element in mosquito cells
A plasmid (pSTI-TagRFP-RhPV-eGFP) was constructed in which the polyubiquitin promoter was used to generate a bicistronic mRNA coding for TagRFP in the first ORF and eGFP in the second ORF. The RhPV IRES element was used to enhance expression of the second ORF. C6/36, U4.4, and Ae cells were transfected with 1 µg of plasmid and TagRFP and eGFP expression examined 48 h p.t.. Combined images were used to determine the-functionality if the IRES. The control images were examined using UV at the TagRFP excitation wavelength. All images were taken at x10 magnification.

three genome segments were further subcloned into the classical pTVT7 plasmid used in standard rescue attempts. These three plasmids were termed pTVT7-GSco, pTVT7-GMco, and pTVT7-GLco for S, M, and L segment respectively.

7.3.3 Minireplicon development in mosquito cells

A minireplicon system in mosquito cells has previously been described for BUNV, although this was restricted to C6/36 cells (Kohl et al. 2004). Constituent T7RNAP expression was driven by the OpIE2 promoter, and selection of the plasmid maintained in cell culture by the use of the blasticidin-resistance gene. Reporter gene activity in this system was reduced approximately 1,000-fold compared to a comparative assay in mammalian cells. Given the disparity in activity between polyubiquitin and OpIE2 promoters demonstrated in Figure 7-1 it was anticipated that using the former in a minireplicon assay would result in increased reporter protein expression levels. Due to the poor transfection efficiency of mosquito cells, a cell line constituently expressing T7RNAP was considered the preferred option to supply the polymerase for the assays. This would ensure a high percentage of cells were expressing the T7RNAP. Attempts were made to generate T7RNAP constituently expressing C6/36 and U4.4 cell lines using a modified pSTI-IRES polyUB hyg-GFP Dcr-2 NTag plasmid in which the Dcr-2 CDS was replaced with that for T7RNAP, yielding pSTI-T7RNAP IRES H/G plasmid. C6/36 and U4.4 cells were transfected with 1 μg of plasmid, and eGFP expression monitored over 5 consecutive passages under selection pressure of hygromycin B (Figure 7-4). Whilst extensive GFP expression was apparent at p1 in both cell lines it rapidly diminished with continued passage. At passage 5, GFP expression was only minimally apparent in C6/36 cells, and not at all in U4.4 cells. Further issues arose concerning cell viability and growth rates when exposed to hygromycin B at any concentration (data not shown). Therefore attempts to create mosquito cells constitutive expressing T7RNAP were discontinued, and the focus moved to performing minireplicon assays in cells transiently expressing the polymerase.

For bunyavirus based minireplicon assays, N and L are both necessary and sufficient for replication and transcription (Kohl et al. 2004); Ikegami:2005hd}. The codon optimised N and L proteins were initially evaluated in the established BSR-T7/5 cell minireplicon

Figure 7-4: Generation of mosquito cell lines constitutively expressing T7RNAP
C6/36 and U4.4 cells were transfected with 1 µg of plasmid containing CDSs for T7 polymerase and the hygromycin B resistance gene fused with eGFP (pST-T7pol etc.). To maintain the plasmid between passages the cells were grown in standard cell culture medium containing 200 mg/mg hygromycin B. Prior to each cell split (4-6 days) GFP expression level was assessed using fluorescent microscopy (passages p1-p5). All images were taken at 10x magnification.

system alongside the parental N and L proteins to assess their relative activities. Assays were performed using an M segment reporter plasmid, containing the *Renilla* luciferase reporter gene in antigenomic orientation (non-coding) between the authentic antigenome 5' (21 nt) and 3' (3615 nt) UTRs, yielding pTVT7-MRENMg. In this orientation the *Renilla* luciferase CDS would be in the negative-sense in the T7RNAP transcripts, and activity would only be detected if functional N and L proteins are present to transcribe the RNA and generate the mRNA. Briefly, BSR-T7/5 cells were transfected with a combination of either pTM1-L or pTM1-Lco, and pTM1-N or pTM1-Nco (0.5 μg or 0.1 μg). Each sample was also transfected with the 1 μg of pTVT7-MRENMg reporter plasmid and 0.05 μg of pTM1-FFLuc transfection control plasmid. Different amounts of L were evaluated as minireplicon activity levels have previously been shown to be affected by concentration of the protein (Benjamin Brennan - personal communication). Results showed that the codon optimised L (Lco) in the minireplicon context increased reporter activity over that determined for the parental L protein. The opposite was true with codon optimized N (Nco) where significant decreases in reporter activity over control were observed. Lower amounts of L protein resulted in reduced activity of the reporter only in samples which utilised the parental protein (Figure 7-5). Differences in observed reporter activity were thought to be due to variations in the intracellular L:N:RNA ratios.

Initial efforts at developing minireplicon assays in mosquito cells attempted to emulate the mammalian system as closely as possible. pTM1 plasmids contain the encephalomyocarditis virus (EMCV) IRES to enhance protein expression from T7RNAP transcripts in mammalian cell lines (Fuerst et al. 1986). However, the EMCV IRES has been shown to be non-functional in mosquito cells (Kohl et al. 1999). The EMCV IRES in pTM1 plasmid was therefore replaced with the RhPV IRES, yielding a plasmid termed pTM1-R. Using this backbone, viral protein CDSs were subcloned in to enhance the expression of N, Nco, L, Lco, and FFLuc in the mosquito cells. C6/36, U4.4, and Ae cells were transfected with the same combinations of N and L (parental and codon optimised) proteins as with the BSR-T7/5 cells, along with pSTI-IRES T7RNAP IRES H/G to express T7RNAP and pTM1-R-FFLuc as the transfection control. Expression levels of the reporter proteins were minimal in both U4.4 and Ae cells, with very low values generated for both *Renilla* and firefly luciferase light units. These low values made resolving differences in

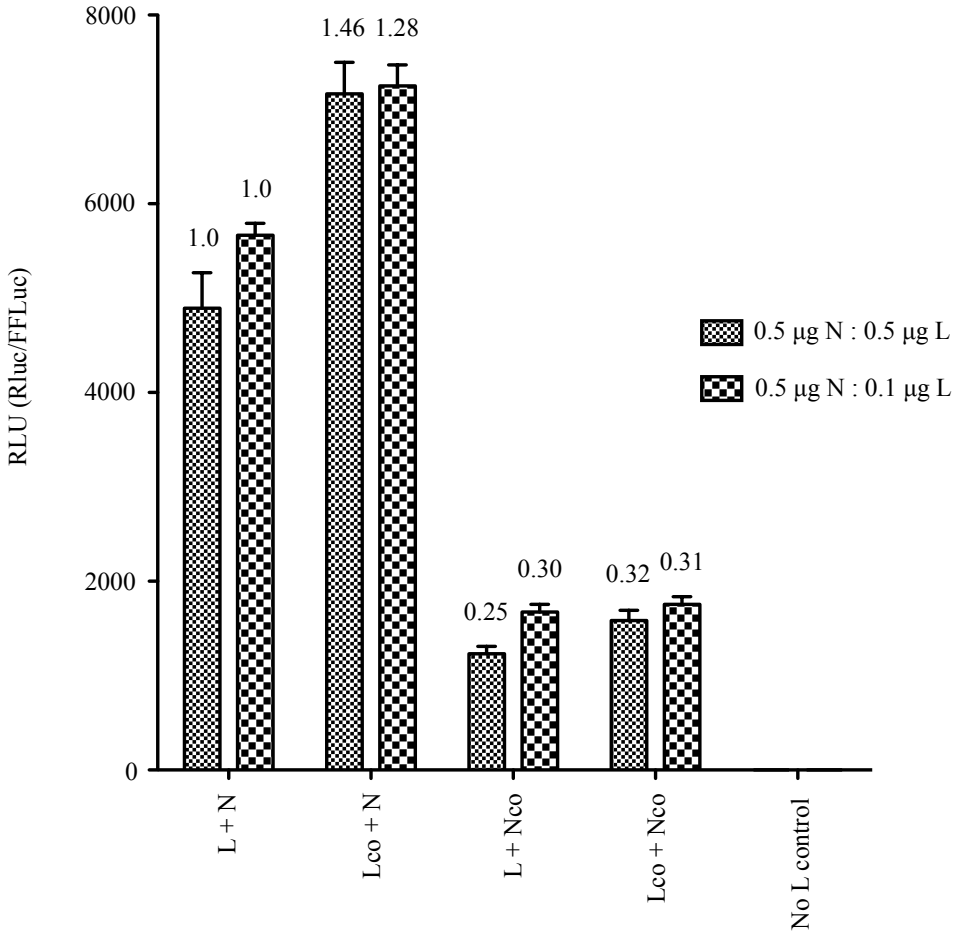

Figure 7-5: Relative activities of the MP12 parental and codon optimised N and L proteins in a BSR-T7/5 cell based minireplicon assay.

BSR-T7/5 cells were transfected with: pTM1-L + pTM1-N (L + N); pTM1-Lco + pTM1-N (Lco + N); pTM1-L + pTM1-Nco (L + Nco); or pTM1-Lco and pTM1-Nco (Lco + Nco) with the indicated amount. Cells were also transfected at the same time with 1 µg of pTVT7-MRENMg and 0.05 µg of pTM1-FFLuc. The control sample was transfected with no source of L protein. Samples were set up in triplicate. Cells were harvested at 24 h p.t. and reporter activities determined. Results are presented as relative light units (RLU) representing the ratio of RLuc activity to FFLuc activity. Number above bars represent the fold increase in activity over the parental N + L sample (L + N). Error bars represent standard deviation.

reporter activity levels difficult in Ae and U4.4 cells, with levels in both only marginally higher than background for several samples. However, a 1.94-fold increase in minireplicon activity was observed for the N and Lco combination in U4.4 cells. In C6/36 cells reporter activity was above background levels in all experimental samples, and a similar 1.87-fold increase in activity was observed in the Lco and N combination over the parental control (Figure 7-6). In all mosquito cell lines evaluated, raw light unit values for both *Renilla* and firefly luciferase were on average reduced approximately 100 to 1000-fold when compared to those in BSR-T7/5 cells. Differences in reporter activity were also observed between the mosquito cell lines, possibly a result of the different transfection efficiencies noted earlier and corroborated here by monitoring of GFP expression from the pSTI-T7RNAP IRES H/G plasmid. Reduced expression could also be a result of the lower T7RNAP activity at 28°C compared to 37°C (Kohl et al. 2004).

As the polyubiquitin promoter was shown to drive high levels of protein expression in mosquito cells, it was decided to use pSTI-based plasmids to express all proteins for the mosquito minireplicon assay. Plasmids generated were pSTI -N, -Nco, -L, -Lco, and -FFLuc. Use of the polyubiquitin promoter resulted in approximate 10-fold increases in both the *Renilla* and firefly luciferase light unit values over those generated by the pTM1-R-based plasmids. The differences in reporter activity levels between the combinations of N and L proteins were similar in C6/36 cells compared to the pTM1-R based minireplicon assay (Figure 7-7). The combination of N with Lco resulted in a 2.22-fold increase in activity, and the combination of Nco with L or Lco resulted in 0.25- and 0.45-fold decreases respectively over parental N and L control. Both U4.4 and Ae cells demonstrated similar increase in reporter activity for the N and Lco combination over parental control samples (2.05- and 1.52-fold increases respectively). The use of Nco in the minireplicon context similarly resulted in a decrease in activity over N and L controls in these two cell lines. However, even with the improved expression levels using the polyubiquitin promoter the overall expression levels or reporter proteins in Ae cells remained significantly reduced compared to C6/36 and U4.4 cells.

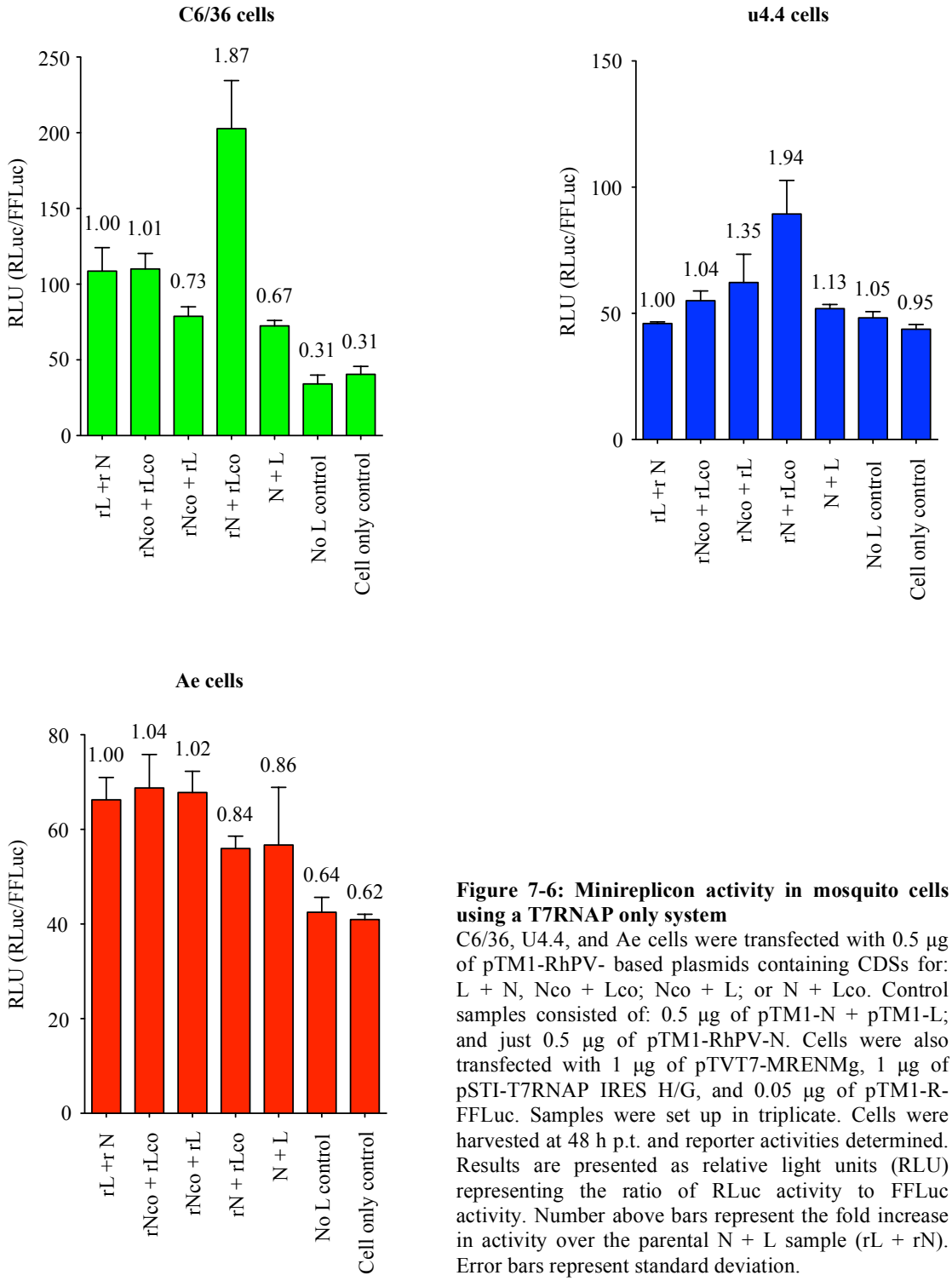

Figure 7-6: Minireplicon activity in mosquito cells using a T7RNAP only system
C6/36, U4.4, and Ae cells were transfected with 0.5 µg of pTM1-RhPV- based plasmids containing CDSs for: L + N, Nco + Lco; Nco + L; or N + Lco. Control samples consisted of: 0.5 µg of pTM1-N + pTM1-L; and just 0.5 µg of pTM1-RhPV-N. Cells were also transfected with 1 µg of pTVT7-MRENMg, 1 µg of pSTI-T7RNAP IRES H/G, and 0.05 µg of pTM1-R-FFLuc. Samples were set up in triplicate. Cells were harvested at 48 h p.t. and reporter activities determined. Results are presented as relative light units (RLU) representing the ratio of RLuc activity to FFLuc activity. Number above bars represent the fold increase in activity over the parental N + L sample (rL + rN). Error bars represent standard deviation.

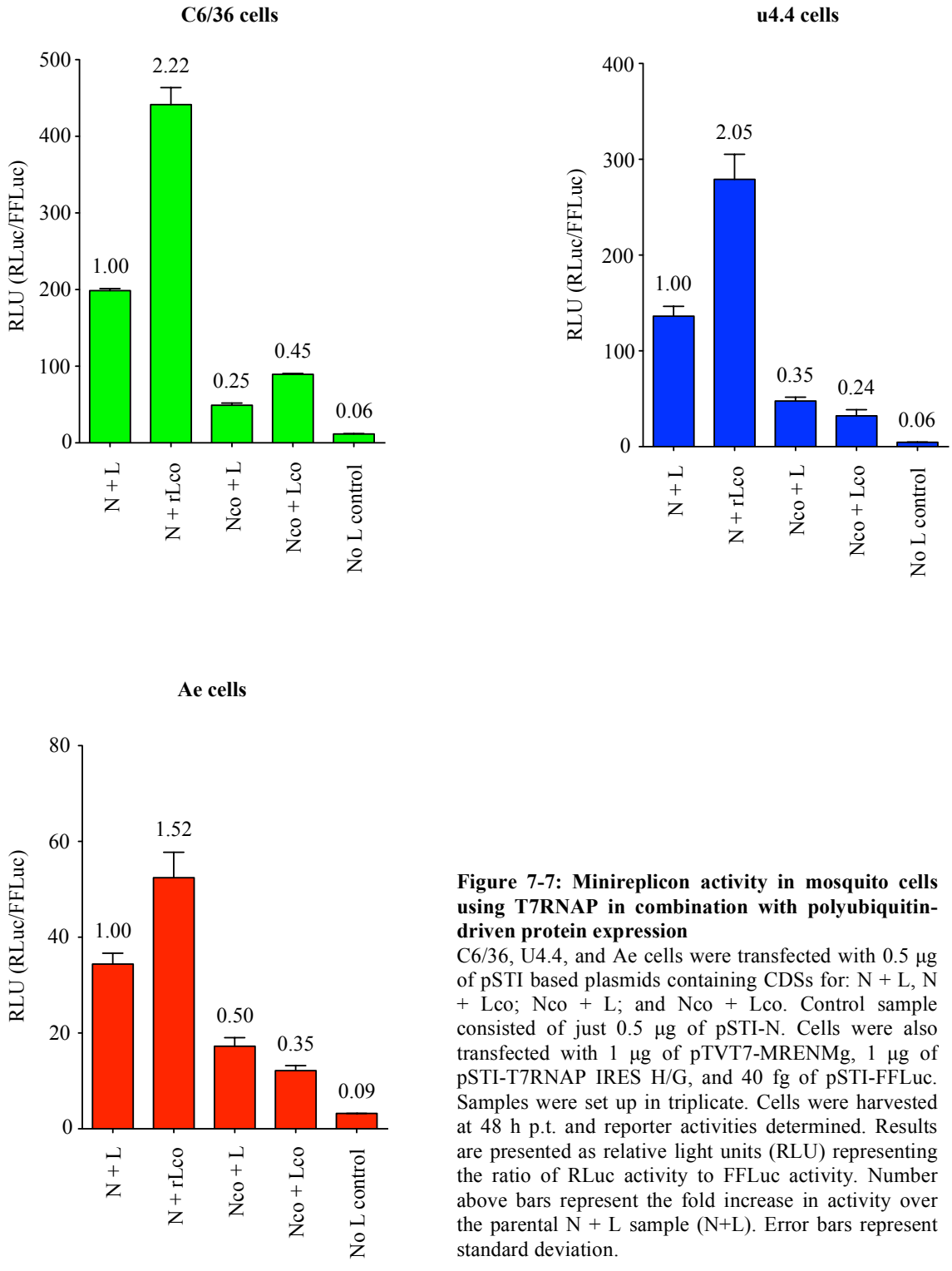

Figure 7-7: Minireplicon activity in mosquito cells using T7RNAP in combination with polyubiquitin-driven protein expression

C6/36, U4.4, and Ae cells were transfected with 0.5 µg of pSTI based plasmids containing CDSs for: N + L, N + Lco; Nco + L; and Nco + Lco. Control sample consisted of just 0.5 µg of pSTI-N. Cells were also transfected with 1 µg of pTVT7-MRENMg, 1 µg of pSTI-T7RNAP IRES H/G, and 40 fg of pSTI-FFLuc. Samples were set up in triplicate. Cells were harvested at 48 h p.t. and reporter activities determined. Results are presented as relative light units (RLU) representing the ratio of RLuc activity to FFLuc activity. Number above bars represent the fold increase in activity over the parental N + L sample (N+L). Error bars represent standard deviation.

7.3.4 Effects of NSs on minireplicon activity

NSs expression has been shown to have modulatory effects on minireplicon behavior in mammalian cells for several bunyaviruses. It was shown to be inhibitory in a BUNV minireplicon assay, and described as both inhibitory (Brennan et al. 2011) and facilitative (Ikegami *et al.*, 2005) in a RVFV minireplicon. When examined in the mosquito cell-based BUNV minireplicon assay no effects on reporter activity were noted when cells were supplemented with BUNV NSs (Kohl et al. 2004). To investigate if RVFV NSs affects reporter activity in mosquito cell, C6/36 and U4.4 cells were transfected with different amounts of pSTI-NSs. These cell lines were chosen as previous described results demonstrated good minireplicon activity, and also because they exhibit differential NSs expression profiles when infected with MP12. Briefly, cells lines were assessed using the minireplicon system described in 7.3.3, namely pSTI- based N and Lco expression with pTVT7-MRENMg plasmid used as the reporter. Cells were also transfected with 5, 10, 50, 100, 250, and 500 μg of pSTI-NSs, and transfection mixes made up to identical DNA concentrations with an empty pSTI- plasmid. Results in C6/36 cells demonstrated 1.41- and 1.38-fold increases in reporter activity with 250 and 500 μg of pSTI-NSs respectively. No significant pattern representing increase or decrease in reporter activity was observed in U4.4 cells (Figure 7-8). This suggested that small concentrations of NSs protein may aid viral replication and transcriptional activity within infected cells, although any increase and decrease in reporter activity was insignificant compared to those described for RVFV minireplicons in mammalian cells.

7.3.5 UTR promoter strength differences in mammalian and mosquito cells

The UTRs are thought to regulate the replication and transcription potential for the individual RVFV genome segments (Bouloy & Weber 2010). The 3' genomic UTR of L and M segment is responsible for promoting both antigenomic strand replication and mRNA transcription. On the ambisense S segment the genome 3' UTR is responsible for both genomic strand replication and transcription of N mRNA, whereas the antigenome 3' UTR is responsible for promoting transcription of NSs mRNA. Previous studies have investigated the relative abilities of genomic UTR promoters using a RVFV minireplicon in mammalian cells (Gauliard et al. 2006). Using the minireplicon developed here the

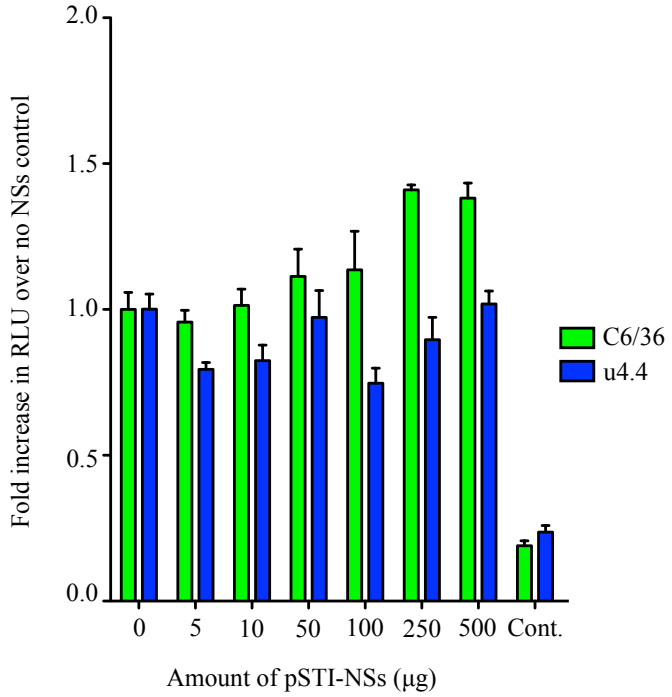

Figure 7-8: Effects of NSs on minireplicon activity in mosquito cells
C6/36 and U4.4 cells were transfected with: pSTI-N and pSTI-Lco, (both 0.5 µg); 1 µg of pTVT7-MRENMg; 1 µg of pSTI-T7RNAP IRES H/G, and 40 fg of pSTI-FFLuc. Included in the transfection mix was pSTI-NSs at 5, 10, 50, 100, 250, 500 µg. Amounts of DNA in the transfection mix were kept constant with empty pSTI plasmid. Control sample (Cont.) contained no pSTI-L or pSTI-NSs. Samples were set up in triplicate. Cells were harvested at 48 h p.t. and reporter activities determined. Results are presented at the fold difference in relative light units (RLuc/FFLuc signals) compared to the activity determined for the sample contained no pSTI-NSs.

promotional activities of segment-specific UTR sequences were examined in both BSR-T7/5 and mosquito cells.

The *Renilla* luciferase reporter gene in antigenome orientation was subcloned between the genomic 5' (110 and 38 nt) and 3' (6298 and 1657 nt) UTRs of the reference MP12 L and S segment respectively, yielding pTVT7-LRENLg and pTVT7-SRENSg. To evaluate the antigenome 3' UTR promoter of S segment the *Renilla* luciferase reporter gene was cloned between the antigenomic 5' (1657 nt) and 3' (38 nt) UTRs of S segment, yielding pTVT7-SRENSag. BSR-T7/5 cells were transfected with pTM1-L, pTM1-N and one of the minireplicon reporter plasmids. Luciferase activity levels were assessed after 24 hours incubation. Mosquito cells were transfected with pSTI-N, pSTI-Lco, and pSTI-T7RNAP IRES H/G and one of the minireplicon reporter plasmids. Luciferase activity levels were assessed after 48 hours incubation. Results for transfected BST-T7/5 cells demonstrated that the relative strengths of the MP12 UTR promoters were M genomic (Mg) > S genomic (Sg) > L genomic (Lg) > S antigenomic (Sag) (highest to lowest) (Figure 7-9). Promoter strengths were similar to this in U4.4 cells, but in C6/36 and Ae cells the pattern altered to Mg > Lg > Sg > Sag (highest to lowest) (Figure 7-10). However, in all mosquito cell lines the relative strengths of both the Lg and Sg promoters were very similar, with Mg significantly stronger and Sag significantly weaker. The relative differences between segment reporter activity were significantly larger in BSR-T7/5 cells compared to those in the mosquito cells. Whilst this does represent differences in UTR promoter strength between the mammalian and mosquito cell lines, the differences in T7RNAP activity at 28°C and 37°C must also be considered.

7.3.6 Rescue attempts of codon optimised MP12 in BSR-T7/5 cells

Attempts were made to rescue codon optimised MP12 in BSR-T7/5 cells. Briefly, cells were transfected with pTM1-N and pTM1-L (0.5 μg of each), and 1 μg of each of the pTVT7 genome rescue plasmids. Attempts were made to rescue an rMP12 recombinant with: three codon optimised genome segments (pTVT7-GLco, pTVT7-GMco, and pTVT7-GSco); two codon optimised segments and one standard rMP12 segment; and one codon optimised segment with two standard rMP12 segments. Success of the rescue was based on both visible CPE in the BSR-T7/5 cells, and visible CPE, titreable virus, and detection of

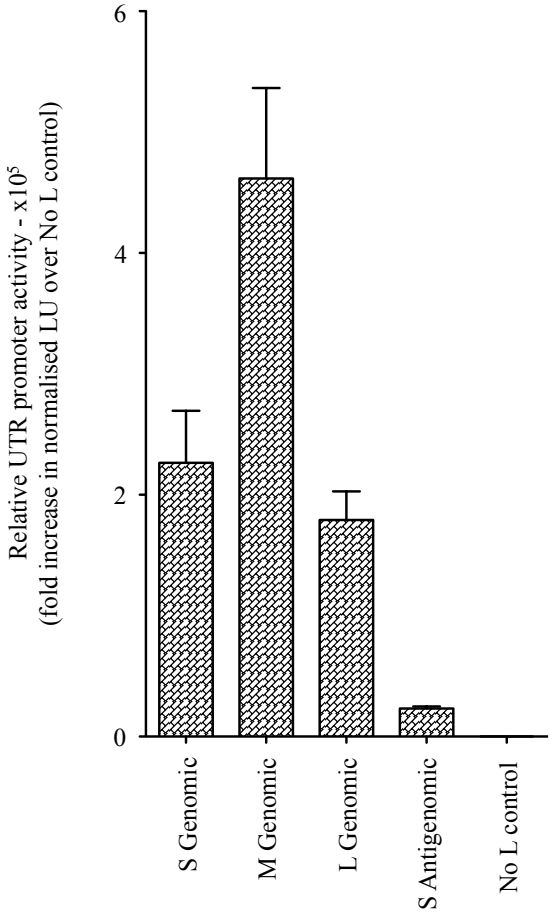

Figure 7-9: Analysis of MP12 UTR promoter strengths in BSR-T7/5 cells
BSR-T7/5 cells were transfected with pTM1-N and pTM1-L (both 0.5 μg); 1 μg of either pTVT7-SRENSg (S Genomic), pTVT7-MRENMg (M Genomic), pTVT7-LRENL (L Genomic), and pTVT7SRENSag (S Antigenomic). Cells were also transfected with 0.05 μg of pTM1-FFLuc. The control samples contained no pTM1-L. Samples were set up in triplicate. Cells were harvested at 24 h p.t. and reporter activities determined. Results are presented at the fold difference in relative light units (RLuc/FFLuc signals) compared to the activity determined for the no L control.

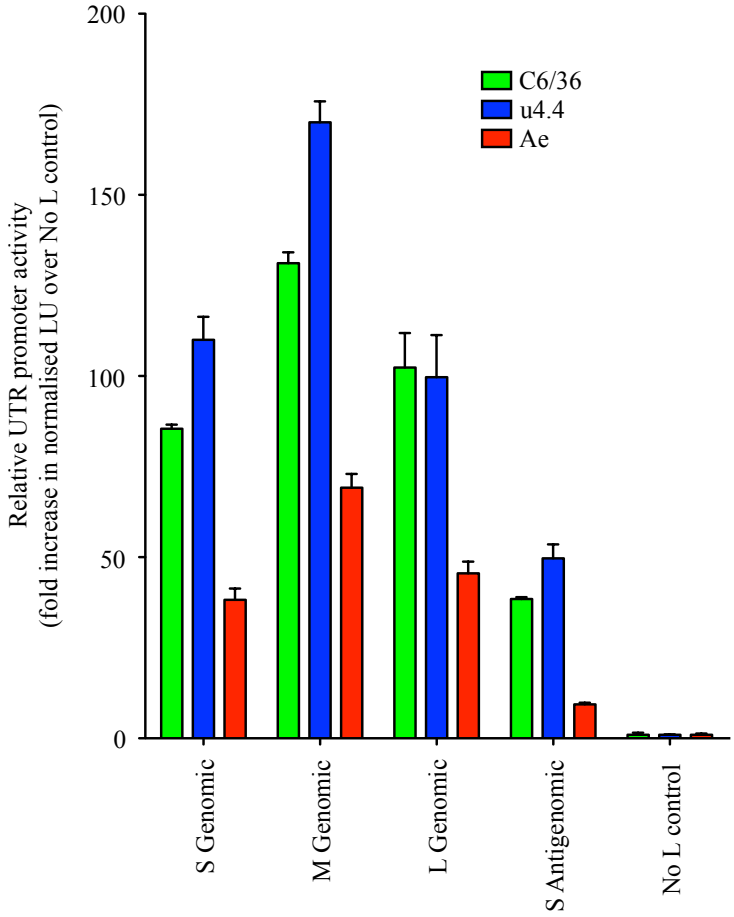

Figure 7-10: Analysis of MP12 UTR promoter strengths in mosquito cell lines
C6/36, U4.4 and Ae cells were transfected with pSTI-N and pSTI-Lco (both 0.5 µg); 1 µg of either pTVT7-SRENSg (S Genomic), pTVT7-MRENMg (M Genomic), pTVT7-LRENL (L Genomic), and pTVT7SRENSag (S Antigenomic). Cells were also transfected with 1 µg of pSTI-IRES polyUB hyg-GFP T7pol and 40 fg of pSTI-FFLuc. The control samples contained no pSTI-Lco. Samples were set up in triplicate. Cells were harvested at 48 h p.t. and reporter activities determined. Results are presented at the fold difference in relative light units (RLuc/FFLuc signals) compared to the activity determined for the no L control.

N and NSs in BHK-21 cells infected with any rescued virus. Despite numerous attempts the only rescue of non-standard rMP12 that was successful was a combination of pTVT7-GL, pTVT7-GM and pTVT7-GSco, yielding a mutant termed rMP12:COGS.

To characterise rMP12:COGS infection BHK-21, C6/36, U4.4, and Ae cells were infected at MOI 5, and growth of the virus investigated over 48 hours. Growth of rMP12:COGS in BHK-21 cells was similar to rMP12, with a yield of $5x10^7$ pfu/ml determined at 48 h p.i.. (Figure 7-11.A). However, no virus replication was detected in any of the mosquito cells lines. Analysis of protein production demonstrated N and NSs expression in BHK-21 cells, but no expression of either protein in mosquito cells (Figure 7-11.B). Minireplicon analysis had demonstrated the reduced activity of Nco compared to parental N protein, but expression of reporter proteins was still noted in both the mammalian (BSR-T7/5) and mosquito cells. A difference in replication potential between the mammalian and mosquito cells examined here was therefore unexpected.

7.3.7 Rescue attempts of MP12 in mosquito cells

Initially it was aimed to rescue both MP12 and the codon optimised recombinant viruses in the mosquito cell lines. However, after the non-growth of rMP12:COGS in mosquito cells, efforts were concentrated on the MP12 rescue attempts only. As a significant increase in reporter activity was noted when using Lco in minireplicon assays, both versions of L protein were in the rescue attempts. Unlike in BSR-T7/5 cell rescues there was no overt CPE or cell death associated with viral replication in mosquito cells. Therefore confirmation of a successful rescue was based on generation of titreable virus in BHK-21 cells, and/or detection of N and NSs protein in BHK-21 cells and mosquito cells infected with any rescued virus.

Numerous experimental conditions were used. Briefly, C6/36, U4.4, and Ae cells were transfected with 1 μg pSTI-T7RNAP IRES H/G 24 hours prior to rescue plasmid transfection. Rescues were attempted with: three plasmids - pTVT7-GS, pTVT7-GM, and pTVT7-GL (1 or 2 μg of each); five plasmids - as with the three plasmid rescue but with either pSTI-N and pSTI-L, or pSTI-N and pSTI-Lco (0.5, 1, or 2 μg of each); and six

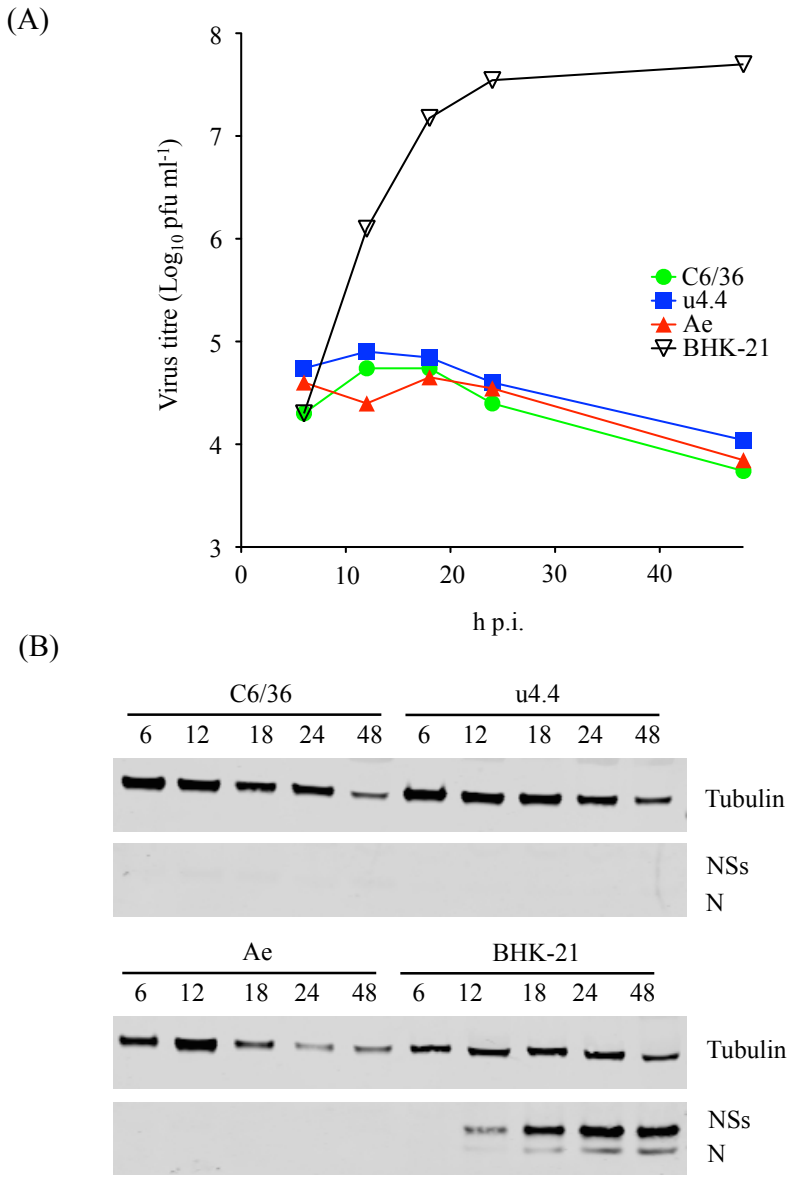

Figure 7-11: Analysis of rMP12:COGS growth in BHK-21 and mosquito cells
The rMP12 recombinant rMP12:COGS containing the pTVT7-GSco segment (codon optimised N and NSs CDSs) was used to infected BHK-21, C6/36, U4.4 and Ae cells at MOI 5. (A) Virus titres at the indicated time points were determined by plaque assay in BHK-21 cells. (B) Cell monolayers were harvested at each point and expression level of N and NSs protein examined. Antibodies targeting RVFV N and NSs (primary antibody concentration 1:1000) were used to probe for viral proteins, and anti-tubulin antibody was used to detect tubulin as loading control for each sample.

plasmids - as with the five plasmid rescue but with addition of pSTI-Gn/Gc (0.5, 1, and 2 μg). Cell culture supernatants were harvested for all experiments after 5, 7, or 14 days, and used to infect BHK-21 cells. None of the conditions resulted in virus rescue. BHK-21 cells treated with the rescue cell culture supernatant demonstrated no evidence of CPE associated with viral replication, and protein analysis revealed no evidence of rMP12 N or NSs expression. Analysis of the C6/36 cells used in the rescue attempts did show evidence of weak NSs expression in the 5-plasmid rescue attempts at both 7 and 14 day harvests, something not observed in U4.4 or Ae cells (data not shown). For NSs to be expressed it suggests that viral replication and transcription processes were occurring in the C6/36 cells, but possibly not at a level necessary for rescues to be successful. High levels of both RNA genome transcripts and protein expression are needed for a successful rescue experiment (Kohl et al. 2004). It is therefore probable that the activity noted in the minireplicon assays was ultimately insufficient to initiate a fully competent replication cycle resulting in release of infectious virions.

7.4 Discussion

This chapter describes the development of a minireplicon assay applicable to all mosquito cell lines analysed in this project. However, the overall aims of this section had to be adjusted as the research progressed due to unforeseen issues arising from manipulation of the cell lines themselves. The T7RNAP-based minireplicon systems in mammalian cells function efficiently due to the high levels of the polymerase expressed in the stably transformed BSR-T7/5 cells. Efficient transcription ensures high concentrations of minireplicon genome segments are available, as well as high concentrations of mRNA transcripts for N and L protein expression. However, it was not possible to generate stably-transformed mosquito cell lines capable of expressing the T7RNAP. Reasons for this were not apparent, although concurrent experiments attempting to create a stably transformed C6/36 cell line constituently expressing Dcr-2 protein also experienced similar difficulties in maintaining selection of the plasmid over continued passages.

Experiments to investigate the use of invertebrate promoters demonstrated two things. The promoters could be employed to express the support proteins required for the minireplicon and rescue attempts, but the maximum plasmid transfection efficiency achievable in mosquito cells was only approximately 50%. The wide disparity noted between the various

promoters was unexpected, but the availability of a strong mosquito polyubiquitin promoter, capable of expressing proteins of interest in all the cell lines analysed here was beneficial. Minireplicon assays relying on IRES-driven expression were only capable of expressing reporter proteins at levels high enough to generate useful results in C6/36 cells. Fortunately, minireplicon assays using the polyubiquitin promoter to drive protein expression produced activity in all mosquito cells that could be compared with that for mammalian cells.

Significantly reduced activity levels noted for the BUNV minireplicon experiments when comparing C6/36 to mammalian cell-based assay was also reported here for MP12 (Kohl et al. 2004). A major contributing factor to this was likely the reduced activity of the T7RNAP at 28^{o}C compared to at 37^{o}C. This may explain why the combination T7RNAP and pSTI- based minireplicon worked more effectively than the T7RNAP only system, as overall reliance on RNA transcripts produced by T7RNAP would be lessened. A combination of lack of T7RNAP availability due to poor transfection efficiency and reduced activity due to temperature may explain the lack of successful rescue attempts in the mosquito cells. Although not reported here, attempts were also made to rescue BUNV in mosquito cells using the pSTI-plasmid based system described here. Like RVFV, the BUNV rescue system is highly efficient in BSR-T7/5 cells, but all attempts in mosquito cells were unsuccessful. These data suggest that until the problem of generating the high levels of RNA transcripts generated in the BSR-T7/5 cells is solved, mosquito cell-based rescue attempts will likely remain unsuccessful. The potential for a RNA pol I/II based minireplicon system was not explored here, but it could have the potential to be a more effective system than the one described here. The two major bottlenecks in the current system, relating to T7RNAP availability and activity, would be overcome as intrinsic polymerases would be used.

Codon optimisation of the proteins encoded by MP12 virus resulted in several differences. In minireplicon assays codon optimized L protein gave higher activity in both mosquito cell lines and in BSR-T7/5 cells. Codon optimised N however had significantly reduced activity in both cell types. Arboviruses are notable amongst the RNA viruses in that their genomes are unusually genetically stable (Jenkins et al. 2002; Nichol et al. 1993; Weaver et al. 1992). The scientific consensus is that their host switching nature means that only changes beneficial or neutral in both the mammalian host and invertebrate vector become

fixed, with changes benefiting only one host rapidly lost due to evolutionary pressures (Ciota & Kramer 2010; Scott & Weaver 1994). This suggest that the current codon usage in RVFV is optimised for a successful arboviral lifecycle, switching between a mosquito vector and vertebrate host. It is possible that RVFV utilises the different codon usage biases between the two hosts as a way of regulating protein expression levels in each species. In conjunction with the different UTR promoter strengths reported here in the mosquito cells, these two factors could possible offer another explanation regarding the different protein and mRNA transcript levels described between the cell lines throughout this research. While the increased minireplicon activity reported for the codon optimised L protein was beneficial *in vitro*, it may have unforeseen and inhibitory effects in the context of a viral infection. Indeed, even with the increased activity associated with Lco a rMP12 recombinant encoding this protein could not be rescued. This may also explain why the majority of attempts to rescue codon optimised virus attempts in BSR-T7/5 cells were unsuccessful.

The differential replication potential of rMP12:COGS in mammalian and mosquito cell lines however was unexpected, and several theories were proposed to explain this result. Alteration of the N and NSs nucleotide sequence during codon optimisation may have disrupted unknown ORFs within the S segment. The current knowledge of RVFV suggests that only two proteins, N and NSs, are encoded on the S segment. It is possible however that smaller, as yet uncharacterised protein species are also encoded within the S segment. Using bioinformatics software to discover potential ORFs (parameters: AUG start codon; minimum codon length of 50; standard genetic code used for translation) in the MP12 and MP12 codon optimised S segment reveals several differences (see Appendix Figure 10-1). The possibility exists that a protein essential to replication within mosquito cells was lost in the MP12:COGS S segment genome, or that a new protein inhibitory to replication was unknowingly encoded. A further consequence of altering nucleotide sequences was a potential to alter regulatory elements within the CDS, or spanning either the UTR-CDS or CDS-IGR boundary regions. The failure of MP12:COGS to grow in mosquito cells may be a result of alteration to a vital mosquito specific regulatory element. Finally, the majority of all RNA viruses demonstrate a marked suppression of CpG dinucleotide frequencies within their genomes (Cheng et al. 2013; Simmonds et al. 2013; Rima & McFerran 1997). The exact reasons for this is not known, but experimental evidence has demonstrated that if CpG ratios are increased in the positive-strand RNA picornoviruses then replication and

growth are impaired (Atkinson et al. 2014). Analysis of the CpG dinucleotide ratios in MP12 and MP12:COGS was conducted using the EMBOSS Cpgplot web-based software (www.ebo.ac.uk) (McWilliam et al. 2013) (see Appendix Figure 10-2) This demonstrated that CpG dinucleotides were as expected under represented in the MP12 S genome. However, the CpG dinucleotide frequencies were markedly different in the altered rMP12:COGS S segment genome, being significantly over-represented in the N CDS region. However, the biological significances of this observations were not explored in this project, and other explanations may still exist as to the cause of the differential replication potential of the codon optimised virus.

In conclusion, this chapter describes the development of an MP12 based minireplicon assay that functions in all the mosquito cell lines evaluated. However, even after extensive modifications and optimisation regarding specific promoters, protein expression mechanisms and codon optimisation of the support protein species, the minireplicon assay remained approximately 10 to 100-fold less active than a similar assay in mammalian cells. The primary stumbling blocks to development remain the T7RNAP delivery mechanisms and poor transfection efficiency of mosquito cells lines. All attempts to rescue MP12 in mosquito cell were unsuccessful, potentially due to reduced protein expression in these cells compared to BSR-T7/5 cells.

7.5 Summary

- Promoter comparison demonstrated that the polyubiquitin promoter was highly efficient in all mosquito cells tested, and RhPV IRES was also fully functional.

- Minireplicon assays based on a combination of T7RNAP-driven reporter genome transcription and polyubiquitin promoter-driven protein expression were functional in C6/36 and U4.4 cells. However, activity was significantly lower than that for mammalian cells, and reduced activity in the Ae cells made results inconsistent

- Promoter strength differences between mammalian and mosquito cells were observed, with overall strengths in mosquito cells markedly reduced compared to the same promoter used in a mammalian cell-based assay.

- Codon optimisation gave unexpected results, with differing activity reported in the minireplicon assay for both L and N proteins. The majority of attempts to rescue codon optimised viruses in BSR-T7/5 cells were unsuccessful. A rescued virus with a codon optimised S segment replicated in BHK-21 cells, but not mosquito cells. The reasons for this are unknown.

- Attempts to rescue MP12 in mosquito cells were unsuccessful. The reasons for this were thought to include poor transfection efficiency of mosquito cells, lack of high levels of T7RNAP expression, and reduced T7RNAP activity at 28^{o}C. Attempts to create a mosquito cell line constituently expressing T7RNAP were also unsuccessful.

8 Investigation of the RNAi response to RVFV infection in mosquito cells

8.1 Introduction

The important roles played by the RNAi pathways in restricting and controlling arboviral replication within invertebrate vectors have recently been established (reviewed in (Blair 2011; Fragkoudis et al. 2009). The majority of this research has been conducted in *D. melanogaster*, and antiviral activity characterised for several viruses (Chotkowski et al. 2008; Galiana-Arnoux et al. 2006; van Rij et al. 2006; Wang et al. 2006; Zambon et al. 2006). RNAi pathways have subsequently been shown to be present in mosquito species (reviewed in Sanchez-Vargas *et al*. (2004)), and antiviral RNAi responses described against several arboviruses including West Nile virus (WNV) (Zambon et al. 2005), DENV (Xi et al. 2008), ONNV (Keene et al. 2004), SFV (Schnettler et al. 2013) and RVFV (Léger et al. 2013).

Two RNAi pathways responding to exogenous RNA species have been identified, the siRNA and piRNA pathways (Karlikow et al. 2014; Morazzani et al. 2012; Vodovar et al. 2012). Virus-induced siRNA species are generated from viral dsRNA substrates, although the specific targets responsible for pathway activation in RVFV infected cells are unclear. Genome strands of NSVs are encapsidated by protein, theoretically preventing RNA secondary structure formation. Nevertheless, siRNAs have been detected following NSV infection (Léger et al. 2013). Potential dsRNA targets for siRNA biogenesis are thought to include replicative intermediates, viral mRNA transcripts, or genome:mRNA duplexes. The piRNA response was originally believed to be germ-line specific, responsible for epigenetic and post-translational gene silencing of transposons (Karlikow et al. 2014). Recent research however has shown evidence of piRNA pathway activity in somatic cells (Yan et al. 2011), and also of a directed response to arboviral infection of mosquito cells (Vodovar et al. 2012, Léger et al. 2013, Schnettler et al. 2013).

Advances in the understanding of invertebrate antiviral RNAi responses were aided by the extensive depth of genome annotation of *D. melanogaster*, allowing identification and study of individual protein components of the pathways. Although annotated genomes of several mosquito species such as *Anopheles gambiae* and *A. aegypti* have recently been

published, our knowledge of mosquito RNAi response still remains incomplete compared to that for *D. melanogaster* (Christophides et al. 2002; Nene et al. 2007). However, RNAi investigations have been performed using some of the mosquito cell lines employed in this project. The U4.4 cell line has been shown to have a competent siRNA pathway with demonstrable antiviral activity, and an active piRNA pathway in RVFV, SNV and LACV infected cells has been described (Léger et al. 2013; Vodovar et al. 2012). The siRNA pathway in C6/36 cells is dysfunctional due to a deletion in the *Dcr-2* gene, but piRNA species have been detected in arbovirus infected cells (Brackney et al. 2010; Vodovar et al. 2012; Léger et al. 2013). C7-10 cells also exhibit a dysfunctional siRNA pathway due to a *Dcr-2* mutation (Morazzani et al. 2012), but have not been extensively studied in RNAi experiments.

8.2 Aims

The aim of this chapter was to analyse the RNAi response in rMP12 and recombinant virus infected mosquito cells. siRNA and piRNA responses to ZH548 infection in the U4.4 and Aag-2 cell lines have been previously described, whereas infected C6/36 cells demonstrated only a piRNA response (Léger et al. 2013). Examination of the RNAi responses in Ae and C7-10 cells to RVFV infection are unreported to date, although Ae cells are known to possess a competent siRNA pathway (Alain Kohl - personal communication).

Léger *et al*. (2013) reported evidence of an siRNA response targeted toward NSs in ZH548 infected mosquito cells. Previous results described here have identified variances in both NSs expression in rMP12 infected mosquito cells, and GFP expression in rMP12ΔNSs:eGFP infected mosquito cells. Therefore these two viruses were used to look for evidence that the RNAi pathway regulates protein expression in infected mosquito cells. By examining differences in the polarity of all virus induced small RNA species (viRNAs) targeting rMP12 or rMP12:S-Swap S segment during infection it was hoped the nature of the virus substrate acting as template for RNAi pathway activation could be determined. BHK-21 cells were included to evaluate if the characterised RNAi pathway responses seen in invertebrate cell lines had potential analogous responses in mammalian cell lines. Finally, all infections were performed and analysed in duplicate to investigate

the reproducibility of the RNAi response to infection, and also to compare any reproducibility between different cell lines.

8.3 Results

8.3.1 Sample preparation

Mosquito cell lines C6/36, U4.4, Ae, and C7-10 were infected with rMP12, rMP12ΔNSs:eGFP, or rMP12:S-Swap at MOI 0.1. BHK-21 cells were infected with rMP12 or rMP12:S-Swap at MOI 0.1. All infections were performed in duplicate. Samples were harvested at 72 h p.i. where supernatant was removed to determine viral titre, and total RNA extraction was performed on cell monolayers. RNA quality was assessed using the Agilent Bioanalyser (Agilent Technologies, USA). For successful Illumina RNA expression sequencing an RNA integrity number (RIN) of >7 is recommended. Although BHK-21 RNA samples generated a RIN of 9.2 or greater, RINs for mosquito cell RNA samples could not be calculated. Electropherogram trace analysis demonstrated disparity in the relative levels of 18S and 28S RNA species in these samples. Whilst in BHK-21 cells samples the levels were equivalent, in mosquito cell samples 18S RNA levels were greater than those for 28S RNA (Figure 8-1). Calculation of the RIN is based on these relative levels, and this disparity meant a value could not be determined. However, further quality control analysis undertaken at ARK Genomics determined the RNA quality was suitable for sequencing. Viral titres determined by plaque assay in BHK-21 cells demonstrated that viral replication had occurred in all samples, although rMP12:S-Swap titres were reduced in Ae and C7-10 cells compared to the other cell lines evaluated (Figure 8-2).

8.3.2 Data analysis

To characterise the RNAi responses small RNA sequences detected in RNA samples obtained from infected mosquito cells were aligned to the three genomic segments. The reference sequences for rMP12 infection were: MP12 S segment (NCBI accession#: DQ380154); MP12 M segment (NCBI accession#: DQ380208); and MP12 L segment (NCBI accession#: DQ375404). For analysis of rMP12:S-Swap virus infection the reference S segment was a modified version of MP12 S segment in which N and NSs CDSs were switched, leaving the terminal UTRs and IGR unaltered (see Chapter 6). For

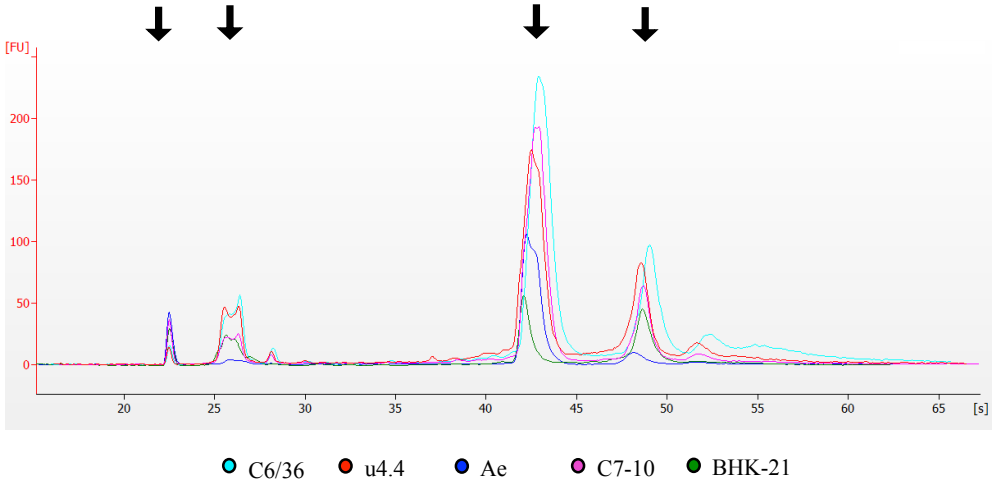

Figure 8-1: RNA analysis from rMP12 or recombinant infected cells
Total RNA was extracted from rMP12, rMP12:S-Swap or rMP12ΔNSs:eGFP infected cells using Trizol. RNA was quality controlled using the Agilent Bioanlyser. The electropherogram displays migration time against fluorescent units (FU). Black arrows indicate peaks relating to (left to right): sample marker; 5s-region; 18s-fragment; 28S-fragment.

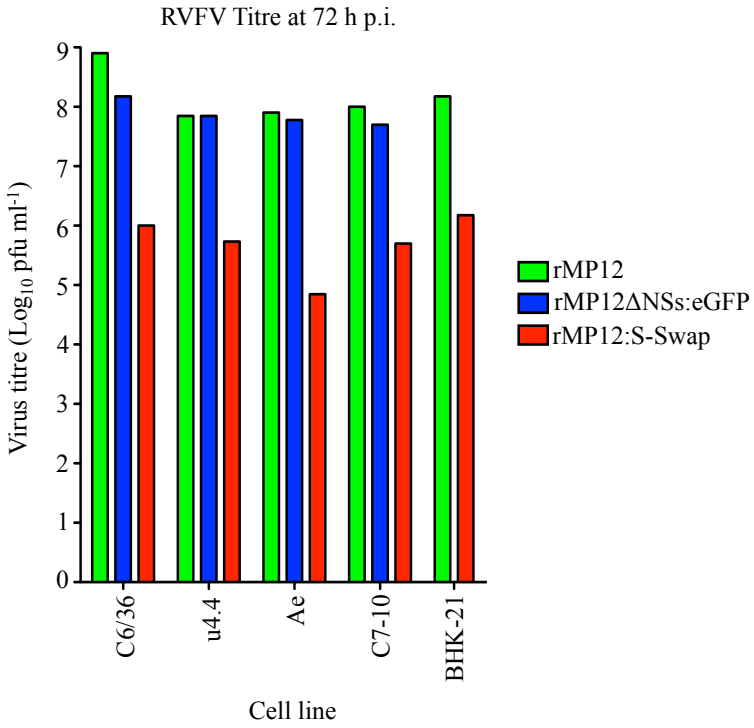

Figure 8-2: rMP12 and recombinant virus titres in cell lines infected for RNAi experiment
C6/36, U4.4, Ae, C7-10, and BHK-21 cells were infected with rMP12, rMP12ΔNSs:eGFP (not BHK-21 cells), or rMP12:S-Swap at MOI 0.1. At 72 h p.i. cell culture supernatant was removed and viral titres determined by plaque assay of BHK-21 cells.

analysis of rMP12ΔNSs:eGFP virus the reference S segment was the modified version of MP12 S segment in which NSs CDS was replaced with eGFP CDS, leaving the terminal UTRs and IGR unaltered (see Chapter 5). Cluster sizes chosen to analyse viRNAs in theinfected cells were: 21 nt to assess the siRNA pathway; 24-25 nt, 27-28 nt, and 29-30 nt to assess individual aspects of the piRNA pathway; and 15-17 nt to analyse the large numbers of very small viRNA species found during this experiment. For the BHK-21 cell analysis the 21 nt size class was increased to incorporate viRNA species in the 21-23 nt range. The siRNA pathway in invertebrate cells is specifically mediated by Dcr-2, generating the characteristic 21 nt RNA species. Other members of the Dicer protein family however will produce viRNA species between 21-23 nt (Svoboda 2014; Kim et al. 2009). As RNAi pathways are not fully characterised in BHK-21 cell this range was chosen to capture all potential products of Dcr-mediated dsRNA cleavage.

Nucleotide frequency biases present in the viRNA species were investigated by logo analysis. This allowed for graphical representation of nucleotide frequency in aligned consensus viRNA sequences (Schneider & Stephens 1990). Previous work investigating the RNAi response in *D. melanogaster* and in mosquito species has identified nucleotide frequency biases in piRNAs, but not in the siRNAs (Brennecke et al. 2007; Morazzani et al. 2012; Vodovar et al. 2012; Léger et al. 2013).

8.3.3 Infection with rMP12 recombinants results in variation in viRNA populations characteristics

Analysis of viRNA species was restricted to those between 15-37 nt that also aligned to one of the three viral genomic segments. Infection with rMP12 or rMP12ΔNSs:eGFP generated the highest numbers of viRNAs, with total read counts greater in U4.4 and Ae cells compared to C6/36 and C7-10 cells. Reduced viRNA numbers have previously been reported in ZH548 infected C6/36 cells, and thought to be due to the dysfunctional siRNA pathway (Léger et al. 2013). Total number reduction in C7-10 cells was even more pronounced although titres remained similar to those from infected C6/36 for both viruses. This possibly suggests total RNAi dysfunctionality was more severe in C7-10 cells compared to others evaluated.

In rMP12 infected cells the percentage of reads aligned to each genome segment remained highly consistent between both replicate samples and the separate mosquito cell lines (Table 8-1.A). The S segment was the most intensely targeted, followed by M and L segments. viRNA species targeting the L segment were predominantly of genomic polarity, whilst those targeting S were predominately of antigenomic polarity. These polarity ratios remained highly consistent between both replicate samples, and the individual mosquito cell lines. viRNA polarity ratios were similar in rMP12ΔNSs:eGFP infected cells, although a small increase in antigenomic S segment species was apparent (Table 8-1.B). However, the proportion of viRNA species targeting the modified S segment of rMP12ΔNSs:eGFP virus was reduced in all cell lines compared to rMP12. Numbers targeting the L and M segment remained consistent with those observed in rMP12 infected cells. The exception was C7-10 cells where distribution of viRNA species targeting the genome segments remained similar to rMP12, although total numbers were severely reduced.

The read numbers generated in rMP12:S-Swap infected cells were significantly reduced. U4.4 cells again generated the highest numbers, followed by C6/36, Ae and then C7-10 cells (Table 8-1C). Even with reduced numbers, the genomic to antigenomic polarity distribution ratios for each genome segment remained similar to rMP12 and rMP12ΔNSs:eGFP infected cells. Genome distribution of these viRNA species however was markedly different however, with an intense targeting of S segment apparent. Again C7-10 cells were the exception, with distribution patterns remaining similar to rMP12 infection. However, overall read numbers were minimal compared to the other cell lines, with the majority of viRNAs in the 15-19 nt range. These data were not comparable to those generated by C6/36, U4.4 or Ae cells.

8.3.4 rMP12 infection produces multiple viRNA species in mosquito cells

Peaks of viRNA species at 21 nt were apparent, targeting all three genomic segments in infected U4.4 and Ae cells. These represented products of the siRNA pathway, and as expected were absent in C6/36 and C7-10 cells (Figure 8-3). A second, broader peak comprising of 24-30 nt viRNA species, presumably products of the piRNA pathway, was also apparent targeting all three genome segments. This peak was observed in all mosquito

8-1: Characteristics of viRNA species detected in rMP12 or recombinant virus infected mosquito cell lines.
Analysis of the viRNA species detected in rMP12, rMP12:S-Swap, or rMP12ΔNSs:eGFP infected C6/36, U4.4, and Ae cells. Samples A and B were duplicate infections. viRNA species between 15 and 37 nt in length, and of 100% homology to reference genome, were included. %Total reads is the proportion of all viRNAs detected in the sample that aligned to the L, M, and S segment

(A) rMP12 infected mosquito cells.

		rMP12							
Cell line	**Sample**	**Segment**	**Total reads**	**Average length (nt)**	**Number reads genomic sense**	**Number reads antigenomic sense**	**% Total genomic sense**	**% Total antigenomic sense**	**% of total reads aligning to segment**
C6/36	**A**	**L**	38,476	20.56	25,755	12,721	66.94%	33.06%	16.48%
		M	90,534	21.48	41,037	49,497	45.33%	54.67%	38.78%
		S	104,442	21.72	26,280	78,162	25.16%	74.84%	44.74%
			233,452		**93,072**	**140,380**			
	B	**L**	34,026	20.56	22,711	11,315	66.75%	33.25%	15.82%
		M	85,741	21.44	38,259	47,482	44.62%	55.38%	39.86%
		S	95,358	21.63	24,602	70,756	25.80%	74.20%	44.33%
			215,125		**85,572**	**129,553**			
u4.4	**A**	**L**	49,316	22.58	31,884	17,432	64.65%	35.35%	7.01%
		M	214,425	24.01	112,163	102,262	52.31%	47.69%	30.49%
		S	439,592	23.55	106,787	332,805	24.29%	75.71%	62.50%
			703,333		**250,834**	**452,499**			
	B	**L**	38,301	22.20	23,774	14,527	62.07%	37.93%	7.60%
		M	165,742	23.59	83,136	82,606	50.16%	49.84%	32.90%
		S	299,657	22.96	77,740	221,917	25.94%	74.06%	59.49%
			503,700		**184,650**	**319,050**			
Ae	**A**	**L**	17,366	20.60	11,893	5,473	68.48%	31.52%	11.60%
		M	62,431	20.71	31,186	31,245	49.95%	50.05%	41.70%
		S	69,926	21.19	22,483	47,443	32.15%	67.85%	46.70%
			149,723		**65,562**	**84,161**			
	B	**L**	22,231	20.22	15,034	7,197	67.63%	32.37%	11.12%
		M	85,104	20.47	41,782	43,322	49.10%	50.90%	42.58%
		S	92,516	21.10	30,024	62,492	32.45%	67.55%	46.29%
			199,851		**86,840**	**113,011**			
C7-10	**A**	**L**	2,504	24.63	1,642	862	65.58%	34.42%	9.93%
		M	8,673	25.27	4,624	4,049	53.31%	46.69%	34.38%
		S	14,051	24.61	3,293	10,758	23.44%	76.56%	55.70%
			25,228		**9,559**	**15,669**			
	B	**L**	1,934	24.26	1,278	656	66.08%	33.92%	9.79%
		M	6,961	25.16	3,755	3,206	53.94%	46.06%	35.24%
		S	10,860	24.33	2,563	8,297	23.60%	76.40%	54.97%
			19,755		**7,596**	**12,159**			

(B) rMP12ΔNSs:eGFP infected mosquito cells

		rMP12ΔNSs:eGFP							
Cell line	**Sample**	**Segment**	**Total reads**	**Average length (nt)**	**Number reads genomic sense**	**Number reads antigenomic sense**	**% Total genomic sense**	**% Total antigenomic sense**	**% of total reads aligning to segment**
C6/36	**A**	**L**	32,225	20.66	19,887	12,338	61.71%	38.29%	16.49%
		M	99,486	21.27	47,408	52,078	47.65%	52.35%	50.90%
		S	63,762	20.50	13,721	50,041	21.52%	78.48%	32.62%
			195,473		**81,016**	**114,457**			
	B	**L**	15,828	19.84	9,443	6,385	59.66%	40.34%	15.46%
		M	53,416	20.18	24,540	28,876	45.94%	54.06%	52.17%
		S	33,139	19.58	7,418	25,721	22.38%	77.62%	32.37%
			102,383		**41,401**	**60,982**			
U4.4	**A**	**L**	32,105	22.42	21,129	10,976	65.81%	34.19%	5.91%
		M	276,160	24.15	140,853	135,307	51.00%	49.00%	50.87%
		S	234,601	22.56	38,776	195,825	16.53%	83.47%	43.22%
			542,866		**200,758**	**342,108**			
	B	**L**	23,187	22.51	15,189	7,998	65.51%	34.49%	5.77%
		M	202,393	24.17	104,866	97,527	51.81%	48.19%	50.35%
		S	176,394	22.61	29,539	146,855	16.75%	83.25%	43.88%
			401,974		**149,594**	**252,380**			
Ae	**A**	**L**	17,551	20.49	9,878	7,673	56.28%	43.72%	9.66%
		M	79,517	20.24	39,884	39,633	50.16%	49.84%	43.78%
		S	84,562	20.13	20,079	64,483	23.74%	76.26%	46.56%
			181,630		**69,841**	**111,789**			
	B	**L**	32,873	20.92	18,926	13,947	57.57%	42.43%	9.07%
		M	152,279	21.27	76,952	75,327	50.53%	49.47%	42.04%
		S	177,104	20.96	39,199	137,905	22.13%	77.87%	48.89%
			362,256		**135,077**	**227,179**			
C7-10	**A**	**L**	862	24.58	544	318	63.11%	36.89%	10.25%
		M	3,954	25.43	2,096	1,858	53.01%	46.99%	47.04%
		S	3,590	24.38	619	2,971	17.24%	82.76%	42.71%
			8,406		**3,259**	**5,147**			
	B	**L**	591	24.56	385	206	65.14%	34.86%	10.12%
		M	2,733	25.25	1,455	1,278	53.24%	46.76%	46.78%
		S	2,518	24.10	442	2,076	17.55%	82.45%	43.10%
			5,842		**2,282**	**3,560**			

(C) rMP12:S-Swap infected mosquito cells.

		rMP12:S-Swap							
Cell line	Sample	Segment	Total reads	Average length (nt)	Number reads genomic sense	Number reads antigenomic sense	% Total genomic sense	% Total antigenomic sense	% of total reads aligning to segment
C6/36	A	L	174	17.64	89	85	51.15%	48.85%	7.51%
		M	213	19.15	106	107	49.77%	50.23%	9.19%
		S	1,931	19.08	479	1,452	24.81%	75.19%	83.30%
			2,318		**674**	**1,644**			
	B	L	173	19.00	86	87	49.71%	50.29%	7.55%
		M	261	20.66	121	140	46.36%	53.64%	11.39%
		S	1,857	19.16	475	1,382	25.58%	74.42%	81.06%
			2,291		**682**	**1,609**			
U4.4	A	L	229	20.93	135	94	58.95%	41.05%	2.29%
		M	862	24.39	443	419	51.39%	48.61%	8.62%
		S	8,906	23.77	2,444	6,462	27.44%	72.56%	89.09%
			9,997		**3,022**	**6,975**			
	B	L	258	21.07	135	123	52.33%	47.67%	2.37%
		M	925	24.31	498	427	53.84%	46.16%	8.50%
		S	9,701	23.29	2,499	7,202	25.76%	74.24%	89.13%
			10,884		**3,132**	**7,752**			
Ae	A	L	105	18.82	55	50	52.38%	47.62%	5.96%
		M	241	20.32	128	113	53.11%	46.89%	13.67%
		S	1,417	18.94	404	1,013	28.51%	71.49%	80.37%
			1,763		**587**	**1,176**			
	B	L	139	18.98	66	73	47.48%	52.52%	5.94%
		M	272	19.93	97	175	35.66%	64.34%	11.62%
		S	1,930	19.44	524	1,406	27.15%	72.85%	82.44%
			2,341		**687**	**1,654**			
C7-10	A	L	33	22.62	20	13	60.61%	39.39%	16.42%
		M	85	22.66	41	44	48.24%	51.76%	42.29%
		S	83	25.25	58	25	69.88%	30.12%	41.29%
			201		**119**	**82**			
	B	L	27	21.78	14	13	51.85%	48.15%	17.31%
		M	68	23.02	27	41	39.71%	60.29%	43.59%
		S	61	23.87	35	26	57.38%	42.62%	39.10%
			156		**76**	**80**			

(A) rMP12 infected C6/36 cells

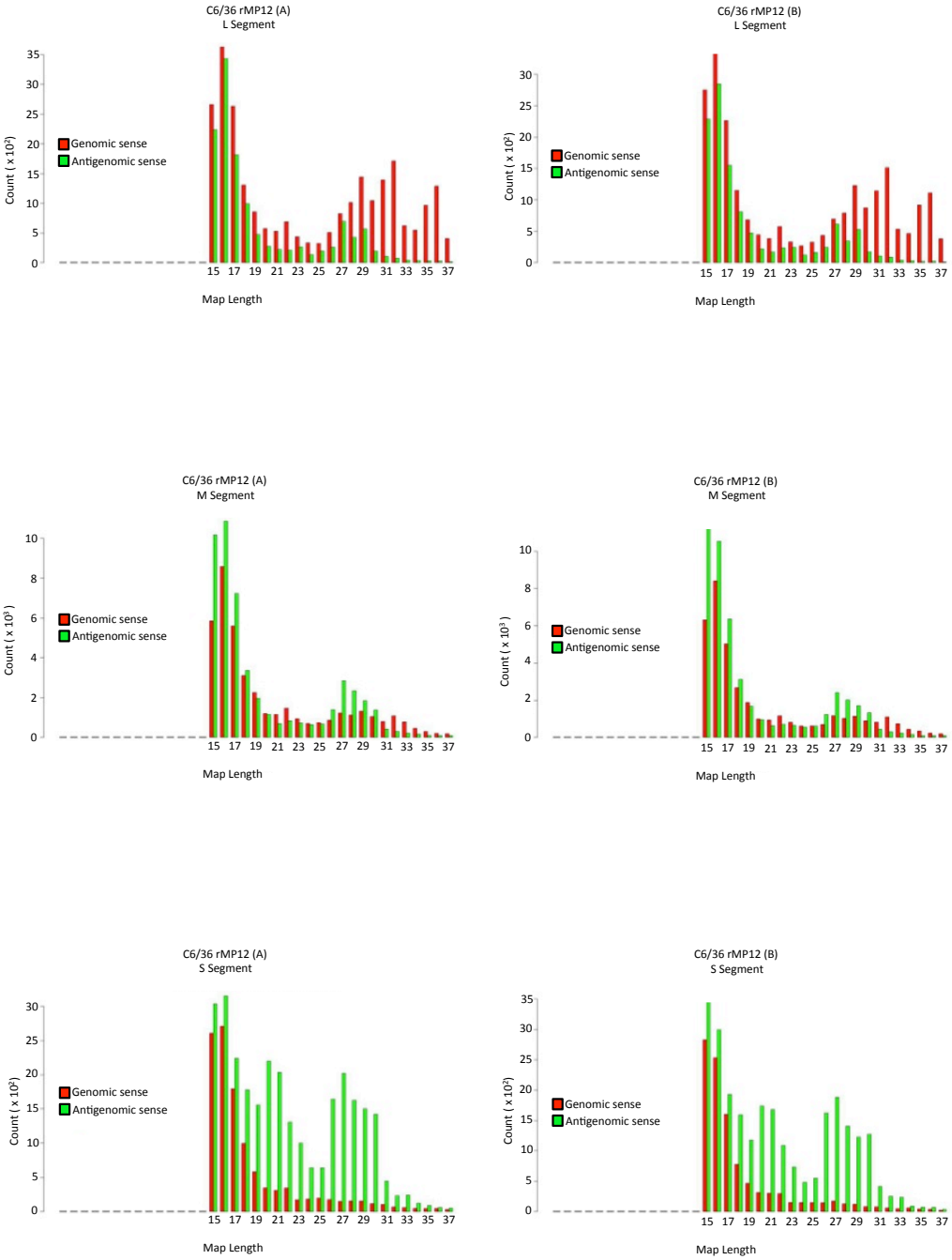

Figure 8-3: viRNA species plot analysis for rMP12 infected mosquito cell lines.
Size distribution and density plots of all 15-37 nt viRNA species detected in rMP12 infected mosquito cells lines aligning to L, M or S segment. Shown are replicate samples A and B taken from duplicate infections. viRNA species aligning to genomic polarity (negative sense) RNA are shown in red, antigenomic polarity (positive sense) RNA in green.

(B) rMP12 infected U4.4 cells

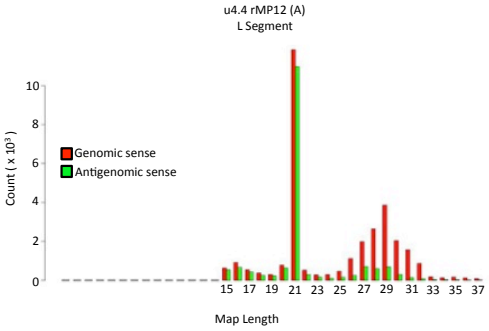

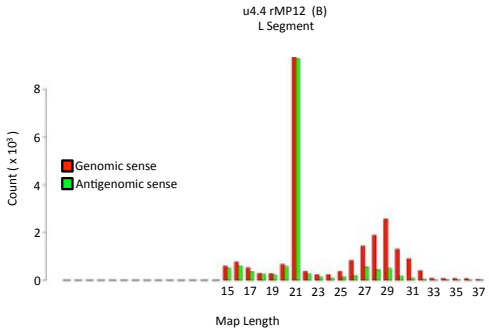

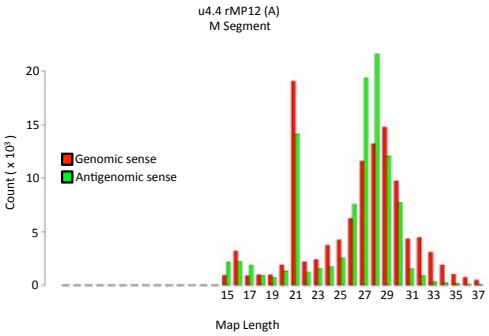

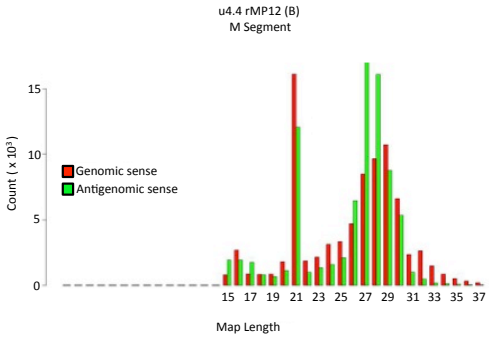

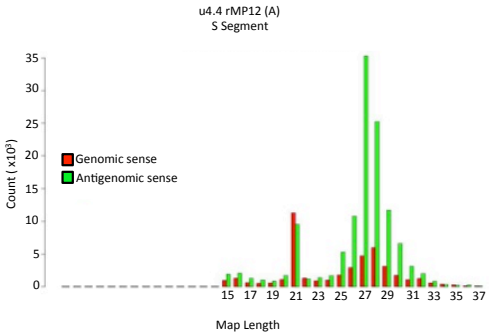

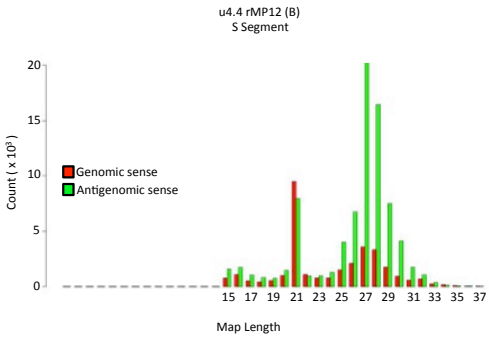

(C) rMP12 infected Ae cells

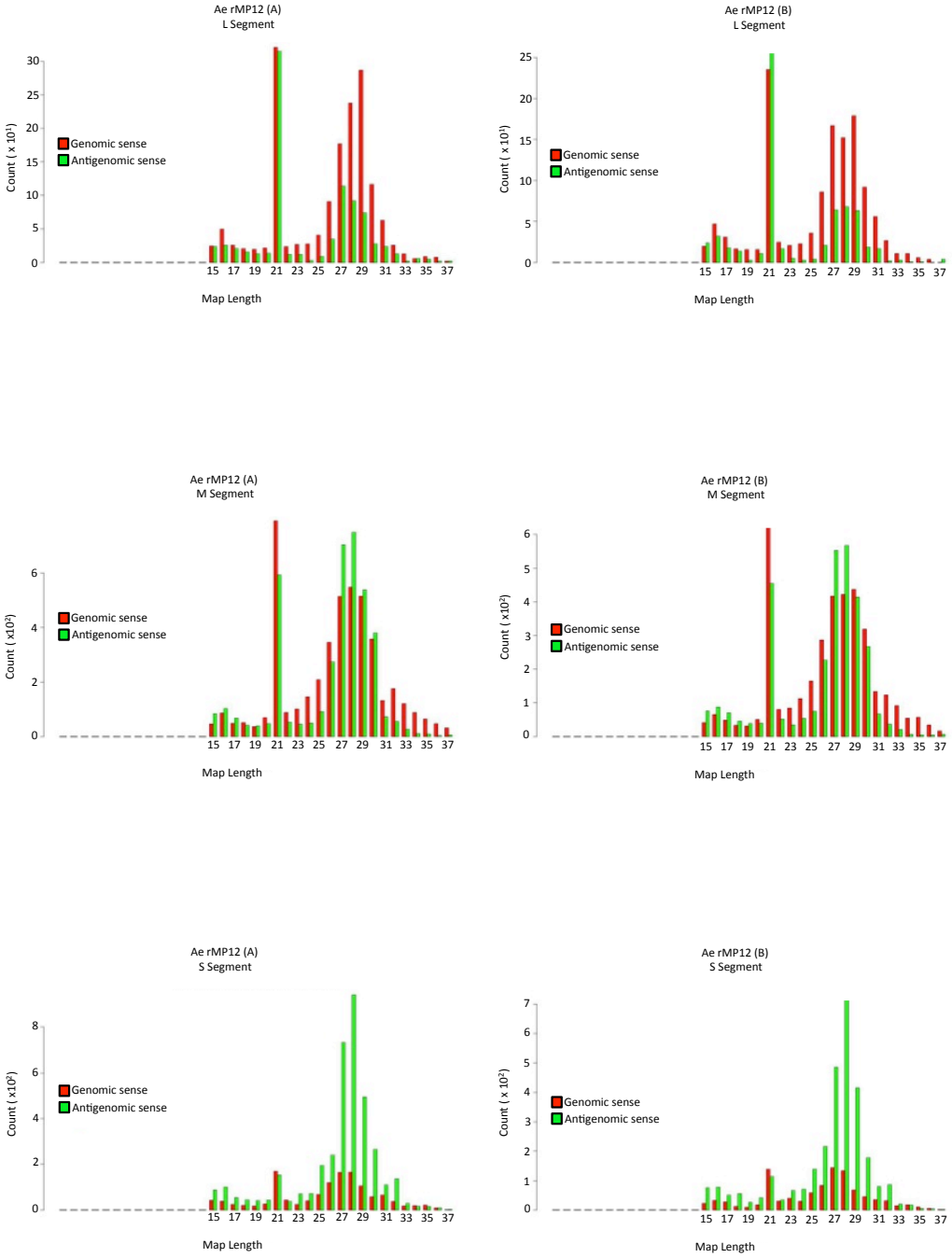

(D) rMP12 infected C7-10 cells

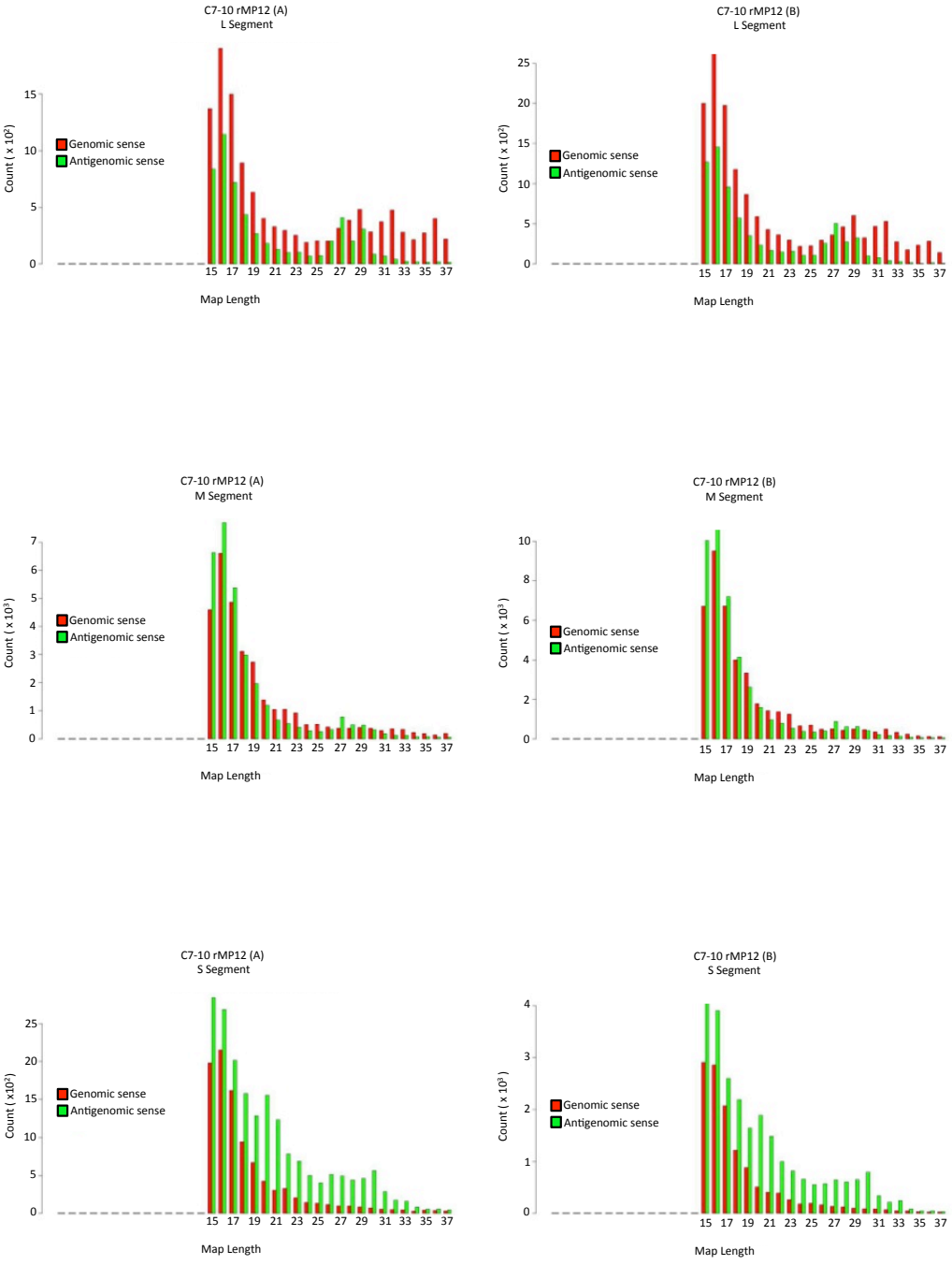

cell lines. Distribution patterns of viRNA species across the L, M, and S genome segments were highly consistent between replicate samples. The relative distributions of siRNA and piRNA species targeting each genome segment varied in U4.4 and Ae cells. siRNA species outnumbered the piRNA species targeting L segment (more pronounced in U4.4 cells), but for M segment the number of both species were similar. In S segment the opposite was observed with piRNA species outnumbering the siRNAs. Polarity differences in both siRNA and piRNA species were also observed. siRNA species were distributed equally between genomic and antigenomic polarity for those targeting S and L segments, but a bias toward genomic sense siRNA species was observed for the M segment. The polarity of piRNA species demonstrated a shift from predominantly genomic to predominantly antigenomic polarity in all those targeting L and S segments respectively. For the M segment the polarity varied between individual size classes of piRNA species.

Although siRNA species were distributed throughout all the genome segments, several regions of intense targeting, termed hotspots, were apparent (Figure 8-4). The NSs coding region of S segment was more intensely targeted than the N coding region, with hotspots in both polarities detected. Two hotspots located in the IGR of both genomic and antigenomic polarity were of interest as these aligned to the 3' terminal ends of both N and NSs mRNA transcripts. viRNA species targeting this region were identified previously as having regulatory effects on the expression of ZH548 NSs protein in mosquito cells (Léger et al. 2013). Their reproduction here indicated a similar siRNA response to both the virulent ZH548 and attenuated MP12 strains. piRNA distribution in S segment was predominantly antigenomic and biased toward the 3' end, with several hotspots apparent in the individual size groups analysed. In L and M segment the piRNA hotspots were distributed more evenly throughout the genome, although 29-30 nt viRNAs were almost exclusively of genomic polarity with a distributional bias toward the 5' end. The distribution and polarity of both siRNA and piRNA species targeting the genome segments were again highly conserved between infected U4.4 and Ae cells.

The viRNA species generated by rMP12 infected C6/36 and C7-10 cells varied considerably from that of U4.4 and Ae cells. Although no siRNA species were apparent, large numbers of antigenomic 19-23 nt viRNA species were detected targeting S segment. These were not observed in L or M segments. The overwhelming majority of viRNA

(A) rMP12 infected C6/36 cells

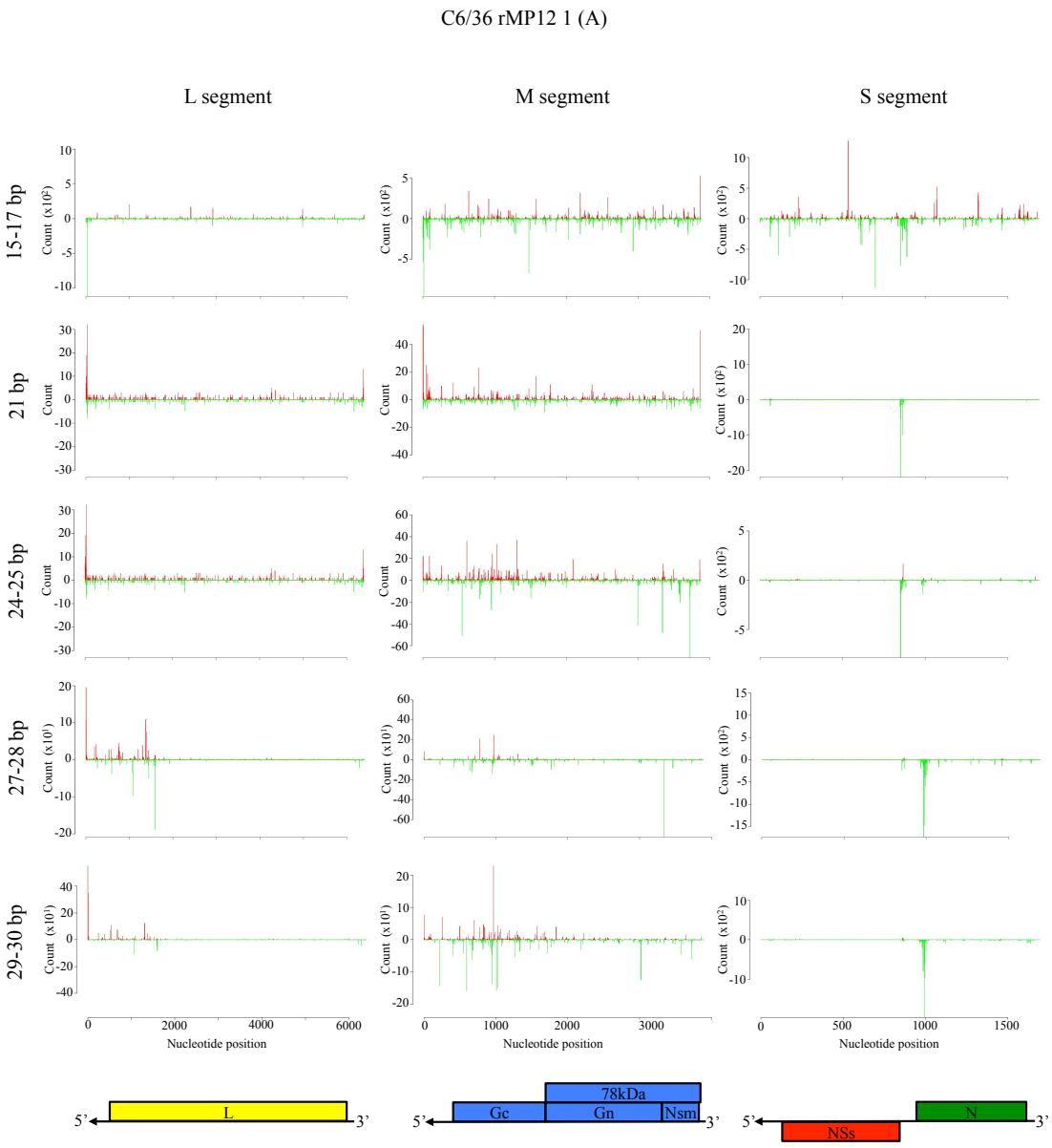

Figure 8-4: Mapping analysis of viRNA species targeting the rMP12 genome segments
Shown are density plots of aligned viRNA species of 15-17nt, 21nt, 24-25nt, 27-28nt, and 29-30nt aligning to the rMP12 L, M, and S genome segments. Upper plots (red) show alignments to genomic polarity (negative sense) and lower plots (green) to antigenomic polarity (positive sense). Also shown are the CDS for MP12 proteins encoded on the L (yellow), M (blue) and S (green and red) segments.

(B) rMP12 infected U4.4 cells

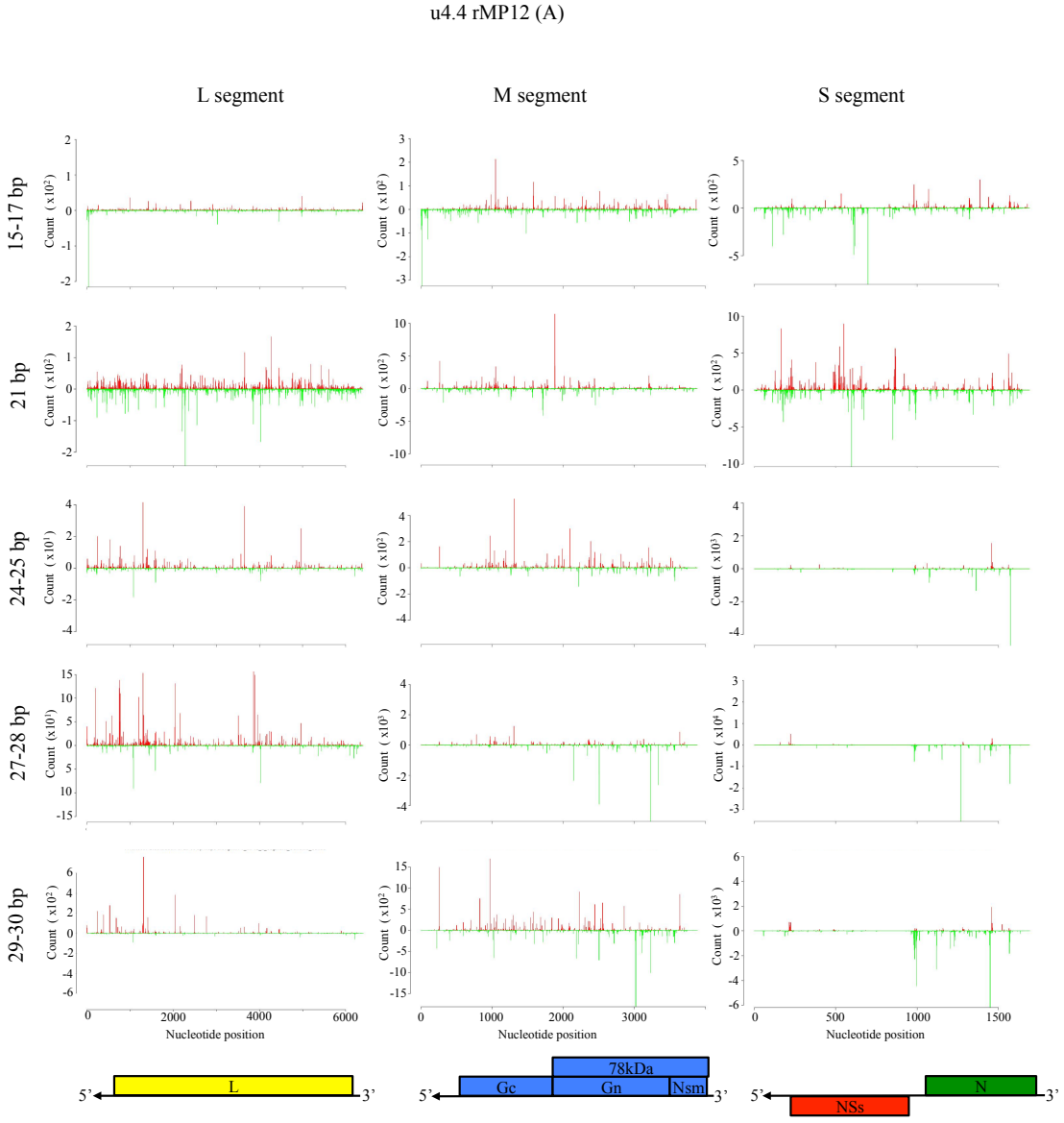

(C) rMP12 infected Ae cells

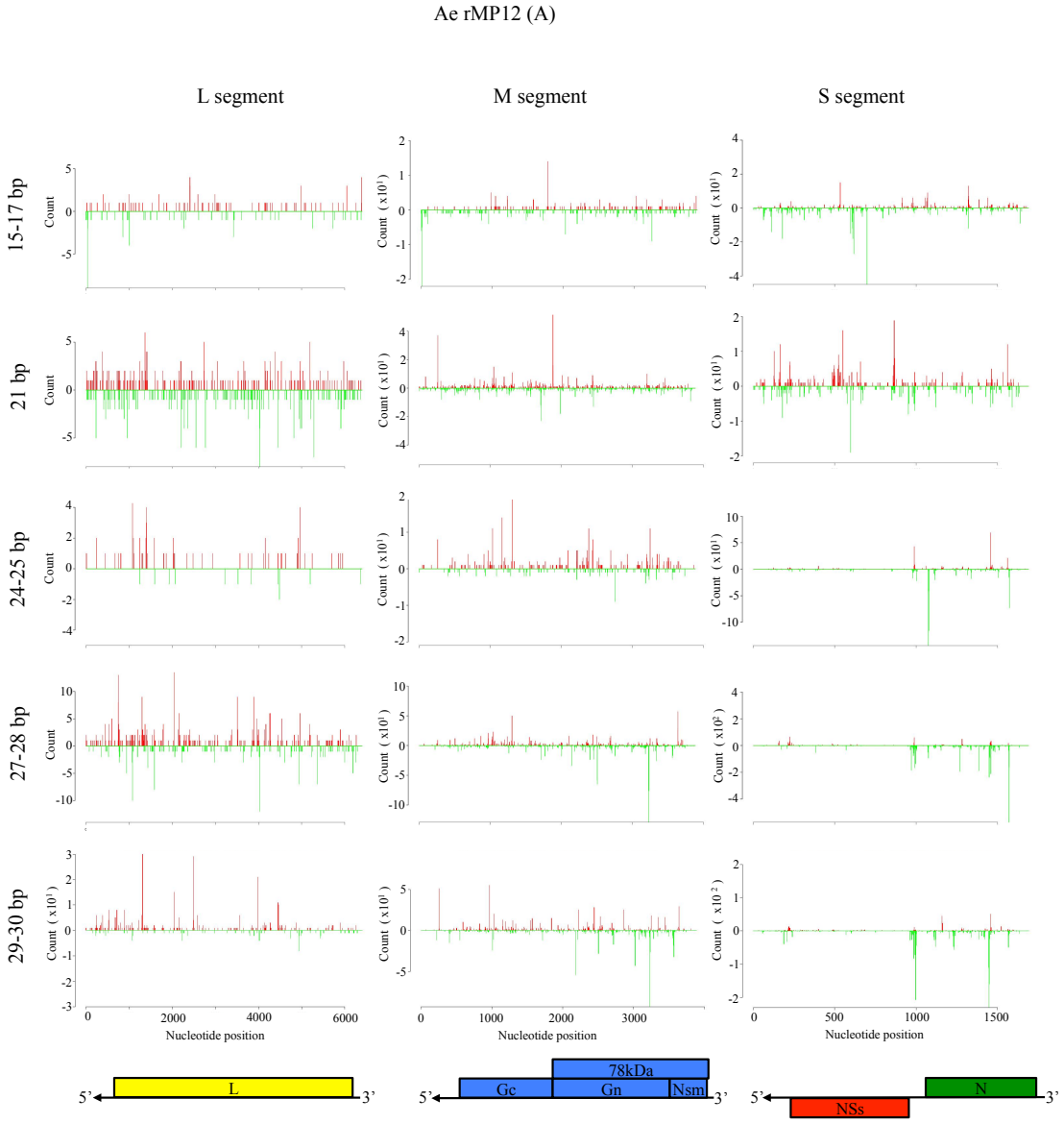

(D) rMP12 infected C7-10 cells

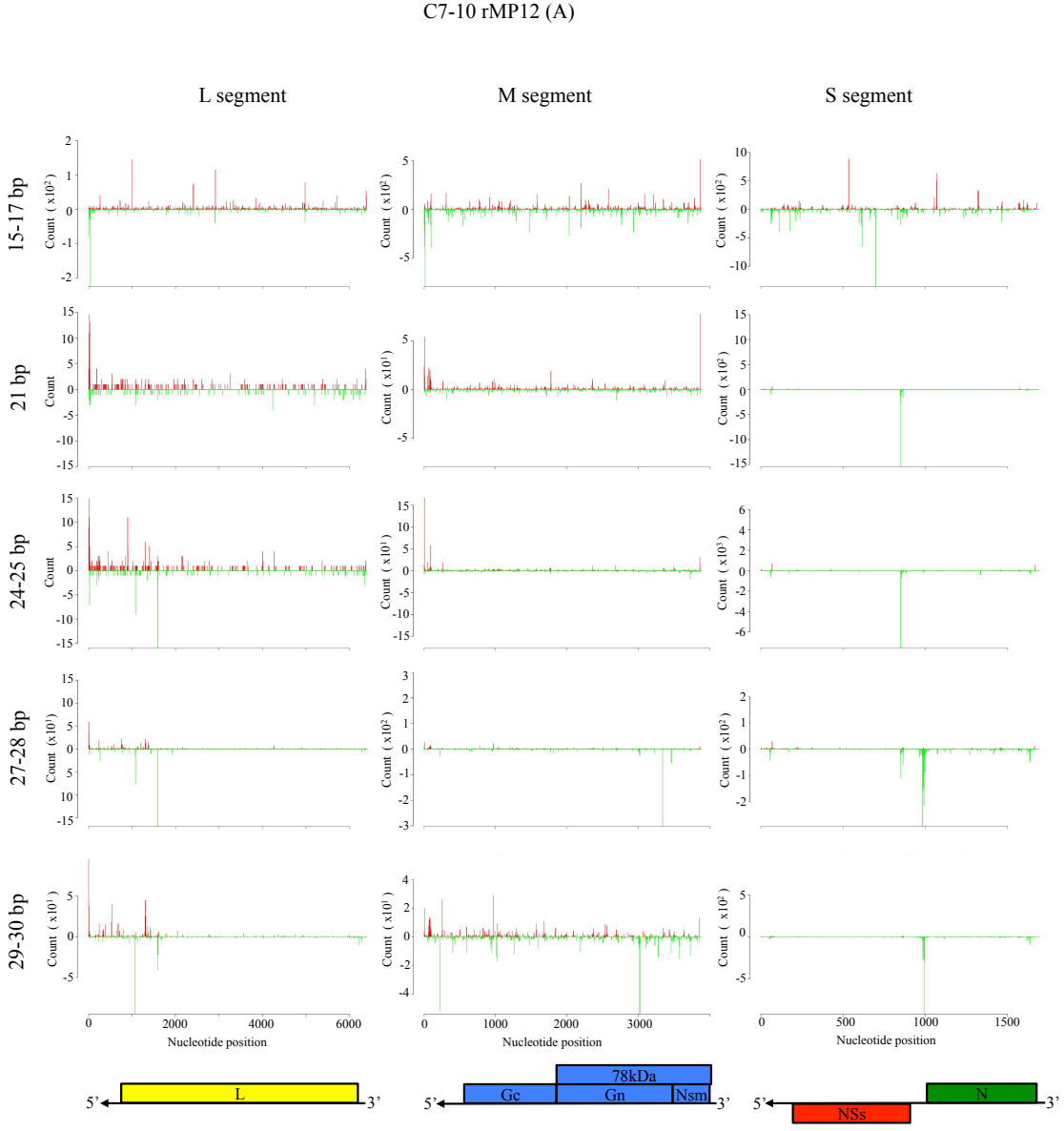

species in this size class however targeted the same region responsible for the strong antigenomic hotspot in rMP12 infected U4.4 and Ae cells. These species were also observed in ZH548 infected C6/36 cells (Léger et al. 2013). This possibly suggests that the viral substrate acting as the target for Dcr-2 in U4.4 and Ae cells may also act as a target for the Dcr-1 protein, which can replace Dcr-2 to some extent. This may indicate that the siRNA dysfunctional C6/36 and C7-10 cells exhibit a degree of redundancy in their ability to respond to dsRNA, although the antiviral potential of this is unknown. The single hotspot distribution pattern was also apparent for the piRNA species, with a large majority targeting a similar region to that observed in the 21 nt species. This hotspot however migrated toward the 3' genomic terminus in the 27-30 nt size classes. piRNA species distribution in L and M segment were also different to U4.4 and Ae cells, with hotspots tending more toward the 5' genomic terminus. However, the piRNA species were remarkably conserved between the rMP12 infected C6/36 and C7-10 cell lines, again indicating similar targets were responsible for their biogenesis (see Appendix Figure 10-3 for replicate sample results). Although piRNA species varied between cell lines, logo analysis demonstrated their characteristic nucleotide frequency biases in all mosquito cell lines (Figure 8-5). Genome polarity (antisense) species demonstrated an increased frequency of adenine at nucleotide position 10, and antigenomic polarity (sense) species demonstrated an increased frequency of uracil at nucleotide position 1 (represented as thymine rather than uracil as DNA was analysed rather than RNA).

An unexpected observation was the large number of 15-17 nt viRNA species targeting the genome segments. These species were present in all cell lines, and outnumbered all other viRNA species in C6/36 and C7-10 cells (Figure 8-3). Density plot analysis demonstrated hotspot locations throughout all the genome segments common between the cell lines (Figure 8-4). In L and M segment they were primarily antigenomic species and targeted to the 5' genome termini. In the S segment, these species aligned to regions spread throughout the genome. Logo analysis demonstrated no patterns of conserved nucleotide frequency bias as seen in the piRNA species. Potential mechanisms of biogenesis for these species remain undefined, and specific analysis of the small viRNA species is performed later in the chapter.

(A) rMP12 infected C6/36 cells

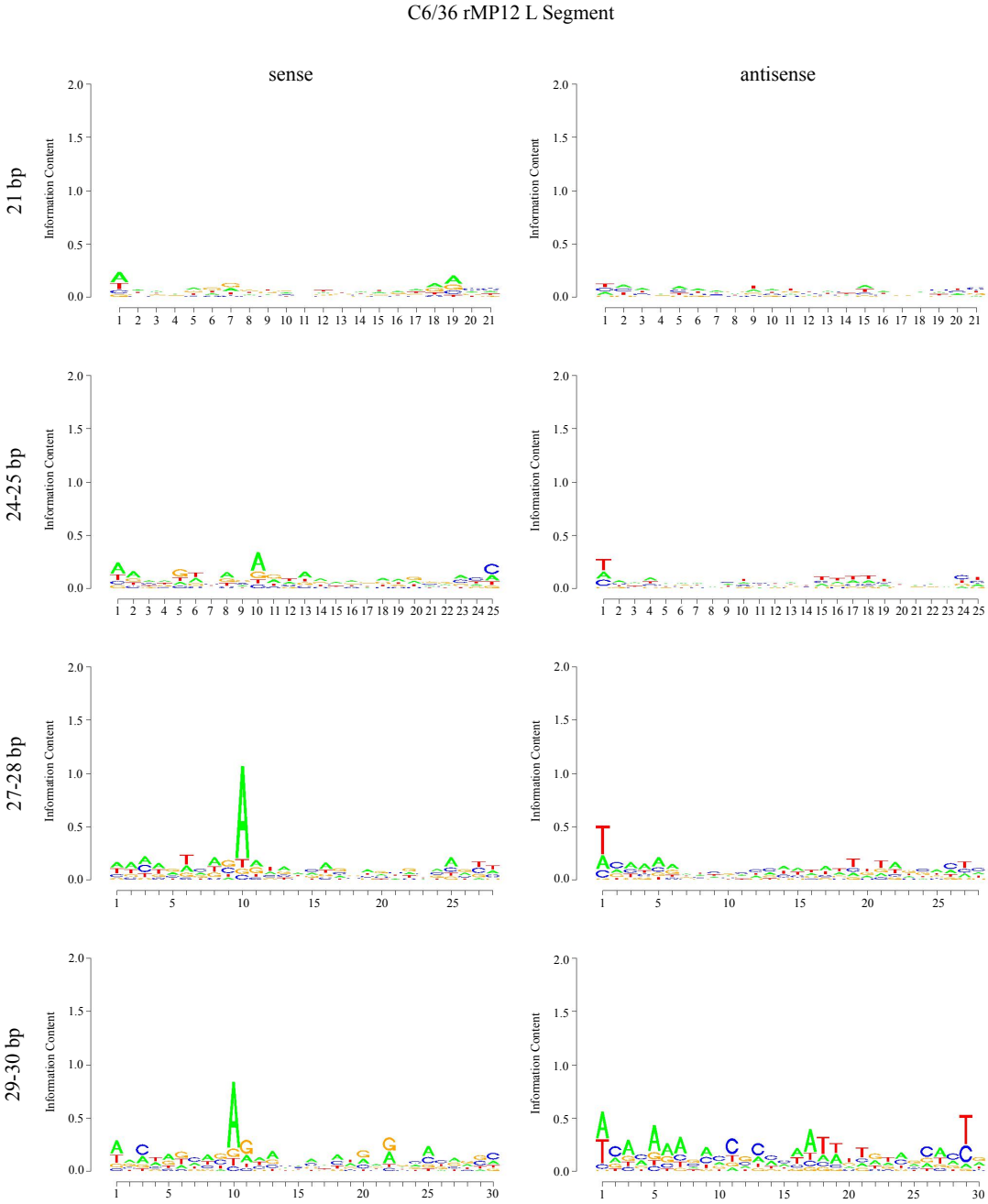

Figure 8-5: Logo analysis of viRNA species detected in rMP12 infected mosquito cells
Logo analysis of rMP12 infected C6/36, U4.4, Ae, and C7-10 cells, with sense and antisense strand species analysis represented for the 21 bp, 24-25 bp, 27-28 bp, and 29-30 bp viRNA size classes. Shown are species aligning to the rMP12 L, M, and S segments,

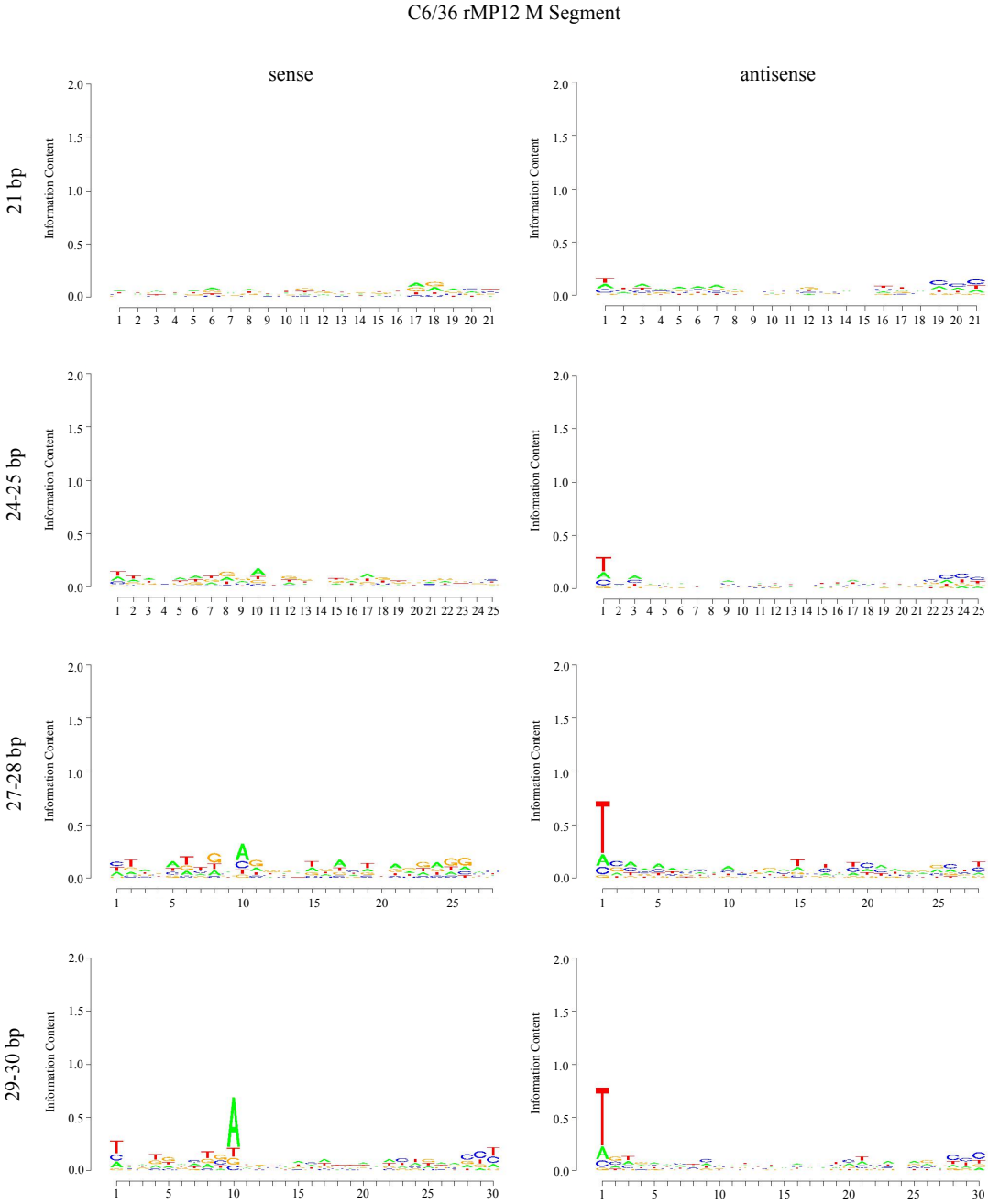
C6/36 rMP12 M Segment
sense
antisense
21 bp
24-25 bp
27-28 bp
29-30 bp
Information Content

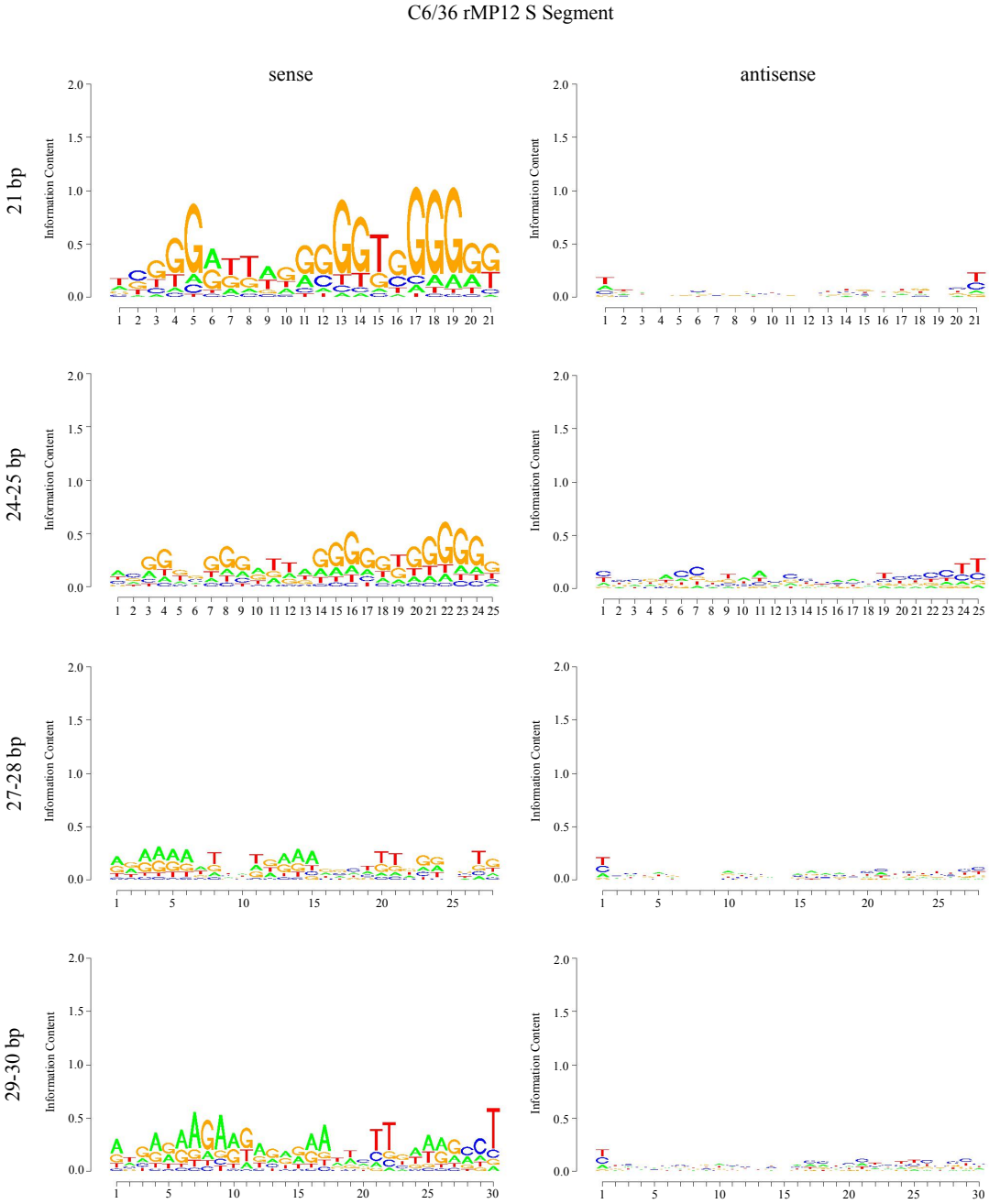
C6/36 rMP12 S Segment
sense
antisense
21 bp
24-25 bp
27-28 bp
29-30 bp
Information Content

(B) rMP12 infected U4.4 cells

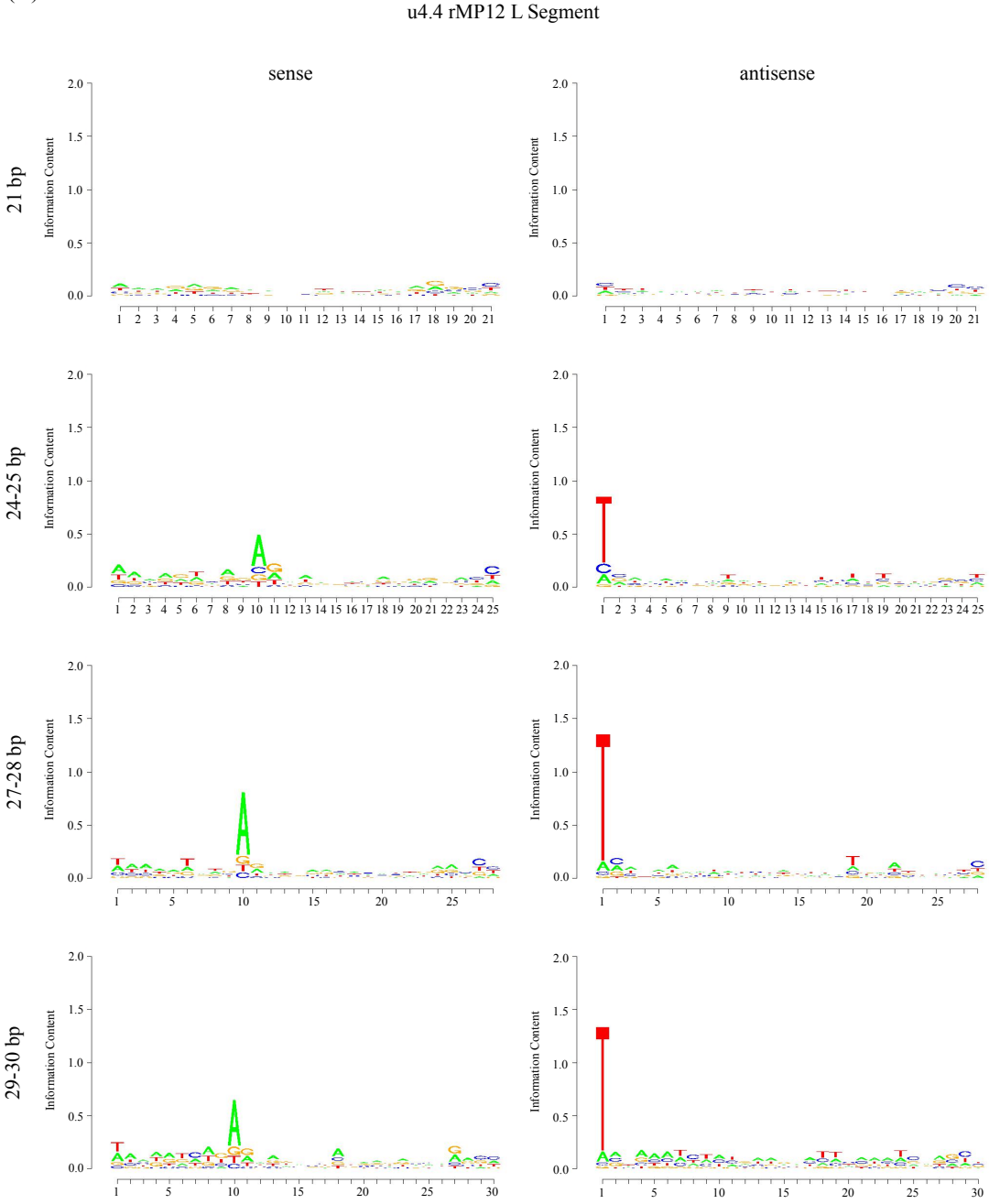

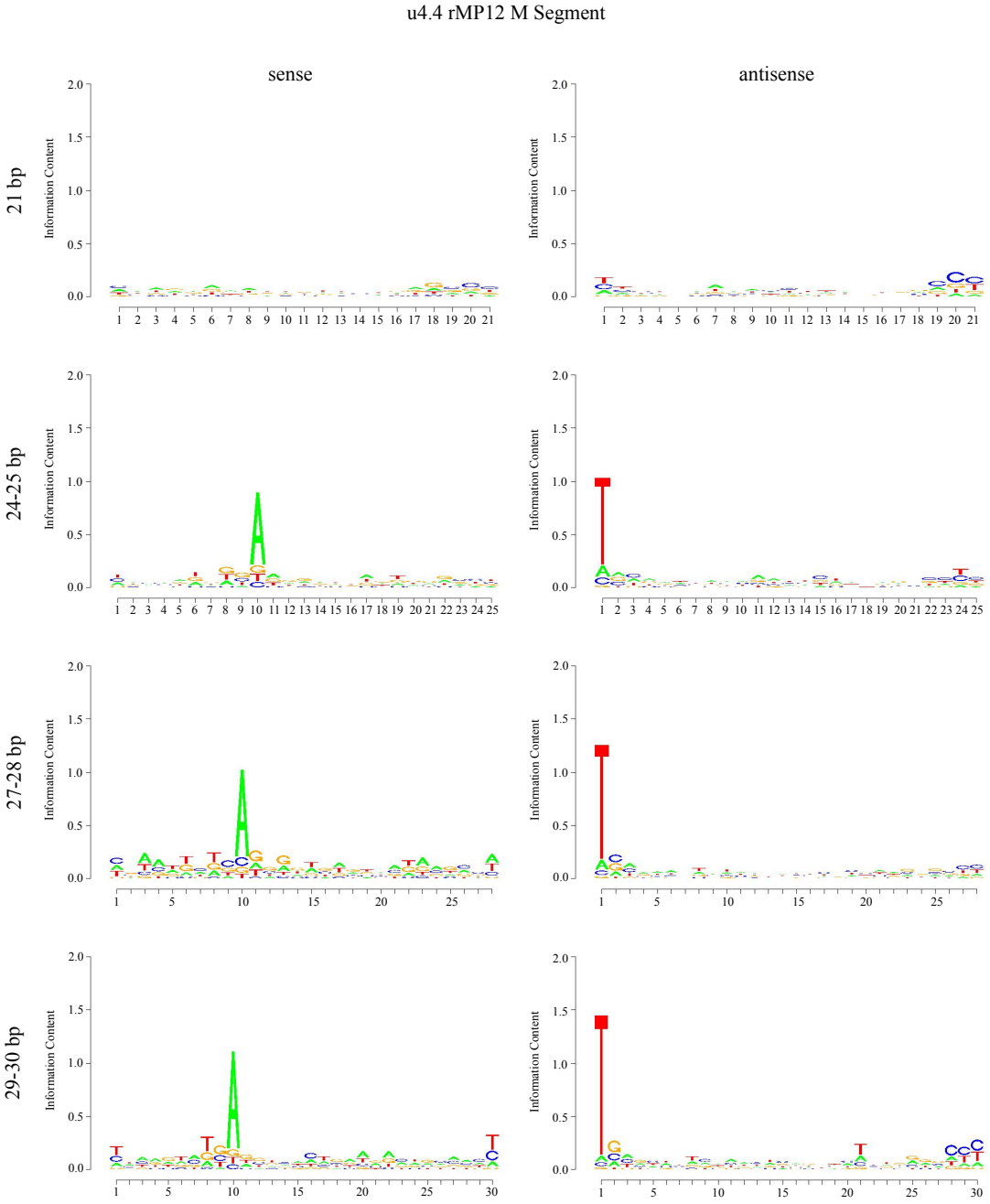
u4.4 rMP12 M Segment
sense
antisense
21 bp
24-25 bp
27-28 bp
29-30 bp
Information Content

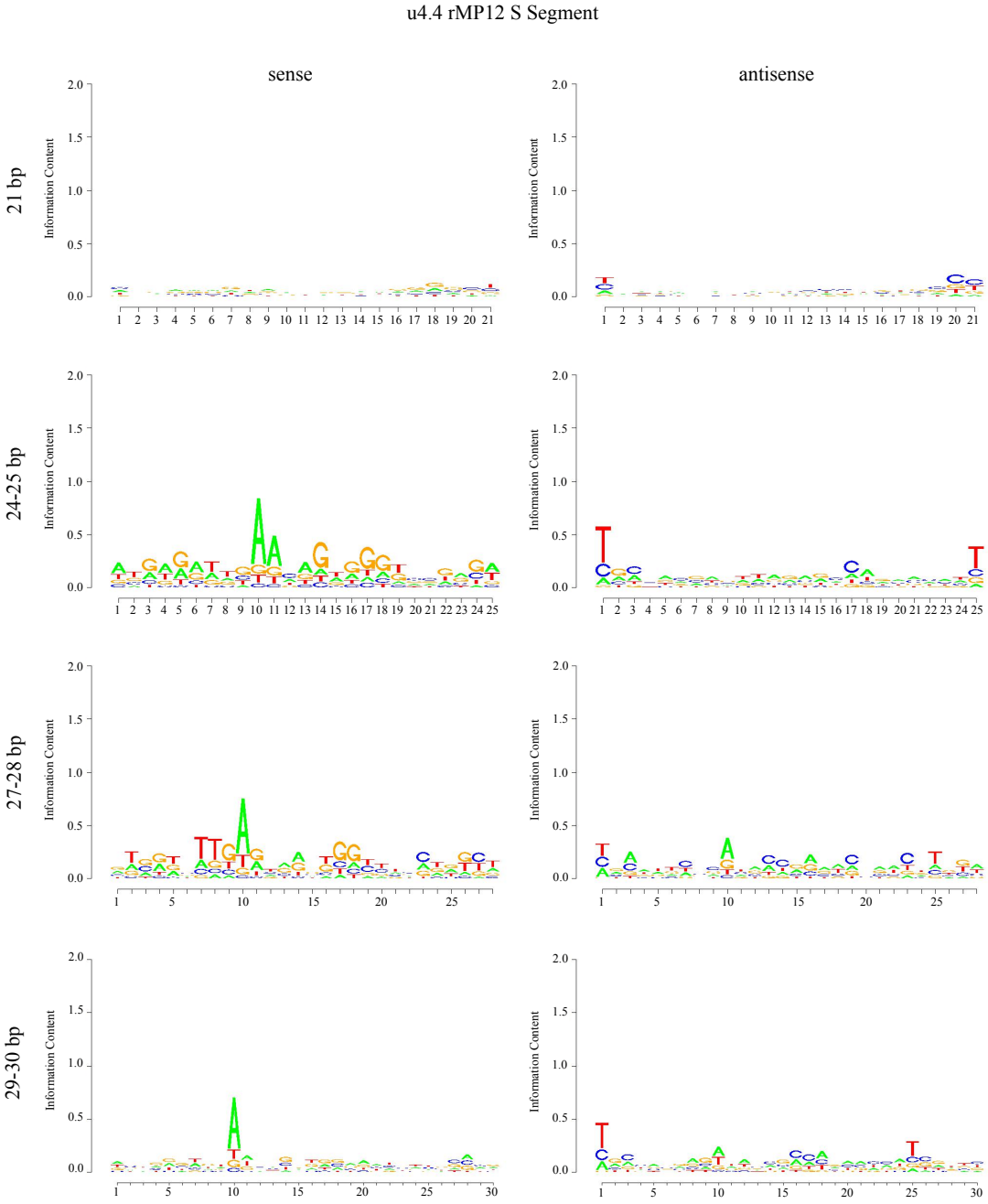
u4.4 rMP12 S Segment
sense
antisense
21 bp
24-25 bp
27-28 bp
29-30 bp
Information Content

(C) rMP12 infected Ae cells

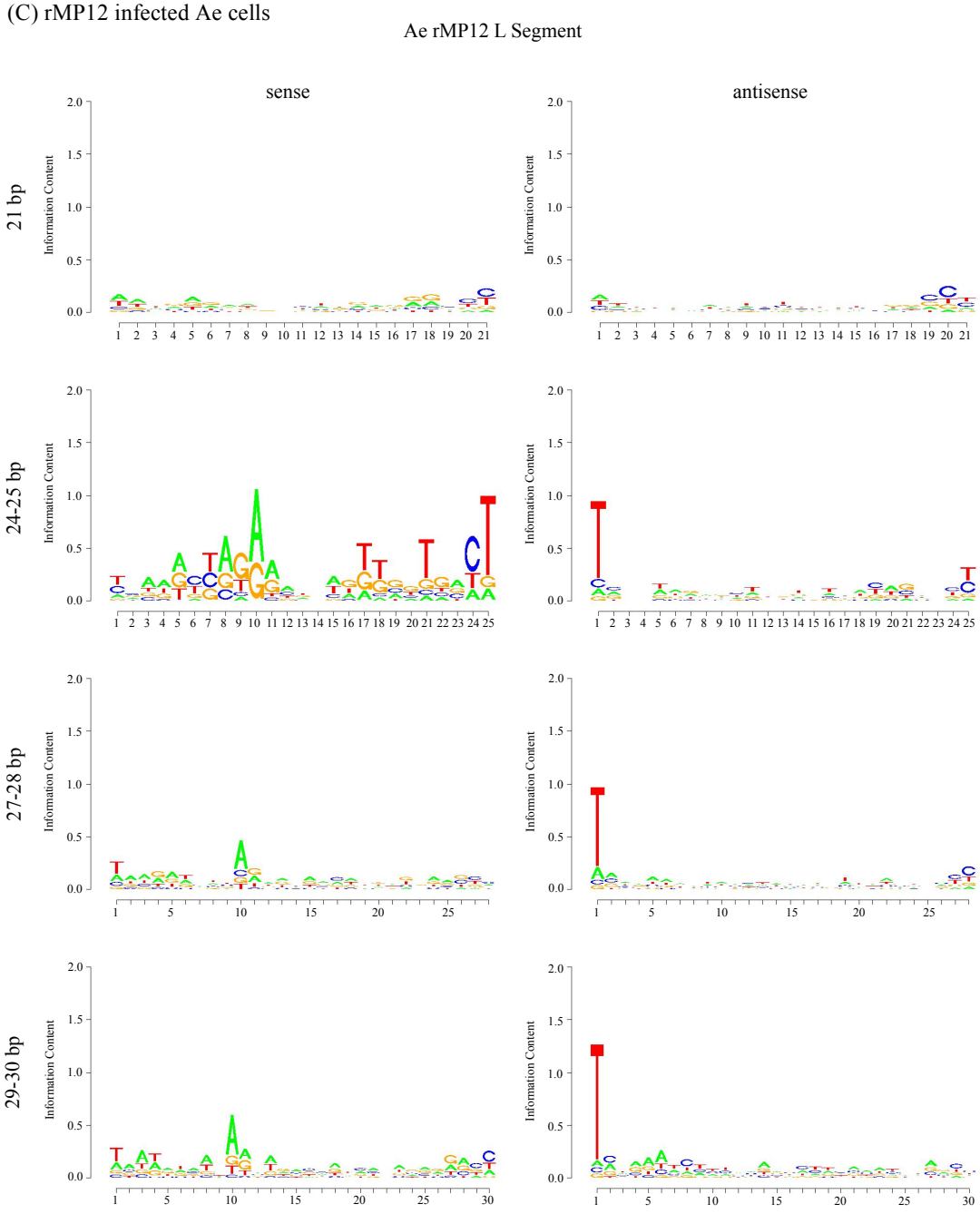

(C) Ae cells infected with rMP12

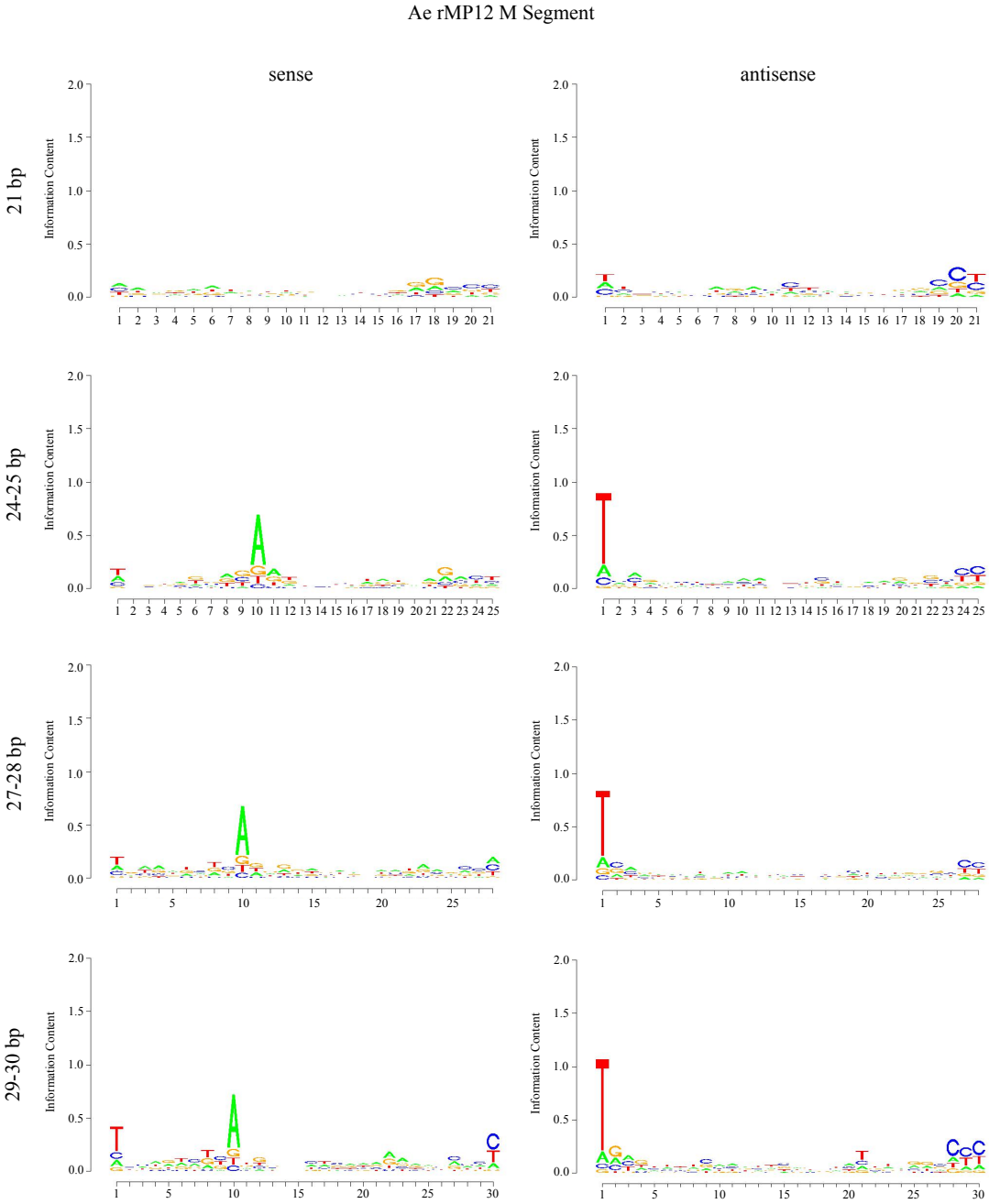
Ae rMP12 M Segment
sense
antisense
21 bp
24-25 bp
27-28 bp
29-30 bp
Information Content

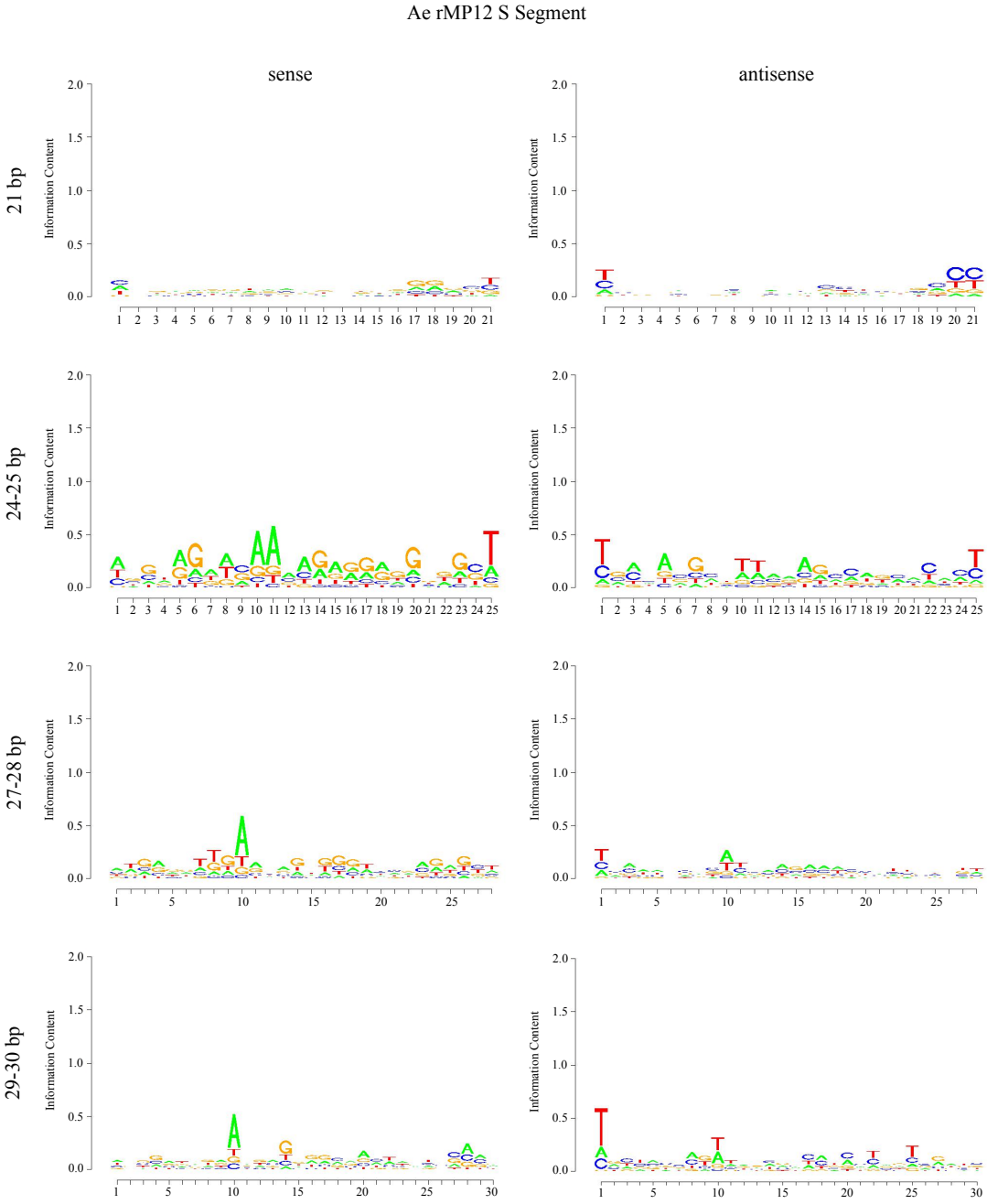
Ae rMP12 S Segment
sense
antisense
21 bp
24-25 bp
27-28 bp
29-30 bp
Information Content

(D) rMP12 infected C7-10 cells

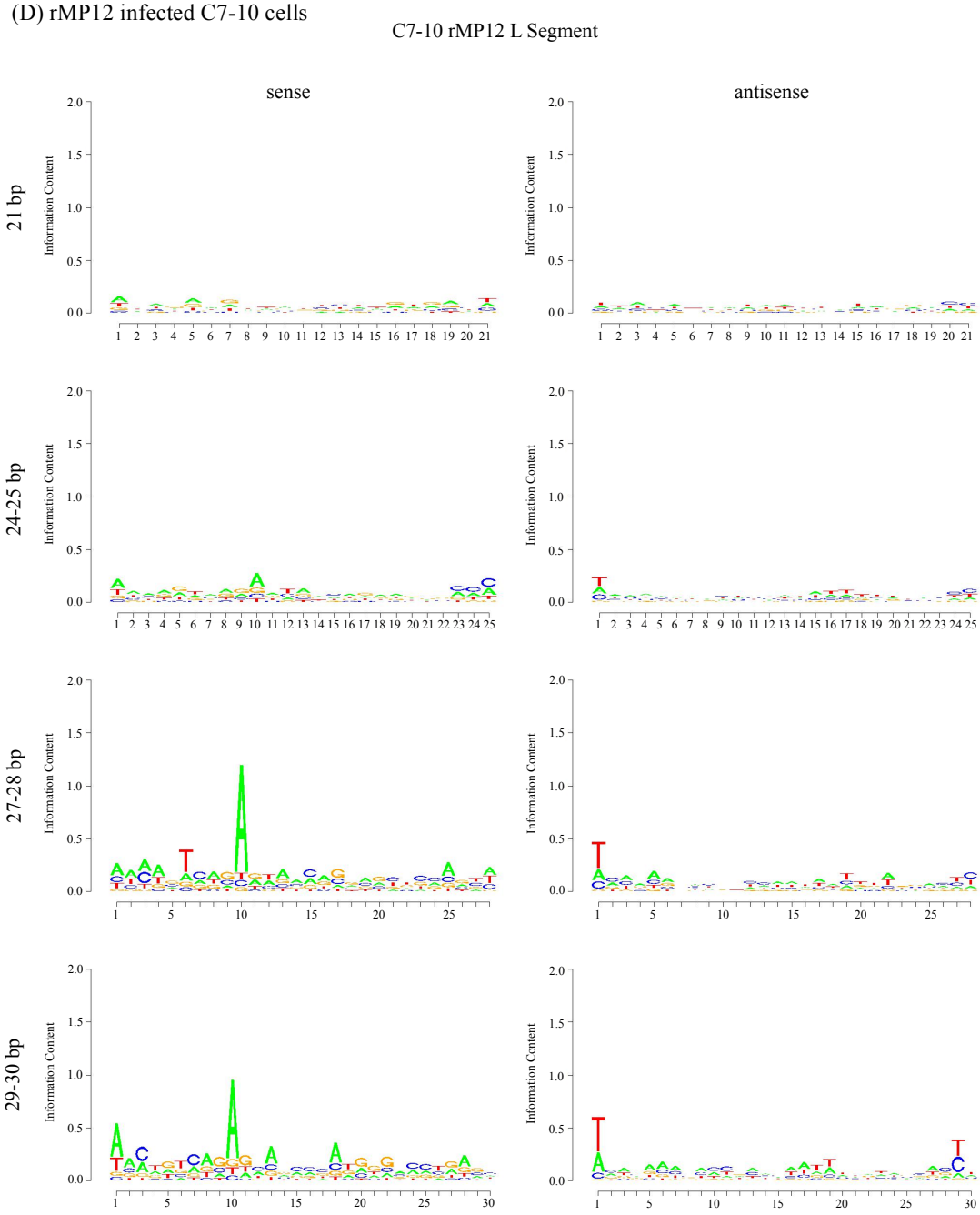

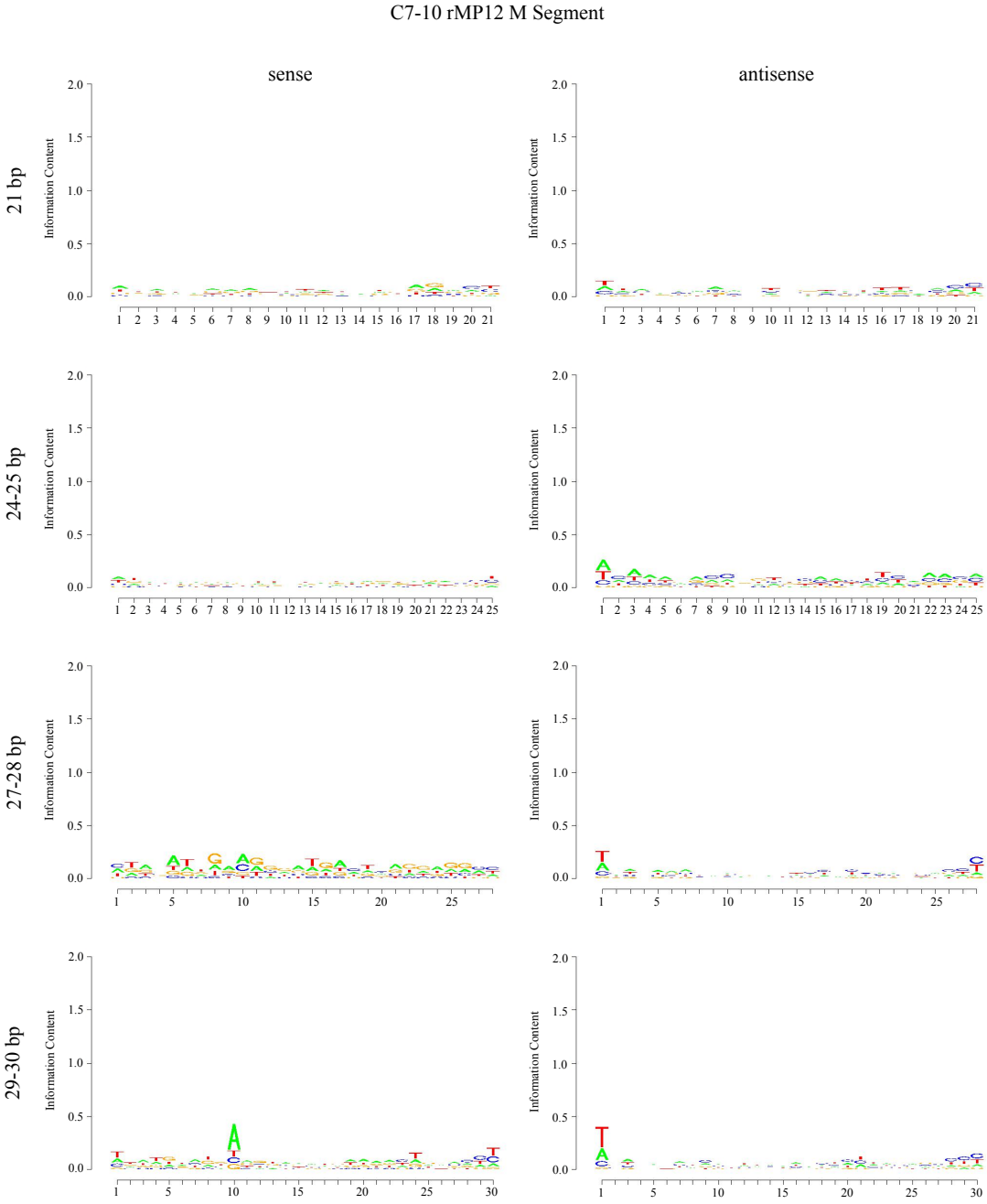
C7-10 rMP12 M Segment
sense
antisense
21 bp
24-25 bp
27-28 bp
29-30 bp
Information Content

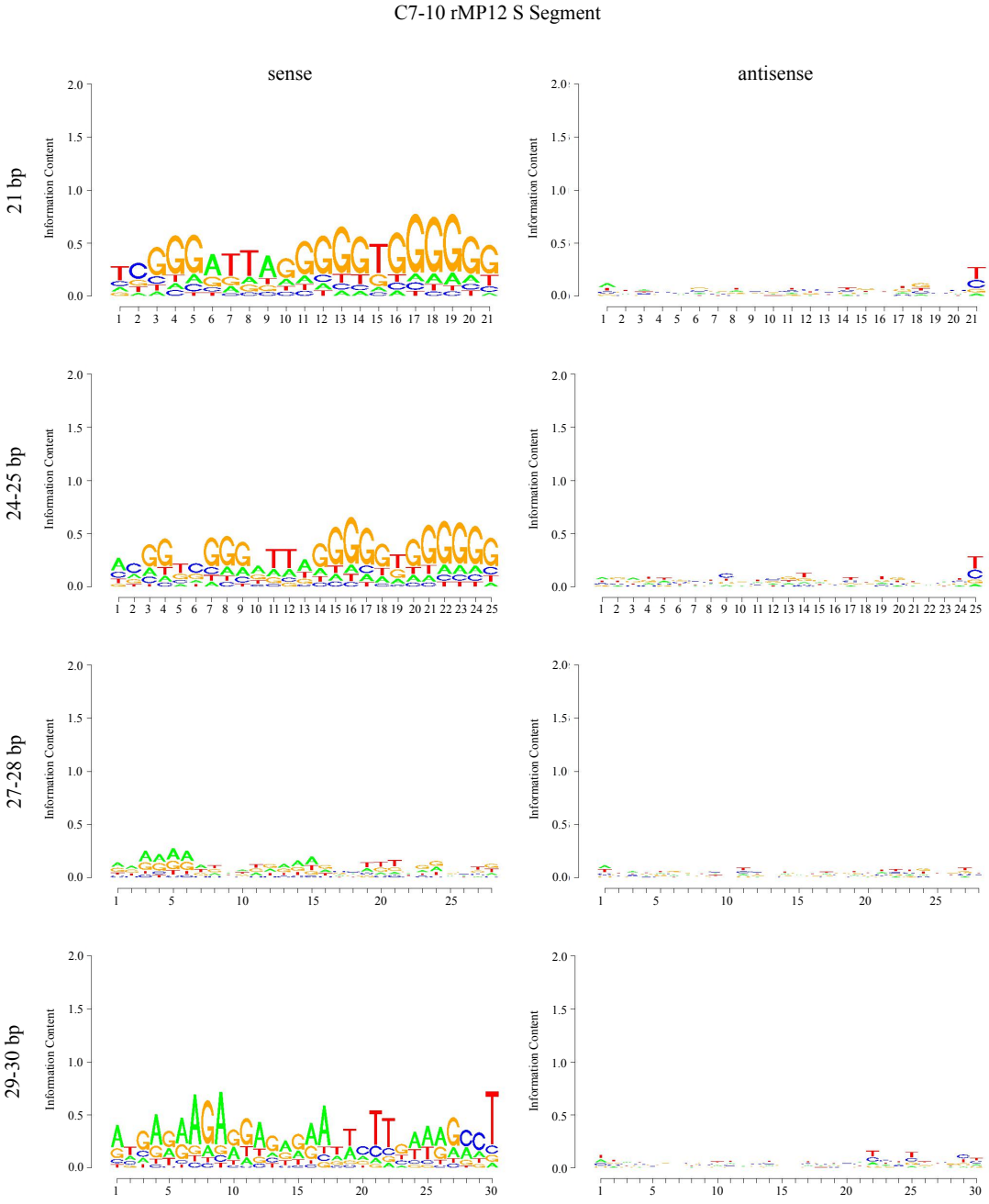
C7-10 rMP12 S Segment
sense
antisense
21 bp
24-25 bp
27-28 bp
29-30 bp
Information Content

8.3.5 Differences in RNAi response to rMP12 and rMP12:S-Swap infection

Previous data have demonstrated the attenuation of rMP12:S-Swap virus replication in mosquito cells. As well as reduced titres, the level of mRNA transcription and protein expression was also markedly lower than that observed in rMP12 infected cells. Similarly, total read numbers of viRNA species were reduced by an average 100-fold in all cell lines. Attenuation was greatest in Ae cells where total numbers were reduced to a level where meaningful data analysis could not be performed. In C6/36 and C7-10 cells the majority of viRNA species detected comprised 15-17 nt species, with no peaks apparent at other size classes. Results for the rMP12:S-Swap infected C6/36, Ae, and C7-10 cells are summarised in: viRNA plots analysis in Appendix Figure 10-4; density plots analysis in Appendix Figure 10-5; and logo analysis in Appendix Figure 10-6. However, in rMP12:S-Swap infected U4.4 cells viRNA numbers generated were sufficient to compare the response to that observed in rMP12 infected cells.

Size and polarity distribution patterns in viRNA species targeting the L and M segments remained similar to those of rMP12 infected cells (Figure 8-6). A small variation in the proportion of antigenomic siRNA species targeting the S segment was apparent compared to rMP12, but no differences in piRNA species were observed. The reduction in viRNA numbers was most apparent for species targeting the L and M segments, and no discernable hotspots were observed (Figure 8-7). viRNA species targeting the S segment were distributed throughout the genome, consisting of both genomic and antigenomic polarity species. However, siRNA species targeting the coding regions were reduced, and the majority now targeted the same IGR sequence observed previously in the rMP12 infected cells. This suggests that this IGR target elicits a preferential and stronger response from the siRNA pathway than those contained within the coding regions. The distribution of piRNA hotspots was similar to that in rMP12 infected cells, demonstrating a bias towards antigenomic polarity species targeting 3’ terminus. Again, the viRNAs were highly conserved between the duplicate samples (see Appendix Figure 10-7) Logo analysis demonstrated similar nucleotide biases for the piRNA species as those observed in rMP12 infected cells, although a bias toward 1’ T and 10’ U residues was observed in both sense and antisense piRNA species (Figure 8-8). The reasons for this are unclear, although as it was only observed in S segment it is possible it was an artifact of the ambisense coding strategy.

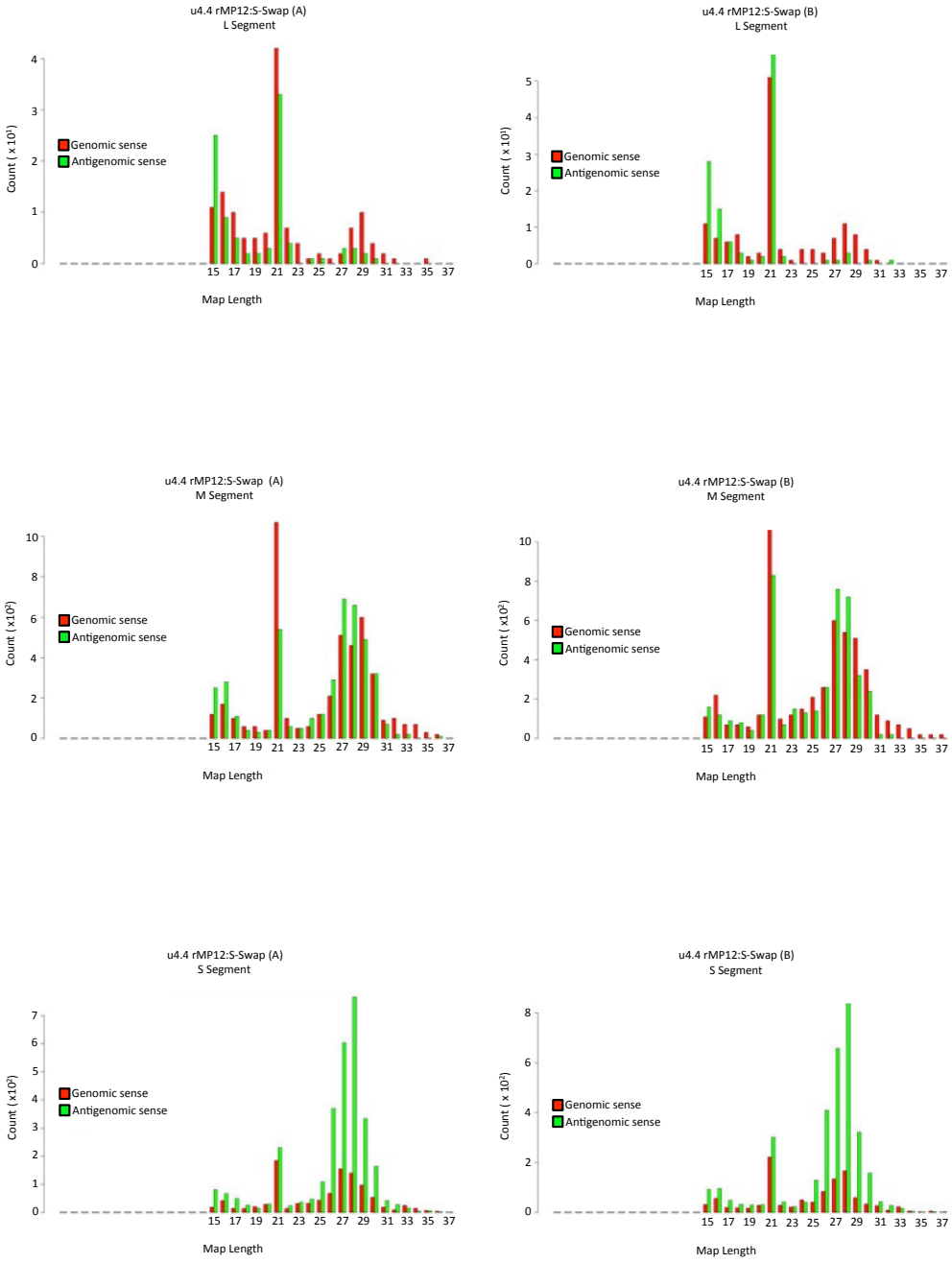

Figure 8-6: viRNA species plot analysis for rMP12:S-Swap infected U4.4 cells.
Size distribution and density plots of all 15-37 nt viRNA species detected in rMP12:S-Swap infected U4.4 cells aligning to the L, M and modified S segment. Shown are replicate samples A and B taken from duplicate infections. viRNA species aligning to genomic polarity (negative sense) RNA are shown in red, antigenomic polarity (positive sense) RNA in green.

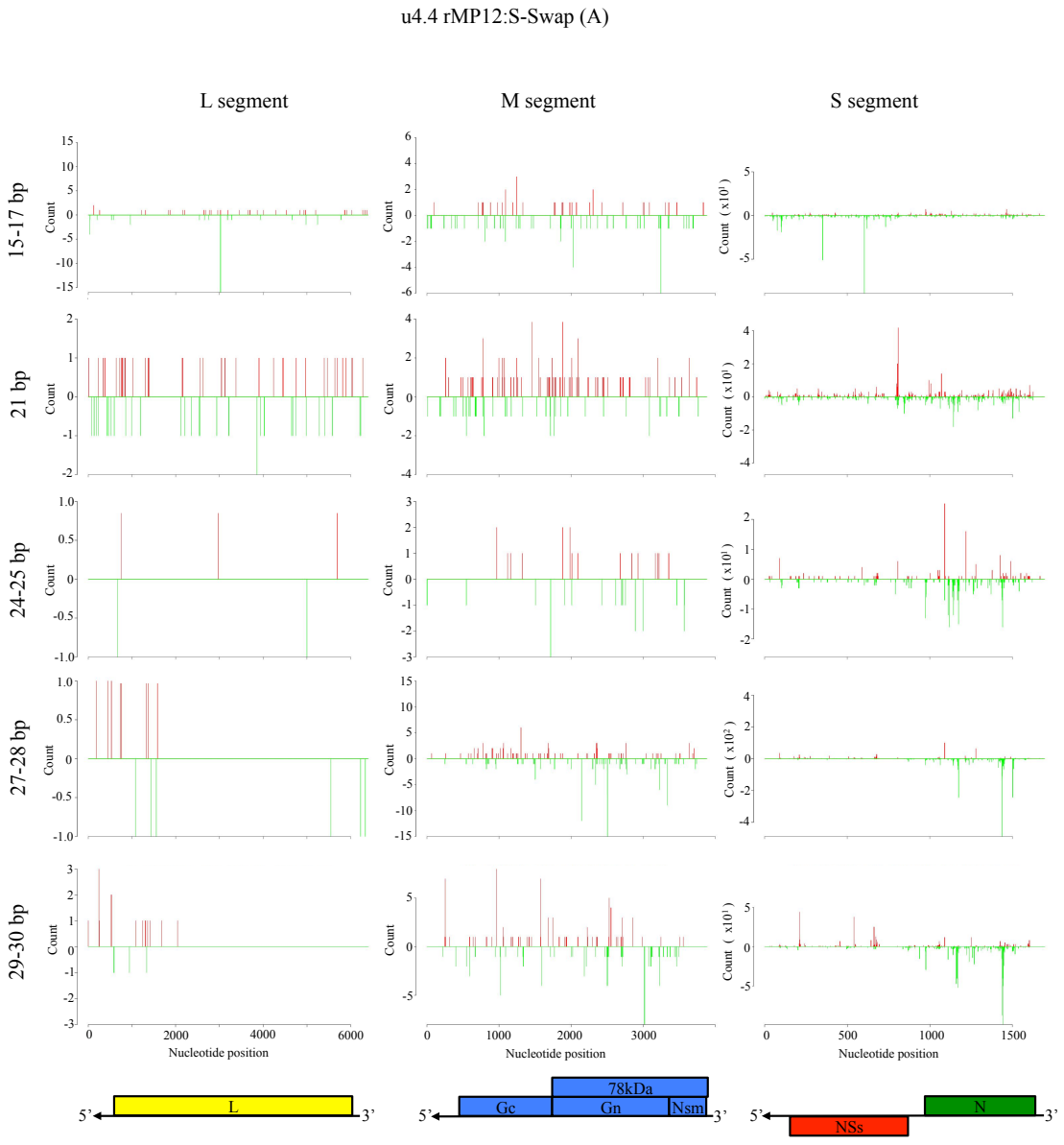

Figure 8-7: Mapping analysis of viRNA species targeting the rMP12:S-Swap genome segments in infected U4.4 cells.
Shown are density plots of aligned viRNA species of 15-17nt, 21nt, 24-25nt, 27-28nt, and 29-30nt aligning to the rMP12:S-Swap L, M, and S genome segments. Upper plots (red) show alignments to genomic polarity (negative sense) and lower plots (green) to antigenomic polarity (positive sense). Also shown are the CDS for MP12 proteins encoded on the L (yellow), M (blue) and S (green and red) segments.

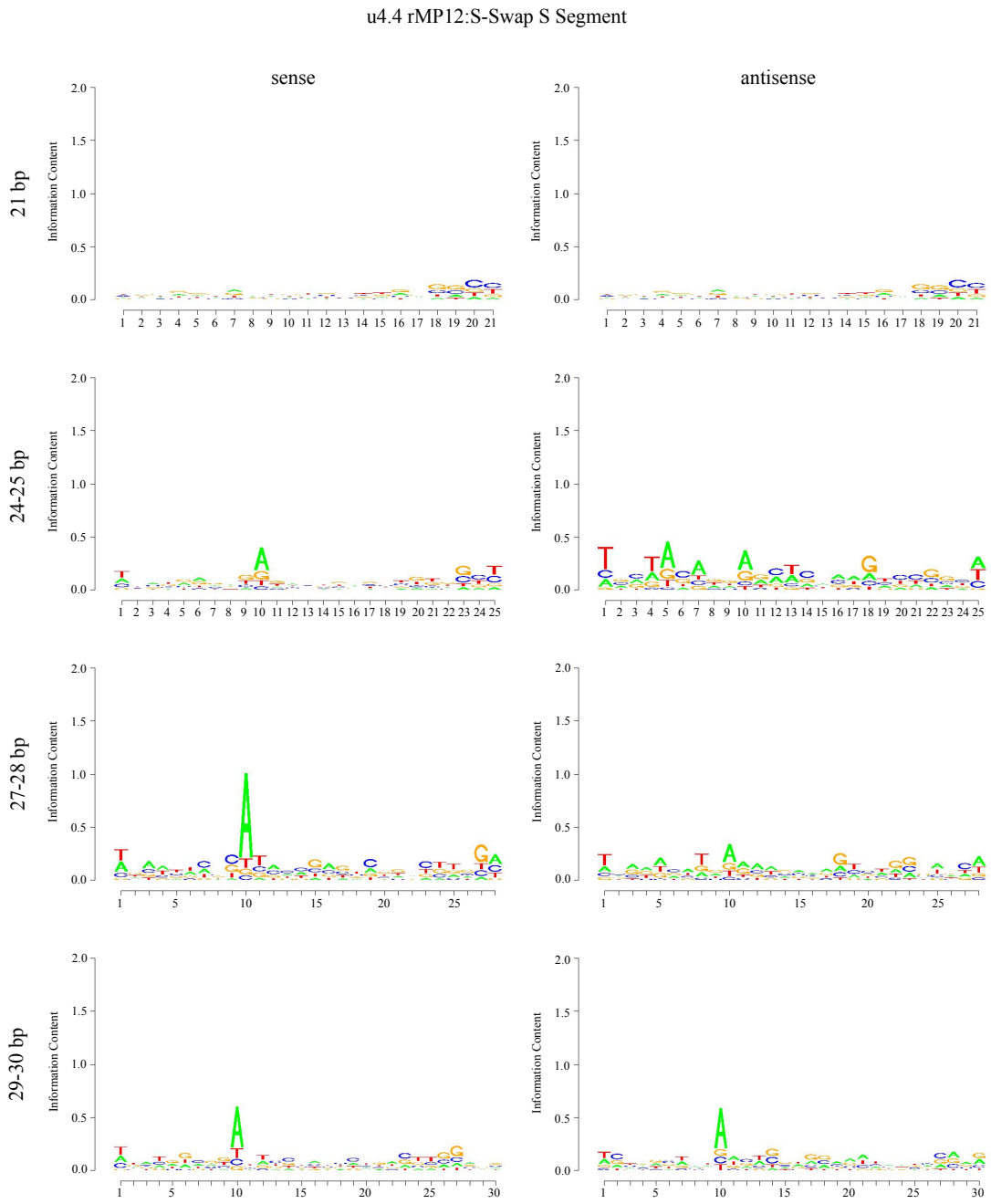

Figure 8-8: Logo analysis of viRNA species detected in rMP12:S-Swap infected U4.4 cells
Logo analysis of rMP12:S-Swap infected U4.4 cells, with sense and antisense strand species analysis represented for the 21 bp, 24-25 bp, 27-28 bp, and 29-30 bp viRNA size classes. Shown are species aligning to the rMP12:S-Swap L, M, and S segments.

To investigate differences in viRNA species targeting the rMP12:S-Swap S segment, the five most numerous siRNA and piRNA species targeting the S segment in the duplicate rMP12 and rMP12:S-Swap samples were identified (summarised in Appendix Table 10-5). Alignments of the siRNA revealed several consensus species were generated in cells infected with both viruses, with the majority targeting the NSs coding region (Figure 8-9). Due to polarity differences in the reference genomes, antigenomic species targeting NSs coding region in rMP12 infected cells, would be of the same sense (positive) as genomic species targeting NSs coding regions in rMP12:S-Swap infected cells. Individual siRNA species comprising the strong NSs hotspots in both rMP12 and rMP12:S-Swap infected cells were identical. However, the species comprising the IGR hotspot were of different polarities between the two viruses. This suggested that the target for the siRNA pathway in both infections had identical polarities in the NSs coding region, but an opposite polarity in the IGR. These results imply that it is the NSs mRNA transcript or mRNA:genome duplex structures acting as the target for both viruses, rather than a replicative intermediate structure.

To investigate if potential dsRNA targets for the siRNA pathway exist within the NSs mRNA transcript, the overall secondary structure was calculated using mFold (Zuker 2003). The five most numerous siRNA species identified previously (see Appendix Table 10-5) were aligned to this structure. The species targeted the NSs CDS aligned to hairpin loop regions, specifically mapping to one strand of the hairpin stem with the end of the siRNA species located in the terminal loop structure. Species targeting the IGR also aligned to a hairpin loop stem, although the terminal loop was not involved (Figure 8-10). NSs mRNA transcribed from rMP12:S-Swap S segment was predicted to have slightly dissimilar overall secondary structure compared to rMP12 NSs mRNA due to sequence differences in the UTR and IGR. However, identical hairpin structures were predicted to form in the rMP12:S-Swap NSs mRNA molecule. Hairpin loop structures within the NSs mRNA acting as dsRNA targets would be a potential target for the biogenesis of the siRNA species, given our current understanding of this pathway.

The distribution pattern of piRNA species in cells infected with rMP12 or rMP12:S-Swap was different to that for the siRNAs. In rMP12 infected cells the majority of piRNA species were of antigenomic polarity and targeted toward the N coding region. In

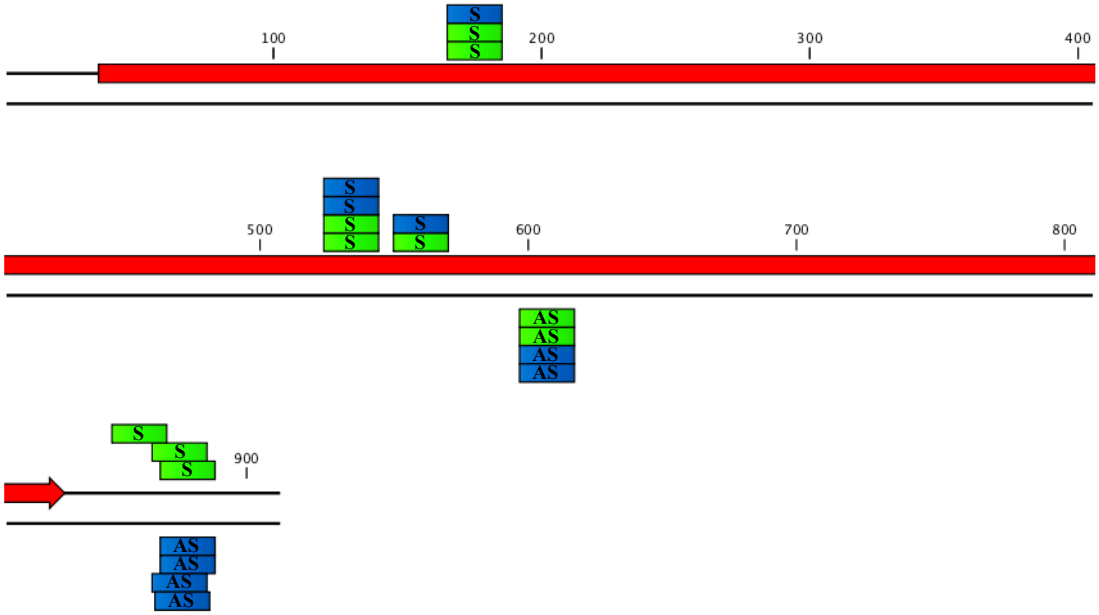

Figure 8-9: siRNA consensus species analysis in rMP12 and rMP12:S-Swap infected of U4.4 cells
The five most populous siRNA species detected in rMP12 (green) and rMP12:S-Swap (blue) infected U4.4 cells (duplicate infections) were aligned to NSs mRNA transcribed from the rMP12 S segment. Each siRNA species was classified as either sense (S) or antisense (AS) dependent on the polarity. Also shown is the NSs CDS (red).

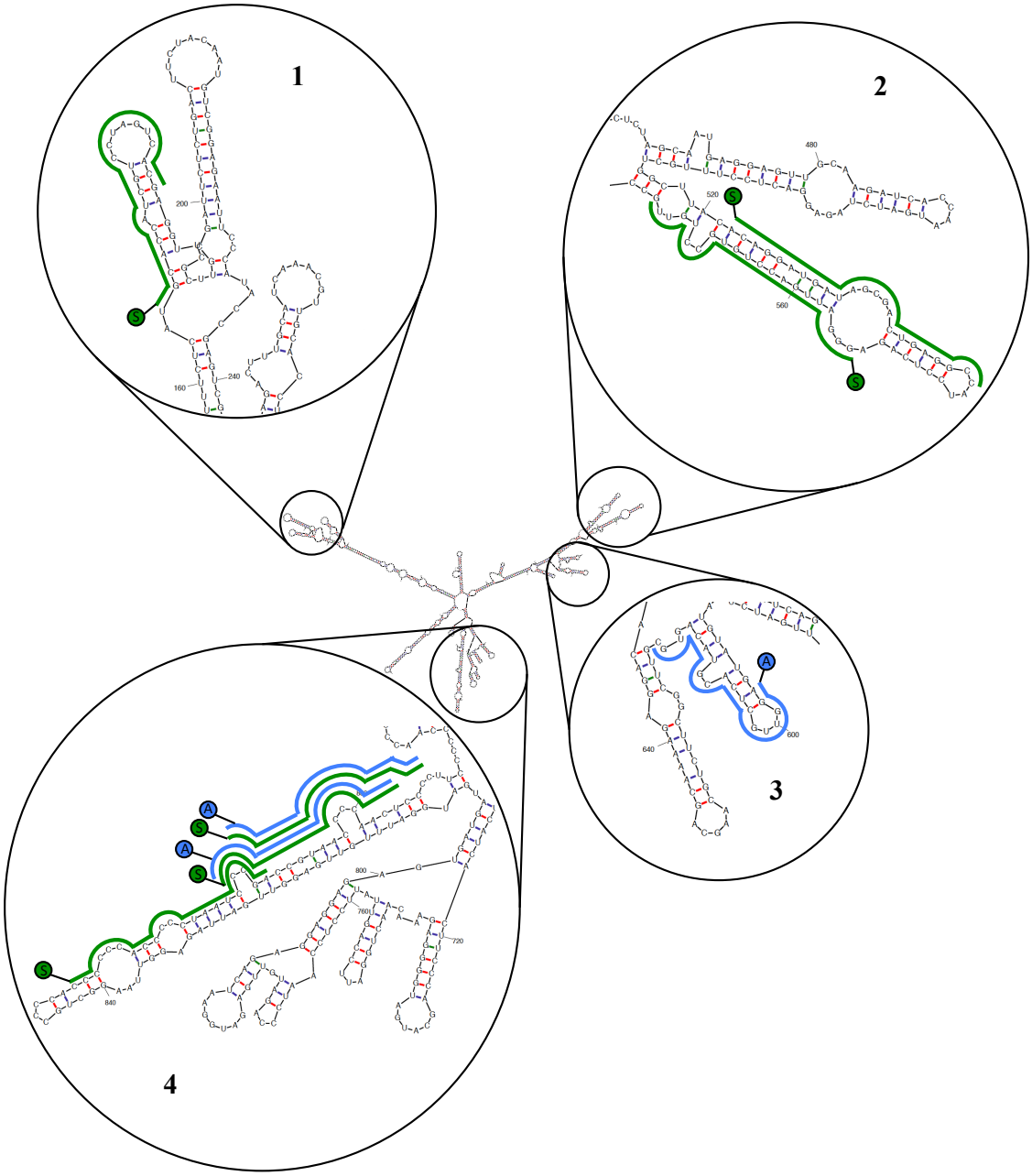

Figure 8-10: Secondary structure of the rMP12 NSs mRNA transcript showing siRNA consensus species

RNA secondary structure of rMP12 NSs mRNA was calculated using mFold web software. rMP12 and rMP12:S-Swap consensus species identified in Figure 8-9 were aligned to the mRNA structure. Identified are the species location and polarity, either sense (S) or antisense (A). Regions 1-3 are located within the CDS for NSs, region 4 is located within the IGR region.

rMP12:S-Swap infected cells the piRNA species generated were again predominately of antigenomic polarity, although these now mainly targeted the NSs coding region (Figure 8-11). Unlike for the siRNA pathways, the specific process or processes responsible for piRNA biogenesis during viral infection are less well defined. They are thought to involve a single stranded RNA target, and production has been shown to be Dicer-independent (Vodovar et al. 2012; Olivieri et al. 2010). The previously described results in Chapter 6 demonstrated an increase in the level of NSs mRNA transcription in rMP12:S-Swap infected cells, and in Chapter 7 the parental N UTR of MP12 was shown to be the stronger of the promoters contained on the S segment. This could suggest that piRNA biogenesis is based on the relative amounts of specific RNA species in infected cells, and the differential piRNA species observed are a result of this response targeting the most populous species in the infected cell.

8.3.6 RNAi pathway consequences of replacing the NSs CDS in rMP12

rMP12ΔNSs:eGFP titres were similar to those for rMP12, although numbers of viRNA species detected were reduced. Patterns in size distribution, polarity biases, and hotspot distributions for both the L and M segments demonstrated little variation to those observed in rMP12 infected cells (Figure 8-12). The decrease in viRNA number was most apparent in those species targeting the S segment, with an average 2-fold reduction in both U4.4 and Ae cells. The distribution of siRNAs targeting the S segment was similar to that observed for rMP12 however. While some species targeted the N coding region, the majority were located in the eGFP coding region (Figure 8-13). This is analogous to rMP12 where the majority of the siRNA species aligned to the NSs coding region. Again there was a high degree of conservation in viRNA species targeting each genome segment (see Appendix Figure 10-8 for results from duplicate samples). Logo analysis demonstrated similar nucleotide biases in the piRNA species as observed in rMP12 infected cells (see Appendix Figure 10-9).

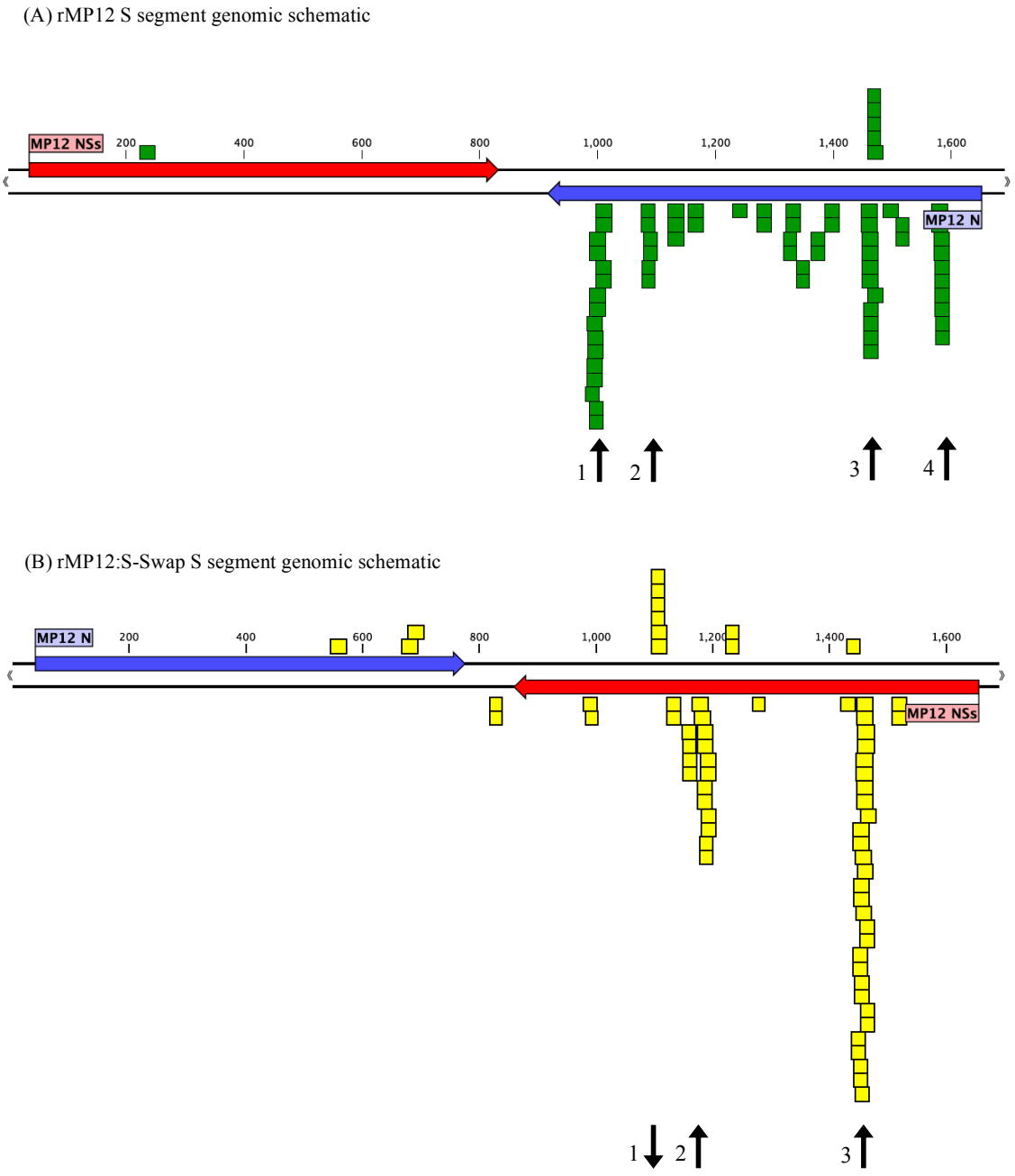

Figure 8-11: piRNA consensus species analysis in rMP12 and rMP12:S-Swap infected U4.4 cells
The 5 most numerous 24-30 nt viRNAs generated in rMP12 (green) or rMP12:S-Swap (yellow) infected U4.4 cell replicate samples were aligned to the (A) rMP12 and (B) rMP12:S-Swap reference genomes. piRNA species alignments shown above the genome segment are of genomic polarity, and below the genome are of antigenomic polarity. Shown are the CDS for the S segment encoded proteins N (blue) and NSs (red). Represented by black arrow are the major consensus species, expanded in Appendix Figure 10-13 and 10-14.

(A) rMP12ΔNSs:eGFP infected C6/36 cells.

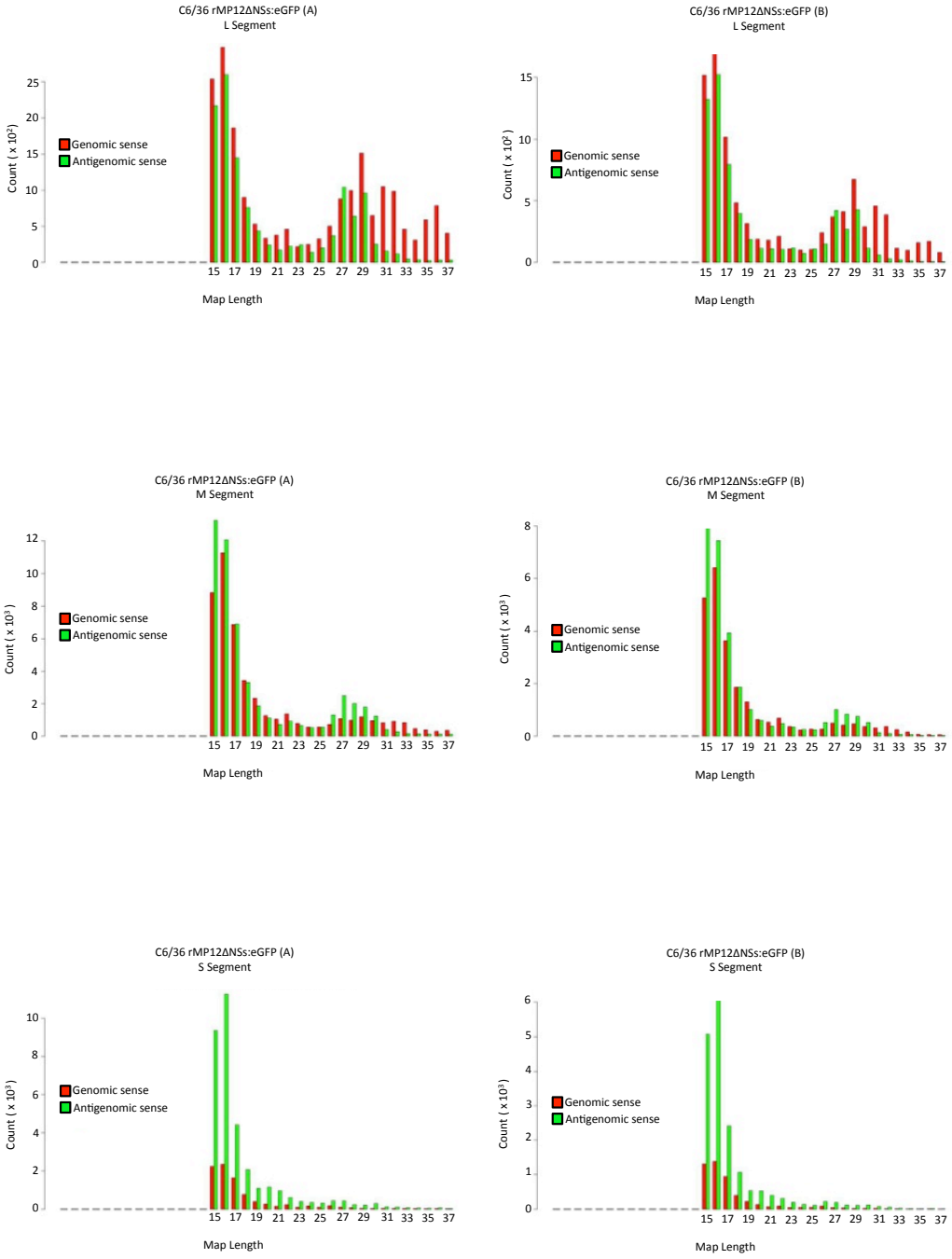

Figure 8-12: viRNA species plot analysis for rMP12ΔNSs:eGFP infected mosquito cells.
Size distribution and density plots of all 15-37 nt viRNA species detected in rMP12ΔNSs:eGFP infected mosquito cells lines aligning to L, M or S segment. Shown are replicate samples A and B taken from duplicate infections. viRNAs aligning to genomic sense RNA are shown in red, antigenomic sense RNA in green.

(B) rMP12ΔNSs:eGFP infected U4.4 cells.

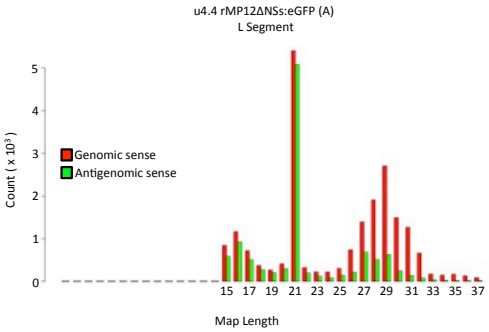

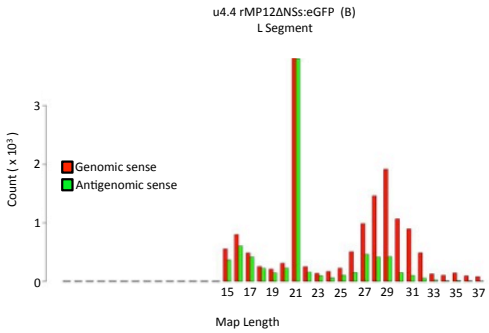

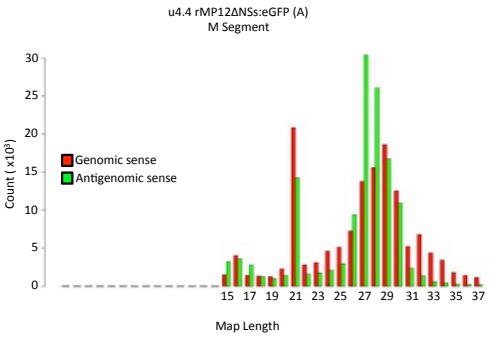

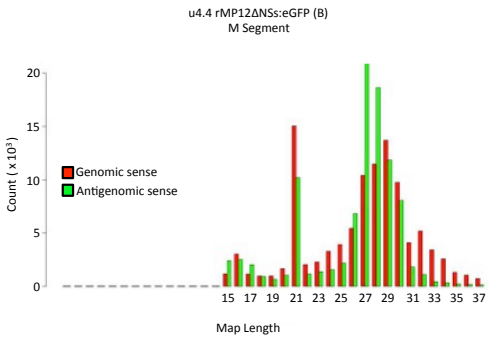

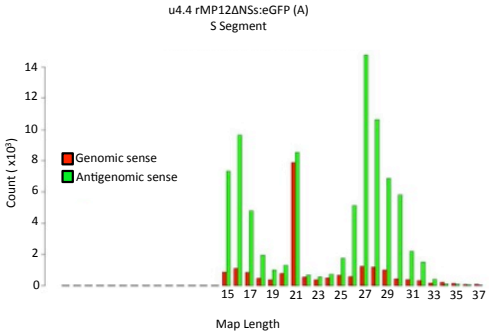

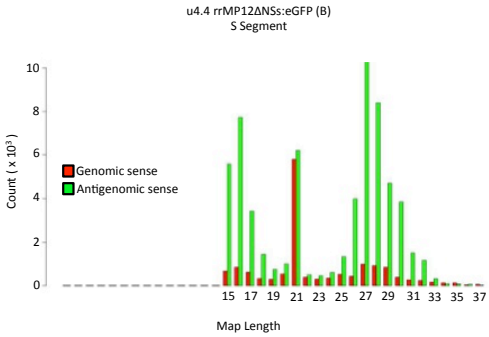

(C) rMP12ΔNSs:eGFP infected Ae cells.

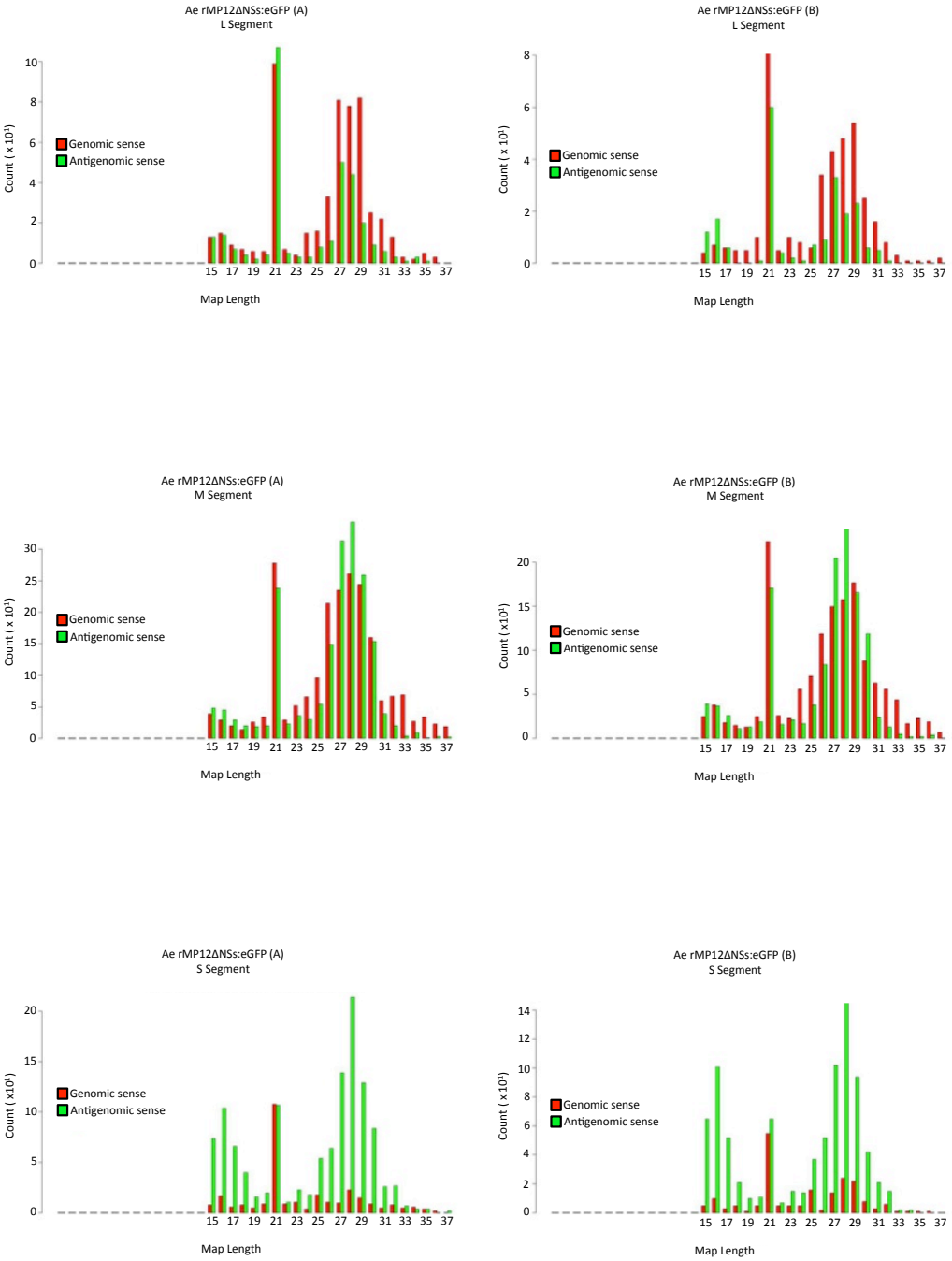

(D) rMP12ΔNSs:eGFP infected C7-10 cells.

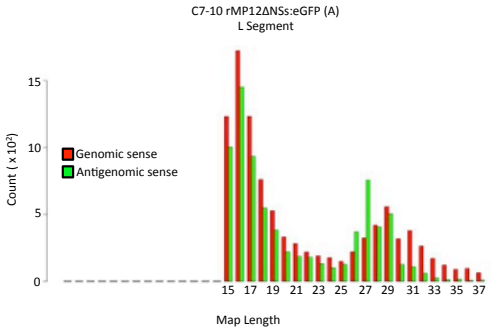

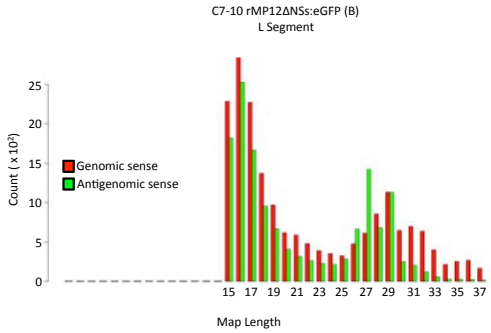

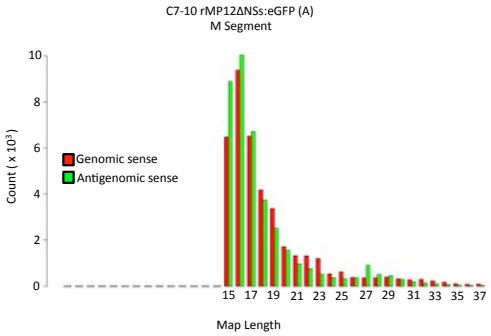

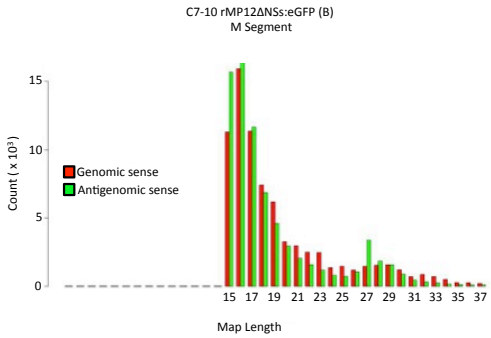

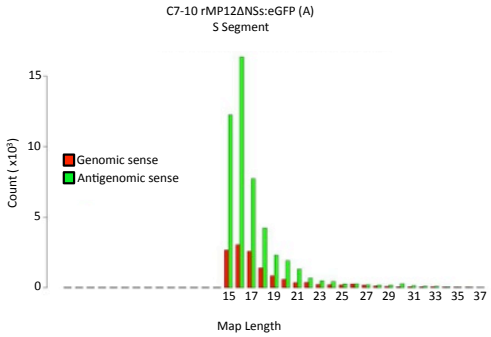

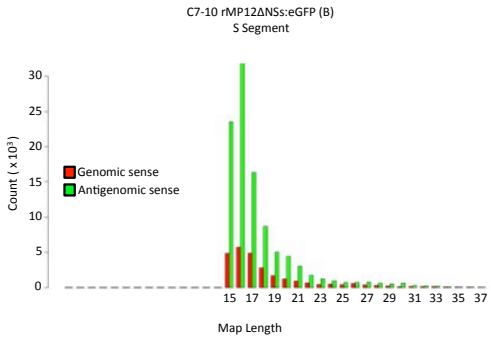

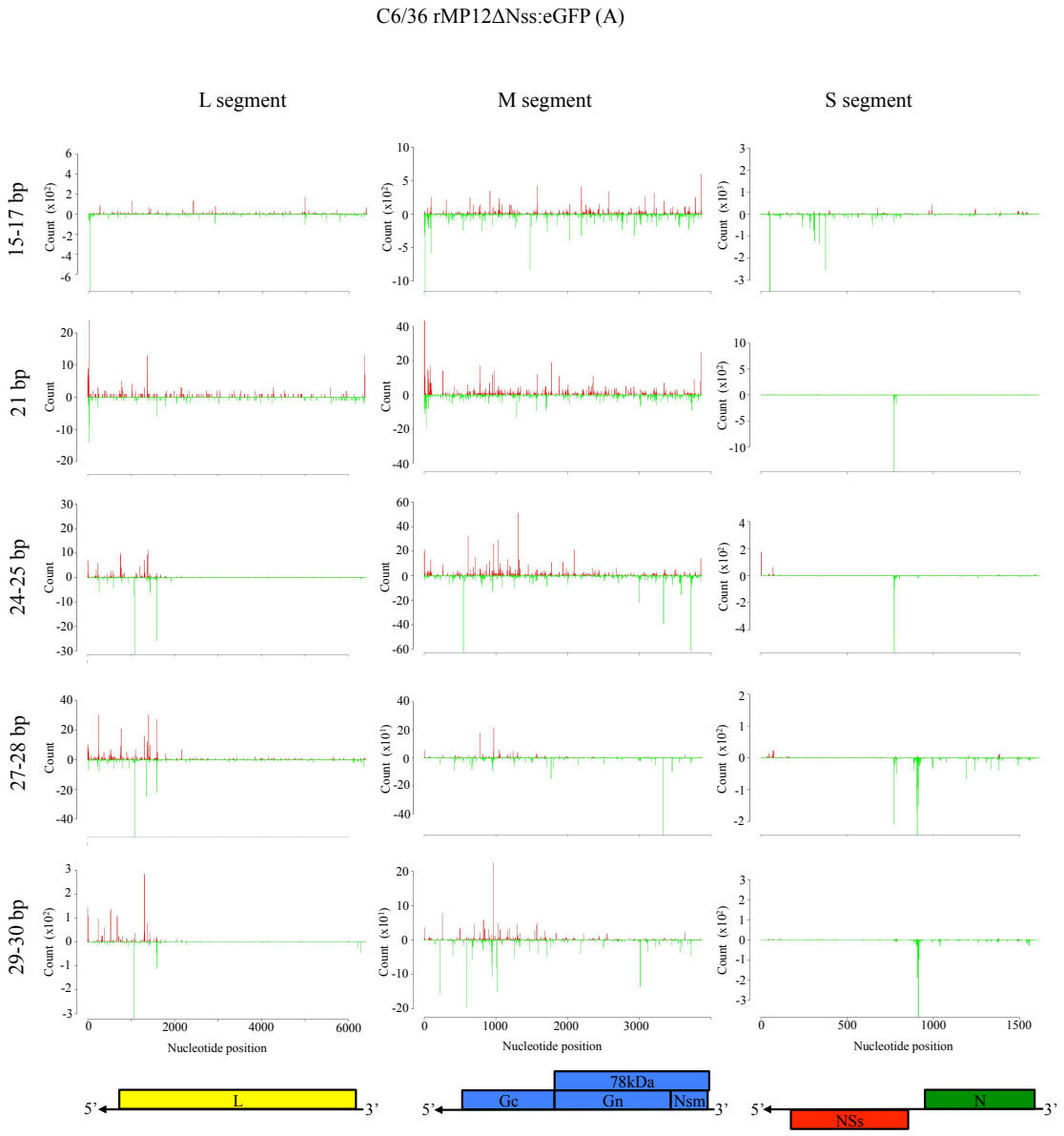

Figure 8-13: Mapping analysis of viRNA species targeting the rMP12ΔNSs:eGFP genome segments
Shown are the density plots of aligned viRNAs of 15-17nt, 21nt, 24-25nt, 27-28nt, and 29-30nt aligning to the rMP12ΔNSs:eGFP L, M, and S genomic segments. Upper plots (red) show alignments to genomic sense and lower plots (green) to antigenomic sense. Also shown are the CDS for MP12 proteins encoded on the L (yellow), M (blue) and S (green and red) segments.

(A) rMP12ΔNSs:eGFP infected C6/36 cells.

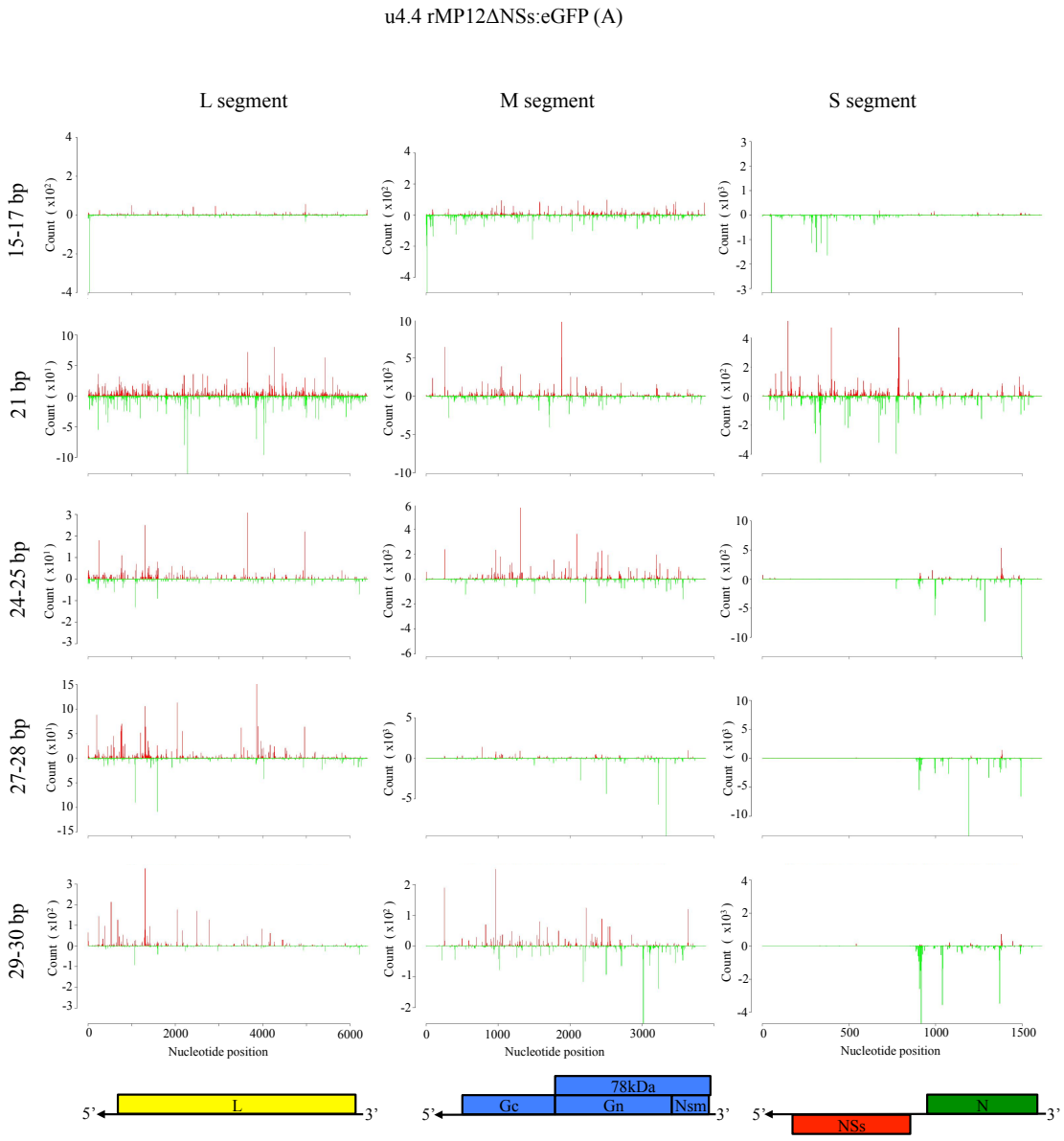

(B) rMP12ΔNSs:eGFP infected U4.4 cells.

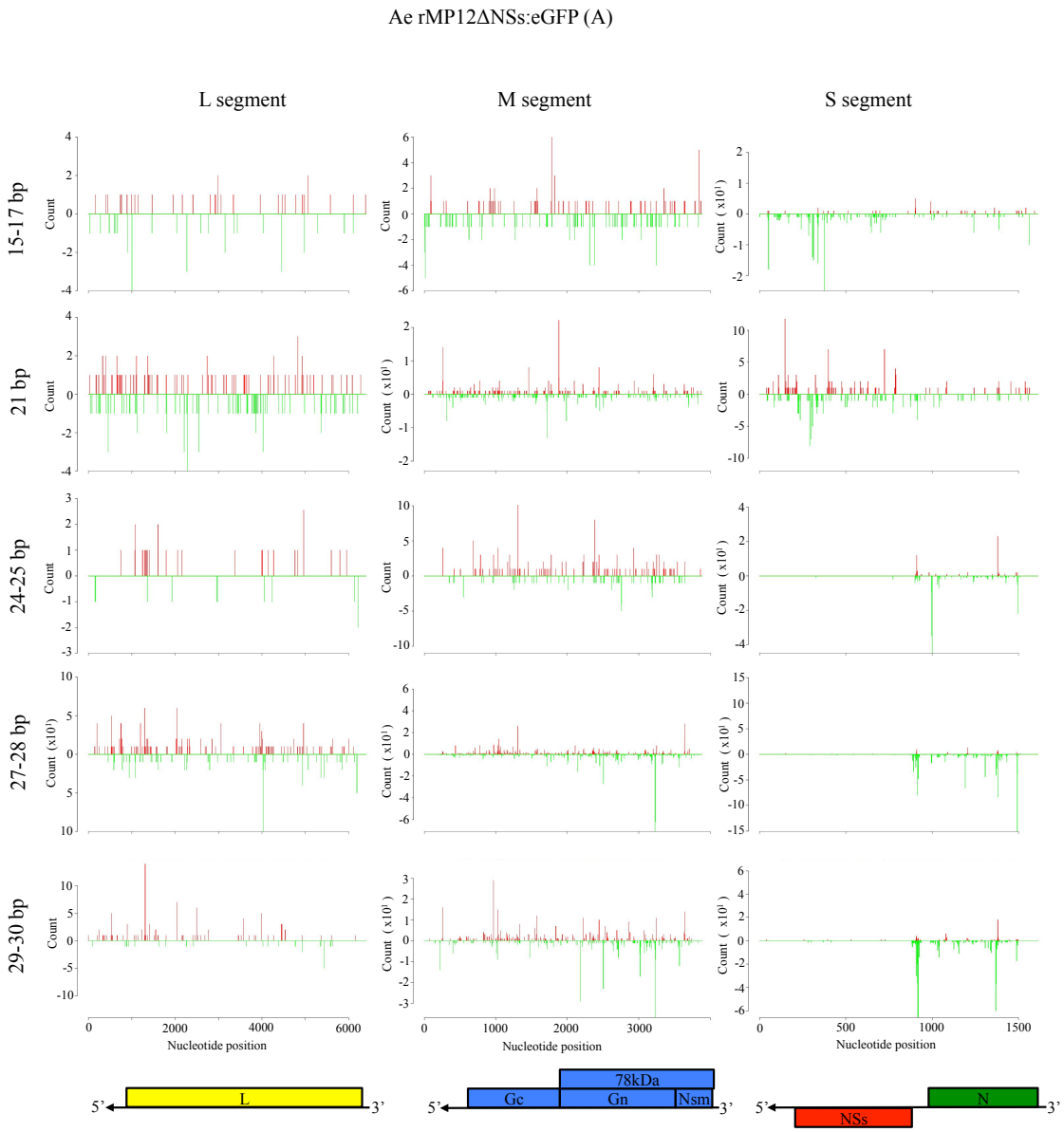

(C) rMP12ΔNSs:eGFP infected Ae cells.

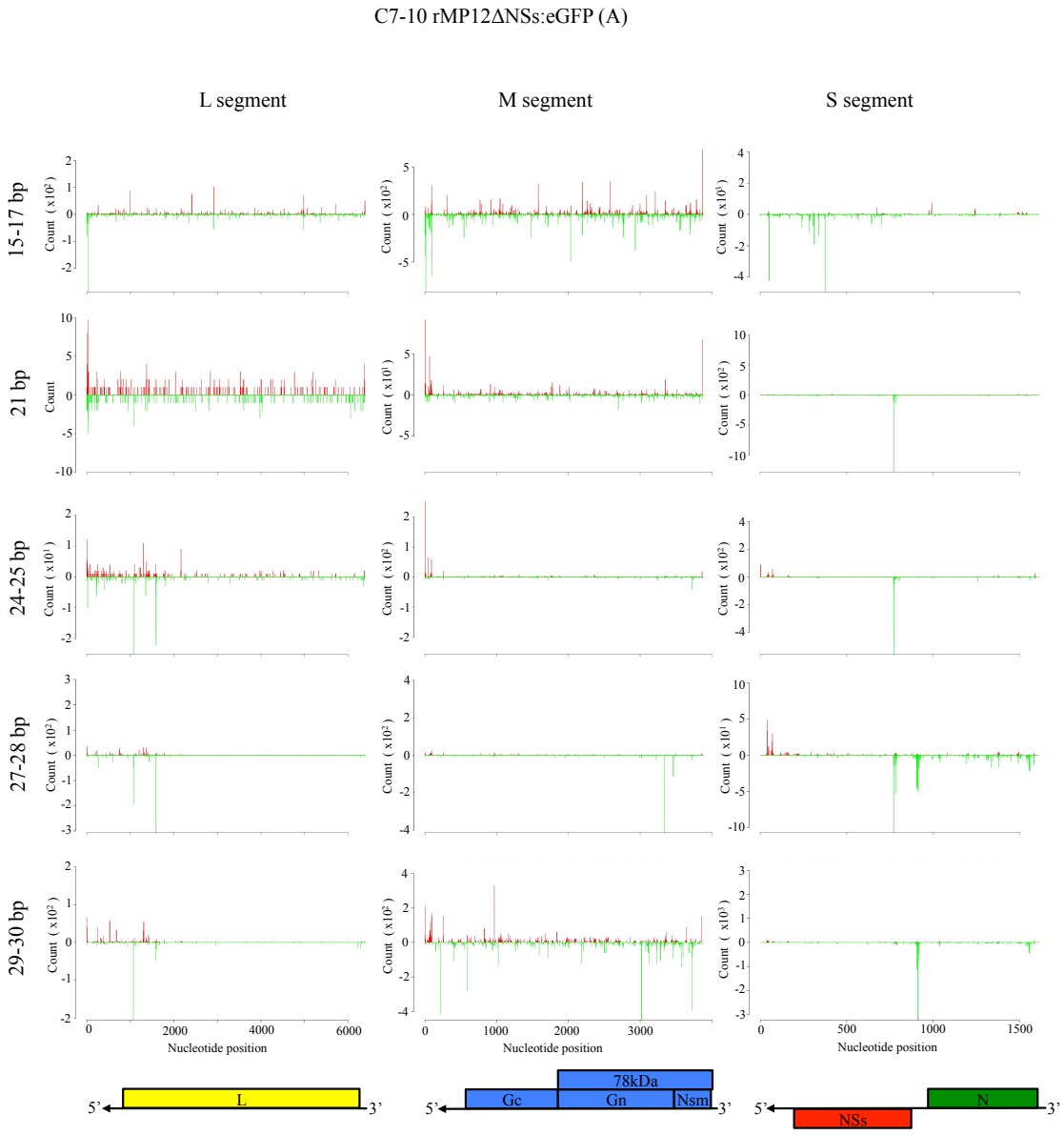

(D) rMP12ΔNSs:eGFP infected C7-10 cells.

To compare the RNAi response to that in rMP12 infected cells, the five most numerous siRNA species in rMP12 and rMP12ΔNSs:eGFP infected U4.4 and Ae cells were identified (summarised in Appendix Table 10-6). Three areas of consensus targeting by siRNAs were recognised between U4.4 and Ae cells. Two were located in the eGFP coding region, and one located in the IGR. The IGR hotspot was the same observed in rMP12 infected cells (Figure 8-14.A). Mapping these hotspots to the predicted eGFP mRNA transcript secondary structure demonstrated a similar pattern to the previously described results. siRNA species aligned to one strand of the hairpin stem structure, with the end of the siRNA located in the terminal loop (Figure 8-14.B). Predicted mRNA secondary structures of the IGR in rMP12 (NSs) and rMP12ΔNSs:eGFP (eGFP) were different however, although identical siRNA species targeted this region. Whilst species targeting the coding region of eGFP mRNA may contribute to the observed reduction of GFP expression, the IGR hotspot is known to cause a reduction in NSs expression level in rMP12 infected cells. Conservation of siRNA species between the two viruses suggests that rMP12ΔNSs:eGFP virus experiences similar transcriptional and translational pressures on GFP expression that rMP12 does for NSs. This would explain the lack of GFP expression in rMP12ΔNSs:eGFP infected U4.4 and Ae cells reported in results Chapter 6. The single antigenomic hotspot in the IGR observed in rMP12 infected C6/36 and C7-10 cells was also apparent in rMP12ΔNSs:eGFP cells. Although piRNA peaks were not apparent in the size analysis, density plots analysis demonstrated that similar species observed in the rMP12 infected cells were present here in the N coding region. The RNAi pathway results obtained from rMP12ΔNSs:eGFP infected C6/36 cells can therefore still not explain the lack of GFP expression reported in Chapter 6.

8.3.7 Analysis of very small viRNA populations targeting virus genomes

An unexpected feature of this research was the abundance of small viRNA species in the 15-17 nt range. viRNA species of these sizes were detected aligning to all three genome segments, and in all the viruses examined (Figure 8-3). These viRNAs were not observed in the uninfected Ae control samples analysed, and were therefore a product of viral replication within the mosquito cells (not shown). Density plot analysis for the small viRNA species targeting the L and M segments demonstrated a strong bias toward the 3’

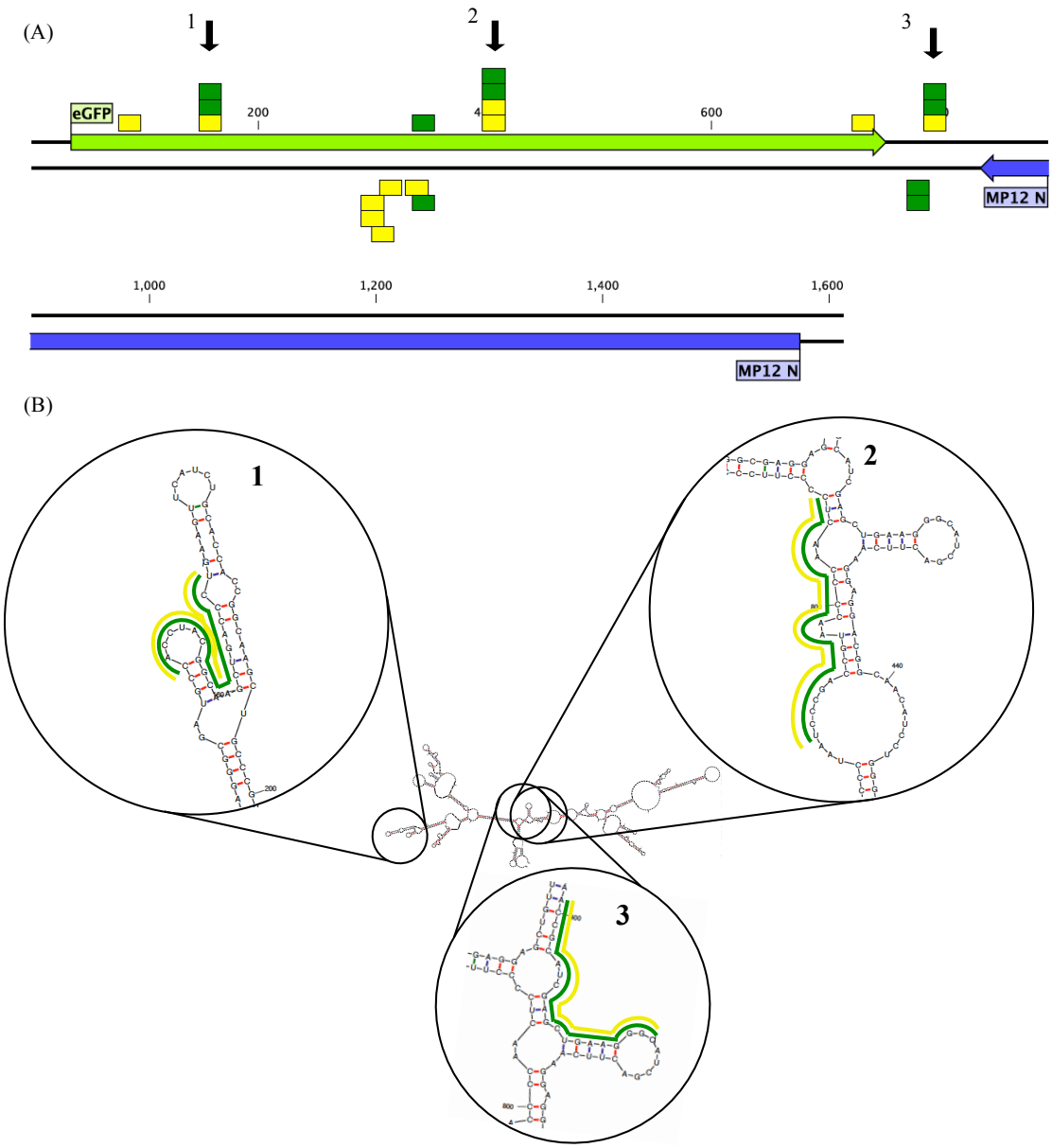

Figure 8-14: siRNA species analysis in rMP12ΔNSs:eGFP infected U4.4 and Ae cells
(A) The locations of the 5 most numerous siRNA products detected in duplicate rMP12ΔNSs:eGFP infected U4.4 (green) and Ae (yellow) cells aligned to the rMP12ΔNSs:eGFP S segment (one Ae sample shows the top 6 most numerous products). siRNA species alignments shown above the genome segment are of genomic polarity, and below the genome are of antigenomic polarity. Also shown are the CDS for proteins N (blue) and eGFP (light green). Arrows represent the 3 major siRNA consensus species. (B) The secondary structure of eGFP mRNA generated from the rMP12ΔNSs:eGFP S segment was calculated using MFold web software, and the three consensus species are shown. The locations of the aligned siRNAs are indicated for U4.4 (green) and Ae (yellow) cells.

antigenomic UTR (Figure 8-4). This hotspot, along with others less prominent throughout the genome, was present in the all the mosquito cell lines. The 3' antigenomic UTR bias for small viRNAs was observed in rMP12ΔNSs:eGFP infected cells. These viRNA species were highly conserved between the samples.

To further investigate the small viRNAs, species targeting the S genome segments of rMP12, rMP12:S-Swap and rMP12ΔNSs:eGFP were examined. Analysis was as with the siRNA and piRNA species, with the five most numerous species in the 15-17 nt range selected, providing the total read number was greater than 2 (see Appendix Table 10-7). A high degree of reproducibility regarding genome position, size and polarity of small viRNA species was apparent between the replicate samples. Several small viRNA species were conserved between all four mosquito cell lines, and several identical regions were targeted by viRNA species of different lengths. This was similar to the pattern observed with piRNA species, where clusters of multiple length piRNA species targeted one region. Large increases in the numbers targeting the modified S segment in rMP12ΔNSs:eGFP virus were observed in both infected C6/36 and C7-10 cells, but in U4.4 and Ae cells the numbers remained similar to those of rMP12 infected cells. Numbers of small viRNA species generated from rMP12:S-Swap infected cells were reduced, although those detected again demonstrated a high degree of conservation between the mosquito cells lines.

Logo analyses of small RNAs targeting the L and M segments were skewed by the consensus species aligning to the 3' antigenomic UTR region. However, hotspot distribution of small viRNA species throughout the S segments allowed for greater resolution of any potential nucleotide frequency bias (Figure 8-15). This demonstrated a small bias for cytosine at the 3' termini of antisense polarity species in all mosquito cells infected with rMP12 or rMP12ΔNSs:eGFP. However this bias was observed more in the sense polarity small viRNAs in rMP12:S-Swap infected cells. Reasons for this variation are unclear as the species targeting this region are antigenomic in both viruses, targeting NSs in rMP12 and N in rMP12:S-Swap.The significance of these small viRNA species in relation to viral replication is unclear. They have been reported in the previous study examining ZH548 replication in mosquito cells, but the majority of published results

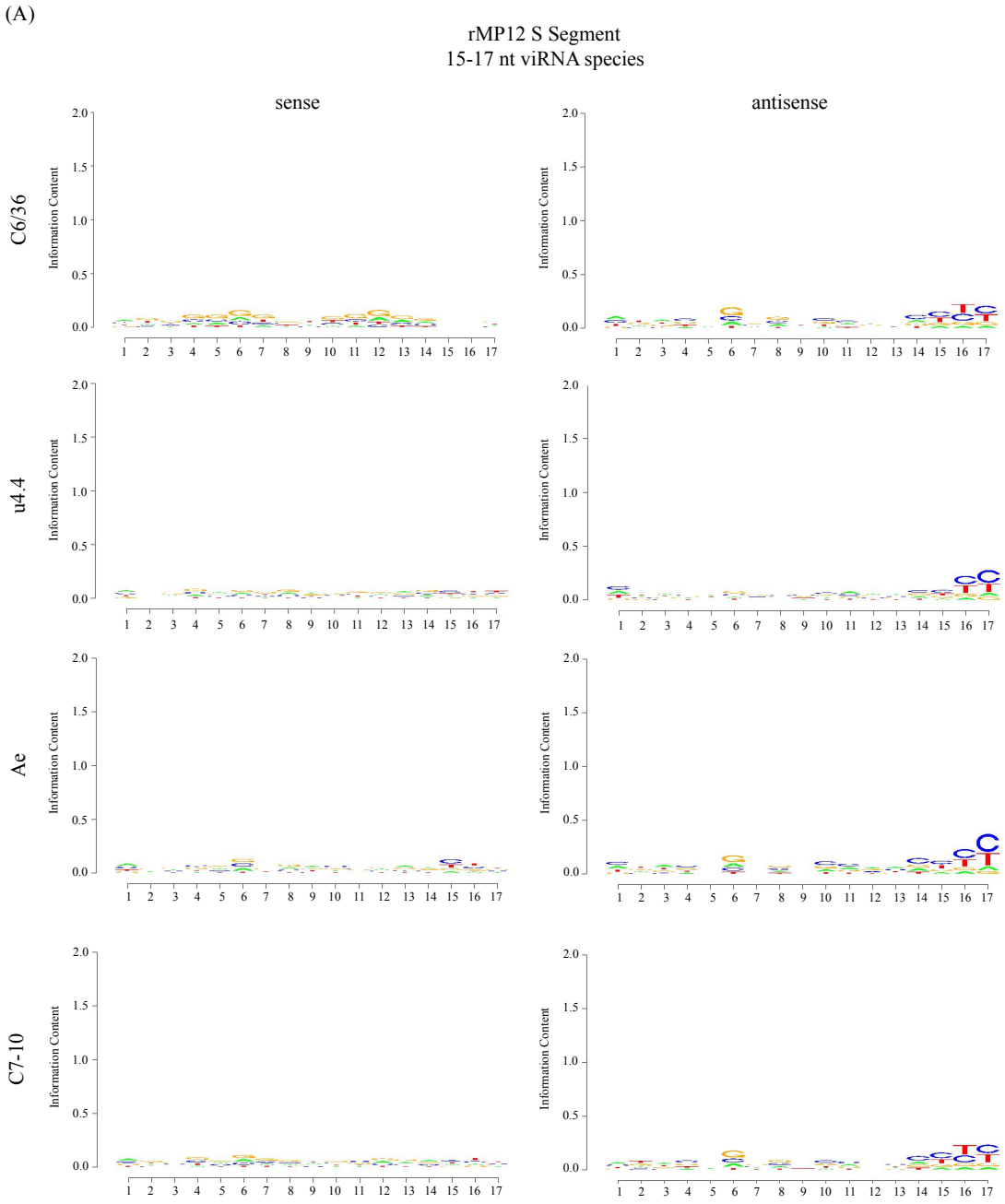

Figure 8-15: Logo analysis of small viRNA species generated in infected mosquito cells.
Logo analysis of small viRNA species produced in C6/36, U4.4, Ae, and C7-10 cells infected with rMP12, rMP12ΔNSs:eGFP or rMP12:S-Swap virus. Sense and antisense strand species analysis represented for the 15-17 nt viRNA size classes. Shown are species aligning to the rMP12 S segments of (A) rMP12, (B) rMP12ΔNSs:eGFP, and (C) rMP12:S-Swap.

(B)

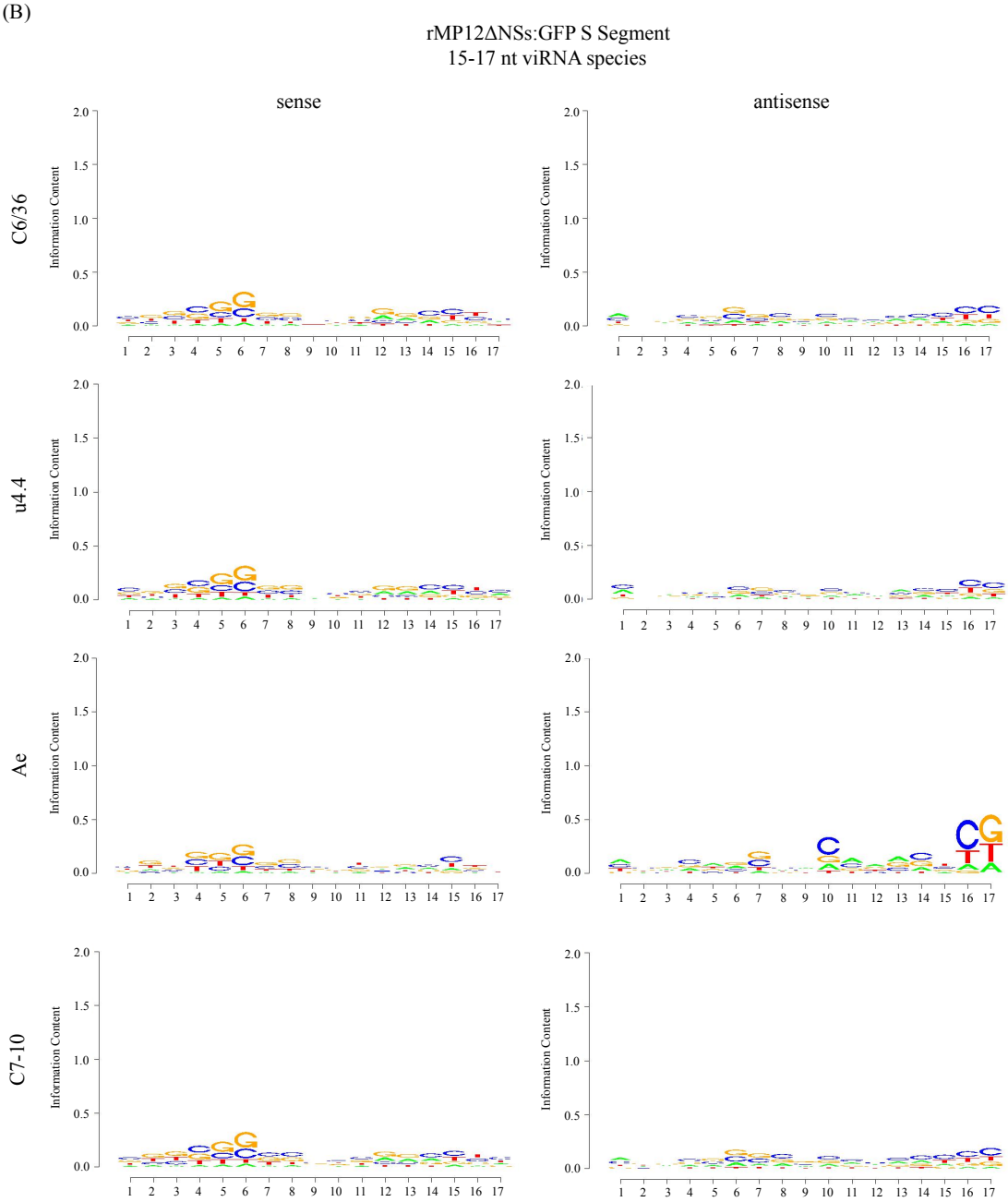
rMP12ΔNSs:GFP S Segment
15-17 nt viRNA species
sense
antisense
C6/36
u4.4
Ae
C7-10
Information Content

(C)

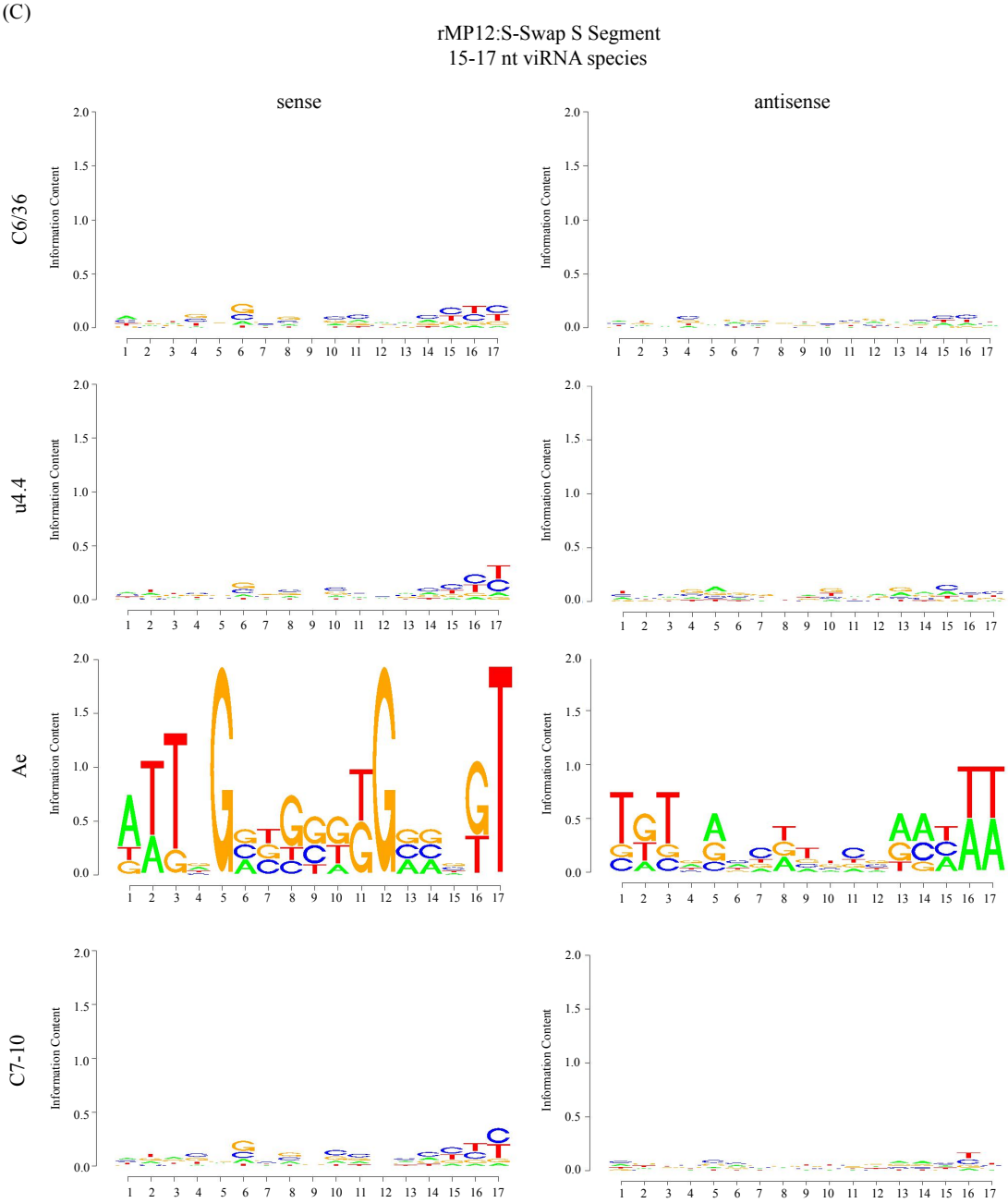
rMP12:S-Swap S Segment
15-17 nt viRNA species
sense
antisense
C6/36
u4.4
Ae
C7-10
Information Content
0.0
0.5
1.0
1.5
2.0
1 2 3 4 5 6 7 8 9 10 11 12 13 14 15 16 17

only present data examining species above 18 nt (Léger et al. 2013). However, the highly conserved nature of these species between replicate samples, different viral sequences, and different cell lines, suggests a controlled process regulating biogenesis deserving of further investigation.

8.3.8 Reproducibility of the RNAi pathway responses in mosquito cells

The highly conserved nature of antiviral RNAi responses to infection was apparent from these data. Duplicate infections allowed the opportunity to examine reproducibility of the response toward viral infection, and also compare the responses of different cell lines and mosquito species. A high degree of conservation in the read numbers generated was observed between duplicate samples. This reproducibility extended between mosquito cell lines when examining distribution of viRNA species between the genome segments, the genomic to antigenomic polarity ratio of the viRNA species targeting each segment, and the distribution of species throughout the genome segments. To investigate the reproducibility between two mosquito species, the siRNA and piRNA species generated by rMP12 infected U4.4 and Ae cells were compared. The five most populous species comprising the 21 nt, and sizes between 24-30 nt were identified for each of the three genomic segments, providing read number was greater than 2. This was performed for both samples, with viRNA species aligning to identical positions on the reference genomic sequence of similar polarity were recorded as identical species. These data are summarized in Appendix Table 10-8.

In U4.4 cells there was striking duplication in viRNA species targeting all three genome segments in the replicate samples. Consensus species predominated for all sizes analysed in all but three examples (Figure 8-16). In several cases the five most numerous species were identical between the replicate samples. Similar reproducibility was observed in Ae cells, although consensus viRNA species were only in the majority for the S segment. Only two size classes (24 and 25 nt) targeting the L segment showed no consensus in viRNA species. However, total read numbers were consistently higher in U4.4 cells compared to Ae cells, and the greater number targeting the L and M segment may explain the increased consistency in targeted regions observed. Of the five most numerous siRNA species, four identical species were identified in both cells lines, with only one unique species observed

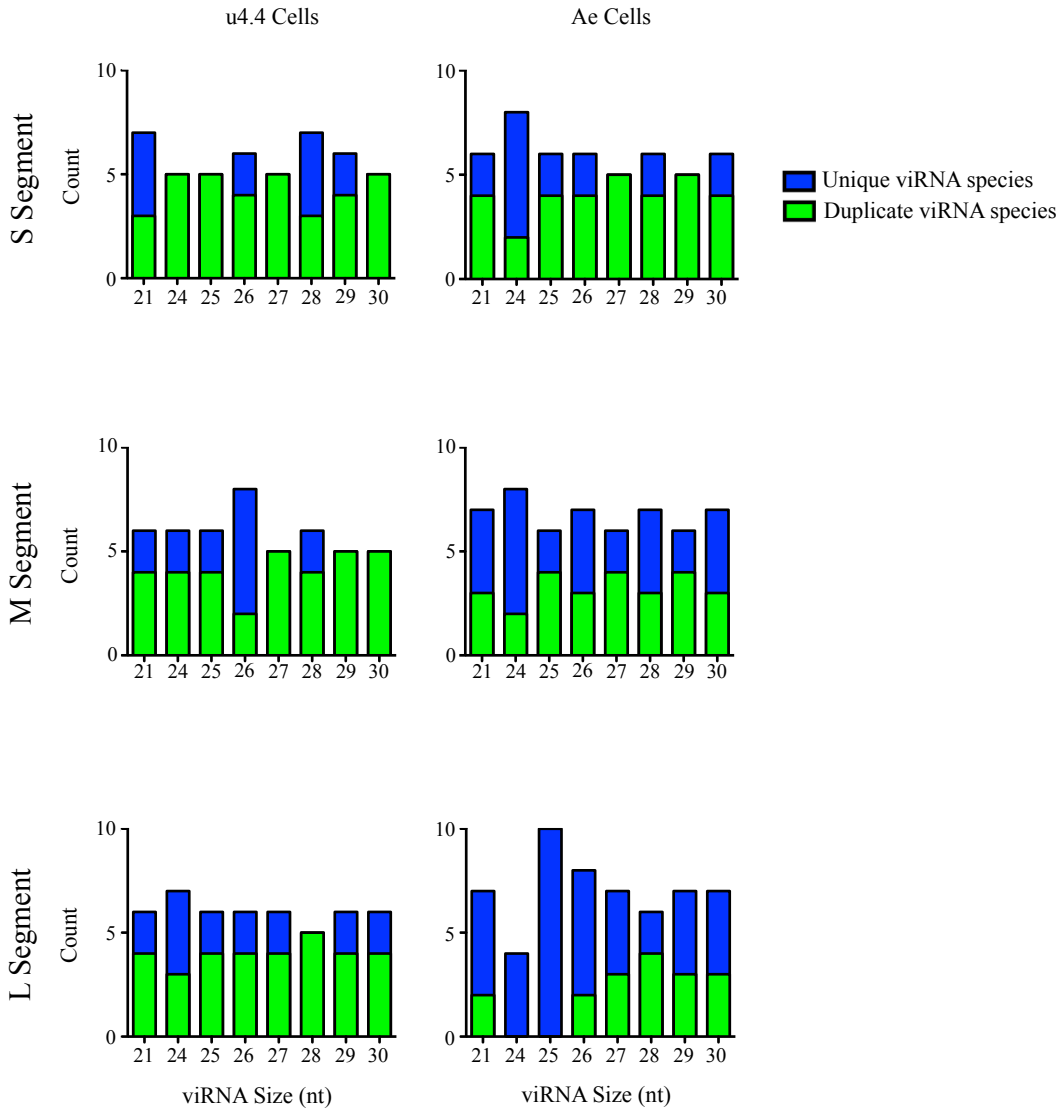

Figure 8-16: viRNA species comparison in the rMP12 infected U4.4 and Ae cells duplicate samples
The 5 most populous siRNA (21 nt) and piRNA (24-30 nt) species were identified for the duplicate rMP12 infections in U4.4 and Ae cells that targeted the L, M and S segments. Of these viRNA species, the total number of unique species in each size class were determined (blue bar). Unique species were those of the same size and polarity that targeted the same region on the reference genome strand. Species identified that were conserved between the replicate infections were identified and superimposed (green bar).

for each cell line (Figure 8-17.A). Consistency between viRNA species was also apparent when analyzing the piRNAs, and several consensus species were apparent targeting identical regions on the S segment (Figure 8-17.B). The reproducibility of the RNAi responses analysed here was not confined to the S segment, with consistency in both pathways targeting the L and M segments also observed. These results indicate that the RNAi system is highly conserved between mosquito species, with common pathways leading to the biogenesis of identical viRNA species.

Differences in the piRNA response between the C6/36 and C7-10 cells compared to that of U4.4 and Ae cells were apparent however. The siRNA-deficient C6/36 and C7-10 cells generated similar piRNA species to each other when infected with rMP12, but these were markedly different from those observed in the infected U4.4 and Ae cells. These differences were also observed in the rMP12ΔNSs:eGFP infected cells. Consistently across all viRNA size classes the responses of the siRNA deficient C6/36 and C7-10 cells were markedly different to the siRNA competent U4.4 cells. However, logo analysis demonstrated the characteristic nucleotide frequencies associated with piRNAs in all these cell lines, suggesting a common pathway of biogenesis. Therefore, the reasons why different piRNA species observed was unclear, although it may represent an as yet unidentified pathway linking the biogenesis of both piRNA and siRNA species.

8.3.9 Analysis of the BHK-21 cell RNAi response to viral infection

Although mammalian cells contain many orthologues to known proteins within the RNAi pathways characterised in *D. melanogaster*, it was assumed they provided little contribution to antiviral activity when compared to acquired immune pathways and the powerful interferon pathways (Svoboda 2014; Fragkoudis et al. 2009). However, interest has grown after detection of viral genome specific viRNA species in infected mammalian cells, with evidence of antiviral RNAi activity reported (Maillard et al. 2013). Genome specific viRNAs were detected in both rMP12 and rMP12:S-Swap infected BHK-21 cells, indicating active pathways within these cells. Analysis of these viRNA species demonstrated clear differences compared to those generated in mosquito cells. However, a high degree of reproducibility between replicates of both rMP12 and rMP12:S-Swap virus infected cells was apparent across all genome segments, indicative of a controlled biogenesis process.

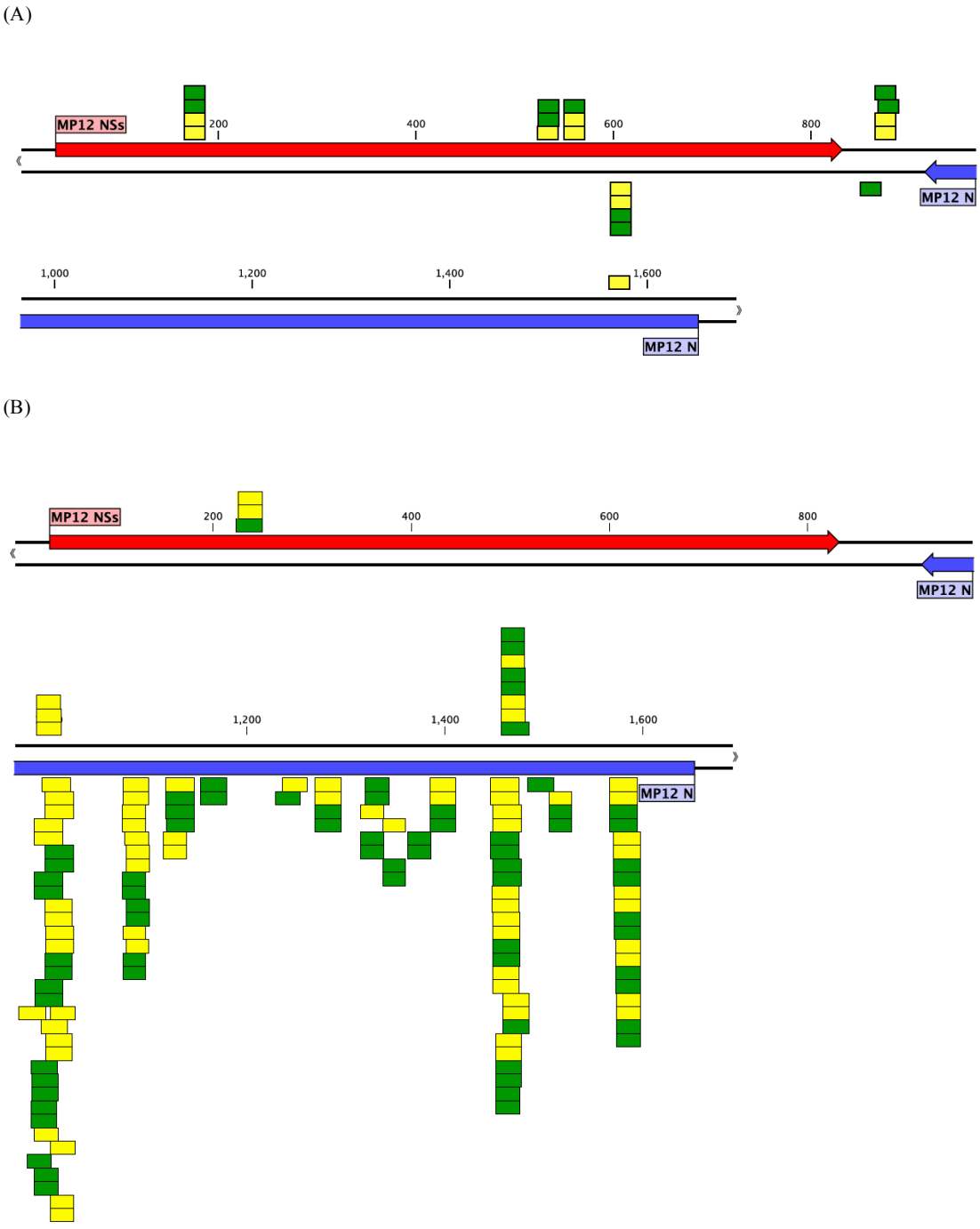

Figure 8-17: Locations of viRNA species on rMP12 S Segment in infected U4.4 and Ae cells.
The 5 most populous viRNA species in the siRNA (21 nt) (A), and piRNA (24-30 nt) (B) ranges were aligned to the reference rMP12 S segment genome. These viRNA species were generated in infected U4.4 (green) and Ae (yellow) cells. Unique species were those of the same size and polarity that targeted the same region on the reference genome strand. viRNA species alignments shown above the genome segment are of genomic polarity, and below the genome are of antigenomic polarity. Also shown are the CDS for the S segment encoded proteins N (blue) and NSs (red).

Total read numbers for individual size classes were reduced in BHK-21 cells compared to all mosquito cell lines aside from C7-10 cells (Table 8-2). The distribution of viRNAs across genome segments was also different to mosquito cells, with the L segment preferentially targeted followed by the M and S segments. While genomic to antigenomic ratios in viRNA species targeting L and S segments were similar to the mosquito cells, a difference was observed in those species targeting the M segment where genomic sense viRNAs predominated.

The reduction in read numbers in rMP12:S-Swap infected cells was not as pronounced as that observed for the mosquito cell lines. This was likely due the increased titres observed in BHK-21 cells increasing the numbers of viral substrates available for RNAi activation (Figure 8-2). The increased targeting of rMP12:S-Swap S segment observed in mosquito cells was repeated here. The distribution of viRNA species amongst the genome segments varied in rMP12:S-Swap infected cells, although the genome to antigenome polarity ratios remained similar to rMP12 infected cells. The peak at 15-17 nt containing small viRNA species apparent in mosquito cells was also observed here (Figure 8-18). Another peak observed in 21-23 nt viRNAs was observed for all segments, although no feature analogous to peaks of piRNA species was present. viRNA species of 21-23 nt targeting the S segment in rMP12 infected cells were predominantly antigenomic, but in rMP12:S-Swap infected cells this polarity was predominantly genomic. Hotspot analysis demonstrated that these 21-23 nt viRNA species were similar to those detected in rMP12 infected C6/36 and C7-10 cells (Figure 8-19). Sequence analysis of these species demonstrated they were identical to those targeting the IGR in all mosquito cells. These species were apparent in both rMP12 and rMP12:S-Swap infected cells, and were conserved between the replicate samples (see Appendix Figure 10-10). viRNA species here may again represent products of a Dcr-like protein in BHK-21 cells, analogous to the predicted Dcr-1 mediated viRNA species detected in the C6/36 and C7-10 cells As previous experiments have demonstrated expression of both S segment encoded proteins in rMP12 and rMP12:S-Swap infected BHK-21 cells, it is unlikely these species exert any significant transcriptional pressures on RVFV replication. Logo analysis revealed no nucleotide frequency biases in viRNA species generated in the infected BHK-21 cells (see Appendix Figure 10-11).

Table 8-2: Characteristics of viRNA species detected in rMP12 and rMP12:S-Swap infected BHK-21 cells.
Analysis of viRNA species detected in rMP12 and rMP12:S-Swap infected BHK-21 cells. Samples A and B were duplicate infections. Species between 15 and 37 nt in length and of 100% homology to reference genomes were included.

		rMP12							
Cell line	**Sample**	**Segment**	**Total reads**	**Average length (nt)**	**Number reads genomic sense**	**Number reads antigenomic sense**	**% Total genomic sense**	**% Total antigenomic sense**	**% of total reads aligning to segment**
BHK-21	**A**	**L**	27,961	22.28	19,634	8,327	70.22%	29.78%	43.65%
		M	24,516	22.67	18,087	6,429	73.78%	26.22%	38.28%
		S	11,574	22.77	4,301	7,273	37.16%	62.84%	18.07%
			64,051		**42,022**	**22,029**			
	B	**L**	26,126	22.51	17,972	8,154	68.79%	31.21%	42.84%
		M	23,683	22.77	17,205	6,478	72.65%	27.35%	38.84%
		S	11,171	22.95	4,054	7,117	36.29%	63.71%	18.32%
			60,980		**39,231**	**21,749**			

		rMP12:S-Swap							
Cell line	**Sample**	**Segment**	**Total reads**	**Average length (nt)**	**Number reads genomic sense**	**Number reads antigenomic sense**	**% Total genomic sense**	**% Total antigenomic sense**	**% of total reads aligning to segment**
BHK-21	**A**	**L**	5,959	21.92	4,284	1,675	71.89%	28.11%	27.44%
		M	4,761	21.93	3,446	1,315	72.38%	27.62%	21.93%
		S	10,993	21.71	4,221	6,772	38.40%	61.60%	50.63%
			21,713		**11,951**	**9,762**			
	B	**L**	10,345	21.15	7,210	3,135	69.70%	30.30%	27.48%
		M	7,729	21.35	5,549	2,180	71.79%	28.21%	20.53%
		S	19,577	21.15	7,344	12,233	37.51%	62.49%	52.00%
			37,651		**20,103**	**17,548**			

(A)

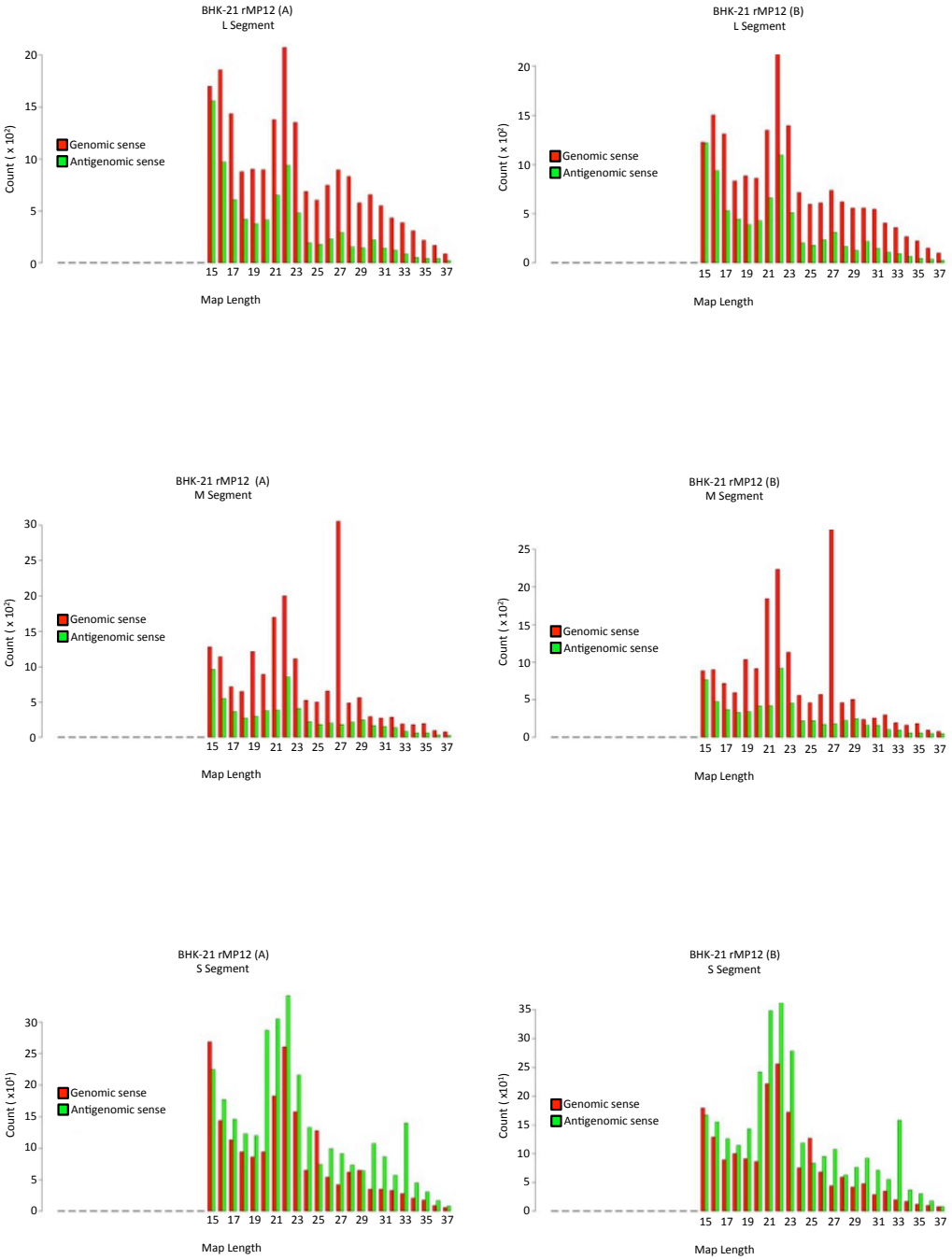

Figure 8-18: viRNA species plot analysis for rMP12 and rMP12:S-Swap infected BHK-21 cells
Size distribution and density plots of all 15-37 nt viRNA species detected in rMP12 and rMP12:S-Swap infected BHK-21 cells lines aligning to L, M or S segment. Shown are replicate sample A and B taken from duplicate infections. viRNA species aligning to genomic polarity (negative sense) RNA are shown in red, antigenomic polarity (positive sense) RNA in green. (A) rMP12 infection, and (B) rMP12:S-Swap infection.

(B)

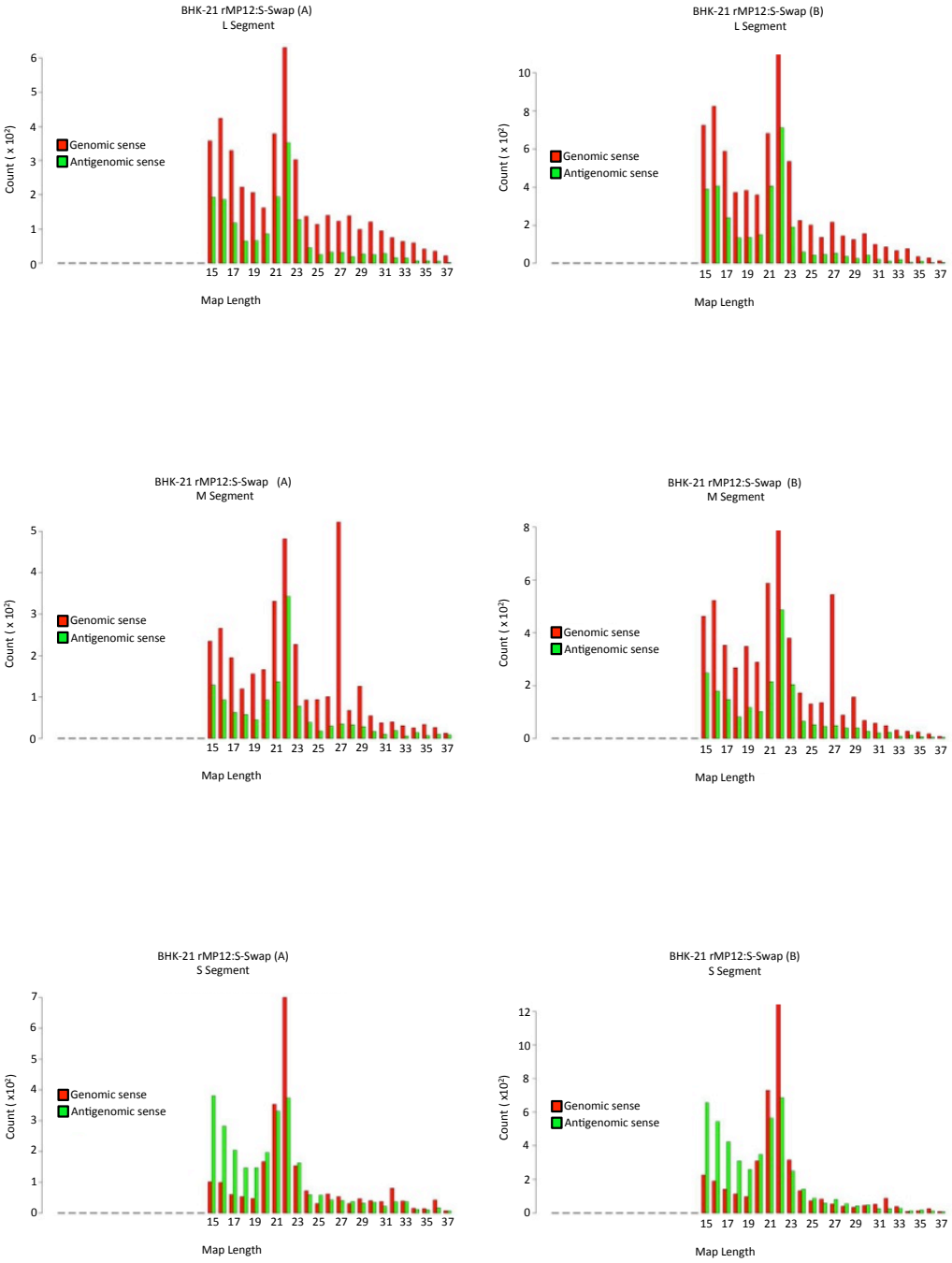
BHK-21 rMP12:S-Swap (A)
L Segment
BHK-21 rMP12:S-Swap (B)
L Segment
BHK-21 rMP12:S-Swap (A)
M Segment
BHK-21 rMP12:S-Swap (B)
M Segment
BHK-21 rMP12:S-Swap (A)
S Segment
BHK-21 rMP12:S-Swap (B)
S Segment
Genomic sense
Antigenomic sense
Count (x 10²)
Count (x10²)
Map Length

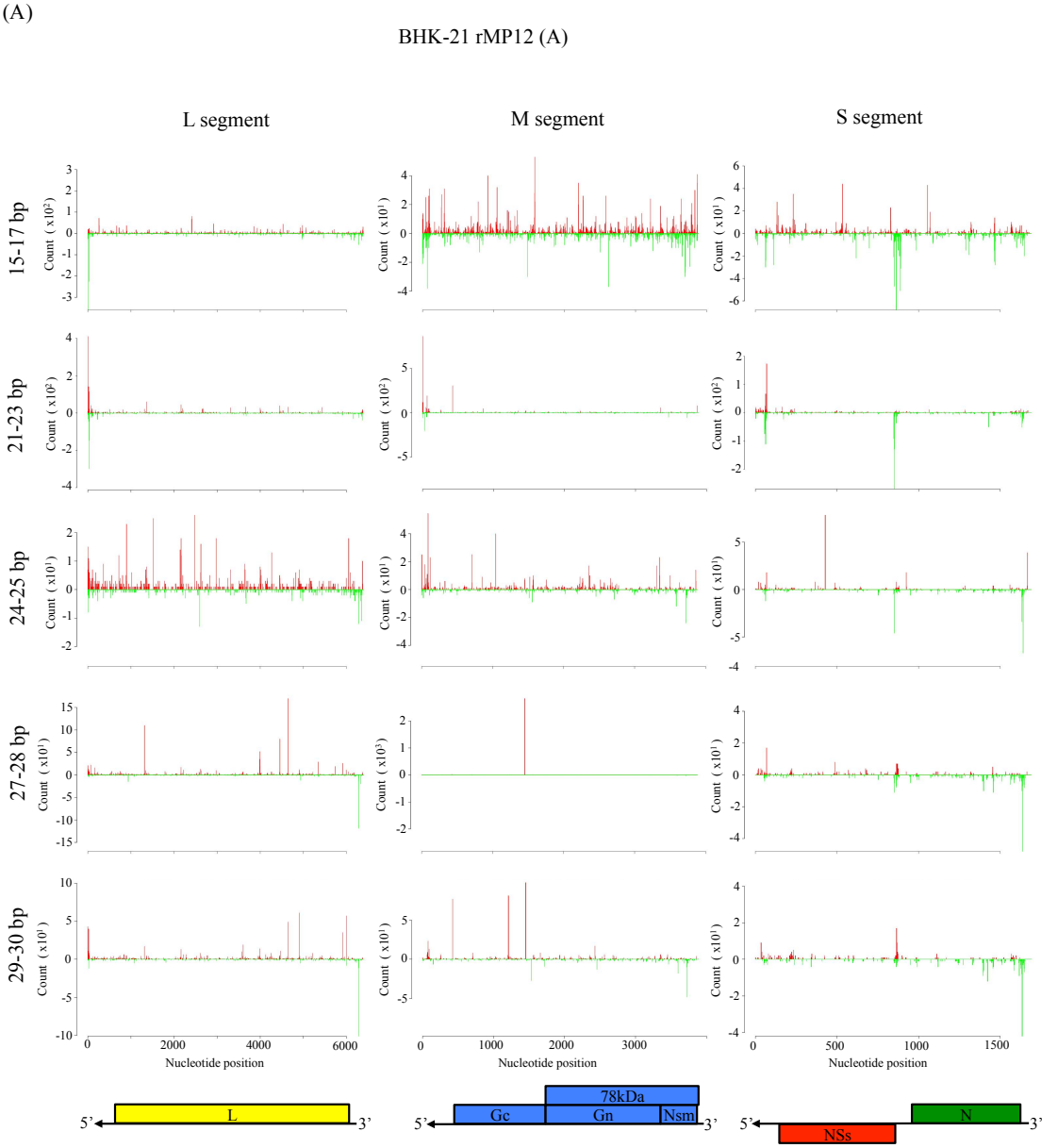

Figure 8-19: Mapping analysis of viRNA species targeting the rMP12 and rMP12:S-Swap genome segments in infected BHK-21 cells.
Shown are density plots of aligned viRNA species of 15-17 nt, 21-23 nt, 24-25 nt, 27-28 nt, and 29-30 nt aligning to the rMP12 L, M, and S genome segments. Upper plots (red) show alignments to genomic polarity (negative sense) and lower plots (green) to antigenomic polarity (positive sense). Shown are duplicate infections (A) rMP12 infection, (B) rMP12:S-Swap infection. Also shown are the CDS for MP12 proteins encoded on the L (yellow), M (blue) and S (green and red) segments.

(B)

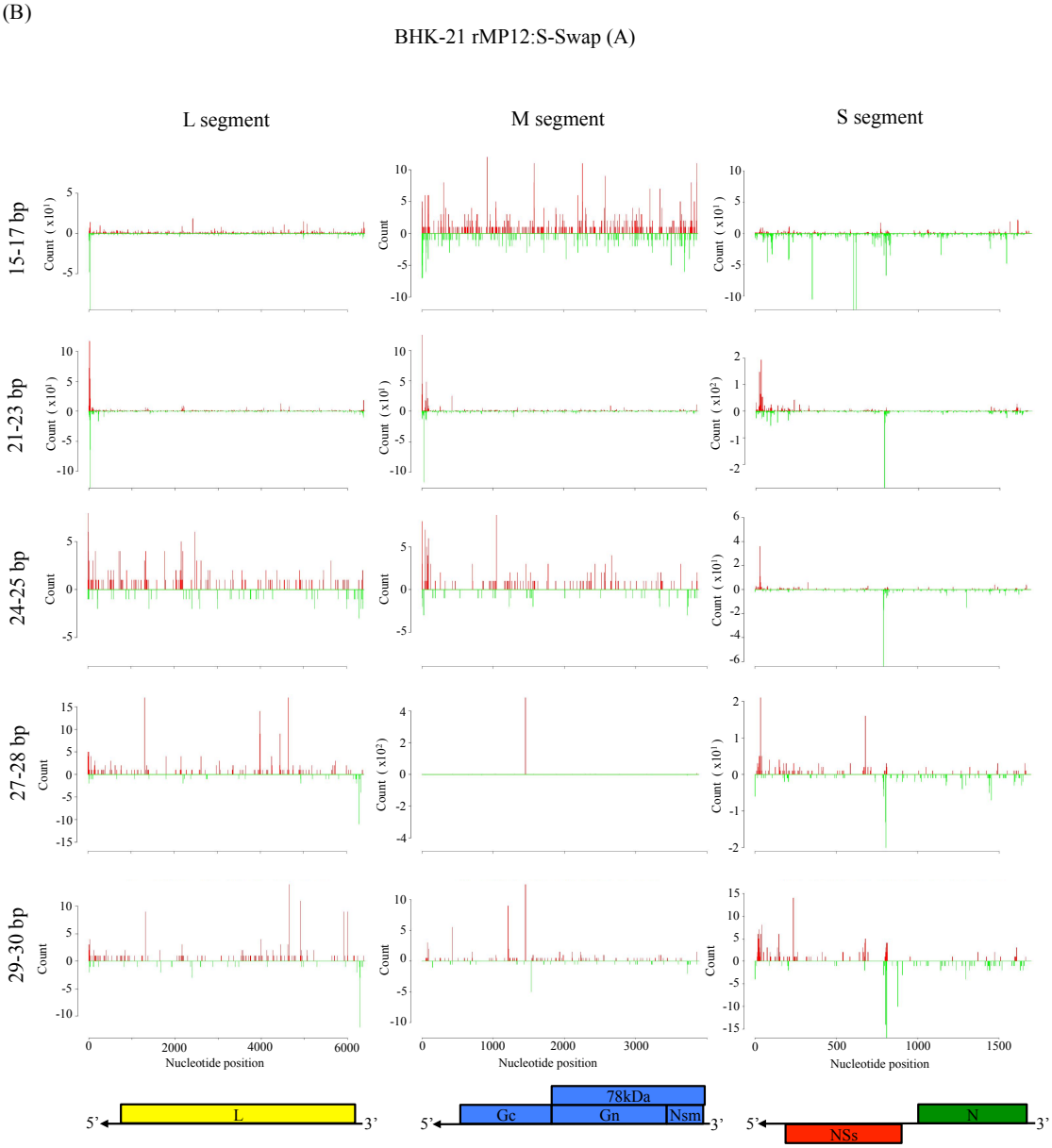
BHK-21 rMP12:S-Swap (A)
L segment
M segment
S segment
15-17 bp
21-23 bp
24-25 bp
27-28 bp
29-30 bp
Count
Nucleotide position
5'
3'
L
78kDa
Gc
Gn
Nsm
N
NSs

8.3.10 Rescue of the siRNA pathway in C6/36 cells

Experiments were performed to examine whether the siRNA pathway in C6/36 cells could be rescued by supplementation with exogenous Dcr-2 protein. This was achieved though transient transfection with the *A. albopictus Dcr-2* gene of U4.4 cells, with protein expression driven by the previously characterized polyubiquitin promoter.

The silencing potential of Dcr-2 transfected C6/36 cells was evaluated by examining the reduction in firefly luciferase (FFLuc) levels after addition of sequence specific dsRNA. One set of C6/36 cells (Set A) was transfected with 1 µg pST-IRES polyUB hyg - GFP DCR2 HA N-tag plasmid and 50 ng pMT-FFLuc, while another set was transfected with only 50 ng pMT-FFLuc (Set B). Both experiments the were transfected with 500 ng of either firefly luciferase specific dsRNA, or non-specific eGFP dsRNA 24 hours later, with Set B also transfected with 1 µg of pST-IRES polyUB hyg - GFP DCR2 HA N-tag. After 12 hours expression FFluc expression was induced by addition of 50 mM $CuSO_4$ (160 µl per ml of cell culture medium). After a further 36 hour incubation cells were lysed and FFLuc levels determined. C6/36 cells expressing Dcr-2 prior to dsRNA addition (Set A) demonstrated a reduction in FFLuc signal compared with untreated cells (Figure 8-20). In C6/36 cells transfected simultaneously with pST-IRES polyUB hyg - GFP DCR2 HA N-tag and dsRNA (Set B) the reduction in FFLuc signal was notably less pronounced. No reduction in FFLuc signal was seen in cells transfected with non-specific eGFP dsRNA. These results indicated that the siRNA response in C6/36 cells can be rescued by addition of Dcr-2, although silencing potential was reduced if intracellular Dcr-2 was not available upon dsRNA addition. Presumably expression of FFluc was induced in Set B at a time where the level of Dcr-2 was not sufficient to initiate an effective siRNA response.

Previous experiments demonstrated a difference in NSs expression between rMP12 infected U4.4 and Ae cells when compared to C6/36 cells. Hotspots in siRNA density targeting the NSs mRNA have previously been reported (Léger et al. 2013), and also demonstrated here. To investigate how rescuing the siRNA response affected NSs expression, Dcr-2 expressing C6/36 cells were infected with rMP12 at MOI 1 and 5, and samples taken to determine virus titre and protein production levels. rMP12 titres at both MOI 1 and 5 were unaffected by Dcr-2 expression (Figure 8-21.A). Expression of Dcr-2 was detected via an N-terminal fused HA tag (Figure 8-21.B). Both N and NSs protein

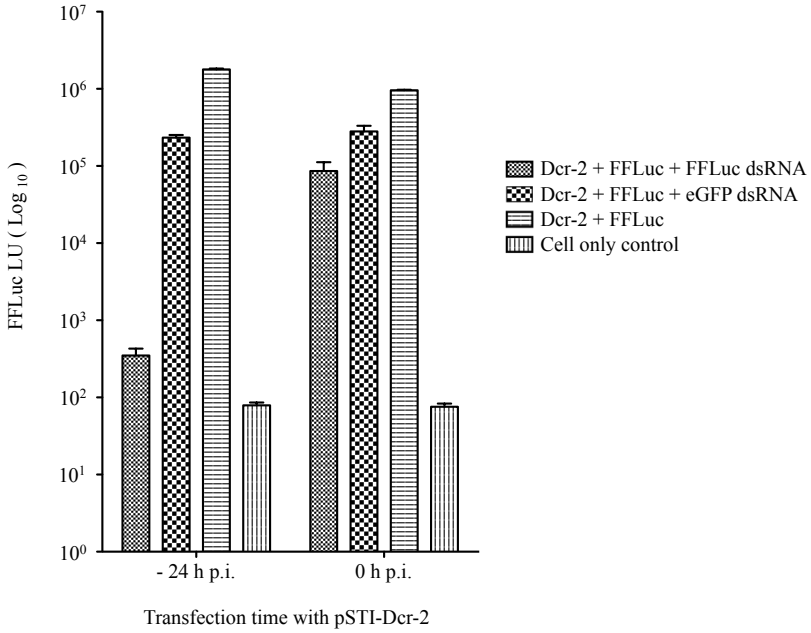

Figure 8-20: Silencing of FFLuc signal in Dcr-2 expressing C6/36 cells
24 hours prior to dsRNA treatment one set of C6/36 cells was transfected with 1 µg of pST-IRES polyUB hyg - GFP DCR2 HA N-tag plasmid and 50 ng pMT-FFLuc (Set A) and another set of C6/36 cells transfected with 50 ng pMT-FFLuc only (Set B). 24 hours later Set A was treated with 500 ng FFLuc sequence specific dsRNA or non-specific (eGFP) dsRNA. Set B was treated with the same concentrations of dsRNA but also 1 µg of pST-IRES polyUB hyg - GFP DCR2 HA N-tag plasmid. After 12 hours FFLuc expression was induced by addition of 50 mM $CuSO_4$ to cell culture media. After a further 36 hours the level of FFLuc expression was determined. In C6/36 cells treated with Dcr-2 plasmid prior dsRNA treatment a reduction in FFLuc signal was observed. This was not seen in cells treated with Dcr-2 and dsRNA at the same time. No silencing was observed with the non-specific dsRNA treatment.

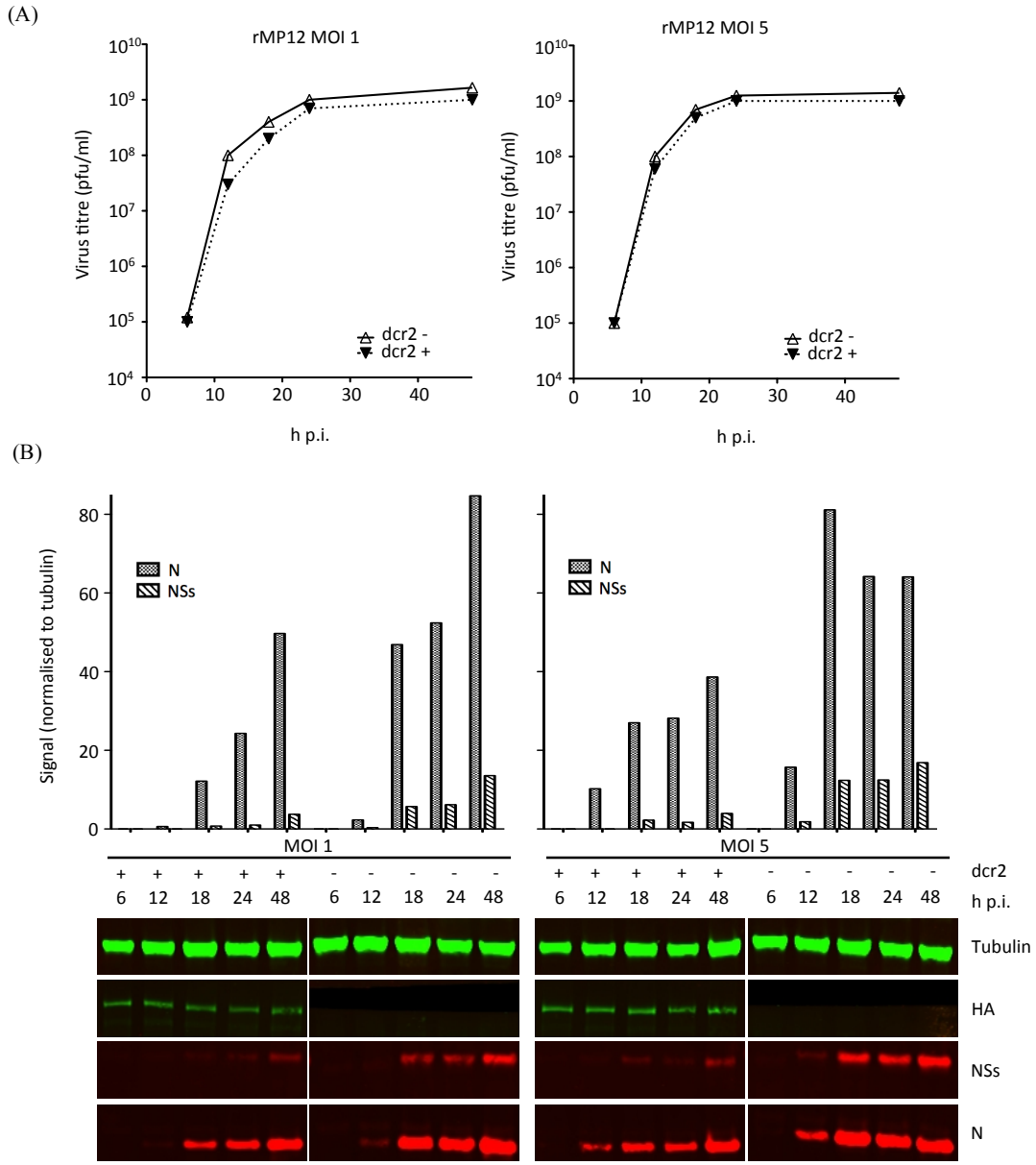

Figure 8-21: rMP12 N and NSs expression in Dcr-2 expressing C6/36 cells
C6/36 cells were transfected with 1µg of pST-IRES polyUB hyg - GFP DCR2 HA N-tag plasmid to express Dcr-2 protein. At six hours post transfection, cells were infected with rMP12 at MOI 5. At specific time points cell lysates and cell culture supernatant was collected and analysed for rMP12 viral titres and protein expression. Duplicate rMP12 infections in un-transfected cells were also performed. (A) Viral titres at each time point were obtained by plaque assay in BHK-21 cells. (B) Cell lysates were analysed using specific RVFV N and NSs antibodies, as well as for the Dcr-2 expression via a N-terminal HA tag. Quantitative analysis of the western blots for RVFV N and NSs were performed using LICOR methodology, with protein signal normalized to tubulin loading control levels to obtain relative N and NSs levels in each sample.

expression levels were reduced in Dcr-2 expressing C6/36 cells. On average a 2.86- and 2.12-fold reduction in N level was observed at MOI 1 and 5 respectively. This reduction was more pronounced at earlier time points, with only a 1.7-fold reduction at both MOI 1 and 5 observed by 48 h p.i.. The reduction in NSs level was more pronounced, with an average 5.82- and 5.69-fold reduction in NSs level at both MOI 1 and MOI 5 respectively compared to C6/36 cells not expressing Dcr-2. These data suggest that the siRNA pathway is responsible in part for the difference in NSs expression level observed between C6/36 cells and the siRNA competent U4.4 and Ae cells.

8.4 Discussion

For the majority of arboviruses, a tightly regulated control over replication within the arthropod vector is vital. If viral replication and dissemination within the vector results in detrimental effects, this will impact negatively on transmission efficiency and subsequent propagation of the virus. Evidence of this control is demonstrated when comparing the cytolytic and persistent RVFV infection phenotypes in mammalian and invertebrate cells respectively. Whilst numerous physical barriers and biological pathways contribute to this regulation, the RNAi pathways have recently been recognised as one of the most important factors controlling viral replication (Blair 2011).

Differences in viral replication between C6/36 cells and the U4.4 and Ae cells have consistently been observed throughout this project. Infection with rMP12 in C6/36 reliably resulted in higher titres, and variances in protein expression and mRNA levels were also apparent. Differences in RNAi responses between the cell lines, notably the impaired siRNA response in C6/36 and C7-10 cells, offered a potential explanation as to these phenotypic variations (Morazzani et al. 2012; Brackney et al. 2010). Previous research identified an siRNA hotspot located in the IGR of ZH548 S segment as being responsible for reducing NSs expression in infected mosquito cells (Léger et al. 2013). This hotspot was recognised here in rMP12 infected cells, and therefore would also be responsible for reducing rMP12 NSs expression. Further evidence indicating the regulatory role the siRNA pathway plays in rMP12 infected cells was demonstrable by the rescue of the siRNA response in C6/36 cells. C6/36 cells supplemented with Dcr-2 protein were able to silence expression of firefly luciferase, and its role in reducing NSs expression level was also demonstrated. Future experiments will be conducted in which individual protein

components of the siRNA response will be "knocked-down" using siRNA silencing methods. These results suggest that impairment of the siRNA pathway in U4.4 or Ae cells should result in increased NSs expression when infected with rMP12.

The altered S segment coding strategies of rMP12 and rMP12:S-Swap virus allowed us to further investigate aspects of the RNAi response. These data demonstrated preferential targeting of the NSs coding region by the siRNA pathway, even after the coding sequences were swapped. Analysis of the siRNA species generated in infected U4.4 cells demonstrated that four out of the five most numerous species in both rMP12 and rMP12:S-Swap infected cells were targeted to the NSs coding region, with the remaining species targeting the IGR. Species aligning to the IGR target NSs mRNA in rMP12 infected cells, but N mRNA in rMP12:S-Swap infected cells. As this hotspot is responsible for modulating NSs expression, it offers an explanation as to why rMP12:S-Swap is attenuated in U4.4 and Ae cells. Whilst data have shown NSs to be dispensable for replication in mosquito cells, a siRNA response targeting N mRNA would effect all aspects of the viral lifecycle, from transcription to genome replication. Examination of the density plots for S segment in rMP12 infected cells show a relatively greater proportion of the siRNAs targeting the IGR region in Ae cells than in U4.4 cells. This may further explain why replication in Ae cells was more attenuated than in U4.4 cells as the reductions in N level may be more pronounced. A relatively stronger silencing effect in Ae cells could explain several observations noted throughout this research: (1) lower levels of NSs expression in Ae cells compared to U4.4 cells at all MOIs; (2) severe attenuation of rMP12:S-Swap replication in Ae cells compared to C6/36 and U4.4; and (3) inability to create a rMP12:S-Swap persistently-infected Ae cell line.

The use of rMP12:S-Swap virus allowed examination of the potential viral substrates acting as targets for the RNAi responses, an area not yet well characterised for the NSVs. Comparative analysis of RNAi responses between positive and negative stranded RNA viruses demonstrates a vastly reduced viRNA read number in the later. This disparity is likely due to fundamental differences in the replication strategies of these two classes of virus. Genomes of positively-stranded RNA viruses act directly as mRNA, and as such exhibit highly ordered secondary-structures such as IRES elements and *cis*-acting replication signals (Liu et al. 2009). These secondary structures represent multiple dsRNA targets for the siRNA pathway to recognise. However, as the genomes of negative-stranded

RNA viruses are closely associated with nucleocapsid protein this limits any potential for extensive secondary structures formation (Bouloy & Weber 2010). Possible sources of viral dsRNA structures generated during NSV infection are considered to be either replicative intermediates, secondary structures within viral mRNA transcripts, or mRNA:genome strand duplex structures.

Identical siRNA species were detected targeting the NSs coding region for both rMP12 and rMP12:S-Swap infected cells. However, the siRNA species targeting the IGR sequence contained within the mRNA terminal 3' sequence were of opposite polarity between the viruses. This suggests that the viral substrate responsible for siRNA activation contained the NSs CDS in the same polarity, but an IGR sequence of opposite polarity between the two viruses. This suggested that the NSs mRNA molecule acts as the substrate for Dcr-2 in infected cells rather than replicative intermediate or mRNA duplex structures. Whilst the target could exist as a genome:transcript duplex this remains unlikely due to the genome encapsidation. Evidence of mRNA transcripts acting as the dsRNA target was strengthened by data showing that the siRNA species aligned to hairpin loop structures in the predicted mRNA secondary structure. Alignment of hotspot species to hairpin loop structures was determined for both rMP12 and rMP12:S-Swap virus N and NSs mRNA transcripts. It remained true in siRNA species aligning to the eGFP mRNA transcribed from rMP12ΔNSs:eGFP virus. The reasons why NSs mRNA was preferentially targeted over N mRNA were not apparent however as numerous hairpin structures also exist within the N mRNA. Furthermore, N mRNA is produced earlier and at a higher level compared to NSs mRNA during a rMP12 infection (Brennan et al. 2014), so relative levels of the individual species can not explain this phenomenon.

All the mosquito cell lines evaluated were shown to generate piRNA species. Our current understanding of piRNA species biogenesis is that it involves a single stranded RNA target. piRNAs have been described in several viral infections with both positive and negative stranded RNA viruses, although the exact role the play in promoting an antiviral state requires further experimental studies (Vodovar et al. 2012). It is likely however that any process capable of degrading a viral RNA will ultimately have a negative impact on the viral lifecycle. While siRNA responses described here were shown to preferentially target the NSs coding region in both rMP12 and rMP12:S-Swap, the piRNA response was independent of the S segment genome arrangement. Species comprising the major hotspots

in all three viral infections were primarily of antigenomic polarity, with a strong bias toward the 5' terminus. Due to the altered coding strategies these biases represented different coding regions in both viruses, and was therefore unlikely to be related to any sequence specific features. Activation of the piRNA pathway may be a consequence of the concentration of certain RNA species within the infected cell. Gauliard *et al.* (2006) described differences in UTR promoter strengths between the genome segments, and also showed that S segment transcripts outnumber those for both M and L in infected mammalian cells. Therefore differences in segment specific transcript levels could explain why the S segment was more intensely targeted than M and L, with targeting intensity of piRNA species a consequence of the concentration of viral substrate acting as the target.

The characteristic nucleotide biases related to the ping-pong amplification process were present in piRNA species detected in all mosquito cells (Siomi et al. 2011), indicating a common biogenesis. However, a large degree of variation in piRNA species distribution between the different size classes was noted. In some areas piRNA species of every size class analysed targeted a common region. In other examples single size piRNA species targeted a unique region where no other species were detected. The biological significance of these findings was unclear, but perhaps indicates the presence of multiple discrete processes comprising the piRNA pathways, each generating different length piRNA species. Interestingly, the most numerous piRNA species targeting the rMP12 N and rMP12:S-Swap coding regions aligned to similar hairpin structures as the siRNA species in N and NSs mRNA transcripts (see Appendix Figure 10-13 and Figure 10-14). Furthermore, the minority of piRNA species aligning the genomic polarity NSs coding region in rMP12 infected cells were identical to those targeting the NSs coding region in rMP12:S-Swap infected cells, and vice versa. This structure-specific alignment was also observed in both rMP12 and rMP12:S-Swap infected BHK-21 cells. The large peak in 27 nt viRNA species observed targeting the M segment comprised an entire hairpin loop in the predicted secondary structure of the M segment polyprotein mRNA transcript (see Appendix Figure 10-14). The reproducibility and consistency of these responses suggests that piRNA biogenesis, similar to siRNA biogenesis, may also involve specific sequences or structures for activation. Furthermore, although piRNA species all contained the characteristic nucleotide frequencies associated with them, their distribution in infected C6/36 and C7-10 cells was dissimilar to that in U4.4 and Ae cells. In the former, piRNA hotspot regions were closely associated with those of the 19-23 nt viRNA species,

although genome location varied slightly for individual size classes. This pattern was not observed in the U4.4 and Ae cells. It is possible that the dysfunctional siRNA pathway in C6/36 and C7-10 cells also has an effects on piRNA biogenesis, resulting in this pattern.

One remarkable feature noted during this research was the highly conserved nature of the individual components of the RNAi response. Performing each infection in duplicate allowed for direct comparison in each cell type, and although total read numbers varied the proportional distribution of viRNA species targeting the genome segments, as well their genomic to antigenomic polarity ratios were highly reproducible. This reproducibility was further maintained when infection between different mosquito cells lines was compared, including those from different species. Hotspots of siRNA and piRNA activity in U4.4 and Ae cells were consistently targeted toward identical sequences in both rMP12 and rMP12ΔNSs:eGFP infected cells. This reproducibility was also apparent in BHK-21 cells tested, indicating a controlled biogenesis process is also present within this cell line. Previous studies had concluded that the evolution of the interferon system in mammalian cells led to the RNAi system becoming redundant and therefore not used by these organisms (Maillard et al. 2013). Recent research however has identified numerous classes of viRNAs produced in mammalian cells following viral infection, and the antiviral properties they possess. The role of the RNAi system in the mammalian hosts of arboviruses awaits experimental validation.

In conclusion, these data indicated that the mosquito cells lines evaluated here all contain RNAi pathways capable of generating RVFV specific viRNAs. Infected Ae cells respond with similar siRNA and piRNA pathways to those described in another *A. aegypti* cell line Aag-2. Both C6/36 and C7-10 cells have dysfunctional siRNA pathways, but are capable of mounting a PIWI-interacting RNAi pathway response to RVFV infection. However, the responses in C7-10 cells were not as efficient as those in C6/36 cells, perhaps indicating further dysfunctionality in other RNAi pathway genes that remain to be characterised. The *Dcr-2* mutation in C6/36 has proved fortunate for researching the Dcr-2 mediated siRNA pathway in mosquitos. If the nature of the dysfunctionality in C7-10 can be characterised then it may prove useful in future experiments in the absence of any current mosquito cell knock-out mutants.

8.5 Summary

- Reduction in NSs expression observed in rMP12 infected U4.4 and Ae cells was likely due to the actions of the siRNA response, with numerous siRNA species shown to target this coding region. The dysfunctional siRNA response in C6/36 cells results in the observed NSs expression when infected with rMP12, but the siRNA response can be rescued by supplementation with exogenous Dcr-2.

- rMP12:S-Swap virus offered clues as the viral substrates responsible for RNAi activation. The siRNA response targeted the NSs coding region in both rMP12 and rMP12:S-Swap viruses, suggesting preferential targeting of the NSs mRNA transcript. Furthermore, siRNA species were shown to align to hairpin loop structure suggesting a potential route of activation. piRNA activation was independent of coding region polarity in rMP12 and rMP12:S-Swap infected cells, and seemingly targeting the most populous RNA species.

- There is evidence of a mammalian RNAi response to rMP12 infected cells, although the antiviral potential of this remains undefined.

- The RNAi responses were highly conserved between the duplicate samples and also between individual cell lines. This suggested that the process was tightly regulated, highly conserved, and involved specific targets for activation.

- A large number of small viRNA species were detected in all cell lines. Similar to the siRNA and piRNA species they displayed a high degree of conservation in size, polarity and genome targeting locations. Whether these are a results of cellular responses to infection, or artifacts viral replication was unexplored, but represents a potential avenue for future research.

Chapter 9

FINAL REFLECTIONS

9 Final reflections

9.1 Fulfillment of aims

The primary aim of this project was to characterise RVFV replication in mosquito cells. Using a combination of different cell lines and RVFV recombinants several interesting observations were made and further experiments performed. Chapter 5 describes the initial characterisation of the rMP12 RVFV strain in three mosquito cell lines. These experiments revealed several differences in the permissiveness to infection, and expression levels of the S segment-encoded proteins. These differences were observed between both the mosquito cells lines, and also when compared to rMP12 infection of mammalian cells. Taking advantage of the highly efficient reverse genetics system for RVFV I was able to design and rescue several recombinant viruses. These aided in the understanding of rMP12 replication in mosquito cells, and the requirements for the non-structural proteins. A question arising from this initial characterisation was why there were differences in NSs expression levels observed between the cell lines. Attempts to answer this question opened up several other avenues of research which were investigated.

The rMP12:S-Swap recombinant virus had been previously shown to exhibit altered levels of both protein expression and mRNA transcription in infected mammalian cells. I was able to parallel this work in the mosquito cell lines and show similar results (Chapter 6). By designing and developing a strand-specific qRT-PCR assay I was also able to demonstrate that the altered coding strategy of the S segment affected the proportion of genomic and antigenomic polarity RNAs packaged into progeny virions. The development of a mosquito cell-based minireplicon assay allowed investigations of viral protein function and segment-specific promoter sequences in these cell lines (Chapter 7). The aim of developing a reverse genetic system unfortunately remained unfulfilled, although the extensive research carried out identified several potential problems that still need to be solved. While unsuccessful, the research described will provide a useful basis for the future continuation of this work.

Finally, I was able to use the mosquito cell lines and rMP12 recombinants to investigate differences in RNAi pathway activation by viral infection. Similar research and results were published during my PhD investigating the RNAi responses to ZH548 infection in

mosquito cells (Léger et al. 2013). I was able to expand on this research and use the various mosquito cell lines and rMP12 recombinants to investigate specific aspects of the RNAi response. I demonstrated that RNAi responses were highly reproducible between duplicate samples, and viRNA species generated were highly conserved between cell lines. I was also able to identify possible candidates for the virus substrates that activate the RNAi pathways.

9.2 The bigger picture: potential for future research

The public health and economic impacts should RVFV be introduced into Europe or North America would be devastating. The need for a safe and effective vaccine, effective in both humans and livestock, is recognised as a being an important step in worldwide control of the disease. It would be interesting to assess the potential of rMP12:S-Swap virus as a vaccine candidate. The virus was shown to be attenuated in cell culture, and interestingly replication was cytotoxic in mosquito cells. A recombinant based on rMP12:S-Swap expressing a marker protein in place of NSs would likely be attenuated in animals, but still capable of inducing protective immunity, as demonstrated for other NSs deleted strains (Bird et al. 2011; Bird et al. 2008). If the marker protein was antigenic then this would also fulfill the differentiation of infected and vaccinated animals (DIVA) requirements for a licensed vaccine. Alternatively, as GFP in the NSs locus was demonstrated to be hyper-expressed a second antigenic protein could be introduced, creating a divalent vaccine strain which would provide protection against a second pathogen. It would also be interesting to investigate the replication of rMP12:S-Swap in mosquitos. If viral replication was shown to be either attenuated in the vector, or if NSs hyper-expression resulted in death of the vector, then rMP12:S-Swap could be used as a live non-transmissible vaccine strain.

The research performed here was successful in the generation of a RVFV-based minireplicon assay that functioned in mosquito cells. Using the assay I was able to perform experiments to investigate the effect of NSs on viral polymerase activity, and study the differential promoters strengths between the cell lines. This assay would easily be adaptable to investigate other mosquito-borne arboviruses. Preliminary experiments performed in parallel demonstrated that a mosquito cell-based minireplicon assay for BUNV using on the same methodology was functional. Minireplicon assays based on the midge-borne OROV and tick-borne UUKV were also demonstrated to be active in

mosquito cell lines demonstrating the adaptability of the system. Finally, a new clade of mosquito-associated bunyaviruses has recently been described (Marklewitz et al. 2013). As these viruses do not have a vertebrate species component to their lifecycle, replication studies can only be performed in mosquito cells. Therefore mosquito-based minireplicon assays represent the only way in which replication and transcription of these species could be easily investigated.

The minireplicon assay required the supply of T7RNAP *in trans* for transcription of the reporter genome segments, and this represented the major bottle-neck in assay development. Low transfection efficiency in mosquito cells and reduced activity of the T7RNAP at 28°C resulted in significantly lower reporter activity when compared to the BSR-T7/5 cell based minireplicon assay. It remains likely that these issues were the ultimate cause of the unsuccessful rescue attempts in mosquito cells. Mosquito cell lines constitutively expressing T7RNAP would increase the effectiveness, although efforts to do this using antibiotic selective pressure were unsuccessful. A possible solution would be the use of CRISPR-Cas gene-editing methods to introduce the T7RNAP gene into a mosquito cell line (Sander & Joung 2014). This powerful technology is already being investigated for its potential to genetically modify mosquito vectors to make them more resistant to malaria and DENV transmission (World Health Organization 2009), demonstrating it potential for use in manipulating mosquito cell lines. A second approach would be to identify cell line specific RNA polymerase-I promoters which would bypass the need for T7RNAP altogether. Instead minireplicons or genome segments cloned under control of a RNA Pol-I promoter could be created, analogous to the Pol-I system widely used in influenza virus rescue (Hoffmann et al. 2000).

The results described here demonstrated that RVFV replication processes within the mosquito vector can differ significantly from that in the mammalian host. Whilst there is an increasing understanding of the essential interactions between arboviral and cellular proteins in mammalian cells, there have been no extensive studies of these interactions during the mosquito cell infection. Indirect evidence of the different roles for the non-structural proteins in a vertebrate or arthropod host were described here. Viral attenuation was more pronounced in mosquito cells infected with rMP12 recombinants unable to express NSm or 78 kDa proteins when compared to mammalian cells. Differences were also observed for the intranuclear NSs phenotypes between infected mosquito and

mammalian cell lines. The use of techniques such as affinity tagging and purification mass spectrometry could be employed to identify new host cell and virus encoded protein-protein interactions (Jäger et al. 2012). At a fundamental level this would increase our understanding of critical factors necessary to maintain the virus life-cycle in mammalian and mosquito hosts, and may also leads to the identification of novel therapeutic targets for the treatment and control of RVFV.

Investigations into the roles the various RNAi pathways play during viral infection have only recently begun to be examined in detail. The research presented here could be expanded on in several areas. The ability to use the siRNA pathway to "knock-down" expression of proteins within the siRNA and piRNA pathways have been investigated for several viruses (Blair 2011; Donald et al. 2012; Schnettler et al. 2013), and could be used to investigate both RNAi pathways in RVFV infected cells. The results I have presented here also described the presence of smaller 15-17 nt viRNA species. These RNA species demonstrated many of the same characteristics of the siRNA and piRNA species, namely a high degree of reproducibility between the cell lines and a high degree of conservation between the viruses. The origin of these viRNAs remains unknown but is deserving of further investigation. It is likely that in the near future the number of fully annotated mosquito genomes available to researchers will increase which will help with these investigations. RNAi research in *D. melanogaster* has been greatly assisted by the development of knock-out mutant strains unable to express individual protein components of the pathways. The ability to generate similar mutants in mosquito species could potentially lead to a similar increase in our knowledge of the mosquito RNAi pathways, and the antiviral roles they play.

Chapter 10

APPENDICES

10 Appendices

Table 10-1: List of primers used in project

Primer Name	Primer Sequence (5' to 3')	Primer Use
delNSm+ACC fwd	GACGGTGCATTAAACCATGGCAGGGATTGC	QC primer to add a stronger kozak sequence (ACC) -1 from the AUG that initiates the GnGc CDS in the pTVT7-GM rescue
delNSm+ACC rev	GCAATCCCTGCCATGGTTTAATGCACCGTC	QC primer to add a stronger kozak sequence (ACC) -1 from the AUG that initiates the GnGc CDS in the pTVT7-GM rescue
delNSm+g fwd	AATACGACTCACTATAGACACAAAGACGGTG C	QC primer to add G +1 from T7 promoter sequence in the pTVT7-GM rescue plasmid
delNSm+g rev	GCACCGTCTTTGTGTCTATAGTGAGTCGTATT	QC primer to add G +1 from T7 promoter sequence in the pTVT7-GM rescue plasmid
FFLuc to pSTI fwd	GATTTCAAGGCGCGTATGTATAGATTTGAAG	In Fusion clone FFLuc CDS into pST-IRES polyUB hyg -GFP DCR2 HA N-tag excised with 1+3
FFLuc to pSTI rev	TCTGGATCGCTCGAGTCAGCTCAGGGGGAGG TG	In Fusion clone FFLuc CDS into pST-IRES polyUB hyg -GFP DCR2 HA N-tag excised with 1+3
GFP to pAC FWD	GGATCGGGGTACCTGCATGGTGAGCAAGGGC	In fusion clone the eGFP CDS into pAC plasmid
GFP to pAC REV	GCCCTCTAGACTCGAGCGGTTACTTGTACAGC TC	In fusion clone the eGFP CDS into pAC plasmid
GFP to pSTI (post IRES) fwd	TATTTATAGGATCCAAATGGTGAGCAAGGGC	In Fusion clone eGFP CDS into pST-IRES polyUB hyg -GFP DCR2 HA N-tag excised with 4+5
GFP to pSTI (post IRES) rev	TGGATCGCTCGAGTTTTACTTGTACAGCTCG	In Fusion clone eGFP CDS into pST-IRES polyUB hyg -GFP DCR2 HA N-tag excised with 4+5
GFP to pSTI fwd	GATTTCAAGGCGCGTATGGTGAGCAAGGGCG	In fusion clone eGFP CDS into pST-IRES polyUB hyg -GFP DCR2 HA N-tag plasmid excised with 1+3
GFP to pSTI rev	TCTGGATCGCTCGAGTTACTTGTACAGCTC	In fusion clone eGFP CDS into pST-IRES polyUB hyg -GFP DCR2 HA N-tag plasmid excised with 1+3
GL3FFLuc to pSTI fwd	GATTTCAAGGCGCGATGGAAGACGCCAAAAA C	In fusion clone FFLuc CDS into pST-IRES polyUB hyg -GFP DCR2 HA N-tag plasmid excised with 1+3
GL3FFLuc to pSTI rev	TCTGGATCGCTCGAGTTACACGGCGATCTTTC CG	In fusion clone FFLuc CDS into pST-IRES polyUB hyg -GFP DCR2 HA N-tag plasmid excised with 1+3
IF L to pTM1-RhPV fwd	TATTTATAGGATCCAAATGGATTCTATATTA	In fusion clone rMP12 L CDS into pTM1-RhPV plasmid excised with 1+2
IF L to pTM1-RhPV rev	ATTAGGCCTCTCGAGTTAGCCTAGCATGTC	In fusion clone rMP12 L CDS into pTM1-RhPV plasmid excised with 1+2
IF Lco to pTM1-RhPV fwd	TATTTATAGGATCCAAATGGACAGCATCTTG	In fusion clone rMP12 Lco CDS into pTM1-RhPV plasmid excised with 1+2
IF Lco to pTM1-RhPV rev	CAGGGTCCTGAAGAGAACCTTGGAAAGGTC	In fusion clone rMP12 Lco CDS into pTM1-RhPV plasmid excised with 1+2
MP12 seqN 1	TGGAGGAGAGCCTGATGCTGCG	Sequencing primer for MP12 S segment
MP12 seqN 2	GGAGGAGAGTGATGATGATGG	Sequencing primer for MP12 S segment
MP12 SeqN 3	GATCCACCATGCCAGCAAAGC	Sequencing primer for MP12 S segment
MP12 seqNSs 1	GCCTTTGGACTTGTGGATTCC	Sequencing primer for MP12 S segment
MP12 seqNSs 2	CAGCAGCCTAAGTGGCTGCCC	Sequencing primer for MP12 S segment
MP12 seqNSs 3	GATCTTGCAACTCCTCATTGC	Sequencing primer for MP12 S segment
MRENM exi 1	ATCAGTGCGTGTAAAAGCAATATG	Excise hRen CDS from pTVT7-MRENg
MRENM exi 2	TTAATGCACCGTCTTTGTGTGG	Excise hRen CDS from pTVT7-MRENg
pSTI IRES exi 1	ACGCGCCTTGAAATCTCTGTTGAGC	Use for excision PCR on pST-IRES polyUB hyg -GFP DCR2 HA N-tag
pSTI IRES exi 2	GGGCCCGGATACCCATACGATGTTCC	Use for excision PCR on pST-IRES polyUB hyg -GFP DCR2 HA N-tag
pSTI IRES exi 3	CTCGAGCGATCCAGACATGATAAG	Use for excision PCR on pST-IRES polyUB hyg -GFP DCR2 HA N-tag
pSTI IRES exi 4	GTTCATTCGGGCCCTTAATTAAG	Use for excision PCR on pST-IRES polyUB hyg -GFP DCR2 HA N-tag

Primer Name	Primer Sequence (5' to 3')	Primer Use
pSTI IRES exi 5	GGTGGCGCGCCGTTGAAATCTC	Use for excision PCR on pST-IRES polyUB hyg -GFP DCR2 HA N-tag
pSTI IRES exi 6	TTGGATCCTATAAATAGATAAAGC	Use for excision PCR on pST-IRES polyUB hyg -GFP DCR2 HA N-tag
pSTI IRES exi 7	GATCCAAATGAAGAAG	Use for excision PCR on pST-IRES polyUB hyg -GFP DCR2 HA N-tag
pSTI IRES exi 8	TTAATTAAGGGCCCGAATGAAC	Use for excision PCR on pST-IRES polyUB hyg -GFP DCR2 HA N-tag
pSTI IRES exi 9	TGAGTCGTATTAAACGCGCCTTGAAATCTCTG TTG	Use for excision PCR on pST-IRES polyUB hyg -GFP DCR2 HA N-tag
pSTI IRES seq 1	TCGTGCTCGAAGCCAAAGGC	Sequence inserts into pSTI plasmid, down from pUB promoter
pSTI IRES seq 2	AGCCGTAATTCCTAATGAGC	Sequence inserts into pSTI plasmid, upstream of IRES
pSTI IRES seq 3	CTAGTTGTGGTTTGTCCAAACTC	Sequence inserts into pSTI plasmid, upstream of SV40
pSTI IRES T7 InF Fwd	GATTTCAAGGCGCGTATGAACACGATTAAC	In fusion clone T7RNAP CDS into pST-IRES polyUB hyg -GFP DCR2 HA N-tag plasmid excised with 1+2
pSTI IRES T7 InF Rev	TGGGTATCCGGGCCCTTACGCGAACGCGAAG	In fusion clone T7RNAP CDS into pST-IRES polyUB hyg -GFP DCR2 HA N-tag plasmid excised with 1+2
pTM1 ires exi 1	TATAGTGAGTCGTATTAATTTCG	Used in primer excision of EMCV IRES from pTM1 plasmid
pTM1 ires exi L	ATGGATTCTATATTATCAAAAC	Used with pTM1 ires exi 1 to primer excise the EMCV IRES from pTM1-L plasmid
pTM1 ires exi Lco	ATGGACAGCATCTTGAGCAAGC	Used with pTM1 ires exi 1 to primer excise the EMCV IRES from pTM1-Lco plasmid
pTM1 ires exi N	ATGGACAACTATCAAGAGCTTG	Used with pTM1 ires exi 1 to primer excise the EMCV IRES from pTM1-N plasmid
pTM1 ires exi Nco	ATGGATAACTACCAGGAACTGG	Used with pTM1 ires exi 1 to primer excise the EMCV IRES from pTM1-Nco plasmid
pTM1-GnGc co fwd	AAACACGATAATACCATGGCCGGCATCGCG	In fusion clone the GnGcco CDS into pTM1 excised plasmid
pTM1-GnGc co rev	ATTAGGCCTCTCGAGTTAGGAGGCCTTCTT	In fusion clone the GnGcco CDS into pTM1 excised plasmid
pTM1-L CO fwd	CTTTGAAAAACACGATAATACCATGGACAGC ATCTTG	In fusion clone the Lco CDS into pTM1 excised plasmid
pTM1-L CO rev	CTTAATTAATTAGGCCTCTCGAGTTAGCCGAG CATATC	In fusion clone the Lco CDS into pTM1 excised plasmid
pTM1-N CO fwd	CTTTGAAAAACACGATAATACCATGGATAAC TACCAGG	In fusion clone the Nco CDS into pTM1 excised plasmid
pTM1-N CO rev	CTTAATTAATTAGGCCTCTCGAGTTAGGCCGC GGTCTTG	In fusion clone the Nco CDS into pTM1 excised plasmid
pTM1-RhPV exi 1	TTGGATCCTATAAATAGATAAAGC	Used to PCR excise pTM1-RhPV, removing CDS after the IRES
pTM1-RhPV exi 2	CTCGAGAGGCCTAATTAATTAAG	Used to PCR excise pTM1-RhPV, removing CDS after the IRES
pTVT7 RVFV CO L Fwd	ATACGACTCACTATAGACACAAAGGCGCCCA ATC	In fusion clone the codon optimised RVFV L segment into BbsI digested pTVT7R
pTVT7 RVFV CO L Rev	ATGCCATGCCGACCCACACAAAGACCGCCC	In fusion clone the codon optimised RVFV L segment into BbsI digested pTVT7R
pTVT7 RVFV CO M Fwd	ATACGACTCACTATAGACACAAAGACGGTGC AT	In fusion clone the codon optimised RVFV M segment into BbsI digested pTVT7R
pTVT7 RVFV CO M Rev	ATGCCATGCCGACCCACACAAAGACCGGTGC AAC	In fusion clone the codon optimised RVFV M segment into BbsI digested pTVT7R
pTVT7 RVFV CO S Fwd	ATACGACTCACTATAGACACAAAGCTCCCTA GAGA	In fusion clone the codon optimised RVFV S segment into BbsI digested pTVT7R
pTVT7 RVFV CO S Rev	ATGCCATGCCGACCCACACAAAGACCCCCTA GTGC	In fusion clone the codon optimised RVFV S segment into BbsI digested pTVT7R
Q M Fwd	CCGGTGCAACTTCAAAGAGT	qPCR Primers for RVFV
Q M Fwd tagged	GGCCGTCATGGTGGCGAATCCGGTGCAACTT CAAAGAGT	qPCR Primers for RVFV
Q M Rev	AGGCAGCAGCAGTCTCAAGT	qPCR Primers for RVFV
Q M Rev tagged	GGCCGTCATGGTGGCGAATAGGCAGCAGCAG TCTCAAGT	qPCR Primers for RVFV
Q N FWD	AACTCTACGGGCATCAAACC	qPCR Primers for RVFV

Primer Name	Primer Sequence (5' to 3')	Primer Use
Q N REV	AAGAGCTTGCGATCCAGTTT	qPCR Primers for RVFV
Q N Rev tagged	GGCCGTCATGGTGGCGAATAAGAGCTTGCGATCCAGTTT	qPCR Primers for RVFV
Q NSs FWD	GGACTCCTTTGCTGGCTTAC	qPCR Primers for RVFV
Q NSs Fwd tagged	GGCCGTCATGGTGGCGAATGGACTCCTTTGCTGGCTTAC	qPCR Primers for RVFV
Q NSs REV	GCACTGTACGTGAGCAACCT	qPCR Primers for RVFV
RhPV IRES Fwd	CGACTCACTATAGGGTAAGATAAAAGAACC	In fusion clone the RhPV IRES into pMT1 plasmid with excised EMCV IRES
RhPV IRES pMT1-L Rev	TAATATAGAATCCATTTGGATCCTATAAATAG	In fusion clone the RhPV IRES into pMT1-L plasmid with excised EMCV IRES
RhPV IRES pMT1-Lco Rev	CAAGATGCTGTCCATTTGGATCCTATAAATAG	In fusion clone the RhPV IRES into pMT1-Lco plasmid with excised EMCV IRES
RhPV IRES pMT1-N Rev	TTGATAGTTGTCCATTTGGATCCTATAAATAG	In fusion clone the RhPV IRES into pMT1-N plasmid with excised EMCV IRES
RhPV IRES pMT1-Nco Rev	CTGGTAGTTATCCATTTGGATCCTATAAATAG	In fusion clone the RhPV IRES into pMT1-Nco plasmid with excised EMCV IRES
RVFV L co to pSTI fwd	GATTTCAAGGCGCGTATGGACAGCATCTTGAG	In Fusion clone RVFV Lco CDS into pST-IRES polyUB hyg -GFP DCR2 HA N-tag excised with 1+3
RVFV L co to pSTI rev	TCTGGATCGCTCGAGTTAGCCGAGCATATC	In Fusion clone RVFV Lco CDS into pST-IRES polyUB hyg -GFP DCR2 HA N-tag excised with 1+3
RVFV L to pSTI fwd	GATTTCAAGGCGCGTATGGATTCTATATTATC	In Fusion clone RVFV L CDS into pST-IRES polyUB hyg -GFP DCR2 HA N-tag excised with 1+3
RVFV L to pSTI rev	TCTGGATCGCTCGAGTTAGCCTAGCATGTC	In Fusion clone RVFV L CDS into pST-IRES polyUB hyg -GFP DCR2 HA N-tag excised with 1+3
RVFV N co to pSTI fwd	GATTTCAAGGCGCGATGGATAACTACCAGG	In Fusion clone RVFV Nco CDS into pST-IRES polyUB hyg -GFP DCR2 HA N-tag excised with 1+3
RVFV N co to pSTI rev	TCTGGATCGCTCGAGTTAGGCTGCTGTCTTG	In Fusion clone RVFV Nco CDS into pST-IRES polyUB hyg -GFP DCR2 HA N-tag excised with 1+3
RVFV N to pSTI fwd	GATTTCAAGGCGCGTATGGACAACTATCAA	In Fusion clone RVFV N CDS into pST-IRES polyUB hyg -GFP DCR2 HA N-tag excised with 1+3
RVFV N to pSTI rev	TCTGGATCGCTCGAGTTAGGCTGCTGTCTTG	In Fusion clone RVFV N CDS into pST-IRES polyUB hyg -GFP DCR2 HA N-tag excised with 1+3
RVFV NSs co to pSTI fwd	GATTTCAAGGCGCGATGGATTATTTTCCAG	In Fusion clone RVFV NSs co CDS into pST-IRES polyUB hyg -GFP DCR2 HA N-tag excised with 1+3
RVFV NSs co to pSTI rev	TCTGGATCGCTCGAGTTAATCTACTTCTAC	In Fusion clone RVFV NSs co CDS into pST-IRES polyUB hyg -GFP DCR2 HA N-tag excised with 1+3
RVFV NSs to pSTI fwd	GATTTCAAGGCGCGTATGGATTACTTTCCTG	In Fusion clone RVFV N CDS into pST-IRES polyUB hyg -GFP DCR2 HA N-tag excised with 1+3
RVFV NSs to pSTI rev	TCTGGATCGCTCGAGCTAATCAACCTCAAC	In Fusion clone RVFV N CDS into pST-IRES polyUB hyg -GFP DCR2 HA N-tag excised with 1+3
T7-GFP-F	TAATACGACTCACTATAGGGAGGAGCTGACCCTGAAGTTCATCTG	Makes a product of the eGFP CDS with T7 promoters at each end, used to create dsRNA
T7-GFP-R	TAATACGACTCACTATAGGGAGAGGTGTTCTGCTGGTAGTGGTC	Makes a product of the eGFP CDS with T7 promoters at each end, used to create dsRNA
T7-Luc-F	TAATACGACTCACTATAGGGAGATATGAAGAGATACGCCCTGGTT	Makes a product of the RLuc CDS with T7 promoters at each end, used to create dsRNA
T7-Luc-R	TAATACGACTCACTATAGGGAGATAAAACCGGGAGGTAGATGAGA	Makes a product of the RLuc CDS with T7 promoters at each end, used to create dsRNA
TagRFP to pSTI fwd	CAACGGCGCGCCACCATGAGCGAGCTGATTAAGG	In Fusion clone TagRFP CDS into pST-IRES polyUB hyg -GFP DCR2 HA N-tag excised with 1+2
TagRFP to pSTI rev	GGGCCCGAATGAACTCACTTGTGCCCCAG	In Fusion clone TagRFP CDS into pST-IRES polyUB hyg -GFP DCR2 HA N-tag excised with 1+2
delNSm+ACC fwd	GACGGTGCATTAAACCATGGCAGGGATTGC	QC primer to add a stronger kozak sequence (ACC) -1 from the AUG that initiates the GnGc CDS in the pTVT7-GM rescue plasmid
delNSm+ACC rev	GCAATCCCTGCCATGGTTTAATGCACCGTC	QC primer to add a stronger kozak sequence (ACC) -1 from the AUG that initiates the GnGc CDS in the pTVT7-GM rescue plasmid
delNSm+g fwd	AATACGACTCACTATAGACACAAAGACGGTGC	QC primer to add G +1 from T7 promoter sequence in the pTVT7-GM rescue plasmid
delNSm+g rev	GCACCGTCTTTGTGTCTATAGTGAGTCGTATT	QC primer to add G +1 from T7 promoter sequence in the pTVT7-GM rescue plasmid
FFLuc to pSTI fwd	GATTTCAAGGCGCGTATGTATAGATTTGAAG	In Fusion clone FFLuc CDS into pST-IRES polyUB hyg -GFP DCR2 HA N-tag excised with 1+3

Primer Name	Primer Sequence (5' to 3')	Primer Use
FFLuc to pSTI rev	TCTGGATCGCTCGAGTCAGCTCAGGGGGAGG TG	In Fusion clone FFLuc CDS into pST-IRES polyUB hyg -GFP DCR2 HA N-tag excised with 1+3
GFP to pAC FWD	GGATCGGGGTACCTGCATGGTGAGCAAGGGC	In fusion clone the eGFP CDS into pAC plasmid

Table 10-2: Analysis of RNA species in virion RNA extracted from rMP12 and rMP12:S-Swap viruses. Table showing the percentage of either genomic or antigenomic polarity S and M segment RNA detected in virion RNA. Samples were taken from rMP12 or rMP12:S-Swap infected C6/36. u4.4, and Ae cells. Each row represents an independent infection. Mean percentage values are indicated in bold at the bottom of each column.

C6/36							
rMP12				rMP12:S-Swap			
S Segment		M Segment		S Segment		M Segment	
Genome	Antigenome	Genome	Antigenome	Genome	Antigenome	Genome	Antigenome
79.63%	20.37%	98.13%	1.87%	25.24%	74.76%	89.21%	10.79%
90.32%	9.68%	96.93%	3.07%	38.70%	61.30%	84.16%	15.84%
83.57%	16.43%	98.34%	1.66%	4.98%	95.02%	88.23%	11.77%
78.75%	21.25%	98.80%	1.20%	34.76%	65.24%	89.47%	10.53%
63.21%	36.79%	90.70%	9.30%	18.43%	81.57%	94.37%	5.63%
85.51%	14.49%			38.12%	61.88%	97.17%	2.83%
80.17%	**19.83%**	**96.58%**	**3.42%**	**26.71%**	**73.29%**	**90.44%**	**9.57%**

u4.4							
rMP12				rMP12:S-Swap			
S Segment		M Segment		S Segment		M Segment	
Genome	Antigenome	Genome	Antigenome	Genome	Antigenome	Genome	Antigenome
76.97%	23.03%	98.43%	1.57%	28.07%	71.93%	97.74%	2.26%
71.15%	28.85%	97.39%	2.61%	17.83%	82.17%	85.30%	14.70%
80.60%	19.40%	98.10%	1.90%	33.14%	66.86%	96.30%	3.70%
81.31%	18.69%	94.71%	5.29%	20.78%	79.22%	89.73%	10.27%
63.05%	36.95%	96.27%	3.73%	22.65%	77.35%	91.64%	8.36%
74.61%	**25.39%**	**96.98%**	**3.02%**	**24.49%**	**75.51%**	**92.14%**	**7.86%**

Ae							
rMP12				rMP12:S-Swap			
S Segment		M Segment		S Segment		M Segment	
Genome	Antigenome	Genome	Antigenome	Genome	Antigenome	Genome	Antigenome
92.61%	7.39%	96.98%	3.02%	27.34%	72.66%	97.20%	2.80%
67.87%	32.13%	98.61%	1.39%	21.86%	78.14%	81.12%	18.88%
84.29%	15.71%	99.33%	0.67%	36.72%	63.28%	82.69%	17.31%
79.34%	20.66%	94.56%	5.44%	35.86%	64.14%	83.44%	16.56%
85.07%	14.93%	94.80%	5.20%	28.78%	71.22%	92.04%	7.96%
						85.46%	14.54%
81.84%	**18.16%**	**96.86%**	**3.14%**	**30.11%**	**69.89%**	**86.99%**	**13.01%**

Table 10-3: Analysis of RNA species in cellular RNA from rMP12 and rMP12:S-Swap infected mosquito cells.
Table showing the percentage of either genomic or antigenomic polarity S and M segment RNA detected in cellular RNA. Samples were taken from rMP12 or rMP12:S-Swap infected C6/36. u4.4, and Ae cells. Each row represents an independent infection. Mean percentage values are indicated in bold at the bottom of each column..

C6/36							
rMP12				rMP12:S-Swap			
S Segment		M Segment		S Segment		M Segment	
Genome	Antigenome	Genome	Antigenome	Genome	Antigenome	Genome	Antigenome
75.51%	24.49%	87.16%	12.84%	36.11%	63.89%	78.13%	21.87%
80.85%	19.15%	90.04%	9.96%	32.58%	67.42%	76.26%	23.74%
99.71%	0.29%	81.78%	18.22%	36.10%	63.90%	76.05%	23.95%
83.52%	16.48%	84.02%	15.98%	46.61%	53.39%	79.25%	20.75%
89.35%	10.65%	77.81%	22.19%	30.09%	69.91%	86.74%	13.26%
68.38%	31.62%	93.60%	6.40%	36.38%	63.62%		
96.03%	3.97%			49.93%	50.07%		
80.88%	19.12%						
84.28%	**15.72%**	**85.74%**	**14.27%**	**38.26%**	**61.74%**	**79.29%**	**20.71%**

u4.4							
rMP12				rMP12:S-Swap			
S Segment		M Segment		S Segment		M Segment	
Genome	Antigenome	Genome	Antigenome	Genome	Antigenome	Genome	Antigenome
86.24%	13.76%	77.77%	22.23%	36.15%	63.85%	78.16%	21.84%
76.60%	23.40%	71.96%	28.04%	36.29%	63.71%	71.02%	28.98%
73.15%	26.85%	69.96%	30.04%	41.82%	58.18%	71.31%	28.69%
85.34%	14.66%	77.20%	22.80%	44.24%	55.76%	76.42%	23.58%
87.53%	12.47%	74.10%	25.90%	39.80%	60.20%	74.10%	25.90%
79.95%	20.05%	71.61%	28.39%	32.50%	67.50%		
		63.11%	36.89%				
81.47%	**18.53%**	**72.24%**	**27.76%**	**38.47%**	**61.53%**	**74.20%**	**25.80%**

Ae							
rMP12				rMP12:S-Swap			
S Segment		M Segment		S Segment		M Segment	
Genome	Antigenome	Genome	Antigenome	Genome	Antigenome	Genome	Antigenome
79.24%	20.76%	79.81%	20.19%	17.61%	82.39%	84.87%	15.13%
75.23%	24.77%	77.12%	22.88%	19.85%	80.15%	79.55%	20.45%
80.07%	19.93%	79.25%	20.75%	41.15%	58.85%	72.10%	27.90%
77.64%	22.36%	82.35%	17.65%	12.51%	87.49%	79.40%	20.60%
87.54%	12.46%	71.96%	28.04%	37.50%	62.50%	69.23%	30.77%
86.40%	13.60%	74.41%	25.59%	26.98%	73.02%		
81.02%	**18.98%**	**77.48%**	**22.52%**	**25.93%**	**74.07%**	**77.03%**	**22.97%**

Table 10-4: Analysis of RNA species in rMP12 and rMP12:S-Swap infected BHK-21 cells.
Table showing the percentage of either genomic or antigenomic polarity S and M segment RNA detected in either (A) virion, or (B) cellular RNA. Samples were taken from rMP12 or rMP12:S-Swap infected BHK-21 cells. Each row represents an independent infection. Mean percentage values are indicated in bold.

(A) RNA species in virion RNA samples

BHK-21							
rMP12				rMP12:S-Swap			
S Segment		M Segment		S Segment		M Segment	
Genome	Antigenome	Genome	Antigenome	Genome	Antigenome	Genome	Antigenome
78.68%	21.32%	93.83%	6.17%	29.16%	70.84%	84.34%	15.66%
80.87%	19.13%	94.93%	5.07%	49.80%	50.20%	87.78%	12.22%
83.23%	16.77%	94.18%	5.82%	42.39%	57.61%	91.76%	8.24%
88.25%	11.75%	94.36%	5.64%	38.00%	62.00%	90.34%	9.66%
78.77%	21.23%	98.13%	1.87%	48.99%	51.01%	89.21%	10.79%
				32.43%	67.57%		
				26.21%	73.79%		
81.96%	**18.04%**	**95.09%**	**4.91%**	**38.14%**	**61.86%**	**88.69%**	**11.31%**

(B) RNA species in cellular RNA samples

BHK-21							
rMP12				rMP12:S-Swap			
S Segment		M Segment		S Segment		M Segment	
Genome	Antigenome	Genome	Antigenome	Genome	Antigenome	Genome	Antigenome
64.53%	35.47%	77.74%	22.26%	27.72%	72.28%	68.92%	31.08%
73.73%	26.27%	94.84%	5.16%	26.24%	73.76%	86.10%	13.90%
61.72%	38.28%	93.92%	6.08%	18.53%	81.47%	90.34%	9.66%
82.12%	17.88%	85.54%	14.46%	26.92%	73.08%	67.89%	32.11%
69.98%	30.02%	82.33%	17.67%	19.93%	80.07%	71.33%	28.67%
79.96%	20.04%	84.12%	15.88%	21.38%	78.62%	72.03%	27.97%
				21.53%	78.47%		
				32.50%	67.50%		
72.01%	**27.99%**	**86.42%**	**13.59%**	**24.34%**	**75.66%**	**76.10%**	**23.90%**

(A) MP12 S segment

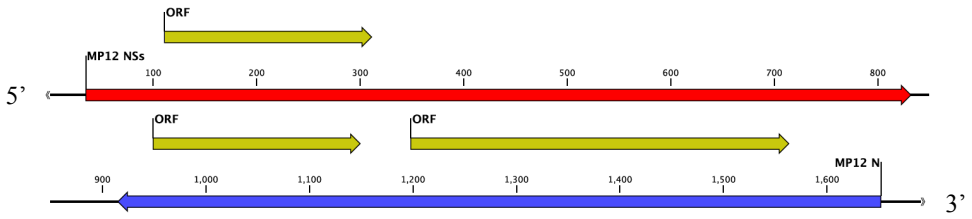

(B) MP12 S segment codon optimsed

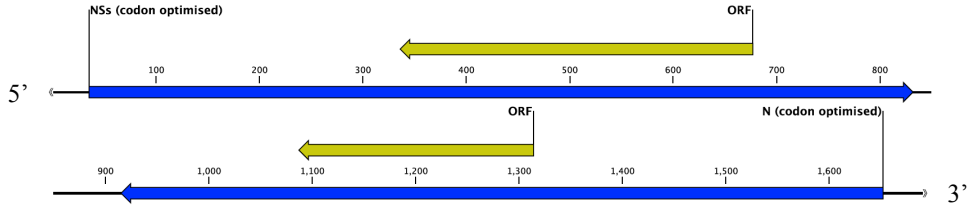

Figure 10-1: Analysis of CDS and ORF regions on the MP12 and codon optimised MP12 S segments. (A) The reference MP12 S segment (Genbank accession# DQ380154) was analysed to look for potential ORFs. Parameters were: AUG start codon; minimum codon length of 50; standard genetic code used for translation. Represented in genomic polarity RNA, with arrow representing coding direction. Known CDs are for N (blue) and NSs (red). Potential ORFs are represented as yellow arrows. (B) The MP12 S segment in which the CDS were codon optimised for *Aedes* species was also examined using the same parameters.

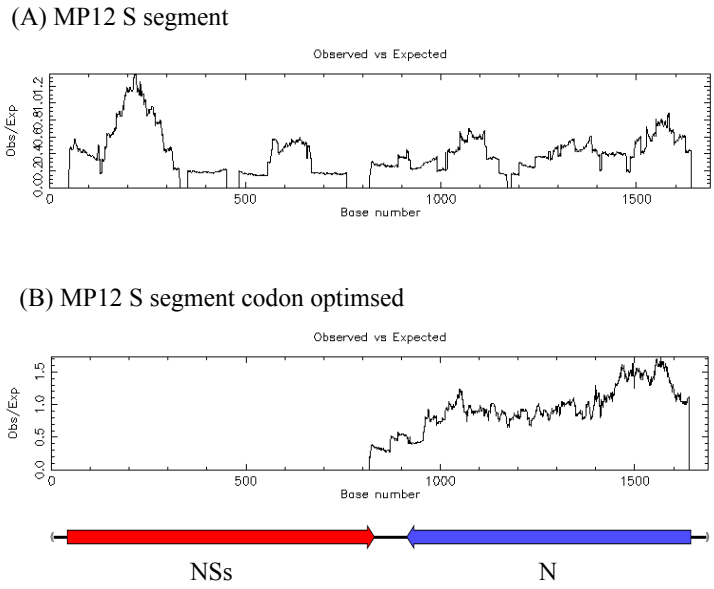

Figure 10-2: Analysis of CpG dinucleotide frequency differences in the MP12 and codon optimised MP12 S segments.
The reference (A) MP12 S segment and *Aedes* species optimised S (B) MP12 S segment were analysed using EMBOSS Cpgplot web-based software to determine CpG dinucleotide frequencies throughout the genome. Below the graphs is the reference S segment showing positions of the CDS for N and NSs (genomic polarity orientation, 5' to 3'). Represented is the observed to expected ratio of C plus G dinucleotides across the genome.

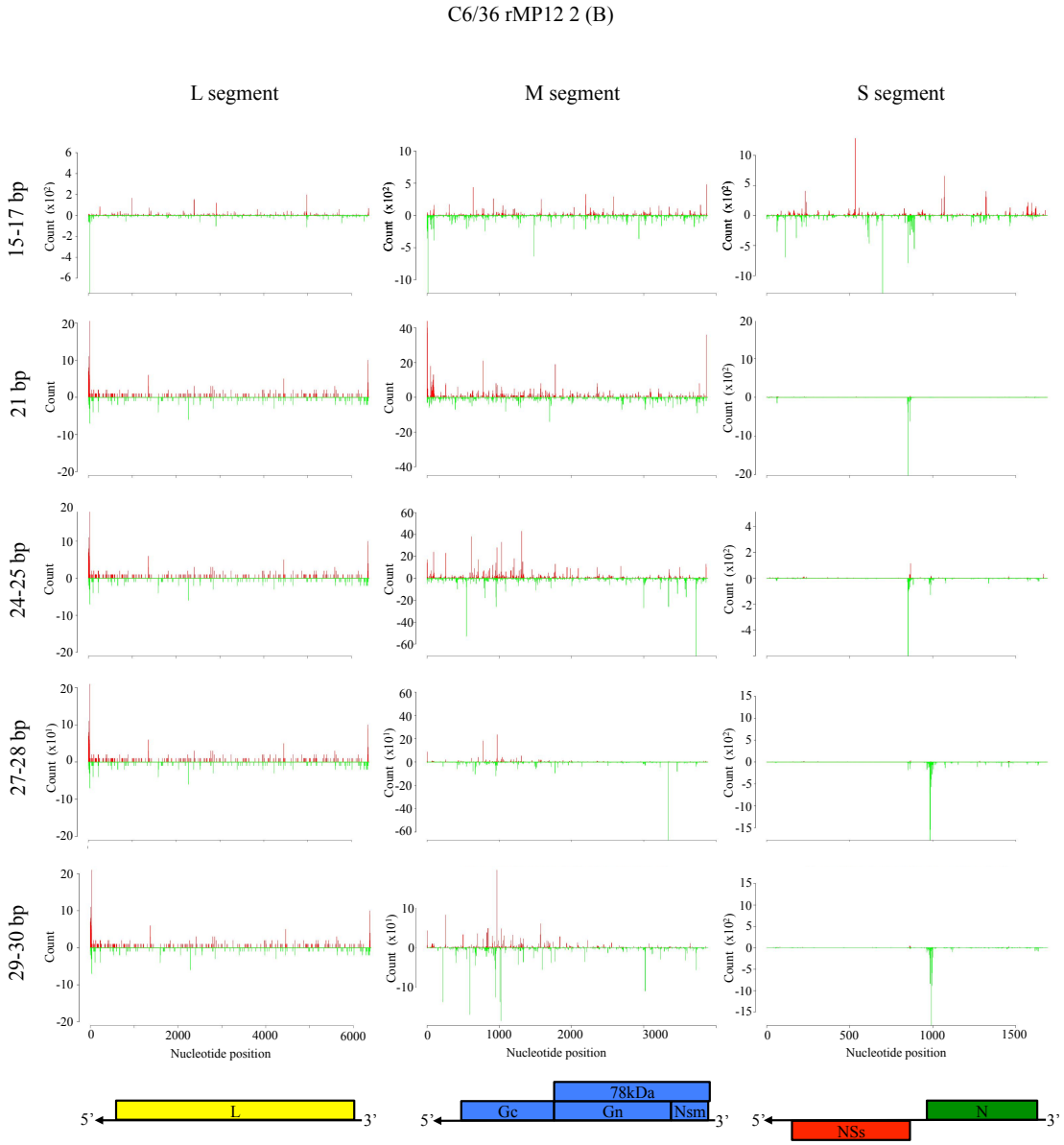

Figure 10-3: Duplicate mapping analysis plots for rMP12 infected mosquito cells
Shown are density plots of aligned viRNA species of 15-17nt, 21nt, 24-25nt, 27-28nt, and 29-30nt aligning to the rMP12 L, M, and S genome segments for the duplicate sample B infections. Upper plots (red) show alignments to genomic polarity (negative sense) and lower plots (green) to antigenomic polarity (positive sense). Also shown are the CDS for MP12 proteins encoded on the L (yellow), M (blue) and S (green and red) segments.

(A) rMP12 infected C6/36 cells.

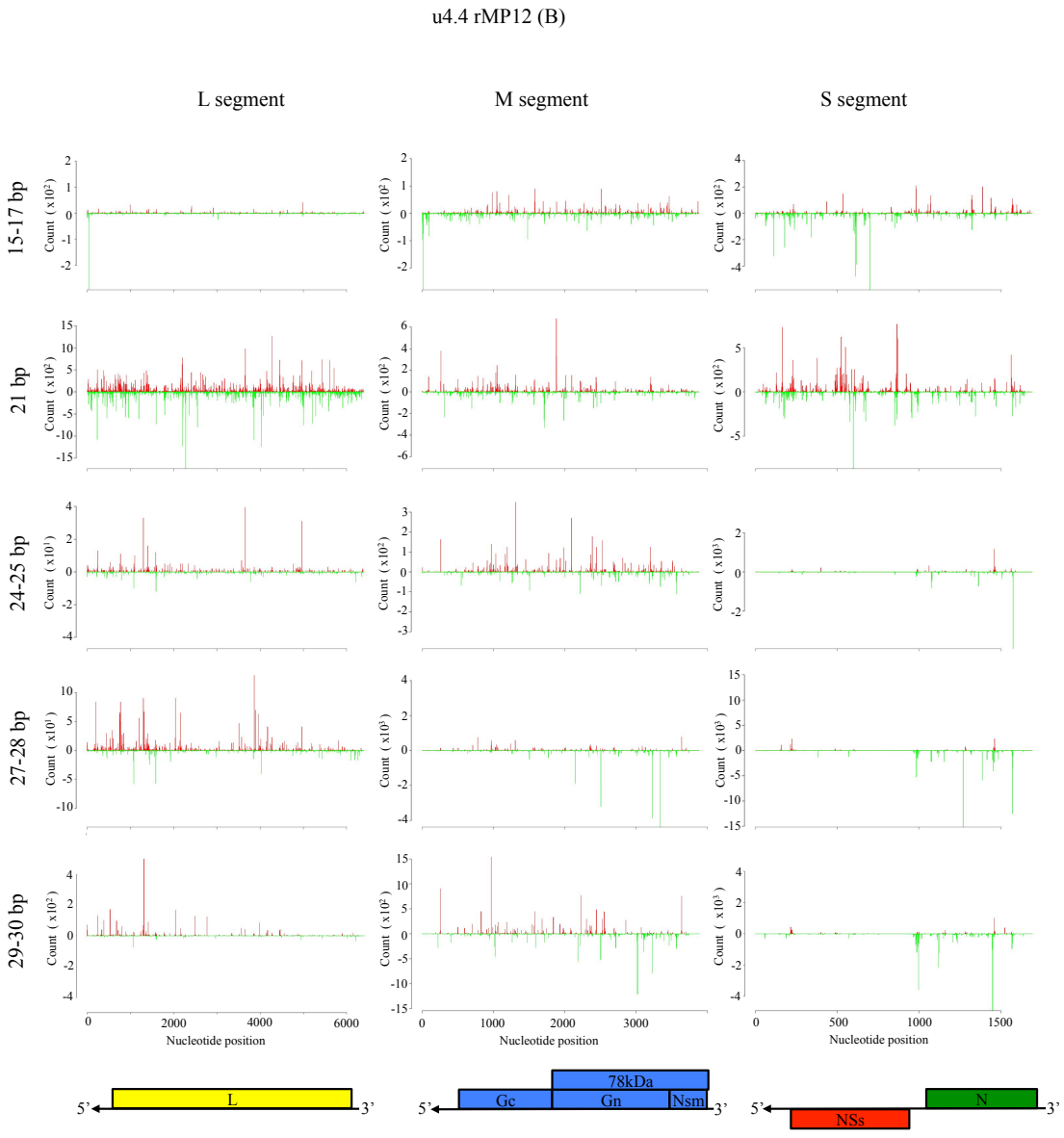

(B) rMP12 infected u4.4 cells

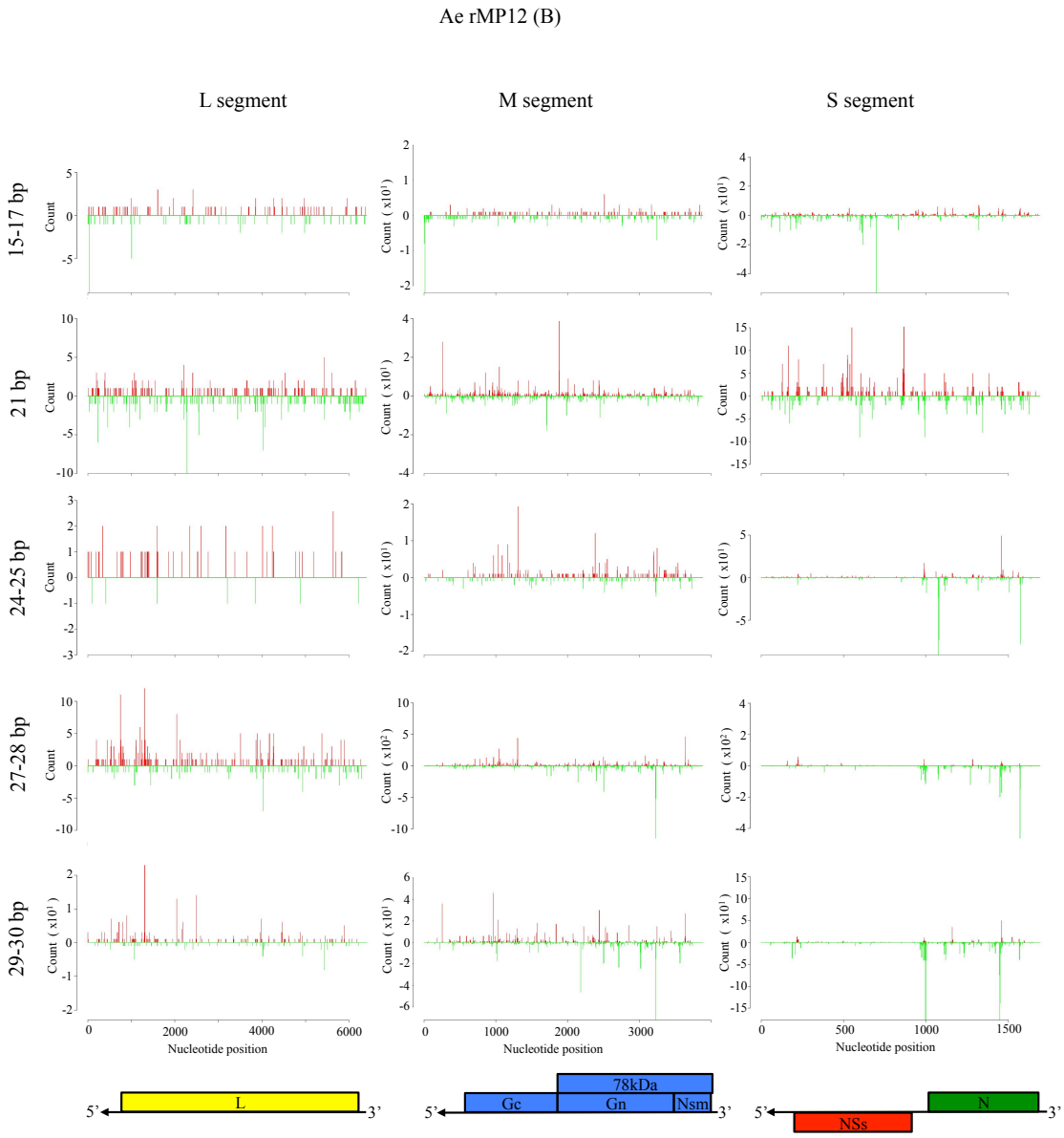

(C) rMP12 infected Ae cells.

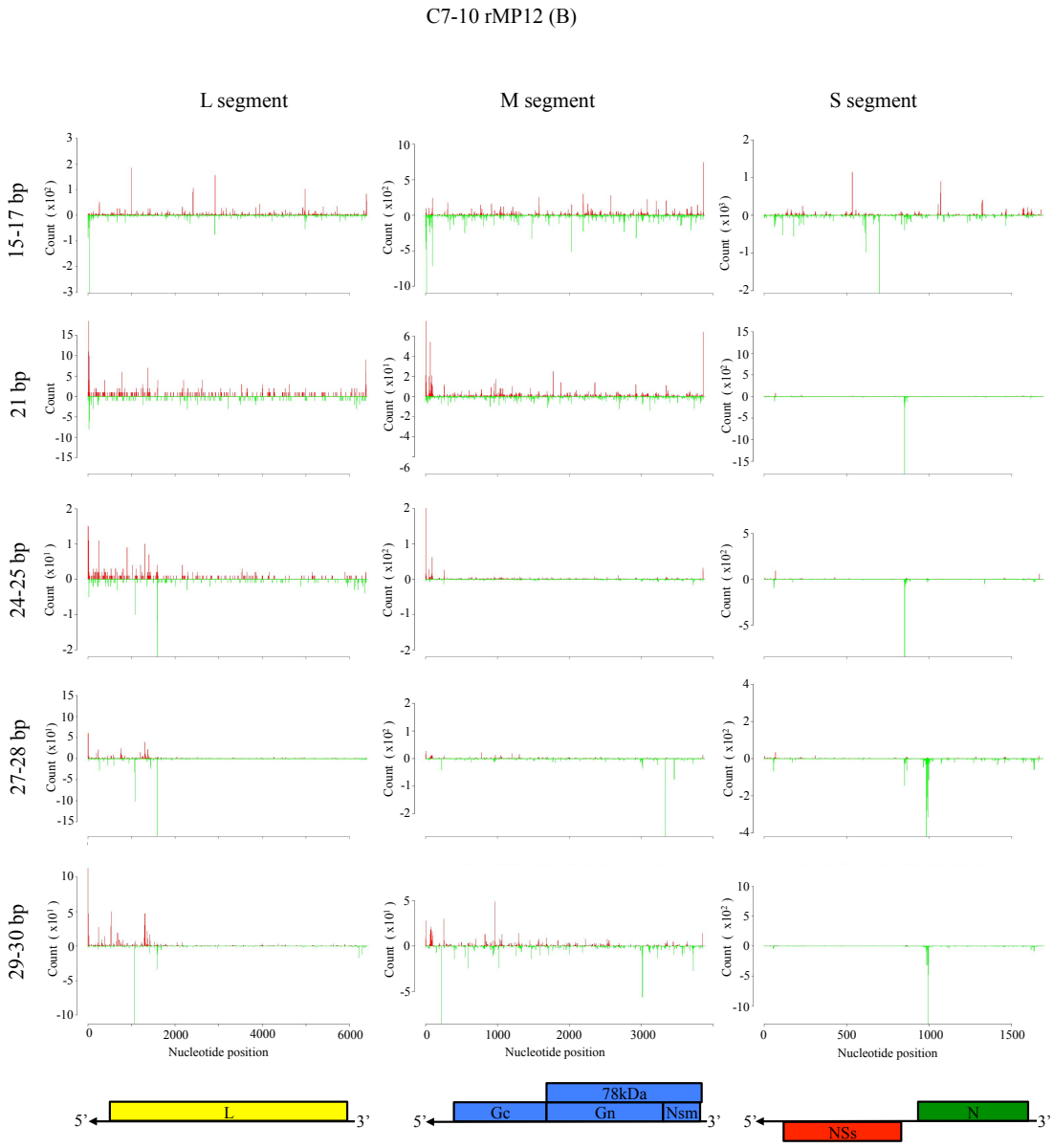

(D) rMP12 infected C7-10 cells.

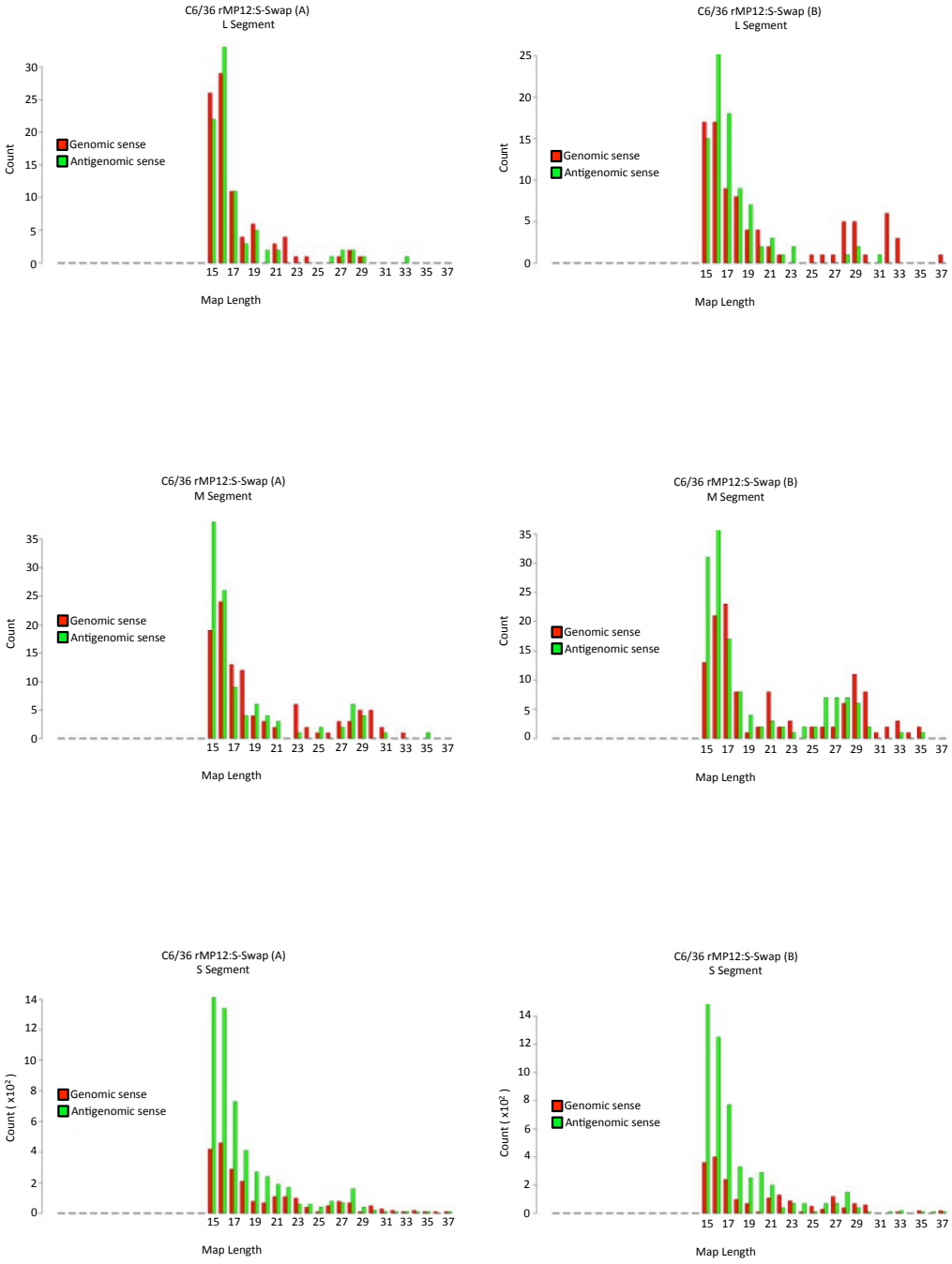

Figure 10-4: viRNA species plot analysis for rMP12:S-Swap infected mosquito cells.
Size distribution and density plots of all 15-37 nt viRNA species detected in rMP12:S-Swap infected C6/36, Ae, and C7-10 cells lines aligning to L, M or S segment. Shown are replicate samples A and B taken from duplicate infections. viRNA species aligning to genomic polarity (negative sense) RNA are shown in red, antigenomic polarity (positive sense) RNA in green.

(A) rMP12:S-Swap infected C6/36 cells

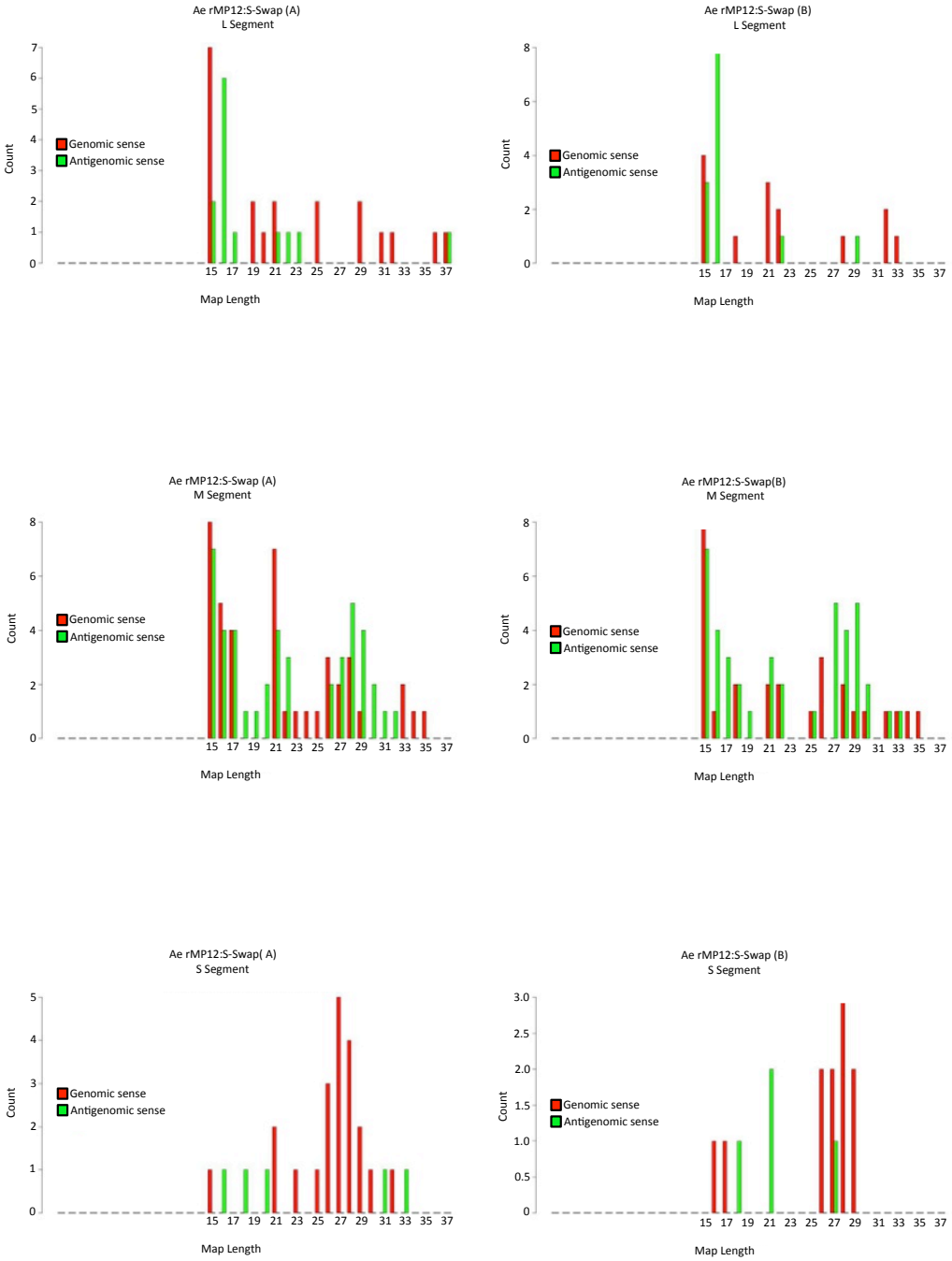

(B) rMP12:S-Swap infected Ae cells

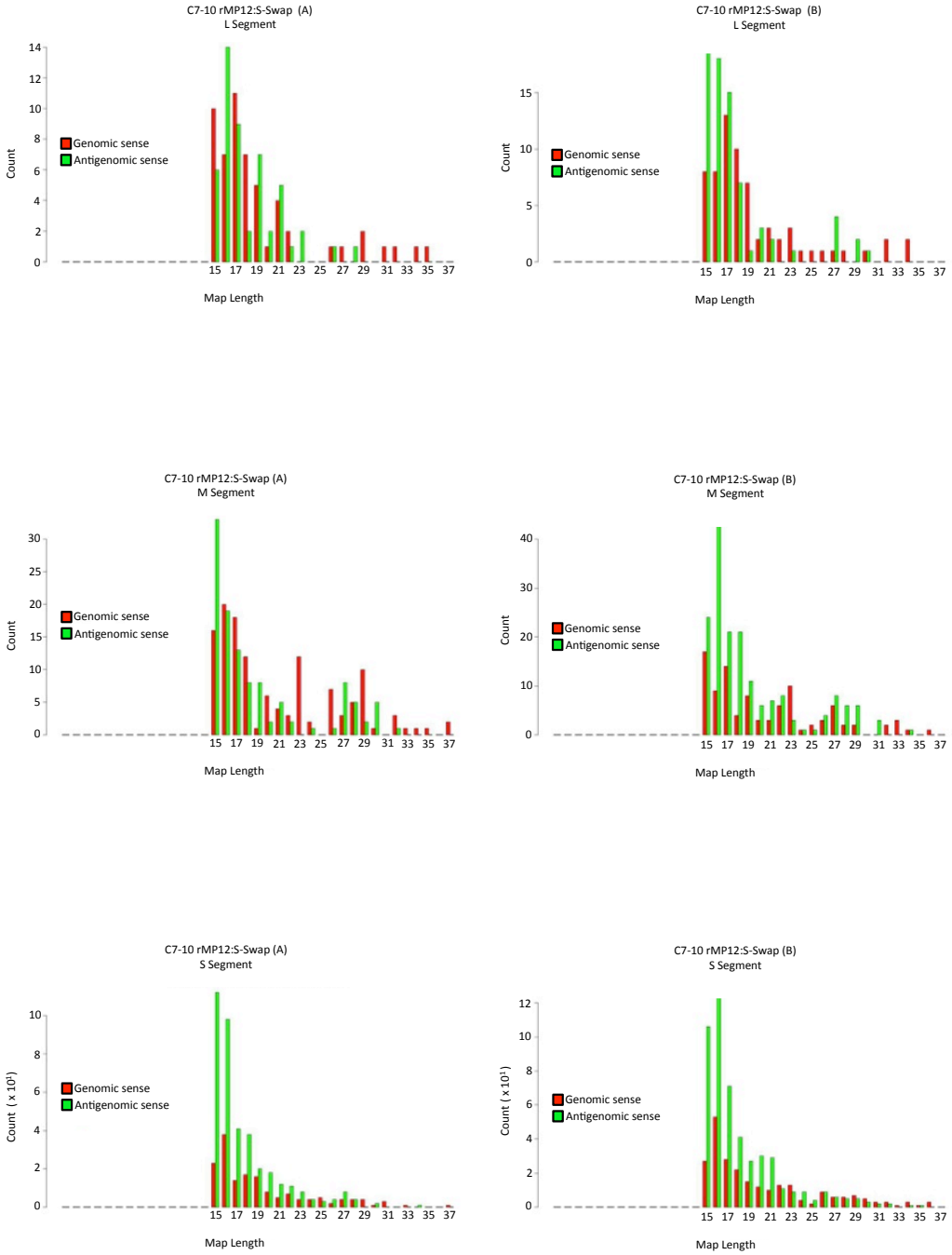

(C) rMP12:S-Swap infected C7-10 cells

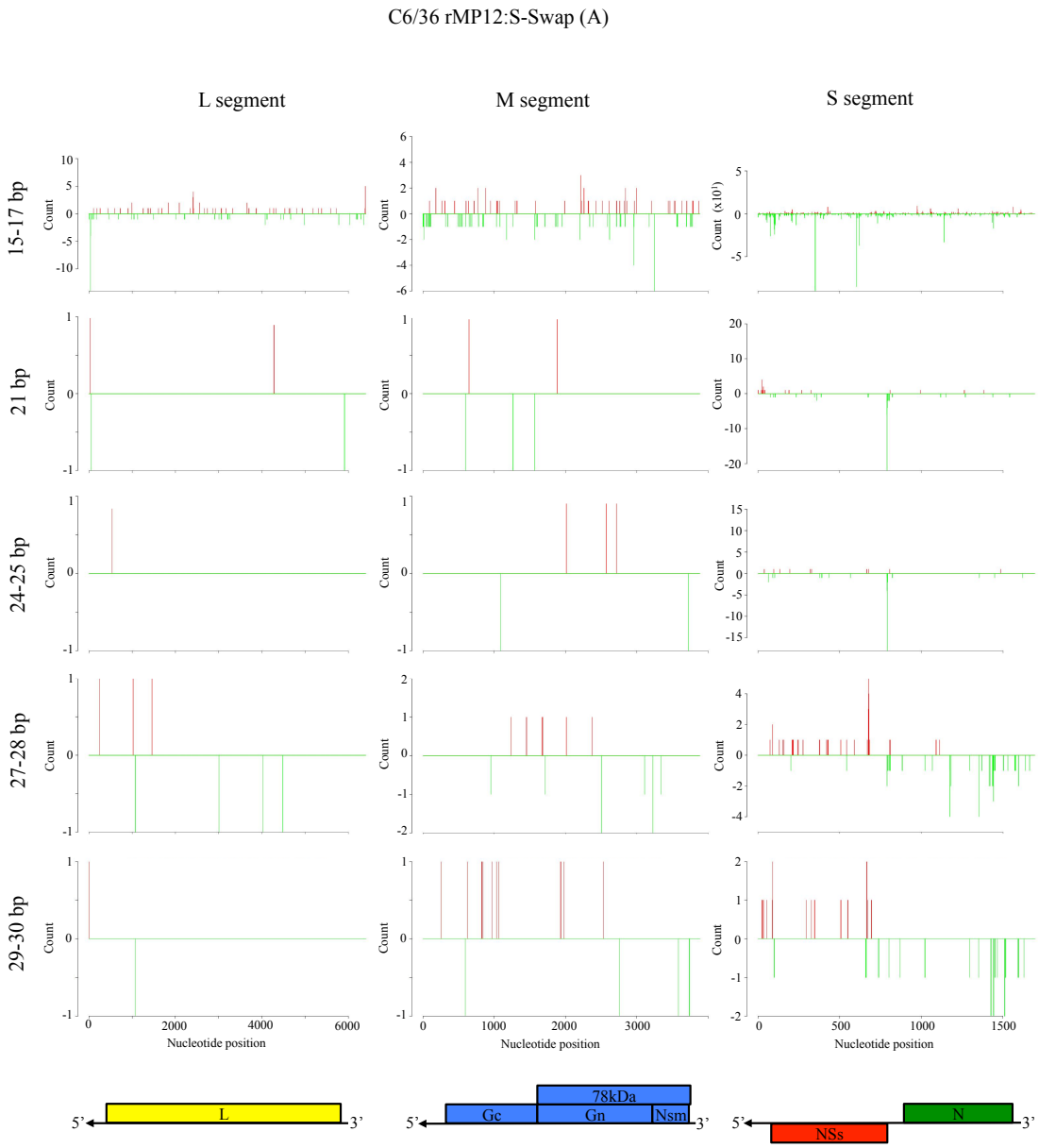

Figure 10-5: Mapping analysis of viRNA species in rMP12:S-Swap infected C6/36, u4.4, and Ae cells
Shown are density plots of aligned viRNA species of 15-17nt, 21nt, 24-25nt, 27-28nt, and 29-30nt aligning to the rMP12 :S-Swap L, M, and S genome segments for the infections in C6/36, u4.4, and Ae cells. Shown are replicate samples A and B taken from duplicate infections. Upper plots (red) show alignments to genomic polarity (negative sense) and lower plots (green) to antigenomic polarity (positive sense). Also shown are the CDS for MP12 proteins encoded on the L (yellow), M (blue) and S (green and red) segments.

(A) rMP12:S-Swap infected C6/36 cells.

C6/36 rMP12:S-Swap (B)

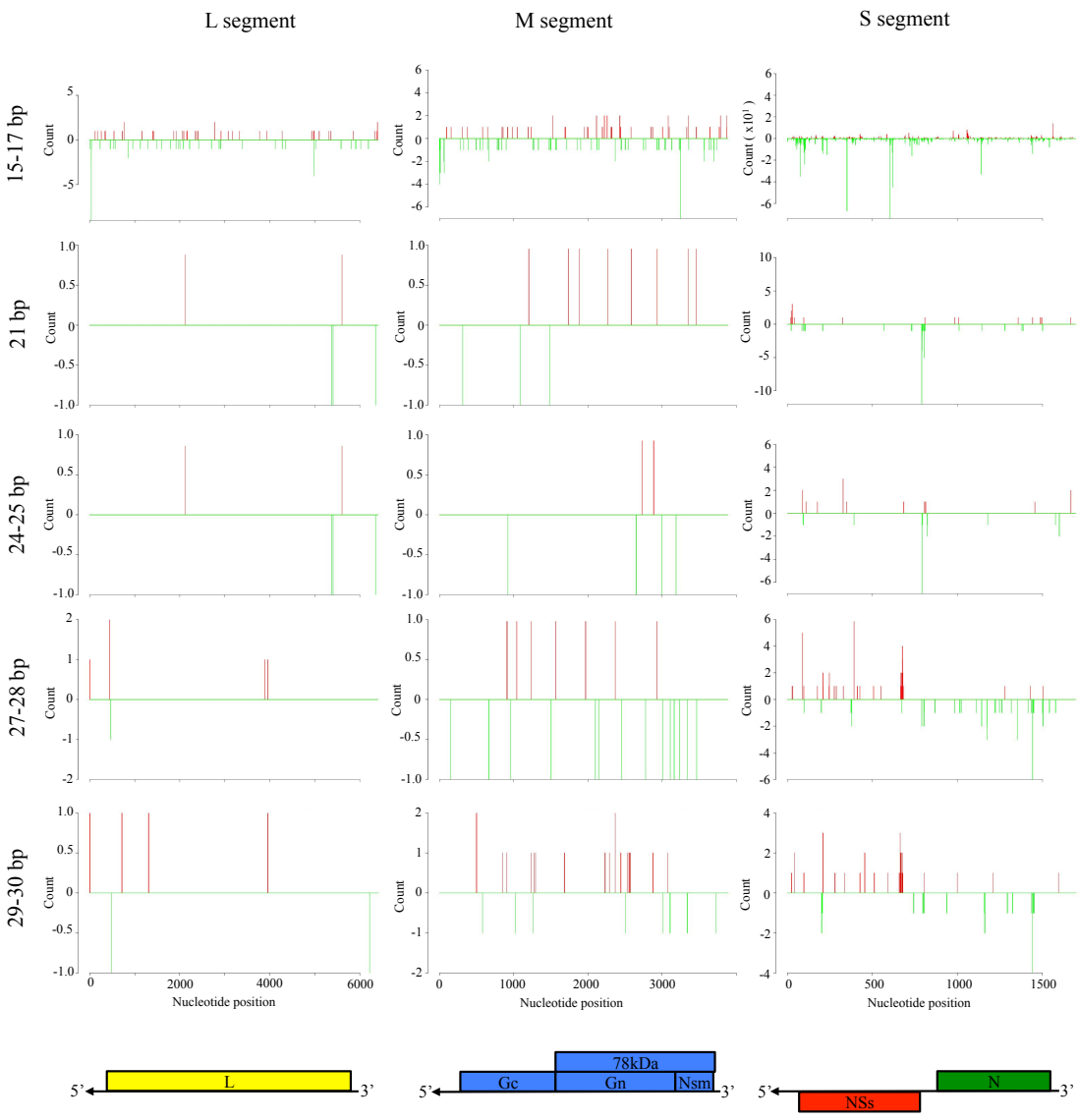

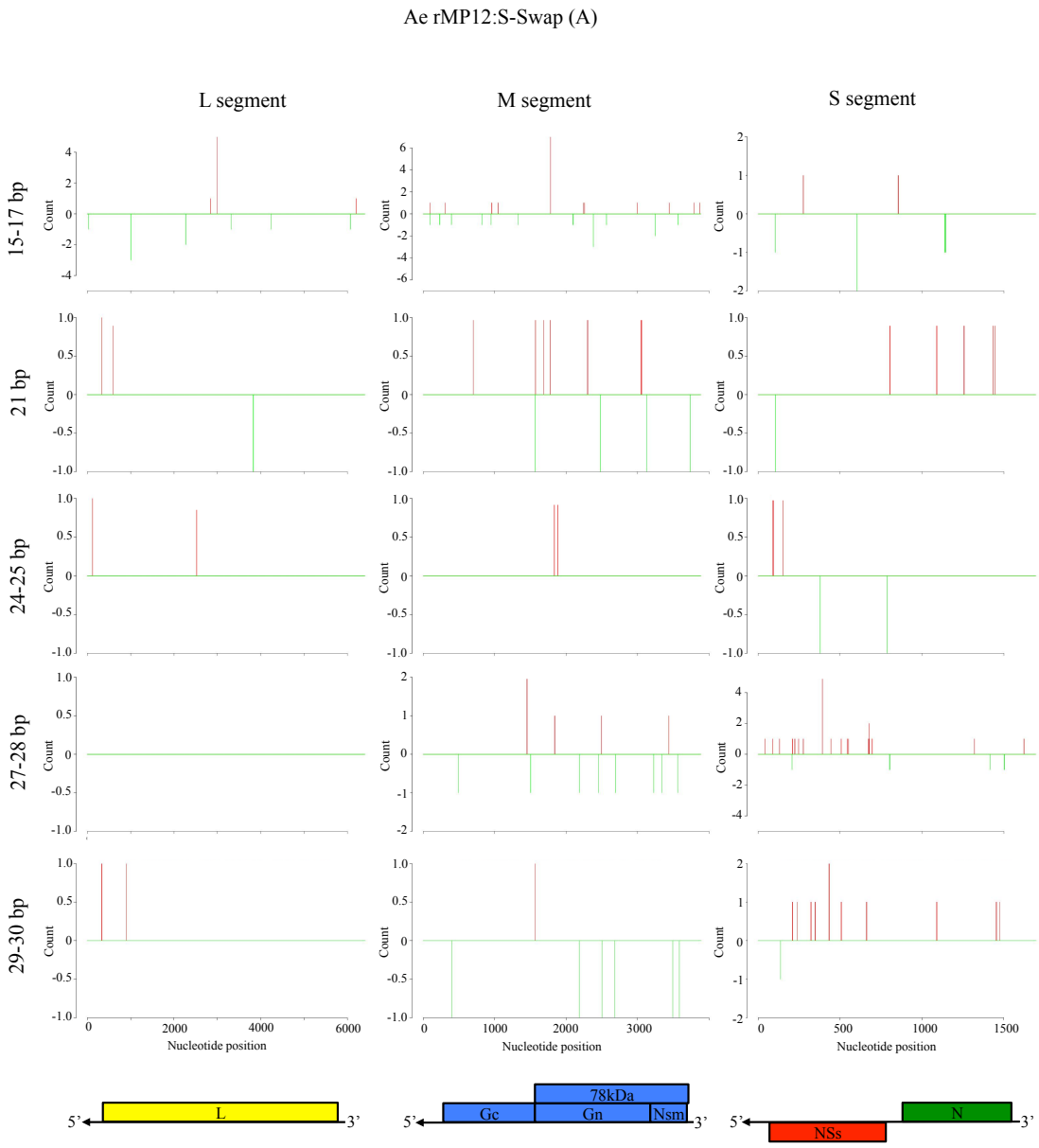

(B) rMP12:S-Swap infected Ae cells.

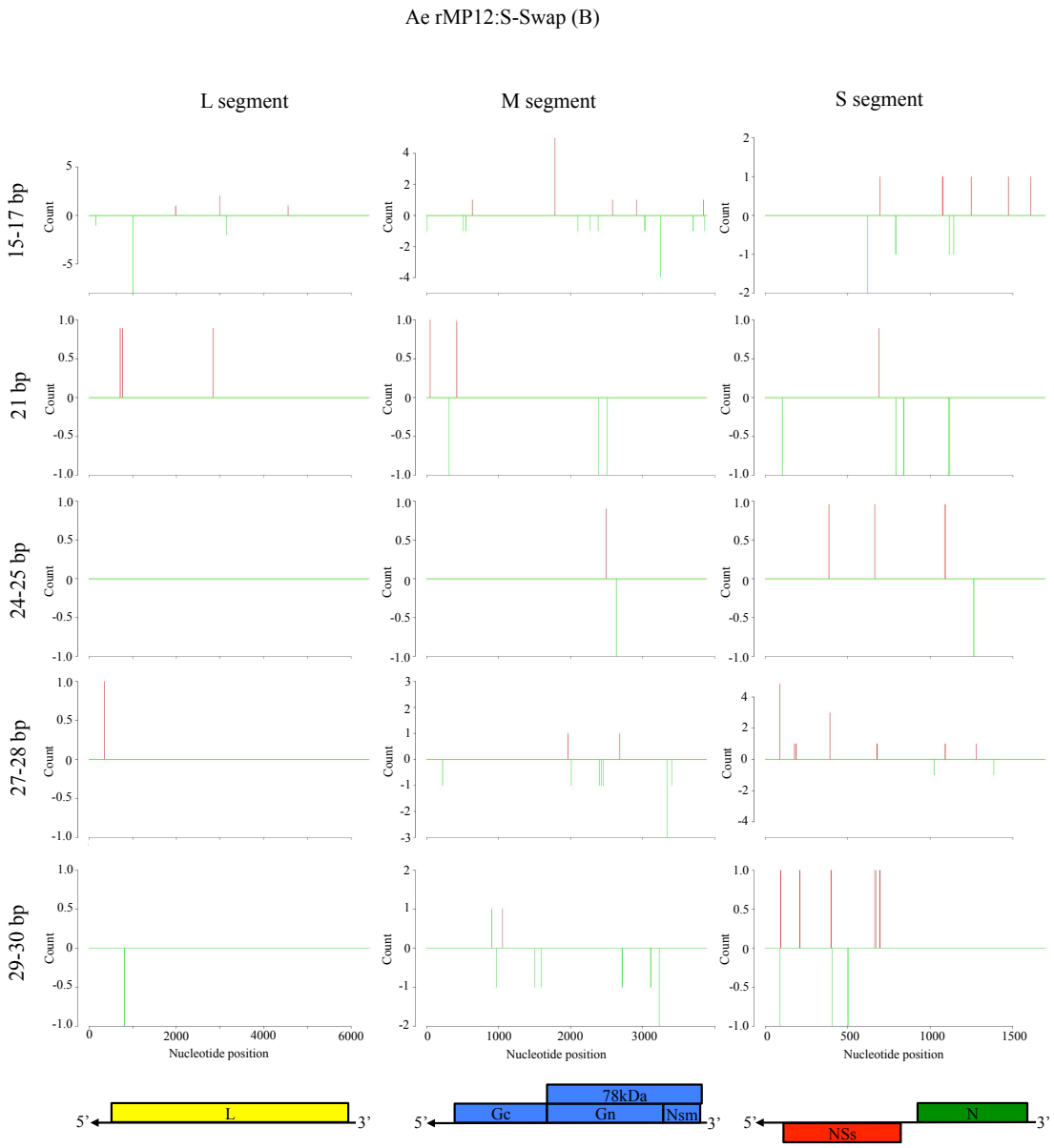
Ae rMP12:S-Swap (B)
L segment
M segment
S segment
15-17 bp
21 bp
24-25 bp
27-28 bp
29-30 bp
Count
Nucleotide position
5'
3'
L
78kDa
Gc
Gn
Nsm
N
NSs

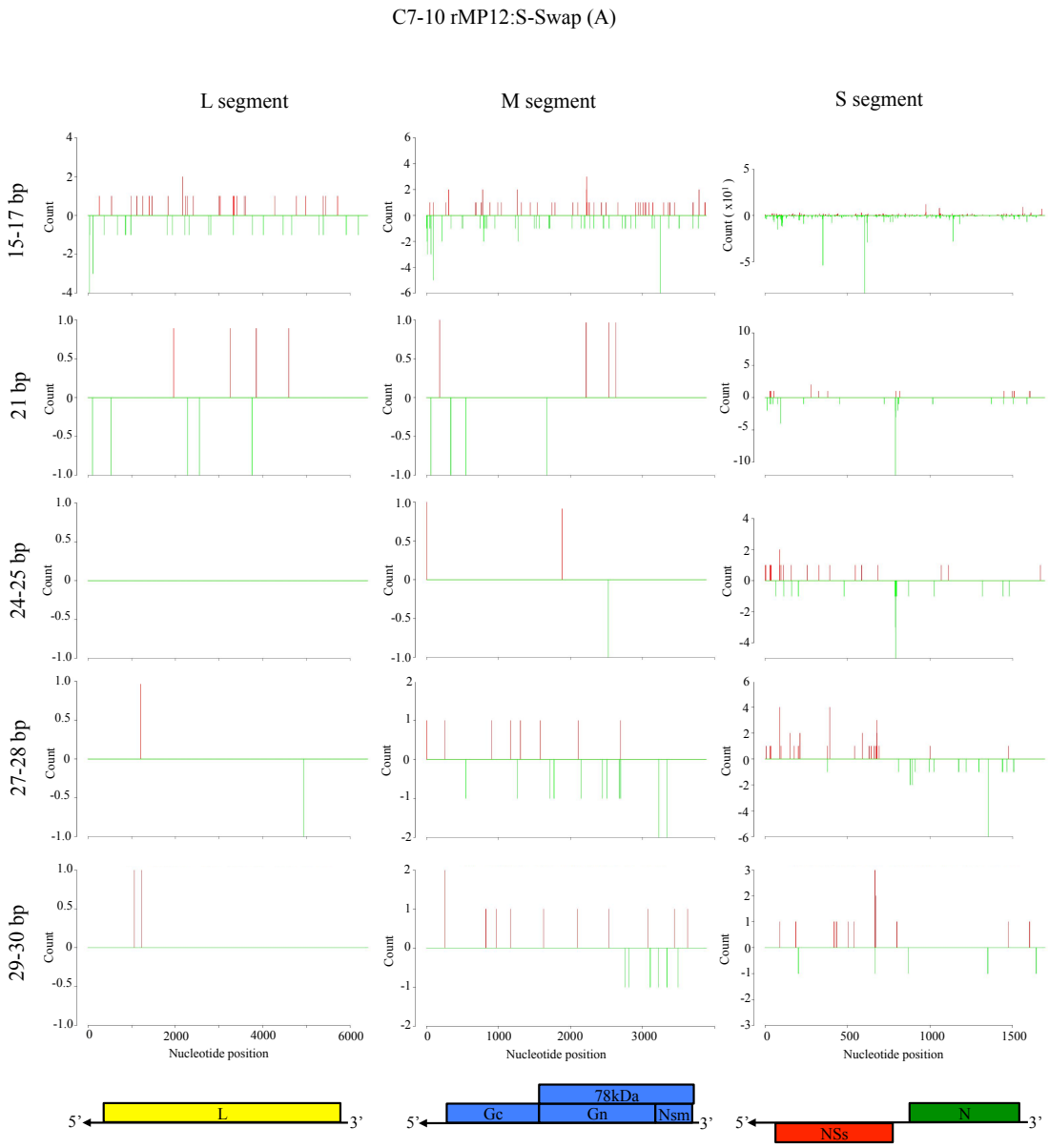

(C) rMP12:S-Swap infected C7-10 cells

C7-10 rMP12:S-Swap (B)

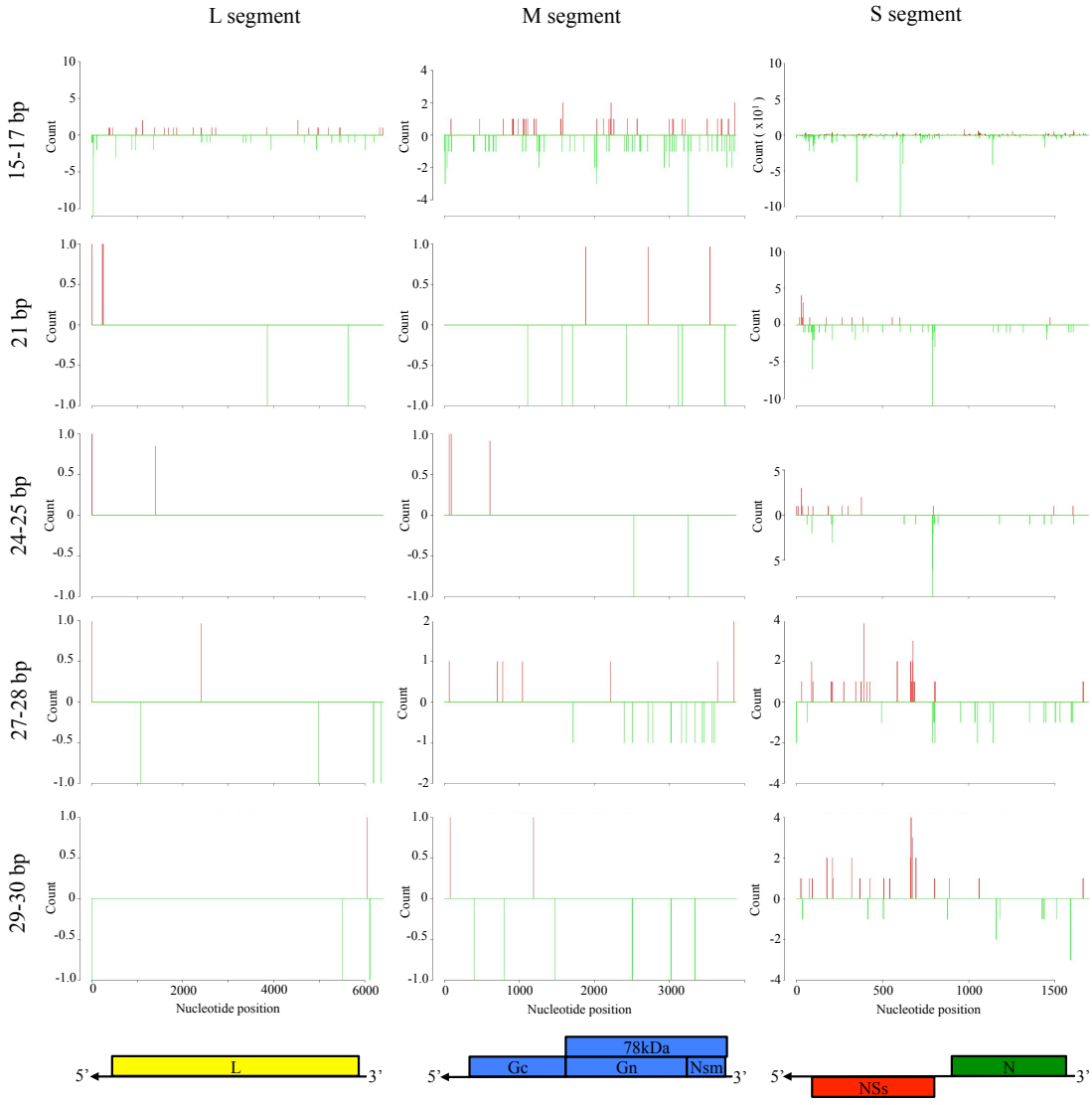

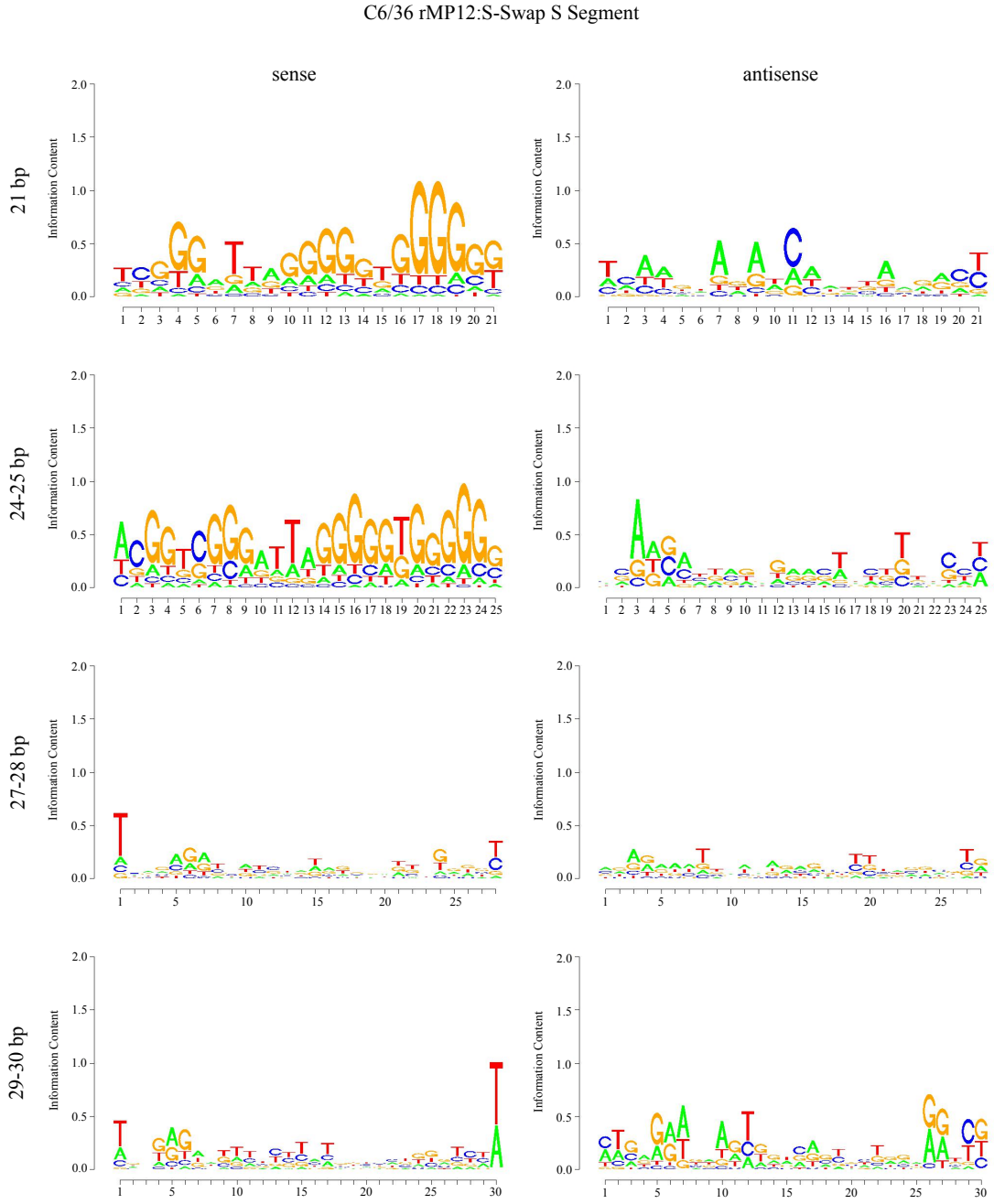

Figure 10-6: Logo analysis of viRNA species generated in rMP12:S-Swap infected mosquito cells
Logo analysis of rMP12:S-Swap infected C6/36, Ae, and C7-10 cells, with sense and antisense strand species analysis represented for the 21 bp, 24-25 bp, 27-28 bp, and 29-30 bp viRNA size classes. Shown are species aligning to the modified S segment.

(A) rMP12:S-Swap infected C6/36 cells

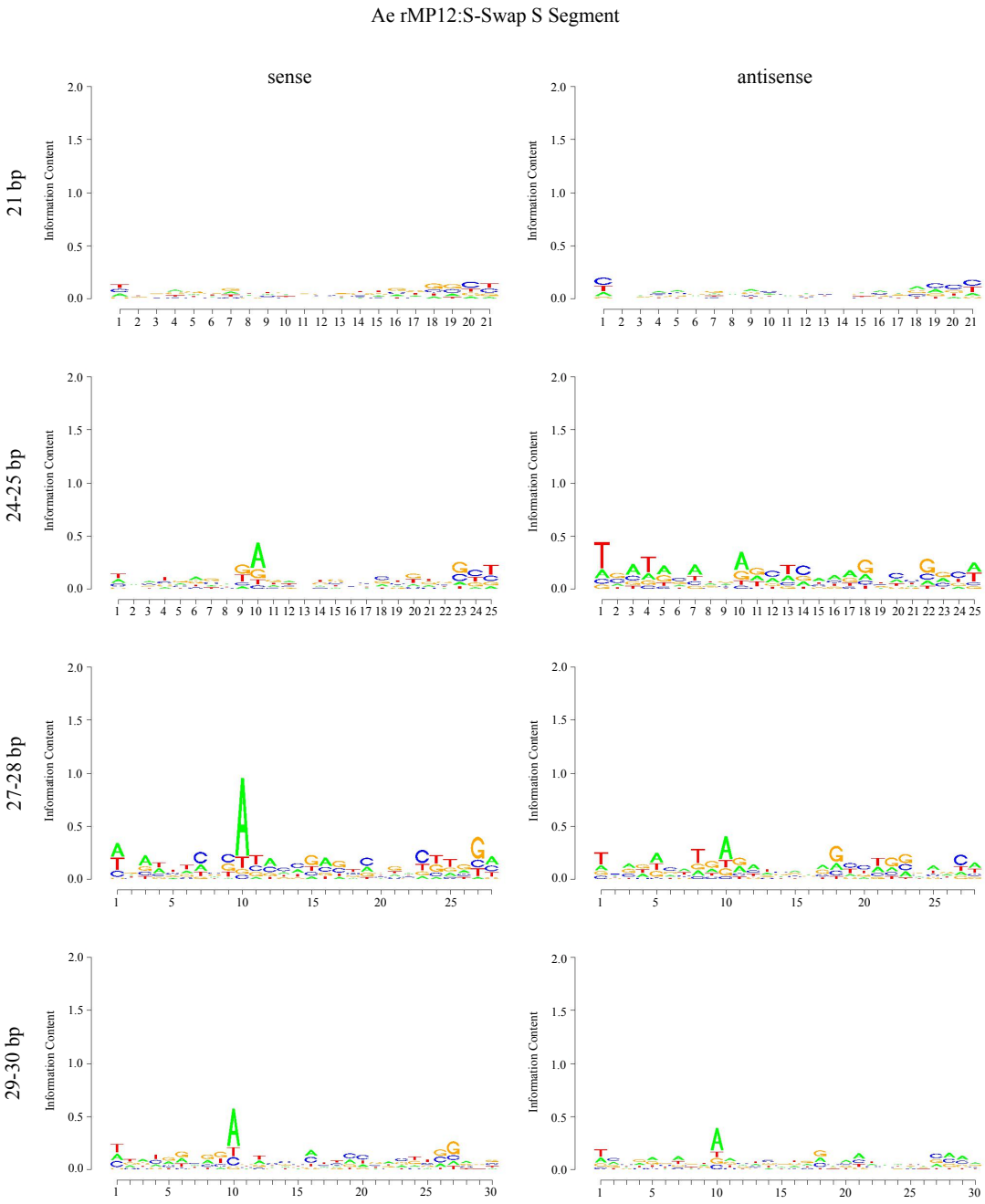

(B) rMP12:S-Swap infected u4.4 cells

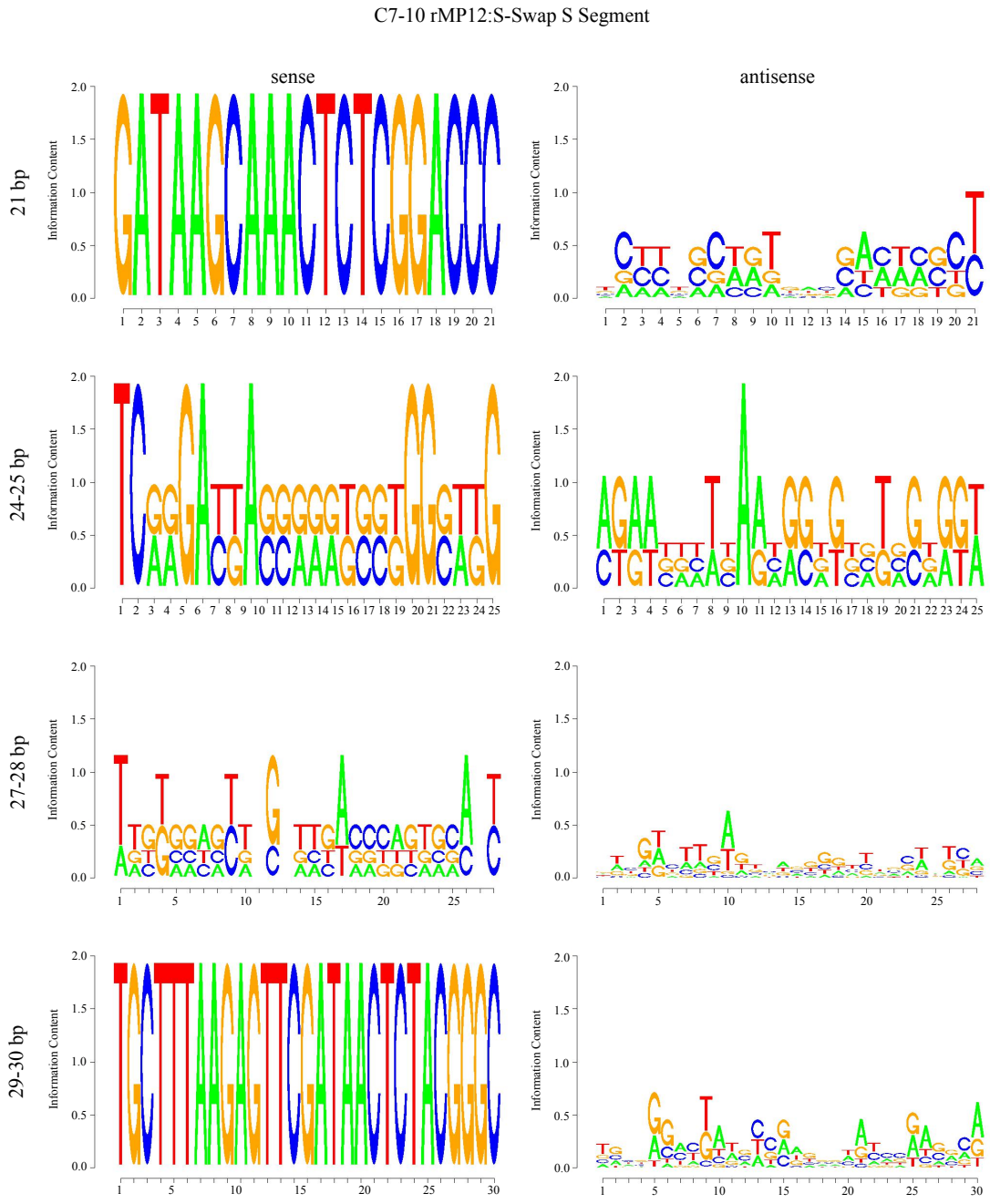

(C) rMP12:S-Swap infected C7-10 cells

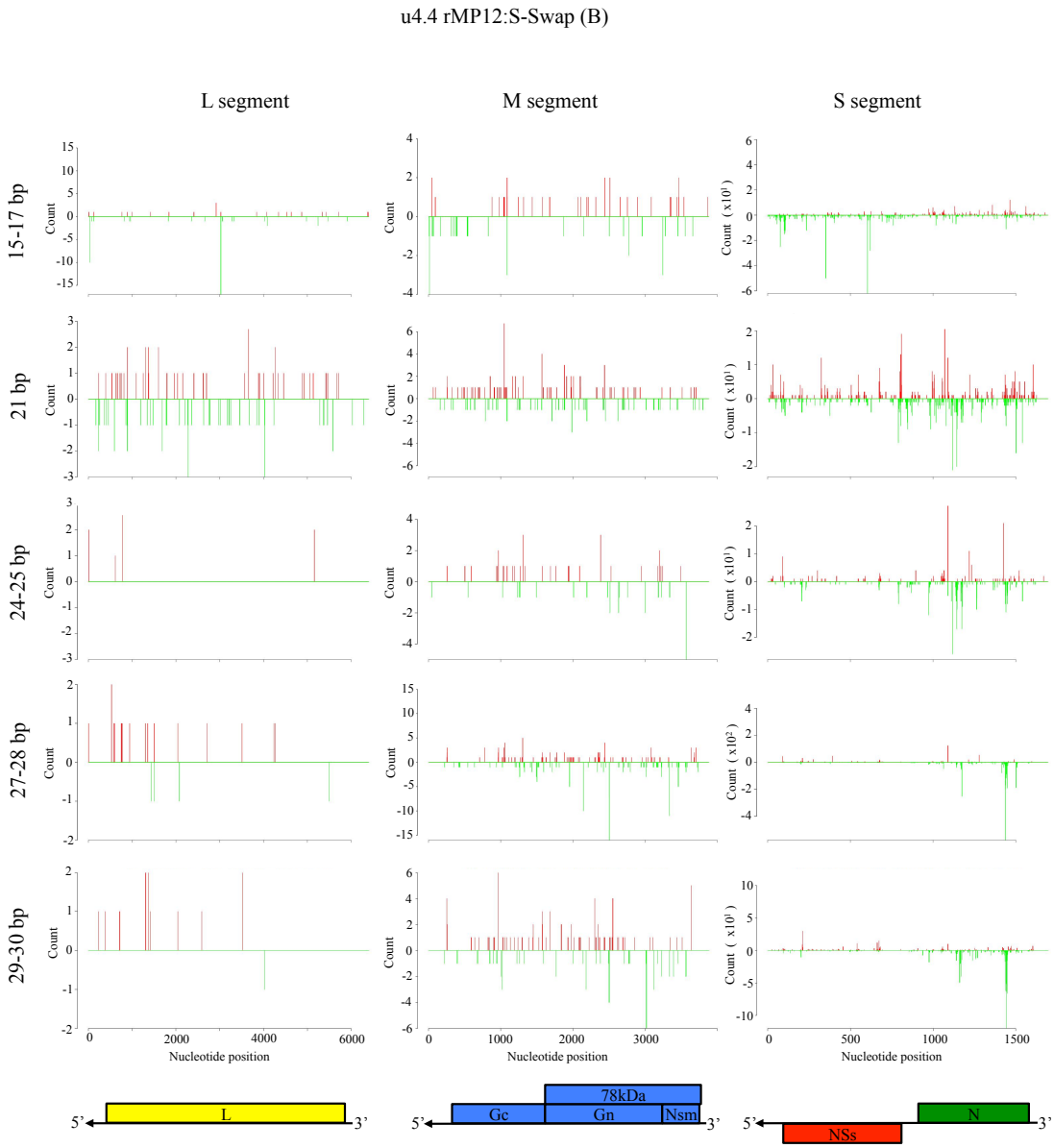

Figure 10-7: Duplicate mapping analysis plot for rMP12:S-Swap infected u4.4 cells
Shown are density plots of aligned viRNA species of 15-17nt, 21nt, 24-25nt, 27-28nt, and 29-30nt aligning to the rMP12:S-Swap L, M, and S genome segments for the duplicate sample B infection. Upper plots (red) show alignments to genomic polarity (negative sense) and lower plots (green) to antigenomic polarity (positive sense).

Table 10-5: Characteristics of viRNA species comprising the top five hotspots targeting S segment in rMP12 and rMP12:S-Swap infected u4.4 cells
viRNA species analysis was performed on rMP12 or rMP12:S-Swap infected u4.4 cells. The five most populous species of viRNA in the 21 nt and 24-30 nt size classes that aligned to the reference S segment were identified. Duplicate infections were labeled (A) and (B). viRNA species polarity (Pol) was recoded either as genomic (g) or antigenomic (ag).Pos. is nucleotide position on the reference genome sequence, % Total is the percentage of total for individual species of that size class

u4.4 rMP12 S Segment

Size.	(A) Pos.	Pol.	Sequence	Count.	% Total	(B) Pos.	Pol.	Sequence	Count.	% Total
	1 597	ag	AGGTTGCTCACGTACAGTGCG	1037	2.15%	1 597	ag	AGGTTGCTCACGTACAGTGCG	869	2.10%
	2 550	g	CAGAGGGATTGACCTGTGCCT	894	1.85%	2 865	g	TCCCGACCGTAACCCCAACTC	857	2.08%
21	3 165	g	TGCACCATCGTCCTAGTCACG	830	1.72%	3 165	g	TGCACCATCGTCCTAGTCACG	731	1.77%
	4 850	ag	CCCCCCACCCCCTAATCCCGA	668	1.38%	4 524	g	AGGATGATAGCGACTGAGGCC	620	1.50%
	5 524	g	AGGATGATAGCGACTGAGGCC	588	1.22%	5 868	g	CGACCGTAACCCCAACTCCCC	602	1.46%
					8.32%					8.91%
	1 1457	g	TGCCACGAGTTAGAGCCAGAACAA	394	6.22%	1 1457	g	TGCCACGAGTTAGAGCCAGAACAA	394	7.50%
	2 1505	ag	AGTCAGCCCCACCATACTGCTTTA	343	5.42%	2 1505	ag	AGTCAGCCCCACCATACTGCTTTA	343	6.53%
24	3 1337	ag	GTGATAGAGTCAACTCATCCCGGG	188	2.97%	3 1337	ag	GTGATAGAGTCAACTCATCCCGGG	188	3.58%
	4 1315	ag	CCAGCCAAGGCGGCAGCAACTCGT	176	2.78%	4 1315	ag	CCAGCCAAGGCGGCAGCAACTCGT	176	3.35%
	5 1075	ag	GCAACCTCCTCTTTTGTTCTACCT	151	2.38%	5 1075	ag	GCAACCTCCTCTTTTGTTCTACCT	151	2.87%
					19.77%					23.83%
	1 1573	ag	TCTCGGACCCACTGTTCAATCTCAT	4625	25.52%	1 1573	ag	TCTCGGACCCACTGTTCAATCTCAT	3897	28.56%
	2 1362	ag	AGGATTCCCTTCCTTTAGCTTATAC	1329	7.33%	2 1074	ag	AGCAACCTCCTCTTTTGTTCTACCT	799	5.86%
25	3 1457	g	TGCCACGAGTTAGAGCCAGAACAAT	1030	5.68%	3 1457	g	TGCCACGAGTTAGAGCCAGAACAAT	768	5.63%
	4 1074	ag	AGCAACCTCCTCTTTTGTTCTACCT	820	4.52%	4 1362	ag	AGGATTCCCTTCCTTTAGCTTATAC	729	5.34%
	5 1078	ag	ACCTCCTCTTTTGTTCTACCTCGGA	421	2.32%	5 1078	ag	ACCTCCTCTTTTGTTCTACCTCGGA	357	2.62%
					45.38%					48.00%
	1 985	ag	AGTCCAAAGGCTTTCAAGAATTCTCT	6544	17.43%	1 1572	ag	CTCTCGGACCCACTGTTCAATCTCAT	3072	11.96%
	2 1572	ag	CTCTCGGACCCACTGTTCAATCTCAT	3524	9.39%	2 985	ag	AGTCCAAAGGCTTTCAAGAATTCTCT	2947	11.47%
26	3 1319	ag	CCAAGGCGGCAGCAACTCGTGATAGA	1687	4.49%	3 1451	ag	GCTTGTTGCCACGAGTTAGAGCCAGA	1397	5.44%
	4 1451	ag	GCTTGTTGCCACGAGTTAGAGCCAGA	1454	3.87%	4 1319	ag	CCAAGGCGGCAGCAACTCGTGATAGA	1250	4.87%
	5 1229	ag	TCGGGTATGCAGGGGATAGGCCGTCC	861	2.29%	5 978	ag	ATCCACAAGTCCAAAGGCTTTCAAGA	653	2.54%
					37.47%					36.28%
	1 1269	ag	GACAGGAAGCCACTCACTCAAGACGAC	35124	33.08%	1 1269	ag	GACAGGAAGCCACTCACTCAAGACGAC	15034	23.11%
	2 1385	ag	ACTTGTTGATGAGAGCCTCCACAGTTG	8175	7.70%	2 1385	ag	ACTTGTTGATGAGAGCCTCCACAGTTG	5860	9.01%
27	3 982	ag	ACAAGTCCAAAGGCTTTCAAGAATTCT	5192	4.89%	3 1451	ag	GCTTGTTGCCACGAGTTAGAGCCAGAA	4056	6.24%
	4 1451	ag	GCTTGTTGCCACGAGTTAGAGCCAGAA	5075	4.78%	4 1571	ag	ACTCTCGGACCCACTGTTCAATCTCAT	3398	5.22%
	5 1571	ag	ACTCTCGGACCCACTGTTCAATCTCAT	4284	4.04%	5 982	ag	ACAAGTCCAAAGGCTTTCAAGAATTCT	2185	3.36%
					54.49%					46.94%
	1 1570	ag	AACTCTCGGACCCACTGTTCAATCTCAT	17584	21.67%	1 1570	ag	AACTCTCGGACCCACTGTTCAATCTCAT	12315	23.55%
	2 1153	ag	TCTAATATTGCCCTTAGATAGTCTCCTG	6732	8.30%	2 983	ag	CAAGTCCAAAGGCTTTCAAGAATTCTCT	3654	6.99%
28	3 983	ag	CAAGTCCAAAGGCTTTCAAGAATTCTCT	5463	6.73%	3 1153	ag	TCTAATATTGCCCTTAGATAGTCTCCTG	2181	4.17%
	4 223	g	AGAATTCCCATACCGAGTCGGACTTGGA	4006	4.94%	4 1458	ag	GCCACGAGTTAGAGCCAGAACAATCATT	2152	4.12%
	5 1483	ag	ATTTTCTTGGCATCCTTCTCCCAGTCAG	2674	3.30%	5 982	ag	ACAAGTCCAAAGGCTTTCAAGAATTCTC	1952	3.73%
					44.94%					42.55%
	1 1448	ag	TGGGCTTGTTGCCACGAGTTAGAGCCAGA	4469	29.38%	1 1448	ag	TGGGCTTGTTGCCACGAGTTAGAGCCAGA	3632	13.52%
	2 996	ag	TTTCAAGAATTCTCTCCTCTTCTCATGGC	2774	8.72%	2 996	ag	TTTCAAGAATTCTCTCCTCTTCTCATGGC	2188	8.15%
29	3 1566	ag	AGCAAACTCTCGGACCCACTGTTCAATCT	1814	5.20%	3 1119	ag	CCGGGAGAACTGCAGCAGATACAGAGAGT	1153	4.29%
	4 986	ag	GTCCAAAGGCTTTCAAGAATTCTCTCCTC	1784	5.13%	4 986	ag	GTCCAAAGGCTTTCAAGAATTCTCTCCTC	956	3.56%
	5 1457	g	TGCCACGAGTTAGAGCCAGAACAATCATT	1554	4.66%	5 1566	ag	AGCAAACTCTCGGACCCACTGTTCAATCT	940	3.50%
					53.08%					33.02%
	1 1118	ag	CCCGGGAGAACTGCAGCAGATACAGAGAGT	3073	13.11%	1 1118	ag	CCCGGGAGAACTGCAGCAGATACAGAGAGT	2104	14.09%
	2 985	ag	AGTCCAAAGGCTTTCAAGAATTCTCTCCTC	2244	9.58%	2 996	ag	TTTCAAGAATTCTCTCCTCTTCTCATGGCT	1379	9.24%
30	3 1448	ag	TGGGCTTGTTGCCACGAGTTAGAGCCAGAA	1713	7.31%	3 1448	ag	TGGGCTTGTTGCCACGAGTTAGAGCCAGAA	1293	8.66%
	4 996	ag	TTTCAAGAATTCTCTCCTCTTCTCATGGCT	1654	7.06%	4 985	ag	AGTCCAAAGGCTTTCAAGAATTCTCTCCTC	1176	7.88%
	5 1446	ag	CCTGGGCTTGTTGCCACGAGTTAGAGCCAG	1161	4.95%	5 1446	ag	CCTGGGCTTGTTGCCACGAGTTAGAGCCAG	977	6.54%
					42.01%					46.41%

u4.4 rMP12:S-Swap S Segment

Size.	(A) Pos.	Pol.	Sequence	Count.	% Total	(B) Pos.	Pol.	Sequence	Count.	% Total
	1 808	g	CGACCGTAACCCCAACTCCCC	47	5.00%	1 1070	g	CGCACTGTACGTGAGCAACCT	23	2.19%
	2 805	g	TCCCGACCGTAACCCCAACTC	20	2.13%	2 1117	ag	AGGCACAGGTCAATCCCTCTG	21	2.00%
21	3 806	g	CCCGACCGTAACCCCAACTCC	20	2.13%	3 1143	ag	GGCCTCAGTCGCTATCATCCT	20	1.90%
	4 1143	ag	GGCCTCAGTCGCTATCATCCT	18	1.91%	4 808	g	CGACCGTAACCCCAACTCCCC	19	1.81%
	5 1070	g	CGCACTGTACGTGAGCAACCT	14	1.49%	5 1502	ag	CGTGACTAGGACGATGGTGCA	16	1.52%
					12.66%					9.42%
	1 1090	g	TCATACATGAGATCAAAGCCTGGC	17	16.19%	1 1090	g	TCATACATGAGATCAAAGCCTGGC	17	11.04%
	2 1425	g	TGATGCAAAGTCTCCAAGTCCGAC	12	11.43%	2 1425	g	TGATGCAAAGTCTCCAAGTCCGAC	12	7.79%
24	3 1218	g	TGCTAGAGTGGCAATCTGATCCCT	10	9.52%	3 1218	g	TGCTAGAGTGGCAATCTGATCCCT	10	6.49%
	4 1264	ag	ACTCTAGTAGAGCTTAGGTCGAAG	6	5.71%	4 1264	ag	ACTCTAGTAGAGCTTAGGTCGAAG	6	3.90%
	5 791	ag	CCCCCACCCCCTAATCCCGACCGT	5	4.76%	5 791	ag	CCCCCACCCCCTAATCCCGACCGT	5	3.25%
					47.62%					32.47%
	1 1090	g	TCATACATGAGATCAAAGCCTGGCA	16	4.98%	1 1117	ag	AGGCACAGGTCAATCCCTCTGAGGA	26	7.65%
	2 1117	ag	AGGCACAGGTCAATCCCTCTGAGGA	16	4.98%	2 1143	ag	GGCCTCAGTCGCTATCATCCTGTGT	17	5.00%
25	3 1440	ag	AAGTCCGACTCGGTATGGGAATCT	16	4.98%	3 1173	ag	AGCAAAGGAGTCCTCTAGATCATTG	17	5.00%
	4 1173	ag	AGCAAAGGAGTCCTCTAGATCATTG	15	4.67%	4 974	ag	AGCGCAGCATCAGGCTCTCCTCCAT	12	3.53%
	5 974	ag	AGCGCAGCATCAGGCTCTCCTCCAT	13	4.05%	5 1090	g	TCATACATGAGATCAAAGCCTGGCA	11	3.24%
					23.68%					24.41%
	1 1437	ag	TCCAAGTCCGACTCGGTATGGGAATT	165	17.78%	1 1437	ag	TCCAAGTCCGACTCGGTATGGGAATT	278	25.27%
	2 1176	ag	AAAGGAGTCCTCTAGATCATTGGTGA	122	13.15%	2 1176	ag	AAAGGAGTCCTCTAGATCATTGGTGA	166	15.09%
26	3 1144	ag	GCCTCAGTCGCTATCATCCTGTGTAA	65	7.00%	3 1433	ag	AGTCTCCAAGTCCGACTCGGTATGGG	60	5.45%
	4 1433	ag	AGTCTCCAAGTCCGACTCGGTATGGG	49	5.28%	4 1144	ag	GCCTCAGTCGCTATCATCCTGTGTAA	53	4.82%
	5 1448	ag	CTCGGTATGGGAATTCTCCGACATTG	24	2.59%	5 1448	ag	CTCGGTATGGGAATTCTCCGACATTG	45	4.09%
					45.80%					54.73%
	1 1502	ag	CGTGACTAGGACGATGGTGCATGAGAA	225	13.82%	1 1436	ag	CTCCAAGTCCGACTCGGTATGGGAATT	195	11.32%
	2 1436	ag	CTCCAAGTCCGACTCGGTATGGGAATT	128	7.86%	2 1447	ag	ACTCGGTATGGGAATTCTCCGACATTG	191	11.09%
27	3 1438	ag	CCAAGTCCGACTCGGTATGGGAATTCT	109	6.70%	3 1502	ag	CGTGACTAGGACGATGGTGCATGAGAA	174	10.10%
	4 1169	ag	AGCCAGCAAAGGAGTCCTCTAGATCAT	69	4.24%	4 1438	ag	CCAAGTCCGACTCGGTATGGGAATTCT	170	9.87%
	5 1447	ag	ACTCGGTATGGGAATTCTCCGACATTG	66	4.05%	5 1169	ag	AGCCAGCAAAGGAGTCCTCTAGATCAT	53	3.08%
					36.67%					45.47%
	1 1437	ag	TCCAAGTCCGACTCGGTATGGGAATTCT	489	25.43%	1 1437	ag	TCCAAGTCCGACTCGGTATGGGAATTCT	574	27.22%
	2 1174	ag	GCAAAGGAGTCCTCTAGATCATTGGTGA	242	12.58%	2 1174	ag	GCAAAGGAGTCCTCTAGATCATTGGTGA	244	11.57%
28	3 1090	g	TCATACATGAGATCAAAGCCTGGCAACA	75	3.90%	3 1441	ag	AGTCCGACTCGGTATGGGAATTCTCCGA	113	5.36%
	4 1414	ag	GGTGCAACGTTTGATGCAAAGTCTCCAA	56	2.91%	4 1090	g	TCATACATGAGATCAAAGCCTGGCAACA	92	4.36%
	5 1441	ag	AGTCCGACTCGGTATGGGAATTCTCCGA	45	2.34%	5 1444	ag	CCGACTCGGTATGGGAATTCTCCGACAT	85	4.03%
					47.17%					52.54%
	1 1436	ag	CTCCAAGTCCGACTCGGTATGGGAATTCT	87	9.86%	1 1436	ag	CTCCAAGTCCGACTCGGTATGGGAATTCT	62	7.86%
	2 1442	ag	GTCCGACTCGGTATGGGAATTCTCCGACA	52	5.90%	2 1448	ag	CTCGGTATGGGAATTCTCCGACATTGTAG	56	7.10%
29	3 1169	ag	AGCCAGCAAAGGAGTCCTCTAGATCATTG	50	5.67%	3 1442	ag	GTCCGACTCGGTATGGGAATTCTCCGACA	53	6.72%
	4 1164	ag	GTGTAAGCCAGCAAAGGAGTCCTCTAGAT	40	4.54%	4 1440	ag	AAGTCCGACTCGGTATGGGAATTCTCCGA	51	6.46%
	5 1440	ag	AAGTCCGACTCGGTATGGGAATTCTCCGA	40	4.54%	5 1169	ag	AGCCAGCAAAGGAGTCCTCTAGATCATTG	39	4.94%
					30.50%					33.08%
	1 1444	ag	CCGACTCGGTATGGGAATTCTCCGACATTG	50	11.55%	1 1442	ag	GTCCGACTCGGTATGGGAATTCTCCGACAT	67	15.58%
	2 1442	ag	GTCCGACTCGGTATGGGAATTCTCCGACAT	47	10.85%	2 1444	ag	CCGACTCGGTATGGGAATTCTCCGACATTG	63	14.65%
30	3 540	g	ACTCTCTGTATCTGCTGCAGTTCTCCCGGG	24	5.54%	3 1441	ag	AGTCCGACTCGGTATGGGAATTCTCCGACA	28	6.51%
	4 1441	ag	AGTCCGACTCGGTATGGGAATTCTCCGACA	20	4.62%	4 1160	ag	TCCTGTGTAAGCCAGCAAAGGAGTCCTCTA	26	6.05%
	5 662	g	AGCCATGAGAAGAGGAGAGAATTCTTGAAA	16	3.70%	5 673	g	GAGGAGAGAATTCTTGAAAGCCTTTGGACT	13	3.02%
					36.26%					45.81%

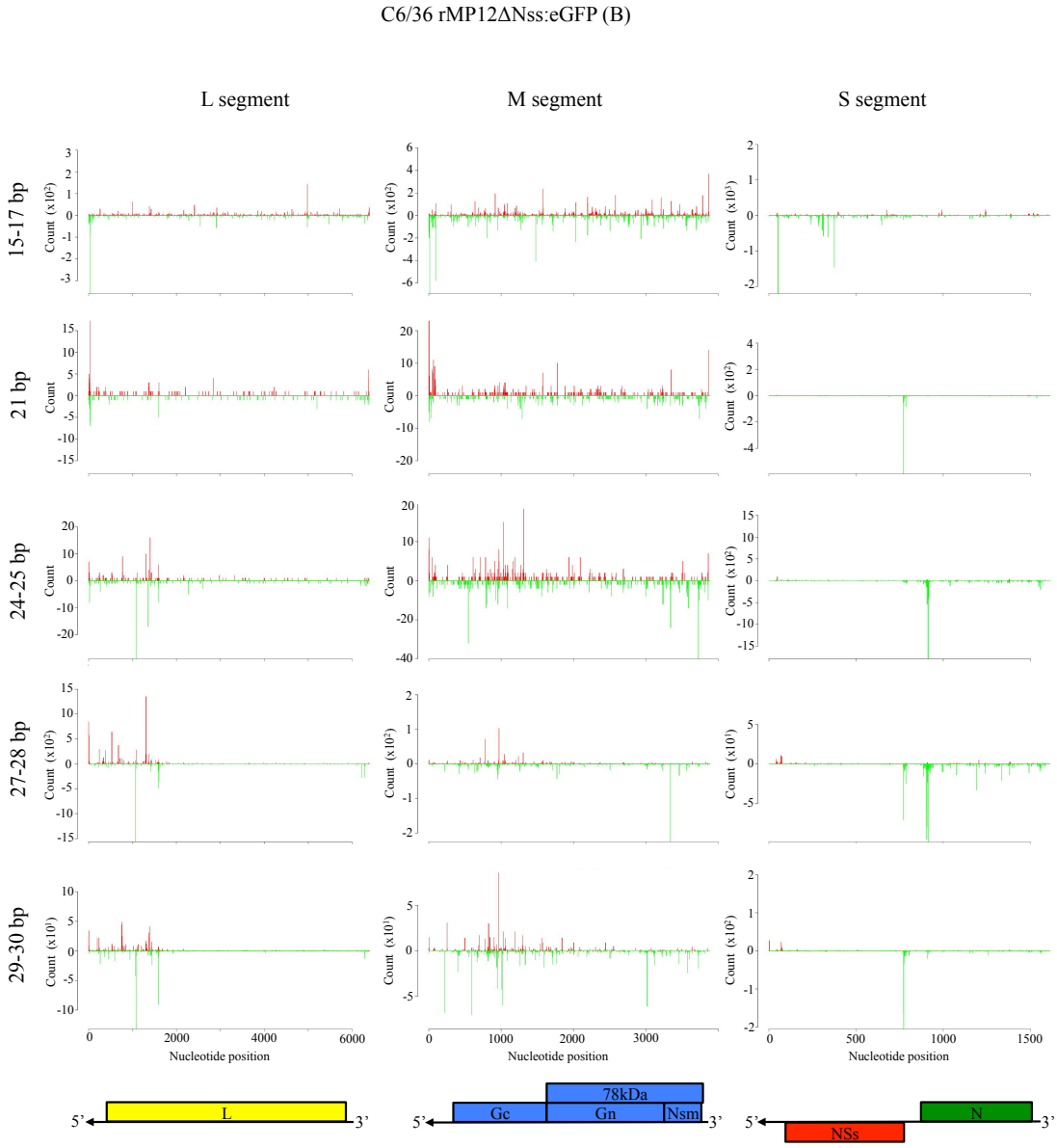

Figure 10-8: Duplicate mapping analysis plots for rMP12ΔNSs:eGFP infected mosquito cells
Shown are density plots of aligned viRNA species of 15-17nt, 21nt, 24-25nt, 27-28nt, and 29-30nt aligning to the rMP12ΔNSs:eGFP L, M, and S genome segments for the duplicate sample B infection. Upper plots (red) show alignments to genomic polarity (negative sense) and lower plots (green) to antigenomic polarity (positive sense). Also shown are the CDS for MP12 proteins encoded on the L (yellow), M (blue) and S (green and red) segments.

(A) rMP12ΔNSs:eGFP infected C6/36 cells.

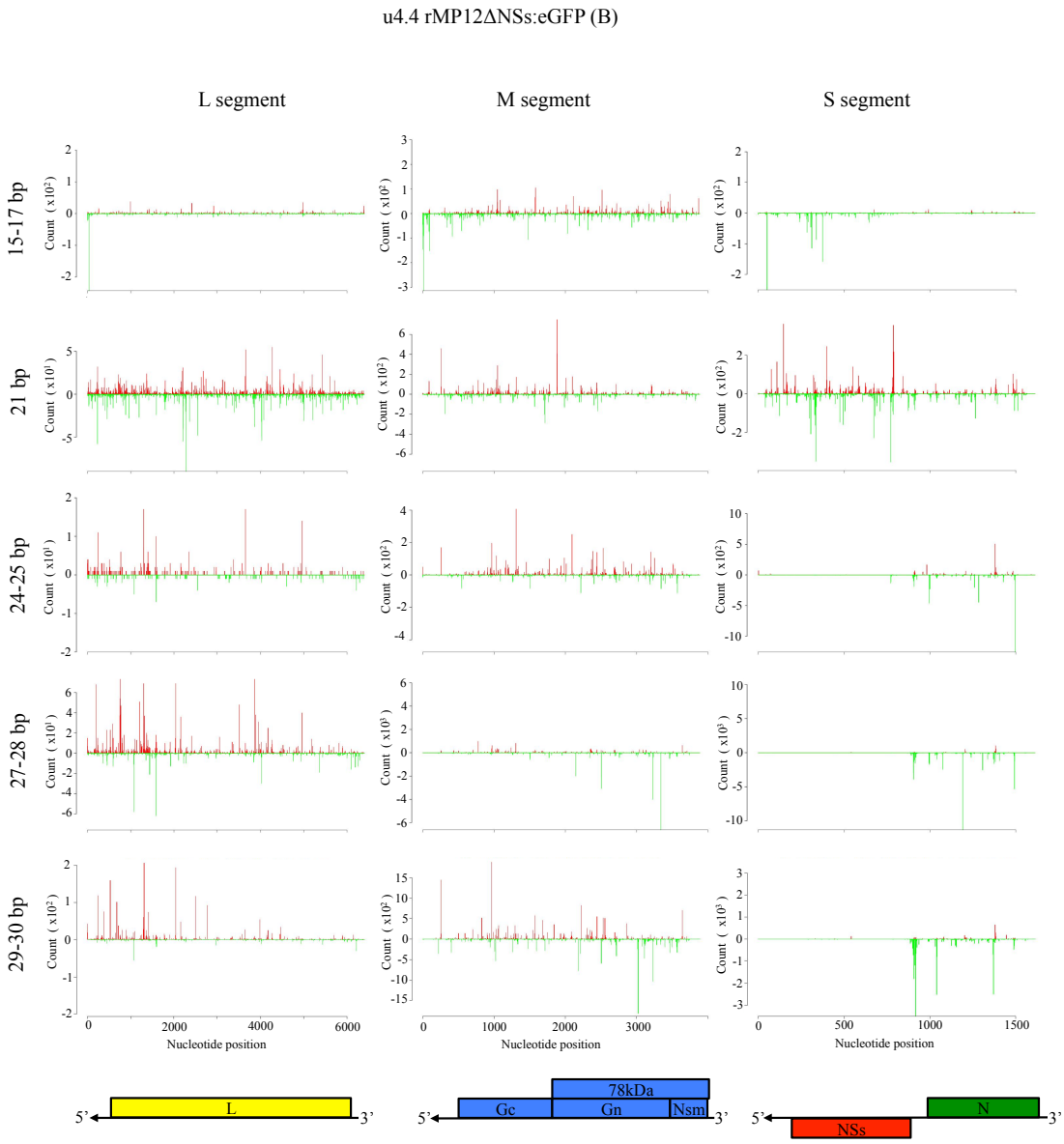

(B) rMP12ΔNSs:eGFP infected u4.4 cells.

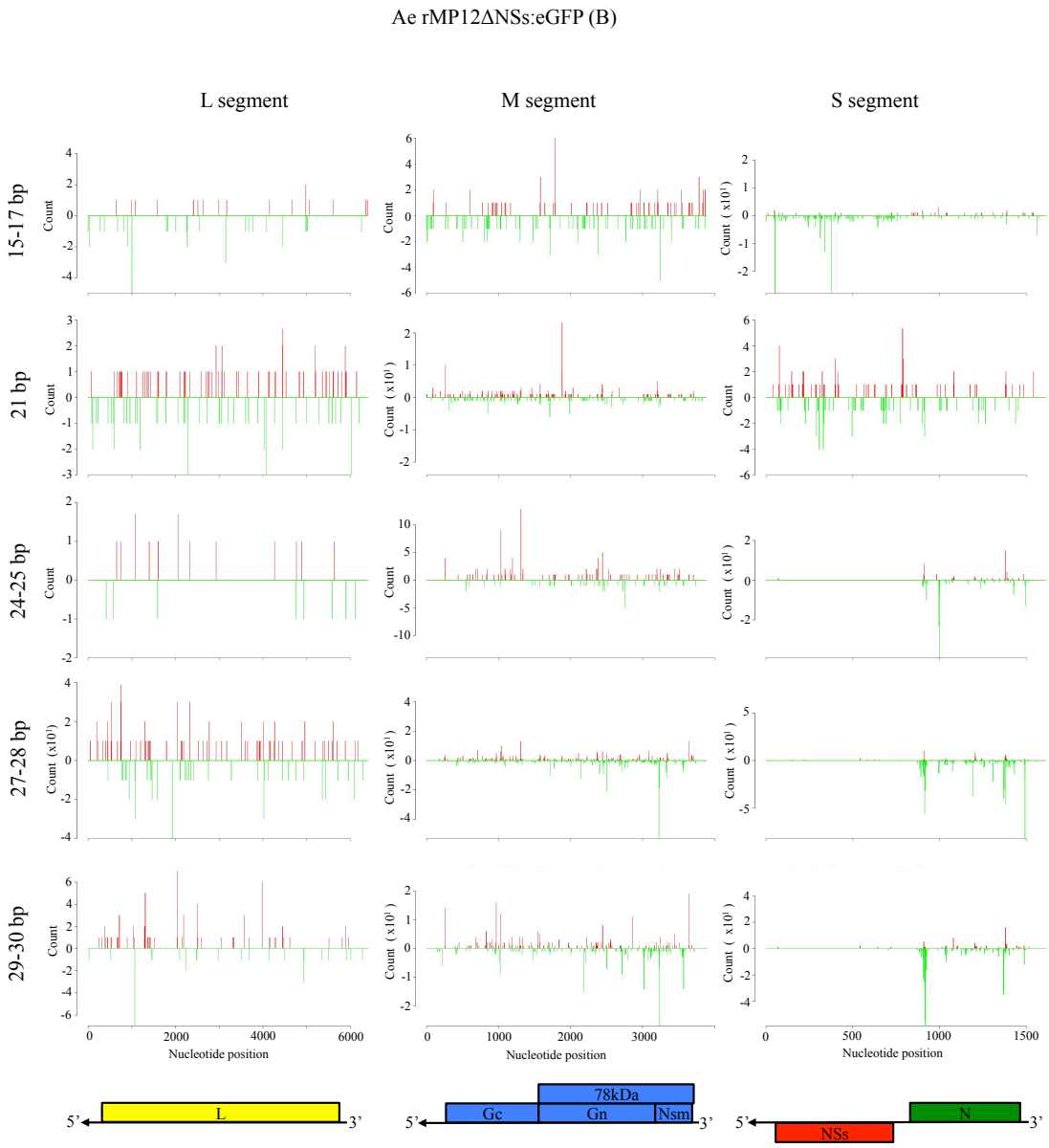

(C) rMP12ΔNSs:eGFP infected Ae cells

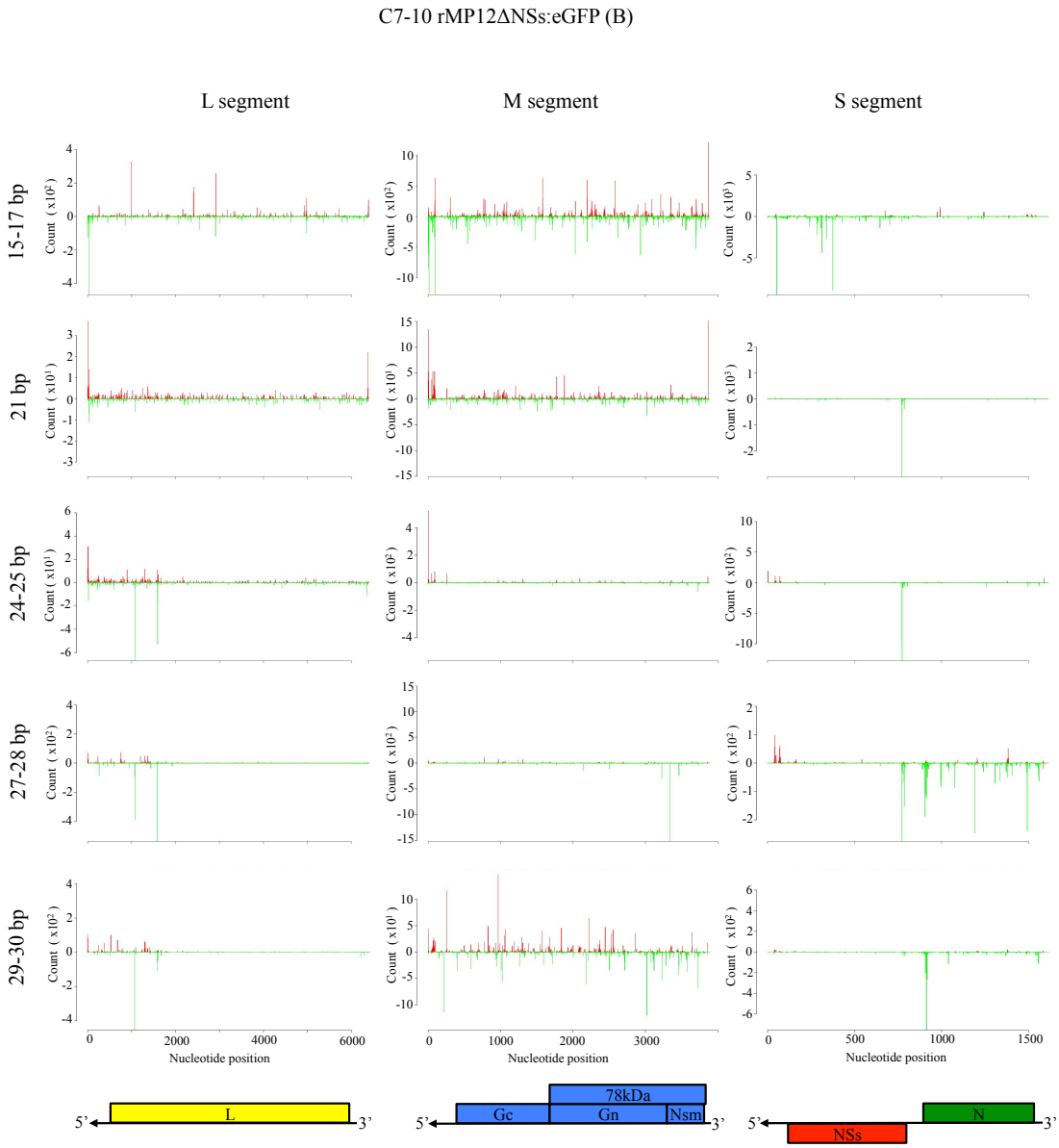

(D) rMP12ΔNSs:eGFP infected C7-10 cells.

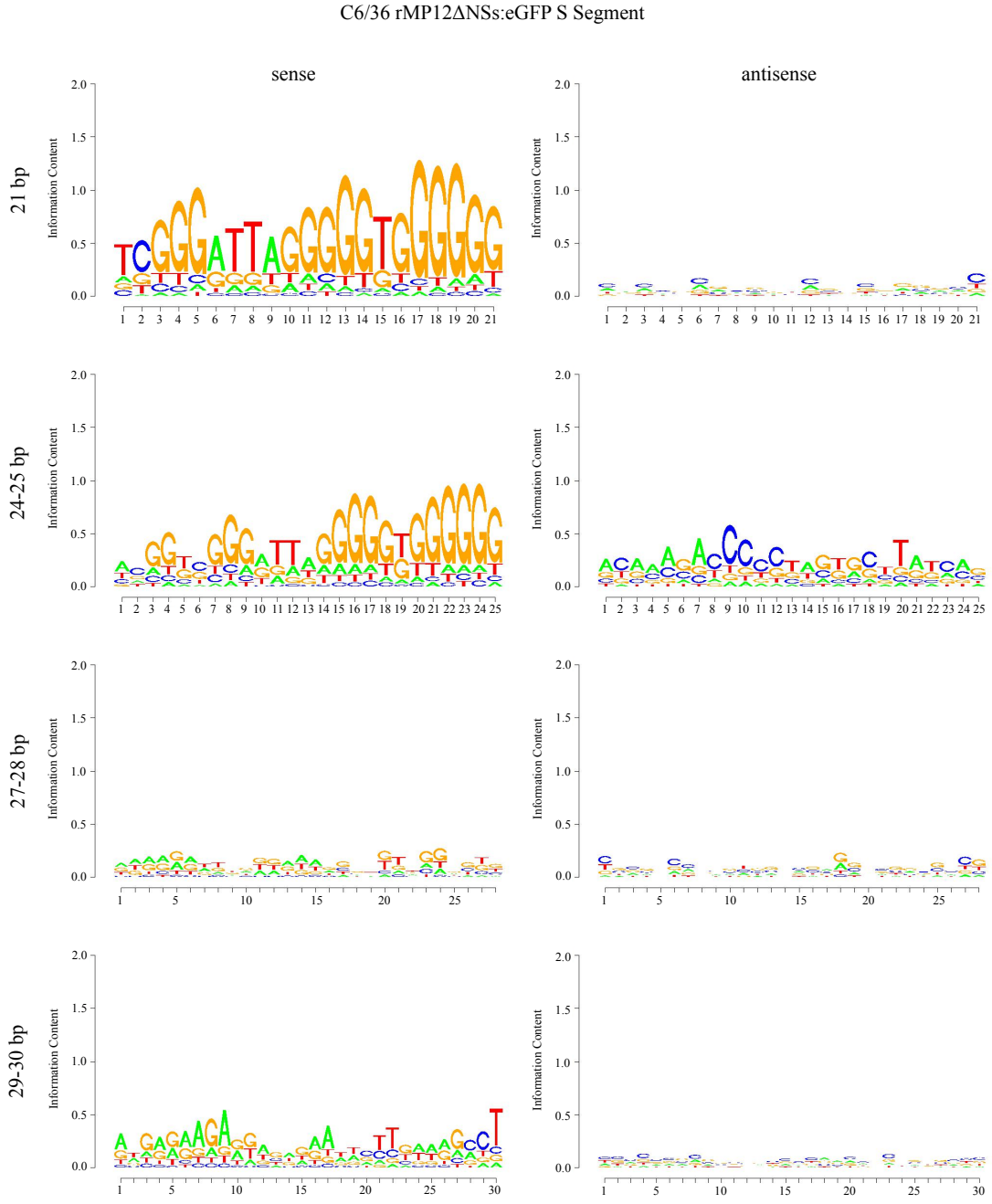

Figure 10-9: Logo analysis of viRNA species detected in rMP12ΔNSs:eGFP infected mosquito cells
Logo analysis of rMP12ΔNSs:eGFP infected C6/36, u4.4, and Ae cells, with sense and antisense strand species analysis represented for the 21 bp, 24-25 bp, 27-28 bp, and 29-30 bp viRNA size classes. Shown are species aligning to the modified S segment.

(A) rMP12ΔNSs:eGFP virus infected C6/36 cells

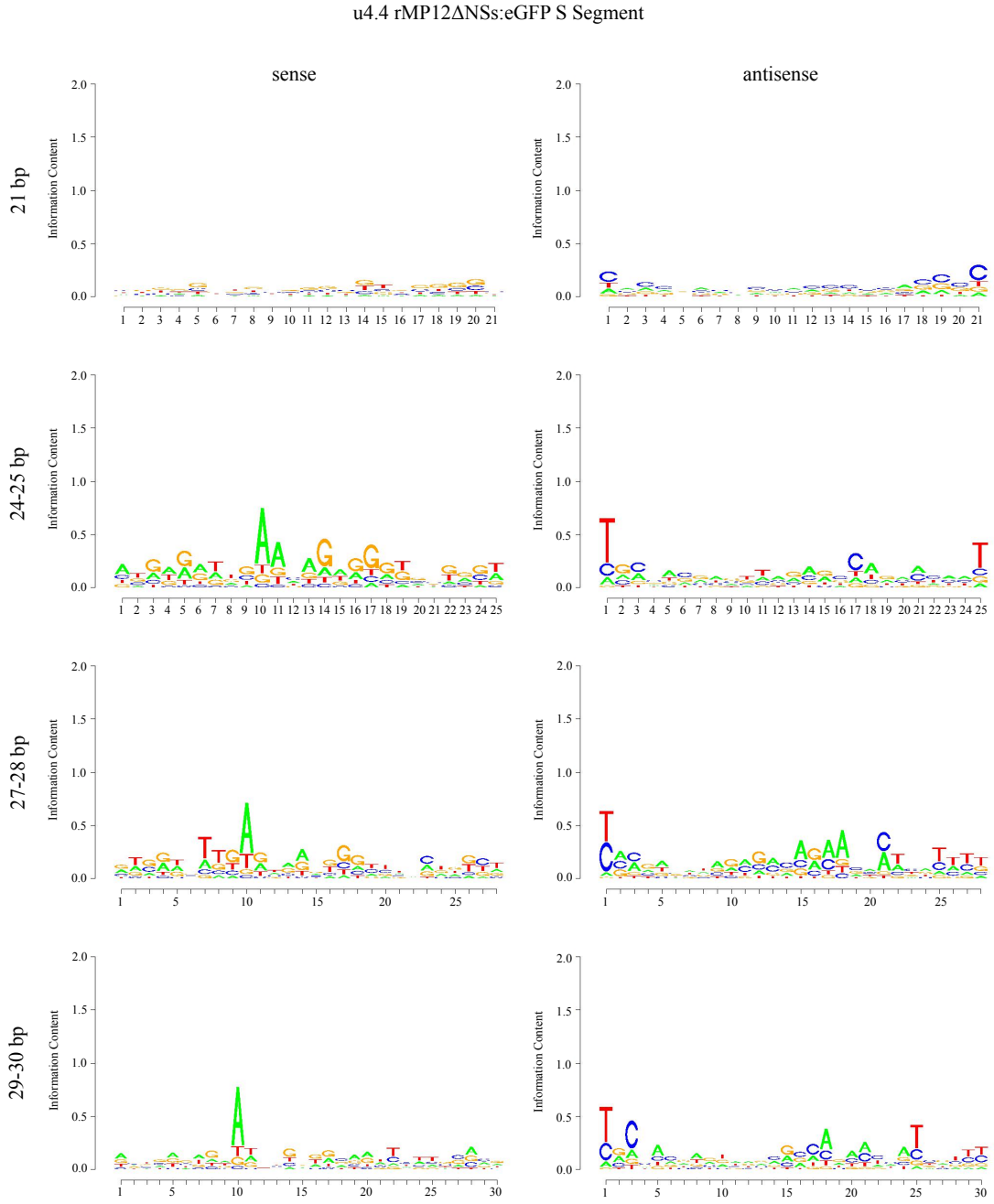

(B) rMP12ΔNSs:eGFP virus infected u4.4 cells

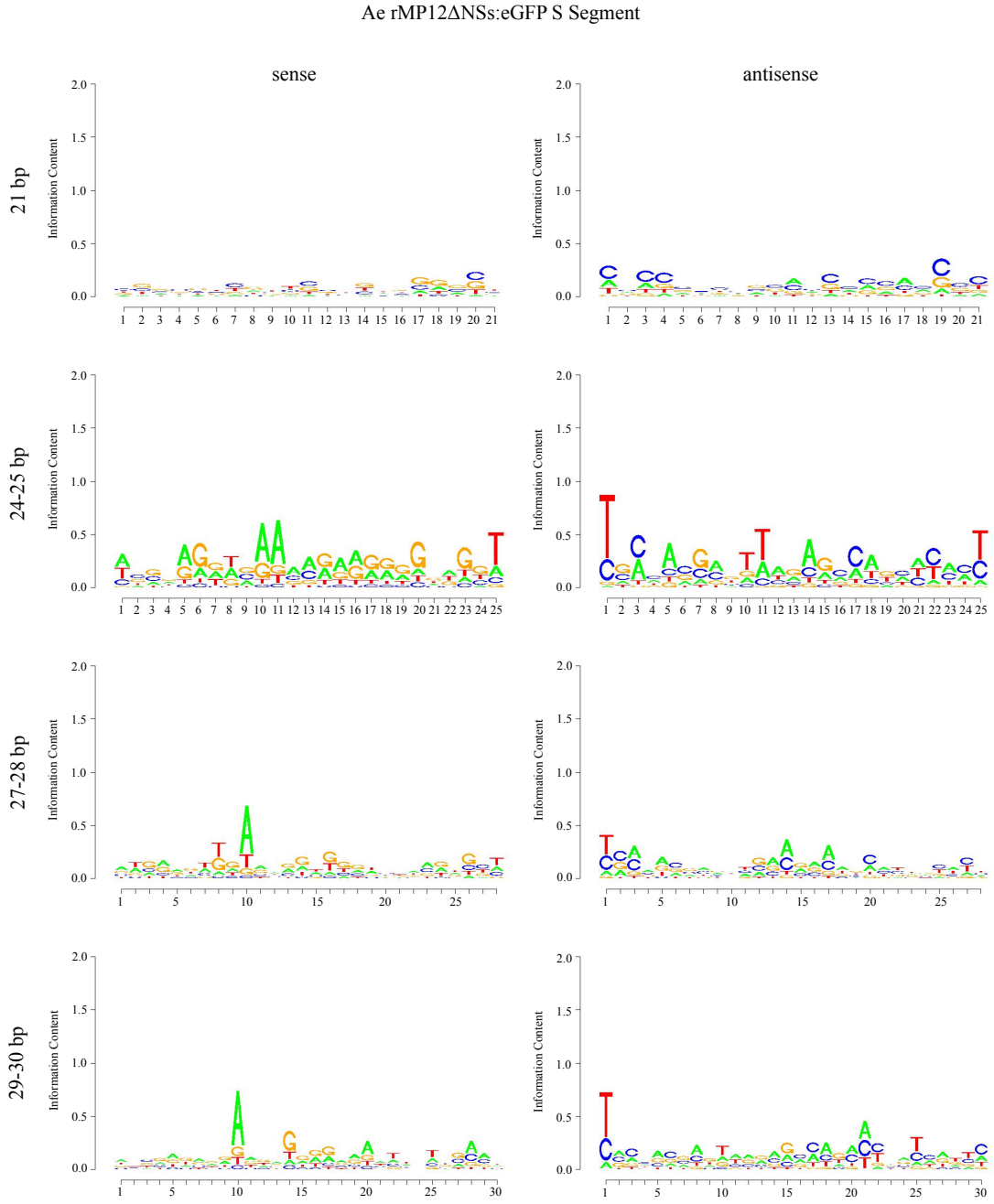

(C) rMP12ΔNSs:eGFP virus infected Ae cells

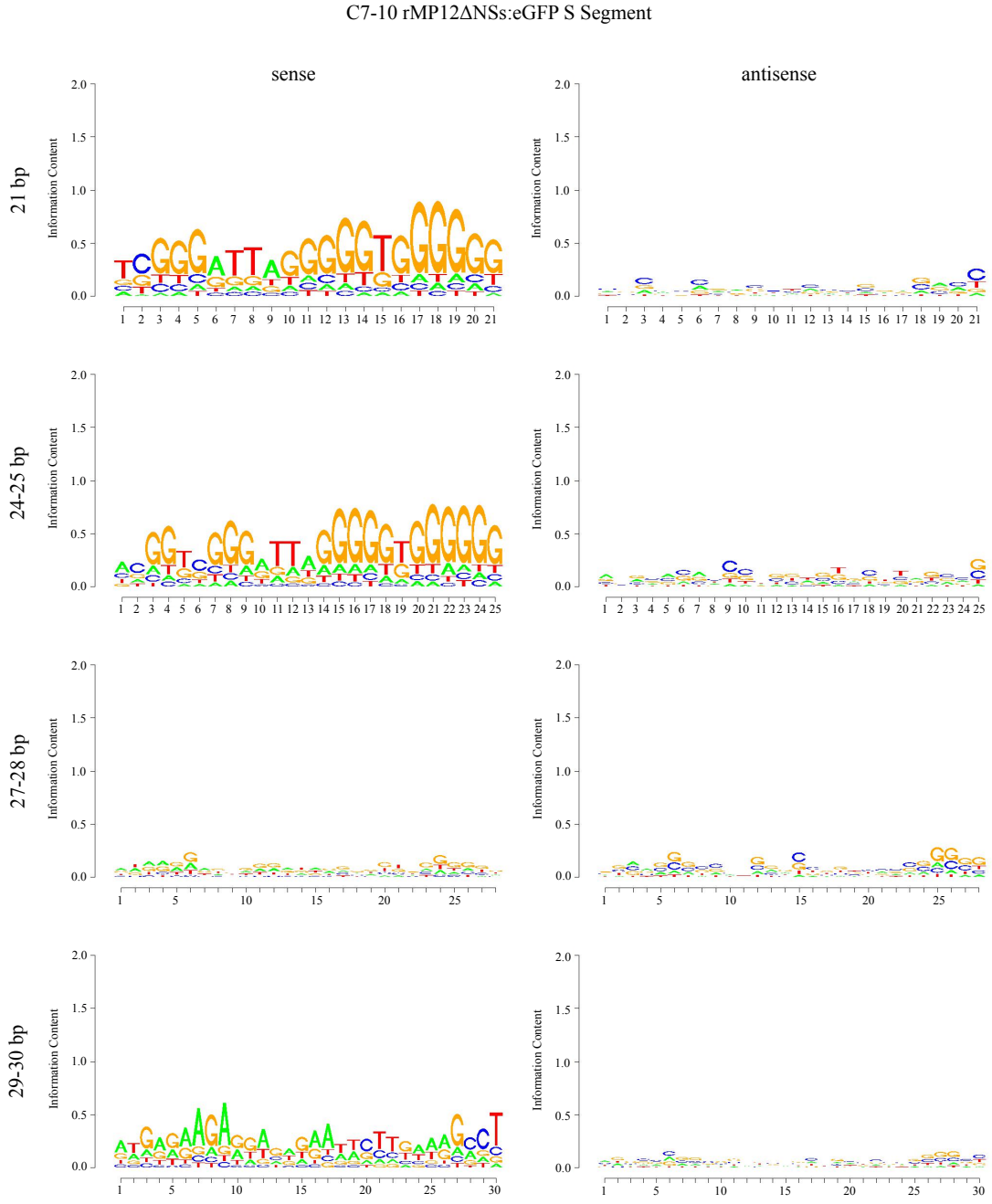

(D) rMP12ΔNSs:eGFP virus infected C7-10 cells

Table 10-6: Characteristics of siRNA species comprising the top five siRNA species in rMP12ΔNSs:eGFP virus infected u4.4 and Ae cells.
viRNA species analysis was performed on rMP12ΔNSs:eGFP infected u4.4 and Ae cells. The five most populous siRNA species aligning to the modified S segment were identified. Duplicate infections were labeled (A) and (B). viRNA species polarity (Pol) is recoded either as genomic (g) or antigenomic (ag). Pos. is nucleotide position on the reference genome sequence, % Total is the percentage of total for individual species of that size class

u4.4 rMP12ΔNSs:eGFP S Segment												
Size.	(A)	Pos.	Pol.	Sequence	Count.	% Total	(B)	Pos.	Pol.	Sequence	Count.	% Total
21	1	787	g	TCCCGACCGTAACCCCAACTC	534	2.42%	1	787	g	TCCCGACCGTAACCCCAACTC	399	2.48%
	2	148	g	CACCTACGGCAAGCTGACCCT	517	2.34%	2	148	g	CACCTACGGCAAGCTGACCCT	363	2.26%
	3	398	g	AACCGCATCGAGCTGAAGGGC	498	2.26%	3	772	ag	CCCCCCACCCCCTAATCCCGA	355	2.21%
	4	336	ag	TCAAGGACGACGGCAACTACA	455	2.06%	4	336	ag	TCAAGGACGACGGCAACTACA	351	2.18%
	5	772	ag	CCCCCCACCCCCTAATCCCGA	395	1.79%	5	398	g	AACCGCATCGAGCTGAAGGGC	246	1.53%
						10.88%						**10.65%**

Ae rMP12ΔNSs:eGFP S Segment												
Size.	(A)	Pos.	Pol.	Sequence	Count.	% Total	(B)	Pos.	Pol.	Sequence	Count.	% Total
21	1	148	g	CACCTACGGCAAGCTGACCCT	12	4.55%	1	787	g	TCCCGACCGTAACCCCAACTC	6	3.64%
	2	291	ag	AGTCCGCCATGCCCGAAGGCT	8	3.03%	2	77	g	ATCCTGGTCGAGCTGGACGGC	4	2.42%
	3	300	ag	TGCCCGAAGGCTACGTCCAGG	7	2.65%	3	307	ag	AGGCTACGTCCAGGAGCGCAC	4	2.42%
	4	398	g	AACCGCATCGAGCTGAAGGGC	7	2.65%	4	330	ag	TCTTCTTCAAGGACGACGGCA	4	2.42%
	5	724	g	CACTCTCGGCATGGACGAGCT	7	2.65%	5	291	ag	AGTCCGCCATGCCCGAAGGCT	3	1.82%
							6	398	g	AACCGCATCGAGCTGAAGGGC	3	1.82%
						10.65%						**12.73%**

Table 10-7: Characteristics of the small viRNA species detected in infected mosquito cells targeting the S segments.
The five most populous viRNA species in the 15-17 nt size range targeting the S genome segment of rMP12, rMP12ΔNSs:eGFP, or rMP12:S-Swap in infected C6/26, u4.4, Ae, and C7-10 cell were identified. Duplicate infections were labeled (A) and (B). viRNA polarity (Pol.) is recorded as either genomic (g) or antigenomic (ag). Pos. is nucleotide position on the reference genome sequence, % Total is the percentage of total for individual species of that size class, Size is the viRNA size in nucleotides.

(A) rMP12 infected cells

C6/36 rMP12 S Segment													
(A)	Pos.	Pol.	Sequence	Size	Count.	% Total	(B)	Pos.	Pol.	Sequence	Size	Count.	% Total
1	534	g	CGACTGAGGCCATCCT	16	1148	3.03%	1	534	g	CGACTGAGGCCATCCT	16	1122	2.99%
2	698	ag	AGCCTGATGCTGCGCT	16	685	1.81%	2	698	ag	AGCCTGATGCTGCGCT	16	762	2.03%
3	1070	g	TTGCAGCAACCTCCT	15	518	1.37%	3	1070	g	TTGCAGCAACCTCCT	15	655	1.74%
4	112	ag	TGGTCCTCCCAGGAT	15	488	1.29%	4	112	ag	TGGTCCTCCCAGGAT	15	600	1.60%
5	850	ag	CCCCCCACCCCCTAA	15	432	1.14%	5	850	ag	CCCCCCACCCCCTAA	15	474	1.26%

u4.4 rMP12 S Segment													
(A)	Pos.	Pol.	Sequence	Size	Count.	% Total	(B)	Pos.	Pol.	Sequence	Size	Count.	% Total
1	698	ag	AGCCTGATGCTGCGCT	16	511	2.66%	1	698	ag	AGCCTGATGCTGCGCT	16	349	2.12%
2	112	ag	TGGTCCTCCCAGGAT	15	342	1.78%	2	112	ag	TGGTCCTCCCAGGAT	15	267	1.62%
3	1386	g	CTTGTTGATGAGAGCC	16	294	1.53%	3	617	ag	GTTCGGCTTCTGCAA	15	248	1.51%
4	617	ag	GTTCGGCTTCTGCAA	15	268	1.40%	4	611	ag	CAGTGCGTTCGGCTTC	16	244	1.48%
5	611	ag	CAGTGCGTTCGGCTTC	16	257	1.34%	5	179	ag	AGTCACGAGGTTCGCT	16	220	1.34%

Ae rMP12 S Segment													
(A)	Pos.	Pol.	Sequence	Size	Count.	% Total	(B)	Pos.	Pol.	Sequence	Size	Count.	% Total
1	698	ag	AGCCTGATGCTGCGC	15	24	3.03%	1	698	ag	AGCCTGATGCTGCGC	15	27	3.84%
2	698	ag	AGCCTGATGCTGCGCT	16	19	2.40%	2	698	ag	AGCCTGATGCTGCGCT	16	21	2.98%
3	617	ag	GTTCGGCTTCTGCAA	15	18	2.27%	3	617	ag	GTTCGGCTTCTGCAA	15	11	1.56%
4	179	ag	AGTCACGAGGTTCGCT	16	15	1.89%	4	179	ag	AGTCACGAGGTTCGCT	16	9	1.28%
5	534	g	CGACTGAGGCCATCCT	16	13	1.64%	5	617	ag	GTTCGGCTTCTGCAAG	16	9	1.28%

C7-10 rMP12 S Segment													
(A)	Pos.	Pol.	Sequence	Size	Count.	% Total	(B)	Pos.	Pol.	Sequence	Size	Count.	% Total
1	534	g	CGACTGAGGCCATCCT	16	779	2.47%	1	698	ag	AGCCTGATGCTGCGCT	16	1195	2.74%
2	698	ag	AGCCTGATGCTGCGCT	16	744	2.36%	2	534	g	CGACTGAGGCCATCCT	16	927	2.13%
3	1070	g	TTGCAGCAACCTCCT	15	628	1.99%	3	1070	g	TTGCAGCAACCTCCT	15	889	2.04%
4	698	ag	AGCCTGATGCTGCGC	15	516	1.64%	4	698	ag	AGCCTGATGCTGCGC	15	684	1.57%
5	1069	g	GTTGCAGCAACCTCCT	16	497	1.58%	5	617	ag	GTTCGGCTTCTGCAA	15	635	1.46%

(B) rMP12ΔNSs:eGFP infected cells

C6/36 rMP12ΔNSs:eGFP S Segment														
(A)	Pos.	Pol.	Sequence	Size	Count.	% Total	(B)	Pos.	Pol.	Sequence	Size	Count.	% Total
1	53	ag	GAGCTGTTCACCGGGG	16	2530	6.55%	1	53	ag	GAGCTGTTCACCGGGG	16	1595	7.42%
2	375	ag	AGTTCGAGGGCGACA	15	1541	3.99%	2	375	ag	AGTTCGAGGGCGACA	15	865	4.03%
3	375	ag	AGTTCGAGGGCGACAC	16	898	2.32%	3	375	ag	AGTTCGAGGGCGACAC	16	552	2.57%
4	339	ag	AGGACGACGGCAACTA	16	730	1.89%	4	307	ag	AGGCTACGTCCAGGAG	16	355	1.65%
5	313	ag	CGTCCAGGAGCGCACC	16	614	1.59%	5	53	ag	GAGCTGTTCACCGGG	15	353	1.64%

u4.4 rMP12ΔNSs:eGFP S Segment														
(A)	Pos.	Pol.	Sequence	Size	Count.	% Total	(B)	Pos.	Pol.	Sequence	Size	Count.	% Total
1	375	ag	AGTTCGAGGGCGACA	15	853	2.99%	1	53	ag	GAGCTGTTCACCGGGG	16	1805	8.32%
2	313	ag	CGTCCAGGAGCGCAC	15	717	2.51%	2	375	ag	AGTTCGAGGGCGACA	15	821	3.78%
3	53	ag	GAGCTGTTCACCGGG	15	591	2.07%	3	375	ag	AGTTCGAGGGCGACAC	16	667	3.07%
4	339	ag	AGGACGACGGCAACT	15	418	1.46%	4	313	ag	CGTCCAGGAGCGCACC	16	584	2.69%
5	314	ag	GTCCAGGAGCGCACC	15	285	1.00%	5	339	ag	AGGACGACGGCAACTA	16	532	2.45%

Ae rMP12ΔNSs:eGFP S Segment														
(A)	Pos.	Pol.	Sequence	Size	Count.	% Total	(B)	Pos.	Pol.	Sequence	Size	Count.	% Total
1	375	ag	AGTTCGAGGGCGACA	15	14	4.27%	1	53	ag	GAGCTGTTCACCGGGG	16	19	6.76%
2	307	ag	AGGCTACGTCCAGGAG	16	13	3.96%	2	375	ag	AGTTCGAGGGCGACA	15	11	3.91%
3	313	ag	CGTCCAGGAGCGCACC	16	10	3.05%	3	375	ag	AGTTCGAGGGCGACAC	16	10	3.56%
4	1560	ag	TTGATAGTTGTCCATTA	17	10	3.05%	4	339	ag	AGGACGACGGCAACTA	16	8	2.85%
5	53	ag	GAGCTGTTCACCGGGG	16	9	2.74%	5	375	ag	AGTTCGAGGGCGACACC	17	7	2.49%

C7-10 rMP12ΔNSs:eGFP S Segment														
(A)	Pos.	Pol.	Sequence	Size	Count.	% Total	(B)	Pos.	Pol.	Sequence	Size	Count.	% Total
1	53	ag	GAGCTGTTCACCGGGG	16	2961	5.47%	1	53	ag	GAGCTGTTCACCGGGG	16	6776	6.42%
2	375	ag	AGTTCGAGGGCGACA	15	2631	4.86%	2	375	ag	AGTTCGAGGGCGACA	15	4339	4.11%
3	375	ag	AGTTCGAGGGCGACAC	16	2120	3.92%	3	375	ag	AGTTCGAGGGCGACAC	16	4141	3.92%
4	313	ag	CGTCCAGGAGCGCACC	16	938	1.73%	4	313	ag	CGTCCAGGAGCGCACC	16	2112	2.00%
5	285	ag	TCTTCAAGTCCGCCATG	17	901	1.67%	5	313	ag	CGTCCAGGAGCGCAC	15	2086	1.98%

(C) rMP12:S-Swap infected cells

C6/36 rMP12:S-Swap S Segment														
(A)	Pos.	Pol.	Sequence	Size	Count.	% Total	(B)	Pos.	Pol.	Sequence	Size	Count.	% Total
1	603	ag	AGGAGGTTGCTGCAA	15	49	4.05%	1	603	ag	AGGAGGTTGCTGCAA	15	40	3.33%
2	351	ag	GAGTTGCTGCCGCCTT	16	44	3.63%	2	351	ag	GAGTTGCTGCCGCCTT	16	40	3.33%
3	1138	ag	AGGATGGCCTCAGTCG	16	33	2.73%	3	619	ag	GTTCACGCAGCCAAT	15	34	2.83%
4	603	ag	AGGAGGTTGCTGCAAC	16	29	2.39%	4	1138	ag	AGGATGGCCTCAGTCG	16	33	2.75%
5	619	ag	GTTCACGCAGCCAAT	15	28	2.31%	5	603	ag	AGGAGGTTGCTGCAAC	16	25	2.08%

u4.4 rMP12:S-Swap S Segment														
(A)	Pos.	Pol.	Sequence	Size	Count.	% Total	(B)	Pos.	Pol.	Sequence	Size	Count.	% Total
1	603	ag	AGGAGGTTGCTGCAA	15	59	8.06%	1	603	ag	AGGAGGTTGCTGCAA	15	34	3.70%
2	603	ag	AGGAGGTTGCTGCAAC	16	23	3.14%	2	603	ag	AGGAGGTTGCTGCAAC	16	23	2.50%
3	351	ag	GAGTTGCTGCCGCCTT	16	20	2.73%	3	619	ag	GTTCACGCAGCCAAT	15	21	2.28%
4	351	ag	GAGTTGCTGCCGCCT	15	17	2.32%	4	351	ag	GAGTTGCTGCCGCCTT	16	21	2.28%
5	619	ag	GTTCACGCAGCCAAT	15	15	2.05%	5	76	ag	AGCAGTGGACCGCAATG	17	20	2.17%

Ae rMP12:S-Swap S Segment														
(A)	Pos.	Pol.	Sequence	Size	Count.	% Total	(B)	Pos.	Pol.	Sequence	Size	Count.	% Total
1	603	ag	AGGAGGTTGCTGCAA	15	2	14.28%	1	619	ag	GTTCACGCAGCCAAT	15	2	16.67%
2			n/a				2			n/a			
3			n/a				3			n/a			
4			n/a				4			n/a			
5			n/a				5			n/a			

C7-10 rMP12:S-Swap S Segment														
(A)	Pos.	Pol.	Sequence	Size	Count.	% Total	(B)	Pos.	Pol.	Sequence	Size	Count.	% Total
1	603	ag	AGGAGGTTGCTGCAA	15	51	5.82%	1	603	ag	AGGAGGTTGCTGCAA	15	75	6.76%
2	1138	ag	AGGATGGCCTCAGTCG	16	28	3.20%	2	1138	ag	AGGATGGCCTCAGTCG	16	40	3.61%
3	603	ag	AGGAGGTTGCTGCAAC	16	27	3.08%	3	619	ag	GTTCACGCAGCCAAT	15	32	2.89%
4	351	ag	GAGTTGCTGCCGCCT	15	22	2.51%	4	603	ag	AGGAGGTTGCTGCAAC	16	28	2.52%
5	619	ag	GTTCACGCAGCCAAT	15	20	2.28%	5	351	ag	GAGTTGCTGCCGCCTTG	17	25	2.25%

Table 10-8: Comparison of viRNA species comprising the top five hotspots in rMP12 infected u4.4 and Ae cells

viRNA species comparative analysis was performed on rMP12 infected u4.4 cells. The five most populous species of viRNA in the 21 nt and 24-30 nt size classes that aligned to the reference rMP12 genome segments were identified. Duplicate infections were labeled (A) and (B). viRNA species polarity (Pol) was recoded either as genomic (g) or antigenomic (ag).. Pos. is nucleotide position on the reference genome sequence, % Total is the percentage of total for individual species of that size class. (A) viRNA species aligning to the rMP12 S segment

u4.4 rMP12 S Segment

Size.	(A) Pos.	Pol.	Sequence	Count.	% Total	(B) Pos.	Pol.	Sequence	Count.	% Total
21	1 597	ag	AGGTTGCTCACGTACAGTGCG	1037	2.15%	1 597	ag	AGGTTGCTCACGTACAGTGCG	869	2.10%
	2 550	g	CAGAGGGATTGACCTGTGCCT	894	1.85%	2 865	g	TCCCGACCGTAACCCCAACTC	857	2.08%
	3 165	g	TGCACCATCGTCCTAGTCACG	830	1.72%	3 165	g	TGCACCATCGTCCTAGTCACG	731	1.77%
	4 850	ag	CCCCCCACCCCCTAATCCCGA	668	1.38%	4 524	g	AGGATGATAGCGACTGAGGCC	620	1.50%
	5 524	g	AGGATGATAGCGACTGAGGCC	588	1.22%	5 868	g	CGACCGTAACCCCAACTCCCC	602	1.46%
					8.32%					8.91%

Size.	(A) Pos.	Pol.	Sequence	Count.	% Total	(B) Pos.	Pol.	Sequence	Count.	% Total
24	1 1457	g	TGCCACGAGTTAGAGCCAGAACAA	529	8.35%	1 1457	g	TGCCACGAGTTAGAGCCAGAACAA	394	7.50%
	2 1505	ag	AGTCAGCCCCACCATACTGCTTTA	390	6.16%	2 1505	ag	AGTCAGCCCCACCATACTGCTTTA	343	6.53%
	3 1337	ag	GTGATAGAGTCAACTCATCCCGGG	348	5.50%	3 1337	ag	GTGATAGAGTCAACTCATCCCGGG	188	3.58%
	4 1315	ag	CCAGCCAAGGCGGCAGCAACTCGT	239	3.77%	4 1315	ag	CCAGCCAAGGCGGCAGCAACTCGT	176	3.35%
	5 1075	ag	GCAACCTCCTCTTTTGTTCTACCT	226	3.57%	5 1075	ag	GCAACCTCCTCTTTTGTTCTACCT	151	2.87%
					27.35%					23.83%

Size.	(A) Pos.	Pol.	Sequence	Count.	% Total	(B) Pos.	Pol.	Sequence	Count.	% Total
25	1 1573	ag	TCTCGGACCCACTGTTCAATCTCAT	4625	25.52%	1 1573	ag	TCTCGGACCCACTGTTCAATCTCAT	3897	28.56%
	2 1362	ag	AGGATTCCCTTCCTTTAGCTTATAC	1329	7.33%	2 1074	ag	AGCAACCTCCTCTTTTGTTCTACCT	799	5.86%
	3 1457	g	TGCCACGAGTTAGAGCCAGAACAAT	1030	5.68%	3 1457	g	TGCCACGAGTTAGAGCCAGAACAAT	768	5.63%
	4 1074	ag	AGCAACCTCCTCTTTTGTTCTACCT	820	4.52%	4 1362	ag	AGGATTCCCTTCCTTTAGCTTATAC	729	5.34%
	5 1078	ag	ACCTCCTCTTTTGTTCTACCTCGGA	421	2.32%	5 1078	ag	ACCTCCTCTTTTGTTCTACCTCGGA	357	2.62%
					45.38%					48.00%

Size.	(A) Pos.	Pol.	Sequence	Count.	% Total	(B) Pos.	Pol.	Sequence	Count.	% Total
26	1 985	ag	AGTCCAAAGGCTTTCAAGAATTCTCT	6544	17.43%	1 1572	ag	CTCTCGGACCCACTGTTCAATCTCAT	3072	11.96%
	2 1572	ag	CTCTCGGACCCACTGTTCAATCTCAT	3524	9.39%	2 985	ag	AGTCCAAAGGCTTTCAAGAATTCTCT	2947	11.47%
	3 1319	ag	CCAAGGCGGCAGCAACTCGTGATAGA	1687	4.49%	3 1451	ag	GCTTGTTGCCACGAGTTAGAGCCAGA	1397	5.44%
	4 1451	ag	GCTTGTTGCCACGAGTTAGAGCCAGA	1454	3.87%	4 1319	ag	CCAAGGCGGCAGCAACTCGTGATAGA	1250	4.87%
	5 1229	ag	TCGGGTATGCAGGGGATAGGCCGTCC	861	2.29%	5 978	ag	ATCCACAAGTCCAAAGGCTTTCAAGA	653	2.54%
					37.47%					36.28%

Size.	(A) Pos.	Pol.	Sequence	Count.	% Total	(B) Pos.	Pol.	Sequence	Count.	% Total
27	1 1269	ag	GACAGGAAGCCACTCACTCAAGACGAC	35124	33.08%	1 1269	ag	GACAGGAAGCCACTCACTCAAGACGAC	15034	23.11%
	2 1385	ag	ACTTGTTGATGAGAGCCTCCACAGTTG	8175	7.70%	2 1385	ag	ACTTGTTGATGAGAGCCTCCACAGTTG	5860	9.01%
	3 982	ag	ACAAGTCCAAAGGCTTTCAAGAATTCT	5192	4.89%	3 1451	ag	GCTTGTTGCCACGAGTTAGAGCCAGAA	4056	6.24%
	4 1451	ag	GCTTGTTGCCACGAGTTAGAGCCAGAA	5075	4.78%	4 1571	ag	ACTCTCGGACCCACTGTTCAATCTCAT	3398	5.22%
	5 1571	ag	ACTCTCGGACCCACTGTTCAATCTCAT	4284	4.04%	5 982	ag	ACAAGTCCAAAGGCTTTCAAGAATTCT	2185	3.36%
					54.49%					46.94%

Size.	(A) Pos.	Pol.	Sequence	Count.	% Total	(B) Pos.	Pol.	Sequence	Count.	% Total
28	1 1570	ag	AACTCTCGGACCCACTGTTCAATCTCAT	17584	21.67%	1 1570	ag	AACTCTCGGACCCACTGTTCAATCTCAT	12315	23.55%
	2 1153	ag	TCTAATATTGCCCTTAGATAGTCTCCTG	6732	8.30%	2 983	ag	CAAGTCCAAAGGCTTTCAAGAATTCTCT	3654	6.99%
	3 983	ag	CAAGTCCAAAGGCTTTCAAGAATTCTCT	5463	6.73%	3 1153	ag	TCTAATATTGCCCTTAGATAGTCTCCTG	2181	4.17%
	4 223	g	AGAATTCCCATACCGAGTCGGACTTGGA	4006	4.94%	4 1458	ag	GCCACGAGTTAGAGCCAGAACAATCATT	2152	4.12%
	5 1483	ag	ATTTTCTTGGCATCCTTCTCCCAGTCAG	2674	3.30%	5 982	ag	ACAAGTCCAAAGGCTTTCAAGAATTCTC	1952	3.73%
					44.94%					42.55%

Size.	(A) Pos.	Pol.	Sequence	Count.	% Total	(B) Pos.	Pol.	Sequence	Count.	% Total
29	1 1448	ag	TGGGCTTGTTGCCACGAGTTAGAGCCAGA	4469	29.38%	1 1448	ag	TGGGCTTGTTGCCACGAGTTAGAGCCAGA	3632	13.52%
	2 996	ag	TTTCAAGAATTCTCTCCTCTTCTCATGGC	2774	8.72%	2 996	ag	TTTCAAGAATTCTCTCCTCTTCTCATGGC	2188	8.15%
	3 1566	ag	AGCAAACTCTCGGACCCACTGTTCAATCT	1814	5.20%	3 1119	ag	CCGGGAGAACTGCAGCAGATACAGAGAGT	1153	4.29%
	4 986	ag	GTCCAAAGGCTTTCAAGAATTCTCTCCTC	1784	5.13%	4 986	ag	GTCCAAAGGCTTTCAAGAATTCTCTCCTC	956	3.56%
	5 1457	g	TGCCACGAGTTAGAGCCAGAACAATCATT	1554	4.66%	5 1566	ag	AGCAAACTCTCGGACCCACTGTTCAATCT	940	3.50%
					53.08%					33.02%

Size.	(A) Pos.	Pol.	Sequence	Count.	% Total	(B) Pos.	Pol.	Sequence	Count.	% Total
30	1 1118	ag	CCCGGGAGAACTGCAGCAGATACAGAGAGT	3073	13.11%	1 1118	ag	CCCGGGAGAACTGCAGCAGATACAGAGAGT	2104	14.09%
	2 985	ag	AGTCCAAAGGCTTTCAAGAATTCTCTCCTC	2244	9.58%	2 996	ag	TTTCAAGAATTCTCTCCTCTTCTCATGGCT	1379	9.24%
	3 1448	ag	TGGGCTTGTTGCCACGAGTTAGAGCCAGAA	1713	7.31%	3 1448	ag	TGGGCTTGTTGCCACGAGTTAGAGCCAGAA	1293	8.66%
	4 996	ag	TTTCAAGAATTCTCTCCTCTTCTCATGGCT	1654	7.06%	4 985	ag	AGTCCAAAGGCTTTCAAGAATTCTCTCCTC	1176	7.88%
	5 1446	ag	CCTGGGCTTGTTGCCACGAGTTAGAGCCAG	1161	4.95%	5 1446	ag	CCTGGGCTTGTTGCCACGAGTTAGAGCCAG	977	6.54%
					42.01%					46.41%

Ae rMP12 S Segment

Size.	(A) Pos.	Pol.	Sequence	Count.	% Total	(B) Pos.	Pol.	Sequence	Count.	% Total
21	1 865	g	TCCCGACCGTAACCCCAACTC	22	2.97%	1 865	g	TCCCGACCGTAACCCCAACTC	17	2.81%
	2 597	ag	AGGTTGCTCACGTACAGTGCG	19	2.56%	2 550	g	CAGAGGGATTGACCTGTGCCT	15	2.48%
	3 550	g	CAGAGGGATTGACCTGTGCCT	16	2.16%	3 165	g	TGCACCATCGTCCTAGTCACG	11	1.82%
	4 165	g	TGCACCATCGTCCTAGTCACG	12	1.62%	4 523	g	CAGGATGATAGCGACTGAGGC	9	1.49%
	5 1561	g	TGATAAGCAAACTCTCGGACC	12	1.62%	5 597	ag	AGGTTGCTCACGTACAGTGCG	9	1.49%
					10.93%					10.08%

Size.	(A) Pos.	Pol.	Sequence	Count.	% Total	(B) Pos.	Pol.	Sequence	Count.	% Total
24	1 1078	ag	ACCTCCTCTTTTGTTCTACCTCGG	21	10.24%	1 1505	ag	AGTCAGCCCCACCATACTGCTTTA	21	11.67%
	2 1116	ag	GACCCGGGAGAACTGCAGCAGATA	20	9.76%	2 1002	ag	GAATTCTCTCCTCTTCTCATGGCTT	20	11.11%
	3 1002	ag	GAATTCTCTCCTCTTCTCATGGCT	19	9.27%	3 1116	ag	GACCCGGGAGAACTGCAGCAGATA	19	10.56%
	4 1457	g	TGCCACGAGTTAGAGCCAGAACAA	19	9.27%	4 1075	ag	GCAACCTCCTCTTTTGTTCTACCT	19	10.56%
	5 1337	ag	GTGATAGAGTCAACTCATCCCGGG	18	8.78%	5 1315	ag	CCAGCCAAGGCGGCAGCAACTCGT	18	10.00%
					47.32%					53.89%

Size.	(A) Pos.	Pol.	Sequence	Count.	% Total	(B) Pos.	Pol.	Sequence	Count.	% Total
25	1 1074	ag	AGCAACCTCCTCTTTTGTTCTACCT	144	18.51%	1 1074	ag	AGCAACCTCCTCTTTTGTTCTACCT	90	16.51%
	2 1078	ag	ACCTCCTCTTTTGTTCTACCTCGGA	95	12.21%	2 1573	ag	TCTCGGACCCACTGTTCAATCTCAT	77	14.13%
	3 1573	ag	TCTCGGACCCACTGTTCAATCTCAT	71	9.13%	3 1078	ag	ACCTCCTCTTTTGTTCTACCTCGGA	64	11.74%
	4 1457	g	TGCCACGAGTTAGAGCCAGAACAAT	50	6.43%	4 1457	g	TGCCACGAGTTAGAGCCAGAACAAT	37	6.79%
	5 988	g	CCAAAGGCTTTCAAGAATTCTCTCC	38	4.88%	5 1077	ag	AACCTCCTCTTTTGTTCTACCTCGG	23	4.22%
					51.16%					53.39%

Size.	(A) Pos.	Pol.	Sequence	Count.	% Total	(B) Pos.	Pol.	Sequence	Count.	% Total
26	1 1572	ag	CTCTCGGACCCACTGTTCAATCTCAT	81	7.77%	1 1572	ag	CTCTCGGACCCACTGTTCAATCTCAT	71	8.42%
	2 225	g	AATTCCCATACCGAGTCGGACTTGGA	72	6.91%	2 225	g	AATTCCCATACCGAGTCGGACTTGGA	41	4.86%
	3 985	ag	AGTCCAAAGGCTTTCAAGAATTCTCT	59	5.66%	3 1002	ag	GAATTCTCTCCTCTTCTCATGGCTTA	39	4.63%
	4 1002	ag	GAATTCTCTCCTCTTCTCATGGCTTA	45	4.32%	4 988	g	CCAAAGGCTTTCAAGAATTCTCTCCT	36	4.27%
	5 988	g	CCAAAGGCTTTCAAGAATTCTCTCCT	40	3.84%	5 1236	ag	TGCAGGGGATAGGCCGTCCATGGTAG	31	3.68%
					28.50%					25.86%

Size.	(A) Pos.	Pol.	Sequence	Count.	% Total	(B) Pos.	Pol.	Sequence	Count.	% Total
27	1 1385	ag	ACTTGTTGATGAGAGCCTCCACAGTTG	187	8.16%	1 1571	ag	ACTCTCGGACCCACTGTTCAATCTCAT	145	8.44%
	2 1269	ag	GACAGGAAGCCACTCACTCAAGACGAC	184	8.03%	2 1269	ag	GACAGGAAGCCACTCACTCAAGACGAC	115	6.69%
	3 1571	ag	ACTCTCGGACCCACTGTTCAATCTCAT	161	7.02%	3 1385	ag	ACTTGTTGATGAGAGCCTCCACAGTTG	110	6.40%
	4 1451	ag	GCTTGTTGCCACGAGTTAGAGCCAGAA	88	3.84%	4 1075	ag	GCAACCTCCTCTTTTGTTCTACCTCGG	75	4.36%
	5 1075	ag	GCAACCTCCTCTTTTGTTCTACCTCGG	79	3.45%	5 1451	ag	GCTTGTTGCCACGAGTTAGAGCCAGAA	69	4.01%
					30.50%					29.90%

Size.	(A) Pos.	Pol.	Sequence	Count.	% Total	(B) Pos.	Pol.	Sequence	Count.	% Total
28	1 1570	ag	AACTCTCGGACCCACTGTTCAATCTCAT	556	18.96%	1 1570	ag	AACTCTCGGACCCACTGTTCAATCTCAT	470	20.71%
	2 1448	ag	TGGGCTTGTTGCCACGAGTTAGAGCCAG	235	8.02%	2 1448	ag	TGGGCTTGTTGCCACGAGTTAGAGCCAG	198	8.73%
	3 1458	ag	GCCACGAGTTAGAGCCAGAACAATCATT	201	6.86%	3 1458	ag	GCCACGAGTTAGAGCCAGAACAATCATT	162	7.14%
	4 970	ag	CCATTGGAATCCACAAGTCCAAAGGCTT	141	4.81%	4 997	ag	TTCAAGAATTCTCTCCTCTTCTCATGGC	113	4.98%
	5 997	ag	TTCAAGAATTCTCTCCTCTTCTCATGGC	133	4.54%	5 992	ag	AGGCTTTCAAGAATTCTCTCCTCTTCTC	80	3.53%
					43.18%					45.09%

Size.	(A) Pos.	Pol.	Sequence	Count.	% Total	(B) Pos.	Pol.	Sequence	Count.	% Total
29	1 997	ag	TTCAAGAATTCTCTCCTCTTCTCATGGCT	205	11.67%	1 997	ag	TTCAAGAATTCTCTCCTCTTCTCATGGCT	177	12.82%
	2 1447	ag	CTGGGCTTGTTGCCACGAGTTAGAGCCAG	186	10.59%	2 1447	ag	CTGGGCTTGTTGCCACGAGTTAGAGCCAG	148	10.72%
	3 996	ag	TTTCAAGAATTCTCTCCTCTTCTCATGGC	128	7.29%	3 996	ag	TTTCAAGAATTCTCTCCTCTTCTCATGGC	104	7.53%
	4 1448	ag	TGGGCTTGTTGCCACGAGTTAGAGCCAGA	94	5.35%	4 1448	ag	TGGGCTTGTTGCCACGAGTTAGAGCCAGA	70	5.07%
	5 1566	ag	AGCAAACTCTCGGACCCACTGTTCAATCT	49	2.79%	5 1457	g	TGCCACGAGTTAGAGCCAGAACAATCATT	40	2.90%
					37.68%					39.03%

Size.	(A) Pos.	Pol.	Sequence	Count.	% Total	(B) Pos.	Pol.	Sequence	Count.	% Total
30	1 1446	ag	CCTGGGCTTGTTGCCACGAGTTAGAGCCAG	109	11.01%	1 1446	ag	CCTGGGCTTGTTGCCACGAGTTAGAGCCAG	74	10.25%
	2 985	ag	AGTCCAAAGGCTTTCAAGAATTCTCTCCTC	77	7.78%	2 1448	ag	TGGGCTTGTTGCCACGAGTTAGAGCCAGAA	68	9.42%
	3 1448	ag	TGGGCTTGTTGCCACGAGTTAGAGCCAGAA	66	6.67%	3 996	ag	TTTCAAGAATTCTCTCCTCTTCTCATGGCT	39	5.40%
	4 996	ag	TTTCAAGAATTCTCTCCTCTTCTCATGGCT	62	6.26%	4 1118	ag	CCCGGGAGAACTGCAGCAGATACAGAGAGT	39	5.40%
	5 993	ag	GGCTTTCAAGAATTCTCTCCTCTTCTCATG	46	4.65%	5 985	ag	AGTCCAAAGGCTTTCAAGAATTCTCTCCTC	35	4.85%
					36.36%					35.32%

(B) viRNA species aligning to the rMP12 M segment

u4.4 rMP12 M Segment

Size.	(A)	Pos.	Pol.	Sequence	Count.	% Total	(B)	Pos.	Pol.	Sequence	Count.	% Total
	1	1881	g	TTCCCTAGAACCAACTGACCT	1169	3.52%	1	1881	g	TTCCCTAGAACCAACTGACCT	712	2.53%
	2	262	g	ACGCACTGATCTATGAGGCCT	422	1.27%	2	262	g	ACGCACTGATCTATGAGGCCT	379	1.34%
21	3	1713	ag	GTGCCAGACAGTCTACACTTG	412	1.24%	3	1713	ag	GTGCCAGACAGTCTACACTTG	330	1.17%
	4	1882	g	TCCCTAGAACCAACTGACCTC	349	1.05%	4	1882	g	TCCCTAGAACCAACTGACCTC	326	1.16%
	5	1048	g	CTGAGGACTCTGAATTGCACC	337	1.01%	5	1884	g	CCTAGAACCAACTGACCTCCT	266	0.94%
						8.10%						**7.14%**

Size.	(A)	Pos.	Pol.	Sequence	Count.	% Total	(B)	Pos.	Pol.	Sequence	Count.	% Total
	1	1309	g	TACAGTTAAAAACTCTAAGGGCCT	547	16.00%	1	1309	g	TACAGTTAAAAACTCTAAGGGCCT	353	12.28%
	2	2384	g	TCGGACAACCAATCCATGAGGCTC	174	5.09%	2	259	g	TACACGCACTGATCTATGAGGCCT	150	5.22%
24	3	259	g	TACACGCACTGATCTATGAGGCCT	159	4.65%	3	2384	g	TCGGACAACCAATCCATGAGGCTC	147	5.11%
	4	1984	g	TGAAGGCTGTGATCCACATTAGTG	134	3.92%	4	1193	g	TGAGAGGCTAACTGAACCCCAGTT	120	4.18%
	5	1193	g	TGAGAGGCTAACTGAACCCCAGTT	125	3.66%	5	2443	g	TCTGGATGGGCTTGGCAGAGAGTT	116	4.04%
						33.31%						**30.83%**

Size.	(A)	Pos.	Pol.	Sequence	Count.	% Total	(B)	Pos.	Pol.	Sequence	Count.	% Total
	1	2093	g	TACAAACACAACAACAAAGGCACTG	297	4.38%	1	2093	g	TACAAACACAACAACAAAGGCACTG	270	4.96%
	2	968	g	TGTGCACTCCAATTGATCTATCATG	239	3.53%	2	968	g	TGTGCACTCCAATTGATCTATCATG	139	2.55%
25	3	2217	ag	GAGCTAACTGACTGATCATCGTGTG	143	2.11%	3	3571	ag	TGTCCTCAGGATCCTTACCATGGCA	109	2.00%
	4	3200	g	TGCAATGATGGTGTCGTGAACTGCC	118	1.74%	4	2217	ag	GAGCTAACTGACTGATCATCGTGTG	108	1.98%
	5	1032	g	TCATGAGCACTCAGGACTGAGGACT	111	1.64%	5	3200	g	TGCAATGATGGTGTCGTGAACTGCC	104	1.91%
						13.40%						**13.40%**

Size.	(A)	Pos.	Pol.	Sequence	Count.	% Total	(B)	Pos.	Pol.	Sequence	Count.	% Total
	1	1063	g	TGCACCTGATCTCCCCCAAGAACCCT	459	3.32%	1	3561	ag	AGGGAAATCTTGTCCTCAGGATCCTT	398	3.56%
	2	3561	ag	AGGGAAATCTTGTCCTCAGGATCCTT	439	3.18%	2	1505	ag	CCTATTCACATGGCATTCCCCGACAA	328	2.93%
26	3	851	ag	GCCCTTAGAGAAAGCTTGAACACCTC	374	2.71%	3	2619	ag	TCCCCAGTGCACTTCTTACTACCATG	305	2.73%
	4	3200	g	TGCAATGATGGTGTCGTGAACTGCCT	337	2.44%	4	545	ag	AGGCCGCTCATCTCCATCACAAGAGT	286	2.56%
	5	2146	ag	GGCCATGAGCACACACTATGCAGTCA	335	2.43%	5	2146	ag	GGCCATGAGCACACACTATGCAGTCA	286	2.56%
						14.08%						**14.34%**

Size.	(A)	Pos.	Pol.	Sequence	Count.	% Total	(B)	Pos.	Pol.	Sequence	Count.	% Total
	1	3339	ag	TCCTCCTGAGTCATCCCGTCAATGTAG	2517	8.14%	1	3339	ag	TCCTCCTGAGTCATCCCGTCAATGTAG	4224	16.16%
	2	2145	ag	AGGCCATGAGCACACACTATGCAGTCA	2347	7.59%	2	2145	ag	AGGCCATGAGCACACACTATGCAGTCA	1889	7.23%
27	3	2505	ag	GGCTTCTTCCAGACCCCTGATACTTGT	1862	6.02%	3	2505	ag	GGCTTCTTCCAGACCCCTGATACTTGT	1754	6.71%
	4	1305	g	TCGATACAGTTAAAAACTCTAAGGGCC	1052	3.40%	4	777	g	TCACAAGATACGGCTGCTCCCACAAAG	616	2.36%
	5	777	g	TCACAAGATACGGCTGCTCCCACAAAG	539	1.74%	5	1305	g	TCGATACAGTTAAAAACTCTAAGGGCC	510	1.95%
						26.88%						**34.40%**

Size.	(A)	Pos.	Pol.	Sequence	Count.	% Total	(B)	Pos.	Pol.	Sequence	Count.	% Total
	1	3225	ag	TCTAGTAGAGTTCTATGATGAGCATACG	5035	14.47%	1	3225	ag	TCTAGTAGAGTTCTATGATGAGCATACG	3865	15.00%
	2	2504	ag	AGGCTTCTTCCAGACCCCTGATACTTGT	3910	11.23%	2	2504	ag	AGGCTTCTTCCAGACCCCTGATACTTGT	3209	12.45%
28	3	3638	g	TGCCCTGTATAACTCCTGGCTTGAGGTC	717	2.06%	3	3638	g	TGCCCTGTATAACTCCTGGCTTGAGGTC	668	2.59%
	4	2339	ag	TCCGCTAGCACAAGCAACTGCTGATGAT	696	2.00%	4	1503	ag	CACCTATTCACATGGCATTCCCCGACAA	493	1.91%
	5	3182	ag	GCTAGGTGGATCAGCCTTTGCAATGATG	511	1.47%	5	2339	ag	TCCGCTAGCACAAGCAACTGCTGATGAT	358	1.39%
						31.23%						**33.35%**

Size.	(A)	Pos.	Pol.	Sequence	Count.	% Total	(B)	Pos.	Pol.	Sequence	Count.	% Total
	1	968	g	TGTGCACTCCAATTGATCTATCATGGGCT	1308	4.87%	1	968	g	TGTGCACTCCAATTGATCTATCATGGGCT	1228	6.29%
	2	3020	ag	GTTGCAGTCTTCAGTGAGCTCATACTTAG	1017	3.79%	2	3020	ag	GTTGCAGTCTTCAGTGAGCTCATACTTAG	753	3.86%
29	3	3638	g	TGCCCTGTATAACTCCTGGCTTGAGGTCT	754	2.81%	3	3638	g	TGCCCTGTATAACTCCTGGCTTGAGGTCT	698	3.58%
	4	2183	ag	CGGGTCCTGGGGAGGGCAGTGAGCTACTA	664	2.47%	4	2183	ag	CGGGTCCTGGGGAGGGCAGTGAGCTACTA	551	2.82%
	5	2503	ag	AAGGCTTCTTCCAGACCCCTGATACTTGT	663	2.47%	5	2503	ag	AAGGCTTCTTCCAGACCCCTGATACTTGT	485	2.49%
						16.41%						**19.04%**

Size.	(A)	Pos.	Pol.	Sequence	Count.	% Total	(B)	Pos.	Pol.	Sequence	Count.	% Total
	1	3019	ag	AGTTGCAGTCTTCAGTGAGCTCATACTTAG	1778	10.17%	1	3019	ag	AGTTGCAGTCTTCAGTGAGCTCATACTTAG	1185	9.90%
	2	3229	ag	GTAGAGTTCTATGATGAGCATACGACTGGA	995	5.69%	2	3229	ag	GTAGAGTTCTATGATGAGCATACGACTGGA	776	6.48%
30	3	253	g	TGCTTTTACACGCACTGATCTATGAGGCCT	861	4.93%	3	2225	g	TGACTGATCATCGTGTGCCATGTGAACCCC	501	4.19%
	4	2225	g	TGACTGATCATCGTGTGCCATGTGAACCCC	605	3.46%	4	253	g	TGCTTTTACACGCACTGATCTATGAGGCCT	460	3.84%
	5	3110	ag	ATTTGGACAGTGTGTCTTCATCACGAGTTT	520	2.98%	5	3110	ag	ATTTGGACAGTGTGTCTTCATCACGAGTTT	347	2.90%
						27.23%						**27.31%**

Ae rMP12 M Segment

Size.	(A)	Pos.	Pol.	Sequence	Count.	% Total	(B)	Pos.	Pol.	Sequence	Count.	% Total
	1	1881	g	TTCCCTAGAACCAACTGACCT	54	3.90%	1	1881	g	TTCCCTAGAACCAACTGACCT	40	3.66%
	2	262	g	ACGCACTGATCTATGAGGCCT	37	2.68%	2	262	g	ACGCACTGATCTATGAGGCCT	28	2.56%
21	3	1713	ag	GTGCCAGACAGTCTACACTTG	23	1.66%	3	1713	ag	GTGCCAGACAGTCTACACTTG	18	1.65%
	4	1987	ag	AGGCTGTGATCCACATTAGTG	18	1.30%	4	1048	g	CTGAGGACTCTGAATTGCACC	15	1.37%
	5	1882	g	TCCCTAGAACCAACTGACCTC	16	1.16%	5	1711	ag	CTGTGCCAGACAGTCTACACT	15	1.37%
						10.70%						**10.60%**

Size.	(A)	Pos.	Pol.	Sequence	Count.	% Total	(B)	Pos.	Pol.	Sequence	Count.	% Total
	1	1309	g	TACAGTTAAAAACTCTAAGGGCCT	20	14.08%	1	1309	g	TACAGTTAAAAACTCTAAGGGCCT	21	15.79%
	2	259	g	TACACGCACTGATCTATGAGGCCT	8	5.63%	2	3198	g	TTTGCAATGATGGTGTCGTGAACT	6	4.51%
24	3	2443	g	TCTGGATGGGCTTGGCAGAGAGTT	6	4.23%	3	1089	g	TGCCGAGGAATTTCTGAGAATGGC	5	3.76%
	4	1166	g	TGAGCCTGAAATGCCCTCTGCGTC	5	3.52%	4	685	g	AGAGAGATCCAGTTCCTGTGGATG	4	3.01%
	5	2384	g	TCGGACAACCAATCCATGAGGCTC	5	3.52%	5	1166	g	TGAGCCTGAAATGCCCTCTGCGTC	3	2.26%
						30.99%						**29.32%**

Size.	(A)	Pos.	Pol.	Sequence	Count.	% Total	(B)	Pos.	Pol.	Sequence	Count.	% Total
	1	3249	g	TACGACTGGAAAAGGGGAAATTTTC	11	3.65%	1	2384	g	TCGGACAACCAATCCATGAGGCTCA	11	4.58%
	2	1032	g	TCATGAGCACTCAGGACTGAGGACT	9	2.99%	2	1032	g	TCATGAGCACTCAGGACTGAGGACT	8	3.33%
25	3	1166	g	TGAGCCTGAAATGCCCTCTGCGTCC	9	2.99%	3	3249	g	TACGACTGGAAAAGGGGAAATTTTC	8	3.33%
	4	2755	ag	AGTCTGGTAGCAGATTCTCCTCAGT	9	2.99%	4	968	g	TGTGCACTCCAATTGATCTATCATG	6	2.50%
	5	2384	g	TCGGACAACCAATCCATGAGGCTCA	6	1.99%	5	1166	g	TGAGCCTGAAATGCCCTCTGCGTCC	6	2.50%
						14.62%						**16.25%**

Size.	(A)	Pos.	Pol.	Sequence	Count.	% Total	(B)	Pos.	Pol.	Sequence	Count.	% Total
	1	3249	g	TACGACTGGAAAAGGGGAAATTTTCC	23	3.71%	1	1063	g	TGCACCTGATCTCCCCCAAGAACCCT	21	4.09%
	2	1063	g	TGCACCTGATCTCCCCCAAGAACCCT	21	3.39%	2	3249	g	TACGACTGGAAAAGGGGAAATTTTCC	16	3.11%
26	3	3562	ag	GGGAAATCTTGTCCTCAGGATCCTTA	19	3.06%	3	851	ag	GCCCTTAGAGAAAGCTTGAACACCTC	14	2.72%
	4	3339	ag	TCCTCCTGAGTCATCCCGTCAATGTA	18	2.90%	4	3339	ag	TCCTCCTGAGTCATCCCGTCAATGTA	14	2.72%
	5	2619	ag	TCCCCAGTGCACTTCTTACTACCATG	17	2.74%	5	2146	ag	GGCCATGAGCACACACTATGCAGTCA	13	2.53%
						15.81%						**15.18%**

Size.	(A)	Pos.	Pol.	Sequence	Count.	% Total	(B)	Pos.	Pol.	Sequence	Count.	% Total
	1	2505	ag	GGCTTCTTCCAGACCCCTGATACTTGT	59	4.85%	1	1305	g	TCGATACAGTTAAAAACTCTAAGGGCC	38	3.92%
	2	3232	ag	GAGTTCTATGATGAGCATACGACTGGA	47	3.86%	2	3232	ag	GAGTTCTATGATGAGCATACGACTGGA	38	3.92%
27	3	1305	g	TCGATACAGTTAAAAACTCTAAGGGCC	46	3.78%	3	2505	ag	GGCTTCTTCCAGACCCCTGATACTTGT	37	3.82%
	4	2145	ag	AGGCCATGAGCACACACTATGCAGTCA	34	2.79%	4	1042	g	TCAGGACTGAGGACTCTGAATTGCACC	26	2.68%
	5	2402	ag	AGGCTCACATTTGGTTATACAAGTTGT	24	1.97%	5	2145	ag	AGGCCATGAGCACACACTATGCAGTCA	26	2.68%
						17.26%						**17.03%**

Size.	(A)	Pos.	Pol.	Sequence	Count.	% Total	(B)	Pos.	Pol.	Sequence	Count.	% Total
	1	3225	ag	TCTAGTAGAGTTCTATGATGAGCATACG	129	9.95%	1	3225	ag	TCTAGTAGAGTTCTATGATGAGCATACG	123	12.44%
	2	2504	ag	AGGCTTCTTCCAGACCCCTGATACTTGT	58	4.47%	2	2504	ag	AGGCTTCTTCCAGACCCCTGATACTTGT	41	4.15%
28	3	3639	g	GCCCTGTATAACTCCTGGCTTGAGGTCT	43	3.32%	3	3639	g	GCCCTGTATAACTCCTGGCTTGAGGTCT	34	3.44%
	4	3232	ag	GAGTTCTATGATGAGCATACGACTGGAA	29	2.24%	4	3085	g	TGAGGTGATGAGCTGACTGGTAGTCATT	15	1.52%
	5	2455	ag	TGGCAGAGAGTTCTCTCTTCACAACCAC	23	1.77%	5	2501	g	TAAAGGCTTCTTCCAGACCCCTGATACT	14	1.42%
						21.74%						**22.95%**

Size.	(A)	Pos.	Pol.	Sequence	Count.	% Total	(B)	Pos.	Pol.	Sequence	Count.	% Total
	1	2183	ag	CGGGTCCTGGGGAGGGCAGTGAGCTACTA	54	5.13%	1	2183	ag	CGGGTCCTGGGGAGGGCAGTGAGCTACTA	46	5.41%
	2	968	g	TGTGCACTCCAATTGATCTATCATGGGCT	52	4.94%	2	968	g	TGTGCACTCCAATTGATCTATCATGGGCT	41	4.82%
29	3	253	g	TGCTTTTACACGCACTGATCTATGAGGCC	40	3.80%	3	3638	g	TGCCCTGTATAACTCCTGGCTTGAGGTCT	25	2.94%
	4	3567	ag	ATCTTGTCCTCAGGATCCTTACCATGGCA	32	3.04%	4	2715	ag	GTTCCTTTGTACTGTCCCTTATGCTCGAA	23	2.70%
	5	3638	g	TGCCCTGTATAACTCCTGGCTTGAGGTCT	28	2.66%	5	253	g	TGCTTTTACACGCACTGATCTATGAGGCC	21	2.47%
						19.56%						**18.33%**

Size.	(A)	Pos.	Pol.	Sequence	Count.	% Total	(B)	Pos.	Pol.	Sequence	Count.	% Total
	1	3229	ag	GTAGAGTTCTATGATGAGCATACGACTGGA	93	12.60%	1	3229	ag	GTAGAGTTCTATGATGAGCATACGACTGGA	72	12.29%
	2	3019	ag	AGTTGCAGTCTTCAGTGAGCTCATACTTAG	41	5.56%	2	3019	ag	AGTTGCAGTCTTCAGTGAGCTCATACTTAG	23	3.92%
30	3	1008	ag	AGGTTTGGTGCCCTAAGGCATGATTCATGA	24	3.25%	3	2443	g	TCTGGATGGGCTTGGCAGAGAGTTCTCTCT	22	3.75%
	4	2443	g	TCTGGATGGGCTTGGCAGAGAGTTCTCTCT	21	2.85%	4	253	g	TGCTTTTACACGCACTGATCTATGAGGCCT	15	2.56%
	5	1028	g	TGATTCATGAGCACTCAGGACTGAGGACTC	19	2.57%	5	2529	g	TGTATCTGCACAATCCCTGACCCATTAGCA	14	2.39%
						26.83%						**24.91%**

(C) viRNA species aligning to the rMP12 L segment

u4.4 rMP12 L Segment

Size.	(A)	Pos.	Pol.	Sequence	Count.	% Total	(B)	Pos.	Pol.	Sequence	Count.	% Total
	1	2278	-	ATGTTCAAACGGTCTCTCAAT	243	1.06%	1	2278	-	ATGTTCAAACGGTCTCTCAAT	174	0.92%
	2	4029	-	AAGGTGCTCAAGTTCTATGAT	167	0.73%	2	4274	+	CTTGCAGCTCTGACCTGAGAA	126	0.67%
21	3	4030	-	AGGTGCTCAAGTTCTATGATT	166	0.73%	3	4030	-	AGGTGCTCAAGTTCTATGATT	124	0.66%
	4	4274	+	CTTGCAGCTCTGACCTGAGAA	166	0.73%	4	2210	-	GGCCTGTTCTGGGAGCCCGAT	123	0.65%
	5	2210	-	GGCCTGTTCTGGGAGCCCGAT	134	0.59%	5	231	-	GGAGCACCGACCTGTTTCTAG	108	0.57%
						3.83%						3.46%

Size.	(A)	Pos.	Pol.	Sequence	Count.	% Total	(B)	Pos.	Pol.	Sequence	Count.	% Total
	1	1300	+	TCACCATCTAGAAATCTCTGAAGG	17	2.06%	1	1300	+	TCACCATCTAGAAATCTCTGAAGG	11	1.71%
	2	1587	+	TACTGGAGCTCCTGTTATTCTGAC	8	0.97%	2	1587	+	TACTGGAGCTCCTGTTATTCTGAC	9	1.40%
24	3	1591	-	GGAGCTCCTGTTATTCTGACTGTT	8	0.97%	3	3779	-	CATCCTTATAGACATACCAATTCT	6	0.93%
	4	4030	-	AGGTGCTCAAGTTCTATGATTTTC	8	0.97%	4	751	+	TCTGATATTGACTTGAAAATGCCT	5	0.78%
	5	751	+	TCTGATATTGACTTGAAAATGCCT	7	0.85%	5	1913	+	TGTAAACTATAGAATCCAGTGATT	5	0.78%
						5.82%						5.61%

Size.	(A)	Pos.	Pol.	Sequence	Count.	% Total	(B)	Pos.	Pol.	Sequence	Count.	% Total
	1	3653	+	TGCATCCTTGTGACTCTATCTGCCT	37	5.93%	1	3653	+	TGCATCCTTGTGACTCTATCTGCCT	46	8.90%
	2	1300	+	TCACCATCTAGAAATCTCTGAAGGA	31	4.97%	2	4963	+	TCACAAGAGAGAGGGCTGTACAGGT	31	6.00%
25	3	4963	+	TCACAAGAGAGAGGGCTGTACAGGT	23	3.69%	3	1300	+	TCACCATCTAGAAATCTCTGAAGGA	22	4.26%
	4	247	+	TCTAGAACTTTCCTAACTGAGGCTC	19	3.04%	4	1399	+	TAGATTAGCTGTAGCTTATAGCTCT	14	2.71%
	5	537	+	TGAGAACATAGATCCGACTTTTGAT	18	2.88%	5	247	+	TCTAGAACTTTCCTAACTGAGGCTC	10	1.93%
						20.51%						23.79%

Size.	(A)	Pos.	Pol.	Sequence	Count.	% Total	(B)	Pos.	Pol.	Sequence	Count.	% Total
	1	246	+	TTCTAGAACTTTCCTAACTGAGGCTC	103	7.42%	1	246	+	TTCTAGAACTTTCCTAACTGAGGCTC	89	8.52%
	2	2978	+	TACTACTATCATCTGATCCTTGCATC	99	7.13%	2	2978	+	TACTACTATCATCTGATCCTTGCATC	51	4.89%
26	3	1078	+	TCCCATGGGCTGCTCTGACAGTTAGT	70	5.04%	3	770	+	TGCCTGGACTGAGATCATTGTCTGAT	39	3.74%
	4	537	+	TGAGAACATAGATCCGACTTTTGATC	47	3.38%	4	1078	+	TCCCATGGGCTGCTCTGACAGTTAGT	39	3.74%
	5	748	+	TCATCTGATATTGACTTGAAAATGCC	47	3.38%	5	748	+	TCATCTGATATTGACTTGAAAATGCC	32	3.07%
						26.35%						23.95%

Size.	(A)	Pos.	Pol.	Sequence	Count.	% Total	(B)	Pos.	Pol.	Sequence	Count.	% Total
	1	3862	+	TCTCGAATAATCTGGTTGTCTATCTGC	159	5.86%	1	3862	+	TCTCGAATAATCTGGTTGTCTATCTGC	131	6.53%
	2	748	+	TCATCTGATATTGACTTGAAAATGCCT	120	4.43%	2	748	+	TCATCTGATATTGACTTGAAAATGCCT	66	3.29%
27	3	1201	+	TAATAGACCACTTTGTTCTGCACAACT	97	3.58%	3	1588	-	ACTGGAGCTCCTGTTATTCTGACTGTT	57	2.84%
	4	1076	-	GGTCCCATGGGCTGCTCTGACAGTTAG	88	3.25%	4	1201	+	TAATAGACCACTTTGTTCTGCACAACT	55	2.74%
	5	770	+	TGCCTGGACTGAGATCATTGTCTGATG	64	2.36%	5	1076	-	GGTCCCATGGGCTGCTCTGACAGTTAG	53	2.64%
						19.48%						#REF!

Size.	(A)	Pos.	Pol.	Sequence	Count.	% Total	(B)	Pos.	Pol.	Sequence	Count.	% Total
	1	1300	+	TCACCATCTAGAAATCTCTGAAGGATTC	148	4.54%	1	2042	+	TAGAATCCTCCAAGAAGTTGAACTCAGG	89	3.81%
	2	3889	+	TCCATGAAATTCTGTCCATAGAGGCTCC	148	4.54%	2	1300	+	TCACCATCTAGAAATCTCTGAAGGATTC	88	3.77%
28	3	756	+	TATTGACTTGAAAATGCCTGGACTGAGA	134	4.11%	3	3889	+	TCCATGAAATTCTGTCCATAGAGGCTCC	68	2.91%
	4	2042	+	TAGAATCCTCCAAGAAGTTGAACTCAGG	130	3.99%	4	751	+	TCTGATATTGACTTGAAAATGCCTGGAC	62	2.66%
	5	751	+	TCTGATATTGACTTGAAAATGCCTGGAC	77	2.36%	5	756	+	TATTGACTTGAAAATGCCTGGACTGAGA	61	2.61%
						19.53%						15.76%

Size.	(A)	Pos.	Pol.	Sequence	Count.	% Total	(B)	Pos.	Pol.	Sequence	Count.	% Total
	1	1308	+	TAGAAATCTCTGAAGGATTCCAATCAAGT	668	14.66%	1	1308	+	TAGAAATCTCTGAAGGATTCCAATCAAGT	452	14.70%
	2	2042	+	TAGAATCCTCCAAGAAGTTGAACTCAGGA	347	7.61%	2	2042	+	TAGAATCCTCCAAGAAGTTGAACTCAGGA	146	4.75%
29	3	243	+	TGTTTCTAGAACTTTCCTAACTGAGGCTC	217	4.76%	3	243	+	TGTTTCTAGAACTTTCCTAACTGAGGCTC	130	4.23%
	4	384	+	TGTATCAAAAGACTCCATCTCGTAAGGGC	182	3.99%	4	527	+	TGGCGACAAATGAGAACATAGATCCGACT	97	3.15%
	5	527	+	TGGCGACAAATGAGAACATAGATCCGACT	150	3.29%	5	678	+	TACAGACTCACATCTCACCCAGCAGTTGC	95	3.09%
						34.31%						29.92%

Size.	(A)	Pos.	Pol.	Sequence	Count.	% Total	(B)	Pos.	Pol.	Sequence	Count.	% Total
	1	526	+	TTGGCGACAAATGAGAACATAGATCCGACT	239	10.15%	1	526	+	TTGGCGACAAATGAGAACATAGATCCGACT	141	9.51%
	2	2771	+	TCCACCTGATCGTTGGTCTAACATGCTGGG	154	6.54%	2	2771	+	TCCACCTGATCGTTGGTCTAACATGCTGGG	103	6.95%
30	3	2496	+	TCTGAAACCTCCCAATCCGCACGCATAAGG	139	5.90%	3	2496	+	TCTGAAACCTCCCAATCCGCACGCATAAGG	93	6.27%
	4	1308	+	TAGAAATCTCTGAAGGATTCCAATCAAGTT	95	4.04%	4	1308	+	TAGAAATCTCTGAAGGATTCCAATCAAGTT	47	3.17%
	5	1408	+	TGTAGCTTATAGCTCTCACTGTATGGACCT	92	3.91%	5	802	+	TAAGATAGAATGTGTAGGTCCTGATGAGAA	45	3.03%
						30.54%						28.93%

Ae rMP12 L Segment

Size.	(A)	Pos.	Pol.	Sequence	Count.	% Total	(B)	Pos.	Pol.	Sequence	Count.	% Total
	1	4029	-	AAGGTGCTCAAGTTCTATGAT	8	1.26%	1	2278	-	ATGTTCAAACGGTCTCTCAAT	10	2.01%
	2	4030	-	AGGTGCTCAAGTTCTATGATT	7	1.10%	2	4030	-	AGGTGCTCAAGTTCTATGATT	7	1.41%
21	3	5284	-	AGGTTTGCAGAGGTGACCACT	7	1.10%	3	231	-	GGAGCACCGACCTGTTTCTAG	6	1.21%
	4	1368	+	CTCAACGTTTGACACTGAGCT	6	0.94%	4	2548	-	AGGCCAGGGTCATTCCACTTC	5	1.01%
	5	2210	-	GGCCTGTTCTGGGAGCCCGAT	6	0.94%	5	5428	+	TCATTGAGGTCCCTAAGGTTG	5	1.01%
						5.35%						6.64%

Size.	(A)	Pos.	Pol.	Sequence	Count.	% Total	(B)	Pos.	Pol.	Sequence	Count.	% Total
	1	1078	+	TCCCATGGGCTGCTCTGACAGTTA	5	13.89%	1	3169	+	TTAAAGGCCCATGGAACTTCTGCC	2	4.76%
	2	1404	+	TAGCTGTAGCTTATAGCTCTCACT	4	11.11%	2	4013	+	CATCTGACTGTGGTCTAAGGTGCT	2	4.76%
24	3	4158	+	CCCTGAAAAAGGATTGAACATGCC	2	5.56%						
						30.56%						9.52%

Size.	(A)	Pos.	Pol.	Sequence	Count.	% Total	(B)	Pos.	Pol.	Sequence	Count.	% Total
	1	4963	+	TCACAAGAGAGAGGGCTGTACAGGT	4	8.00%	1	5636	+	TAAACCTGTCAAACATTTCTCTGCT	3	7.50%
	2	1399	+	TAGATTAGCTGTAGCTTATAGCTCT	3	6.00%	2	336	+	TGAACTGATGTCCTTGTAATGGGCT	2	5.00%
25	3	247	+	TCTAGAACTTTCCTAACTGAGGCTC	2	4.00%	3	1587	+	TACTGGAGCTCCTGTTATTCTGACT	2	5.00%
	4	1100	+	TAGTTGTGACATTCCTAAGCCTTGG	2	4.00%	4	2339	+	TAAGAATTAGAGCGCCACCTGGGCT	2	5.00%
	5	1389	+	TAGGACTCTGTAGATTAGCTGTAGC	2	4.00%	5	2599	+	TCAGACACTCCCATGCCCATCAGCA	2	5.00%
						26.00%						27.50%

Size.	(A)	Pos.	Pol.	Sequence	Count.	% Total	(B)	Pos.	Pol.	Sequence	Count.	% Total
	1	1076	-	GGTCCCATGGGCTGCTCTGACAGTTA	6	4.76%	1	246	+	TTCTAGAACTTTCCTAACTGAGGCTC	6	5.61%
	2	246	+	TTCTAGAACTTTCCTAACTGAGGCTC	5	3.97%	2	753	+	TGATATTGACTTGAAAATGCCTGGAC	5	4.67%
26	3	537	+	TGAGAACATAGATCCGACTTTTGATC	3	2.38%	3	1078	+	TCCCATGGGCTGCTCTGACAGTTAGT	5	4.67%
	4	1795	+	TCTGACACCAACTTCTCTGGAGATGT	3	2.38%	4	748	+	TCATCTGATATTGACTTGAAAATGCC	3	2.80%
	5	3998	+	TGTAACCCAAGAAGGCATCTGACTGT	3	2.38%	5	1076	-	GGTCCCATGGGCTGCTCTGACAGTTA	3	2.80%
						15.87%						20.56%

Size.	(A)	Pos.	Pol.	Sequence	Count.	% Total	(B)	Pos.	Pol.	Sequence	Count.	% Total
	1	4030	-	AGGTGCTCAAGTTCTATGATTTTCTTA	12	4.12%	1	748	+	TCATCTGATATTGACTTGAAAATGCCT	11	4.76%
	2	1076	-	GGTCCCATGGGCTGCTCTGACAGTTAG	10	3.44%	2	4030	-	AGGTGCTCAAGTTCTATGATTTTCTTA	7	3.03%
27	3	3509	+	TACAGAGGGTATCAGAAGCAAAGAACT	9	3.09%	3	1201	+	TAATAGACCACTTTGTTCTGCACAACT	6	2.60%
	4	748	+	TCATCTGATATTGACTTGAAAATGCCT	8	2.75%	4	3509	+	TACAGAGGGTATCAGAAGCAAAGAACT	5	2.16%
	5	1588	-	ACTGGAGCTCCTGTTATTCTGACTGTT	8	2.75%	5	5377	+	TCGACATCATGATAGGACAGCCAGGGA	5	2.16%
						16.15%						14.72%

Size.	(A)	Pos.	Pol.	Sequence	Count.	% Total	(B)	Pos.	Pol.	Sequence	Count.	% Total
	1	2042	+	TAGAATCCTCCAAGAAGTTGAACTCAGG	14	4.24%	1	1300	+	TCACCATCTAGAAATCTCTGAAGGATTC	12	5.45%
	2	751	+	TCTGATATTGACTTGAAAATGCCTGGAC	12	3.64%	2	2042	+	TAGAATCCTCCAAGAAGTTGAACTCAGG	8	3.64%
28	3	1300	+	TCACCATCTAGAAATCTCTGAAGGATTC	9	2.73%	3	3889	+	TCCATGAAATTCTGTCCATAGAGGCTCC	5	2.27%
	4	3889	+	TCCATGAAATTCTGTCCATAGAGGCTCC	9	2.73%	4	751	+	TCTGATATTGACTTGAAAATGCCTGGAC	4	1.82%
	5	4934	-	TCCTCTGGGCTGCCAATCTAAGCTCTTT	7	2.12%	5	756	+	TATTGACTTGAAAATGCCTGGACTGAGA	4	1.82%
						15.45%						15.00%

Size.	(A)	Pos.	Pol.	Sequence	Count.	% Total	(B)	Pos.	Pol.	Sequence	Count.	% Total
	1	1308	+	TAGAAATCTCTGAAGGATTCCAATCAAGT	29	8.03%	1	1308	+	TAGAAATCTCTGAAGGATTCCAATCAAGT	22	9.09%
	2	3988	+	TCTGGATCTTTGTAACCCAAGAAGGCATC	21	5.82%	2	2042	+	TAGAATCCTCCAAGAAGTTGAACTCAGGA	10	4.13%
29	3	2496	+	TCTGAAACCTCCCAATCCGCACGCATAAG	17	4.71%	3	5435	-	GGTCCCTAAGGTTGTCTTCTGCTCTATAC	8	3.31%
	4	2042	+	TAGAATCCTCCAAGAAGTTGAACTCAGGA	14	3.88%	4	527	+	TGGCGACAAATGAGAACATAGATCCGACT	7	2.89%
	5	4453	+	TCCATTGCTGCAGAGTCTGAAGACCTGAA	11	3.05%	5	3988	+	TCTGGATCTTTGTAACCCAAGAAGGCATC	7	2.89%
						25.48%						22.31%

Size.	(A)	Pos.	Pol.	Sequence	Count.	% Total	(B)	Pos.	Pol.	Sequence	Count.	% Total
	1	2496	+	TCTGAAACCTCCCAATCCGCACGCATAAGG	12	8.28%	1	2496	+	TCTGAAACCTCCCAATCCGCACGCATAAGG	8	7.21%
	2	4461	+	TGCAGAGTCTGAAGACCTGAACAAGTCACC	10	6.90%	2	802	+	TAAGATAGAATGTGTAGGTCCTGATGAGAA	6	5.41%
30	3	893	+	TCAGTCTGATGACATCTGACATATCACCCT	5	3.45%	3	893	+	TCAGTCTGATGACATCTGACATATCACCCT	6	5.41%
	4	3571	+	TGAACAATTCTTTCCTCTGCACCCATCACA	5	3.45%	4	4461	+	TGCAGAGTCTGAAGACCTGAACAAGTCACC	6	5.41%
	5	526	+	TTGGCGACAAATGAGAACATAGATCCGACT	3	2.07%	5	2041	+	TTAGAATCCTCCAAGAAGTTGAACTCAGGA	5	4.50%
						24.14%						27.93%

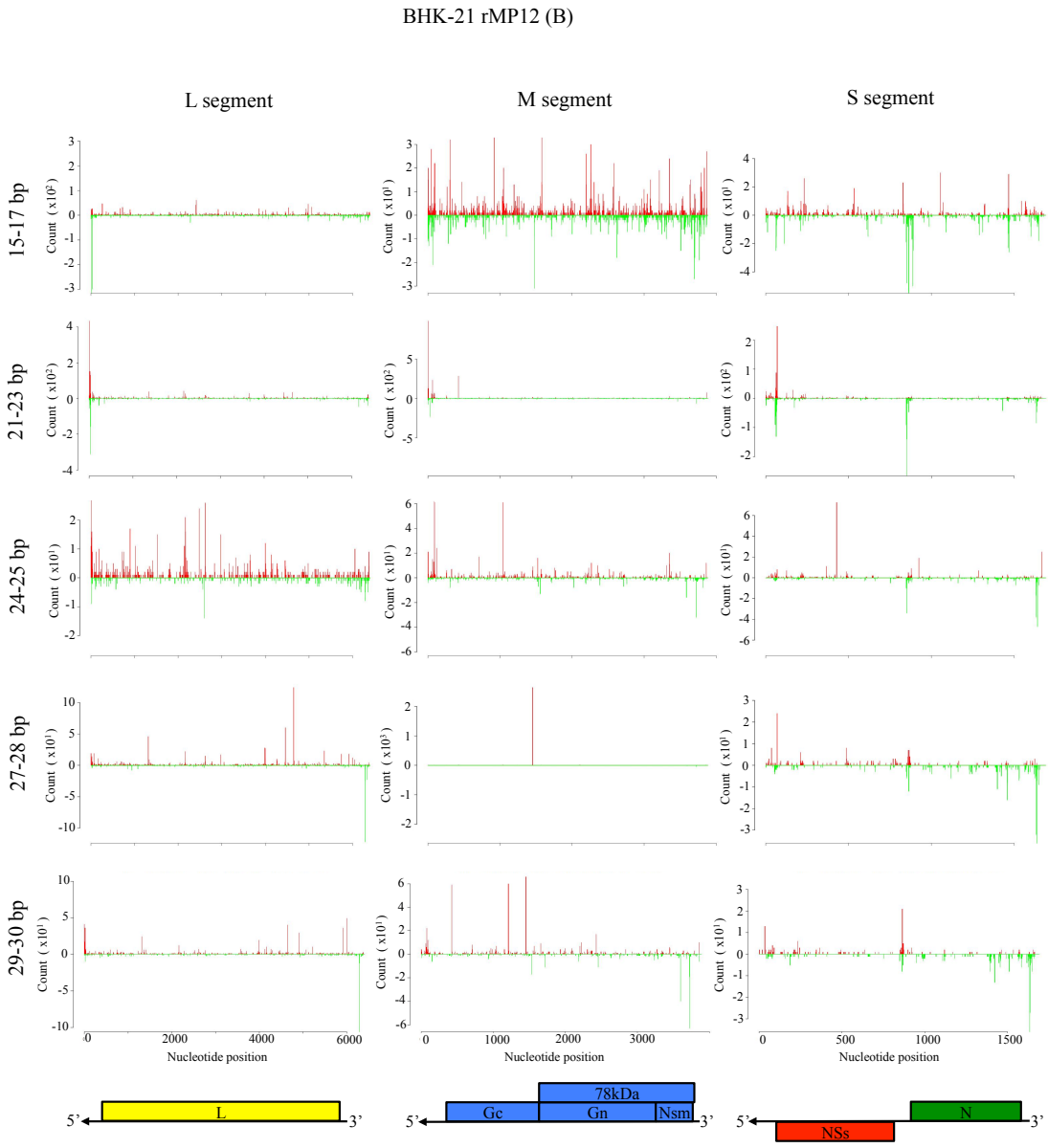

Figure 10-10: Duplicate mapping analysis plots for rMP12 and rMP12:S-Swap infected BHK-21 cells
Shown are density plots of aligned viRNA species of 15-17nt, 21nt, 24-25nt, 27-28nt, and 29-30nt aligning to the L, M, and S genome segments for the duplicate sample B BHK-21 cell infection. Upper plots (red) show alignments to genomic polarity (negative sense) and lower plots (green) to antigenomic polarity (positive sense). Also shown are the CDS for MP12 proteins encoded on the L (yellow), M (blue) and S (green and red) segments.

(A) rMP12 infected BHK-21 cells

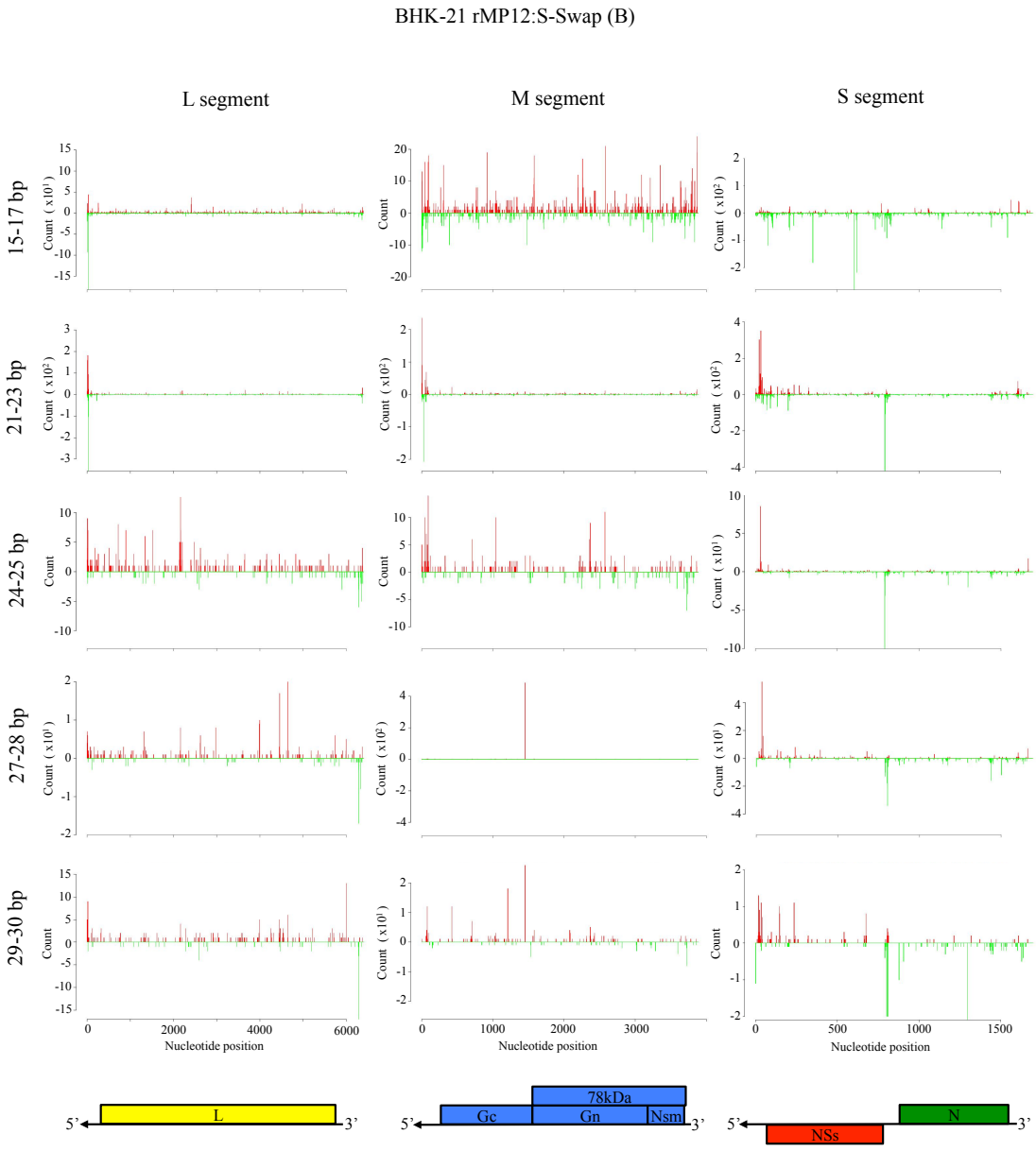

(B) rMP12:S-Swap infected BHK-21 cells

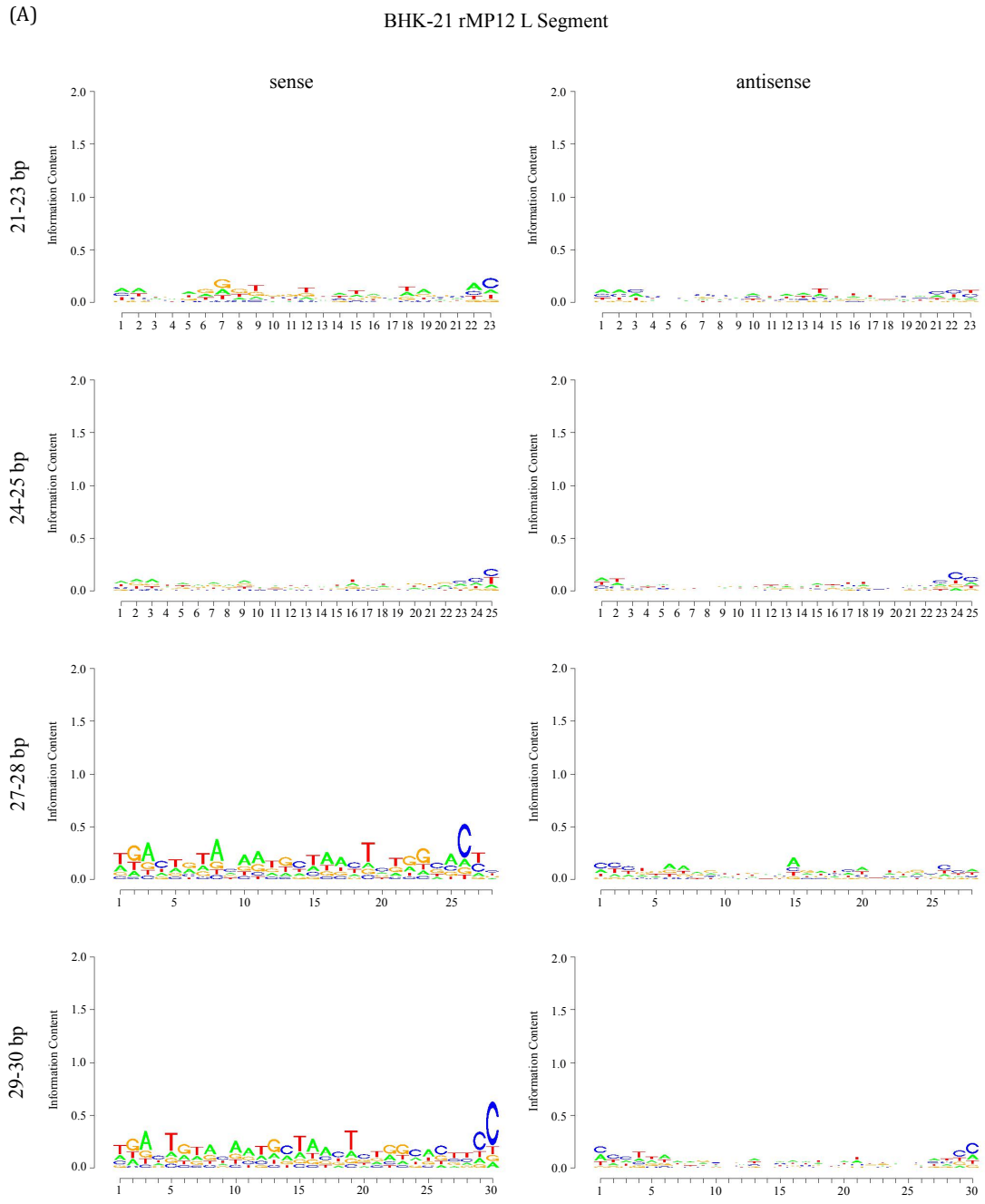

Figure 10-11: Logo analysis of viRNA species generated in rMP12 and rMP12:S-Segment infected BHK-21 cells.
Logo analysis of rMP12 or rMP12:S-Swap infected BHK-21 cells, with sense and antisense strand species analysis represented for the 21-23bp, 24-25bp, 27-28bp, and 29-30bp viRNA size classes. Presented are the (A) L, (B) M, and (C) S segment for rMP12 or the (D) S segment for rMP12:S-Swap infected cells.

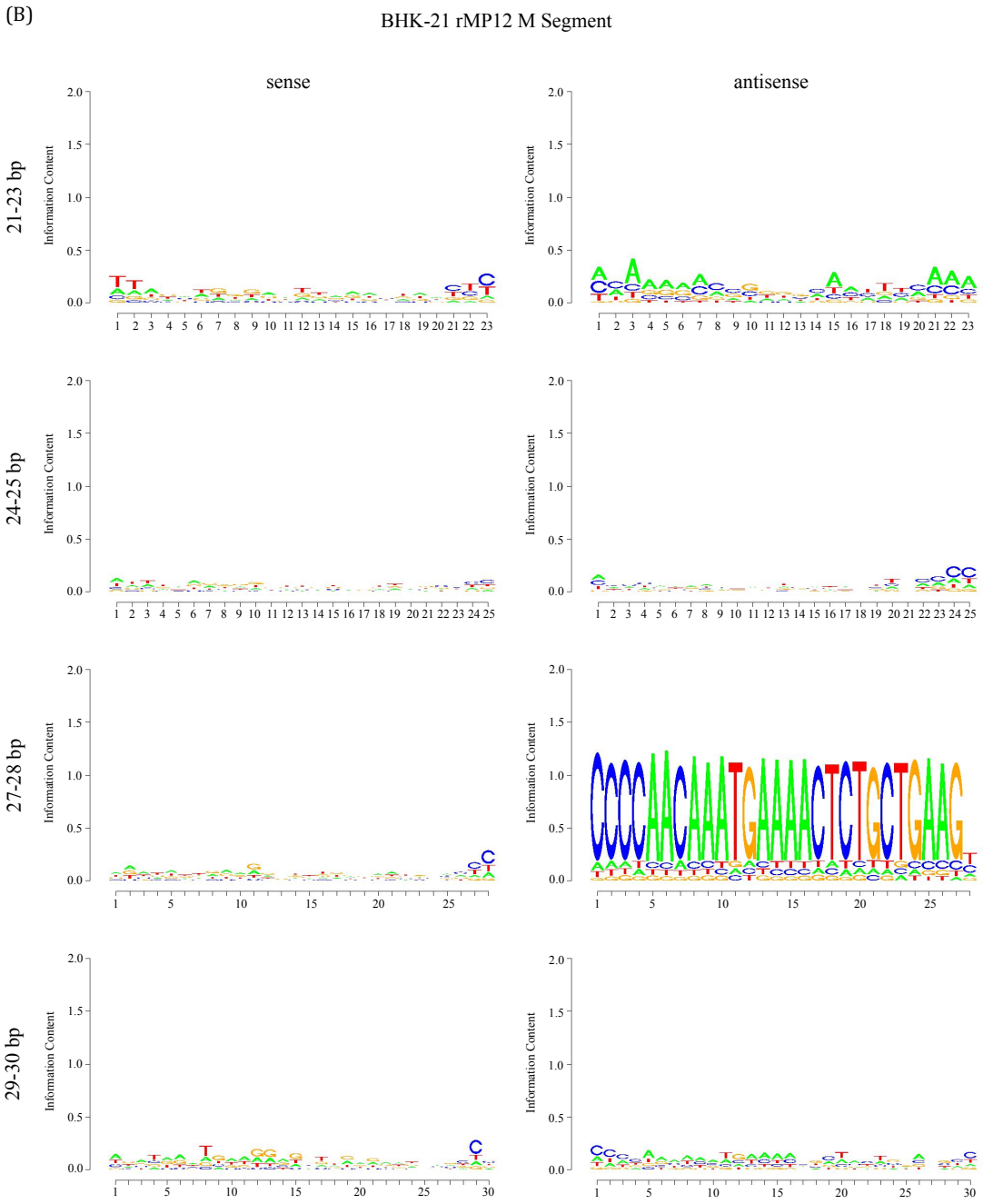
(B)
BHK-21 rMP12 M Segment
sense
antisense
21-23 bp
24-25 bp
27-28 bp
29-30 bp
Information Content

(C) BHK-21 rMP12 S Segment

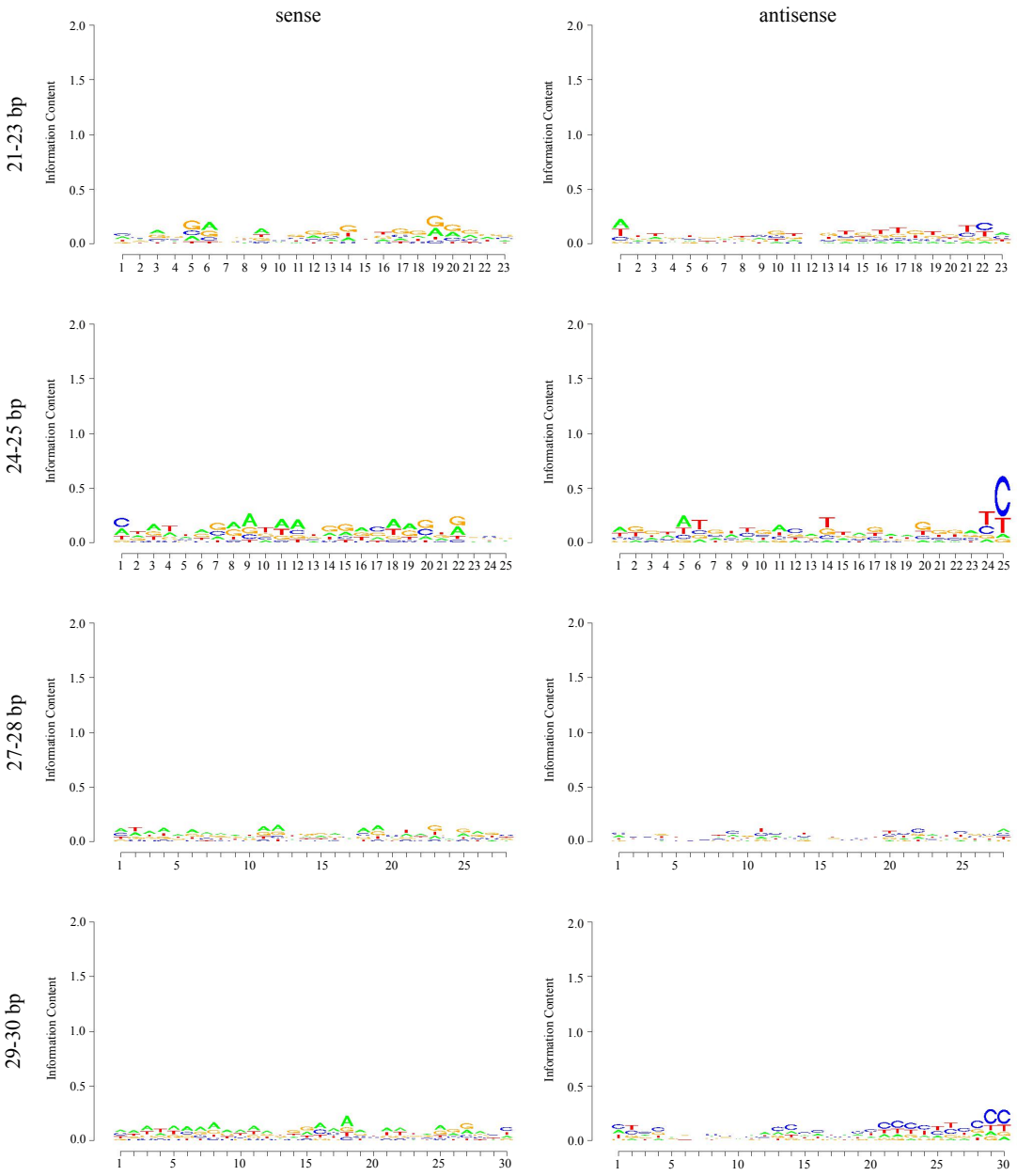

(D) BHK-21 rMP12:S-Swap S Segment

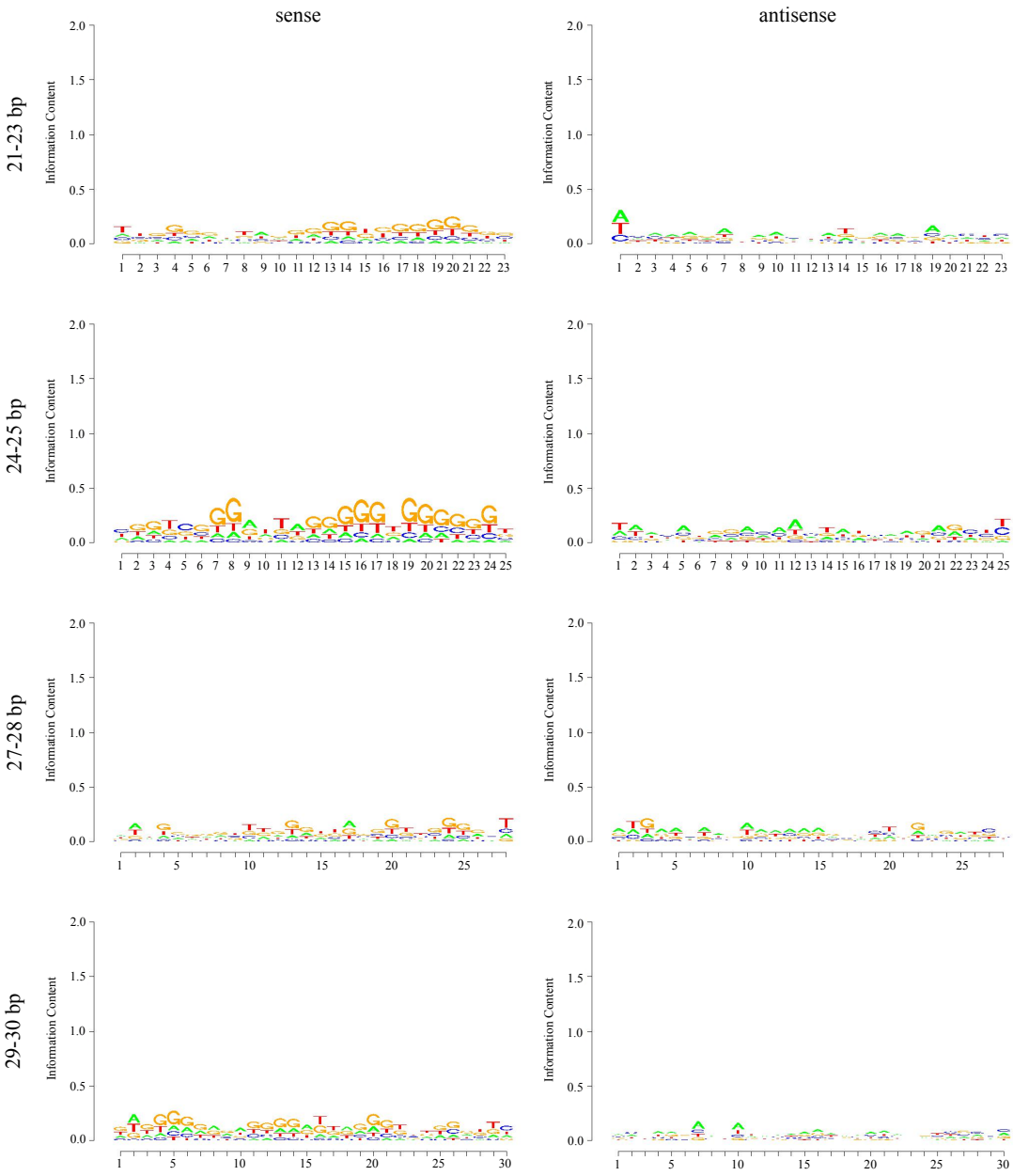

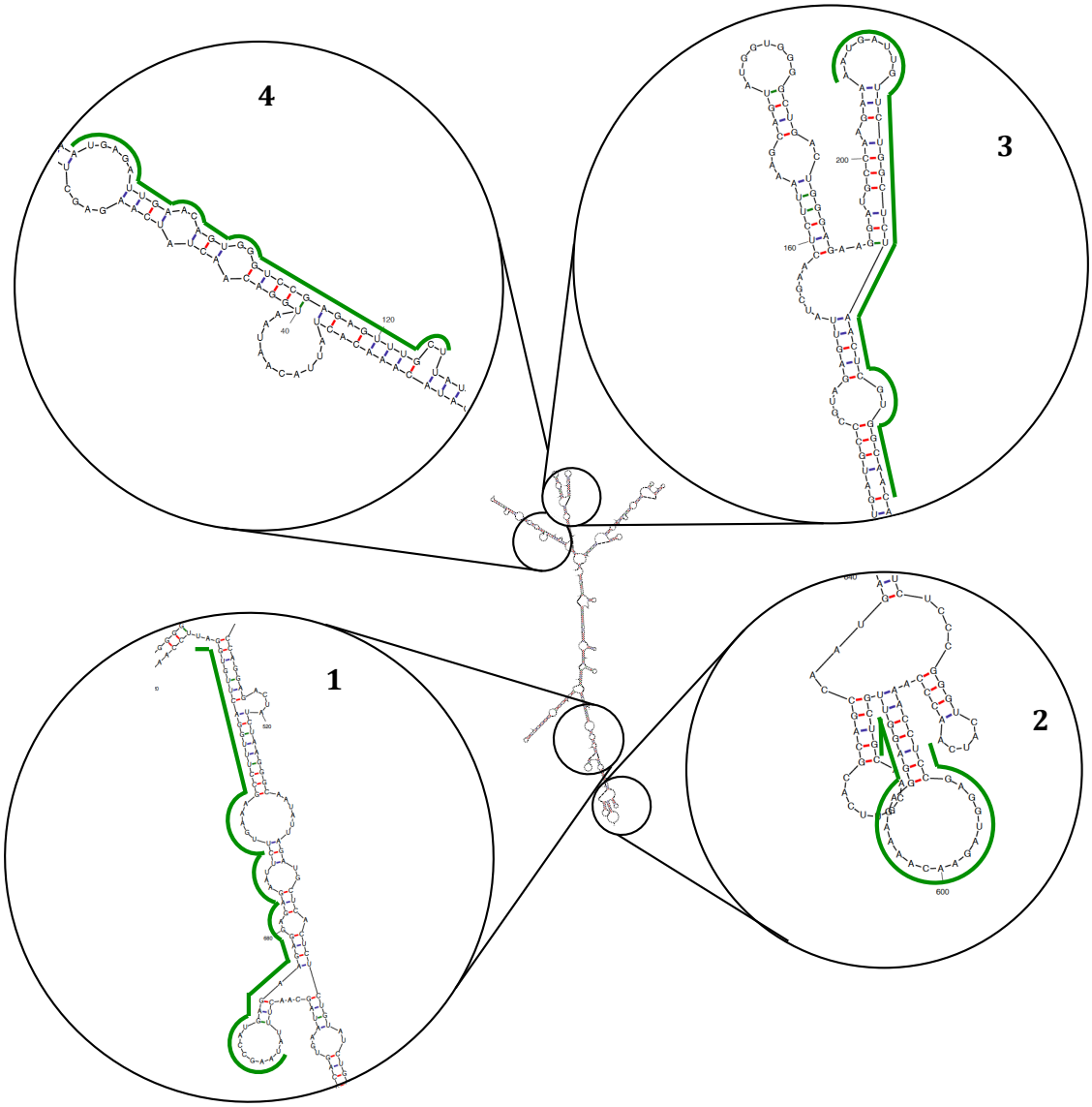

Figure 10-12: Location of 24-30 piRNA species on the rMP12 N mRNA transcript
RNA structure for rMP12 N mRNA was calculated using MFold web software. The four regions that had the highest concentration of piRNA alignments (see Figure 8-11.A) were identified (number 1-4) and are represented here by the green line.

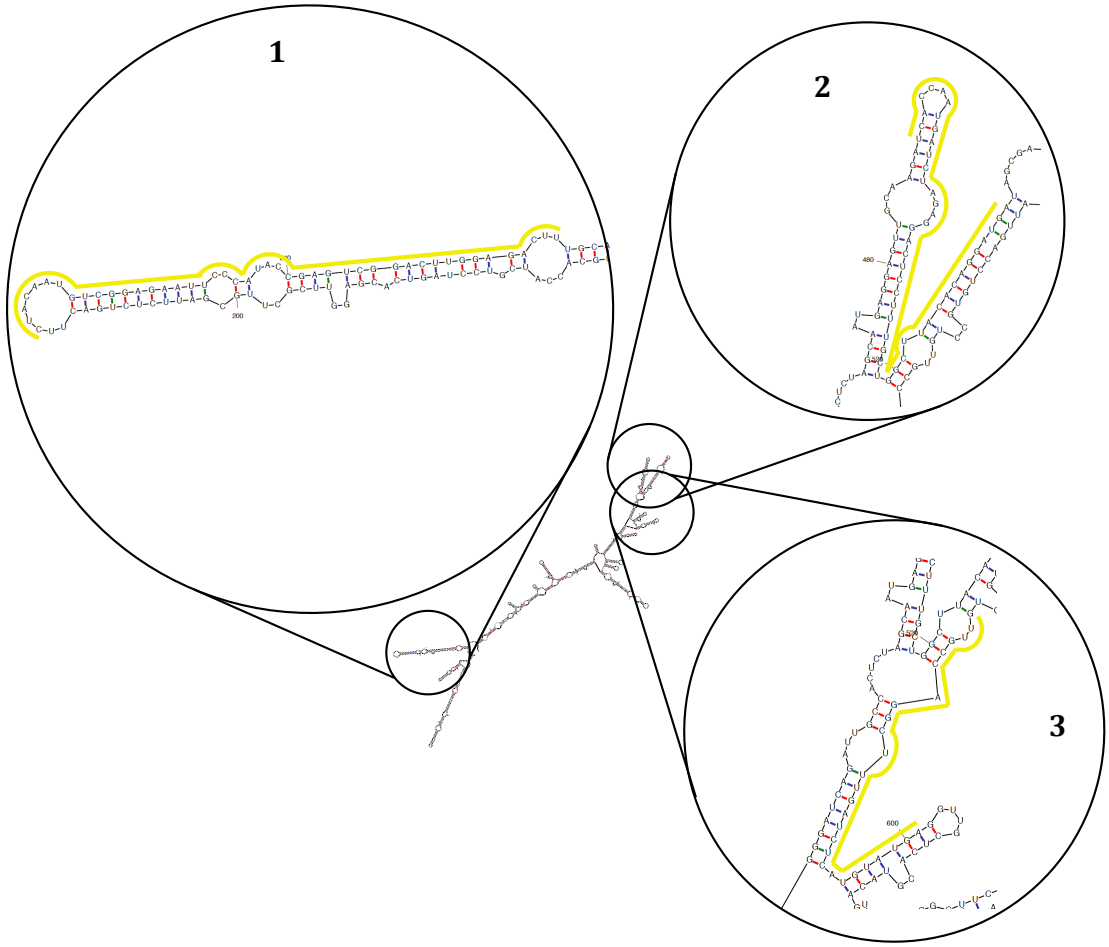

Figure 10-13: Location of the 24-30 piRNA species on rMP12:S-Swap NSs mRNA transcript
RNA secondary structure was calculated for rMP12:S-Swap mRNA using MFold web software. The three regions that had the highest concentration of piRNA alignments (see Figure 8-11B) were identified (numbers 1-3) and are represented here by the yellow lines.

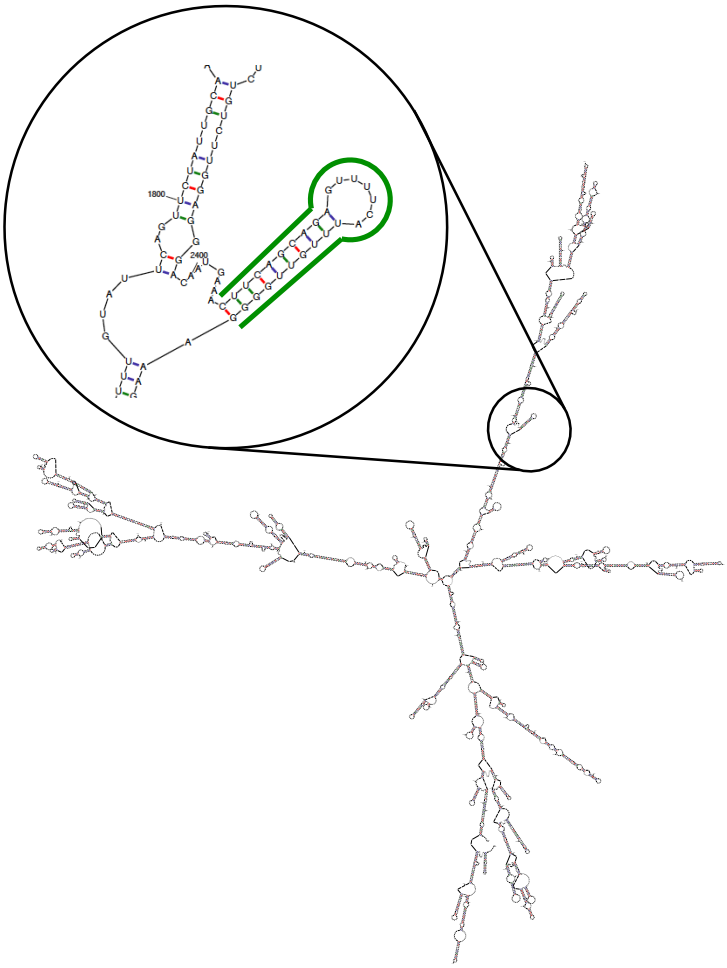

Figure 10-14: Location of 27 nt piRNA species on rMP12 M segment mRNA transcript
RNA secondary structure of rMP12 M segment mRNA was calculated using mFold web software. The location of the antigenome species of the 27 nt viRNA peak is shown in green, located between 2407-2433nt in antigenomic sense RNA.

Chapter 11
REFERENCES

11 References

Abdo-Salem, S., Waret-Szkuta, A., Roger, F., Olive, M.-M., Saeed, K. & Chevalier, V. (2011). Risk assessment of the introduction of Rift Valley fever from the Horn of Africa to Yemen via legal trade of small ruminants. *Trop Anim Health Prod* **43**, 471–480.

Afonso, A., Abrahantes, J. C., Conraths, F., Veldhuis, A., Elbers, A., Roberts, H., Van der Stede, Y., Méroc, E., Gache, K. & Richardson, J. (2014). The Schmallenberg virus epidemic in Europe-2011-2013. *Prev Vet Med*.

Al-Khuwaitir, T. S., Al-Moghairi, A. M., Sherbeeni, S. M. & Al-Ghamdi, A. S. (2004). Rift Valley fever hepatitis complicated by disseminated intravascular coagulation and hepatorenal syndrome. *Saudi Med J* **25**, 528–531.

Albariño, C. G., Bird, B. H., Chakrabarti, A. K., Dodd, K. A., Erickson, B. R. & Nichol, S. T. (2011). Efficient rescue of recombinant Lassa virus reveals the influence of S segment noncoding regions on virus replication and virulence. *J Virol* **85**, 4020–4024. American Society for Microbiology.

Anderson, G. W. & Smith, J. F. (1987). Immunoelectron microscopy of Rift Valley fever viral morphogenesis in primary rat hepatocytes. *Virology* **161**, 91–100.

Anderson, M. A. E., Gross, T. L., Myles, K. M. & Adelman, Z. N. (2010). Validation of novel promoter sequences derived from two endogenous ubiquitin genes in transgenic Aedes aegypti. *Insect Mol Biol* **19**, 441–449.

Aquino, V. H., Moreli, M. L. & Moraes Figueiredo, L. T. (2003). Analysis of oropouche virus L protein amino acid sequence showed the presence of an additional conserved region that could harbour an important role for the polymerase activity. *Arch Virol* **148**, 19–28. Springer-Verlag.

Atkinson, N. J., Witteveldt, J., Evans, D. J. & Simmonds, P. (2014). The influence of CpG and UpA dinucleotide frequencies on RNA virus replication and characterization of the innate cellular pathways underlying virus attenuation and enhanced replication. *Nucleic Acids Res* **42**, 4527–4545. Oxford University Press.

Attarzadeh-Yazdi, G., Fragkoudis, R., Chi, Y., Siu, R. W. C., Ulper, L., Barry, G., Rodriguez-Andres, J., Miller, A. A., Bouloy, M. & other authors. **(2009).** Cell-to-cell spread of the RNA interference response suppresses Semliki Forest virus (SFV) infection of mosquito cell cultures and cannot be antagonized by SFV. *J Virol* **83**, 5735–5748.

Azevedo, R. S. D. S., Nunes, M. R. T., Chiang, J. O., Bensabath, G., Vasconcelos, H. B., Pinto, A. Y. D. N., Martins, L. C., Monteiro, H. A. de O., Rodrigues, S. G. & Vasconcelos, P. F. D. C. (2007). Reemergence of Oropouche fever, northern Brazil. *Emerging Infect Dis* **13**, 912–915.

Barr, J. N., Rodgers, J. W. & Wertz, G. W. (2006). Identification of the Bunyamwera bunyavirus transcription termination signal. *J Gen Virol* **87**, 189–198. Society for General Microbiology.

Battisti, A. J., Chu, Y.-K., Chipman, P. R., Kaufmann, B., Jonsson, C. B. & Rossmann, M. G. (2011). Structural studies of Hantaan virus. *J Virol* **85**, 835–841.

Behura, S. K. & Severson, D. W. (2013). Codon usage bias: causative factors, quantification methods and genome□wide patterns: with emphasis on insect genomes. *Biological Reviews* **88**, 49–61. Blackwell Publishing Ltd.

Bembom, O. (2008). *seqLogo: Sequence logos for DNA sequence alignments*. R package version.

Benferhat, R., Josse, T., Albaud, B., Gentien, D., Mansuroglu, Z., Marcato, V., Souès, S., Le Bonniec, B., Bouloy, M. & Bonnefoy, E. (2012). Large-scale chromatin immunoprecipitation with promoter sequence microarray analysis of the interaction of the NSs protein of Rift Valley fever virus with regulatory DNA regions of the host genome. *J Virol* **86**, 11333–11344.

Bente, D. A., Forrester, N. L., Watts, D. M., McAuley, A. J., Whitehouse, C. A. & Bray, M. (2013). Crimean-Congo hemorrhagic fever: history, epidemiology, pathogenesis, clinical syndrome and genetic diversity. *Antiviral Res* **100**, 159–189.

Bernstein, E., Caudy, A. A., Hammond, S. M. & Hannon, G. J. (2001a). Role for a bidentate ribonuclease in the initiation step of RNA interference. *Nature* **409**, 363–366.

Bernstein, E., Denli, A. M. & Hannon, G. J. (2001b). The rest is silence. *RNA* **7**, 1509–1521.

Best, S. M. (2008). Viral subversion of apoptotic enzymes: escape from death row. *Annu Rev Microbiol* **62**, 171–192.

Billecocq, A., Gauliard, N., Le May, N., Elliott, R. M., Flick, R. & Bouloy, M. (2008). RNA polymerase I-mediated expression of viral RNA for the rescue of infectious virulent and avirulent Rift Valley fever viruses. *Virology* **378**, 377–384.

Billecocq, A., Spiegel, M., Vialat, P., Kohl, A., Weber, F., Bouloy, M. & Haller, O. (2004). NSs protein of Rift Valley fever virus blocks interferon production by inhibiting host gene transcription. *J Virol* **78**, 9798–9806.

Bird, B. H., Albariño, C. G., Hartman, A. L., Erickson, B. R., Ksiazek, T. G. & Nichol, S. T. (2008). Rift valley fever virus lacking the NSs and NSm genes is highly attenuated, confers protective immunity from virulent virus challenge, and allows for differential identification of infected and vaccinated animals. *J Virol* **82**, 2681–2691.

Bird, B. H., Ksiazek, T. G., Nichol, S. T. & Maclachlan, N. J. (2009). Rift Valley fever virus. *http://dxdoiorg/102460/javma2347883* **234**, 883–893. American Veterinary Medical Association 1931 North Meacham Road - Suite 100, Schaumburg, IL 60173 USA 847-925-8070 847-925-1329 avmajournals@avma.org.

Bird, B. H., Maartens, L. H., Campbell, S., Erasmus, B. J., Erickson, B. R., Dodd, K. A., Spiropoulou, C. F., Cannon, D., Drew, C. P. & other authors. **(2011).** Rift Valley fever virus vaccine lacking the NSs and NSm genes is safe, nonteratogenic, and confers protection from viremia, pyrexia, and abortion following challenge in adult and pregnant sheep. *J Virol* **85**, 12901–12909. American Society for Microbiology.

Bishop, D. H. (1986a). Ambisense RNA viruses: positive and negative polarities combined in RNA virus genomes. *Microbiol Sci* **3**, 183–187.

Bishop, D. H. (1986b). Ambisense RNA genomes of arenaviruses and phleboviruses. *Adv Virus Res* **31**, 1–51.

Bishop, D. H. (1989). Infection and coding strategies of arenaviruses, phleboviruses, and nairoviruses. *Rev Infect Dis* **11 Suppl 4**, S722–9.

Blackmore, C. G. M. & Grimstad, P. R. (2008). Evaluation of the eastern cottontail Sylvilagus floridanus as an amplifying vertebrate host for Cache Valley virus (Bunyaviridae) in Indiana. *J Wildl Dis* **44**, 188–192.

Blair, C. D. (2011). Mosquito RNAi is the major innate immune pathway controlling arbovirus infection and transmission. *Future Microbiology* **6**, 265–277.

Blakqori, G., Delhaye, S., Habjan, M., Blair, C. D., Sanchez-Vargas, I., Olson, K. E., Attarzadeh-Yazdi, G., Fragkoudis, R., Kohl, A. & other authors. **(2007).** La Crosse bunyavirus nonstructural protein NSs serves to suppress the type I interferon system of mammalian hosts. *J Virol* **81**, 4991–4999.

Blakqori, G., Lowen, A. C. & Elliott, R. M. (2012). The small genome segment of Bunyamwera orthobunyavirus harbours a single transcription-termination signal. *J Gen Virol* **93**, 1449–1455. Society for General Microbiology.

Blakqori, G. & Weber, F. (2005). Efficient cDNA-based rescue of La Crosse bunyaviruses expressing or lacking the nonstructural protein NSs. *J Virol* **79**, 10420–10428. American Society for Microbiology.

Bouloy, M., Janzen, C., Vialat, P., Khun, H., Pavlovic, J., Huerre, M. & Haller, O. (2001). Genetic evidence for an interferon-antagonistic function of rift valley fever virus nonstructural protein NSs. *J Virol* **75**, 1371–1377. American Society for Microbiology.

Bouloy, M. & Weber, F. (2010). Molecular biology of rift valley Fever virus. *Open Virol J* **4**, 8–14.

Bowden, T. A., Bitto, D., Mclees, A., Yeromonahos, C., Elliott, R. M. & Huiskonen, J. T. (2013). Orthobunyavirus ultrastructure and the curious tripodal glycoprotein spike. *PLoS Pathog* **9**, e1003374 (T. C. Pierson, Ed.). Public Library of Science.

Bowers, D. F., Coleman, C. G. & Brown, D. T. (2003). Sindbis virus-associated pathology in Aedes albopictus (Diptera: Culicidae). *J Med Entomol* **40**, 698–705.

Brackney, D. E., Scott, J. C., Sagawa, F., Woodward, J. E., Miller, N. A., Schilkey, F. D., Mudge, J., Wilusz, J., Paskewitz, S. M. & other authors. **(2010).** C6/36 Aedes albopictus cells have a dysfunctional antiviral RNA interference response. *PLoS Negl Trop Dis* **4**, e856.

Brennan, B., Li, P. & Elliott, R. M. (2011a). Generation and characterization of a recombinant Rift Valley fever virus expressing a V5 epitope-tagged RNA-dependent RNA polymerase. *J Gen Virol* **92**, 2906–2913. Society for General Microbiology.

Brennan, B., Welch, S. R. & Elliott, R. M. (2014). The consequences of reconfiguring the ambisense S genome segment of Rift Valley fever virus on viral replication in mammalian and mosquito cells and for genome packaging. *PLoS Pathog* **10**, e1003922.

Brennan, B., Welch, S. R., McLees, A. & Elliott, R. M. (2011b). Creation of a recombinant Rift Valley fever virus with a two-segmented genome. *J Virol* **85**, 10310–10318.

Brennan, B., Welch, S. R., Mclees, A. & Elliott, R. M. (2011c). Creation of a recombinant Rift Valley fever virus with a two-segmented genome. *J Virol* **85**, 10310–10318.

Brennecke, J., Aravin, A. A., Stark, A., Dus, M., Kellis, M., Sachidanandam, R. & Hannon, G. J. (2007). Discrete small RNA-generating loci as master regulators of transposon activity in Drosophila. *Cell* **128**, 1089–1103.

Bridgen, A. & Elliott, R. M. (1996). Rescue of a segmented negative-strand RNA virus entirely from cloned complementary DNAs. *Proc Natl Acad Sci U S A* **93**, 15400–15404.

Bridgen, A., Weber, F., Fazakerley, J. K. & Elliott, R. M. (2001). Bunyamwera bunyavirus nonstructural protein NSs is a nonessential gene product that contributes to viral pathogenesis. *Proc Natl Acad Sci U S A* **98**, 664–669.

Brown, D. T. (1984). *Alphavirus growth in cultured vertebrate and invertebrate cells*. Special publications of the Society for General ….

Buchholz, U. J., Finke, S. & Conzelmann, K. K. (1999). Generation of bovine respiratory syncytial virus (BRSV) from cDNA: BRSV NS2 is not essential for virus replication in tissue culture, and the human RSV leader region acts as a functional BRSV genome promoter. *J Virol* **73**, 251–259.

Campbell, C. L., Black, W. C., Hess, A. M. & Foy, B. D. (2008a). Comparative genomics of small RNA regulatory pathway components in vector mosquitoes. *BMC Genomics* **9**, 425.

Campbell, C. L., Keene, K. M., Brackney, D. E., Olson, K. E., Blair, C. D., Wilusz, J. & Foy, B. D. (2008b). Aedes aegypti uses RNA interference in defense against Sindbis virus infection. *BMC Microbiol* **8**, 47.

Caplen, H., Peters, C. J. & Bishop, D. H. (1985). Mutagen-directed attenuation of Rift Valley fever virus as a method for vaccine development. *J Gen Virol* **66 (Pt 10)**, 2271–2277.

Capodagli, G. C., McKercher, M. A., Baker, E. A., Masters, E. M., Brunzelle, J. S. & Pegan, S. D. (2011). Structural analysis of a viral ovarian tumor domain protease from the Crimean-Congo hemorrhagic fever virus in complex with covalently bonded ubiquitin. *J Virol* **85**, 3621–3630. American Society for Microbiology.

Carlini, D. B. & Stephan, W. (2003). In vivo introduction of unpreferred synonymous codons into the Drosophila Adh gene results in reduced levels of ADH protein. *Genetics* **163**, 239–243.

Carnec, X., Baize, S., Reynard, S., Diancourt, L., Caro, V., Tordo, N. & Bouloy, M. (2011). Lassa virus nucleoprotein mutants generated by reverse genetics induce a robust type I interferon response in human dendritic cells and macrophages. *J Virol* **85**, 12093–12097. American Society for Microbiology.

Carthew, R. W. (2001). Gene silencing by double-stranded RNA. *Curr Opin Cell Biol* **13**, 244–248.

Cheng, X., Virk, N., Chen, W., Ji, S., Ji, S., Sun, Y. & Wu, X. (2013). CpG usage in RNA viruses: data and hypotheses. *PLoS ONE* **8**, e74109 (R. D. Burk, Ed.). Public Library of Science.

Chevalier, V., la Rocque, de, S., Baldet, T., Vial, L. & Roger, F. (2004). Epidemiological processes involved in the emergence of vector-borne diseases: West Nile fever, Rift Valley fever, Japanese encephalitis and Crimean-Congo haemorrhagic fever. *Rev - Off Int Epizoot* **23**, 535–555.

Chevalier, V., Pépin, M., Plée, L. & Lancelot, R. (2010). Rift Valley fever--a threat for Europe? *Euro Surveill* **15**, 19506.

Choi, Y., Kwon, Y.-C., Kim, S.-I., Park, J.-M., Lee, K.-H. & Ahn, B.-Y. (2008). A hantavirus causing hemorrhagic fever with renal syndrome requires gC1qR/p32 for efficient cell binding and infection. *Virology* **381**, 178–183.

Chotkowski, H. L., Ciota, A. T., Jia, Y., Puig-Basagoiti, F., Kramer, L. D., Shi, P.-Y. & Glaser, R. L. (2008). West Nile virus infection of Drosophila melanogaster induces a protective RNAi response. *Virology* **377**, 197–206.

Christophides, G. K., Zdobnov, E. M., Barillas-Mury, C., Birney, E., Blandin, S., Blass, C., Brey, P. T., Collins, F. H., Danielli, A. & other authors. **(2002).** Immunity-related genes and gene families in Anopheles gambiae. *Science* **298**, 159–165.

Ciota, A. T. & Kramer, L. D. (2010). Insights into arbovirus evolution and adaptation from experimental studies. *Viruses* **2**, 2594–2617. Molecular Diversity Preservation International.

Clarke, T. E. & Clem, R. J. (2003). Insect defenses against virus infection: the role of apoptosis. *Int Rev Immunol* **22**, 401–424.

Condreay, L. D. & Brown, D. T. (1986). Exclusion of superinfecting homologous virus by Sindbis virus-infected Aedes albopictus (mosquito) cells. *J Virol* **58**, 81–86.

Condreay, L. D. & Brown, D. T. (1988). Suppression of RNA synthesis by a specific antiviral activity in Sindbis virus-infected Aedes albopictus cells. *J Virol* **62**, 346–348.

Crabtree, M. B., Kent Crockett, R. J., Bird, B. H., Nichol, S. T., Erickson, B. R., Biggerstaff, B. J., Horiuchi, K. & Miller, B. R. (2012). Infection and transmission of Rift Valley fever viruses lacking the NSs and/or NSm genes in mosquitoes: potential role for NSm in mosquito infection. *PLoS Negl Trop Dis* **6**, e1639 (M. J. Turell, Ed.). Public Library of Science.

Crescenzo-Chaigne, B. & van der Werf, S. (2007). Rescue of influenza C virus from recombinant DNA. *J Virol* **81**, 11282–11289. American Society for Microbiology.

Daubney, R. & Hudson, J. (1931). Enzootic hepatitis or Rift Valley fever. An undescribed virus disease of sheep cattle and man from East Africa. *The Journal of Pathology* ….

Davies, F. G. & Karstad, L. (1981). Experimental infection of the African buffalo with the virus of Rift Valley fever. *Trop Anim Health Prod* **13**, 185–188.

Davies, F. G. & Martin, V. (2003). *Recognizing rift valley fever*.

Di Bonito, P., Nicoletti, L., Mochi, S., Accardi, L., Marchi, A. & Giorgi, C. (1999). Immunological characterization of Toscana virus proteins. *Arch Virol* **144**, 1947–1960.

Dias, A., Bouvier, D., Crépin, T., McCarthy, A. A., Hart, D. J., Baudin, F., Cusack, S. & Ruigrok, R. W. H. (2009). The cap-snatching endonuclease of influenza virus polymerase resides in the PA subunit. *Nature* **458**, 914–918.

Donald, C. L., Kohl, A. & Schnettler, E. (2012). New Insights into Control of Arbovirus Replication and Spread by Insect RNA Interference Pathways. *Insects 2012, Vol 3, Pages 511-531* **3**, 511–531. Molecular Diversity Preservation International.

Dostert, C., Jouanguy, E., Irving, P., Troxler, L., Galiana-Arnoux, D., Hetru, C., Hoffmann, J. A. & Imler, J.-L. (2005). The Jak-STAT signaling pathway is required but not sufficient for the antiviral response of drosophila. *Nat Immunol* **6**, 946–953.

Dungu, B., Louw, I., Lubisi, A., Hunter, P., Teichman, von, B. F. & Bouloy, M. (2010). Evaluation of the efficacy and safety of the Rift Valley Fever Clone 13 vaccine in sheep. *Vaccine* **28**, 4581–4587.

Dunn, E. F., Pritlove, D. C., Jin, H. & Elliott, R. M. (1995). Transcription of a recombinant bunyavirus RNA template by transiently expressed bunyavirus proteins. *Virology* **211**, 133–143.

Eifan, S. A. & Elliott, R. M. (2009). Mutational analysis of the Bunyamwera orthobunyavirus nucleocapsid protein gene. *J Virol* **83**, 11307–11317.

Elliott, R. M. (1996). *The Bunyaviridae.* Plenum Press.

Elliott, R. M. & Wilkie, M. L. (1986). Persistent infection of *Aedes albopictus* C6/36 cells by Bunyamwera virus. *Virology*.

Elliott, R. M. (2009). Bunyaviruses and climate change. *Clin Microbiol Infect* **15**, 510–517.

Elliott, R. M. (2012). Bunyavirus Reverse Genetics and Applications to Studying Interactions with Host Cells. In *Reverse Genetics of RNA Viruses*, Applications and Perspectives, pp. 200–223. Chichester, UK: John Wiley & Sons, Ltd.

Elliott, R. M., Blakqori, G., van Knippenberg, I. C., Koudriakova, E., Li, P., Mclees, A., Shi, X. & Szemiel, A. M. (2013). Establishment of a reverse genetics system for Schmallenberg virus, a newly emerged orthobunyavirus in Europe. *J Gen Virol* **94**, 851–859. Society for General Microbiology.

Elliott, R. M. & Schmaljohn, C. (2013). *Bunyaviridae*. In *Fields Virology*, 6 edn. Lippincott Williams & Wilkins.

Emonet, S. F., Seregin, A. V., Yun, N. E., Poussard, A. L., Walker, A. G., la Torre, de, J. C. & Paessler, S. (2011). Rescue from cloned cDNAs and in vivo characterization of recombinant pathogenic Romero and live-attenuated Candid #1 strains of Junin virus, the causative agent of Argentine hemorrhagic fever disease. *J Virol* **85**, 1473–1483. American Society for Microbiology.

Fazakerley, J. K., Gonzalez-Scarano, F., Strickler, J., Dietzschold, B., Karush, F. & Nathanson, N. (1988). Organization of the middle RNA segment of snowshoe hare Bunyavirus. *Virology* **167**, 422–432.

Firtel, R. A. (1981). Multigene families encoding actin and tubulin. *Cell* **24**, 6–7.

Flint, S. J., Enquist, L. W. & Racaniello, V. R. (2008). *Principles of Virology 2 Volume Set*.

Fodor, E., Devenish, L., Engelhardt, O. G., Palese, P., Brownlee, G. G. & García-Sastre, A. (1999). Rescue of influenza A virus from recombinant DNA. *J Virol* **73**, 9679–9682.

Fontana, J., López-Montero, N., Elliott, R. M., Fernández, J. J. & Risco, C. (2008). The unique architecture of Bunyamwera virus factories around the Golgi complex. *Cell Microbiol* **10**, 2012–2028. Blackwell Publishing Ltd.

Fontenille, D., Traore-Lamizana, M., Diallo, M., Thonnon, J., Digoutte, J. P. & Zeller, H. G. (1998). New vectors of Rift Valley fever in West Africa. *Emerging Infect Dis* **4**, 289–293.

Foundation for the National Institutes of Health. **(2010).** *Progress and Prospects for the Use of Genetically Modified Mosquitoes to Inhibit Disease Transmission*.

Fragkoudis, R., Attarzadeh-Yazdi, G., Nash, A. A., Fazakerley, J. K. & Kohl, A. (2009). Advances in dissecting mosquito innate immune responses to arbovirus infection. *J Gen Virol* **90**, 2061–2072. Society for General Microbiology.

Fragkoudis, R., Chi, Y., Siu, R. W. C., Barry, G., Attarzadeh-Yazdi, G., Merits, A., Miller, A. A., Fazakerley, J. K. & Kohl, A. (2008). Semliki Forest virus strongly reduces mosquito host defence signaling. *Insect Mol Biol* **17**, 647–656.

Freiberg, A. N., Sherman, M. B., Morais, M. C., Holbrook, M. R. & Watowich, S. J. (2008). Three-dimensional organization of Rift Valley fever virus revealed by cryoelectron tomography. *J Virol* **82**, 10341–10348.

Frias-Staheli, N., Giannakopoulos, N. V., Kikkert, M., Taylor, S. L., Bridgen, A., Paragas, J., Richt, J. A., Rowland, R. R., Schmaljohn, C. S. & other authors. **(2007).** Ovarian tumor domain-containing viral proteases evade ubiquitin- and ISG15-dependent innate immune responses. *Cell Host Microbe* **2**, 404–416.

Fuerst, T. R., Niles, E. G., Studier, F. W. & Moss, B. (1986). Eukaryotic transient-expression system based on recombinant vaccinia virus that synthesizes bacteriophage T7 RNA polymerase. *Proc Natl Acad Sci U S A* **83**, 8122–8126.

Galiana-Arnoux, D., Dostert, C., Schneemann, A., Hoffmann, J. A. & Imler, J.-L. (2006). Essential function in vivo for Dicer-2 in host defense against RNA viruses in drosophila. *Nat Immunol* **7**, 590–597.

Gao, Q., Chou, Y.-Y., Doğanay, S., Vafabakhsh, R., Ha, T. & Palese, P. (2012). The influenza A virus PB2, PA, NP, and M segments play a pivotal role during genome packaging. *J Virol* **86**, 7043–7051.

Gargan, T. P., Jupp, P. G. & Novak, R. J. (1988). Panveld oviposition sites of floodwater Aedes mosquitoes and attempts to detect transovarial transmission of Rift Valley fever virus in South Africa. *Med Vet Entomol* **2**, 231–236.

Gauliard, N., Billecocq, A., Flick, R. & Bouloy, M. (2006). Rift Valley fever virus noncoding regions of L, M and S segments regulate RNA synthesis. *Virology* **351**, 170–179.

Gavrilovskaya, I. N., Brown, E. J., Ginsberg, M. H. & Mackow, E. R. (1999). Cellular entry of hantaviruses which cause hemorrhagic fever with renal syndrome is mediated by beta3 integrins. *J Virol* **73**, 3951–3959.

Gavrilovskaya, I. N., Shepley, M., Shaw, R., Ginsberg, M. H. & Mackow, E. R. (1998). beta3 Integrins mediate the cellular entry of hantaviruses that cause respiratory failure. *Proc Natl Acad Sci U S A* **95**, 7074–7079.

Gentleman, R. C., Carey, V. J., Bates, D. M., Ben Bolstad, Dettling, M., Dudoit, S., Ellis, B., Gautier, L., Ge, Y. & other authors. **(2004).** *Bioconductor: open software development for computational biology and bioinformatics*. *Genome Biol*. BioMed Central Ltd.

Gentsch, J., Bishop, D. H. & Obijeski, J. F. (1977). The virus particle nucleic acids and proteins of four bunyaviruses. *J Gen Virol* **34**, 257–268.

Gergova, I., Kunchev, M. & Kamarinchev, B. (2012). Crimean-Congo hemorrhagic fever virus-tick survey in endemic areas in Bulgaria. *J Med Virol* **84**, 608–614. Wiley Subscription Services, Inc., A Wiley Company.

Gerrard, S. R., Bird, B. H., Albariño, C. G. & Nichol, S. T. (2007). The NSm proteins of Rift Valley fever virus are dispensable for maturation, replication and infection. *Virology* **359**, 459–465.

Gerrard, S. R. & Nichol, S. T. (2007). Synthesis, proteolytic processing and complex formation of N-terminally nested precursor proteins of the Rift Valley fever virus glycoproteins. *Virology* **357**, 124–133.

Gillies, S. & Stollar, V. (1982). Protein synthesis in lysates of Aedes albopictus cells infected with vesicular stomatitis virus. *Mol Cell Biol* **2**, 1174–1186.

Giorgi, C., Accardi, L., Nicoletti, L., Gro, M. C., Takehara, K., Hilditch, C., Morikawa, S. & Bishop, D. H. (1991). Sequences and coding strategies of the S RNAs of Toscana and Rift Valley fever viruses compared to those of Punta Toro, Sicilian Sandfly fever, and Uukuniemi viruses. *Virology* **180**, 738–753.

Girard, Y. A., Popov, V., Wen, J., Han, V. & Higgs, S. (2005). Ultrastructural study of West Nile virus pathogenesis in Culex pipiens quinquefasciatus (Diptera: Culicidae). *J Med Entomol* **42**, 429–444.

Gould, E. A. & Higgs, S. (2009). Impact of climate change and other factors on emerging arbovirus diseases. *Trans R Soc Trop Med Hyg* **103**, 109–121. Oxford University Press.

Grobbelaar, A. A., Weyer, J., Leman, P. A., Kemp, A., Paweska, J. T. & Swanepoel, R. (2011). Molecular epidemiology of Rift Valley fever virus. *Emerging Infect Dis* **17**, 2270–2276.

Gu, S. H., Lim, B. K., Kadjo, B., Arai, S., Kim, J.-A., Nicolas, V., Lalis, A., Denys, C., Cook, J. A. & other authors. **(2014).** Molecular phylogeny of hantaviruses harbored by insectivorous bats in Côte d'Ivoire and Vietnam. *Viruses* **6**, 1897–1910. Multidisciplinary Digital Publishing Institute.

Guillet, P., Germain, M. C., Giacomini, T., Chandre, F., Akogbeto, M., Faye, O., Kone, A., Manga, L. & Mouchet, J. (1998). Origin and prevention of airport malaria in France. *Trop Med Int Health* **3**, 700–705.

Gunning, P., Mohun, T., Ng, S.-Y., Ponte, P. & Kedes, L. (1984). Evolution of the human sarcomeric-actin genes: Evidence for units of selection within the 3′ untranslated regions of the mRNAs. *J Mol Evol* **20**, 202–214. Eukaryotic Genes: Their Structure.

Habjan, M., Penski, N., Spiegel, M. & Weber, F. (2008). T7 RNA polymerase-dependent and -independent systems for cDNA-based rescue of Rift Valley fever virus. *J Gen Virol* **89**, 2157–2166. Society for General Microbiology.

Habjan, M., Pichlmair, A., Elliott, R. M., Overby, A. K., Glatter, T., Gstaiger, M., Superti-Furga, G., Unger, H. & Weber, F. (2009a). NSs protein of rift valley fever virus induces the specific degradation of the double-stranded RNA-dependent protein kinase. *J Virol* **83**, 4365–4375. American Society for Microbiology.

Habjan, M., Pichlmair, A., Elliott, R. M., Overby, A. K., Glatter, T., Gstaiger, M., Superti-Furga, G., Unger, H. & Weber, F. (2009b). NSs protein of rift valley fever virus induces the specific degradation of the double-stranded RNA-dependent protein kinase. *J Virol* **83**, 4365–4375.

Hacker, J. K. & Hardy, J. L. (1997). Adsorptive endocytosis of California encephalitis virus into mosquito and mammalian cells: a role for G1. *Virology* **235**, 40–47.

Hacker, J. K., Volkman, L. E. & Hardy, J. L. (1995). Requirement for the G1 protein of California encephalitis virus in infection in vitro and in vivo. *Virology* **206**, 945–953.

Heng, X., Kharytonchyk, S., Garcia, E. L., Lu, K., Divakaruni, S. S., LaCotti, C., Edme, K., Telesnitsky, A. & Summers, M. F. (2012). Identification of a minimal region of the HIV-1 5'-leader required for RNA dimerization, NC binding, and packaging. *J Mol Biol* **417**, 224–239.

Hewlett, M. J. & Chiu, W. (1991). Virion Structure. In *Bunyaviridae*, Current Topics in Microbiology and Immunology, pp. 79–90. Berlin, Heidelberg: Springer Berlin Heidelberg.

Hewlett, M. J., Pettersson, R. F. & Baltimore, D. (1977). Circular forms of Uukuniemi virion RNA: an electron microscopic study. *J Virol* **21**, 1085–1093.

Hoffmann, E., Neumann, G., Kawaoka, Y., Hobom, G. & Webster, R. G. (2000). A DNA transfection system for generation of influenza A virus from eight plasmids. *Proc Natl Acad Sci U S A* **97**, 6108–6113. National Acad Sciences.

Hoffmann, E., Mahmood, K., Yang, C.-F., Webster, R. G., Greenberg, H. B. & Kemble, G. (2002). Rescue of influenza B virus from eight plasmids. *Proc Natl Acad Sci U S A* **99**, 11411–11416. National Acad Sciences.

Hofmann, H., Li, X., Zhang, X., Liu, W., Kühl, A., Kaup, F., Soldan, S. S., González-Scarano, F., Weber, F. & other authors. **(2013).** Severe fever with thrombocytopenia virus glycoproteins are targeted by neutralizing antibodies and can use DC-SIGN as a receptor for pH-dependent entry into human and animal cell lines. *J Virol* **87**, 4384–4394. American Society for Microbiology.

Holt, R. A., Subramanian, G. M., Halpern, A., Sutton, G. G., Charlab, R., Nusskern, D. R., Wincker, P., Clark, A. G., Ribeiro, J. M. C. & other authors. **(2002).** The genome sequence of the malaria mosquito Anopheles gambiae. *Science* **298**, 129–149.

Honig, J. E., Osborne, J. C. & Nichol, S. T. (2004). Crimean-Congo hemorrhagic fever virus genome L RNA segment and encoded protein. *Virology* **321**, 29–35.

Huang, N. E., Lin, C. H., Lin, Y. S. & Yu, W. C. Y. (2003). Modulation of YY1 activity by SAP30. *Biochem Biophys Res Commun* **306**, 267–275.

Huiskonen, J. T., Hepojoki, J., Laurinmäki, P., Vaheri, A., Lankinen, H., Butcher, S. J. & Grünewald, K. (2010). Electron cryotomography of Tula hantavirus suggests a unique assembly paradigm for enveloped viruses. *J Virol* **84**, 4889–4897. American Society for Microbiology.

Huiskonen, J. T., Overby, A. K., Weber, F. & Grünewald, K. (2009). Electron cryo-microscopy and single-particle averaging of Rift Valley fever virus: evidence for GN-GC glycoprotein heterodimers. *J Virol* **83**, 3762–3769. American Society for Microbiology.

Hunter, P., Erasmus, B. J. & Vorster, J. H. (2002). Teratogenicity of a mutagenised Rift Valley fever virus (MVP 12) in sheep. *Onderstepoort J Vet Res* **69**, 95–98.

Igarashi, A. (1978). Isolation of a Singh's Aedes albopictus cell clone sensitive to Dengue and Chikungunya viruses. *J Gen Virol* **40**, 531–544.

Ihara, T., Akashi, H. & Bishop, D. H. (1984). Novel coding strategy (ambisense genomic RNA) revealed by sequence analyses of Punta Toro Phlebovirus S RNA. *Virology* **136**, 293–306.

Ikegami, T. & Makino, S. (2009). Rift valley fever vaccines. *Vaccine* **27 Suppl 4**, D69–72.

Ikegami, T. & Makino, S. (2011). The Pathogenesis of Rift Valley Fever. *Viruses* **3**, 493–519. Molecular Diversity Preservation International.

Ikegami, T., Narayanan, K., Won, S., Kamitani, W., Peters, C. J. & Makino, S. (2009a). Rift Valley fever virus NSs protein promotes post-transcriptional downregulation of protein kinase PKR and inhibits eIF2alpha phosphorylation. *PLoS Pathog* **5**, e1000287.

Ikegami, T., Narayanan, K., Won, S., Kamitani, W., Peters, C. J. & Makino, S. (2009b). Dual functions of Rift Valley fever virus NSs protein: inhibition of host mRNA transcription and post-transcriptional downregulation of protein kinase PKR. *Ann N Y Acad Sci* **1171 Suppl 1**, E75–85.

Ikegami, T., Peters, C. J. & Makino, S. (2005a). Rift valley fever virus nonstructural protein NSs promotes viral RNA replication and transcription in a minigenome system. *J Virol* **79**, 5606–5615.

Ikegami, T., Won, S., Peters, C. J. & Makino, S. (2005b). Rift Valley fever virus NSs mRNA is transcribed from an incoming anti-viral-sense S RNA segment. *J Virol* **79**, 12106–12111.

Ikegami, T., Won, S., Peters, C. J. & Makino, S. (2006). Rescue of infectious rift valley fever virus entirely from cDNA, analysis of virus lacking the NSs gene, and expression of a foreign gene. *J Virol* **80**, 2933–2940.

Ikegami, T., Won, S., Peters, C. J. & Makino, S. (2007). Characterization of Rift Valley fever virus transcriptional terminations. *J Virol* **81**, 8421–8438.

Imam, El, M., Sabiq, El, M., Omran, M., Abdalkareem, A., Gaili Mohamed, El, M. A., Elbashir, A. & Khalafala, O. (2009). Acute renal failure associated with the Rift Valley fever: a single center study. *Saudi J Kidney Dis Transpl* **20**, 1047–1052.

Jääskeläinen, K. M., Kaukinen, P., Minskaya, E. S., Plyusnina, A., Vapalahti, O., Elliott, R. M., Weber, F., Vaheri, A. & Plyusnin, A. (2007). Tula and Puumala hantavirus NSs ORFs are functional and the products inhibit activation of the interferon-beta promoter. *J Med Virol* **79**, 1527–1536. Wiley Subscription Services, Inc., A Wiley Company.

Jääskeläinen, K. M., Plyusnina, A., Lundkvist, A., Vaheri, A. & Plyusnin, A. (2008). Tula hantavirus isolate with the full-length ORF for nonstructural protein NSs survives for more consequent passages in interferon-competent cells than the isolate having truncated NSs ORF. *Virol J* **5**, 3. BioMed Central Ltd.

Jäger, S., Cimermancic, P., Gulbahce, N., Johnson, J. R., McGovern, K. E., Clarke, S. C., Shales, M., Mercenne, G., Pache, L. & other authors. **(2012).** Global landscape of HIV-human protein complexes. *Nature* **481**, 365–370.

Jenkins, G. M., Rambaut, A., Pybus, O. G. & Holmes, E. C. (2002). Rates of Molecular Evolution in RNA Viruses: A Quantitative Phylogenetic Analysis. *J Mol Evol* **54**, 156–165. Springer-Verlag.

Jin, H. & Elliott, R. M. (1991). Expression of functional Bunyamwera virus L protein by recombinant vaccinia viruses. *J Virol* **65**, 4182–4189.

Jin, H. & Elliott, R. M. (1992). Mutagenesis of the L protein encoded by Bunyamwera virus and production of monospecific antibodies. *J Gen Virol* **73 (Pt 9)**, 2235–2244.

Jin, H. & Elliott, R. M. (1993). Non-viral sequences at the 5' ends of Dugbe nairovirus S mRNAs. *J Gen Virol* **74 (Pt 10)**, 2293–2297.

Jin, M., Park, J., Lee, S., Park, B., Shin, J., Song, K.-J., Ahn, T.-I., Hwang, S.-Y., Ahn, B.-Y. & Ahn, K. (2002). Hantaan virus enters cells by clathrin-dependent receptor-mediated endocytosis. *Virology* **294**, 60–69.

Johnson, B. K., Chanas, A. C., el-Tayeb, E., Abdel-Wahab, K. S., Sheheta, F. A. & Mohamed A el-D. **(1978).** Rift Valley fever in Egypt, 1978. *Lancet* **2**, 745.

Jones, D. R. (2005). Plant Viruses Transmitted by Thrips. *Eur J Plant Pathol* **113**, 119–157. Kluwer Academic Publishers.

Jonsson, C. B., Figueiredo, L. T. M. & Vapalahti, O. (2010). A global perspective on hantavirus ecology, epidemiology, and disease. *Clin Microbiol Rev* **23**, 412–441. American Society for Microbiology.

Josse, T., Mokrani-Benhelli, H., Benferhat, R., Shestakova, E., Mansuroglu, Z., Kakanakou, H., Billecocq, A., Bouloy, M. & Bonnefoy, E. (2012). Association of the interferon-β gene with pericentromeric heterochromatin is dynamically regulated during virus infection through a YY1-dependent mechanism. *Nucleic Acids Res* **40**, 4396–4411.

Jup, P. G., Kemp, A., Grobbelaar, A., Lema, P., Burt, F. J., Alahmed, A. M., Mujalli, Al, D., Khamees, Al, M. & Swanepoel, R. (2002). The 2000 epidemic of Rift Valley fever in Saudi Arabia: mosquito vector studies. *Med Vet Entomol* **16**, 245–252.

Jupp, P. G., Kemp, A., Grobbelaar, A., LEMAN, P., Burt, F. J., Alahmed, A. M., MUJALLI, D. A., KHAMEES, M. A. & Swanepoel, R. (2002). The 2000 epidemic of Rift Valley fever in Saudi Arabia: mosquito vector studies. *Med Vet Entomol* **16**, 245–252. Blackwell Science Ltd.

Kading, R. C., Crabtree, M. B., Bird, B. H., Nichol, S. T., Erickson, B. R., Horiuchi, K., Biggerstaff, B. J. & Miller, B. R. (2014). Deletion of the NSm virulence gene of Rift Valley fever virus inhibits virus replication in and dissemination from the midgut of Aedes aegypti mosquitoes. *PLoS Negl Trop Dis* **8**, e2670 (M. J. Turell, Ed.).

Kalveram, B., Lihoradova, O. & Ikegami, T. (2011). NSs protein of rift valley fever virus promotes posttranslational downregulation of the TFIIH subunit p62. *J Virol* **85**, 6234–6243.

Karlikow, M., Goic, B. & Saleh, M.-C. (2014). RNAi and antiviral defense in Drosophila: setting up a systemic immune response. *Dev Comp Immunol* **42**, 85–92.

Karpf, A. R. & Brown, D. T. (1998). Comparison of Sindbis virus-induced pathology in mosquito and vertebrate cell cultures. *Virology* **240**, 193–201.

Kasari, T. R., Carr, D. A., Lynn, T. V. & Weaver, J. T. (2008). Evaluation of pathways for release of Rift Valley fever virus into domestic ruminant livestock, ruminant wildlife, and human populations in the continental United States. *J Am Vet Med Assoc* **232**, 514–529.

Kascsak, R. J. & Lyons, M. J. (1978). Bunyamwera virus. II. The generation and nature of defective interfering particles. *Virology* **89**, 539–546.

Kaukinen, P., Vaheri, A. & Plyusnin, A. (2003). Mapping of the regions involved in homotypic interactions of Tula hantavirus N protein. *J Virol* **77**, 10910–10916.

Keene, K. M., Foy, B. D., Sanchez-Vargas, I., Beaty, B. J., Blair, C. D. & Olson, K. E. (2004). RNA interference acts as a natural antiviral response to O'nyong-nyong virus (Alphavirus; Togaviridae) infection of Anopheles gambiae. *Proc Natl Acad Sci U S A* **101**, 17240–17245.

Kemp, C. & Imler, J.-L. (2009). Antiviral immunity in drosophila. *Curr Opin Immunol* **21**, 3–9.

Khoo, C. C. H., Piper, J., Sanchez-Vargas, I., Olson, K. E. & Franz, A. W. E. (2010). The RNA interference pathway affects midgut infection- and escape barriers for Sindbis virus in Aedes aegypti. *BMC Microbiol* **10**, 130.

Kim, V. N., Han, J. & Siomi, M. C. (2009). Biogenesis of small RNAs in animals. *Nat Rev Mol Cell Biol* **10**, 126–139.

King, A. M. Q., Adams, M. J., Lefkowitz, E. J. & Carstens, E. B. (2012). *Virus Taxonomy*. Elsevier.

Kinsella, E., Martin, S. G., Grolla, A., Czub, M., Feldmann, H. & Flick, R. (2004). Sequence determination of the Crimean-Congo hemorrhagic fever virus L segment. *Virology* **321**, 23–28.

Kittelberger, R., McFadden, A. M. J., Kirkland, P. D., Hannah, M. J., Orr, D., Bueno, R., Swainsbury, R., Keen, D., Jenner, J. & other authors. **(2013).** Evaluation of two commercial enzyme-linked immunosorbent assay kits for the detection of serum antibodies against Akabane virus in cattle. *J Vet Diagn Invest* **25**, 645–648.

Kohl, A., Billecocq, A., Prehaud, C., Yadani, F. Z. & Bouloy, M. (1999a). Transient gene expression in mammalian and mosquito cells using a recombinant Semliki Forest virus expressing T7 RNA polymerase. *Appl Microbiol Biotechnol* **53**, 51–56.

Kohl, A., di Bartolo, V. & Bouloy, M. (1999b). The Rift Valley fever virus nonstructural protein NSs is phosphorylated at serine residues located in casein kinase II consensus motifs in the carboxy-terminus. *Virology*.

Kohl, A., Hart, T. J., Noonan, C., Royall, E., Roberts, L. O. & Elliott, R. M. (2004). A bunyamwera virus minireplicon system in mosquito cells. *J Virol* **78**, 5679–5685. American Society for Microbiology.

Krautkrämer, E. & Zeier, M. (2008). Hantavirus causing hemorrhagic fever with renal syndrome enters from the apical surface and requires decay-accelerating factor (DAF/CD55). *J Virol* **82**, 4257–4264. American Society for Microbiology.

Kukkonen, S. K. J., Vaheri, A. & Plyusnin, A. (2004). Tula hantavirus L protein is a 250 kDa perinuclear membrane-associated protein. *J Gen Virol* **85**, 1181–1189.

Labuda, M. & Nuttall, P. A. (2004). Tick-borne viruses. *Parasitology* **129 Suppl**, S221–45.

Lappin, D. F., Nakitare, G. W., Palfreyman, J. W. & Elliott, R. M. (1994). Localization of Bunyamwera bunyavirus G1 glycoprotein to the Golgi requires association with G2 but not with NSm. *J Gen Virol* **75 (Pt 12)**, 3441–3451.

Le May, N., Dubaele, S., Proietti De Santis, L., Billecocq, A., Bouloy, M. & Egly, J.-M. (2004). TFIIH transcription factor, a target for the Rift Valley hemorrhagic fever virus. *Cell* **116**, 541–550.

Le May, N., Mansuroglu, Z., Léger, P., Josse, T., Blot, G., Billecocq, A., Flick, R., Jacob, Y., Bonnefoy, E. & Bouloy, M. (2008). A SAP30 complex inhibits IFN-beta expression in Rift Valley fever virus infected cells. *PLoS Pathog* **4**, e13.

Lemaitre, B. & Hoffmann, J. A. (2007). The host defense of Drosophila melanogaster. *Annu Rev Immunol* **25**, 697–743.

Léger, P., Lara, E., Jagla, B., Sismeiro, O., Mansuroglu, Z., Coppée, J. Y., Bonnefoy, E. & Bouloy, M. (2013). Dicer-2- and Piwi-mediated RNA interference in Rift Valley fever virus-infected mosquito cells. *J Virol* **87**, 1631–1648.

Li, C., Vagin, V. V., Lee, S., Xu, J., Ma, S., Xi, H., Seitz, H., Horwich, M. D., Syrzycka, M. & other authors. **(2009a).** Collapse of germline piRNAs in the absence of Argonaute3 reveals somatic piRNAs in flies. *Cell* **137**, 509–521. Elsevier.

Li, D. (2013). A highly pathogenic new bunyavirus emerged in China. *Emerging Microbes & Infections* **2**, e1.

Li, W., Lewandowski, D. J., Hilf, M. E. & Adkins, S. (2009b). Identification of domains of the Tomato spotted wilt virus NSm protein involved in tubule formation, movement and symptomatology. *Virology* **390**, 110–121.

Lin, C.-C., Chou, C.-M., Hsu, Y.-L., Lien, J.-C., Wang, Y.-M., Chen, S.-T., Tsai, S.-C., Hsiao, P.-W. & Huang, C.-J. (2004). Characterization of two mosquito STATs, AaSTAT and CtSTAT. Differential regulation of tyrosine phosphorylation and DNA binding activity by lipopolysaccharide treatment and by Japanese encephalitis virus infection. *J Biol Chem* **279**, 3308–3317.

Liu, S., Chai, C., Wang, C., Amer, S., Lv, H., He, H., Sun, J. & Lin, J. (2014). Systematic review of severe fever with thrombocytopenia syndrome: virology, epidemiology, and clinical characteristics. *Rev Med Virol* **24**, 90–102.

Liu, Y., Wimmer, E. & Paul, A. V. (2009). Cis-acting RNA elements in human and animal plus-strand RNA viruses. *Biochim Biophys Acta* **1789**, 495–517.

Lopez, N., Muller, R., Prehaud, C. & Bouloy, M. (1995). The L protein of Rift Valley fever virus can rescue viral ribonucleoproteins and transcribe synthetic genome-like RNA molecules. *J Virol* **69**, 3972–3979.

Lopez-Velez, R. & Molina Moreno, R. (2005). [Climate change in spain and risk of infectious and parasitic diseases transmitted by arthropods and rodents]. *Rev Esp Salud Publica* **79**, 177–190.

Lowen, A. C., Boyd, A., Fazakerley, J. K. & Elliott, R. M. (2005). Attenuation of bunyavirus replication by rearrangement of viral coding and noncoding sequences. *J Virol* **79**, 6940–6946.

Lozach, P.-Y., Kühbacher, A., Meier, R., Mancini, R., Bitto, D., Bouloy, M. & Helenius, A. (2011). DC-SIGN as a receptor for phleboviruses. *Cell Host Microbe* **10**, 75–88.

Lozach, P.-Y., Mancini, R., Bitto, D., Meier, R., Oestereich, L., Overby, A. K., Pettersson, R. F. & Helenius, A. (2010). Entry of bunyaviruses into mammalian cells. *Cell Host Microbe* **7**, 488–499. Elsevier.

Lu, K., Heng, X. & Summers, M. F. (2011). Structural determinants and mechanism of HIV-1 genome packaging. *J Mol Biol* **410**, 609–633.

Ludwig, G. V., Christensen, B. M., Yuill, T. M. & Schultz, K. T. (1989). Enzyme processing of La Crosse virus glycoprotein G1: a bunyavirus-vector infection model. *Virology* **171**, 108–113.

Ludwig, G. V., Israel, B. A., Christensen, B. M., Yuill, T. M. & Schultz, K. T. (1991). Role of La Crosse virus glycoproteins in attachment of virus to host cells. *Virology* **181**, 564–571.

MacNeil, A., Ksiazek, T. G. & Rollin, P. E. (2011). Hantavirus pulmonary syndrome, United States, 1993-2009. *Emerging Infect Dis* **17**, 1195–1201.

Madani, T. A., Al-Mazrou, Y. Y., Al-Jeffri, M. H., Mishkhas, A. A., Al-Rabeah, A. M., Turkistani, A. M., Al-Sayed, M. O., Abodahish, A. A., Khan, A. S. & other authors. (2003). Rift Valley fever epidemic in Saudi Arabia: epidemiological, clinical, and laboratory characteristics. *Clin Infect Dis* **37**, 1084–1092. Oxford University Press.

Maillard, P. V., Ciaudo, C., Marchais, A., Li, Y., Jay, F., Ding, S. W. & Voinnet, O. (2013). Antiviral RNA interference in mammalian cells. *Science* **342**, 235–238. American Association for the Advancement of Science.

Malone, C. D., Brennecke, J., Dus, M., Stark, A., McCombie, W. R., Sachidanandam, R. & Hannon, G. J. (2009). Specialized piRNA pathways act in germline and somatic tissues of the Drosophila ovary. *Cell* **137**, 522–535. Elsevier.

Mandell, R. B. & Flick, R. (2011). Rift Valley fever virus: a real bioterror threat. *J Bioterr Biodef*.

Mansuroglu, Z., Josse, T., Gilleron, J., Billecocq, A., Léger, P., Bouloy, M. & Bonnefoy, E. (2010). Nonstructural NSs protein of rift valley fever virus interacts with pericentromeric DNA sequences of the host cell, inducing chromosome cohesion and segregation defects. *J Virol* **84**, 928–939.

Marczinke, B. I. & Nichol, S. T. (2002). Nairobi sheep disease virus, an important tick-borne pathogen of sheep and goats in Africa, is also present in Asia. *Virology* **303**, 146–151.

Marklewitz, M., Zirkel, F., Rwego, I. B., Heidemann, H., Trippner, P., Kurth, A., Kallies, R., Briese, T., Lipkin, W. I. & other authors. **(2013).** Discovery of a unique novel clade of mosquito-associated bunyaviruses. *J Virol* **87**, 12850–12865. American Society for Microbiology.

Martin, M. (2011). Cutadapt removes adapter sequences from high-throughput sequencing reads. *EMBnet journal*.

Martin, M. L., Lindsey-Regnery, H., Sasso, D. R., McCormick, J. B. & Palmer, E. (1985). Distinction between Bunyaviridae genera by surface structure and comparison with Hantaan virus using negative stain electron microscopy. *Arch Virol* **86**, 17–28. Springer-Verlag.

Matranga, C., Tomari, Y., Shin, C., Bartel, D. P. & Zamore, P. D. (2005). Passenger-strand cleavage facilitates assembly of siRNA into Ago2-containing RNAi enzyme complexes. *Cell* **123**, 607–620. Elsevier.

McElroy, A. K., Albariño, C. G. & Nichol, S. T. (2009). Development of a RVFV ELISA that can distinguish infected from vaccinated animals. *Virol J* **6**, 125.

McIntosh, B. M., Dickinson, D. B. & Santos, dos, I. (1973). Rift Valley fever. 3. Viraemia in cattle and sheep. 4. The susceptibility of mice and hamsters in relation to transmission of virus by mosquitoes. *J S Afr Vet Assoc* **44**, 167–169.

McJunkin, J. E., de los Reyes, E. C., Irazuzta, J. E., Caceres, M. J., Khan, R. R., Minnich, L. L., Fu, K. D., Lovett, G. D., Tsai, T. & Thompson, A. (2001). La Crosse encephalitis in children. *N Engl J Med* **344**, 801–807.

McLean, J. E., Ruck, A., Shirazian, A., Pooyaei-Mehr, F. & Zakeri, Z. F. (2008). Viral manipulation of cell death. *Curr Pharm Des* **14**, 198–220.

McWilliam, H., Li, W., Uludag, M., Squizzato, S., Park, Y. M., Buso, N., Cowley, A. P. & Lopez, R. (2013). Analysis Tool Web Services from the EMBL-EBI. *Nucleic Acids Res* **41**, W597–600. Oxford University Press.

Meegan, J. M. (1979). The Rift Valley fever epizootic in Egypt 1977-78. 1. Description of the epizzotic and virological studies. *Trans R Soc Trop Med Hyg* **73**, 618–623.

Meegan, J. M. (1981). *Rift Valley fever in Egypt: an overview of the epizootics in 1977 and 1978*. Proceedings... Rift Valley fever; a workshop.

Meegan, J. M., Hoogstraal, H. & Moussa, M. I. (1979). An epizootic of Rift Valley fever in Egypt in 1977. *Vet Rec* **105**, 124–125.

Mellor, P. S. (2000). Replication of arboviruses in insect vectors. *J Comp Pathol* **123**, 231–247.

Mims, C. A., Day, M. F. & Marshall, I. D. (1966). Cytopathic effect of Semliki Forest virus in the mosquito Aedes aegypti. *Am J Trop Med Hyg* **15**, 775–784.

Mir, M. A., Brown, B., Hjelle, B., Duran, W. A. & Panganiban, A. T. (2006). Hantavirus N protein exhibits genus-specific recognition of the viral RNA panhandle. *J Virol* **80**, 11283–11292.

Mir, M. A., Duran, W. A., Hjelle, B. L., Ye, C. & Panganiban, A. T. (2008). Storage of cellular 5' mRNA caps in P bodies for viral cap-snatching. *Proc Natl Acad Sci USA* **105**, 19294–19299. National Acad Sciences.

Morazzani, E. M., Wiley, M. R., Murreddu, M. G., Adelman, Z. N. & Myles, K. M. (2012). Production of virus-derived ping-pong-dependent piRNA-like small RNAs in the mosquito soma. *PLoS Pathog* **8**, e1002470 (S.-W. Ding, Ed.). Public Library of Science.

Morrill, J. C. & Peters, C. J. (2011). Protection of MP-12-Vaccinated Rhesus Macaques Against Parenteral and Aerosol Challenge With Virulent Rift Valley Fever Virus. *J Infect Dis* **204**, 229–236.

Morvan, J., Rollin, P. E. & Roux, J. (1992). [Rift Valley fever in Madagascar in 1991. Sero-epidemiological studies in cattle]. *Rev Elev Med Vet Pays Trop* **45**, 121–127.

Morvan, J., Saluzzo, J. F., Fontenille, D., Rollin, P. E. & Coulanges, P. (1991). Rift Valley fever on the east coast of Madagascar. *Res Virol* **142**, 475–482.

Mourãão, M. P. G., Bastos, M. S., Gimaqu, J. B. L., Mota, B. R., Souza, G. S., Grimmer, G. H. N., Galusso, E. S., Arruda, E. & Figueiredo, L. T. M. (2009). Oropouche fever outbreak, Manaus, Brazil, 2007-2008. *Emerging Infect Dis* **15**, 2063–2064.

Moutailler, S., Roche, B., Thiberge, J.-M., Caro, V., Rougeon, F. & Failloux, A.-B. (2011). Host alternation is necessary to maintain the genome stability of rift valley Fever virus. *PLoS Negl Trop Dis* **5**, e1156.

Muller, R., Poch, O., Delarue, M., Bishop, D. H. & Bouloy, M. (1994). Rift Valley fever virus L segment: correction of the sequence and possible functional role of newly identified regions conserved in RNA-dependent polymerases. *J Gen Virol* **75 (Pt 6)**, 1345–1352.

Muller, R., Saluzzo, J. F., Lopez, N., Dreier, T., Turell, M., Smith, J. & Bouloy, M. (1995). Characterization of clone 13, a naturally attenuated avirulent isolate of Rift Valley fever virus, which is altered in the small segment. *Am J Trop Med Hyg* **53**, 405–411.

Murakami, S., Terasaki, K., Narayanan, K. & Makino, S. (2012). Roles of the coding and noncoding regions of rift valley Fever virus RNA genome segments in viral RNA packaging. *J Virol* **86**, 4034–4039. American Society for Microbiology.

Nene, V., Wortman, J. R., Lawson, D., Haas, B., Kodira, C., Tu, Z. J., Loftus, B., Xi, Z., Megy, K. & other authors. **(2007).** Genome sequence of Aedes aegypti, a major arbovirus vector. *Science* **316**, 1718–1723.

Neumann, G., Watanabe, T., Ito, H., Watanabe, S., Goto, H., Gao, P., Hughes, M., Perez, D. R., Donis, R. & other authors. **(1999).** Generation of influenza A viruses entirely from cloned cDNAs. *Proc Natl Acad Sci U S A* **96**, 9345–9350.

Newton, S. E., Short, N. J. & Dalgarno, L. (1981). Bunyamwera virus replication in cultured Aedes albopictus (mosquito) cells: establishment of a persistent viral infection. *J Virol* **38**, 1015–1024.

Nguyen, M. & Haenni, A.-L. (2003). Expression strategies of ambisense viruses. *Virus Res* **93**, 141–150.

Nichol, S. T., Rowe, J. E. & Fitch, W. M. (1993). Punctuated equilibrium and positive Darwinian evolution in vesicular stomatitis virus. *Proc Natl Acad Sci U S A* **90**, 10424–10428. National Acad Sciences.

Noton, S. L., Cowton, V. M., Zack, C. R., McGivern, D. R. & Fearns, R. (2010). Evidence that the polymerase of respiratory syncytial virus initiates RNA replication in a nontemplated fashion. *Proc Natl Acad Sci USA* **107**, 10226–10231. National Acad Sciences.

Novoa, R. R., Calderita, G., Arranz, R., Fontana, J., Granzow, H. & Risco, C. (2005a). Virus factories: associations of cell organelles for viral replication and morphogenesis. *Biol Cell* **97**, 147.

Novoa, R. R., Calderita, G., Cabezas, P., Elliott, R. M. & Risco, C. (2005b). Key Golgi factors for structural and functional maturation of bunyamwera virus. *J Virol* **79**, 10852–10863.

Núñez, J. J., Fritz, C. L., Knust, B., Buttke, D., Enge, B., Novak, M. G., Kramer, V., Osadebe, L., Messenger, S. & other authors. **(2014).** Hantavirus infections among overnight visitors to Yosemite National Park, California, USA, 2012. *Emerging Infect Dis* **20**, 386–393.

Obijeski, J. F., Bishop, D. H., Murphy, F. A. & Palmer, E. L. (1976a). Structural proteins of La Crosse virus. *J Virol* **19**, 985–997. American Society for Microbiology.

Obijeski, J. F., Bishop, D. H., Palmer, E. L. & Murphy, F. A. (1976b). Segmented genome and nucleocapsid of La Crosse virus. *J Virol* **20**, 664–675.

Ogawa, Y., Kato, K., Tohya, Y. & Akashi, H. (2007a). Characterization of temperature-sensitive Akabane virus mutants and their roles in attenuation. *Arch Virol* **152**, 1679–1686. Springer-Verlag.

Ogawa, Y., Sugiura, K., Kato, K., Tohya, Y. & Akashi, H. (2007b). Rescue of Akabane virus (family Bunyaviridae) entirely from cloned cDNAs by using RNA polymerase I. *J Gen Virol* **88**, 3385–3390. Society for General Microbiology.

Olaleye, O. D., Tomori, O., Fajimi, J. L. & Schmitz, H. (1996). Experimental infection of three Nigerian breeds of sheep with the Zinga strain of the Rift Valley Fever virus. *Rev Elev Med Vet Pays Trop* **49**, 6–16.

Oliveira, V. C., Bartasson, L., de Castro, M. E. B., Corrêa, J. R., Ribeiro, B. M. & Resende, R. O. (2011). A silencing suppressor protein (NSs) of a tospovirus enhances baculovirus replication in permissive and semipermissive insect cell lines. *Virus Res* **155**, 259–267.

Olivieri, D., Sykora, M. M., Sachidanandam, R., Mechtler, K. & Brennecke, J. (2010). An in vivo RNAi assay identifies major genetic and cellular requirements for primary piRNA biogenesis in Drosophila. *EMBO J* **29**, 3301–3317.

Osborne, J. C. & Elliott, R. M. (2000). RNA binding properties of bunyamwera virus nucleocapsid protein and selective binding to an element in the 5' terminus of the negative-sense S segment. *J Virol* **74**, 9946–9952.

Overby, A. K., Pettersson, R. F. & Neve, E. P. A. (2007a). The glycoprotein cytoplasmic tail of Uukuniemi virus (Bunyaviridae) interacts with ribonucleoproteins and is critical for genome packaging. *J Virol* **81**, 3198–3205.

Overby, A. K., Popov, V. L., Pettersson, R. F. & Neve, E. P. A. (2007b). The cytoplasmic tails of Uukuniemi Virus (Bunyaviridae) G(N) and G(C) glycoproteins are important for intracellular targeting and the budding of virus-like particles. *J Virol* **81**, 11381–11391.

Överby, A. K., Pettersson, R. F., Grünewald, K. & Huiskonen, J. T. (2008). Insights into bunyavirus architecture from electron cryotomography of Uukuniemi virus. *Proc Natl Acad Sci USA* **105**, 2375–2379.

Pappu, H. R., Jones, R. A. C. & Jain, R. K. (2009). Global status of tospovirus epidemics in diverse cropping systems: successes achieved and challenges ahead. *Virus Res* **141**, 219–236.

Pepin, M., Bouloy, M., Bird, B. H., Kemp, A. & Paweska, J. (2010). Rift Valley fever virus (Bunyaviridae: Phlebovirus): an update on pathogenesis, molecular epidemiology, vectors, diagnostics and prevention. *Veterinary research* **41**, 61.

Persson, R. & Pettersson, R. F. (1991). Formation and intracellular transport of a heterodimeric viral spike protein complex. *J Cell Biol* **112**, 257–266.

Pfeiffer, D., Ppin, M. & Wooldridge, M. (2005). *The risk of a Rift Valley fever incursion and its persistence within the community*. EFSA J.

Piper, M. E., Sorenson, D. R. & Gerrard, S. R. (2011). Efficient cellular release of Rift Valley fever virus requires genomic RNA. *PLoS ONE* **6**, e18070.

Plassmeyer, M. L., Soldan, S. S., Stachelek, K. M., Martín-García, J. & González-Scarano, F. (2005). California serogroup Gc (G1) glycoprotein is the principal determinant of pH-dependent cell fusion and entry. *Virology* **338**, 121–132.

Plyusnin, A., Beaty, B. J., Elliott, R. M., Kormelink, R., Schmaljohn, C. & Tesh, R. B. (2012). The Negative Sense Single Stranded RNA Viruses - Bunyaviridae. In *Virus Taxonomy*, pp. 725–741. Edited by A. M. Q. King, M. J. Adams, E. B. Carstens & E. J. Lefkowitz. Elsevier.

Poch, O., Sauvaget, I., Delarue, M. & Tordo, N. (1989). Identification of four conserved motifs among the RNA-dependent polymerase encoding elements. *EMBO J* **8**, 3867–3874.

Prins, M. & Goldbach, R. (1998). The emerging problem of tospovirus infection and nonconventional methods of control. *Trends Microbiol* **6**, 31–35. Elsevier.

Pudney, M., Varma, M. G. R. & Leake, C. J. (1979). Establishment of cell lines from larvae of culicine (Aedes species) and anopheline mosquitoes. *Tca Manual* **5**, 997–1002. Kluwer Academic Publishers.

Rand, T. A., Petersen, S., Du, F. & Wang, X. (2005). Argonaute2 cleaves the anti-guide strand of siRNA during RISC activation. *Cell* **123**, 621–629. Elsevier.

Randall, R. E. & Goodbourn, S. (2008). Interferons and viruses: an interplay between induction, signalling, antiviral responses and virus countermeasures. *J Gen Virol* **89**, 1–47. Society for General Microbiology.

Ravkov, E. V., Nichol, S. T. & Compans, R. W. (1997). Polarized entry and release in epithelial cells of Black Creek Canal virus, a New World hantavirus. *J Virol* **71**, 1147–1154.

Raymond, D. D., Piper, M. E., Gerrard, S. R. & Smith, J. L. (2010). Structure of the Rift Valley fever virus nucleocapsid protein reveals another architecture for RNA encapsidation. *Proc Natl Acad Sci USA* **107**, 11769–11774.

RCore, T. (2012). *R: A language and environment for statistical computing. R Foundation for Statistical Computing, Vienna, Austria*.

Reguera, J., Malet, H., Weber, F. & Cusack, S. (2013). Structural basis for encapsidation of genomic RNA by La Crosse Orthobunyavirus nucleoprotein. *Proc Natl Acad Sci USA* **110**, 7246–7251. National Acad Sciences.

Reguera, J., Weber, F. & Cusack, S. (2010). Bunyaviridae RNA polymerases (L-protein) have an N-terminal, influenza-like endonuclease domain, essential for viral cap-dependent transcription. *PLoS Pathog* **6**, e1001101 (F. A. Rey, Ed.). Public Library of Science.

Reynolds, S. H. & Ruohola-Baker, H. (2009). PIWI goes solo in the soma. *Dev Cell* **16**, 627–628. Elsevier.

Riley, D. G., Joseph, S. V., Srinivasan, R. & Diffie, S. (2011). Thrips Vectors of Tospoviruses. *j integ pest manage* **2**, 1–10.

Rima, B. K. & McFerran, N. V. (1997). Dinucleotide and stop codon frequencies in single-stranded RNA viruses. *J Gen Virol*.

Rolin, A. I., Berrang-Ford, L. & Kulkarni, M. A. (2013). The risk of Rift Valley fever virus introduction and establishment in the United States and European Union. *Emerging Microbes & Infections* **2**, e81. Nature Publishing Group.

Rossier, C., Patterson, J. & Kolakofsky, D. (1986). La Crosse virus small genome mRNA is made in the cytoplasm. *J Virol* **58**, 647–650.

Sadler, A. J. & Williams, B. R. G. (2008). Interferon-inducible antiviral effectors. *Nat Rev Immunol* **8**, 559–568.

Salanueva, I. J., Novoa, R. R. & Cabezas, P. (2003). Polymorphism and structural maturation of bunyamwera virus in Golgi and post-Golgi compartments. *J Virol* **77**, 1368-1381.

Sanchez, A. J., Vincent, M. J., Erickson, B. R. & Nichol, S. T. (2006). Crimean-congo hemorrhagic fever virus glycoprotein precursor is cleaved by Furin-like and SKI-1 proteases to generate a novel 38-kilodalton glycoprotein. *J Virol* **80**, 514–525. American Society for Microbiology.

Sanchez-Vargas, I., Scott, J. C., Poole-Smith, B. K., Franz, A. W. E., Barbosa-Solomieu, V., Wilusz, J., Olson, K. E. & Blair, C. D. (2009). Dengue virus type 2 infections of Aedes aegypti are modulated by the mosquito's RNA interference pathway. *PLoS Pathog* **5**, e1000299 (C. M. Rice, Ed.).

Sanchez-Vargas, I., Travanty, E. A., Keene, K. M., Franz, A. W. E., Beaty, B. J., Blair, C. D. & Olson, K. E. (2004). RNA interference, arthropod-borne viruses, and mosquitoes. *Virus Res* **102**, 65–74.

Sander, J. D. & Joung, J. K. (2014). CRISPR-Cas systems for editing, regulating and targeting genomes. *Nat Biotechnol* **32**, 347–355.

Sanders, H. R., Foy, B. D., Evans, A. M., Ross, L. S., Beaty, B. J., Paskewitz, S. M. & Gill, S. S. (2005). Sindbis virus induces transport processes and alters expression of innate immunity pathway genes in the midgut of the disease vector, Aedes aegypti. *Insect Biochem Mol Biol* **35**, 1293–1307.

Santos, R. I. M., Rodrigues, A. H., Silva, M. L., Mortara, R. A., Rossi, M. A., Jamur, M. C., Oliver, C. & Arruda, E. (2008). Oropouche virus entry into HeLa cells involves clathrin and requires endosomal acidification. *Virus Res* **138**, 139–143.

Sánchez, A. B. & la Torre, de, J. C. (2006). Rescue of the prototypic Arenavirus LCMV entirely from plasmid. *Virology* **350**, 370–380.

Scallan, M. F. & Elliott, R. M. (1992). Defective RNAs in mosquito cells persistently infected with Bunyamwera virus. *J Gen Virol*.

Schneider, T. D. & Stephens, R. M. (1990). Sequence logos: a new way to display consensus sequences. *Nucleic Acids Res* **18**, 6097–6100.

Schnettler, E., Donald, C. L., Human, S., Watson, M., Siu, R. W. C., McFarlane, M., Fazakerley, J. K., Kohl, A. & Fragkoudis, R. (2013a). Knockdown of piRNA pathway proteins results in enhanced Semliki Forest virus production in mosquito cells. *J Gen Virol* **94**, 1680–1689. Society for General Microbiology.

Schnettler, E., Ratinier, M., Watson, M., Shaw, A. E., McFarlane, M., Varela, M., Elliott, R. M., Palmarini, M. & Kohl, A. (2013b). RNA interference targets arbovirus replication in Culicoides cells. *J Virol* **87**, 2441–2454. American Society for Microbiology.

Scott, J. C., Brackney, D. E., Campbell, C. L., Bondu-Hawkins, V., Hjelle, B., Ebel, G. D., Olson, K. E. & Blair, C. D. (2010). Comparison of dengue virus type 2-specific small RNAs from RNA interference-competent and -incompetent mosquito cells. *PLoS Negl Trop Dis* **4**, e848.

Scott, T. W. & Weaver, S. C. (1994). Evolution of mosquito-borne viruses. In Evolutionary Biology of Viruses, Morse, S.S., ed. (New York, NY, Raven Press).

Seufi, A. M. & Galal, F. H. (2010). Role of Culex and Anopheles mosquito species as potential vectors of rift valley fever virus in Sudan outbreak, 2007. *BMC Infect Dis* **10**, 65. BioMed Central Ltd.

Severson, W. E., Xu, X. & Jonsson, C. B. (2001). cis-Acting signals in encapsidation of Hantaan virus S-segment viral genomic RNA by its N protein. *J Virol* **75**, 2646–2652. American Society for Microbiology.

Shi, X., Brauburger, K. & Elliott, R. M. (2005). Role of N-linked glycans on bunyamwera virus glycoproteins in intracellular trafficking, protein folding, and virus infectivity. *J Virol* **79**, 13725–13734. American Society for Microbiology.

Shi, X. & Elliott, R. M. (2004). Analysis of N-linked glycosylation of hantaan virus glycoproteins and the role of oligosaccharide side chains in protein folding and intracellular trafficking. *J Virol* **78**, 5414–5422.

Shi, X. & Elliott, R. M. (2009). Generation and analysis of recombinant Bunyamwera orthobunyaviruses expressing V5 epitope-tagged L proteins. *J Gen Virol* **90**, 297–306.

Shi, X., Kohl, A., Léonard, V. H. J., Li, P., Mclees, A. & Elliott, R. M. (2006). Requirement of the N-terminal region of orthobunyavirus nonstructural protein NSm for virus assembly and morphogenesis. *J Virol* **80**, 8089–8099.

Shoemaker, T., Boulianne, C., Vincent, M. J., Pezzanite, L., Al-Qahtani, M. M., Al-Mazrou, Y., Khan, A. S., Rollin, P. E., Swanepoel, R. & other authors. (2002). Genetic analysis of viruses associated with emergence of Rift Valley fever in Saudi Arabia and Yemen, 2000-01. *Emerging Infect Dis* **8**, 1415–1420.

Sim, S. & Dimopoulos, G. (2010). Dengue virus inhibits immune responses in Aedes aegypti cells. *PLoS ONE* **5**, e10678 (R. F. Speck, Ed.). Public Library of Science.

Simmonds, P., Tuplin, A. & Evans, D. J. (2004). Detection of genome-scale ordered RNA structure (GORS) in genomes of positive-stranded RNA viruses: Implications for virus evolution and host persistence. *RNA* **10**, 1337–1351. Cold Spring Harbor Lab.

Simmonds, P., Xia, W., Baillie, J. K. & McKinnon, K. (2013). Modelling mutational and selection pressures on dinucleotides in eukaryotic phyla--selection against CpG and UpA in cytoplasmically expressed RNA and in RNA viruses. *BMC Genomics* **14**, 610. BioMed Central Ltd.

Simon, M., Johansson, C. & Mirazimi, A. (2009). Crimean-Congo hemorrhagic fever virus entry and replication is clathrin-, pH- and cholesterol-dependent. *J Gen Virol* **90**, 210–215. Society for General Microbiology.

Simons, J. F., Hellman, U. & Pettersson, R. F. (1990). Uukuniemi virus S RNA segment: ambisense coding strategy, packaging of complementary strands into virions, and homology to members of the genus Phlebovirus. *J Virol* **64**, 247–255.

Sims, D., Bursteinas, B., Jain, E., Gao, Q., Baum, B. & Zvelebil, M. (2010). The flight Drosophila RNAi database: 2010 update. *Fly* **4**.

Siomi, M. C., Sato, K., Pezic, D. & Aravin, A. A. (2011). PIWI-interacting small RNAs: the vanguard of genome defence. *Nat Rev Mol Cell Biol* **12**, 246–258.

Smith, M. C. & Sherman, D. M. (2011). *Goat Medicine*. John Wiley & Sons.

Stalder, J., Reigel, F. & Koblet, H. (1983). Defective viral RNAs in Aedes albopictus C6/36 cells persistently infected with Semliki Forest virus. *Virology* **129**, 247–254.

Sumibcay, L., Kadjo, B., Gu, S. H., Kang, H. J., Lim, B. K., Cook, J. A., Song, J.-W. & Yanagihara, R. (2012). Divergent lineage of a novel hantavirus in the banana pipistrelle (Neoromicia nanus) in Côte d'Ivoire. *Virol J* **9**, 34. BioMed Central Ltd.

Svoboda, P. (2014). Renaissance of mammalian endogenous RNAi. *FEBS Lett* **588**, 2550–2556. Elsevier.

Swanepoel, R. & Blackburn, N. K. (1977). Demonstration of Nuclear Immunofluorescence in Rift Valley Fever Infected Cells. *J Gen Virol* **34**, 557–561. Society for General Microbiology.

Swanepoel, R. & Coetzer, J. (2004). Infectious diseases of livestock. Cape Town: Oxford University Press Southern Africa.

Szemiel, A. M., Failloux, A.-B. & Elliott, R. M. (2012). Role of Bunyamwera Orthobunyavirus NSs protein in infection of mosquito cells. *PLoS Negl Trop Dis* **6**, e1823 (B. Bird, Ed.). Public Library of Science.

Talmon, Y., Prasad, B. V., Clerx, J. P., Wang, G. J., Chiu, W. & Hewlett, M. J. (1987). Electron microscopy of vitrified-hydrated La Crosse virus. *J Virol* **61**, 2319–2321.

Tarlinton, R., Daly, J., Dunham, S. & Kydd, J. (2012). The challenge of Schmallenberg virus emergence in Europe. *Vet J* **194**, 10–18.

Tchurikov, N. A. & Kretova, O. V. (2011). Both piRNA and siRNA pathways are silencing transcripts of the suffix element in the Drosophila melanogaster germline and somatic cells. *PLoS ONE* **6**, e21882 (P. Michalak, Ed.). Public Library of Science.

Terasaki, K., Murakami, S., Lokugamage, K. G. & Makino, S. (2011). Mechanism of tripartite RNA genome packaging in Rift Valley fever virus. *Proc Natl Acad Sci USA* **108**, 804–809.

Tomari, Y., Du, T. & Zamore, P. D. (2007). Sorting of Drosophila small silencing RNAs. *Cell* **130**, 299–308. Elsevier.

Uchil, P. D. & Satchidanandam, V. (2003). Characterization of RNA synthesis, replication mechanism, and in vitro RNA-dependent RNA polymerase activity of Japanese encephalitis virus. *Virology* **307**, 358–371.

Uhrig, J. F., Soellick, T. R., Minke, C. J., Philipp, C., Kellmann, J. W. & Schreier, P. H. (1999). Homotypic interaction and multimerization of nucleocapsid protein of tomato spotted wilt tospovirus: identification and characterization of two interacting domains. *Proc Natl Acad Sci U S A* **96**, 55–60.

Vaidyanathan, R. & Scott, T. W. (2006). Apoptosis in mosquito midgut epithelia associated with West Nile virus infection. *Apoptosis* **11**, 1643–1651. Kluwer Academic Publishers.

van Cleef, K. W. R., van Mierlo, J. T., van den Beek, M. & van Rij, R. P. (2011). Identification of viral suppressors of RNAi by a reporter assay in Drosophila S2 cell culture. *Methods Mol Biol* **721**, 201–213.

van Knippenberg, I., Fragkoudis, R. & Elliott, R. M. (2013). The transient nature of Bunyamwera orthobunyavirus NSs protein expression: effects of increased stability of NSs protein on virus replication. *PLoS ONE* **8**, e64137 (V. Thiel, Ed.). Public Library of Science.

van Mierlo, J. T., van Cleef, K. W. R. & van Rij, R. P. (2011). Defense and counterdefense in the RNAi-based antiviral immune system in insects. *Methods Mol Biol* **721**, 3–22. Totowa, NJ: Humana Press.

van Rij, R. P., Saleh, M.-C., Berry, B., Foo, C., Houk, A., Antoniewski, C. & Andino, R. (2006). The RNA silencing endonuclease Argonaute 2 mediates specific antiviral immunity in Drosophila melanogaster. *Genes Dev* **20**, 2985–2995.

Varela, M., Schnettler, E., Caporale, M., Murgia, C., Barry, G., McFarlane, M., McGregor, E., Piras, I. M., Shaw, A. & other authors. **(2013).** Schmallenberg virus pathogenesis, tropism and interaction with the innate immune system of the host. *PLoS Pathog* **9**, e1003133 (F. Weber, Ed.). Public Library of Science.

Vasilakis, N., Deardorff, E. R., Kenney, J. L., Rossi, S. L., Hanley, K. A. & Weaver, S. C. (2009). Mosquitoes Put the Brake on Arbovirus Evolution: Experimental Evolution Reveals Slower Mutation Accumulation in Mosquito Than Vertebrate Cells. *PLoS Pathog* **5**, e1000467 (R. Andino, Ed.). Public Library of Science.

Vera-Otarola, J., Solis, L., Soto-Rifo, R., Ricci, E. P., Pino, K., Tischler, N. D., Ohlmann, T., Darlix, J.-L. & López-Lastra, M. (2012). The Andes hantavirus NSs protein is expressed from the viral small mRNA by a leaky scanning mechanism. *J Virol* **86**, 2176–2187. American Society for Microbiology.

Vera-Otarola, J., Soto-Rifo, R., Ricci, E. P., Ohlmann, T., Darlix, J.-L. & López-Lastra, M. (2010). The 3' untranslated region of the Andes hantavirus small mRNA functionally replaces the poly(A) tail and stimulates cap-dependent translation initiation from the viral mRNA. *J Virol* **84**, 10420–10424. American Society for Microbiology.

Vialat, P., Billecocq, A., Kohl, A. & Bouloy, M. (2000). The S segment of rift valley fever phlebovirus (Bunyaviridae) carries determinants for attenuation and virulence in mice. *J Virol* **74**, 1538–1543.

Vialat, P., Muller, R., Vu, T. H., Prehaud, C. & Bouloy, M. (1997). Mapping of the mutations present in the genome of the Rift Valley fever virus attenuated MP12 strain and their putative role in attenuation. *Virus Res* **52**, 43–50.

Vodovar, N., Bronkhorst, A. W., van Cleef, K. W. R., Miesen, P., Blanc, H., van Rij, R. P. & Saleh, M.-C. (2012). Arbovirus-Derived piRNAs Exhibit a Ping-Pong Signature in Mosquito Cells. *PLoS ONE* **7**, e30861 (S. Pfeffer, Ed.). Public Library of Science.

Wang, H., Gort, T., Boyle, D. L. & Clem, R. J. (2012). Effects of manipulating apoptosis on Sindbis virus infection of Aedes aegypti mosquitoes. *J Virol* **86**, 6546–6554. American Society for Microbiology.

Wang, X.-H., Aliyari, R., Li, W.-X., Li, H.-W., Kim, K., Carthew, R., Atkinson, P. & Ding, S.-W. (2006). RNA interference directs innate immunity against viruses in adult Drosophila. *Science* **312**, 452–454. American Association for the Advancement of Science.

Waterhouse, R. M., Kriventseva, E. V., Meister, S., Xi, Z., Alvarez, K. S., Bartholomay, L. C., Barillas-Mury, C., Bian, G., Blandin, S. & other authors. (2007). Evolutionary dynamics of immune-related genes and pathways in disease-vector mosquitoes. *Science* **316**, 1738–1743.

Watson, M., Schnettler, E. & Kohl, A. (2013). viRome: an R package for the visualization and analysis of viral small RNA sequence datasets. *Bioinformatics* **29**, 1902–1903. Oxford University Press.

Weaver, S. C., Lorenz, L. H. & Scott, T. W. (1992a). Pathologic changes in the midgut of Culex tarsalis following infection with Western equine encephalomyelitis virus. *Am J Trop Med Hyg* **47**, 691–701.

Weaver, S. C., Rico-Hesse, R. & Scott, T. W. (1992b). Genetic Diversity and Slow Rates of Evolution in New World Alphaviruses. In *Genetic Diversity of RNA Viruses*, Current Topics in Microbiology and Immunology, pp. 99–117. Edited by J. J. Holland. Berlin, Heidelberg: Springer Berlin Heidelberg.

Weill, L., Shestakova, E. & Bonnefoy, E. (2003). Transcription factor YY1 binds to the murine beta interferon promoter and regulates its transcriptional capacity with a dual activator/repressor role. *J Virol* **77**, 2903–2914.

Weiss, S., Witkowski, P. T., Auste, B., Nowak, K., Weber, N., Fahr, J., Mombouli, J.-V., Wolfe, N. D., Drexler, J. F. & other authors. (2012). Hantavirus in bat, Sierra Leone. *Emerging Infect Dis* **18**, 159–161.

Whitfield, A. E., Ullman, D. E. & German, T. L. (2004). Expression and characterization of a soluble form of tomato spotted wilt virus glycoprotein GN. *J Virol* **78**, 13197–13206. American Society for Microbiology.

Won, S., Ikegami, T., Peters, C. J. & Makino, S. (2007). NSm protein of Rift Valley fever virus suppresses virus-induced apoptosis. *J Virol* **81**, 13335–13345.

Xi, Z., Ramirez, J. L. & Dimopoulos, G. (2008). The Aedes aegypti toll pathway controls dengue virus infection. *PLoS Pathog* **4**, e1000098 (D. S. Schneider, Ed.). Public Library of Science.

Yadani, F. Z., Kohl, A., Prehaud, C., Billecocq, A. & Bouloy, M. (1999). The carboxy-terminal acidic domain of Rift Valley Fever virus NSs protein is essential for the formation of filamentous structures but not for the nuclear localization of the protein. *J Virol* **73**, 5018–5025.

Yan, Z., Hu, H. Y., Jiang, X., Maierhofer, V., Neb, E., He, L., Hu, Y., Hu, H., Li, N. & other authors. (2011). Widespread expression of piRNA-like molecules in somatic tissues. *Nucleic Acids Res* **39**, 6596–6607. Oxford University Press.

Zambon, R. A., Nandakumar, M., Vakharia, V. N. & Wu, L. P. (2005). The Toll pathway is important for an antiviral response in Drosophila. *Proc Natl Acad Sci USA* **102**, 7257–7262. National Acad Sciences.

Zambon, R. A., Vakharia, V. N. & Wu, L. P. (2006). RNAi is an antiviral immune response against a dsRNA virus in Drosophila melanogaster. *Cell Microbiol* **8**, 880–889. Blackwell Publishing Ltd.

Zuker, M. (2003). Mfold web server for nucleic acid folding and hybridization prediction. *Nucleic Acids Res* **31**, 3406–3415.